THIRD

INTERNATIONAL

CONFERENCE

ON

STABILITY

OF

SHIPS

AND

OCEAN VEHICLES

VOLUME I
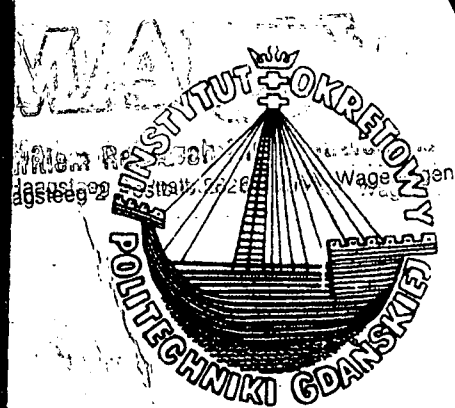
STAB'86

22-26

September 1986

GDAŃSK-POLAND

STAB'86

Third
International
Conference
on

Stability
of
Ships
and
Ocean Vehicles

22-26
September 1986
Gdańsk-Poland

Volume I

ABOUT THE CONFERENCE

As long as shipping existed ships were exposed to the hostile environment
and shipbuilders from the oldest times lerned that in order to survive
in this environment ships had to stable. They developed also by trial and
error method the practical knowledge how to build comparatively stable
ships, however not stable enough to ensure safe completion of the voyage.
In modern times understanding of basic laws of ship's geometry and static
stability enabled naval architects to make calculations during the design
stage, then developments in ship hydrodynamics allowed to calculate the
behaviour of ship in a seaway and the effect of external forces on stabi-
lity. Nevertheless from time to time ships were lost as a result of cap-
sizing quite often with all hands onboard. Even introduction by some na-
tions of stability regulations which also included certain stability cri-
teria did not eliminate casualties.

For more than two decades International Maritime Organization have at-
tempted to establish international stability requirements. It partly suc-
ceded in adopting in 1968 the Recommendation on Intact Stability for Pa-
ssenger and Cargo Ships under 100 metres in length and similar Recommen-
dation for fishing vessels. However those recommendations are not fully
satisfactory and IMO is continuing its work towards development of more
rational criteria. Achievement of this goal will be possible probably ma-
ny years from now, because development of stability criteria belongs to
the most difficult problems of ship design and hydrodynamics. In spite of
many efforts there still is lack of basic understanding and of mathemati-
cal description of the basic physical phenomena leading to ship capsizing,
the philosophical problem of establishing critical limits for different
stability parameters taking due account of the human factor is still un-
solved and definite programmes of work toward development of rational sta-
bility requirements still do not exist.

Although the Subcommittee on Stability and Load Lines and of Fishing
Vessels Safety of IMO is currently working in this direction it is felt
that other, more broader forum is necessary where scientific problems con-
nected with stability could be considered at length and where all invol-
ved in stability work - whether in design, operation, research or regula-
tory activities could discuss research programmes and results achieved and
to consider how those results could be applied in practice.

With the view of this the First International Conference on Stability
of Ships and Ocean Vehicles was held in Glasgow in 1975 and the Second was
held in Tokyo in 1982.
At both conferences a number of papers were presented showing that there
is great interest throughout the world in stability problems and that ma-
ny research programmes concerning stability are under way in various pla-
ces. The present Conference is a follow-up to both previous conferences.

The Conference programme will be divided in seven separate sections to facilitate comprehensive discussion. Section 1 will consider the Basic Theoretical Studies which will include mathematical modelling and computer programmes of the behaviour of ships in a seaway. Section 2 will consider Experiments with Models which form equally important basis for understanding physical phenomena. Sections 3-6 will cover Stability Criteria, Stability and Design and Stability of Special Ship Types, Stability in Operation and Stability of Semi-Submersibles. Section 7 will discuss papers which are outside of the scope of first six sections. There will be also time for panel discussions on the following subjects:

1. Outline of programme of research aimed at stability criteria

2. Relationship between stability requirements and design.

As the emphasis of the Conference is to encourage wide exchange of ideas it is expected that the presentations of technical papers will be brief to allow maximum time for general discussion.

International Programme Committee

Dr P. Bogdanov	Bulgarian Ship Hydrodynamic Centre, Varna
Mr W.A. Cleary, Jr	United States Coast Guard
Dr J. Dudziak	Ship Hydrodynamic Centre, Gdańsk
Professor A. Kholodilin	Leningrad Shipbuilding Institute
Professor L. Kobyliński	Ship Research Institute; Gdańsk Technical University
Professor O. Krappinger	Shipbuilding Institute; Hamburg University
Professor C. Kuo	University of Strathclyde
Mr J.A. Manum	Norwegian Maritime Directorate
Dr A. Morrall	British Maritime Technology
Professor S. Motora	University of Tokyo
Real Admiral P. O'Dogherty	Experimental Towing Tank; El Pardo
Professor T. Özalp	Turkish Register of Shipping
Professor J.A. Paulling	University of California
Dr N.N. Rakhmanin	Krylov Shipbuilding Research Institute

CONTENTS

SHIP CAPSIZING IN STEEP HEAD SEAS: A FEASIBILITY STUDY
FOR COMPUTER SIMULATION

P. Kaplan, J. Bentson

ABSTRACT

A mathematical model is established that
represents the basis for a computer simulation
procedure to predict capsizing of ships in head
sea operation. Various physical mechanisms that
could be responsible for capsize are considered,
with mathematical representations and/or proce-
dures described that would account for such
physical influences. The constituent forces due
to hydrostatic, hydrodynamic, and wave effects,
as well as external environmental effects (wind
and gusts) are included, with consideration of
important nonlinearities. The limits and approx-
imations of mathematical representations of
various elements entering the equations and
methods of computation are described, with
recommended areas of further study and/or up-
dating also indicated. All six degrees of
freedom are included, with a time domain simula-
tion procedure described that accounts for these
effects within the present state of the art.
Recommended computational procedures are pre-
sented which will allow reasonably fast computer
simulation without excessive computer costs,
thereby providing an efficient means of
simulation.

1. INTRODUCTION

Most of the work that has been applied to the
study of capsize stability for surface ships
primarily involves the evaluation of stability by
generally static means, i.e. in terms of the GM,
a measures of initial stability. As well as the
full range variation with heel angle of the
righting arm or righting moment. These techni-
ques are applicable to consideration of various
types of disturbances, and have been the primary
tools used in assessing vessel stability. More
recent efforts have concentrated upon the basic
dynamics of the ship in regard to its interaction
with environmental disturbances due to waves and
wind, with the primary emphasis in those cases
being the effect of waves. Model test studies
have been made to evaluate the capsize stability
of small towing and fishing vessels [1], which
considered operation in both head and following
seas. In addition a combined experimental and
theoretical study was carried out at the

University of California [2] in order to study
vessel capsizing, with the main emphasis on
following and stern quartering seas since the
encounter frequencies in that case would be
relatively low, thereby having some general prox-
imity to the natural frequency of roll of the
vessel.

Although large concern has been devoted in
the past to the problems of capsize in astern
seas, as well as the general case of beam seas in
many investigations (see Proc. of previous ship
stability conferences), concern is now directed
toward the problem of different types of ships in
large head seas. This concern is based upon the
fact that there are new types of ships such as
container ships, LNG tankers, offshore supply
vessels, etc. as well as more unusual methods of
operations by the more conventional vessels,
where there is an insufficient degree of past
experience to establish appropriate stability
criteria. The capsize occurrence in head seas,
as demonstrated in [1], while only shown for
small towing and fishing vessels, indicates that
the possible occurrence with other types of ships
should also be investigated. There is thus a
need for an analytical method to predict stabil-
ity by means of a mathematical simulation tool
that will allow application of results from such
methods to be used as a means of establishing
stability criteria for many different types of
ships.

The present paper describes work aimed at
establishing the basis and feasibility for such a
numerical simulation technique that can be used
for this purpose, with specific application to
the case of extreme head and bow quartering
seas. A limited description of the methods that
can be used to investigate ship capsize stability
under these operating conditions is outlined
here. The complete study is described in [3].

2. PHYSICAL MECHANISMS FOR VESSEL CAPSIZE ANALYSIS

The different physical mechanisms that can
cause a vessel to capsize in head sea operations
were identified, and such mechanisms have to be
represented within the mathematical simulation
models. These mechanisms were determined from

examination of available analytical methods and
model test results.

A listing of these physical mechanisms is
given by the following:

  a) Water on the deck
  b) The general loss of stability for a ship
     as a result of its motion in the verti-
     cal plane, i.e. the relative motion of
     the ship due to heave and pitch with
     respect to the incident wave system.
     Such effects include the static influ-
     ence of the wave crest location relative
     to the ship (e.g. [4]), as well as
     dynamic effects due to the relation of
     natural frequencies of heave and pitch
     relative to the roll natural frequency
     (as in [5]). These motion couplings
     must include random seas, as well as
     include wave groups in the incident wave
     system.
  c) Wind forces, including effects of random
     gusts
  d) Rudder forces

3. GENERAL APPROACH

In view of the mechanisms described above,
and the overall problem of determining capsize
stability by means of computer simulation, there
are a number of particular procedures that are
used. The vessel motions are considered in all
six (6) degrees of freedom, in order to incorpor-
ate all possible coupling effects into the basic
equations. The methods of analysis also includ-
ing primary nonlinear effects, since pure linear-
ity will not be sufficient in this case.

The analysis and simulation are carried out
in the time domain, rather than the frequency
domain, since the time domain technique has a
direct means of allowing for nonlinearity. For
the present problem of simulating capsizing it is
expected that strong non-linearities due to the
large amplitude roll motion as well as discontin-
uous phenomena such as the appearance of water on
the deck will make the frequency domain approach
impractical.

3.1 Computational Methods

Any domain mathematical model for predicting
the capsizing of a ship in steep head seas will
be quite complex due to the diverse number of
causes and effects operating on the ship (e.g.
water on the deck, aerodynamic gust loads, rudder
action, etc.). To add to the difficulty, addi-
tional computational constraints such as speed of
computation, size of any resulting computer code,
etc., are necessary if the model is to be imple-
mented as a usable computer simulation program.

These constraints require a judicious use of any
possible simplifying assumptions in the mathe-
matical model as well as a structuring of the
computer logic so that any complex calculations
can be arranged in such a way as to minimize the
impact on computational efficiency.

Based on past experience with large time
domain simulation models of complex systems [6],
a useful method of building an efficient time
domain model is to create what might be termed a
"data base" simulation. Here the computer pro-
gram is structured so that those variables which
require time consuming calculations, and which
can be expressed in terms of a limited number (2
or 3) of parameters, are evaluated off-line and
stored as data tables for subsequent interpola-
tion by the simulation model during the time
domain run. As an illustration, the hydrostatic
roll moment may be pre-calculated as a function
of local immersion and water slope and stored as
a data array, and then interpolated at each time
point given the current value of the two required
parameters. The advantage is a significant in-
crease of computation speed, as well as a large
degree of flexibility in possible upgrading of
segments of the mathematical model.

4. COORDINATE SYSTEM AND AXES

Due to the expected occurrence of large pitch
and roll angles in the simulation model, a body-
fixed coordinate system is used for the differen-
tial equations of motion and the initial reaction
forces. However, since the primary excitation is
hydrostatic and hydrodynamic, a water level coor-
dinate system is used for evaluating these forces
and moments. The external forces and moments in
the water level coordinate system are then trans-
formed to a body-fixed axis system for use in
solution of the equations of motion.

The water level coordinate system has the
axis system parallel to the undisturbed calm
water free surface, with the ship allowed to
pitch and roll relative to the coordinate system.
This is the usual axis system, used in most ship
motion studies (e.g. [7]), which only consider
first order small angular motions. An illustra-
tion of these axis systems is given in Fig. 1,
with an inertial axis system also shown which is
used to find the ship spacial trajectories.

To transform a vector quantity such as a
force, given in a water level coordinate system
by components X_L, Y_L, Z_L, into the appropriate
body axis components X_B, Y_B, Z_B, the transfor-
mation equations are

$$X_B = X_L \cos\phi - Z_L \sin\theta$$

$$Y_B = X_L \sin\phi\sin\theta + Y_L \cos\phi + Z_L \sin\phi\cos\theta$$

$$Z_B = X_L \cos\phi \sin\theta - Y_L \sin\phi + Z_L \cos\phi\cos\theta \quad (1)$$

where

θ = pitch angle

ϕ = roll angle
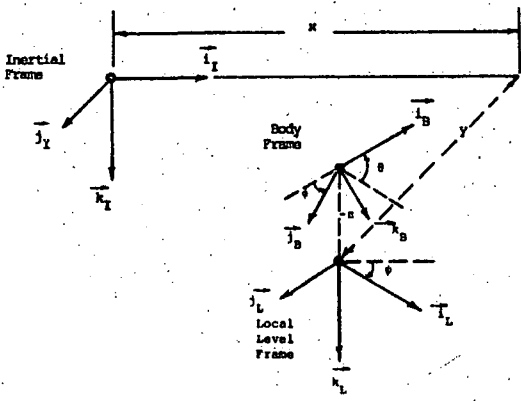
Figure 1. Relative Orientation of Reference Frames

5. EQUATIONS OF MOTION (BODY COORDINATES)

The equations of motion in body coordinates, with translational and rotational velocities given by u_B, v_B, w_B, p_B, q_B, r_B, are written in matrix form as

$$\begin{vmatrix} m & 0 & 0 & & & \\ 0 & m & 0 & & \mathbf{0} & \\ 0 & 0 & m & & & \\ & & & I_{xx} & -I_{xy} & -I_{xz} \\ & \mathbf{0} & & -I_{xy} & I_{yy} & -I_{yz} \\ & & & -I_{xz} & -I_{yz} & I_{zz} \end{vmatrix} \begin{vmatrix} \dot{u}_B \\ \dot{v}_B \\ \dot{w}_B \\ \dot{p}_B \\ \dot{q}_B \\ \dot{r}_B \end{vmatrix} = \begin{vmatrix} X \\ Y \\ Z \\ K \\ M \\ N \end{vmatrix} \quad (2)$$

The terms on the right hand side represent the total forces and moments, including the additional velocity terms arising from rotations of the axis system in inertial space. Each of the forces and moments represent the sum of the individual force components arising from the various applied loads. For this study the total force or moment in any direction is considered to be given by

$$F = F_{inertial} + F_{aerodynamic} + F_{hydrostatic} \quad (3)$$
$$+ F_{hydrodynamic} + F_{steering} + F_{propulsion}$$

The various transformations of body velocities to inertial velocities, in order to determine the ship trajectory in inertial space are given in standard references such as [8]. The inertial reactions, which are the cross products of velocities arising from rotation of the body axes, are also obtained from [8] or any textbook in dynamics or aircraft stability and control.

6. AERODYNAMIC FORCES AND MOMENTS

The aerodynamic forces and moments of importance in a capsize simulator are primarily those associated with the lateral plane since the aerodynamic vertical force (lift) and pitch moment should be negligibly small compared to the hydrostatic effects for those quantities.

The mathematical model for the aerodynamic forces is in the standard form of a coefficient multiplied by the product of an area and the dynamic pressure. For the case where the coefficients are known (from empirical data measurements) as a function of the relative wind heading angle , the forces and moments are given by

$$X_{aero} = -C_x \frac{\rho}{2} V_w |V_w| A_x$$

$$Y_{aero} = -C_y \frac{\rho}{2} V_w |V_w| A_y$$

$$N_{aero} = -C_N \frac{\rho}{2} V_w |V_w| A_y L$$

$$K_{aero} = -C_K \frac{\rho}{2} V_w |V_w| A_y H \quad (4)$$

where

ρ = mass density of air

V_w = velocity of wind relative to ship

A_x = frontal projected area

A_y = lateral projected area

L = ship length

H = height of centroid of A_y above waterline

The aerodynamic forces and moments are determined with respect to water level coordinates.

The relative wind velocity and the wind heading angle are given by

$$V_w^2 = U_s^2 + 2U_sU_w \cos(\psi_w - \psi_s) + U_w^2 \quad (5)$$

$$\mu = \tan \frac{U_w \sin(\psi_w - \psi_s)}{U_w \cos(\psi_w - \psi_s) + U_s} \quad (6)$$

where
U_w = instantaneous wind speed over ground, including gusts

U_s = ship forward speed

ψ_s = ship heading angle in inertial space (relative to x_i)

ψ_w = wind heading angle relative to ship x-axis

The equations for the aerodynamic loads are valid for both steady wind velocity and for gusting conditions (i.e. quasisteady assumption). For conditions involving gusts, the inertial wind velocity U_w is given by

$$U_w = \bar{U}_w + U_{gust} \quad (7)$$

where $\bar{U}_w$ = mean wind speed

U gust = gust speed

The sectional roll movement is defined by

$$f_k = \int \bar{\rho} g \, h_1 \, D_1 \, dt/\cos_w \qquad (11)$$

where $h_1 = x_B \sin(\alpha_w + \phi) - y_B \cos(\alpha_w + \phi)$ in terms of the roll angle ϕ and the wave slope α_w. The value of the roll moment of a ship rolled in calm water at the angle $(\alpha_w + \phi)$ can be precalculated in tables and used for interpolation using the appropriate value of $(\alpha_w + \phi)$. All of the sectional values found above are used to find the total forces and moments by integration over the ship length.

Since all the hydrostatic forces and moments depend on the underwater shape, the sectional draft must also be known and used. The time domain simulation procedure accounts for the draft changes due to heave, pitch and wave elevation.

9. HYDRODYNAMIC FORCES AND MOMENTS

The hydrodynamic forces are effectively represented by added mass and damping terms, as well as different coupling terms that arise from these basic quantities. While these forces are expected to be more important for head sea operation then in the case of following seas [2], in carrying out a time domain simulation certain approximations are made. For vertical plane motions (i.e. heave and pitch) the most important dynamic aspects allowing simplified mathematical modeling involve proper matching of the natural frequencies and the damping in the resonance region. Thus the added mass and damping in heave and pitch can be approximated by the values corresponding to their natural frequencies. Since there is no large dependence of heave and pitch motions on immersion depth (due to almost wall-sided ship forms), values of added mass and damping in those modes are those corresponding to the calm water equilibrium immersion.

For lateral motions a different treatment is used since the lateral added mass and other inertial terms have a significant dependence on the immersion, particularly upon the immersed draft. The sectional lateral added mass terms (using the low frequency approximation) are expressed as functions of the 2-parameter Lewis form family, using continuous variation of the section area and draft throughout the time history. All of these procedures do not specifically account for direct dependence on the roll angular orientation of the section. An approximate way to account for roll angle influence (which may not be that large for the hydrodynamic force terms in head sea operations generally) is to assume that the hydrodynamic forces described above are applied to dynamic variables in the body axis system.

In addition to potential flow-type forces, other hydrodynamic forces are present due to nonlinear cross-flow drag effects. These terms apply to the lateral force, yawing moment and roll moment, due to the body motions of lateral velocity, yaw angular velocity and roll angular velocity. Bilge keel roll damping terms are also included in the model.

Other hydrodynamic forces due to waves excitation forces are found in terms of the water level coordinate system, primarily in terms of the inertial force contributions using added masses and fluid accelerations. The sectional added mass for a rolled body, in water level coordinates, is represented (for the particular case of vertical added mass) by

$$A_{33_L}' = A_{33}' \cos^2 + A_{22}' \sin^2 \qquad (12)$$

where the vertical and lateral added mass (A_{22}') are found in the manner described above, with a continuous evaluation of these quantities as the body section changes immersion. All of the sectional inertial terms are found this way, integrated over the ship length to obtain total forces, and then these water level coordinate terms are transformed to effective forces in body coordinates.

Further hydrodynamic forces acting on the ship are those due to any rudders on the craft. Propulsion force components due to propeller thrust are other forces acting on the ship. No discussion or illustration of these forces is given here, but more detail is presented in [3].

10. WATER ON THE DECK

No complete model for the amount of water on the deck was available for use in this simulation development, when considering the three-dimensional unsteady nature of such effects. Some discussion of the use of information on two-dimensional analyses [10] was given in [3], where possible effects of water on the deck could be represented as a retarding influence on pitch for conditions during bow region submersion and re-emergence. Since no dependence on roll orientation of shipped water is given in [10], no further consideration of such effects was made.

11. NUMERICAL INTEGRATION

The suggested method of numerical integration for digital computer simulation is a variable time step method, viz. Runge-Kutta-Merson [11], which provides speed, accuracy and numerical stability. This variable time step method automatically adjusts itself during the computation to adapt to the frequencies inherent in the

Gust velocities are random in nature, and are obtained from a velocity spectrum which is implemented in the time domain by means of spectral decomposition (the same method used for seaway wave representation). The given spectrum is decomposed into a sum of appropriately weighted sinusoidal time history components, including random phases.

7. WAVES AND WAVE PROPERTIES

The wave system is assumed to be composed of a series of unidirectional sine waves, with the waves travelling in inertial space with an angle β relative to the ship initial heading as shown in Fig. 2.
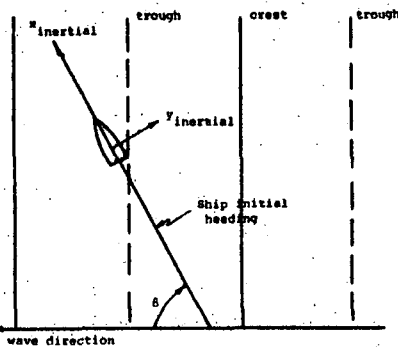
Figure 2. Wave Heading Convention

The various wave properties at a point (i.e. elevation, velocities, slopes, and acceleration) are found by computing the values for each component wave and then linearly summing the effects. The governing equations for the ith component are

$$\eta_i = a_i \sin \alpha_i$$
$$\dot{\eta}_i = a_i \omega_i \cos \alpha_i$$
$$\ddot{\eta}_i = - a \omega_i^2 \sin \alpha_i$$
$$\frac{\partial \eta}{\partial y_i} = -a_i \frac{2\pi}{\lambda_i} \sin \gamma \cos \alpha_i$$
$$u_i = a_i \omega_i \cos \gamma \sin \alpha_i \qquad (8)$$
$$v_i = a_i \omega_i \sin \gamma \sin \alpha_i$$
$$w_i = a_i \omega_i \cos \alpha_i$$

where $\alpha_i = f_i(t) - \frac{2\pi}{\lambda_i} (x_j \cos \gamma + y_j \sin \gamma) + \phi_i$

$$\gamma = \beta - \psi$$

$$f_i(t) = \omega_i t + \frac{2\pi}{\lambda_i} (-x_o \cos \beta - y_o \sin \beta)$$

ϕ_i = wave phase angle

In these equations it is understood that x_o and y_o here represent the values of the CG coordinates of the ship with respect to the inertial reference frame, and that they are time-varying

quantities as the craft moves. The terms x_j, y_j, appearing in the definition of α_i are the coordinates of a point on the ship in water level coordinates, measured relative to the ship CG.

A given wave spectrum is decomposed into a sum of sinusoidal waves by a straightforward procedure which eliminates frequencies that are integer multiples, and also includes a random phase angle. The effect of wave groups in this random seaway representation is also modeled, using the method of [9].

8. HYDROSTATIC EFFECTS INCLUDING WAVES

The total hydrostatic pressure at any point below the surface is composed of the normal hydrostatic pressure and an exponentially decaying part due to wave elevation. Paulling [4] has shown that for wavelengths of the order of the ship length, the effects of the exponential variation can be approximated by a linear variation in the pressure gradient. This leads to the evaluation of the hydrostatic pressure in terms of an effective density so that at any point below the water surface

$$p = \bar{\rho} g z \qquad (9)$$

where $\bar{\rho} = 1 - \sum k_i \eta_i e^{-k_i \bar{z}}$

with $\bar{z}$ = depth of centroid of sectional underwater area.

Using this procedure, applied to a ship section as shown in Fig. 3, the sectional forces (in water level coordinates) are found to be

$$f_z = - g A$$
$$f_y = - g A \frac{\partial \eta}{\partial y} \qquad (10)$$

with A the immersed underwater area of the section.
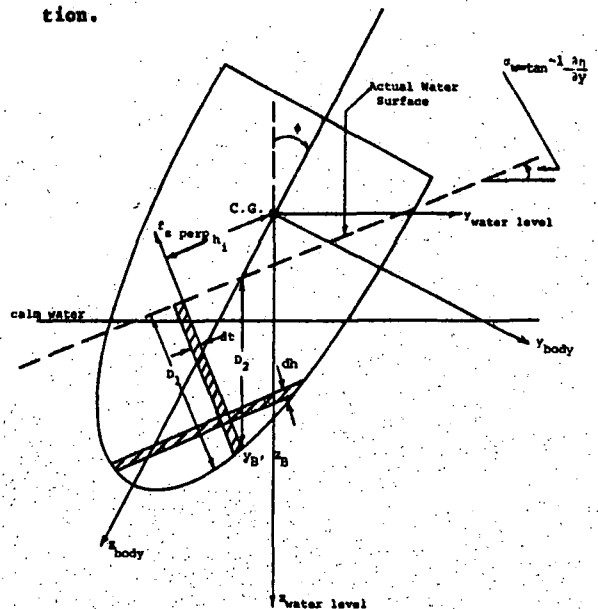
Figure 3. Sectional Geometry of Rolled Ship

phenomena, and is thereby useful when applied to systems that exhibit varying types of response. As a result it is expected that, for slowly-varying phenomena, the computations can be carried out very quickly since larger time steps will be taken, while higher frequency effects will cause an increase in computation time that may exceed real-time. This integration technique has been applied in the time domain simulation of motions of surface effect ships, which considers many state variables with different relative time scales (see [6]).

12. CONCLUDING REMARKS

This paper provides a mathematical model that represents the basis for a computer simulation procedure for predicting the occurrence of capsizing in head seas for different ships.

Different possible mechanisms have been considered that could result in ship capsizing, but no particular mechanism has been favored in the formulation and no specific criteria established for stability. The mathematical model encompasses all of the possible physical mechanisms, and the general structure of the basic computer representations will allow more detailed analysis of constituent force elements, degree of immersion, etc. within simulation runs if such efforts are desired by an investigator using the simulator that can evolve from the model described here.

The simulator itself can be used to investigate the occurrence of capsizing under various operational conditions (e.g. speed, sea state, GM, displacement, etc.). As a result of repeated runs covering different parametric conditions, some insight can then be obtained into predominant influences and/or mechanisms. This will allow evaluation of different stability criteria, as well as aid in the establishment of new stability criteria, if such are required.

13. REFERENCES

1. Miller, E.R. et al: "Evaluation of Current Towing Vessel Stability Criterion and Proposed Fishing Vessel Stability Criteria", Vols. I-III, U.S. Coast Guard Reports by Hydronautics, Inc., 1975-1976.
2. Paulling, J.R. and Wood, P.D.: "Numerical Simulation of Large-Amplitude Ship Motions in Astern Seas", Proceedings of Seakeeping 1953-1973, SNAME T & R Symposium S-3, June 1974.
3. Kaplan, P. and Bentson, J.: "Ship Capsizing in Steep Head Seas: A Feasibility Study for Computer Simulation," Hydromechanics, Inc. Rpt. No. 82-51, November 1982 (also published as U.S. Coast Guard Report).
4. Paulling, J.R.: "The Transverse Stability of a Ship in a Longitudinal Seaway", J. of Ship Research. March 1961.
5. Paulling, J.R. and Rosenberg, R.M.: "On Unstable Ship Motions Resulting from Nonlinear Coupling", J. of Ship Research, June 1959.
6. Bentson, J., Kaplan, P. and Davis, S.: "Simulation of Surface Effect Ship Motions and Loads", Proc. of Summer Computer Simulation Conf., July 1976.
7. Raff, A.I., "Program SCORES — Ship Structural Response in Waves", Ship Structure Committee Report No. SSC-230, 1972.
8. Nomenclature for Treating the Motion of a Submerged Body through a Fluid, SNAME T & R Bull. 1-5, 1952.
9. Spangenberg, B., Jacobsen, B.K.: "The Effect of Wave Grouping on Slow Drift Oscillations of an Offshore Structure", Int. Sump. on Ocean Eng. Ship Handling, Swedish Mar. Res. Centre, SSPA, Gothenburg, Sweden, 1980.
10. Oliver, J.C. and Van Mater, P.R.: "Development of an Analytical Technique for Predicting Deck Wetness", (Vols. I-IV) Giannotti & Assoc. Inc., Report No. 78-030-01, July 1981.
11. Martens, H.R.: "A Comparative Study of Digital Integration Methods", Simulation, Vol. 12, No. 2, Feb. 1969.

P. Kaplan
Professor
Aerospace and Ocean Engineering Department
Virginia Polytechnic Institute and State Univ.
Blacksburg, Virginia 24061
USA

J. Bentson
Assoc. Prof.
Aerospace and Mechanical Eng. Dept.
Polytechnic Institute of New York
Farmingdale, New York
USA

TRANSVERSE STABILITY OF SHIPS IN A QUARTERING SEA

M. Hamamoto

ABSTRACT

This paper is concerned with an analytical method for calculating the righting arm GZ of ships in a quartering sea. Based on this method, the calculations are carried out for the following items.

Fisrt, the righting arm curves in a wave with crest amidship are computed for a container ship and a trawler with several heading angle in order to investigate the influences of them on the pure loss of intact stability.

Next, the maximum righing arms in a wave with crest amidship are computed for the container ship to consider the influences due to the wave to ship length ratios, the wave-length ratios and the BG's.

Finally, a captive model test is carried out for the trawler's model to measure the heeling moment acting on the heeled model towed in quartering seas, in the condition where the model has a given heading angle equal to drift angle. The calculation rendered rusults consistent with those of the experiments.

1. INTRODUCTION

The pure loss of intact stability is considered as one of the causes for capsizing of a ship in a heavy sea. And also it has been pointed out that this would usually occur in a following sea of about the same wave length as the ship length when the crest of a wave is amidship for a long time enough to capsize.

Furthermore, as an actual problem, it would be important to investigate the pure loss of intact stability in a quartering sea, because a ship may be forced to yaw off cource from the direction of waves.

It is not easy to obtain a complete analytical solution making account of the hydrodynamic forces acting on a ship in the present case. But it seems to be typical of a ship in following and quatering seas that the frequency of wave encounter will be low and the ship motion will be determined approximately by the hydrostatic part of the force.

In this paper, an approximate approach focusing on such a typical behaviour is employed for calculating the position of static equilibrium and the righting arms of a ship in a quartering sea. The comparison between the calculations and experimental results is made for a ship model.

2. FORMULATION OF THE PROBLEM

In order to describe the motion of a ship moving in a seaway, the following orthogonal right-hand co-ordinate systems are adopted as shown in Fig. 1.
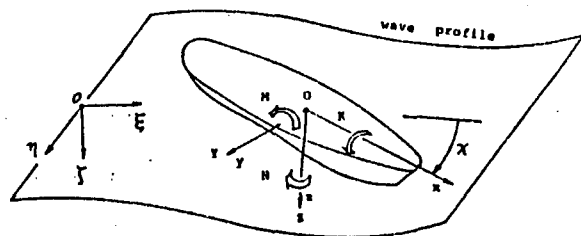
Fig. 1 Co-ordinate systems

A Newtonian co-ordinate system $O-\xi, \eta, \zeta$ is fixed in space with the orgin O located at an arbitrary point in the calm water surface and a body co-ordinate system $o-x, y, z$ is set in the ship such that the orgin o coincides with the intersection of the midship section, the centre plane and the water plane of the ship in an upright condition.

Based on the fundamental principles of rigid body dynamics, the equations describing the six degrees of freedom motion are as follows:

Linear motions and forces

$$m(\dot{u}+wq-vr)+mz_G(\dot{q}+pr)-mx_G(q^2+r^2)$$
$$=X-mg\sin\theta$$
$$m(\dot{v}+ur-wp)+mx_G(\dot{r}+pq)-mz_G(\dot{p}-qr)$$
$$=Y+mg\cos\theta\sin\phi \tag{1}$$
$$m(\dot{w}+vp-uq)-mx_G(\dot{q}-pr)-mz_G(p^2+q^2)$$
$$=Z+mg\cos\theta\cos\phi$$

Angular motions and moments

$$I_{xx}\dot{p}+(I_{zz}-I_{yy})qr-I_{xz}(\dot{r}+pq)-mz_G(\dot{v}+ur-wp)$$
$$=K-mgz_G\cos\theta\sin\phi$$

$$I_{yy}\dot{q}+(I_{xx}-I_{zz})pr-I_{xz}(r^2-p^2)+mz_G(\dot{u}+wq-vr)$$
$$-mx_G(\dot{w}+vp-uq)=M-mg(z_G\sin\theta+x_G\cos\theta\cos\phi) \qquad (2)$$

$$I_{zz}\dot{r}+(I_{yy}-I_{xx})pq-I_{xz}(\dot{p}+qr)+mx_G(\dot{v}+ur-wp)$$
$$=N+mgx_G\cos\theta\sin\phi$$

where m is mass of the ship, g is the gravitational acceleration, u, v and w are linear velocity components along the x, y and z axes, p, q and r are angular velocity components about the x, y and z axes, x_G and z_G are positions of the mass centre in the body co-ordinate system, X, Y and Z are the components of the external fluid and wave forces acting on the ship in the body axes direction x, y and z respectively, I_{xx}, I_{yy}, I_{zz} and I_{xz} are the moments of inertia and the product of intertia in the usual definitions, K, M and N represent the moments about the orgin o of the external forces acting on the ship and χ, θ and φ are the Eulerian angles such that the ship is given yaw χ about oz, trim θ about oy and heel φ about ox, in that order.

The forces X, Y, Z and moments K, M, N in equations (1) and (2) result from the interaction between the ship and the sea and, in general, depend on the time history of the motion of the ship in the sea. The motion may be characterized by the position, velocity and acceleration of the ship. In general, as functions of motion variables, the force and moment are written in the form

$$X=T(1-t)-R+X_{HD}(A.M\ and\ D.F\ including\ W.D.F)$$
$$+X_{HS}(\zeta_0,\theta,\phi)+X_{FK}(a,\Lambda,\chi,\zeta_0,t)$$
$$Y=Y_{HD}(A.M\ and\ D.F\ including\ W.D.F)$$
$$+Y_{HS}(\zeta_0,\theta,\phi)+Y_{FK}(a,\Lambda,\chi,\zeta_0,t) \qquad (3)$$
$$Z=Z_{HD}(A.M\ and\ D.F\ including\ W.D.F)$$
$$+Z_{HS}(\zeta_0,\theta,\phi)+Z_{FK}(a,\Lambda,\chi,\zeta_0,t)$$

and

$$K=K_{HD}(A.M\ and\ D.F\ including\ W.D.F)$$
$$+K_{HS}(\zeta_0,\theta,\phi)+K_{FK}(a,\Lambda,\chi,\zeta_0,t)$$
$$M=M_{HD}(A.M\ and\ D.F\ including\ W.D.F)$$
$$+K_{HS}(\zeta_0,\theta,\phi)+K_{FK}(a,\Lambda,\chi,\zeta_0,t) \qquad (4)$$
$$N=N_{HD}(A.M\ and\ D.F\ including\ W.D.F)$$
$$+N_{HS}(\zeta_0,\theta,\phi)+N_{FK}(a,\Lambda,\chi,\zeta_0,t)$$

where T is the thrust of propller, t is thrust reduction, R is ship resistance, X_{HD}, Y_{HD} and Z_{HD} are hydrodynamic components of the force proportional to velocity and acceleration of the ship and the wave,

X_{HS}, Y_{HS} and Z_{HS} are hydrostatic components of the force proportional to position of the ship, X_{FK}, Y_{FK} and Z_{FK} are components of the Froude-Krilov force based on the Froude-Krilov hypothesis and also the moments K, M and N are specified by the same suffix as forces.

Solution of the hydrodynamic problems have heretofore been obtained only under assumption of small motion amplitudes. This assumption cannot be used in the present case. Instead, as noted previously, we shall focus on an exact computation only of the hydrostatic part of the fluid force and the wave displacement force of the wave excitation. Neglecting all the terms of; the velocity and acceleration of the ship and the sea in equations (1) and (2), the equations for instantaneous equilibrium position of the ship in a wave are obtained as follows:

$$(Y_{HS}+Y_{FK})\sin\phi+(Z_{HS}+Z_{FK})\cos\phi$$
$$+mg\cos\theta=0$$

$$(M_{HS}+M_{FK})\cos\phi-(N_{HS}+N_{FK})\sin\phi \qquad (5)$$
$$-mg(x_G\cos\theta+z_G\sin\theta\cos\phi)=0$$

$$(K_{HS}+K_{FK})-mgz_G\cos\theta\sin\phi=0$$

3. ANALYSIS OF FORCES AND MOMENTS

For analyzing the forces and moments acting on the submerged surface of the ship in a quartering sea, we assume a regular sinusoidal wave travelling with amplitude a, wave number k and phase velocity c in the direction of the oξ axis. At the any time t the elevation ζ_w is

$$\zeta_w=a\cos k(\xi-ct) \qquad (6)$$

and the pressure is approximately

$$p=\rho g\zeta-\rho ga\cos k(\xi-ct) \qquad (7)$$

where ρ g is the specified weight of the water. In equation (7), the so-called Smith's effect due to the orbital motion of water particles is neglected. It is actually possible to take into account this effect, but it is known that the error arising from the neglection is not so great. And also, the wave elevation ζ_w and pressure p may be refered to the body axes, oxyz by replacing ξ and ζ by the components

$$\xi-\xi_0 \approx x\cos\chi-(y\cos\phi-z\sin\phi)\sin\chi$$
$$\zeta-\zeta_0 \approx -x\theta+y\sin\phi+z\cos\phi \qquad (8)$$

then

$$\zeta_w = a\cos k[\xi_0 + x\cos\chi - (y\cos\phi - z\sin\phi)\sin\chi - ct] \quad (9)$$

and

$$p = \rho g(\zeta_0 - x\theta + y\sin\phi + z\cos\phi) \quad (10)$$
$$-\rho g a\cos k[\xi_0 + x\cos\chi - (y\cos\phi - z\sin\phi)\sin\chi - ct]$$

where ξ_0 and ζ_0 are the initial position of the origin of the body axes measured along the oξ and oζ axes respectively and equation (9) is approximately induced under an assumption that the trim angle θ is small and the breadth and depth of the ship are small compared with the length of it.

The force and moment of equation (6) are given by integrals of the pressure gradient over the submerged volume V of the ship. The components of the force and moment in the body axes oxyz are

$$(Y_{HS} + Y_{FK})\sin\phi + (Z_{HS} + Z_{FK})\cos\phi$$
$$= -\iiint_V [(\frac{dp}{dy})\sin\phi + (\frac{dp}{dz})\cos\phi]dV = -\rho g\iiint_V dV$$

$$(M_{HS} + M_{FK})\cos\phi - (N_{HS} + N_{FK})\sin\phi$$
$$= \iiint x[(\frac{dp}{dy})\sin\phi + (\frac{dp}{dz})\cos\phi]dV \quad (11)$$
$$- \iiint_V (y\sin\phi + z\cos\phi)\frac{dp}{dx}dV \sim -\rho g\iiint_V xdV$$

$$(K_{HS} + K_{FK}) = -\iiint_V \{y(\frac{dp}{dz}) - z(\frac{dp}{dy})\}dV$$
$$\sim -\rho g\iiint_V (y\cos\phi - z\sin\phi)dV$$

The integrals are taken over all volume up to the sea surface.

Making the ζ_w of equation (9) equal to the ζ of equation (8), the sea surface in the body axes oxyz can be given by

$$\zeta_0 - x\theta + y\sin\phi + z\cos\phi = a\cos k[\xi_0 + x\cos\chi$$
$$-(y\cos\phi - z\sin\phi)\sin\chi] \quad (12)$$

Then the sea surface at port and starboard sides, z_p and z_s, are

$$\zeta_0 - x\theta - b(z_p)\sin\phi + z_p\cos\phi = a\cos k[\xi_0 + x\cos\chi$$
$$+(b(z_p)\cos\phi + z_p\sin\phi)\sin\chi] \quad (13)$$

and

$$\zeta_0 - x\theta + b(z_s)\sin\phi + z_s\cos\phi = a\cos k[\xi_0 + x\cos\chi$$
$$-(b(z_s)\cos\phi - z_s\sin\phi)\sin\chi] \quad (14)$$

where $b(z_p)$ and $b(z_s)$ are the half breadth at z_p and z_s as shown in Fig. 2.

Since the sectional area A(x) and heeling moment H(x) of the station x are given by
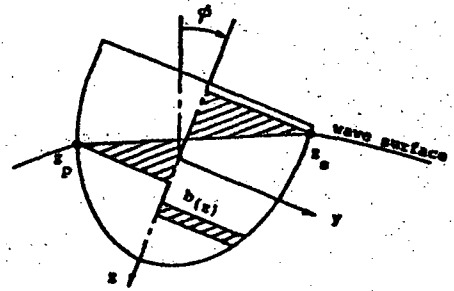
Fig. 2 Sea surface at port and starboard sides

$$A(x) = \int_{z_p}^{d} b(z)dz + \int_{z_s}^{d} b(z)dz$$
$$+\frac{1}{2}(z_p - z_s)[b(z_p) - b(z_s)] \quad (15)$$

and

$$H(x) = \rho g\cos\phi\int_{z_s}^{z_p}\frac{1}{2}b^2(z)dz$$
$$-\rho g\cos\phi\frac{1}{6}(z_p - z_s)[b^2(z_p) - b(z_p)b(z_s) + b^2(z_s)]$$
$$-\rho g\sin\phi[\int_{z_p}^{0} zb(z)dz + \int_{z_s}^{0} zb(z)dz] \quad (16)$$
$$-\rho g\sin\phi\frac{1}{6}(z_p - z_s)[(2z_p + z_s)b(z_p) - (z_p + 2z_s)b(z_s)]$$

the force and moment of equation (11) are represented by

$$\iiint_V dV = \int_L A(x)dx \quad (17)$$

and

$$\rho g\iiint_V (y\cos\phi - z\sin\phi)dV = \int_L H(x)dx \quad (18)$$

Then we have, from equation (5)

$$-\rho g\int_L A(x)dx + mg = 0$$
$$\rho g\int_L xA(x)dx - mgx_G = 0 \quad (19)$$
$$\int_L H(x)dx + mgz_G\sin\phi = 0$$

where L is all over the submerged length of the ship.

We can compute the instantaneous equilibrium position on the righting moment of the ship according to equation (19).

4. EQUATIONS FOR COMPUTATION OF POSITION AND RIGHTING MOMENT

At the beginning of these computations, as noted previously, it is necessary to obtain the sea surface at port and starboard sides, z_p and z_s in equations (13) and (14). A convenient way for computation of them will be to use the perturbation

method.

In this method, the sea surface elevation is given by the sum of infinitely small amplitude waves as follows:

$$\zeta_w = \sum_{n=1}^{N} \Delta a_n \cos k[\xi_0 + x\cos\chi - (y\cos\phi - z\sin\phi)\sin\chi - ct] \qquad (20)$$

where Δa_n is equal to a/N.

For perturbed variables of $\Delta\zeta_0, \Delta\theta, \Delta\phi, \Delta z_p$ and Δz_s in equations (13) and (14) caused by infinitely small amplitude wave Δa, we obtain

$$\Delta\zeta_0 - x\Delta\theta - C_\phi(z_p)\Delta\phi - C_z(z_p)\Delta z_p = \Delta a\cos\alpha(z_p)$$

$$\Delta\zeta_0 - x\Delta\theta - C_\phi(z_s)\Delta\phi - C_z(z_s)\Delta z_s = \Delta a\cos\alpha(z_s) \qquad (21)$$

where

$$C_\phi(z_p) = b(z_p)\cos\phi + z_p\sin\phi + ak[b(z_p)\sin\phi - z_p\cos\phi]\sin\chi\sin\alpha(z_p)$$

$$C_z(z_p) = b'(z_p)\sin\phi - \cos\phi - ak[b'(z_p)\cos\phi + \sin\phi]\sin\chi\sin\alpha(z_p) \qquad (22)$$

$$\alpha(z_p) = k[\xi_0 + x\cos\chi + (b(z_p)\cos\phi + z_p\sin\phi)\sin\chi]$$

and

$$C_\phi(z_s) = -b(z_s)\cos\phi + z_s\sin\phi + ak[-b(z_s)\sin\phi - z_s\cos\phi]\sin\chi\sin\alpha(z_s)$$

$$C_z(z_s) = -b'(z_s)\sin\phi - \cos - ak[-b'(z_s)\cos\phi + \sin\phi]\sin\chi\sin\alpha(z_s) \qquad (23)$$

$$\alpha(z_s) = k[\xi_0 + x\cos\chi + (-b(z_s)\cos\phi + z_s\sin\phi)\sin\chi]$$

Then, for small changes in A(x) and H(x) of equation (19), $\Delta A(x)$ and $\Delta H(x)$, caused by the Δz_p and Δz_s of equation (21), we obtain

$$\int_L \Delta A(x)dx = 0$$

$$\int_L x\Delta A(x)dx = 0 \qquad (24)$$

$$\int_L \Delta H(x)dx + mgz_G\Delta\phi\cos\phi = 0$$

and

$$\Delta A(x) = A_1(x)\Delta\zeta_0 - A_2(x)\Delta\theta - A_3(x)\Delta\phi - A_4(x)\Delta a$$

$$\Delta H(x) = H_1(x)\Delta\zeta_0 - H_2(x)\Delta\theta - H_3(x)\Delta\phi - H_4(x)\Delta a \qquad (25)$$

where $A_1(x), \ldots, H_4(x)$ are the coefficients of perturbed variables $\Delta\zeta_0, \Delta\theta, \Delta\phi$ and Δa which are given in analytical form by making perturbations of equations (13), (14), (15) and (16). The terms of them, however, is too long to describe here. Finally, equation (20) can be decomposed as

$$\Delta\zeta_0\int_L A_1(x)dx - \Delta\theta\int_L A_2(x)dx - \Delta\phi\int_L A_3(x)dx = \Delta a\int_L A_4(x)dx$$

$$\Delta\zeta_0\int_L xA_1(x)dx - \Delta\theta\int_L xA_2(x)dx - \Delta\phi\int_L xA_3(x)dx = \Delta a\int_L xA_4(x)dx \qquad (26)$$

$$\Delta\zeta_0\int_L H_1(x)dx - \Delta\theta\int_L H_2(x)dx - \Delta\phi(\int_L H_3(x)dx - mgz_G\cos\phi) = \Delta a\int_L H_4(x)dx$$

In practical computation of equation (26), we have to start from the upright condition of a ship in still water and by starting from next condition in a wave of amplitude Δa, we can reach an another condition in that of $2\Delta a$. By repeating these step by step approximations up to the desired wave amplitude a, we can obtain the sinkage ζ_0^*, trim angle θ^* and heel angle ϕ^* of the final position.

The ship hull is approximated by a number of polygons representing the station of the ship. Each polygon is in a plane defined by a constant value of x in the body axes.

Next, we shall think of the righting moment of the ship in a quatering sea. Although the righting moment of a ship in still water is, in general, calculated for the anlge of inclination measured from the upright condition, as mentioned above, the position of a ship in a quatering sea may be deviated from the upright condition. That is to say, the ship may be balanced in the condition with an initial heeling angle where the righting moment is equal to zero as shown in Fig. 3. This is a
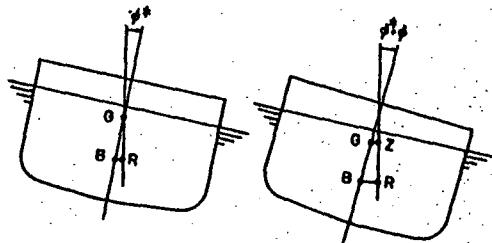
Fig. 3 Righting arm in a wave

different point with respect to the starting condition to calculate it. This initial heeled condition relatively correspond to the upright condition of the ship in still water.

Then the righting arm GZ(ϕ) is geometrically given by, from Fig. 3,

$$GZ(\phi) = BR(\phi^* + \phi) - BG\sin(\phi^* + \phi) \qquad (27)$$

where BR and BG are the same as one given by the traditional definition and have to satisfy the following condition

$$BR(\phi^*) - BG\sin\phi^* = 0 \qquad (28)$$

So that, we can obtain a formula to compute the

righting moment $mgGZ(\phi)$ as follows:

$$mgGZ(\phi)=\int_L H(x;\phi^*+\phi)dx+mgz_G sin(\phi^*+\phi) \quad (29)$$

where

$$z_G=OB-BG \quad (30)$$

On the other hand, the sinkage ζ_0 and trim angle θ caused by the angle of inclination ϕ are obtained by integrals of the equation leading to a step-by-step approximation with respect to the perturbed angle $\Delta\phi$ of ϕ. From equation (26), the equation is given by

$$\Delta\zeta_0\int_L A_1(x)dx-\Delta\theta\int_L A_2(x)dx=\Delta\phi\int_L A_3(x)dx$$

$$\Delta\zeta_0\int_L xA_1(x)dx-\Delta\theta\int_L xA_2(x)dx=\Delta\phi\int_L xA_3(x)dx \quad (31)$$

Here, ϕ should be measured from the initial heeling angle ϕ^*.

5. RESULTS OF NUMERICAL COMPUTATION

In obtaining solutions, the ship is now assumed not to deviate from a given heading angle χ and to be in the relative position defined by ξ_0 which is the position of ship to wave at the time equal to zero. The sinkage ζ_0, trim angle θ and heel angle ϕ which are caused by the wave excitation, are given as a solution of equation (26). Then, we can compute the righting arm GZ, the sinkage ζ_0 and trim angle θ which are caused by the angle of inclination ϕ.

Some numerical computations are presented here for two ships. One is a container ship and another is a trawler.

First, for the pure loss of intact stability of the ships with several heading angles, the righting arm curves, sinkage and trim angle are given in Figs. 4 and 5 compared with that in still water where the wave to ship length ratio Λ/L is 1.0 and the wave-length ratio H/Λ is 1/20.

The influence of heading angles on the righting arm curves can be significant. That is to say, the righting arm curve in a beam sea with crest amidshsip is about the same as that in still water. But they are smaller for smaller heading angles and the smallerst one is that in a following sea.

The variation of the righting arm is more remarkable for the container ship than that for the trawler. The nature of GZ in a quartering sea seems to be strongly dependent on the ratios B/D and B/d of hull form.

Next, let us focus on the maximum righting arm of the container ship with an arbitrary heading angle χ about the influence of wave to ship length ratio Λ/L, wave-length ratio H/Λ and the change of BG.

The maximum righting arms for various ratios Λ/L against heading angle χ are shown in Fig. 6, those for various ratios H/Λ are in Fig.7, those for various ratios Λ/L in constant H/Λ are in Fig. 8 and those for various BG are in Fig. 9 where the maximum righting arm in wave with crest amidship is divided by that of BG equal to 3m in still water.

Finally, to measure the heeling moment acting on the heeled model towed in quartering seas, a captive model test is carried out for the trawler's model in the condition where the model has a given heading angle equal to drift angle and is free with respect to sinkage and trim. Fig. 10 shows an example of the experimental results compared with calculations.
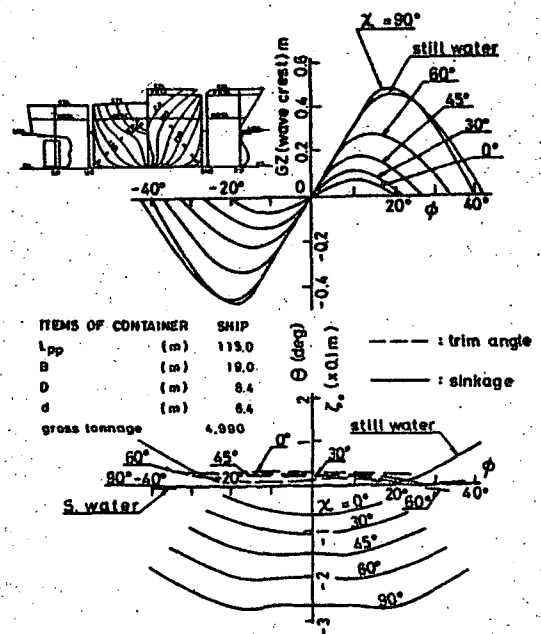
Fig. 4 Righting arm curves, sinkage and trim in wave with crest amidship for a container ship
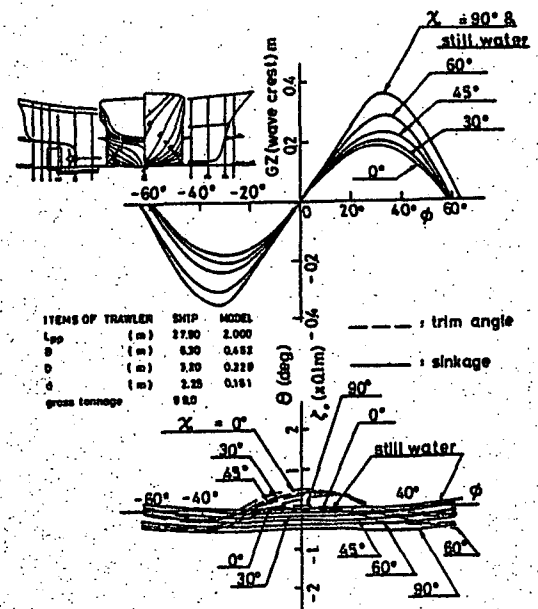
Fig. 5 Righting arm curves, sinkage and trim in wave with crest amidship for a trawler

- 11 -
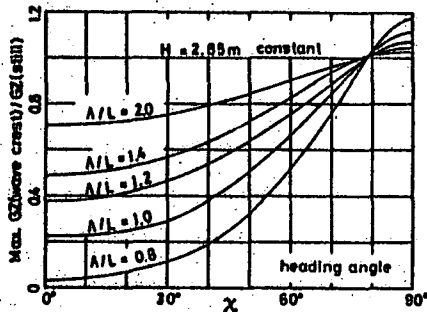
Fig. 6 Maximum righting arms for various ratio Λ/L
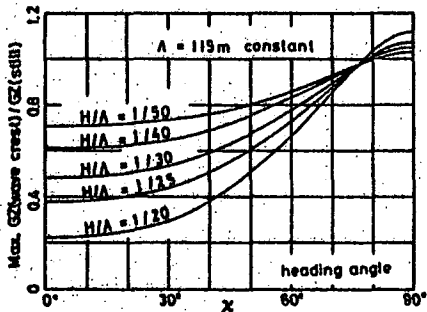
Fig. 7 Maximum righting arms for various ratio H/L
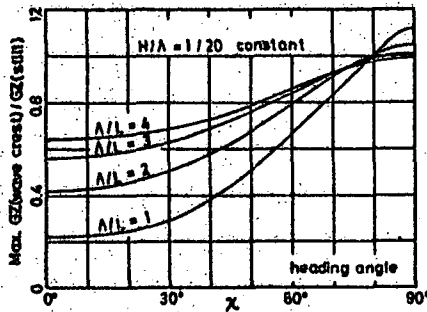
Fig. 8 Maximum righting arms for various ratio Λ/L in constant H/Λ
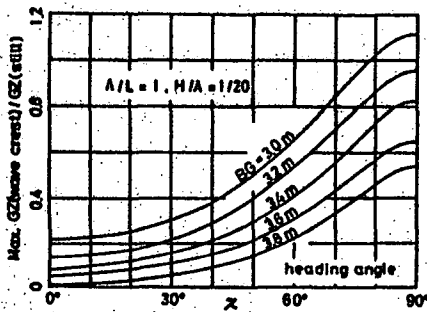
Fig. 9 Maximum righting arms for various BG
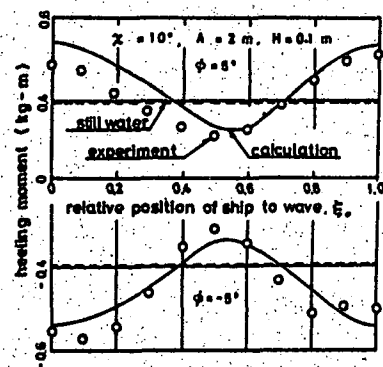
Fig. 10 An example of experimental results

6. CONCLUDING REMARKS

By reference to the diagrams of Figs. 4 to 10, the following deductions can be made:

(1) All the maximum righting arms in wave with crest amidship are close to that in still water as the heading angle of a ship to wave approaches to a beam sea.

(2) For the maximum righting arm, the rate of the change is small for the range of heading angle $0° < \chi < 30°$ and fairly steep for $30° < \chi < 90°$.

(3) The change of BG makes a sensitive influence on the maximum righting arm for the ship in a beam sea but not so much for the ship in a following sea.

(4) The change of BG for a ship in a wave may be expected exactly because the apparent density of water is lighter in wave crest and heavier in wave trough than that in still water. This is the so-called Smith's effect caused by the orbital motion of water particles. Thus, the BG of a ship in a beam sea may become smaller than that in still water and the influence of BG on the righting arm will be equivalent to the Smith's effect.

(6) The calculation rendered results consistent with those of the experiment.

7. ACKNOWLEDGEMENTS

REFERENCES

[1] Chou, S., Oakley, O. and Paulling, R., "Ship motion and capsizing in an astern sea", U.S. Coast Guard, Office of Research and Development, Report No. CG-D-103-75.

[2] Grim, O., "The ship in a following sea", DTMB, AD, No. 458.

[3] Hamamoto, M. and Nomoto, K., "Transverse stability of ships in a following sea", Proc. of Second International Conference on Stability of Ships and Ocean Vehicles, Tokyo, Oct. 1982.

[4] Kerwin, J. E., "Notes on rolling in longitudinal waves", I.S.P., Vol.2, No.16, 1955.

[5] Paulling, J. R., "The transverse stability of a ship in a longitudinal seaway", J.S.R., Vol.4, 1961.

[6] Shipbuilding Reaserch Association of Japan, Reports No.91R, 99R and 108R.

[7] Weinblum, G. and St. Denis, M., "On the motions of ships at sea", Trans. SNAME, 1950.

M. Hamamoto graduated from the University of Osaka Prefecture, Japan, in 1959. He then worked at the Research and Development Centre of Japan Defence Agency as a research engineer for seventeen years. He received the masster's and doctor's degrees of engineering in naval architecture from Osaka University, Japan, in 1966 and 1975. He was appointed to Osaka University in 1976 and has been a professor at that University since 1984. He is interested in ship motions in following seas and hydrodynamics for manoeuvrability of ships.

ON THE PROBLEM OF PEAK-ROLL-RESPONSE OF A SHIP UNDER A WIND-GUST

L.R. Raheja

ABSTRACT

A modification over the conventional energy balance method for the determination of peak-roll-response under a wind gust is suggested so as to take some of the characteristics of the seaway directly into account. it is pointed out that the kinetic energy of the ship rolling in a seaway, just before the windward heeling starts is an important factor in the determination of the maximum angel of roll. The conventional assumption that the wave action ceases to exit when the gust strikes, is modified. It is now assumed that the wave action continues even after the gust strikes and ends just before the windward heeling starts. Consequently, the kinetic energy as mentioned above could be estimated from the seakeeping analysis of the ship in place of conventional righting moment curve and weather criterion. Finally, a graphical method to determine the maximum angle of roll using energy curves in place of conventional moment curves is proposed.

1. INTRODUCTION

One of the essential requirement of stability deals with the maximum angle of roll suffered by the ship when a wind gust strikes the ship. This angle is estimated conventionally by an energy balance approach using the curve of statical stability and a weather criterion which may be different in different nations [1,2]. Besides the differences in the assessment of wind gust moment, various national criteria also differ in their approach in the calculation of the initial angle of roll at which the gust is assumed to start acting.

The problem of rolling subject to the influence of a sudden wind gust is quite complicated one. The ship is supposed to be rolling in waves before the gust strikes. The gust moment itself varies nonlinearily with angle of roll. Consequently, the formulation of the problem requires an unsteady, dynamic and nonlinear mathematical model [3] and therefore complicated. The conventional energy balance approach seems inadequate as it takes no direct consideration of the dynamics of the ship rolling in irregular waves before it is influenced by the gust. However, this approach still remeins a convenient alternative for the calculation of the maximum angle of roll under a wind gust.

In the present work, an attempt is made

to modify this conventional approach in order to incorporate some dynamic aspects of the pre-gust motion through the assessment of the kinetic energy of the ship before it starts heeling windward. The modification is directed towards making the calculation more realistic and reduce the dependence upon arbitrary weather criteria.

The conventional approach is discussed from the point of view of kinetic energy of the ship. The modification in the assessment of the same is explained. Finally, the calculation of the maximum angle of roll using the modification is described. The proposed method of calculation makes use of energy curves in place of conventional moment curves as the former are simpler and convenient for the purpose.

2. CONVENTIONAL ENERGY BALANCE APPROACH

Fig. 1 represents the usual diagram for the conventional energy balance method to calculate the maximum angle of roll under a wind gust. In this approach, the ship is assumed to be rolling in waves and is heeled to an angle φ_i when the wind gust strikes and simultaneously the action of the waves ceases to exist. The wind moment W is assumed to be constant and is represented by the straight line CF. The wind moment as well as the angle φ_i are prescribed by a weather criterion.
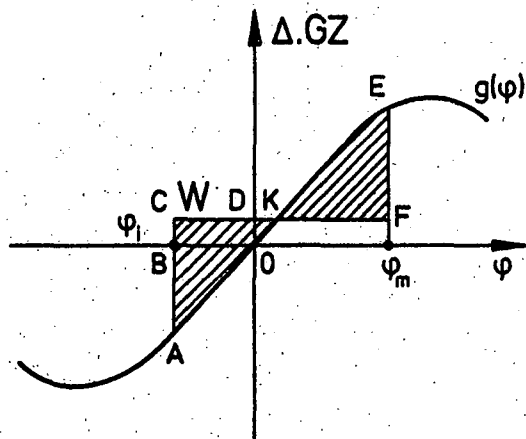
Fig. 1 Conventional Energy Balance Diagram

The maximum angle of roll φ_m is then calculated by the equation

$$\int_{-\varphi_1}^{\varphi_m} \{g(\varphi) - W\}\, d\varphi = 0 \qquad (1)$$

where $g(\varphi)$ is restoring moment of the ship. In terms of areas, the above expression is finally equivalent to

$$\Delta ABCK = \Delta KEF$$

The equation (1) can also be written as

$$\int_{-\varphi_1}^{0} \{g(\varphi) - W\}\, d\varphi = \\ -\int_{0}^{\varphi_m} \{g(\varphi) - W\}\, d\varphi \qquad (2)$$

The left side of this equation represents the $\Delta ABCDOA$ which in turn represents the total energy of the ship in upright position just before it starts heeling windward and should be considered a major factor in deciding the maximum roll response φ_m. This kinetic energy is gained by the ship partly by the action of wind gust on the ship i.e. $\Delta OBCD(=K_1$ say) and partly by its motion in waves i.e. $\Delta AOB(=K_2$ say). It is the estimation of latter in which the modification is proposed.

3. PROPOSED MODIFICATION

In the conventional diagram (Fig. 1), K_2 appears to be equivalent to the maximum kinetic energy of the ship executing natural roll oscillations with an amplitude φ_1 in calm water provided $g(\varphi)$ is considered as usual linear in the φ_1 range, and can be written as

$$K_2 = \frac{1}{2} I \omega_n^2 \varphi_1^2 \quad,$$

where I is virtual mass moment of inertia of the ship in rolling and ω_n its natural fre-

quency. This is a direct consequence of the assumption that the wave action ceases to exist at position B i.e. when the gust strikes. The estimation of K_2 in this way is perhaps oversimplified as it depends upon pre-gust motion which is its origin, only through the value of φ_1 prescribed by the weather criterion. The pre-gust motion of the ship must be that of rolling in an irregular seaway and its characteristics must be known from the seakeeping analysis of the ship. In order to use this information, we modify our basic assumption. It may now be assumed that the wave action continues even after the gust strikes and ceases to exist just before the windward heeling starts, i.e. at the mean position 0 (Fig. 1). Subsequently, the kinetic energy K_2 gained by the ship due to its motion will now be given by the seakeeping analysis of the ship. The estimate of K_2 could now be modified in one of the following ways in the given sea state,

(i) $\quad K_2 = \frac{1}{2} I \tilde{\dot{\varphi}}_{1/3}^2$

where $\tilde{\dot{\varphi}}_{1/3}$ is the significant amplitude of the roll angular velocity,

(ii) $\quad K_2 = \frac{1}{2} I \omega_\varphi^2 \tilde{\varphi}_{1/3}^2$

where $\tilde{\varphi}_{1/3}$ is the significant roll amplitude and ω_φ may be taken as average frequency of the sea spectrum or the one with highest energy density ordinate.

The modification of the assumption and therby the estimate of kinetic energy K_2 should make the calculation of φ_m more realistic. The dependence upon the weather criterion is now reduced and φ_1 in the weather criterion may accordingly be modified.

4. MODIFIED CALCULATION PROCEDURE

One requires to calculate the value of φ_1 and W from weather criterion, duly modified, as because the value of φ_1 will no longer be used to calculate K_2. This gives

$$K_1 = W \varphi_1$$

Next, one calculates K_2 from seakeeping analysis of the ship as described in the previous section. Let us take

$$K_2 = \frac{1}{2} I \tilde{\varphi}_{1/3}^2$$

It would now be convenient to use integral curves i.e. the curves of energy instead of curves of moment as used in the conventional diagram, in order to find the graphical solution of the equation (2) for φ_m. Let us define

$$f_1(\varphi) = \int_0^\varphi g(\varphi)\, d\varphi$$

$$f_2(\varphi) = \int_0^\varphi W\, d\varphi$$

Equation (2) can now be written as

$$-K_1 - K_2 = -f_1(\varphi_m) + f_2(\varphi_m)$$

Rearranging the above equation, we can finally write

$$f_1(\varphi_m) = f_2(\varphi_m) + f_3 ,$$

where $f_3 = K_1 + K_2$.
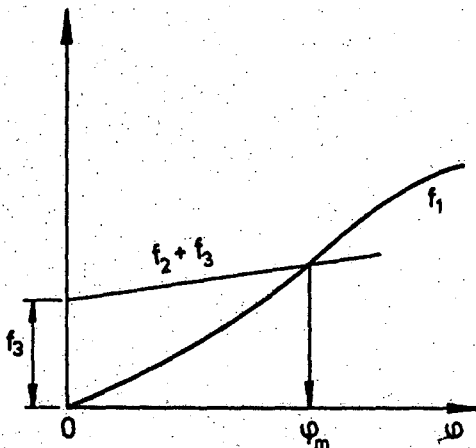
Fig. 2 Calculation of φ_m with modified
approach using energy curves

Now, the maximum angle of roll φ_m is obtained graphically as shown in Fig. 2, which is self explainatory.

5. CONCLUSIONS

The modified approach suggested above
- makes the basic assumption more realistic,
- takes into account the seakeeping characteristics directly,
- reduces the dependence upon weather criteria which suffer of arbitraryness
and therefore is expected to make the calculation for peak-roll-response under a wind gust more rational and realistic.

6. REFERENCES

[1] 'Intact stability, including analysis of intact stability casuality records - weather criterion', IMCO Document STAB 27/5/4, Submitted by Japan in 1982.

[2] 'Intact stability, including analysis of intact stability casuality records - weather criterion', IMCO Dosument STAB 27/5/3, submitted by USSR, 1982.

[3] Odabasi, A.Y.: 'Roll respohse of a ship under the action of a sudden excitation', International Shipbuilding Progress, Vol. 29, p. 327, 1982.

Professor, Department of Naval Architecture
Indian Institute of Technology, Kharagpur, India
Presently at
Institut für Schiffbau der Universität
Hamburg, Hamburg, West Germany

STABILITY AND PARAMETRIC ROLL OF SHIPS IN WAVES

I.K. Boroday, V.A. Morenschildt

1. ABSTRACT

In this report, the results of an experimental investigation of the conditions giving rise to the ship parametric roll in regular and irregular waves are presented. It is shown that the main cause of this dangerous phenomenon is periodic variation of metacenter position due to the ship heave in relation to the wave which, as a rule, takes place if the ship has a large broadside flare in way of the water-line. An approximate method is proposed for computing the parametric roll of the ship on the beam wave. The data obtained by this method are in satisfactory agreement with the experimental results. This method increases the reliability of predicting the ship rolling motions in steep short-period waves.

2. RESULTS OF MATHEMATICAL SIMULATION OF THE PHENOMENON

It is well known that ship stability at large heeling angles is the most important characteristic of her safety in still water and in waves. In particular, substantial broadside flare makes for an increase in stability. However, as is shown below, this kind of flaring can lead to such an extremely undesirable phenomenon as parametric rolling motions.

Though a relatively large number of works is concerned with the investigation of parametric roll, up to now there has been a diversity of opinions about the causes of this phenomenon and possibility of its occurrence in irregular waves.

Various researchers stated that the possibility of occurrence and the character of parametric rolling depended on the following factors: involvement of the ship in orbital wave motion, periodical changes in stability due to relative heave, center of gravity elevation above water-plane, form of stability curve, and magnitude of linear or quadratic damping. Identification of the effect of each of these factors by model testing in towing

tanks requires too much research effort. Therefore, in order to evaluate the effect of individual factors and to take the most important of them for subsequent physical investigation, it was decided to simulate on an analog computer a set of equations giving the most general representation of parametric rolling. The result of this part of work which are given in [1] have shown that:

- parametric roll whose frequency is half the frequency of excitation arises in the cases when the ship heave in relation to the wave leads to changes in the position of transverse metacenter;

- the amplitudes of parametric roll do not increase infinitely; their intensity depends on the linear and quadratic components of damping;

- parametric roll can exist both under regular and irregular excitation (see Figure 1);

- in the frequency range typical of the conditions which give rise to parametric roll there is no immediate effect of the wave-induced excitation leading to oscillations at the excitation frequency, therefore, the rolling motions within this frequency range can be described by the following equation with sufficient accuracy for practical use:

$$\ddot{\theta}+(m+\kappa\theta_o)\dot{\theta}+n_\theta^2(1-\beta\sin\omega t)\theta=0 \qquad (1)$$

3. RESULTS OF MODEL TESTS IN REGULAR WAVES

In order to verify the results of the mathematical simulation, two models were tested on the beam wave at zero speed in the towing tank of the Krylov Shipbuilding Research Institute. The form of model 1 was close to the side-walled one, whereas model 2 had a large flare in way of the water-line. Figure 2 shows the positions of transverse metacenter, Z_m, as functions of the draft, T, for the

two models. The loading of the both mo-
dels was performed so that the natural
heaving period, τ_z , was equal to 1s and
the natural rolling period, τ_θ , was
equal to 2s. In the wave range, λ , ge-
nerated by the wavemaker ($1,5$ m $\leq \lambda \leq$ 10 m)
such values of the periods made it pos-
sible to investigate both the main reso-
nance (that at excitation frequency) and
parametric resonance conditions. Prior to
each test series, the dependence of the
nondimensional linearized roll damping
coefficient, $\nu_{\theta\theta}$, on the roll amplitude,
θ_0 , was determined using the method of
free oscillations. The curves obtained
for the two models were close to each
other.

As is seen from Figure 2, the vari-
ation of the draft from the designed one
for model 1 was not accompanied by a
change in metacenter position, whereas
for model 2 it caused a significant change.
Therefore, based on the results of the
mathematical simulation, one would expect
the occurrence of parametric rolling for
model 2 and its absence for model 1. This
was fully borne out by the model test re-
sults, see Figure 3. It can be seen that
model 1 had no parametric roll, whereas
for model 2 the roll amplitude was as
large as $\sim 25°$.

4. METHOD FOR COMPUTING PARAMETRIC ROLL AMPLITUDES

According to [2], the condition ne-
cessary for the occurrence of regular pa-
rametric oscillations is provided by satis-
fying the inequality:

$$\beta > \frac{2m}{n_\theta} . \qquad (2)$$

In this case, parametric roll would occur
in a frequency range described by the
formula:

$$\omega \approx 2\sqrt{n_\theta^2 - \frac{1}{2}m^2 \pm \sqrt{-n_\theta^2 m^2 + \frac{1}{4}m^4 + \frac{1}{4}\beta^2 n_\theta^4}} . \qquad (3)$$

Since the condition $m \ll n_\theta$ is always
satisfied, damping has practically no
effect on the boundaries of parametric
oscillation occurrence, and condition (3)
can be represented in a simple form:

$$2 n_\theta \sqrt{1 - \frac{\beta}{2}} \leq \omega \leq 2 n_\theta \sqrt{1 + \frac{\beta}{2}} . \qquad (4)$$

Inequality (4) is valid for $\beta \ll 1$, that

is, the ship stability during a heave re-
mains essentially positive. For the real
values of „β" the frequency range where
parametric oscillations occur is found to
be very narrow. For example, for Δ h=0,2h
it satisfies the condition

$$0,95 \leq \frac{\omega}{2} \leq 1,05 . \qquad (5)$$

The parametric roll amplitudes, $\theta_0{}^{par}$,
in the frequency range satisfying the
condition (4) can be calculated using the
formula [2]:

$$\theta_0^{par} = \frac{\omega}{2\kappa} \sqrt{\frac{2}{x^2} + \frac{\frac{\beta^2}{4} - 1}{x^4} - 1} - \frac{m}{\kappa}, \ rad. \qquad (6)$$

where

$$x = \frac{\omega}{2 n_\theta} .$$

The maximum amplitude of parametric
roll for $\frac{\omega}{2 n_\theta}$ = 1 (parametric resonance)
is:

$$\left(\theta_0^{par} \right)_{max} = \frac{\beta \omega}{4\kappa} - \frac{m}{\kappa}, \ rad. \qquad (7)$$

It should be borne in mind that pa-
rametric oscillations have the frequency
$\omega/2$, hence, the amplitude of angular velo-
city is

$$\dot{\theta}_0^{par} = \theta_0^{par} \left(\frac{\omega}{2} \right) . \qquad (8)$$

So, for the prediction of parametric
roll knowledge of the values of β , m , κ
is required.

If the amplitude of the ship heave in
relation to the wave, q_0 , and the rela-
tionship between metacenter elevation and
the draft $z_m = f(T)$ are known then
the value of β is defined by the expres-
sion:

$$\beta = \frac{\left| \frac{d z_m}{d T} \right| q_0}{h} , \qquad (9)$$

where $\frac{d z_m}{d T}$ is the angular coefficient
of a straight line approximating the curve
$z_m = f(T)$ for the region of the still-
water waterline with respect to the axis
of drafts.

It should be noted that the possibi-
lity of occurrence and intensity of para-
metric oscillations does not depend on whe-
ther ship stability increases or decreases
with an increase in draft.

Equation (1) suggests that the plot

of the damping moment as a function of roll amplitude is a straight line which does not pass through the origin, and the plot of the coefficient $\gamma_{0\theta} = f(\theta_0)$ has a similar form. The coefficients m and κ then can be expressed in terms of $\gamma_{0\theta}$ by the formulae:

$$m = (2\gamma_{0\theta})_{\theta_0=0} \cdot n_\theta ; \quad \kappa = 2 \frac{d\gamma_{0\theta}}{d\theta_0} \cdot n_\theta , \quad (10)$$

where $(\gamma_{0\theta})_{\theta_0=0}$ is the value of the nondimensional roll damping coefficient with $\theta_0 = 0$; $\frac{d\gamma_{0\theta}}{d\theta_0}$ is the angular coefficient of a straight line approximating the relationship $\gamma_{0\theta} = f(\theta_0)$ with respect to the θ_0 -axis (when calculating the derivative $\frac{d\gamma_{0\theta}}{d\theta_0}$ the value of θ_0 should be expressed in radians).

The relationship $\gamma_{0\theta} = f(\theta_0)$ for real ships may be rather far from being a straight line. However, parametric rolling is only dependent on the value of κ which corresponds to a given amplitude, and the curve form at other points is practically of no importance. Therefore, for the calculation of parametric roll amplitudes a method of successive approximations can be used similar to that used in calculations of usual resonance in case of nonlinear damping [3].

Together with the experimental values of roll amplitudes, Figure 3 gives their predicted values. Outside the frequency range governed by the condition (5) the calculation was performed using the conventional method [3], whereas within this range use was made of the method described above. The agreement between the predicted and experimental values is quite satisfactory.

As a criterion of the possibility of parametric roll occurrence for a ship characterized by linear damping in the following or head seas, I.K.Boroday has proposed the inequality

$$\gamma_{0\theta} < \frac{\pi}{8} n_\theta S_\beta (2n_\theta) \quad (11)$$

where $S_\beta (2n_\theta)$ is the spectral density of β at the frequency $\omega = 2n_\theta$.

This criterion had to be additionally improved, since in the mathematical simulation, when excitation spectral density was specified as the sum of a finite number of harmonics, parametric roll was also observed when there were no harmonics with the

frequency $\omega = 2n_\theta$, that is, formally, $S_\beta (2n_\theta) = 0$. Yet, parametric oscillations occurred if the harmonics within the range determined by the conditions (4) or (5) had enough energy. Therefore, the criterion (11) should be extended by writing it in the form:

$$(\gamma_{0\theta})_{\theta_0=0} < \frac{\pi}{8} n_\theta S_\beta (n_{pa\imath}.) , \quad (12)$$

where $S_\beta (n_{pa\imath}.)$ is the maximum value of the spectral density of β in the frequency range determined by the conditions (4) or (5).

Based on the above considerations a method for predicting ship parametric roll in irregular waves was suggested. The concept of an equivalent wave was introduced as the basic one which denotes a regular wave with the frequency $\omega = 2n_\theta$ and the amplitude ζ_e determined by the energy of an irregular sea spectrum in the range of parametric resonance, namely,

$$\zeta_e = \sqrt{2 D_\zeta'} , \quad (13)$$

where $D_\zeta' = \int\limits_{\omega=0.95(2n_\theta)}^{\omega=1.05(2n_\theta)} S_\zeta (\omega) d\omega \approx 0.2 n_\theta S_\zeta (n_m), \quad (14)$

$S_\zeta (n_m)$ = mean value of the sea spectrum in the frequency range defined by the condition (5).

For this equivalent wave, the amplitude of ship heave in relation to the wave and the relative change in stability, β'', are computed using formula (9), and the possibility of the occurrence of parametric oscillations according to inequality (11) is verified. Further computations of parametric rolling are performed only if this inequality is satisfied. It is advisable to use the grapho-analytical method for these computations which are performed in the following order.

Several values of the parametric roll amplitude $\theta_0^{pa\imath}$ are prescribed, for each of the values the coefficient κ is calculated by formula (10), and the relationship $\kappa = f(D_\theta)$ with

$$D_\theta = \frac{\theta_0^2}{2} \quad (rad^2) \quad (15)$$

is plotted.

For the value of β'' corresponding to the "equivalent wave" and for several

values of K, the amplitude θ_0^{par} as a function of the frequency ω is calculated using equation (6). The results of the calculations are represented as the square of the transfer function modulus of parametric roll with respect to the value of β:

$$\left| \varphi_{\theta^{par}\beta}(\omega) \right|^2 = \frac{(\theta_0^{par})^2}{\beta^2} . \quad (16)$$

For several values of K the parametric roll spectral density S_θ^{par} and variance $\mathcal{D}_\theta^{par}$ are calculated

$$S_\theta^{par} = \left| \varphi_{\theta^{par}\beta} \right|^2 S_\beta = \left| \varphi_{\theta^{par}\beta} \right|^2 \left| \varphi_{\beta q} \right|^2 \left| \varphi_{q\varsigma} \right|^2 S_\varsigma \quad (17)$$

$$\mathcal{D}_\theta^{par} = \int_{\omega=2n_0\sqrt{1-\frac{\beta}{2}}}^{\omega=2n\sqrt{1+\frac{\beta}{2}}} S_\theta^{par}(\omega)\, d\omega , \quad (18)$$

where $\left| \varphi_{\beta q} \right| = \frac{(dz_m)^2}{h^2}$ is the square of the transfer function modulus of the value of β with respect to the ship heave in relation to the wave;

$\left| \varphi_{q\varsigma} \right|^2$ is the square of the transfer function modulus of the heave with respect to the wave elevation.

On the same diagram where the relationship $K = f(\mathcal{D}_\theta)$ used in the computations has been plotted, and at the same scale, the relationship $\mathcal{D}_\theta^{par} = f(K)$ obtained by equation (18) is plotted. The intersection point of the two curves defines the final value of K, for which, using the above method, the resulting spectral density and variance of the parametric roll are calculated.

For several values of the relative damping coefficient, $\gamma_\theta = \gamma_{0\theta} \cdot n_\theta$, the spectral density of the ordinary roll having the excitation frequency, S_θ, is calculated. The calculation is carried out according to [3], with the difference that the frequency range determined by the condition (4) is excluded.

For the chosen values of γ_θ the spectral densities of the total roll, S_θ^Σ, are plotted as functions of the excitation frequency ω. Outside the frequency range defined by the condition (4) they are the spectra of the ordinary roll, and within that range they represent parametric roll spectra. The spectra $S_\theta^\Sigma = f(\omega)$ have the form shown in Figure 4. The area bounded by the curve and the axis of ω define the variance of the roll angles, $\mathcal{D}_\theta^\Sigma$, for a given value of γ_θ.

The spectral density of the total roll angular velocities, $S_{\dot\theta}^\Sigma = f(\omega)$, is calculated as the sum of two components, one of which corresponds to oscillations at excitation frequency and the other refers to parametric roll. Taking into consideration the characteristic properties of each type of oscillations, one can write:

$$S_{\dot\theta}^\Sigma(\omega) = S_\theta\, \omega^2 + S_\theta^{par}\frac{\omega^2}{4} \quad (19)$$

The variance of the total rolling velocity, $\mathcal{D}_{\dot\theta}^\Sigma$, is defined by the area bounded by the curve $S_{\dot\theta}^\Sigma(\omega)$ and the ω-axis.

Further determination of the energy-statistical linearized coefficient of damping, significant amplitudes, and mean rolling period is carried out in the same way as for the ordinary roll [3].

It should be noted that the spectrum shown in Figure 4 is essentially a pseudospectrum, since it represents the distribution of the energy of oscillations by excitation frequency, and not by the frequency of oscillations, as the spectral density definition implies. These pseudospectra can be used to calculate the variance of oscillations, but not to make comparisons with the spectra obtained from mathematical or physical simulation. For the parametric roll spectral density to be applicable for the purposes of comparison, this must be shown at the actual parametric roll frequency, that is, at half the frequency defined by the condition (4). Since the frequency range of oscillations is half as wide as the frequency range of excitation, the ordinates of parametric roll spectrum should be doubled in order to retain the variance. The total roll spectrum, S_θ^H, takes the form shown in Figure 5. The angular velocity spectrum is then defined by the expression:

$$S_{\dot\theta}(\omega) = S_\theta^H \cdot \omega^2 . \quad (20)$$

5. RESULTS OF MODEL TESTS IN IRREGULAR WAVES

Since the proposed computational method involves a number of assumptions, it was considered reasonable to carry out the tests with model 2 in artificial irregular waves generated by a pneumatic wavemaker. The wave spectra were varied within wide limits both in frequency

content and intensity. The test results have shown that whenever the spectrum had enough energy to satisfy the condition (12), there was a sharp increase in the roll amplitudes, and the roll mean period was close to twice the period of the waves, which indicated to the occurrence of parametric oscillations.

By way of additional illustration, one example will here be examined. In the towing tank, the model was tested in waves having the spectrum shown in Figure 6. It can be seen that the maximum of the energy of this spectrum is concentrated near the frequency $\omega = 2n_\theta$, and that near the main resonance ($\omega = n_\theta$) the spectral density does not exceed 5 per cent of the maximum. Figure 6 also shows the spectrum obtained from the analysis of the waves realization; the spectrum is in satisfactory agreement with the specified one.

If parametric resonance in irregular waves did not show up, the model roll with the spectrum given in Figure 6 would be very weak. According to the calculations in [3], the roll amplitude of 3 % probability of exceedance in this case must not be in excess of 2°. In practice, during the model test the roll was very intensive and the amplitudes exceeded 30°.

Figure 7 shows spectral densities of rolling angles; the experimental spectral density, that calculated following the proposed procedure, and that calculated without taking into consideration parametric oscillations. According to the experimental data, the rolling motion variance was $\mathcal{D}_\theta = 151$ deg.^{2} Calculation by the proposed method gives $\mathcal{D}_\theta = 108$ deg.^{2} which leads to a discrepancy of the order of 20 per cent between the roll amplitudes. At the same time, the calculation without taking into account the parametric oscillations for the given wave spectrum yields the variance $\mathcal{D}_\theta = 1$ deg.^{2} which is by two orders of magnitude less than the experimental value.

6. CONCLUSION

Taking into consideration parametric oscillations substantially increases the accuracy of the prediction of ship roll under the action of comparatively short-period waves. The investigations made it possible to establish relationship between the ship stability characteristics and the possibility of the occurrence of paramet-

ric roll. It has been confirmed that this kind of oscillations can exist both in regular and irregular waves. In order to exclude the possibility of this phenomenon, it is advisable to design the above-water hull form so that during the ship's heave in relation to the wave the position of metacenter remains possibly constant, and for this purpose the undue flaring should be avoided. The proposed computational method makes possible considerable increase in the accuracy of predicting ship roll in the waves of relatively short periods.

7. NOMENCLATURE

n_θ = natural roll frequency,

$\beta = \dfrac{|\Delta h|}{h}$ = change in transverse metacentric height h ($\mathcal{YM}$) due to the ship heave in relation to the wave,

m, κ = coefficients for the linear and quadratic components of the damping moment, respectively,

ω = wave frequency,

$\gamma_{\theta\theta}$ = nondimensional roll damping coefficient,

S_x = spectral density of x,

$\mathcal{D}_x$ = variance of x.

8. REFERENCES

1. Morenschildt, V.A., and Smirnov, B.N., "Analog computers in the investigation of subharmonic rolling motions of a ship in waves", Conference on computer technique and advanced scientific instrumentation in ship hydrodynamics. Proceedings, Vol.1, Oct.2-5, 1984.

2. Kerwin, I.E., "Notes on rolling in longitudinal waves". Int.Ship.Pr., Vol.2, No.16.

3. "Handbook of ship theory", edited by Voitkunsky Y.I. V.2, "Statics and oscillatory motions of the ship" (in Russian)., L., Sudostroenie, 1985.

I.K.Boroday

Born in 1933, I.K.Boroday graduated from the Leningrad Shipbuilding Institute. He specializes in ship seakeeping and dynamics in waves.

Krylov Shipbuilding Research Institute, Leningrad, USSR

V.A.Morenschildt

Born in 1924, V.A.Morenschildt graduated from the Leningrad Shipbuilding Institute. She is engaged in ship seakeeping and ship motions stabilization.

Krylov Shipbuilding Research Institute, Leningrad, USSR
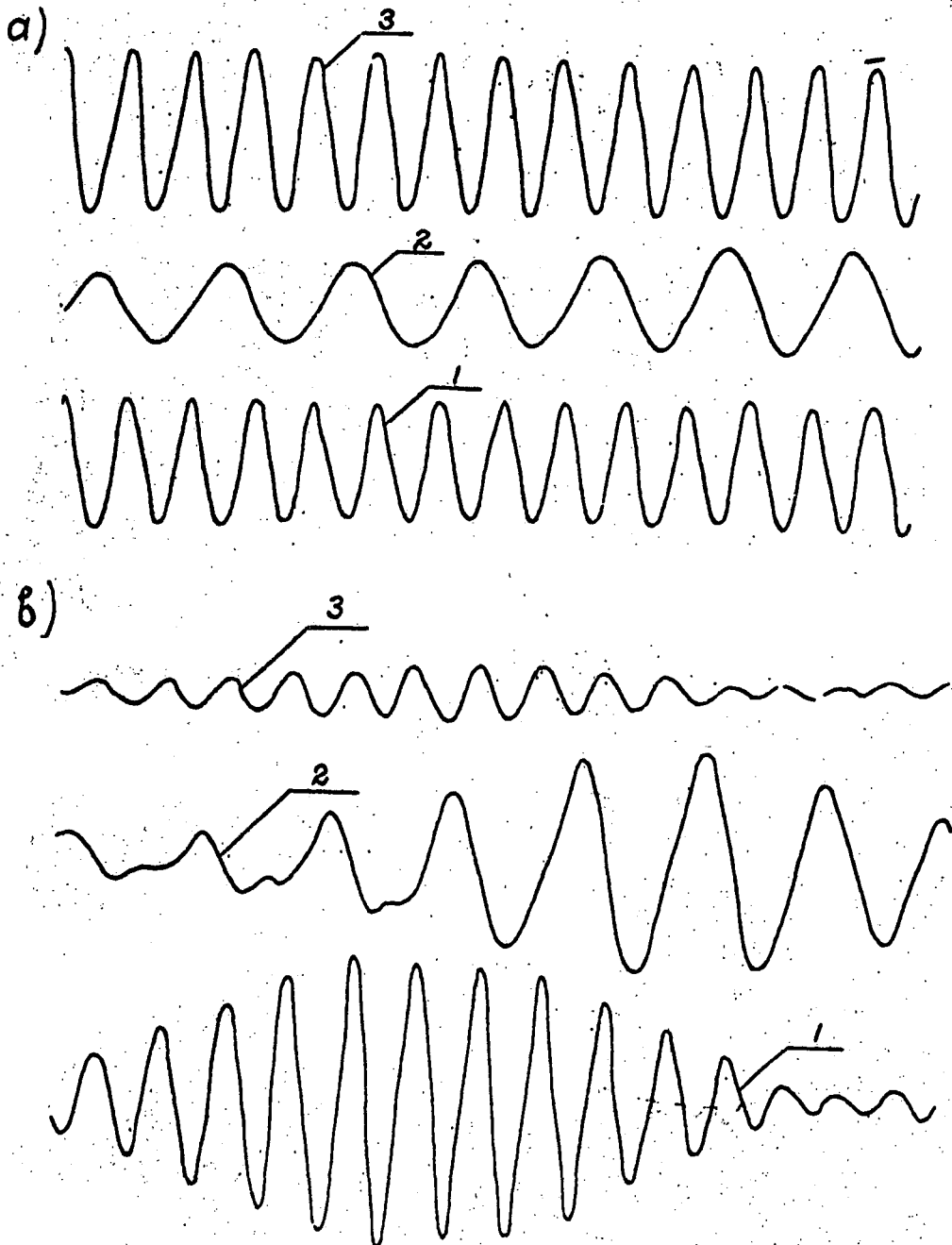
Figure 1. Sample of mathematical simulation of ship rolling motions.
a) Regular excitation; b) irregular excitation;
1) waves; 2) parametric roll; 3) heave in relation to the wave.
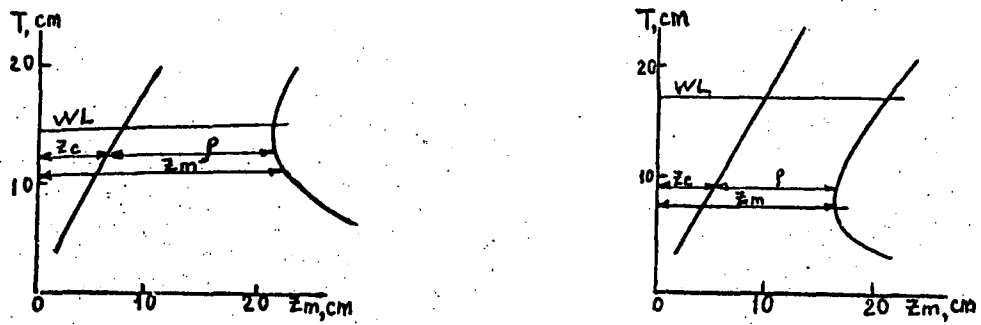
Figure 2. Transverse metacenter position as a function of draft.
a) Model 1;   b) model 2.
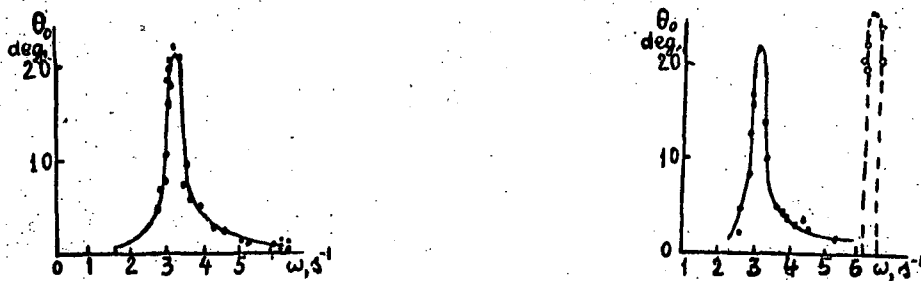
Figure 3. Roll amplitude θ_0 as a function of the wave frequency ω.
a) Model 1;   b) model 2;   ●, oscillations at the frequency ω;
○, oscillations at the frequency $\omega/2$; ——, predicted.
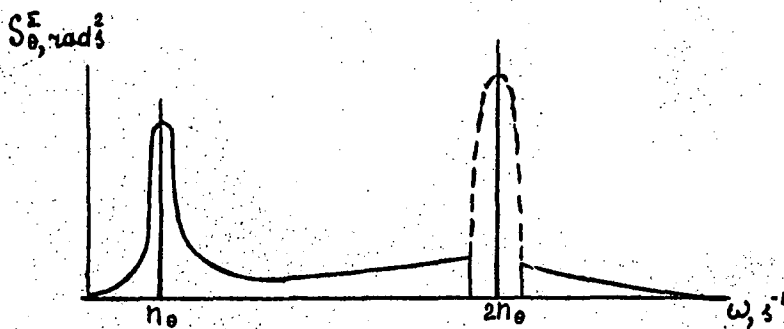
Figure 4. Pseudospectrum of total roll as a function of
excitation frequency. ——, spectrum of ordi-
nary roll for γ_θ = const.; — — —, pseudospect-
rum of parametric roll for K = const.
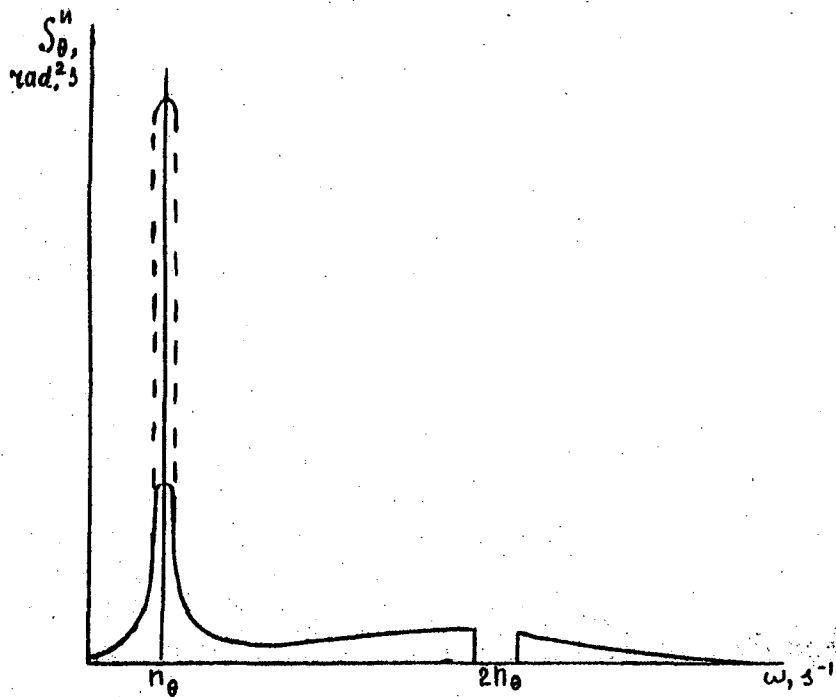
Figure 5. Actual spectrum of total roll as a function of oscillation frequency.
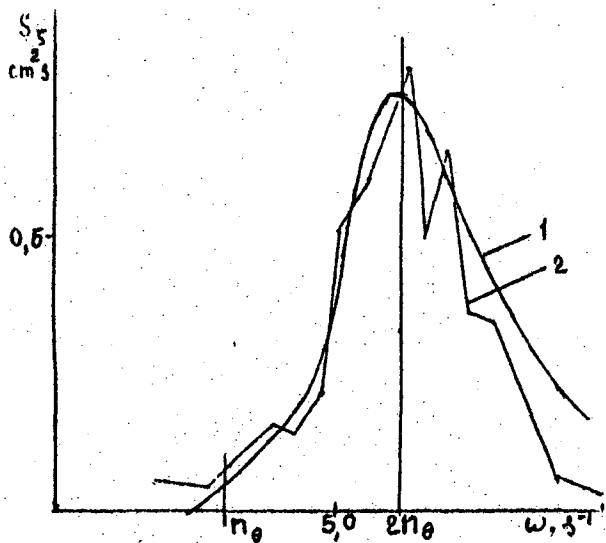
Figure 6. Irregular wave spectra.
1) Prescribed; 2) obtained.
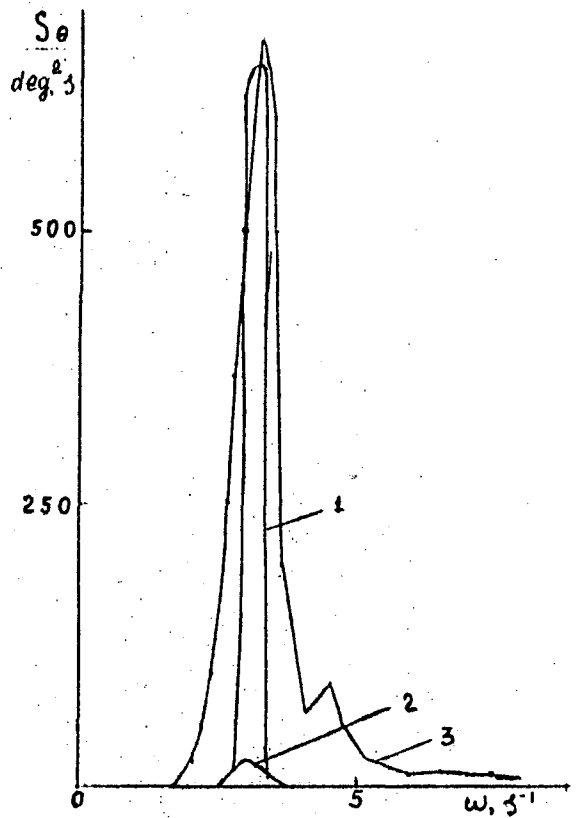
Figure 7. Roll spectra. 1) Computation by the proposed method; 2) computation without taking into account parametric oscillations; 3) experiment.

APPROXIMATE DESIGN PROCEDURE OF NONLINEAR ROLLING
IN ROUGH SEAS

V. Shestopal, Yu. Pashchenko

ABSTRACT

This procedure is based on the joint use of the auxiliary diagrams and programmed microcomputers. The diagrams enable to determine the rolling characteristics in the linear approximation and further to improve them by the method of successive approximation in terms of statistical linearization.

Application of programmed microcomputers provides for the approximation of nonlinear functions by polynomials, as well as calculation of the coefficients of statistical linearization of restoring and damping moments.

The avantages result in almost complete elimination of manual calculations, considerable shortening of calculation time and securing the sufficient practical accuracy.

1. INTRODUCTION

The determination of nonlinear rolling characteristics in irregular waves is executed now by means of statistical linearization method.

It is known that statistical equivalent gain factors, describing the form of both restoring and damping moments, are the functions of output coordinates of the system. Therefore one should execute the calculation either by graphoanalitical method or succesive approximations.

The new procedure is offered for the reduction of volume and time of calculations of statistical characteristics of motions. It is based on using the auxilliary diagrams and programmed microcomputers of different types.

2. DESCRIBING OF THE DIAGRAMS.

The two diagrams are constructed for each sea condition. The first diagram determines roll angle variance D_θ and the second – roll velocity variance $D_{\dot\theta}$ for different values of breadth B, frequency of free rolling oscillations ω_θ and damping coefficient $2\nu_\theta$.

As an example in Fig. 1 and Fig. 2 the diagrams for sea condition force 7 are given. Besides, in those figures the technique of determination D_θ and $D_{\dot\theta}$ for ship with $B = 15.5$ m, $\omega_\theta = 0.645$ s^{-1}, $2\nu_\theta = 0.087$ s^{-1} is shown.

The results of calculation of the rolling parameters of the given ship at sea condition force 7 are shown in /1/. These values are represented in Table 1 (first line), while the diagram values are represented in the second line.

Thus it may be stated that if the rolling of ship is described by means of linear differential equation, then the use of diagrams require no other calculations, except the preparation of initial data.

In a general case the results obtained must be considered as zero estimate of rolling characteristics, necessary for the calculations of statistical linearization coefficients of restoring and damping moments.

3. STATISTICAL LINEARIZATION'S COEFFICIENTS.

If a diagram of statical stability will be approximated by means of a polynomial with respect to odd-numbered degrees of θ :
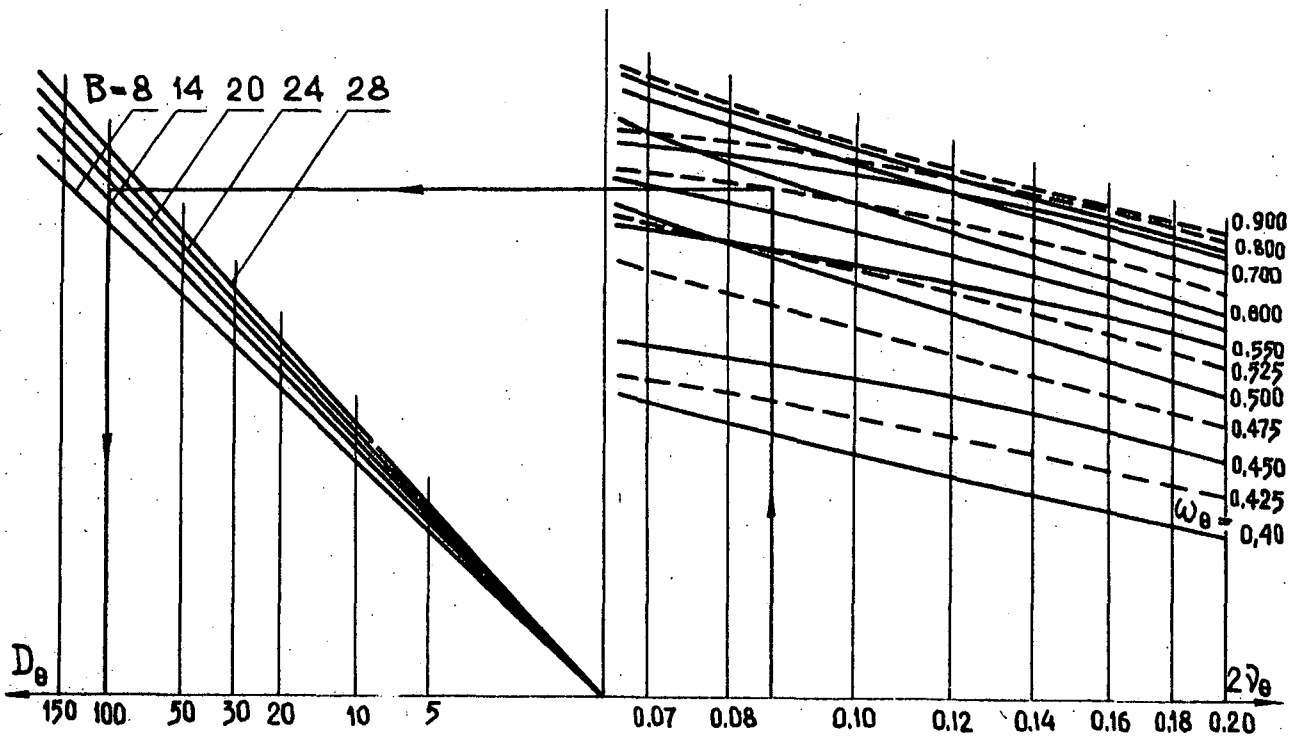
Fig. 1. Diagram for determining roll angle variance
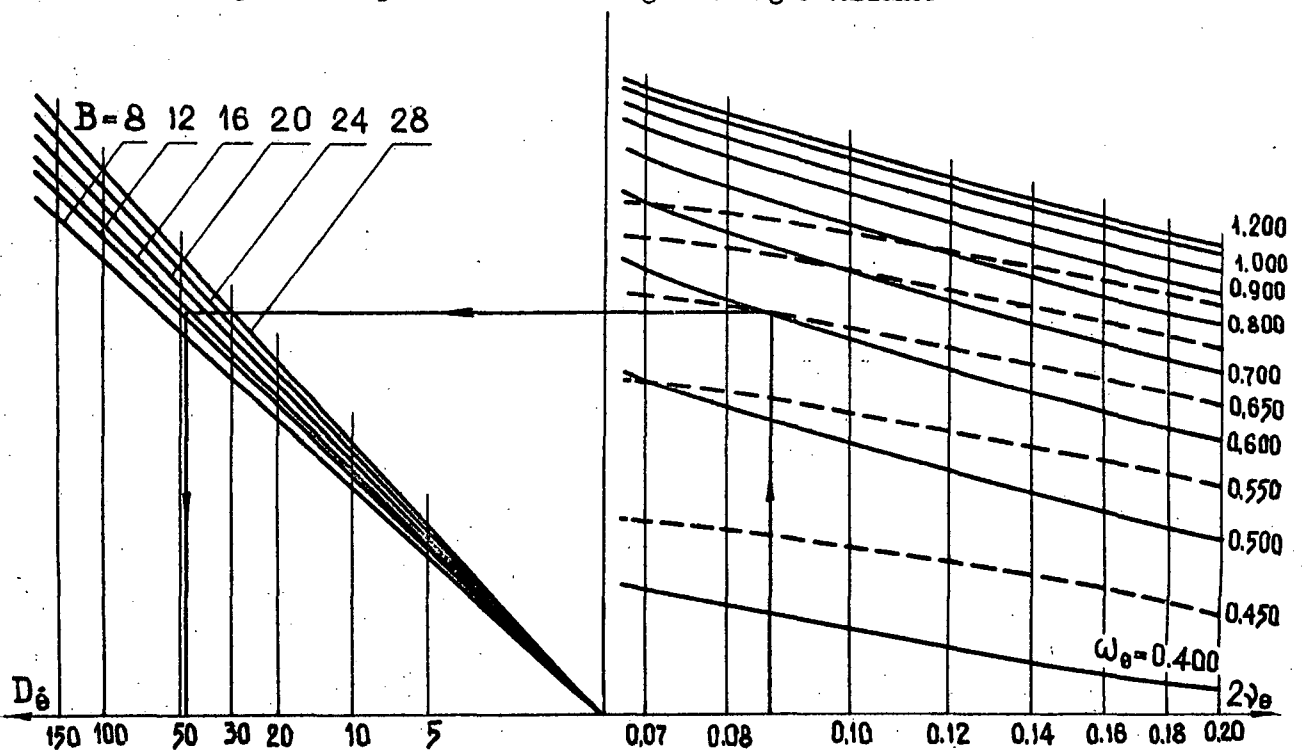
Fig. 2. Diagram for determining roll velocity variance

Table 1.

D_θ	$D_{\dot\theta}$	$\bar\theta$	$\bar{\dot\theta}$	$\theta_{3\%}$	$\theta^0_{3\%}$	$\bar\sigma$	$\bar\tau$
deg^2	deg	deg	deg/s	deg	deg/s	1/s	s
109.7	46.1	13.0	8.51	27.6	18.1	0.65	9.66
100.0	48.0	12.5	8.66	26.4	18.3	0.69	9.10

$$\frac{l(\theta)}{h} = a_1\theta + a_3\theta^3 + a_5\theta^5 \qquad (1)$$

then the formula of linearization's coefficient ω_6^2 becomes

$$\omega_6^2 = \omega_\theta^2\left\{a_1 + 3a_3 D_\theta + 15a_5 D_\theta^2\right\} \qquad (2)$$

The coefficients a_i can be obtained from the condition of equality of values of the true curve $l(\theta)$ and function approximating it in three points over a range of angle of heel from nought to θ_{max}. The corresponding system of three equations with three unknowns is easy solved with the help of programmed microcomputers of different types.

The program, instruction and control example are shown in /4/.

From the square-law linearization of resistance

$$W(\dot\theta) = w\,\dot\theta^2\,sign\,\dot\theta \qquad (3)$$

we have the formula for coefficient

$$2\dot\gamma_\theta^* = w\sqrt{2.55\,D_{\dot\theta}} \qquad (4)$$

If the damping coefficient values, obtained experimentally in form $2\gamma_\theta = f(\theta_m)$ are used for the calculation of rolling, then equivalent statistical linearization coefficient is determined by the same f function, but the argument being equal $1.9\,D_\theta^{1/2}\,\omega_\theta^{-1}$ /2/.

In this case, for the program for coefficient $2\gamma_\theta^*$ composition, f function must be approximated with a polynomial for degrees θ, as stated above.

4. DESIGN PROCEDURE PARAMETERS OF ROLLING

Thus, having D_θ and $D_{\dot\theta}$ values of linear approximation obtained from diagrams, we calculate by formulas (2) and (4) the statistical linearization coefficients ω_6^2 and $2\gamma_\theta^*$ in the first approximation. In spite of relative simplicity of expressions (2) and (4) it is more reasonable to use a programmed microcomputer, because analogous calculations are necessary to be carried out in the next steps.

In this case, the whole calculation of linearization coefficients are reduced to the input of D_θ and $D_{\dot\theta}$ previous approximation into the memory register of a microcomputer.

After calculating ω_6^2 and $2\gamma_\theta^*$ in the first approximation, we again apply to the diagrams, using scale ω_θ for input by ω_6^2, and curve $2\gamma_\theta$ for input by $2\gamma_\theta^*$. Thus we determine the parameters of nonlinear rolling in the first approximation. Then the procedure is repeated until results are obtained with accuracy required for our purposes.

In some cases, especially for large sea condition force, the process of successive approximations may be divergent. For improving the convergency one can make use of the recommendation /3/. When calculating statistical linearization coefficient ω_{6n}^2 and $2\gamma_{\theta n}^*$ one should take as quality arguments not D_θ and $D_{\dot\theta}$ of the previous approximation, but values determined by formulas

$$D_{\theta(n-1)}^* = 0.25\,D_{\theta(n-1)} + 0.75\,D_{\theta(n-2)};$$

$$D_{\dot\theta(n-1)}^* = 0.25\,D_{\dot\theta(n-1)} + 0.75\,D_{\dot\theta(n-2)}.$$

When plotting the diagram the following assumptions were used.

1. Ship is turned broadside on to the twodimensional irregular seas which spectrum is determined by formula of 12 ITTC

$$S_\zeta(\sigma) = 8.10 \cdot 10^{-3}\,g^2\,\sigma^{-5}\exp\left(-\frac{3.11 \cdot 10^4}{\tilde h_{1/3}^2}\,\sigma^{-4}\right) \qquad (5)$$

where $\tilde h_{1/3}$ – significant wave height (corresponding to 14% probability of excess),

$$\tilde h_{1/3} = 4\sqrt{D_\zeta}$$

2. The amplitude – frequency characteristic of the system was based on the simplified equation of the ship's rolling.

$$(J_x + \mu_{44})\ddot\theta + \lambda_{44}\dot\theta + Dh\theta = \\ = \ae_\theta\,\alpha_0\,Dh\,\sin\sigma t, \qquad (6)$$

where designations are those as generally accepted in the theory of ship motion.

3. Reduction coefficient α_θ for the Froude-Krylov force was calculated by Blagowetsjenskij method.

The trial operation of the proposed method testities to a sufficient precision, simplicity and comfort in the estimation of the parameters of both linear and nonlinear rolling.

The total calculation time depends on the number of approximations and averages 10 - 20 min.

NOMENCLATURE

a_i	– Coefficient of approximating polynomial
B	– Breadth of ship
D_θ	– Roll angle variance
$D_{\dot\theta}$	– Roll velocity variance
D_ζ	– Variance of wave ordinates
g	– Acceleration of gravity
h	– Initial transverse metacentric height
$\tilde{h}_{1/3}$	– Significant wave height
J_x	– Mass moment of inertia
$l(\theta)$	– Lever of statical stability
M	– Mass of ship
$S_\zeta(\sigma)$	– Spectrul of dencity of waves ordinate
W	– Statistical linearization coefficient
α_0	– Wave slope
α_θ	– Roll reduction coefficient
Λ_{44}	– Damping coefficient
M_{44}	– Added mass coefficient
ω_θ	– Frequency of free rolling motion
σ	– Wave frequency
$\bar\sigma$	– Mean quantity of roll frequency
$\bar\tau$	– Mean quantity of roll period
θ	– Roll angle
$\bar\theta$	– Mean quantity of roll angle
$\theta_{3\%}$	– Roll amplitude of three persent probability of excess

REFERENCES

1. Blagowetsjenskij, S.N., Golodilin, A.N. "A book of reference static and dynamic of the ship. v.II, Dynamic of the ship", Publishing office "Shipbuilding", 1975, Leningrad, 176 pp.
2. Gerasimov, A.V., Book: "Energy-statistical theory of nonlinear irregular ships motion", Publishing office "Shipbuilding", 1979, Leningrad, 228 pp.
3. Golodilin, A.N., Schmyryov, A.I., Book: "Seakiping and stability of ships in rough seas", Publishing office "Shipbuilding", 1976, Leningrad, 328 pp.
4. Trohimenko, Y.K., Ljubech, F.D. "The radiotechnical calculating on microcomputers", Publishing office "Radio and communication", 1983, Moskow, 325 pp.

Dr. Shestopal, V.
Dr. Pashchenko, Y.
Nikolayev Shipbuilding Institute
Prospekt Geroyev Stalingrada, 9,
327001, Nikolayev, USSR.

INCLINATIONS OF A SHIP DUE TO ARISING SEAS

Yu. Remez, I. Kogan

ABSTRACT

For the calculations of ship motions by the methods of stationary random process theory the parameters of wave spectrum corresponding to some force of sea are chosen. But the wave force scale conforms to the wind force scale only for fully arisen seas. For other stages of seas development such coordination is absent. At the same time for the estimation of the danger of capsizing and elaboration of criteria of stability it is necessary to consider the simultaneous action of wind and waves, not neglecting the dependence between them. In the paper the investigation of ship's inclinations and danger of her capsizing under the action of both the wind with constant average speed and waves of different development stages up to fully arisen is made. The probability of capsizing within some period of navigation time under certain conditions and summarized probability of capsizing in given region are obtained.

1. INTRODUCTION

The Register of the USSR and other classification societies use chiefly the deterministic procedures for estimation and elaboration of criteria of stability. The probabilistic approach is used only in some certain parts of the calculations. At the same time it is possible that the probabilistic approach to estimation of stability will be found perspective. In any case one may use the probability of capsizing as a comparative characteristic of safety of different ships. The determination of the probability of capsizing of a ship, being in heavy seas, includes two different problems. The content of one of

them is the determination of capsizing probability within some period of navigation time under certain hydrometeorological conditions. For the first time this problem was formulated and solved by Firsov. The second problem includes the determination of capsizing probability of ship being in the above-mentioned hydrometeorological conditions.

2. PROBABILITY OF CAPSIZING DUE TO ARISING SEAS

According to Firsov's general ideas, we consider the problem of capsizing probability of a ship, due to arising seas. We introduce the assumption that the storm is developed under action of steady wind, having a constant average speed and the seas excites only rolling motion.

Capsizing is understood as an excess of some dangerous angle of heel due to rolling. This angle θ_0 is considered to be known.

Application of the hydrodynamic and spectral theories of motions allows to determine the statistical characteristics of rolling in oblique seas. With solving the problem of capsizing both the variance and the average period of rolling are considered to be known.

The time of growth of the storm is divided into some intervals. Each of them is specified by its duration and degree of seas development. The latter numerically equals the ratio of average speed of wave running to average speed of wind. According to experimental data the value of this ratio lies within the limits of 0.27 and 0.82.

Both the parameters of wave spectrum γ and $h_{3\%}$ are connected with the average

speed V of wind and the degree β of seas development by the following Titov's formulas:

$$\tau = 0,64 \, v \beta,$$

$$h_{3\%} = 0,0321 \, v^2 \beta^{3/2}.$$

Having obtained the statistical characteristics of motion $D_{\theta\beta}$ and $\tau_{\theta\beta}$ for every degree of seas development, it is possible to calculate both the probability of excess of dangerous angle of heel

$$P_{0\beta} = \exp\left(-\frac{\theta_0^2}{2 D_{\theta\beta}}\right)$$

and the quantity n of excess of this angle with some interval of time T

$$n = \frac{T}{\tau_{\theta\beta}} P_{0\beta}.$$

Since we suppose that the excess of dangerous angle causes the capsizing of a ship we are interested in the first and unique excess only.

Equalling n to one we obtain the time T_0 in which with the probability $P_{0\beta}$ the capsizing of ship will occur.

The safety of a ship under fixed degree of seas development is characterised by the value of probability of capsizing within the time interval from nought to T_β

$$P_\beta(\theta > \theta_0, T_0 < T_\beta) = 1 - \exp(-\mu T_\beta).$$

Parameter μ is determined from the condition that the probability of capsizing P_β equals $P_{0\beta}$ when T_β equals T_0. Thus

$$\mu = -\frac{1}{T_0} \ln(1 - P_{0\beta})$$

and

$$P_\beta(\theta > \theta_0, T_0 < T_\beta) = 1 - (1 - P_{0\beta})^{\frac{T_\beta}{T_0}}. \quad (1)$$

If $P_{0\beta}$ is sufficiently small, the latter expression will be as follows

$$P_\beta = P_{0\beta} \frac{T_\beta}{T_0}. \quad (2)$$

Further we shall obtain the probability of capsizing of a ship being in consecutive order under action of all stages of seas by the wind with constant average speed. Let A_i be a random event consisting in the capsizing of a ship during i-th stage of seas development while A is a random event being the capsizing during all the storm duration. The probability $P_{\beta i}$ of A_i event is determined by the formulas (1) or (2). It is necessary to obtain the probability of an event A denoted by P_A:

$$P_A = P(A) = P(\theta > \theta_0, T_0 < T_s).$$

The following events favour A-event:

1) A_1 - the ship capsized at the first stage of seas development,

2) $\bar{A}_1 A_2$ - the ship did not capsize at the first stage of seas development, but capsized at the second stage,

3) $\bar{A}_1 \bar{A}_2 A_3$ - the ship did not capsize at the first and second stages of seas development, but capsized at the third stage, etc.

Thus, it is evident that

$$P(A) = P(A_1) + P(\bar{A}_1, A_2) + P(\bar{A}_1, \bar{A}_2 A_3) + \dots$$

or

$$P_A = P_{\beta 1} + \sum_{i=2}^{m} P_{\beta i} \prod_{j=1}^{i-1} (1 - P_{\beta i}), \quad (3)$$

where m is the quantity of seas development stages.

The solution of the first problem is terminated by formula (3) given the probability of ship capsizing during the whole storm duration:

$$T_s = \sum_{i=1}^{m} T_{\beta i}.$$

Further, knowing the repetition of occurence of steady wind having the average speed V_k, it is possible to calculate the summarized probability of ship capsizing during the whole duration of her navigation in the given region:

$$P_c = \sum_{k=1}^{N} q_k P_{Ak},$$

where the probabilities P_{Ak} are determined by formula (3).

3. RESULT OF CALCULATIONS

Applied the obtained formulas we have executed the calculations for the ship having the length 45 m, displacement 357 tons and metacentric height 1 m in a three-dimensional beam seas. The results of calculations of average amplitudes and average periods of rolling depending on the degree of seas development and average speed of wind are shown in Fig.1. The probability of excess of different dangerous angles of heel depending on the average speed of wind is represented in Fig.2.
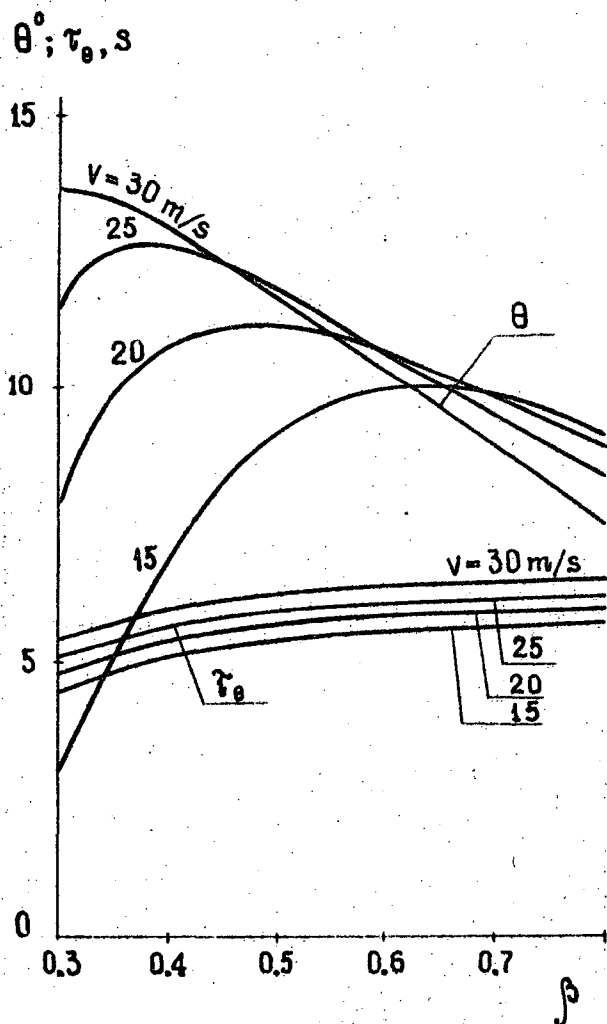
Fig.1. Average amplitudes and average periods of rolling in arising seas

One should note the following circumstance. At the initial stages of seas development greater average amplitudes of rolling are caused by greater speed of wind; in fully arisen seas the dependence is of the contrary character. Besides,

each average wind speed conforms to the most dangerous particular degree of seas development. It confirms the necessity of rigorous accounting all the stages of seas development when the summarized probability of ship capsizing in storm duration is calculated.
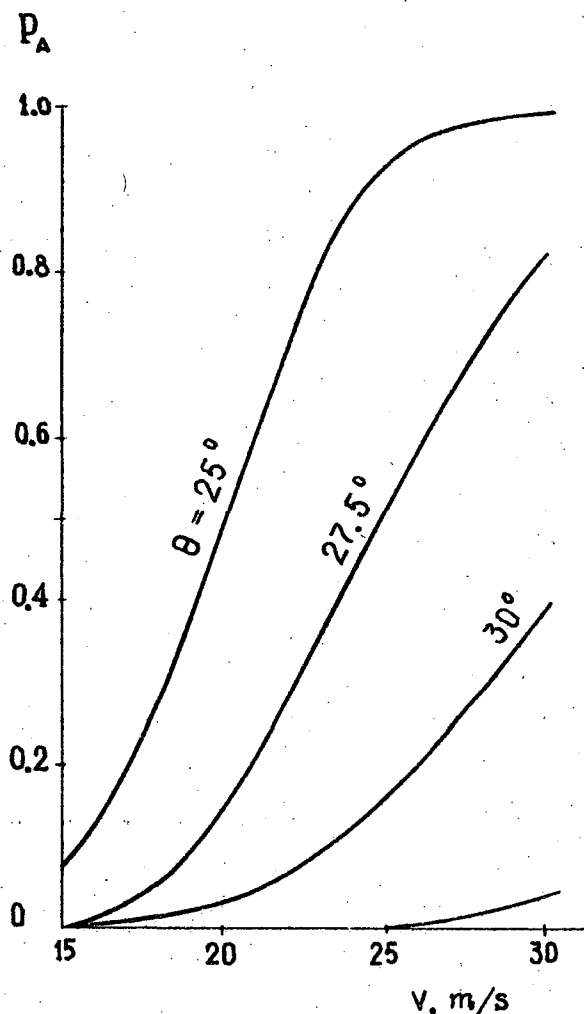
Fig.2. Probability of excess of different heel angles

Having obtained the value of dangerous heel angle and knowing from damage statistics the magnitude of critical capsizing probability, it is possible, using the graph like Fig.2, to make the conclusion if the wind and corresponding seas are safe for the ship or they are able to capsize her.

NOMENCLATURE

V — average speed of wind;

θ_0 — dangerous heel angle (angle of capsizing);

τ — average period of wave spectrum;

$h_{1/3}$ — significant wave height;

$h_{3\%} = 1,32\ h_{1/3}$ – wave height of three percent probability of excess;

D_θ – variance of rolling;

τ_θ – average period of rolling;

T_s – time of storm duration;

β – degree of seas development;

T_β – time of β – degree seas existance;

c – average speed of wave running;

$D_{\theta\beta}$ – variance of rolling on β – degree seas;

$\tau_{\theta\beta}$ – average period of rolling on β – degree seas;

$P_{0\beta}$ – probability of excess of dangerous heel angle on β – degree seas;

T – arbitrary time interval;

n – quantity of excess of dangerous heel angle within T – time;

T_0 – time in which with the probability $P_{0\beta}$ the capsizing of a ship will occur;

P_β – probability of capsizing within the time interval from nought to T_β;

A_i – random event consisting in the capsizing during i -th stage of seas development;

$\bar{A}_i$ – random event contrary to A_i;

A – random event consisting in the capsizing during the whole storm;

P_A – probability of A - event;

$P_{\beta i}$ – probability of capsizing during i -th stage of seas development;

Π – symbol of product;

m – quantity of seas development stages;

q_k – repetition of occurence of steady wind, having the average speed V_k;

P_c – summarized probability of capsizing in the given region.

REFERENCES

1.Titov L.F. Wind wave. L. Gidrometeoizdat, 1969.

Yu. Remez, Prof., Sc. Dr.
I. Kogan, Dipl. Eng.
Nikolayev Shipbuilding Institute,
Prospect Geroev Stalingrada, 9,
327001, Nikolayev, USSR.

ON THE FLOATING DOCK'S DYNAMICAL BEHAVIOUR
UNDER WIND SQUALL IN A SEAWAY

Yu. Bilyansky, L. Dykhta, V. Kozlyakov

ABSTRACT

In order to estimate a dock load carrying capacity, to design its reliable mooring system, to carry out well-founded strength calculations etc. under well-known assumption of the hydrodynamical ship-motion theory and the theory of flexible heavy thread, a study is made of the floating dock oscillatory motions excited by wind squall and incident waves in anchorage. The dock, anchor cables and surrounding fluid are considered as interacting members of a single mechanical system with disturbed and lumped parameters.

Computed numerical results for one environment condition combination are presented as plots both of time functions and point spectra for the dock sway-, heave- and roll-motion.

INTRODUCTION

The up-to-date state of the hydrodynamical ship-motion theory and the modern high-speed computers capabilities make it possible to formulate and to solve the complicated engineering problems of considerable importance from viewpoint of applying the results obtained in design and operation practice of such expensive floating structures as offshore platforms, floating docks, drilling ships etc.

Unlike an ordinary ship the characteristic feature of the mentioned structures is availability of N $(N \geqslant 3)$ anchor cables influencing essentially on its mechanical properties, therefore for reasonable information on structure behaviour under heavy environment conditions to be received it is necessary to account the interaction between surrounding wa-

ter, structure body and anchor cables.

Taking this interaction into consideration complicates, to some degree, the problem on structure behaviour by making it non-linear, the computer-generated analysis being appropriate only.

In this paper there are outlined some points of the problem on definition of the floating dock oscillatory motion in anchorage under wind squall and incident waves having been solved to estimate the operational possibilities and to carry out some design calculations for the real structure in operation.

1. EQUATIONS OF DOCK MOVEMENT

The dynamical behaviour of the considered mechanical system being affected by exciting forces due to wind squall and incident waves is investigated under the following assumptions:

- the dock is a rigid body with six degrees of freedom and its submerged volume forms a parallelepiped;

- the surrounding water is incompressible inviscid fluid under gravity and its disturbed motion is supposed to be described in the scope of the linear wave theory;

- each of the anchor cables is homogeneous flexible heavy thread which tensile deformation is sufficiently small to use Hooke's law;

- the only category of the hydrodynamic disturbed forces the cable being acted upon is considered: namely, those associated with cable's added mass and applied in the cable normal plane;

- the time scales of dynamical processes caused by squall and waves are incommensurable (the wind-squall dock vibra-

tions' period considerably exceeds that of waves);

   - the incident waves are two-dimensional regular waves of small amplitude-length ratio;

   - the wave-excited displacements, velocities and accelerations of the system under consideration are first-order small quantities, their squares and products being neglected;

   - the squall is simulated by time step-function with a known wind-velocity's jump.

   Owing to the above mentioned incommensurability in time scales of the system oscillatory motions due to squall and waves it is permitable to use separation principle for the system motions and to subdivide the undertaken study into two some easier problems: 1) the non-linear problem on the determination of "slow" dock movements and quasi-static stresses in anchor cables forced by squall; 2) the linear problem on the description of the system's "fast" vibrations about its changing equilibrium position and dynamical tensions in the cables' cross-sections.

   For mathematical formulation and solution of these problems two Curtesian co-ordinate systems are used: 1) X, Y, Z - system is fixed in space, X, Y -plane coinciding with basin bottom and Z -axis vertically upwarf; 2) x, y, z -system is fixed in the dock, its origin being in the intersection point of the dock central longitudinal plane, midstation plane and waterline plane, the latter is considered as x, y -plane with x - and y -axis directed to the dock bow and to the port respectively, while z -axis is directed upward. When waves and a wind vanishes, the Z - and z -axis are coinciding with the same vertical line and other ones are mutually parallel and unidirectional.

   Hereafter the nomenclature in Section 4 will be adopted.

   The system of differential equations for determination dock movement due to squall may be written in matrix form as follows:

$$(M+\mu_0)\ddot{R}_0 + CR_0 = F_\alpha + \sum_{j=1}^N T_j \quad (1)$$

with the added mass matrix elements being calculated by strip-method based on the solution of boundary-value problem on the determination fluid motion disturbed by a uniformly moving single rectangular contour (when $h \gg T$) or a grill of such contours (when $h \sim T$).

   There are not any principle difficulties in the problem on determination of the anchor cable tension T_j which may be obtained by means of the equations well known in the flexible heavy thread mechanics. In particular, the quantities G_j, V_j may be found from the relationships

$$l_j \, sh \, \lambda_j = \lambda_j (1+e_j G_j L_j)(L_j^2 - Z_j^2)^{1/2} ;$$

$$V_j = \frac{g \, m_j}{2} \frac{L_j + Z_j \, ch \, \lambda_j}{sh \, \lambda_j + \lambda_j e_j G_j L_j \, ch \, \lambda_j} ; \quad (2)$$

$$\lambda_j = \frac{g \, l_j \, m_j}{2 \, G_j}$$

provided that inequality

$$l_j > \frac{L_j^2 - Z_j^2}{2 Z_j} \, ln \, \frac{L_j + Z_j}{L_j - Z_j}$$

is satisfied. This inequality means that angle of tangent to the anchor cable in its low end with the ground is non-zero; in the opposite case the quantities G_j, V_j and L_j are the solutions of equations

$$L_j^* = \frac{G_j}{g \, m_j} \, sh(\lambda_j^* - 2\lambda_j e_j G_j L_j) ;$$

$$1 + \frac{g \, m_j Z_j}{G_j} = ch(\lambda_j^* - 2\lambda_j e_j G_j L_j); \quad (3)$$

$$V_j = -g \, m_j L_j^* ; \quad \lambda_j = \frac{l_j - L_j + L_j^*}{g \, m_j G_j}$$

where

$$T_{j1} = G_j \, sin \, \alpha_j ; \quad T_{j2} = G_j \, cos \, \alpha_j ; \quad T_{j3} = V_j ;$$
$$T_{j4} = T_{j3}(Y_j - \eta_0) - T_{j2}(Z_j - h - \zeta_0);$$
$$T_{j5} = T_{j1}(Z_j - h - \zeta_0) - T_{j3}(X_j - \xi_0); \quad (4)$$
$$T_{j6} = T_{j2}(X_j - \xi_0) - T_{j1}(Y_j - \eta_0);$$

$$X_j = x_j - y_j \chi_0 + z_j \psi_0 + \xi_0 ;$$

$$Y_j = x_j \chi_0 + y_j - z_j \theta_0 + \eta_0 ;$$

$$Z_j = -x_j \psi_0 + y_j \theta_0 + z_j + h + \zeta_0 .$$

The wind loads on the dock are to be calculated by using the formulae

$$F_{ar} = \frac{1}{2} \rho_a V^2 C_a S_a \nu_r , \quad r = 1, 2, 3;$$

$$F_{a4} = y_a F_{a3} - z_a F_{a2} ;$$

$$F_{a5} = z_a F_{a1} - x_a F_{a3} ; \qquad (5)$$

$$F_{a6} = x_a F_{a2} - y_a F_{a1} .$$

Written formulae (1) - (5) form the closed system of non-linear equations in respect to the unknown dock displacements and to the anchor cables tensions due to squall, the solution being obtained by numerical method only.

Assuming time dependance of unknown kinematic and dynamic parameters defined by factor e^{i6t} (the real part is only to be taken into account in expressions containing this factor), it is possible to reduce the description of considered mechanical system's small vibrations about its equilibrium position to the calculation of their complex amplitudes.

Before writing the dock motion equations it is necessary to consider question on the anchor cable reaction applied to the dock for its complex amplitude to represent as a linear combination of those of dock motion.

The following system of ordinary differential equations

$$G_1 u_1 + Q_1' = \vartheta Q_2 ; \quad u_1' = \vartheta' u_2 ;$$

$$G_2 u_2 + Q_2' = -\vartheta' Q_1 ;$$

$$u_2' = -\vartheta' u_1 + \frac{Q_2}{Q_0} ; \qquad (6)$$

$$G_3 u_3 + Q_3' = 0 ; \quad u_3 = Q_3 / Q_0 ,$$

is found to define the complex amplitudes

of the cable's steady-state oscillations and of the dynamical stresses in its cross-sections (the prime is used to denote the differentiation on dimensionless curvilinear cable's coordinate ε , the $\varepsilon = 0$ and $\varepsilon = 1$ corresponding respectively the lower and upper cable ends). In order to account dynamical interaction between an anchor cable and the dock, the vector u with components u_1, u_2, u_3 is to be satisfied to boundary conditions.

$$u(0) = 0 ; \quad u(1) = w_j ,$$

when $\varepsilon = 0$ and $\varepsilon = 1$ respectively. It should be stressed here, that w_j is the dock's j-th hawse velocity vector referred to the cable moving trihedral. As it may be shown by methods of the analytical theory for differential equations the solution of the system (G) is represented by power series [1].

On the basis of the computations, which are simple but some long, it may be found the complex amplitudes' column vector P_j of the dynamical cable tensions acted upon dock in the j-th hawse point to be represented by

$$P_j = B_j R$$

where elements of matrix B_j are dependant on geometric parameters of j-th anchor cable, on the vibration frequency and on the mutual dock and cable arrangement.

The system of six algebraic equations for determination of the dock motion complex amplitudes may be presented in form of matrix equality

$$\left\{ -6^2 (M + \mu) + i 6 \lambda + C - \sum_{j=1}^{N} B_j \right\} R = F, \qquad (7)$$

where the dock damping coefficients matrix λ and added mass elements matrix μ are to be calculated by strip-method based on the solution of boundary-value problem on determination of the finite depth fluid's motion disturbed by a rectangular contour oscillating on the fluid free surface.

To make the paper shorter it should

be only noted that the latter problem may be shown by ship-motion theory [3] conventional methods to reduce to the solution of an infinite algebraic system with respect to the Fourier series expansion coefficients of the hydrodynamical singularities unknown density to be disturbed on the contour.

The limits of the presented approach applicability is mainly defined by the validity of the assumption that the time scales of dynamical processes caused by squall and waves are to be incommensurable, the mentioned property of the system under consideration being dependant upon the anchor system stiffness (defined by lengthes of the anchor cables provided the water depth is constant): for the "soft" anchor system characteristic the incommensurability is available, for the "hard" one it is absent.

In the latter case the study undertaken may be made on the basis of system (1) which is to be defined more exactly by introducing exciting forces due to waves, damping coefficients matrix λ and by changing the added mass matrix μ_0 on that of μ.

2. RESULTS

In this Section there are represented some illustrative results on the oscillatory motion of the floating dock having been built by a Yugoslavian shipyard and established on the water area of Novorossiisk ship-repair plant. One of the most interesting, from practical viewpoint, cases of environment conditions under beam waves and wind is considered, the input waves, dock and anchor system data being presented in Tables 1, 2 and 3.

Table 1. Wave data

Wave length	λ_0	93 m
Wave height	H	3.7 m
Frequency	σ	0.65 sec^{-1}
Wave number	k	0.0676 m^{-1}
Water depth	h	11.2 m

In addition to the information contained in Table 3 it is important to state the following: 1) in the Table the anchors' coordinates in X, Y, Z -system are written assuming the wind's absence; 2) for the anchor cable unit length mass the same value m_j = 238 kg/m have to be

taken for all $j = 1,2,...,12$; 3) the anchor cables material Young's modulus is adopted equal to 1.8×10^{11} N/m^2.

Table 2. Dock data

Length	L	275 m
Breadth	B	63 m
Draught	T	5.3 m
Mass	m	8.86x10^7 kg
Mass moment of inertia	I_x	3.77x10^{10} kg
Added mass coefficients	μ_{22}	4.43x10^7 kg
	μ_{33}	2.66x10^8 kg
	μ_{44}	3.77x10^{10} kgm^2
	μ_{24}	2.1x10^8 kgm
Damping coefficients	λ_{22}	1.53x10^7 kg/sec
	λ_{33}	9.18x10^7 kg/sec
	λ_{44}	9x10^8 kgm^2/sec
Coordinate of CB	z_c	-2.65 m
Coordinate of CG	z_g	4.7 m
Waterplane area	S	1.84x10^4 m^2
Waterplane area moment of inertia	J_x	7.05x10^6 m^4
Above-water centerplane projected area	S_a	7.8x10^3 m^2
Coordinate of	z_a	8.5 m

Table 3. Anchor system data

j	L_j	X_{Aj}	Y_{Aj}	x_j	y_j	G_{0j}
	m	m	m	m	m	kN
1	88	87	54	87	-32	220
2	88	82	-54	82	32	220
3	88	25	54	18	-32	220
4	88	27	-54	27	32	220
5	88	-25	54	-18	-32	220
6	88	-27	-54	-27	32	220
7	88	-87	54	-87	-32	220
8	88	-82	-54	-82	32	220
9	146	30	64	133	-37	350
10	145	30	64	133	-37	350
11	146	-30	64	-433	-37	350
12	145	-30	-64	-131	37	350

On the basis of computer-generated numerical results for dock motion in Figure 1 there are represented the dock displacements under swaying, heaving and rolling motion as a function of time and in Figure 2 there are given the mentioned processes' point spectra normalized by the maximal spectra ordinates. The availability of anchor system, as seen from Figures 1, 2, affects weakly dock heaving

motion and influences greatly its swaying and rolling motions; the latter makes vibrations more complicated and their spectra includes some additional harmonies besides main ones.

3. NOMENCLATURE

B – dock breadth;

B_j – matrix of coefficients for representation of the cable dynamical reaction;

C – restoring force coefficient matrix;

C_a – airforce coefficient;

e_j – anchor cable elongation;

$F_a = \{F_{ar}\}_{r=1}^{6}$ – column vector of airforces due to wind squall;

G_j – cable horizontal tension component;

G_{0j} – initial cable tension;

g – gravitational acceleration;

H – wave height;

h – water depth;

I_x – dock mass moment of inertia;

J_x – waterplane area moment of inertia;

j – subscript for referring to a quantity associated with j-th anchor;

k – wave number;

L – dock length;

L_j – anchor cable length;

L_j^* – saging part of anchor cable;

l_j – projection of L_j^* on the bottom;

M – matrix of dock inertia elements;

m – dock mass;

m_j – mass in water of the anchor cable unit length;

N – number of anchors;

n_j – added mass of cable unit length;

$P_j = \{P_{jr}\}_{r=1}^{6}$ – column vector cable reactions applied to dock under motion;

$Q = \{Q_r\}_{r=1}^{3}$ – dynamical stress vector in cable cross-section referred to cable moving trihedral;

Q_0 – tension in cable due to squall;

$R = \{\xi, \eta, \zeta, \theta, \psi, \chi\}$ – column vector of dock motion displacements;

$R_0 = \{\xi_0, \eta_0, \zeta_0, \theta_0, \psi_0, \chi_0\}$ – column vector vector of dock displacements due to squall;

r, S – dummy indices;

S – waterplane area;

S_a – dock above-water centerplane projected area;

T – dock draught;

$T_j = \{T_{jr}\}_{r=1}^{6}$ – column vector cable loads acting on dock under squall;

X, Y, Z – fixed in space coordinate system;

$u = \{u_r\}_{r=1}^{3}$ – thread vibration amplitudes vector referred to moving trihedral;

V_j – cable vertical tension component in hawse point;

v – wind velocity;

w_j – hawse velocity referred to cable moving trihedral;

X_j, Y_j, Z_j – hawse point coordinates in X, Y, Z -system;

X_{Aj}, Y_{Aj} – anchor coordinates x, y, z - fixed in dock coordinate system;

$x_j, y_j, z_j = -T$ – hawse point coordinates in x, y, z -system;

x_a, y_a, z_a – coordinates of centre wind pressure in x, y, z -system;

z_c, z_g – z - coordinate of the dock center of buoyancy and gravity, respectively, in x, y, z -system;

α_j – angle made by cavle plane and Y, Z -plane;

ε – dimensionless curvilinear coordinate;

ϑ – angle made by a tangent to thread and bottom plane;

$\lambda = \{\lambda_{rs}\}_{r,s=1}^{6}$ – dock damping coefficients matrix;

λ_0 – wave length;

λ_j, λ_j^* – auxiliary variables in (2) and (3);

$\mu = \{\mu_{rs}\}_{r,s=1}^{6}$ – dock added mass matrix under motion;

$\mu_0 = \{\mu_{0rs}\}_{r,s=1}^{6}$ – dock added mass matrix under squall motion;

$\nu = \{\nu_r\}_{r=1}^{3}$ – unit vector of the wind force principal vector;

ρ_a – air density;

σ – circular frequency;

$$\sigma_1 = \sigma^2 L_j / g \ ;$$

$$\sigma_2 = \sigma_1 \left(1 + n_j / m_j \right);$$

ξ, η, ζ – dock surge-, sway- and heave-motion displacements;

ξ_0, η_0, ζ_0 – dock displacements along x-, y -axis, respectively, due to squall;

θ, ψ, χ – dock roll-, pitch- and yaw-motion displacements;

θ_0, ψ_0, χ_0 – dock angular displacements due to squall.

A dot denotes differentiation with respect to time.
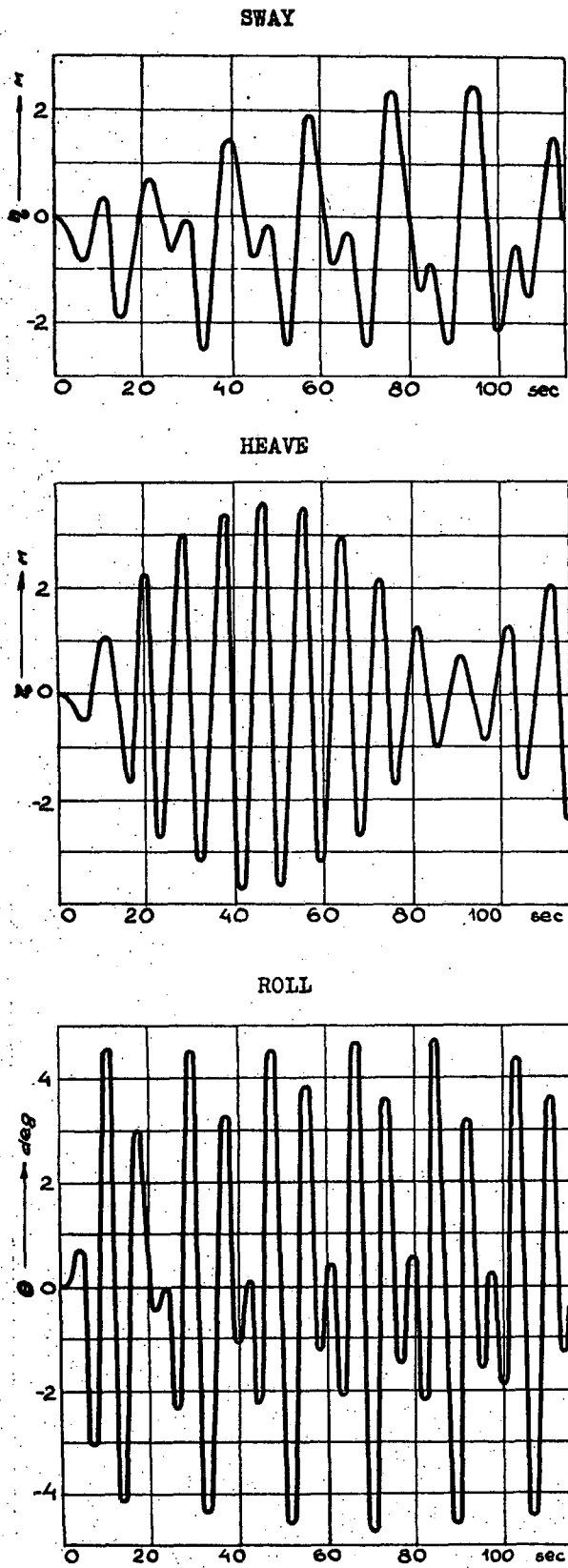
Figure 1. The dock
oscillations under motion
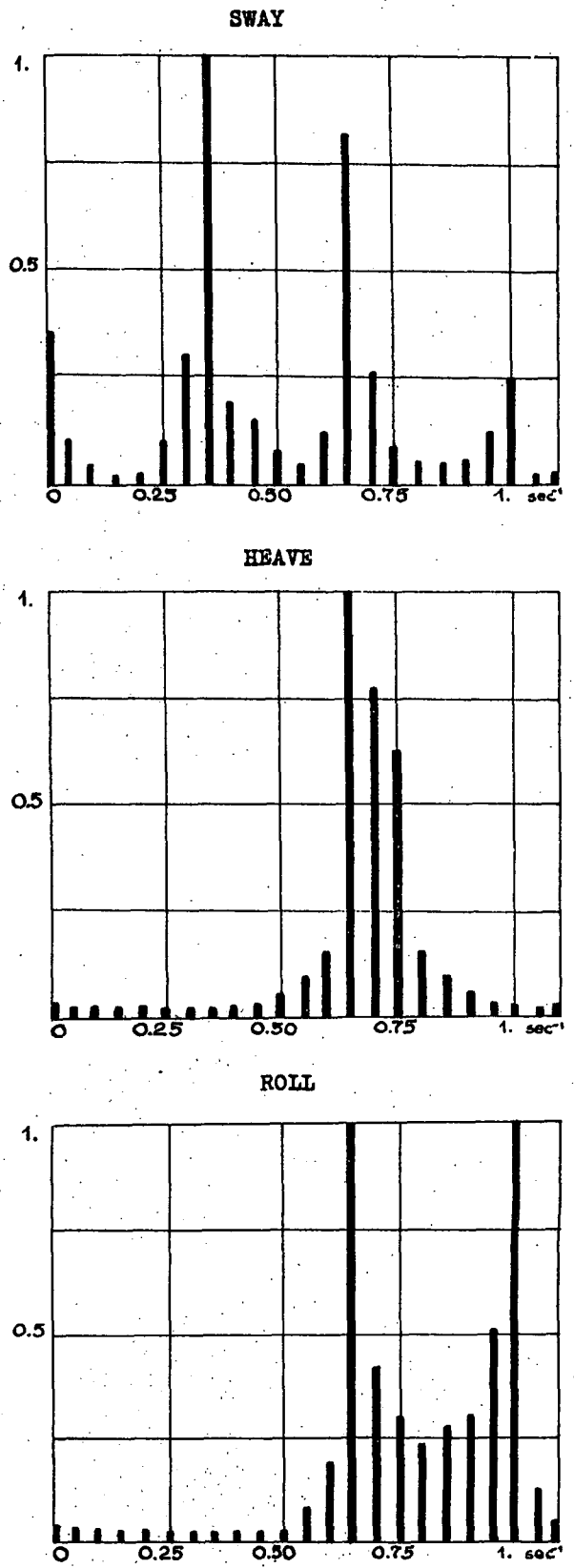
Figure 2. The dock
oscillations point spectra

A prime denotes differentiation with respect to dimentionless variable $\mathcal{E}$.

4. REFERENCES

1. Bilyansky Yu., Dykhta L. Determination of the small vibration forms for a heavy thread in ideal fluid. Hydrodynamics of ship. Sbornik nauchnykh trudov, Nikolayev Shipbuilding Institute, 1984, pp.84-91.
2. Gurevich M. Added masses for a grill of rectangulars, Prikladnaya matematika i mekhanika, vol.4, No.2, 1940, pp.93-100.
3. Haskind M. The hydrodynamical ship-motion theory. "Nauka", 1973, pp.1-327.

Yu. Bilyansky, Dipl. Eng.
L. Dykhta, Dr.
V. Kozlyakov, Prof., Sc. Dr.
Nikolayev Shipbuilding Institute,
Prospect Geroev Stalingrada, 9,
327001, Nikolayev, USSR.

THE PREDICTION OF LONG-TERM SHIP ROLLING FOR INTACT STABILITY

AND ANTI-ROLLING SYSTEM ASSESSMENT

by

Y.S. Tao[*]

Abstract

In this paper it is suggested that ship roll performance in irregular waves, including vessels with anti-rolling systems, ought to use long-term predictions of roll motion using an accumulation of the short-term roll response with a conditional probability. In this approach the ship roll response for short-term prediction is calculated by a non-linear method. The authors have analysed a number of long-term prediction methods of roll and suggest that the roll damping can be given by means of progressively approximate methods corresponding to significant roll angle which is calculated from the roll response amplitude operator. It is suggested that the rules for stability of sea-going ships should adopt long-term predictions of extreme value in roll angle as a basis for ship stability criteria.

1. INTRODUCTION

The rolling motion of a ship in irregular wave is a important index for dynamic stability and seakeeping.

Although a comparison of rolling performance between ships of different designs can be made from ship motion prediction programs or from model tests these are normally based on short term predictions in irregular waves.

If short term prediction techniques are used for roll prediction the comparison between different ship designs can only be made for specific parameters. However, a more meaningful comparison can be made if the variables of loading condition, speed, heading, sea state etc are combined with the encounter probabilities of the factors involved over the ship's entire lifetime.

Ship Hydrodynamics Laboratory,
Shanghai Jiao Tong University,
China

So as would be expected in a number of intact stability rules for some existing sea-going ships stability criteria for the roll angle is based on short-term rather than long prediction.

The calculation of roll response amplitude operator is usually based on linear theory although rolling is finely tuned phenomena and is highly non-linear as a result non-linear damping and non-linear restoring moment. However, it is now practical to make use of non-linear prediction techniques using the equivalent linearisation technique, the perturbation method, the Fokker-Planck equation method and the functional representation method for the prediction of non-linear ship roll motion.

It is therefore possible to calculate a vessel's rolling performance in irregular waves, and assess the effectiveness of a vessel with an anti-rolling system, using non-linear methods and long-term prediction techniques. The rolling motion obtained in this way is an accumulation of the short-term roll motion obtained by the conditional probability. The roll damping can be estimated by means of an approximate method based on the significant roll angle calculated from the roll response amplitude operator. The criteria for the

stability of sea-going ships can then be formulated using long-term predictions of the extreme value of roll amplitude.

2. LONG-TERM ROLL ANGLE AMPLITUDE PREDICTION METHODS

It is of considerable interest to assess the magnitude or roll angle amplitude experienced by a ship in her lifetime while the ship is still in the design stage. This is achieved by evaluating the long-term rolling response of a vessel which is i.e. essentially the application of the conditional probability to the short-term response.

In order to evaluate roll amplitude the lifetime of a ship in a seaway, the amplitude of roll for various short-terms are computed and are accumulated taking into account the frequency of occurrence of each short-term. Because the amplitude of a roll in the short-term follows the Rayleigh probability law, and the sea condition can be represented by the significant wave height and wave period modal, then the probability that the amplitude of a roll, ϕ, will exceed a specified ϕ_1 in the lifetime of the ship can be given [1] as

$$P_{\phi L}(\phi > \phi_1) = \frac{\sum_W \sum_H \sum_{T_O} \sum_V \sum_X n^* e^{\frac{-\phi_1^2}{2\sigma^2}} \cdot P(X,V|H,T_O,W) \cdot P(T_O|H) \cdot P(H) \cdot P(W)}{\sum_W \sum_H \sum_{T_O} \sum_V \sum_X n^* \cdot P(X,V|H,T_O,W) \cdot P(T_O|H) \cdot P(H) \cdot P(W)} \quad (1)$$

Where, σ is standard deviation of roll amplitude (short-term), X is heading to waves, V is ship speed, H is significant wave height, T_O is modal period, W is loading, and n^* is the average number of zero-crossings per unit time for each steady-state short-term response. It is obtained as follows

$$n^* = \frac{1}{2\pi} \sqrt{m_2/m_0} \quad (2)$$

Where, m_0 is area under the short-term response spectrum, m_2 is second moment of the short-term response spectrum.

2.1 Full Scale Ship Measurement Method

The ship's roll motion in seaway is effected by very many environmental and operational factors, and it is not possible to include all of these in some of which have not or cannot been considered practical studies of ship motion.

Furthermore it is not practical to collect long term data from ship trials taking into account all environmental and operational conditions a vessel may encounter during her lifetime. In the initial ship design stage it is very useful to assess the motion and stability of a ship to use an analytical expression from the probability distribution of roll motion based on full-scale data. Although there have been very many roll full scale tests for many kinds of ships, most of them were short

term tests, and show very large data dispersion, and insufficient to be dealt statistically. It is gratifying that Takahashi [2] carried out full scale measurements on a container carrier, for about 52 months from October 1976 to January 1981.

The cumulative probability of maximum, minimum and RMS values of roll amplitude are shown in Fig. 1. The ratio of the frequency of wave encounter angle for this vessel was approximately as follows

Head : Bow : Beam : Quarter : Follow
= 2 : 3 : 2 : 2 : 1.
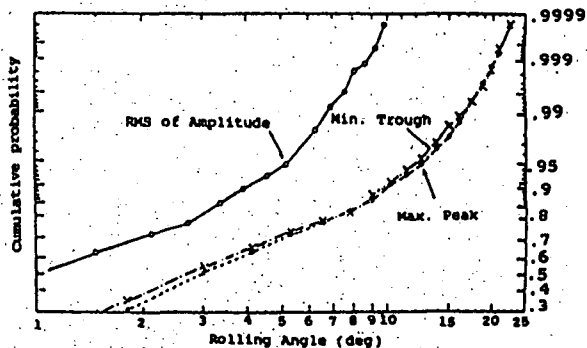
Fig.1 Cumulative probability of rolling angle

2.2 Roberts et al. Method

Roberts et al. hold [3] that in the most general case for specific ship, long-term the standard deviation of roll, σ_L, is a function of four variables - i.e. H, T_O, X and V, as

$$\sigma_L = f(H, T_o, X, V) \qquad (3)$$

and these four variables will be governed by a four-dimensional joint density function $P(H, T_o, X, V)$. If X and V are assumed to be mutually independent, and also independent of h and T_o thus

$$P_L(H, T_o, X, V) = P_L(H, T_o)P_L(X)P_L(V) \qquad (4)$$

Where, $P_L(H, T_o)$ is joint density function for H and T_o, $P_L(X)$ is density function for X, $P_L(V)$ is density function for V.

To evaluate the distribution of σ, a particular case, ship speed V, which is not a random variable. The heading to waves, X, has a known probability distribution, one can then approximate by considering a number, n, of descrete headings, such as X_1, X_2, ..., X_n. The final density function for σ is then obtained by summing over all the headings. Thus

$$P_L(\sigma) = \frac{1}{n} \sum_{i=1}^{n} P(\sigma|X_i)$$

$$(5)$$

It is shown, the cumulative probability distribution of σ, we can regard σ as a joint density function of H and T_o and a simple numerical integration technique has been proposed from Roberts etal which can be used to compute the corresponding probability distribution of σ.

Finally, a long-term probability that the standard deviation, σ, will exceed a specified value, σ_1, we can be found by

$$P_L(\sigma > \sigma_1) = \frac{1}{n} \sum_{i=1}^{n} \exp\left(- (\frac{\sigma}{\alpha_i})^{c_1}\right) \cdot P_i(H, T_o)$$

$$(6)$$

Where, σ is standard deviation for a specific loading, a specific ship speed, a specific heading to wave and wave spectrum value of a specific H and T_o. C_i and α_i are a specific Weibull parameter that the simplest case could be constant values of equation (6).

2.3 Nordenströn Method

A simple and convenient approximately calculation have been given by Nordenströn [4].

When long-term probability distribution of wave height and wave period are not too exactly known, we can be according to Nordenström idea for ship wave induced bending moment, assumption the ratio of significant roll amplitude (double)

to significant wave height is constant, d, in a specific apparent wave period zone. i.e

$$d = \sqrt{8 \ R_\phi}/H$$

$$(7)$$

Where, d is function for mean apparent wave period, $\overline{T}_o$, which can be found by ship mode test, ship full scale test or analytical calculation methods. R_ϕ is value mean square of ship roll amplitude, H is significant wave height. And assumption a specific shipping route expected maximum value of $\overline{T}_o$, as shown in Fig. 2, have also been known.
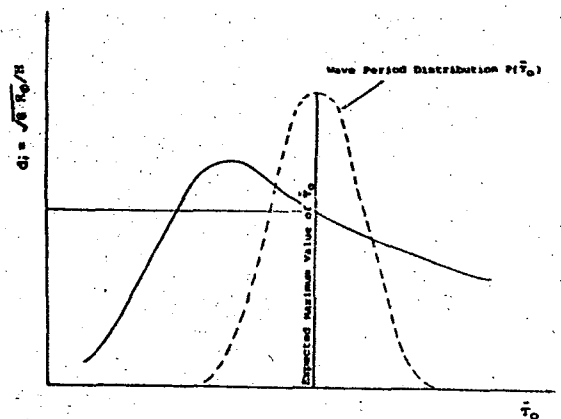
Fig.2   Distribution of di Function

Based on the assumption wave amplitude long-term probability which is Weibull distribution for all $\overline{T}_o$ value, the ship roll amplitude long-term probability distribution can be given by

$$P_L(\phi_a) = 1 - \exp\left(- (\frac{\phi_a}{\alpha d \sqrt{b}})^c\right)$$

$$(8)$$

where, α, b and c are Weibull parameter, d is ratio value which can be given by equation (7).

Finally, long-term probability that ship roll amplitude, ϕ_a, will exceed a specific value, ϕ_{a1}, one can be found by

$$P_L(\phi_a > \phi_{a1}) = \sum_{i=1}^{n} P_i(\overline{T}_o) \cdot \exp\left(- (\frac{\phi_a}{\alpha_i d_i \sqrt{b_i}})^c\right)$$

$$(9)$$

Where, $P_i(\overline{T}_o)$ is ship encounter wave period probability for i set, α_i, b_i and c_i are ship roll amplitude Weibull distribution parameter for i set of wave period, d_i is ratio of ship significant roll amplitude to significant for i set of wave period.

We can be rapidly and convenient estimated ship roll amplitude long-term excess probability from equation (9), which is only wanted wave period long-term probability distribution on ship shipping route.

2.4 Wave Height Replacement Method

In Fig. 3, cumulative probability of observed wave height have been illustrated during Takahashi full-scale measurements. The results shows that RMS of roll amplitude is very nearly with observed wave height but have need to exchange metre of wave height unit for degree of roll amplitude unit, or opposed exchange them.
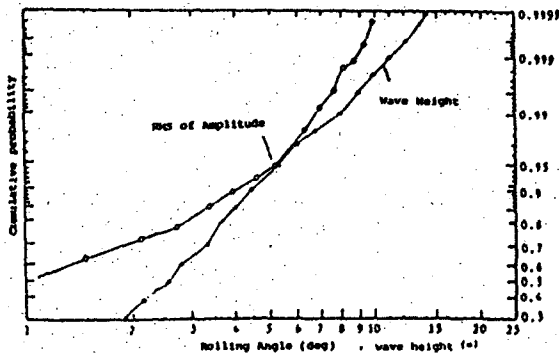

Fig.3 Cumulative probability of rolling angle and observed wave height

Fig. 3 shows simple and convenient estimates of RMS roll amplitude for long-term cumulative probability from a ship on a shipping route with observed wave height (or significant wave height). Then we can obtain significant roll amplitude of long-term probability and the expected extreme of long-term roll amplitude.

2.5 Various Method Comparisons

In order to compare the above various methods for estimation ship roll amplitude long-term probability distribution characteristic, the results of long-term probability of four methods have been shown in Fig. 4.

The Fig. 4 shows, (1) roll amplitude long-term probability distribution is close to that Weibull distribution.

(2) Roll amplitude long-term probability is as good as 2-parameter Weibull distribution, that is, the Rayleigh type. Therefore, so long as parameter is selected good for various conditions that Rayleigh distribution is suitable to predict roll amplitude long-term

probability.

(3) All above methods for estimated roll amplitude long-term cumulative probability is not too largely different, except Roberts etal method, which mainly has large differences in wave parameters between Roberts' calculation and Takahashi full-scale measurements on ship shipping route.
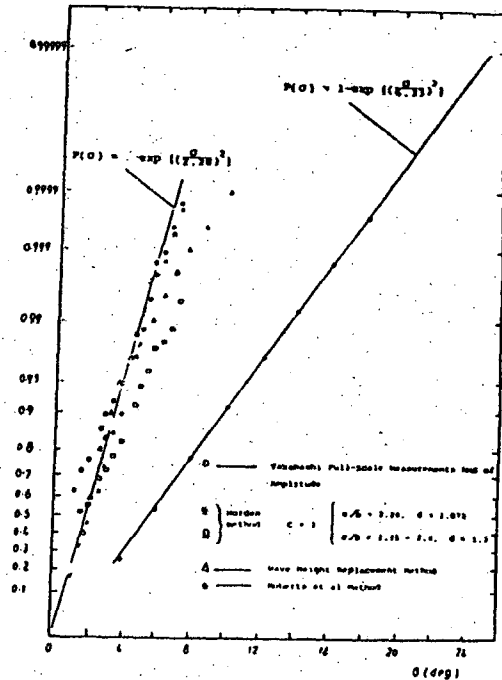
Fig.4 Long-term probability distribution for σ

2.6 Expected Maximum Peak Value

For evaluating the long-term expected maximum peak value probability distribution, one can evaluate expected maximum peak value frequency of occurrence of each short-term for various sea state, ship speed, loading and heading to wave etc.. By means of exactly the same way as in the treatment of σ or RMS, one could determine the distribution of expected maximum peak value, $E(A_{max})$.

Based on Takahashi full-scale measurements data, one can derive the relationship between the long-term distribution of $E(A_{max})$ and long-term distribution of σ or RMS.

From as shown in Fig. 1 curves, the probability density function of $E(A_{max})$ can be given by

$$P(E(A_{max})) = \frac{\lambda}{K_R} P(R_\phi) = \frac{\lambda}{K_\sigma} P(\sigma)$$

(10)

where, $P(R_\phi)$ and $P(\sigma)$ represent probability, distribution of RMS of roll amplitude and σ of roll respectively.

On the assumption that roll amplitude probability distribution accord with Rayleigh type, thus coefficient K_R and K_σ can be respectively by

$$K_R = 1.58 - 0.05 \ R_\phi \qquad (11)$$

$$K_\sigma = 1.58 - 0.071 \ \sigma \qquad (12)$$

Where R_ϕ is the RMS of roll amplitude, σ is the standard deviation of roll.

The coefficient K usually is a function of σ roll or RMS of roll amplitude.

$$N = \sum_{W}\sum_{H}\sum_{T_0} \sum_{V}\sum_{X} n \cdot P(X, \ V|H, \ T_0, \ W) \cdot P(T_0|H) \cdot P(H) \cdot P(W) \cdot T \cdot (60)^2 \qquad (13)$$

Where, T is total exposure time of a ship in seas in her lifetime (in hours). The other symbols are meaning same as equation (1) and (2).

Roberts etal has also been given [3] as

Return period $N = \dfrac{1}{P(\sigma > \sigma_1)}$

$$\qquad (14)$$

Where N is measured in number of sea states, $P(\sigma > \sigma_1)$ is probability that the σ will exceed a specified value, σ_1.

3. **Analytical Approach To Non-linear Ship Rolling**

In order to evaluate long-term roll amplitude according to previous section have to know specified condition short-term standard deviation of roll.

In random seas many ships have a natural roll frequency of similar magnitude to the frequencies at which wave energy is dominant.

2.7 Estimation Of The Extreme Value Of Roll

The probabilistic extreme value of roll is defined as the largest value of the maxima (amplitude or peak-to-trough excursions) which will occur in a specified number of observations or in a specified period of time.

For this reason, the total number of roll, N, experienced by a ship in her lifetime has been proposed by Ochi [1][5] which are arbitrarily in the long-term prediction methods developed to date. Ochi holds that they can be evaluated from the numerator of equation (1) as follows:

Moreover, the hydrodynamic damping associated with rolling moiton is usually relatively small. It is possible for a ship, when operating in a random sea state, to exhibit severe roll motion which nature to behave non-linear. Several analytical methods [6,7,8,9,10,11,12,13,14,15,16 17], have received some attention and is found corresponding results in the field of ship rolling motion.

3.1 Equivalent Linearisation Techniques

The use of this method reduces the problem to a linear one by replacing the non-linearity by a suitable linear term. For example, Vassilapoulos method [6] is given as follows:

For the case in which both non-linear damping and restoration are present, one solve the resulting second-degree algebraic equation in σ_ϕ. The result for the positive square root of that equation can be shown to be:

$$\sigma_{\phi_N} = \frac{-\sqrt{(2/\pi)}\beta\omega_\phi\sigma_{\phi_L}^2 + \sqrt{[(2\beta^2\omega_\phi^2/\pi + 3\gamma]\sigma_{\phi_L}^4 + \sigma_{\phi_L}^2}}{(1 + 3\gamma \ \sigma_{\phi_L}^2)}$$

$$\qquad (15)$$

Where,

σ_{ϕ_N} is the standard deviations for the non-linear roll

σ_{ϕ_L} is the standard deviations for the linear roll

β is the ratio of non-linear and linear damping coefficient

γ is the ratio of non-linear and linear restoring moment

ω_ϕ is the roll undamping natural frequency

Equation (15) permit the estimation of non-linear roll statistics given the values of linear roll variance, $\sigma_{\phi_L}^2$, and those of the mixture ratios β and γ, together with the undamped natural roll frequency ω_ϕ.

3.2 Perturbation Methods

Here the solution is expressed in a series expansion in powers of a small parameter, usually related to the magnitude of the non-linearity. This reduces the problem to the solution of several linear problems. The method is expected to yield a good approximation when the non-linearity is small.

Yamanouchi investigated the effect of quadratic damping on the roll spectrum on the basis of a perturbation method [9]. One can be given as follows:

Accordingly the roll spectrum $S_{\phi_1\phi_1}(\omega)$ of the 1st approximation, $\phi_1(t)$, it were calculated by this author, is taken as

$$S_{\phi_1\phi_1}(\omega) = S_{\phi_0\phi_0}(\omega) - 2\sqrt{\frac{2}{\pi}}\,\sigma_{\dot{\phi}_0}\,\beta\,S_{\phi_0\phi_0}(\omega)\,\omega\,q_g(\omega)$$

$$+\ \beta^2|H_g(\omega)|^2\{\frac{8}{\pi}\sigma_{\dot{\phi}_0}^2\,\omega^2\,S_{\phi_0\phi_0}(\omega) + \frac{4}{3\pi\sigma_{\dot{\phi}_0}^2}\,S(\omega)\}$$

$$(16)$$

Where, $S_{\phi_0\phi_0}(\omega)$ is the linear rolling spectrum,

$$S_{\phi_0\phi_0}(\omega) = |H(\omega)|^2\,S_{\zeta\zeta}(\omega)$$

$$= \left(H_0(\omega)\,I\,\frac{\omega^2}{g}\,\omega_\phi^2\,\gamma(\omega)\right)^2\cdot S_{\zeta\zeta}(\omega)$$

$$= \left(H_g(\omega)\,\frac{\omega^2}{g}\,\omega_\phi^2\,\gamma(\omega)\right)^2\cdot S_{\zeta\zeta}(\omega)$$

$$(17)$$

$$q_g(\omega) = \Phi_m(H_g(\omega))\,\frac{2\alpha\omega}{(\omega_\phi^2 - \omega^2)^2 + 4\alpha^2\omega^2}$$

$$(18)$$

$$H_g(\omega) = \frac{1}{-\omega^2 + \omega_\phi^2 + 2j\alpha\omega} = I\cdot H_0(\omega)$$

$$(19)$$

$$S(\omega) = \int_{-\infty}^{\infty}\int_{-\infty}^{\infty} S_{\dot{\phi}_0\dot{\phi}_0}(\omega_1)\cdot S_{\dot{\phi}_0\dot{\phi}_0}(\omega_2)\cdot S_{\dot{\phi}_0\dot{\phi}_0}(\omega-\omega_1-\omega_2)d\omega_1d\omega_2 \qquad (20)$$

and $S_{\zeta\zeta}(\omega)$ and $S_{\dot{\phi}_0\dot{\phi}_0}(\omega)$ are wave and linear rolling velocity spectral density respectively.

Thus, one can be calculated non-linear rolling variance from integrating equation while ship linear roll characteristics and non-linear rolling damping have been given.

The random response of roll with non-linear restoring function or non-linear damping have also been obtained by Crandall applying the classical perturbation method [11].

If the wave is a stationary random process with known statistical properties, the non-linear restoring function $g(\phi) = \phi^3$. We consider only the first-order perturbation, and take the case of Gaussian white excitation, the simple form for the approximate mean square value, σ_{ϕ_N}, of the non-linear roll can be given by

$$\sigma_{\phi_N}^2 = \sigma_{\phi_L}^2 - 3\,\epsilon\,\sigma_{\phi_L}^4$$

$$(21)$$

Where,

$\sigma_{\phi_L}^2$ is mean square value of the linear roll,

ϵ is the parameter for the non-linear restoring function.

For the ship with small, but non-linear, roll damping, is given

$$\sigma_{\phi_N}^2 = \sigma_{\phi_L}^2 - 3\alpha\omega_\phi^2\,\sigma_{\phi_L}^4$$

$$(22)$$

for the first order perturbation approximation to the mean square of roll with non-linear roll damping. Where α is damping coefficient of non-linear roll.

3.3 Fokker-planck Equation Methods

Robest [12] demonstrated that a suitable theory could be constructed provided that the roll motion can be modelled as a single degree of freedom equation. It was shown, by combining Markov process theory with an averaging technique, that the energy envelope of the roll motion could be approximated as a one-dimensional markov process, governed by an appropriate Fokker-Planck equation. The

stationary solution of this equation yields the probability density function of the roll amplitude. An advantage of this approach is that the non-linear components of the damping and restoring moment terms, in the equation of motion, need not be small and can be of arbitrary form.

The standard deviation, σ, of roll response, $\phi(t)$, is given by

$$\sigma^2 = \int_0^\infty p(V) \, D_2(V) dV \qquad (23)$$

Where

$$D_2(V) = \frac{\sqrt{2}}{T(V)} \int_{-\infty}^\infty \frac{\phi^2 d\phi}{[V - U(\phi)]^{1/2}} \qquad (24)$$

$$V = \frac{\dot\phi^2}{2} + U(\phi) \qquad (25)$$

Where $\dot\phi^2/2$ is the kinetic energy and

$$U(\phi) = \int_0^\phi G(\xi) d\xi \qquad (26)$$

is the potential energy.

The stationary density function can be given by

$$p(V) = \frac{C}{D(V)} \exp\left(2 \int_0^V \frac{m(\xi)}{D(\xi)} d\xi \right) \qquad (27)$$

Where C is a normalisation constant such that:

$$\int_0^\infty p(V) \, dV = 1 \qquad (28)$$

It is evident that, one can calculate the variance of non-linear roll based on equation (23). But a modified theory has also been applied by Roberts. The idea is to replace $S_\chi(\omega)$ in drift and diffusion coefficients by a modified spectrum:

$$S'_\chi(\omega) = \gamma[Q(V)] \, S_\chi(\omega) \qquad (29)$$

Where $\gamma[Q(V)]$ will depend on the damping function $Q(V)$ and the shape of the input spectrum. $Q(V)$ can be regarded as an amplitude dependent damping factor.

If restoring moment is linearity and is considered only non-linear damping of roll, one can be used to correct the spectral level, at each value of V by equation (29).

4. <u>Estimation Of Wave Long-term Probability Distribution</u>

As previous mentioned on long-term roll prediction, one of it should be known the ship seaway shipping route long-term wave characteristics.

The various sea zones or shipping route wave data can be estimated by long-term statistic results which are given as follows:

4.1 Hogben – Lumb And Walden Wave Observed Values

Hogben – Lumb [18] according to altogether about, 1 million sets of observations made in years 1953-1961 have been used to produce the wave data tables. Sea areas in great detail most of the shipping routes of the world for which tables are presented have been arranged into 50 groups, but the North Pacific are not covered.

Walden [19] based on nine weather ships in the North Atlantic Sea zones have also been given the wave height and period observed values. The whole year wave frequency have been tabulated in Table 1.

4.2 North Sea Around And Off Northern Norway Wave Probability

Fang and Hogben [20] based on North Sea around observed data have been developed a joint probability of wave height and period and the corresponding regression. In fact, for another shipping route can also been calculated by Fang – Hogben equation when wave height data is known.

The wave climate off Northern Norway have been measured and investigated by Haver [21] at the Tromsoflaket area in the years 1977-1981, while the hindcast values cover the years 1955-1981. The long-term variation in the wave climate is given by the joint probability distribution of the significant wave height and the spectral peak period. Haver holds that the reason for choosing the spectral peak period instead of other characteristic periods is that this period is less correlated to the significant wave height than the other periods.

4.3 North Pacific Ocean Wave Probability

Yamanouchi [22] based on about four hundred thousand sets of observed wave values for the

Table 1 Wave Frequency in the North Atlantic (According to Walden's Data)

| | | Wave Period (sec) | | | | | | | Sum over All Periods |
		5	7	9	11	13	15	17	
	0.75	20.91	11.79	4.57	2.24	0.47	0.06	0.00	0.60	40.64
	1.75	72.78	133.06	63.00	17.26	2.39	0.33	0.11	0.77	387.00
	2.75	21.24	126.41	118.31	30.24	3.68	0.47	0.09	0.56	301.00
	3.75	3.28	49.60	92.69	32.99	5.46	0.68	0.12	0.27	185.09
	4.75	0.53	16.19	44.36	22.28	4.79	1.14	0.08	0.29	89.66
Wave Height (m)	5.75	0.12	4.34	17.30	12.69	3.13	0.56	0.13	0.04	38.51
	6.75	0.07	2.90	9.90	8.86	3.03	0.59	0.08	0.03	25.46
	7.75	0.03	1.39	4.47	5.22	1.93	0.38	0.04	0.04	13.50
	8.75	0.00	1.09	2.55	3.93	1.98	0.50	0.03	0.02	10.09
	9.75	0.00	0.54	1.36	2.36	1.54	0.68	0.20	0.04	6.62
	10.75	0.01	0.01	0.10	0.11	0.10	0.05	0.02	0.00	0.40
	11.75	0.00	0.00	0.03	0.08	0.17	0.06		0.00	0.34
	12.75		0.05	0.00	0.14	0.22	0.06	0.01		0.48
	13.75		0.02		0.07	0.09	0.03		0.01	0.22
	14.75				0.02	0.06	0.02	0.00	0.01	0.11
	15.75	0.00	0.02	0.00	0.01	0.01	0.02	0.01	0.01	0.08
Sum over All Heights		118.97	345.43	358.72	138.59	29.05	5.63	0.92	2.69	1000.00

Whole Year (for All Nine Weather Ships)   (227,497 Obs.)

North Pacific Ocean by Japanese ships in ten years were compiled marine meteorological tables.

The 163th Research Committee of the Japan Ship Research Association [23] observation North Pacific Ocean which is same observed sea zone as Yamanouchi, about two million sets of wave values in ten years by Japanese ships, have also been given the wave frequency in the North Pacific. The annual results is as shown in Table 2.

Fig. 5 shows that the cumulative distribution function of wave height from Yamanouchi and SR163, all period.

Table 2 Wave frequency in the North Pacific (30° N-55° N, 110° E-110° W) (Data from SR 163) Annual

| Wave Height (m) | Wave Period (sec) | | | | | | Sum over All Period |
	0 - 5	5 - 7	7 - 9	9 - 11	11 - 13	13 -	
0.75	7.367	0.734	0.315	0.210	0.015	0.013	8.654
1.75	22.043	9.886	4.135	0.985	0.639	0.232	37.920
2.75	8.347	9.507	7.108	2.190	0.832	0.432	28.416
3.75	2.531	4.639	4.475	1.714	0.941	0.359	14.659
4.75	0.626	1.494	2.324	0.874	0.579	0.281	6.178
5.75	0.091	0.365	0.760	0.332	0.252	0.073	1.878
6.75	0.031	0.142	0.317	0.199	0.187	0.096	0.972
7.75	0.021	0.218	0.188	0.116	0.113	0.058	0.724
8.75	0.012	0.035	0.065	0.048	0.064	0.036	0.260
9.75	0.007	0.021	0.038	0.030	0.039	0.034	0.169
10.75	0.002	0.011	0.035	0.016	0.027	0.017	0.108
11.75		0.001	0.003	0.003	0.003	0.003	0.013
12.75		0.002	0.004	0.012	0.004	0.005	0.027
13.75		0.001	0.001	0.001	0.001	0.001	0.005
14.75		0.001	0.001	0.001	0.001	0.001	0.005
14.75 <		0.001	0.002	0.002	0.004	0.003	0.012
Sum over All Height	41.073	27.053	19.771	6.733	3.791	1.659	100.000
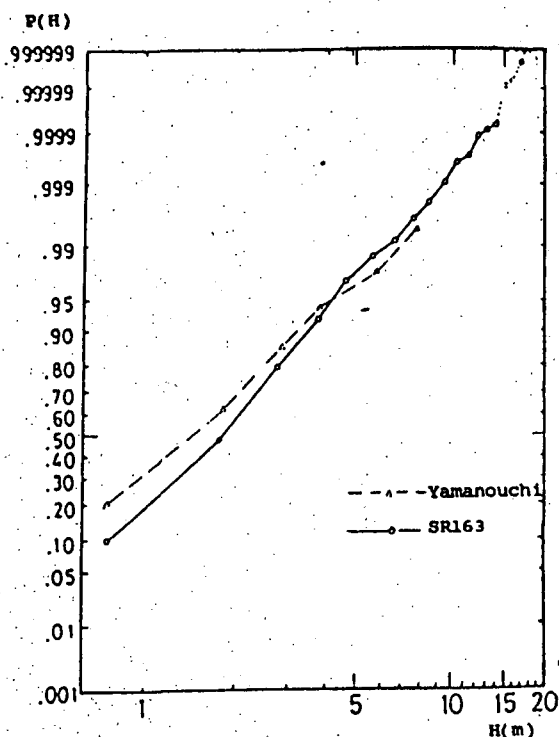
Fig.5 Cumulative distribution function of wave
height in the North pacific plotted on
long-normal probability paper.

Mano and Kawabe [24][25] studied on the
statistical characters of wave statistics in the
North Pacific Ocean which is showed that the
frequency distribution of both wave height and

period can be described by the log-normal
distribution. The long-term joint probability
of wave height and period formula, the
probability density of wave period equation and
the probability density of wave height for
condition period equation have been given
respectively in those papers.

4.4 The Family Of Wave Spectra

Ochi [26] is proposed the design extreme
value based on the long-term prediction approach
using a family of wave spectra in each sea
severity.

Therefore, the six-parameter spectra have
been developed by Ochi [27]. The wave spectra
are decomposed into two parts - one which
includes primarily the lower frequency
components of the wave energy and the second
which covers primarily the higher frequency
components of the energy. The entire spectrum
is expressed by a combination of two sets of
three-parameter spectrum. These parameters are
significant wave height, modal period and shape
parameter.

By combining two sets of three-parameter
spectra, one representing the low frequency
components and the other the high frequency
components of the wave energy, the following
six-parameter spectral representation can be
derived:

$$S(\omega) = \frac{1}{4} \sum_j \frac{(\frac{4\lambda_j + 1}{4} \omega_{mj})^{\lambda_j}}{\Gamma(\lambda_j)} \frac{H_j^2}{\omega^{4\lambda_j + 1}} \exp - (\frac{4\lambda_j + 1}{4})(\frac{\omega_{mj}}{\omega})^4 \qquad (30)$$

Where, j = 1,2 stands for the lower and
higher frequency components, respectively. H is
significant wave height, ω_m is modal frequency
and λ is spectrum shape parameter.

The parameters for six-parameter spectral
families are tabulated in Table 3 so that a
family of spectra for a desired sea can be
generated from equation (30).

5. ASSESSMENT OF SHIP ROLL PERFORMANCE

So far, the rules for stability of sea-going
ships in Japan, USSR, P.R. China and other a
number of shipping register, while with respect
to the stability criterion, it is necessary to
prolong symmetrically the curve of dynamical (or
statical) stability towards the negative
direction of the roll angle, φ. Then can be
concerned through this roll angle that is given

minimum capsizing lever (or moment). The problem
is in calculation present roll angle, though
some irregular wave characteristics have been
concerned, but it is based on the short-term
predicted roll angle which without respect to
the possible maximum roll angle in ship's
lifetime.

We hold that the reasonable way ought to
consider the possible ship loading, ship speed,
sea state of encounter and heading to waves in
the lifetime of the ship, i.e. for the stability
criterion in the rules for stability of
sea-going ships is to be given long-term roll
angle.

Assessment of ship general roll performance
and anti-rolling effectiveness for various
anti-rolling devices, it also is given based on
short-term predicted roll angle for special ship
conditions and specific sea state so far. It is

Table 3   Values of six-parameters (m-units)

	H_1	H_2	ω_{m1}	ω_{m2}	λ_1	λ_2
Most Probable Spectrum	$0.84\ H$	$0.54\ H$	$0.70\ e^{-0.046}\ H$	$1.15\ e^{-0.039}\ H$	3.00	$1.94\ e^{-0.062}\ H$
95% Confidence Spectra	$0.95\ H$	$0.31\ H$	$0.70\ e^{-0.046}\ H$	$1.50\ e^{-0.046}\ H$	1.35	$2.48\ e^{-0.102}\ H$
	$0.65\ H$	$0.76\ H$	$0.61\ e^{-0.039}\ H$	$0.94\ e^{-0.036}\ H$	4.95	$2.48\ e^{-0.102}\ H$
	$0.84\ H$	$0.54\ H$	$0.93\ e^{-0.056}\ H$	$1.50\ e^{-0.046}\ H$	3.00	$2.77\ e^{-0.112}\ H$
	$0.84\ H$	$0.54\ H$	$0.41\ e^{-0.016}\ H$	$0.88\ e^{-0.026}\ H$	2.55	$1.82\ e^{-0.089}\ H$
	$0.90\ H$	$0.44\ H$	$0.81\ e^{-0.052}\ H$	$1.60\ e^{-0.033}\ H$	1.80	$2.95\ e^{-0.105}\ H$
	$0.77\ H$	$0.64\ H$	$0.54\ e^{-0.039}\ H$	$0.61\ H$	4.50	$1.95\ e^{-0.082}\ H$
	$0.73\ H$	$0.68\ H$	$0.70\ e^{-0.046}\ H$	$0.99\ e^{-0.039}\ H$	6.40	$1.78\ e^{-0.069}\ H$
	$0.92\ H$	$0.39\ H$	$0.70\ e^{-0.046}\ H$	$1.37\ e^{-0.039}\ H$	0.70	$1.78\ e^{-0.069}\ H$
	$0.84\ H$	$0.54\ H$	$0.74\ e^{-0.052}\ H$	$1.30\ e^{-0.039}\ H$	2.65	$3.90\ e^{-0.085}\ H$
	$0.84\ H$	$0.54\ H$	$0.62\ e^{-0.039}\ H$	$1.03\ e^{-0.030}\ H$	2.60	$0.53\ e^{-0.069}\ H$

H = significant wave height in meters

evident that should be lead to not correct conclusion. For example, Morenshildt [28] and Williams [29] full-scale ships tests for with various passive anti-rolling tank shows that the anti-rolling effectiveness is very different for the same identical anti-rolling tank in differential ship speed, sea state of encounter and heading to wave.

Therefore, 14th ITTC Seakeeping Committee recommends a standard measure for the effectiveness of passive roll stabiliser tanks should be developed, standard methods of predicting roll in irregular waves also be established.

The reasonable way for comparison ship roll performance and anti-rolling effectiveness of various type stabilisation system is to be taken the long-term ship roll angle and long-term anti-rolling effectiveness.

5.1   Evaluation Of Ship Roll Angle In Rules For Stability Of Sea-going Ships

In case the ship principal parameters and conditions have been known, the standard deviation of roll for various ship situation, wave parameter, heading to wave and ship speed etc. can be calculated by means of non-linear method which is given in Section 3. Based on wave data of ship shipping route which is given in Section 4. Thus, the long-term excess probability distribution of the standard deviation of roll or mean square value of ship roll amplitude can be given by means of any method in Section 2 and to integrate it.

The long-term excess probability distribution of the expected maximum peak value

by means of the method which is given in Section 2.6, and to integrate it can also been given.

In Fig. 6, the typical long-term excess probability distribution (or return period) of significant roll amplitude and expected maximum peak value have been given which is calculated from Fig. 1 Takahashi's full-scale measured data.
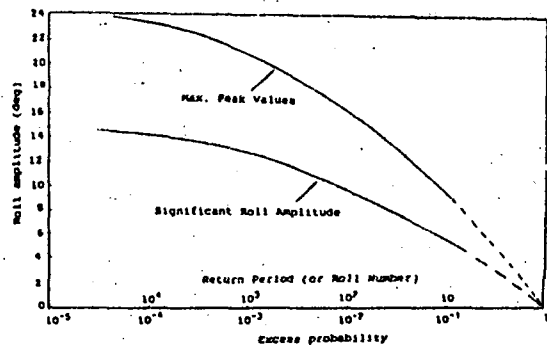

Fig.6   Long-term probability distribution for roll amplitude

One can be taken a specific excess probability or return period for the long-term probability distribution of the standard deviation, σ, or mean square root of roll amplitude, R, thus the corresponding σ or R can be given. The probability that standard deviation, σ, of roll will exceed a specified value, σ_1, can be calculated from equation (14).

Based on different excess probability level, σ_1, one can be given corresponding σ from the long-term probability distribution of the standard deviation. Thus one can be found other

mean maximum amplitude of roll according to Rayleigh distribution law. For example, the excess probability level is 0.5% mean maximum amplitude of roll which can be applyed to the requirements of roll angle in the rules for stability of sea-going ships.

Supposing one applies the expected maximum peak of roll for long-term excess probability distribution, for example the excess probability level which can be taken 0.5%. Thus the critical level for ship experienced roll number (or return period) in her lifetime can be given by means of equation (13) or equation (14) and to calculate extreme value which can be applied to the requirements of the roll angle in the rules for stability of sea-going ships.

In fact, the total number of roll (or return period), N, experienced by a ship in her lifetime usually lies between 10^4 and 10^6.

5.2 Assessment Of Roll Performation And Anti-rolling System Effectiveness

The ship roll performation can be calculated by means of long-term probability distribution for the standard deviation of roll, σ, or mean square root of roll amplitude, R, and significant roll amplitude $\phi_{1/3}$. If a specific excess probability, σ_1, or the total roll number, N, have been known, thus the corresponding σ, R or $\phi_{1/3}$ can be given from their probability distribution respectively, then make a comparison between the σ (R or $\phi_{1/3}$) of different design plan or ship condition.

For ship with anti-rolling system, the calculation for short-term standard deviation, σ, of roll have to consider anti-rolling characteristics, but it don't have to use non-linear method, if there is a good anti-rolling effectiveness.

The typical result is shown in Fig. 7. Where $(\phi_{1/3})A_1$, $(\phi_{1/3})B_1$ and $(\phi_{1/3})A_2$, $(\phi_{1/3})B_2$ are significant roll amplitude for Ship A and Ship B corresponding to $N = 10^2$ and $N = 10^4$. The ϕ_{0A} and ϕ_{0B} represents the roll angle extreme value for Ship A and Ship B which is applicable to stability criteria in rules for stability of sea-going ships.

5.3 Progressively Approximate Method For Roll Damping

In the case of the calculation for short-term standard deviation of roll, the selection of roll damping is of great importance to roll response amplitude operator. Because
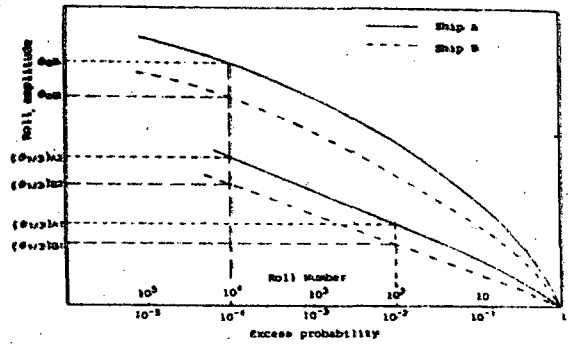

Fig.7 Long-term probability distribution of roll amplitude for Ship A and B

the roll damping is function of roll amplitude. So the calculation for roll damping usually is taken a specific roll damping corresponding to a specific roll amplitude, thus the corresponding roll response amplitude operator can be given from roll decayed curve.

But in case of the ship roll in irregular wave, the roll amplitude is a variable for the same sea state, thus the roll damping also is a variable. it is evident that calculate roll response amplitude operator by the constant roll damping which is not in agreement with the actual situation.

Therefore, we suggest that the roll damping and corresponding roll amplitude can be given by progressively approximate method for ship in irregular wave.

The first approximate. One can be taken the roll damping $N_0 = f(\phi_0)$ corresponding to a specific roll amplitude ϕ_0 which is applicable to calculate roll response amplitude operator. Thus, the standard deviation of roll corresponding to a specific sea state can be given by spectral analysis, and the corresponding significant roll amplitude $(\phi_{1/3})_1$, as shown in Fig. 8.
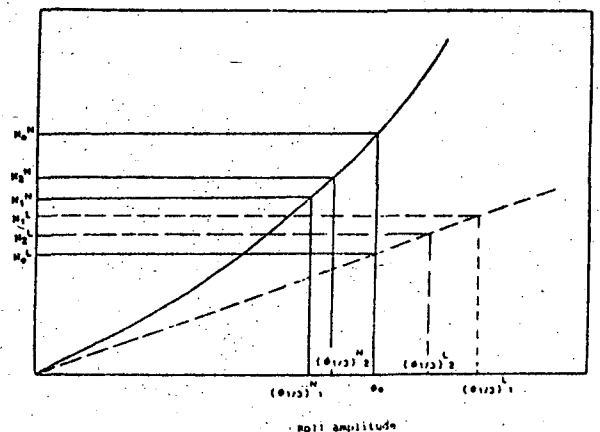

Fig.8 Decline curves for rolling

- 53 -

The second approximate. By means of the first approximate roll damping, $N_1 = f((\phi_{1/3})_1)$, corresponding to significant roll amplitude $(\phi_{1/3})_1$, the roll response amplitude operator and significant roll amplitude, which is in same with present sea state, can be given.

The standard deviation of roll corresponding to roll damping $N_2 = f((\phi_{1/3})_2)$ can be given by means of the step by step calculation. Usually, it will be sufficed trough three times calculation.

We also suggest that the roll damping corresponding to significant roll amplitude can be calculated by progressively approximate method for the roll response amplitude.

We make a comparison between roll response amplitude operator with non-linear and one with linear which ought to calculate based on non-linear damping $N_2^N = f((\phi_{1/3})_2^N)$ and linear damping $N_2^L = f((\phi_{1/3})_2^L)$ respectively. It is evident that assessment the roll damping effect on roll ought not to use $N_0^N = f(\phi_0)$ and $N_0^L = f(\phi_0)$.

REFERENCES

1. Ochi, M.K. & Chang, M.S., "Note on the Statistical Long-term Response Prediction". International Shipbuilding Progress, Vol. 25, Oct. 1978, No.290, pp. 270-271.

2. Takohoshi, Y., "Full Scale Measurements of a Container Ship". The 2nd Internl. Sympo. on Practical Design in Shipbuilding, 1983, Tokyo & Seoul, Proceeding, pp. 517-524 or J. of Soc. Nav. Arch. of Japan, Vol. 150, Dec. 1981, pp. 327-332 and Vol. 152, Jan. 1983, pp. 268-274.

3. Roberts J.B., Dacunha N.M.C. and Hogben., "The Estimation of the Long Term Roll Response of a Ship at Sea". NMI Report No. 169, Dec. 1983.

4. Nordenström, N., "Methods for Predicting Long Term Distributions of Wave Loads and Probability of Failure for Ship". Det Norske Veritas, Res. & Dev. Rep. 71-2-S, 1971.

5. Ochi, M.K., "Probabilistic Extreme Values and their Implication for Offshore Structure Design". Proc. 10th Offshore Techn. Conference, OTC 3161, 1978. pp. 987-989.

6. Vassilopoulos, L., "Ship Rolling at Zero Speed in Random Beam Seas with Non-linear Damping and Restoration". Journal of Ship research, Dec. 1971. pp. 289-294.

7. Yamanouchi, Y., "Some Remarks on the Statistical Estimation of Response Function of a Ship". Proceedings, Fifth Symposium on Naval Hydrodynamics, Bergen, Norway, 1964. p.97.

8. Caughey, T.K., "Equivalent Linearisation Techniques". Journal of the Acoustical Society of America, Vol.35, No 11, Nov. 1963, p. 1706.

9. Yamanouchi, Y., "On the Effect of Non-linearity of Response on Calculation of the Spectrum". Proceedings, 11th ITTC, Tokyo, Japan, 1966, pp.3897-390.

10. Flower, J.O., "A Perturbational Approach to Non-linear Rolling in a Stochastic Sea". ISP Vol. 23, 1976, pp. 209-212.

11. Crandall. S.H., "Perturbation Techniques for Random Vibrations of Non-linear Systems". Journal of the Acoustical Society of America, Vol. 35, No.11, 1963, pp. 1700-1705.

12. Roberts, J.B., "A Stochastic Theory for Non-linear Ship Rolling in Irregular Seas". JSR Vol. 26, No.4, Dec. 1982, pp. 229-245.

13. Haddara, M.R., "A Modified Approach for the Application of Fokker-Planck Equation to Non-linear Ship Motion in Random Waves". ISP Vol. 21, No. 242, 1974, pp. 283-288.

14. Caughey, T.K., "Derivation and Application of the Fokker-Planck Equation to Discrete Non-linear Dynamic Systems Subjected to White Random Excitation", Journal of the Acoustical Society of America, Vol. 35, No. 11, 1963, pp. 1683-1692.

15. Haddara, M.R., "A Note on the Power Spectrum of Non-linear Rolling Motion". ISP Vol. 30, No. 342, 1983, pp. 41-44.

16. Vassilopoulos, L., "The Application of Statistical Theory of Non-linear Systems to Ship Motion Performance in Random Seas". ISP Vol. 114, No. 150, Feb. 1967, pp. 54-65.

17. Hasselman, K., "On Non-linear Ship Motion in Irregular Waves". JSR Vol. 10, No. 1, March 1966, pp. 64-68.

18. Hogben, N. & Lumb, F.E.: <<Ocean Wave Statistics>>. National Physical Laboratory, H.M. Stationery Office, London, 1967.

19. Walden, H.: "Die Eigenschaften der Meerswellen in Nordatlantischen Ozean". Deulscher Wetterdienst, Seewetterant, Einzervoeroffentlichungen Nr. 41, Hamburg (1964).

20. Fang, Z.S. & Hogben.: "Analysis and Prediction of Long Term Probability Distributions of Wave Heights and Periods". NMI R146, Oct. 1982.

21. Haver, S.: "Wave Climate off Northern Norway". Applied Ocean Research, 1985, Vol. 7 No. 2.

22. Yamanouchi, Y. & Ogawa, A.: "Statistical Diagrams on the Winds and Wave on the North Pacific Ocean " Papers of Ship Research Institute, No. 2, 1970, Japan.

23. SR163: <<Wind and Waves of the North Pacific Ocean, 1964-1973 - Statistical and Tables", The Japan Ship research Association, 1980.

24. Mano, H. & Kawabe, H.: "The Severity of Supposed Wave Conditions in Estimating Extreme Values of Wave Induced Response Variables of a Ship (fourth report) - Wave Condition in the North Pacific Ocean - J. of Soc. Nav. Arch. of Japan. Vol. 147 June 1980.

25. Kawabe, H., Mano, H. and Awa, K.: "On the Variety of Wave Conditions Encountered by Ships Sailing in the Same Sea Zone". J. of Soc. Nav. Arch. of Japan, Vol. 152, Dec. 1982.

26. Ochi, M.K.: "Probabilistic Extreme Values and their Implication for Offshore Structure Design". Proc. 10th Offshore Techn. Conference, OTC 3161, 1978.

27. Ochi, M.K. and Hubble, E.N.: "six-parameter Wave Spectra". Proceedings of the 15th Conference on Coastal Engineering, Hawaii, 1976.

28. Morenshildt, V.A.: "An Analysis of the Results of Model and Full-scale tests with Various Types of Stabilizing Tanks". 14th ITTC Proceedings, Vol. 4 OTTAWA, 1975.

29. Williams, I.M.: "Sea trials on the Fisheries Research Vessel "Corella". BSRA, Report NS.363 or Naval Architecture Report No. 93, 1972.

THREE DIMENSIONAL NUMERICAL SIMULATION OF
GREEN WATER ON DECK

J.T. Dillingham, J.M. Falzarano

ABSTRACT

A method is described to model the motion of a ship with water on deck. Previously, the method of Glimm was applied by the first author to solve the problem of water sloshing on the deck of a small fishing vessel in order to study the effect of the deck water on the vessel's stability and motion in waves. Glimm's method is a numerical scheme for solving the hyperbolic equations associated with the shallow water flow and is noted for its ability to handle complicated jump phenomenon efficiently. In this paper continuing work is described which extends Glimm's method from the restrictive two dimensional problem solved previously to the more general three dimensional case. The method has application to the prediction of the effect of deck water on various type of vessels, especially those with large flat deck areas. The results of three dimensional flow simulations are presented for selected cases. In order to make Glimm's method useable for evaluating the safety of small vessels, the deck water simulation has been combined with a ship motion simulation. Limited results are presented along with a description of the program and its suggested application.

1.0 BACKGROUND

The greatest peril to ships at sea is inadequate stability and the possibility of capsizing. Today, most ships which are designed according to national and international stability standards are safe for the most part. However, there are ships, especially the smaller ships, which do capsize. The safety situation for ships has improved since the classical work of Rahola in 1939 [20] yet the methods of analysis have changed little since Moseley [12] (1850).

Typically ship dynamic stability analysis is still based on the assumption that all upsetting moments are applied statically. To account for dynamic effects factors of safety are applied. These correction factors are arrived at by examination of successful ships and ship casualties (i.e. experience). Yet corrections upon corrections are applied so that one quickly loses sight of the physics of the phenomenon which is being modeled.

An alternative approach to evaluate vessel stability is the use of computer simulation to predict vessel motions under various conditions. Unfortunately the majority of computer simulations are based on small amplitude motions of the vessel as well as small amplitude wave theory, and are therefore likely to be in serious error when the motions are large enough to endanger the ship.

Early researchers found the need to use time domain ship motion programs to accurately model non-linear motion leading to capsizing. One of the projects investigated the so-called synchronous rolling phenomena experienced by ships in a following sea. Between 1970 and 1979 the U.S. Coast Guard sponsored an extensive amount of advanced stability research at the University of California, Berkeley under the direction of Prof. J.R. Paulling. Along with numerous experimental results and technical reports this research produced the computer program CAPSIZE. CAPSIZE is a time-domain ship-motion computer program which models the phenomenon of autoparametric excitation. This phenomenon may have caused the loss of at least one general cargo ship (the S.S. Poet) [13].

CAPSIZE is capable of simulating various types of nonlinearities, particularly the nonlinear changes in hydrostatic righting moment which result from large amplitude roll motions and from the change in waterplane shape during the passage of a wave crest. Linear frequency-domain ship motion programs must assume constant coefficients, and consequently cannot account for such phenomenon.

The phenomenon of autoparametric excitation and the computer program used to model it have been mentioned for two reasons. First, the existence of autoparametric excitation reminds Naval Architects of the complexity of modeling the extreme motions leading to ship capsizing. Also, time-domain simulation programs like CAPSIZE are the only methods by which one can hope to accurately model

multiple, complicated non-linear phenomena leading to capsize events.

The development of the program CAPSIZE and the associated research represent the most extensive investigation of its time. Since that time the United Kingdom and Norway have undertaken other extensive research programs into the causes of ship capsizing. The United Kingdom's Board of Trade has sponsored numerous theoretical, applied and experimental investigations for over ten years under the title of SAFESHIP. The SAFESHIP project is described in [21] and by Odabassi [18], including a summary flowchart of the investigation plan and an analysis of the numerous capsizings which prompted the research. The specific casualty that prompted the project is the capsize of the M/T Edith Terkol which apparently met or exceeded all applicable stability regulations. The emphasis of most work has been on the application of classical rigid-body dynamic stability models to ship stability analysis. The Norwegian research was prompted by the capsizing of the M/S Helland-Hansen, which also apparently met all applicable Norwegian and international (IMO; Torremolinos) standards [7]. The Norwegian "Ships in Rough Seas Project" has focused its emphasis on breaking waves and modeling realistic extreme sea conditions leading to capsizing. This work is summarized in [22].

This paper describes ongoing work to improve methods for simulation of green water on the decks of vessels at sea. The motivation for this work began with the desire to explain the numerous capsizings of small fishing vessels (see Storch [25]) and to generally improve the understanding of the stability of those types of vessels. However, it has broader applications since the method described can in principle be used to numerically determine the behavior of water on the deck of any vessel. In some cases water on deck may have a significant effect on safety or operations.

The solution of the water-on-deck problem will by no means completely solve the ship safety problem, since casualites usually happen because of a number of extreme situations which occur simultaneously. Some typical documented capsizing incidents seem to substantiate this claim.

PATTI-B [14] capsized while anchored close to shore. At least three effects are believed to have caused the incident. The PATTI-B was anchored by the stern, limiting its freedom, and anchored in shallow water where waves steepen due to shoaling. A Coast Guard life-boat was standing by when the vessel capsized. The events leading to the capsize were as follows: the vessel took water over the stern, which was momentarily trapped between the bulwalks enclosing the large open after deck; the vessel became poised on a wave, lost stability, down-flooded and capsized. All of these events

occurred in a very short time interval, suggesting that dynamics were important. Furthermore, the PATTI-B met or exceeded all existing criteria including the Coast Guard weather criteria and IMO Torremolinos.

The JOAN-LA-RIE III also capsized because of water on deck and other effects. The JOAN-LA-RIE III was fishing close to a number of other vessels when she was hit by a breaking wave, heeled over, accumulated water into her cockpit, swamped and sank [15]. In general, ships that capsize do so without numerous other vessels looking on. Because of this many vessels that capsize do so without a trace. Two such incidents where the U.S. National Transportation Safety Board (NTSB) believes vessels probably sunk due to water on deck are the sinking of the M/V HOLOHOLO [16] and the F/V AMAZING GRACE [17]. In the AMAZING GRACE incident the NTSB believes that the most reasonable explanation of its loss is that water became trapped on deck due to the stern ramp door and freeing ports being closed. A wave hit the vessel and the vessel capsized.

A final incident where water on deck was a major contributing factor was the loss of the M/S Helland Hansen [7]. The vessel was hit by a breaking wave which momentarily poised the vessel at a 60' heel angle. Water filled the open deck area reducing the vessels stability so that when the vessel was hit by another wave it capsized.

Other documented losses of U.S., U.K., Norwegian and other vessels capsizing due to water on deck are too numerous to mention; yet all seem to involve small vessels with large open decks enclosed by bulwarks. A typical scenario in a capsizing incident involves the occurrence of two or more steep waves in a short period of time. It may be, for example, that the deck water which is present as a result of the first wave reduces the vessel's stability sufficiently that the second wave, may cause a capsize. The time constants for the water leaving the deck, the phasing of the vessel's rolling motion, the motion of the deck water and the sea surface elevation are all important. Since the system is nonlinear, neither a static analysis nor a linear frequency domain analysis can determine this crucial phase information.

The phasing of the motion of the deck water with respect to the ship may be such that it will act as an anti-roll tank, which for moderate motions will actually reduce the amplitude of roll. This was shown by the previous work of Dillingham [9,10]. However, there is strong evidence based on records of actual capsizings that under certain circumstances the reduction of stability caused by the deck water, occuring coincidentally with large overturning moments, may contribute to likelihood of capsize.

Yamakoshi, et. a. [21] have conducted model

experiments to ascertain the effect of shipping of water on the stability and likelihood of capsize of small fishing vessels. Based on their own experiments and the results of other Japanese research groups they conclude that shipping of water on deck plays an important role in the capsizing of fishing vessels.

2.0 PROGRESS IN THE SOLUTION OF THE DECK WATER PROBLEM

Up until a few years ago analytical studies of the effects of deck water were mainly confined to pseudo-static approximations due to the difficulty in accurately simulating the complicated nonlinear behavior of the flow. Because of difficulty and inaccuracy many investigators have opted for costly experiments. Recently Dillingham [9] applied an accurate numerical time domain method for solving the shallow water wave equations which describe the deck water motion.

The so-called Glimm's method provides a means to solve hyperbolic systems of equations approximately by a discretization of the flow region into finite cells. In [10] Glimm's method was developed as a two-dimensional computational tool. By this we mean that the problem is geometrically two-dimensional. Mathematically it is actually one-dimensional since the shallow water approximation reduces the number of independent space variables describing the wave motion to one, namely the transverse coordinate. This simplification is justified when considering only the transverse motions of the vessel (roll, sway and heave).

For fishing vessels which are assymetric for and aft, their motion may not be well predicated by a two-dimensional model. We have, therefore, chosen to expand our simulation to six degrees-of-freedom, although the roll motion is of principle concern.

2.1 Two-Dimensional Problem

The problem of computing the flow of water in a confined area such as on the deck of a boat has not been studied very extensively. For large depths, typical of almost full ballast tanks, the boundary integral technique of Faltinsen [27] is applicable even for large motions of the fluid, since the nonlinear free surface condition is satisfied exactly. However the technique is not suitable for the shallow water case where hydraulic jumps are formed. This specific problem was investigated by Dillingham [10]. In a study of the dynamic stability of fishing vessels he considered the effect of shallow water sloshing back and forth on the aft deck as the vessel rolls.

In [10] only a two-dimensional problem was considered. It was assumed that the vessel was constrained to heave, sway and roll and that the
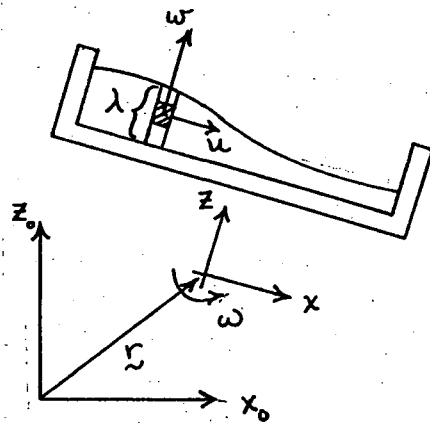

Fig. 1   Two dimensional sloshing
problem definition

predominant flow of the deck water was in the athwart direction. The problem was then formulated as a nonlinear hyperbolic system of equations using the shallow water wave theory. In two dimensions the problem is visualized in Figure 1.

If the deck water is shallow then the following equations result from satisfying the conditions of conservation of mass and momentum, and the kinematic boundary conditions on the bottom (see Stoker [24]):

$$\frac{\partial u}{\partial t} + u\frac{\partial u}{\partial x} + a_z\frac{\partial \lambda}{\partial x} = f_x$$
$$\frac{\partial \lambda}{\partial t} + u\frac{\partial \lambda}{\partial x} + \lambda\frac{\partial u}{\partial x} = 0 \qquad (1)$$

where

u = the horizontal velocity of a water column

a_z = the vertical acceleration of the deck at a point resulting from heave and roll and gravity

λ = the local water depth on deck

f_x = the horizontal (transverse) body force exerted on the fluid by gravity as the deck rolls

t = time variable

The main difficulty associated with finding the solution to such equations is the handling of the hydraulic jumps which inevitably appear. Prior to the appearance of jumps the solution may be computed numerically using the method of characteristics. If the motions of the vessel are small enough the problem can be linearized and solved analytically. Unfortunately smallness in this case means that the motions of the deck in the vertical direction are the vertical direction are small compared to the depth of the deck water. The linear theory is

therefore useless when a part of the deck becomes completely dry.

In [10] a relatively new numerical technique was applied to solve these equations. This method, known either as the random choice method or Glimm's method, was first introduced by Glimm [11] as part of a proof that solutions exist for such systems of equations. It was later developed into a useful numerical tool by Chorin [2,3]. Collela [4] investigated methods for optimizing the accuracy and rate of convergence of the numerical scheme. The details of this method may also be found in Concus and Proskurowski [5], Sod [23], and Wigton [26] and the references cited therein. We mention here only some of the significant features.

Glimm's method proceeds as a time stepping scheme in which the state variables, the depth and the horizontal water velocity in each cell, are determined at each time step on the basis of their values in the previous time step. The attractiveness of Glimm's method lies in the fact that it automatically treats hydraulic jumps of arbitrary number, size and location without requiring any special tracking algorithm. In this respect it is vastly superior to the method of characteristics which breaks down when the characteristic lines converge, corresponding to the formation of a jump. Glimm's method is unconditionally stable and numerical errors can be quantified and reduced to any arbitrarily small size by utilizing smaller cell dimensions and smaller time steps. At each time step the solution is advanced by randomly sampling a series of explicit solutions which describe the interactions between the flows in pairs of adjacent cells. The resulting estimates of depth and velocity, which are random over short time spans converge to the exact solution of (1) as the number of time steps becomes large.

Caglayan [1] performed experiments to test the accuracy of the numerical results. In these experiments he subjected a two-dimensional shallow tank of water to oscillations in roll. The water depth was measured photographically at several points in time and compared with the results of numerical calculations. Typical results are shown in Figure 2. These experiments indicated that the accuracy of the predictions was quite good for short time durations. There was some evidence that over a long time span the numerical solution did not conserve mass precisely. This was not critical in the case of the fishing vessel motion simulation since the amount of deck water varied rapidly due to flow over the bulwarks and through the scuppers. Small variations in mass should not affect the overall behavior.

If we presume that the equations (1) describe the physical processes accurately then we can examine the accuracy of Glimm's method by
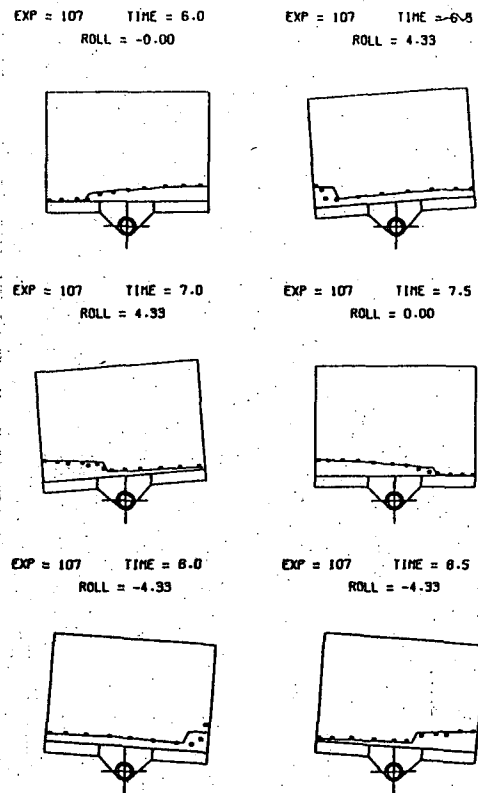

Fig. 2 Comparison between numerical predictions (solid line) and experimental results [1]

comparing the numerical predictions of depth and velocity to an analytical solution of these equations which is known for a specific test case. The test case is the Riemann problem, also known as the dam breaking problem, which is depicted in Figure 3. We assume that the water depth is known on the two sides of a dam. The dam is removed instantaneously at time, t = 0, and a solution describing the resulting flow is sought. The exact analytical solution to this problem may be found in references [8] and [9].

Using Glimm's method the Riemann problem can be solved numerically. Values of depth and velocity are computed at grid points which are equally spaced along the x-axis. Figure 3 shows the values of water depth obtained analytically and numerically for one instant in time. In this test case the water depths are taken to be 4 ft. and 2 ft. on the left and right sides of the dam respectively. The grid spacing in the horizontal direction is one foot. The numerical results are quite accurate in spite of the apparently coarse mesh. The time step was taken to be .01 seconds.

3.2 Three-Dimensional Problem

In three dimensions the shallow water equations

TWO DIMENSIONAL RIEMAN PROBLEM
NO VISCOSITY
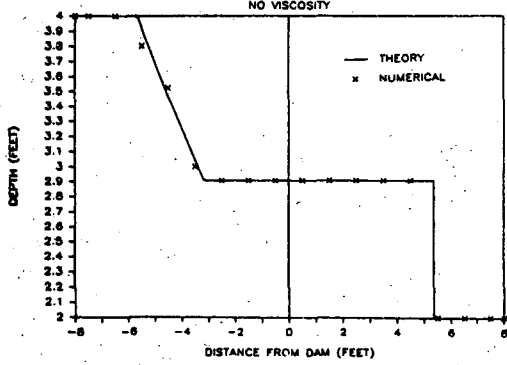
Fig. 3 Comparison between analytical
and numerical solutions of two
dimensional Riemann problem

take the following form (refer to the definition
sketch in Figure 4):

$$\frac{\partial u}{\partial t} + v\frac{\partial u}{\partial y} + u\frac{\partial u}{\partial x} = -a_z\frac{\partial \lambda}{\partial x} + f_x \qquad (2a)$$

$$\frac{\partial v}{\partial t} + v\frac{\partial v}{\partial y} + u\frac{\partial v}{\partial x} = -a_z\frac{\partial \lambda}{\partial y} + f_y \qquad (2b)$$

$$\frac{\partial \lambda}{\partial t} + v\frac{\partial \lambda}{\partial y} + u\frac{\partial \lambda}{\partial x} + \lambda\frac{\partial v}{\partial y} + \lambda\frac{\partial u}{\partial x} = 0 \qquad (2c)$$

where

v = the longitudinal velocity of a fluid
column

f_y = the horizontal longitudinal body force
exerted on the fluid by gravity
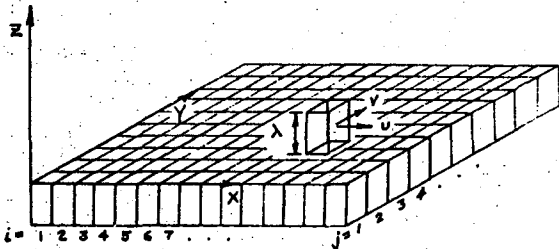
Fig. 4 Three dimensional
sloshing problem definition

To extend Glumm's method to three dimensions
the method of operator splitting is used as
suggested by Collela [4]. Operator splitting calls
for separating the multidimensional problem into
two separate problems for the transverse and
longitudinal flow. The deck area, which for
illustrative purposes is taken to be square, is
divided into a rectangular mesh in two dimensions as
shown in Figure 4. A single time step of duration
Δt consists of first a step of duration Δt in the
x-direction followed by a step of duration Δt in
the y-direction. During the x time step the
following equations are solved:

$$\frac{\partial u}{\partial t} + u\frac{\partial u}{\partial x} = -a_z\frac{\partial \lambda}{\partial x} + f_x \qquad (3a)$$

$$\frac{\partial \lambda}{\partial t} + u\frac{\partial \lambda}{\partial x} = -\lambda\frac{\partial u}{\partial x} \qquad (3b)$$

which express the requirements of conservation of
momentum and mass in the x-direction. During the
y time step the following equations are solved:

$$\frac{\partial v}{\partial t} + v\frac{\partial u}{\partial y} = -a_z\frac{\partial \lambda}{\partial y} + f_y \qquad (4a)$$

$$\frac{\partial \lambda}{\partial t} + v\frac{\partial \lambda}{\partial y} = -\lambda\frac{\partial v}{\partial y} \qquad (4b)$$

which correspond to conservation of momentum and
mass in the y-direction. Each time step consists of
an x-sweep across each row (constant j value)
followed by a y sweep across each column (constant
i value). During the x-sweeps the y-component of
velocity is transported as a passive scalar, while
during the y sweeps the x velocity is
transported as a passive scalar.

A fairly demanding test of the three-
dimensional version of Glumm's method is the three-
dimensional Riemann problem with the dam oriented at
an angle to the mesh. Analytically the solution is
the same, except that the velocities are vectors
perpendicular to the initial dam position and the
depths are constant along any line parallel to the
initial dam position.

Numerically, this represents a fairly general
case, since there will be interaction between waves
propagating in the x and y directions which must
ultimately average out to produce a well defined
disturbance propagating in a direction perpendicular
to the dam. Figure 5 shows the numerical results
for this test case compared with the theoretical
results (which are the same as in Figure 3).

In Figure 5 the depth is shown as a function of
distance from the dam along a line perpendicular to

THREE DIMENSIONAL RIEMAN PROBLEM
### WITH VISCOSITY
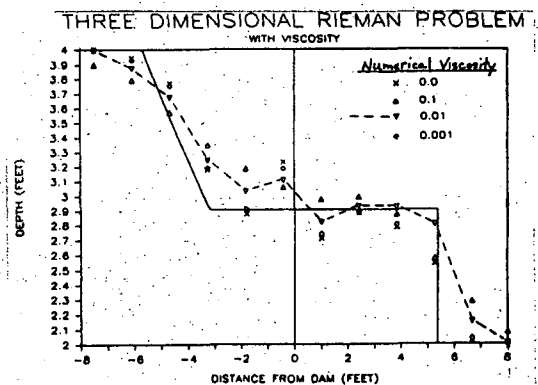
Fig. 5 Comparison between
analytical and numerical solutions
to three dimensional Riemann problem

the dam.

The results indicate that the operator splitting technique is quite successful as a method to extend the capabilities of Glimm's method to three-dimensions although the accuracy is not as good as for the two-dimensional problem. Some discrepancies are seen between the exact and numerical solutions in Figure 5. However these are not severe and appear to be random in nature as expected. This is not entirely undesireable since the real flow will be turbulent and hence random in the vicinity of the jump.

Figure 6 shows a sequence of numerical snapshots of the flow at intervals of one half second. Qualitatively the reflection of the shock waves from the side walls seems correct although analytical results are not available for comparison. This figure also shows the interaction between two shock waves, one being the original shock and one being the reflection from the side wall.

A small amount of numerical viscosity has been introduced into the calculation procedure. This is essentially a rather simple spatial smoothing function. It was suggested by Collela [4] that this would improve the numerical accuracy, however, we observed that the principle effect was to make the graphical representation in Figure 6 more pleasing to look at. Figure 5 shows a comparison of results for various values of the nondimensional viscosity parameter.

3.0 Application

Now that we have a method to compute the behaviour of the deck water numerically it is relatively straightforward to incorporate this procedure into any time-domain ship-motion program. The forces exerted by the deck water on the vessel can be easily computed and the effect on the vessel motions thereby determined. The motions of the deck water are in turn affected by the vessel motion. A simple procedure for approximating the change in volume of the deck water resulting from flow over the bulwarks and through the scuppers is decribed in [10].

At the University of Michigan we have just begun a project in which we will try to utilize the numerical methods described above for simulating the behaviour of water on deck in order to improve our understanding of stability criteria for small vessels. This project is being sponsored by the U.S. Coast Guard. The approach which we intend to take is summarized by the following steps:

1) Identify well documented incidents of vessel capsizing, especially those where water on the deck is suspected to have been part of the cause.

2) Utilizing numerical simulation try to recreate the incidents.

3) Identify the mechanism or primary forces
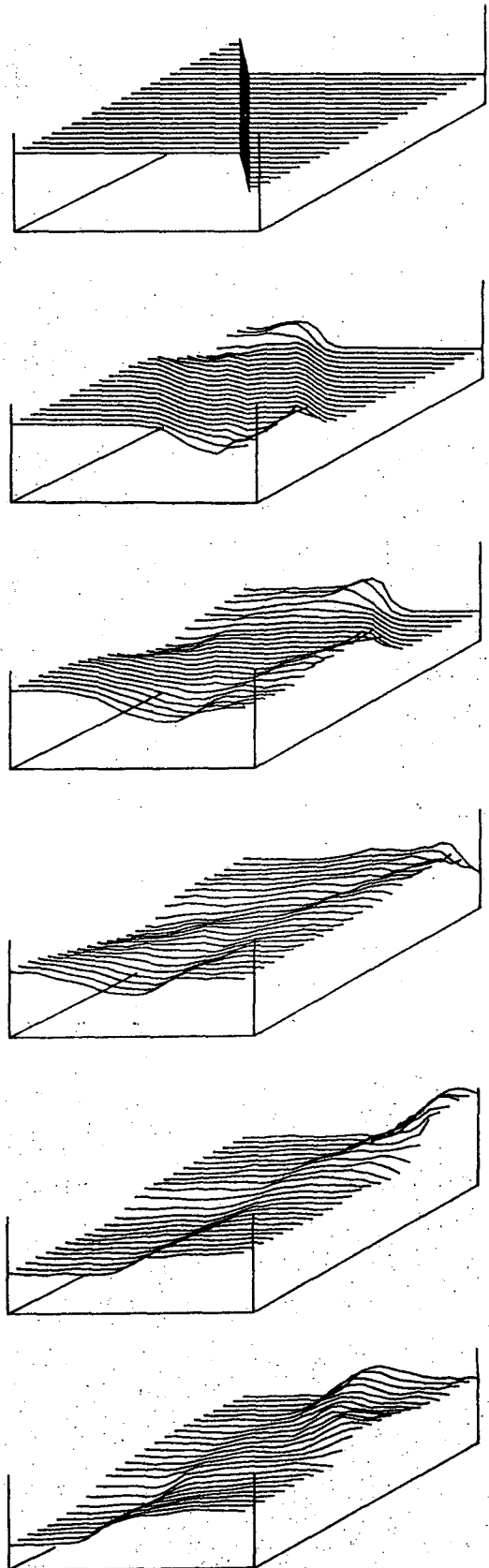
Fig. 6 Three Dimensional Riemann problem solution with viscosity = 0.01

which resulted in the capsizing as determined by the simulation.

4) By parameter variations identify changes in the design which might have prevented the capsize.

5) Determine the applicability of existing stability criteria to the given situation and vessel type. Identify reasonable changes in the stability criteria which might have prevented the accidents.

We feel it is necessary to include as many of the real nonlinearities in the equations of vessel motion as possible. Where exact methods are not available we will use reasonable empirical formulations. At the present time a six degrees-of-freedom ship motion simulation based on the impulse response method (Cummins [6], Perez y Perex [12]) is being used to refine and test the various algorithms for the deck water flow simulation. The impulse response method has the advantage of being a time domain simulation technique which accounts properly for the frequency dependence of the added mass and damping coefficients of the ship hull. Since the simulation is in the time domain any type of force which can be described as a function of time or of the state variables can easily be incorporated. Such forces might arise from a mooring line with nonlinear characteristics, nonlinear hydrostatic restoring forces, wind heeling moments, etc..

At a later point in this project we intend to attach the subroutine GLIMM, which simulates the flow of the deck water, to the original CAPSIZE program. CAPSIZE will provide a more accurate simulation of some of the important nonlinear effects resulting from the time dependence of the shape of the displaced volume of the ship.

Failure of stability criteria to prevent capsizing in certain instances is likely to be a result of either oversimplification (i.e. use of simple empirical formulae for stability criteria) or overgeneralization (i.e. applying the same formula to different types of vessels). Unfortunately the methods which we are suggesting to use are not accessible to naval architects or operators as rules of thumb or simple formulae. Such simple formulae are useless, however if they do not reflect physical reality over the range of circumstances to which they are applied. It may be that the most reliable stability criteria will ultimately be achieved by requiring that each vessel design pass through a "standard" computer simulation without capsizing.

ABOUT THE AUTHORS

Dr. Jeffrey T. Dillingham is an assistant professor in the Department of Naval Architecture and Marine Engineering at The University of Michigan. Mr. Jeffrey M. Falzarano is a graduate student in the same department.

REFERENCES

1. Cayanhan, I., "Effect of Water on Deck on the Motions and Stability of Small Ships," Doctoral Dissertation, University of Washington, 1983.

2. Chorin, Alexandre J., "Random Choice Solution of Hyperbolic Systems," Journal of Computational Physics, Vol. 22, No. 4, December 1976, pp. 517-533.

3. Chorin, Alexandre J., "Random Choice Methods with Applications to Reacting Gas Flow," Journal of Computational Physics, Vol. 25, No. 3, November 1977, pp. 253-272.

4. Collela, Phillip, "An Analysis of the Effect of Operator Splitting and of the Sampline Procedure on the Accuracy of Glimm's Method," Ph.D. Dissertation, Department of Mathematics, University of California, Berkeley, 1979.

5. Concus, Paul and Proskurowski, Wlodzimeierz, "Numerical Solution of a Nonlinear Hyperbolic Equation by a Random Choice Method," LBL-6487 Rev., Lawrence Berkeley Laboratories, Berkeley, California, December 1977.

6. Cummins, W.E., "The Impulse Response Function and Ship Motion," Schiffstechnik, Band 9, Heft 47, June 1962.

7. Dahle, E.A. and Kjaerland, O., "Capsizing of the M/S HELLAND HANSEN," RINA Transactions, 1979.

8. Dillingham, J.T. and Falzarano, J.M., "A Numerical Method for Simulating Sloshing," to be published: SNAME Spring Meeting, 1986.

9. Dillingham, J.T., "Motion Prediction for a Vessel with Shallow Water on Deck," Ph.D. Thesis, Department of Naval Architecture, University of California, Berkeley, 1979.

10. Dillingham, J.T., "Motion Studies of a Vessel with Water on Deck," SNAME Marine Technology, February 1981.

11. Glimm, J., "Solutions in the Large for Nonlinear Hyperbolic Systems of Equations," Communications on Pure and Applied Mathematics, Vol. 18, 1965.

12. Mosely, C., "On Dynamic Stability and the Oscillation of Floating Bodies," Philosophical Transactions of the Royal Society, London, 1850.

13. National Transportation Safety Board Report, "Disappearance of the U.S. Freighter SS Poet in North Atlantic Ocean, About October 25, 1980."

14. National Transportation Safety Board Marine Accident Report, "Grounding and Capsizing of the Clam Dredge PATTI-B, Ocean City Inlet, Ocean City, Maryland, May 9, 1978," NTSB-MAR-79-9.

15. National Transportation Safety Board Marine
    Accident Report, "Sinking of the Charter
    Fishing Vessel JOAN LA RIE III, off Manasquan
    Inlet, New Jersey, on October 24, 1982,"
    NTSB-MAR-84/02.

16. National Transportation Safety Board Marine
    Accident Report, "Sinking of the M/V HOLOHOLO
    in the Pacific Ocean near the Hawaiian Islands,
    December 1978," NTSB-MAR-80-15.

17. National Transportation Safety Board Marine
    Accident Report, "Loss of the U.S. Fishing
    Vessel AMAZING GRACE about 80 miles east of
    Cape Henelopen, Delaware about November 14,
    1984," NTSB/MAR-85-07.

18. Odabassi, A.Y., "Ultimate Stability of Ships,"
    RINA, Transactions, 1976.

19. Perez y Perez, Leonardo, "A Time Domain
    Solution to The Motions of a Steered Ship in
    Waves," U.S. Coast Guard Report No. CGD-19-73,
    November 1972.

20. Rahola, J., "The Judging of the Stability of
    Ships and Determination of the Minimum Amount
    of Stability," Doctoral Thesis, Technical
    University of Finland, 1939.

21. Safeship Seminar Proceedings, National Maritime
    Institute, Feltham, March 4, 1982.

22. "Ships in Rough Seas: Project Proceedings,"
    RINA Occasional Publication #5, February 5,
    1982.

23. Sod, Gary A., "A Numerical Study of a
    Converging Cylindrical Shock," Journal of Fluid
    Mechanics, Vol. 83, Part 4, 1977, pp. 785-794.

24. Stoker, J.J., Water Waves, Outerscrend
    Publishers, Inc., New York, 1957.

25. Storch, R.L., "Alaskan King Crab Boat
    Casualties," Marine Technology, SNAME, January
    1978.

26. U.S. Coast Guard, "Marine Casualty Report: M/V
    JOAN LA RIE III," Washington, DC, 1984.

27. Wigton, Larry, "Glimm's Method for Humans,"
    lecture notes prepared for course on numerical
    methods, Department of Mechanical Engineering,
    University of California, Berkeley, California,
    1979.

28. Faltinsen, Odd M., "A Numerical Nonlinear
    Method of Sloshing in Tanks with Two-
    Dimensional Flow," Journal of Ship Research,
    Vol. 22, No. 3, September 1978, pp. 193-202.

APPLYING LYAPUNOV METHODS TO INVESTIGATE ROLL STABILITY

S.R. Phillips

ABSTRACT

This paper describes how a roll bound may be obtained for any ship, without recourse to iterative techniques. It concludes that a large scale statistical analysis of ships will produce a realistic and usable stability criterion, based upon Lyapunov theory.

1 INTRODUCTION

This paper will consider, in practical terms, the problem of existence of a Lyapunov bound for the roll motion of a vessel in beam seas, obeying the simple second order equation

$$\ddot{\theta} + f(\theta)\,\dot{\theta} + g(\theta) = e(t) \qquad (1)$$

where

$f(\theta)$ = the linearised damping function
$g(\theta)$ = the restoring function
$e(t)$ = the excitation function

Our Lyapunov function will take the form:

$$V(\theta,\dot{\theta}) = \frac{1}{2}\left[\dot{\theta} + F(\theta) - h(\theta)\right]^2 + G(\theta) \qquad (2)$$

where

$$F(\theta) = \int_{x=0}^{\theta} f(x)\,dx$$

$$G(\theta) = \int_{x=0}^{\theta} g(x)\,dx$$

$h(\theta) = a\theta + b\theta^3$ where a,b are arbitrary constants to be discussed in more detail later.

2 FORMULATION OF THE LYAPUNOV BOUND

Reference [1] proves that for a Lyapunov bound to exist it is necessary that there be a region of θ in which

$$-h'(F-h) - 2\sqrt{g h'(F-h)} < e(t) < -h'(F-h) + $$
$$+ 2\sqrt{g h'(F-h)}$$

This bound may be expressed as:

$$-\psi_2 < e(t) < \psi_1 \qquad \text{if } g > 0$$
$$-\psi_1 < e(t) < \psi_2 \qquad \text{if } g < 0$$

where

$$\psi_1 = \sqrt{h'(F-h)}\,\left(2\sqrt{|g|} - \sqrt{h'(F-h)}\right)$$

$$\psi_2 = \sqrt{h'(F-h)}\,\left(2\sqrt{|g|} + \sqrt{h'(F-h)}\right) \qquad (3)$$

We can eliminate the dependence of the excitation on time by considering that $e(t)$ always assumes its maximum absolute value. Call this value the "Excitation Lever".

Plots of ψ_1, ψ_2 and the excitation lever are shown in Fig.1.
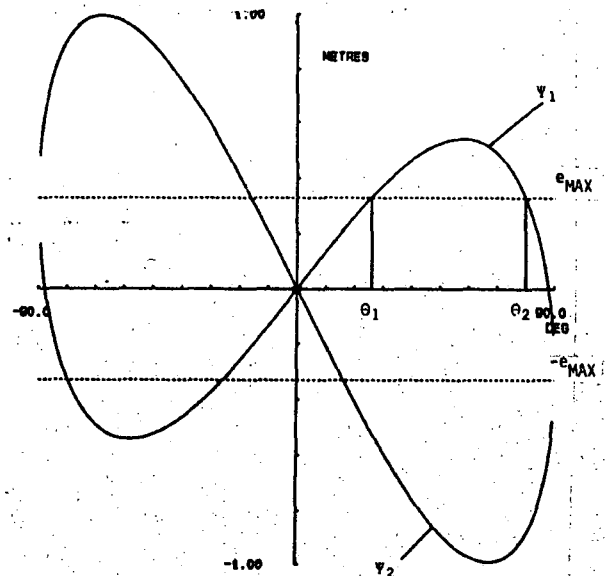

Figure 1   Characteristics of Lyapunov Diagram

Equation (3) is a necessary but not a sufficient condition for stability. Reference [1] goes on to discuss other necessary conditions, but these are all dependent on the distance between θ_1 and θ_2 being reasonably large. This distance, which decreases with increased excitation, we will call the "Stability Range", and its size may be considered as an indication of the likelihood of stability.

As the Stability Range is dependent on the ψ_1 curve alone, and the Lyapunov diagram is symmetrical, then it is usual to confine our study to the positive quadrant alone.

3 VALIDATION

Because the h function is arbitrary, there are an infinite number of ϕ curves that may be plotted. Our aim must be to choose an h function which forces ϕ_1 to be large and therefore maximises the likelihood of obtaining a large stability range.

At BMT, software has been developed that employs the above theory to calculate the stability range for a number of values of a and b (the h coefficients), and iterates in a fashion tending to maximize this range. A Lyapunov bound may then be fitted if the range of stability is large enough.

This criterion can be relied upon to produce a realistic roll-bound for any given vessel. Time simulations of the equation of motion (1) assuming a triangular wave profile, repeatedly produce a roll motion exceeding 90% of the Lyapunov bound calculated. Model tests are planned for more rigorous verification of the method.

As a simple demonstration of the robustness of the method, take Example Ship No.5 (particulars in Table 2, section 4.2) rolling in a beam sea of maximum wave slope 14°. Figure 2 demonstrates that a reasonable stability range is obtained, and the methods of Ref.[1] show the ship to be stable. Now decrease the damping coefficient by 25% (e.g. remove bilge keels) and the diagram alters in such a way that no Lyapunov bound may be found - the ship is now unstable (Fig.3).
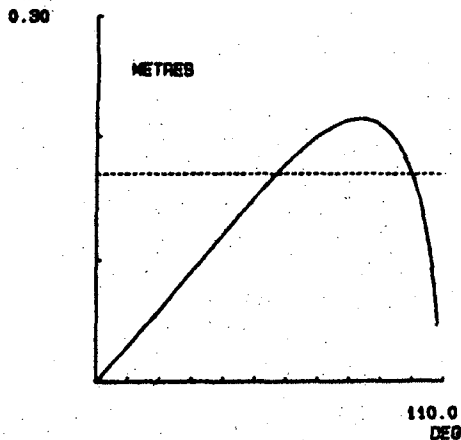
Figure 2   Ship No.5   Normal Damping

4   SIMPLIFYING THE CRITERIA

Work is now in progress towards simplifying the technique in order that it may be possible to rigidly formulate a criterion for ship stability. Any fixed criterion will be dependent on:

  (i) Guidelines for the choice of the coefficients of the h function, a and b.
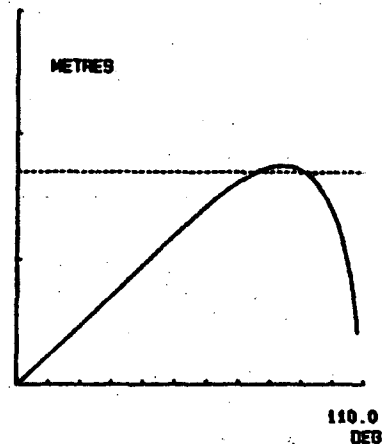
Figure 3   Ship No.5 - Low Damping

  (ii) Guidelines for assessing the implications for stability of any given Lyapunov diagram.

4.1 Guidelines for the h Function

If the h function is to have the required characteristics [1], i.e.

$h' > 0$ and
$g(\theta) [F(\theta) - h(\theta)] > 0$

for some region $-\theta_h < \theta < \theta_h$

then it can be shown that the following constraints must be observed:

$a > 0$
$b > 0$
$c > a$ where $c = f(\theta)$

and θ_h will be defined by

$$\theta_h = \sqrt{\frac{c - a}{b}}$$

Formal experiments performed on 8 ships confirmed an earlier impression that coefficients a and b, although arbitrary, tend to iterate towards a narrow range of values when a Lyapunov bound is searched for by using the methods of section 2. The results of these experiments may be summarised

  (i) a tends to lie in the range
       $(c - 0.1) < a < (c - 0.01)$

  (ii) b tends to lie in the range
       $0.1 E-6 < b < 0.1 E-5$

  (iii) a and b tend to decrease with increased excitation

  (iv) As a consequence of (iii) θ_h tends to increase with excitation.

4.2 Assessing the Lyapunov Diagram

If

A$_1$ = Area bounded by excitation lever and ϕ_1 curve

and

A$_2$ = Area bounded by θ axis and ϕ_1 curve

Then define a new parameter A, where

$$A = \frac{A_1}{A_2} \times 100\%$$

As the excitation is increased then A will naturally decrease until a critical value is reached coinciding with the point at which the ship becomes unstable. Define

A$_c$ = Lowest value of A for which ship remains stable.

Figures 4 to 11 show the Lyapunov diagrams of 8 ships at this critical point. Values of A$_c$ were obtained from these diagrams and recorded in Table 1, along with the Stability Range. The general particulars of the ships are given in Table 2.

Ship No	θ_1 (deg)	θ_2 (deg)	Stability Range (deg)	A$_c$ (%)
1	23.5	59.0	35.5	10.5
2	41.0	78.0	37.0	11.7
3	40.5	77.5	37.0	7.5
4	46.0	88.0	42.0	2.0
5	57.0	99.5	42.5	8.8
6	26.5	57.5	31.0	12.0
7	25.5	49.0	23.5	5.9
8	65.0	93.5	28.5	7.0

Table 1   Parameters Obtained From the Lyapunov Diagrams of Figs.4-11

Ship No.	LBP (m)	B (m)	T (m)	Δ (tonne)	GM (m)	f (s^{-1})
1	52.6	12.2	4.89	2122	1.72	0.36
2	56.8	12.2	4.27	1567	0.70	0.26
3	134.1	20.4	4.02	7912	3.78	0.10
4	67.1	11.0	4.29	2344	1.26	0.66
5	64.0	11.6	9.60	1532	0.78	0.13
6	135.0	23.0	8.20	16098	1.70	0.02
7	20.0	6.7	2.50	160	0.75	0.26
8	80.0	16.0	3.90	2706	0.38	0.07

Table 2   Ship Particulars

It may be possible to develop a criterion for stability in terms of stability range, but parameter A$_c$ is chosen here on the basis that simple geometry constrains it to be the more stable parameter.
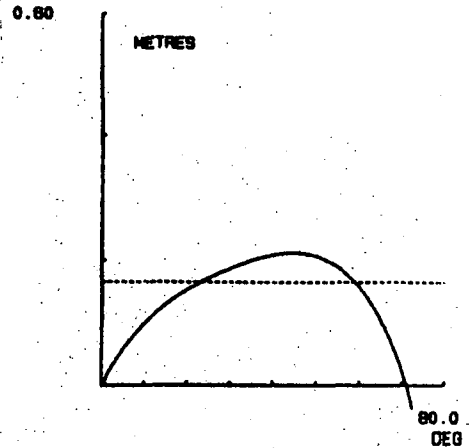

Figure 4   Ship No.1
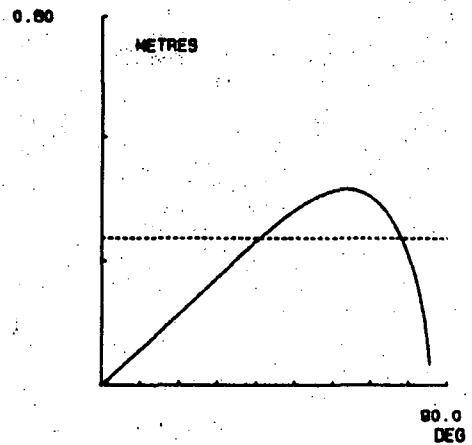
Figure 5   Ship No.2
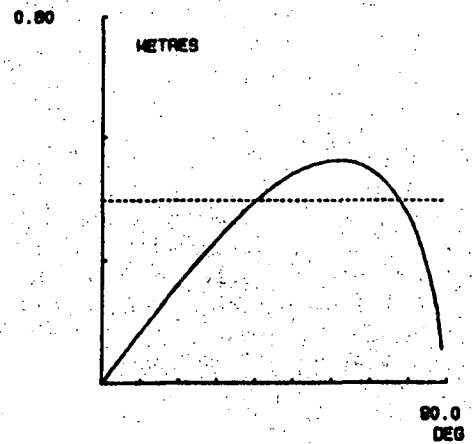
Figure 6   Ship No.3
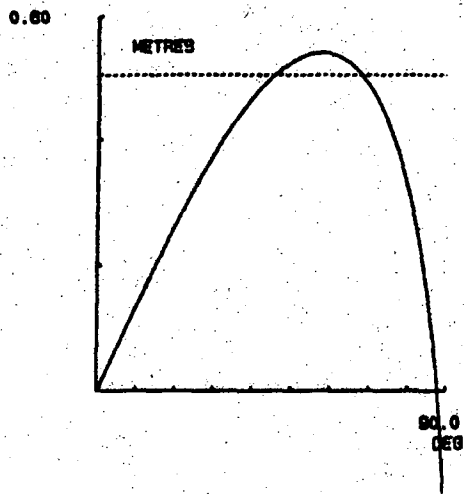
Figure 7   Ship No. 4
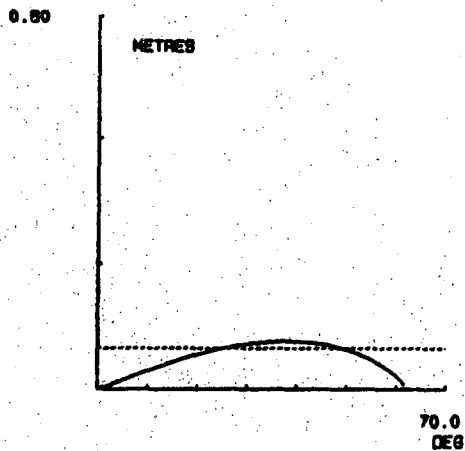

Figure 10   Ship No. 7
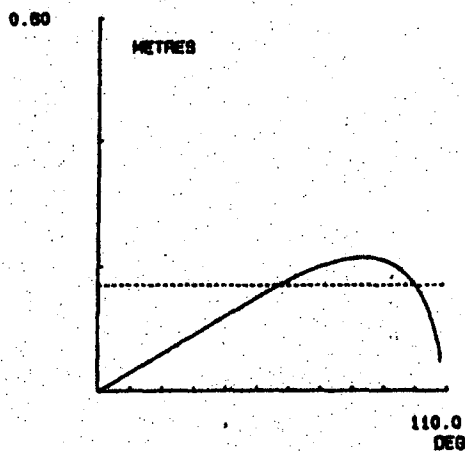

Figure 8   Ship No. 5
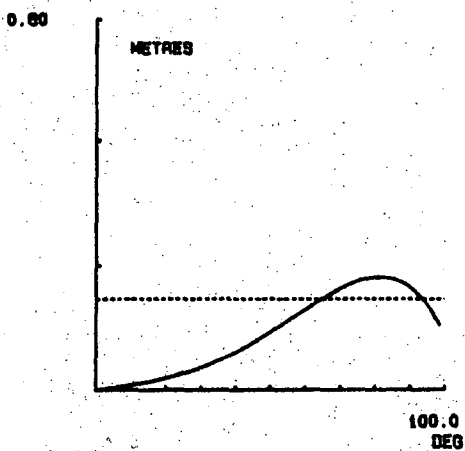
Figure 11   Ship No. 8
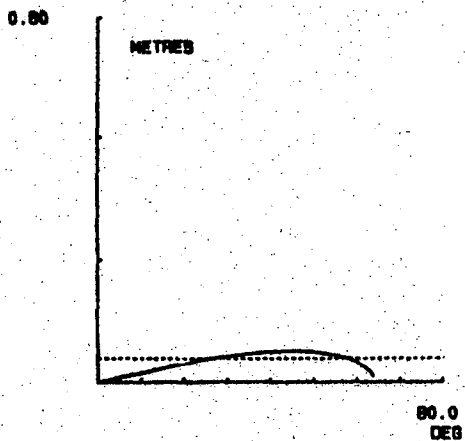
Figure 9   Ship No. 6
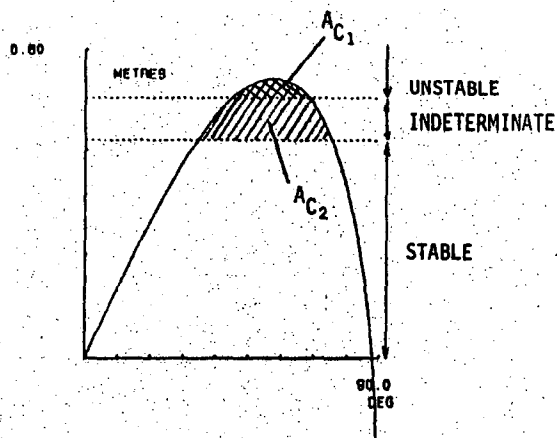
Figure 12   Ranges of Stability Defined by Area Criteria

The task is now to determine statistically a value for A_c applicable to any given ship. It can be seen from Table 1 that A_c is not constant, but we may define

A_{c_1} = Lower limit of A_c

A_{c_2} = Upper limit of A_c

The sample of 8 ships yields values of 2% and 12% for A_{c_1} and A_{c_2} respectively. Therefore, for any given ϕ curve, a stability range in terms of the excitation on a vessel may now be defined (Fig.12).

Examining Fig.12, the practical implication of this diagram for any excitation lever projected onto it is clear. Without recall to iterative techniques, any given vessel may be pronounced stable, unstable or indeterminate. Our aim must be to work towards making the indeterminate range as small as possible.

5   CONCLUSIONS AND EXTENSIONS

At this stage, iterative techniques performed either manually or (more preferably) by computer, have a significant role to play in the method. More precise guidelines for the choice of the h function and interpretation of the area criteria, will follow from a comprehensive statistical study of many ships. Such a survey may reveal a link between these two parameters and a ship characteristic, such as the GZ curve.

Progress is also being made towards extending this method to vessels in following seas. Here, parametric excitation is regarded as the difference between the sagging or hogging GZ curves and the calm water GZ curve, implying an excitation lever varying with θ as shown in Fig.13.

7   REFERENCES

[1] CALDEIRA-SARAIVA, F.   'A Stability Criterion for Ships Using Lyapunov's Method.' RINA International Conference on 'The Safeship Project: Ship Stability and Safety'. London, June, 1986.
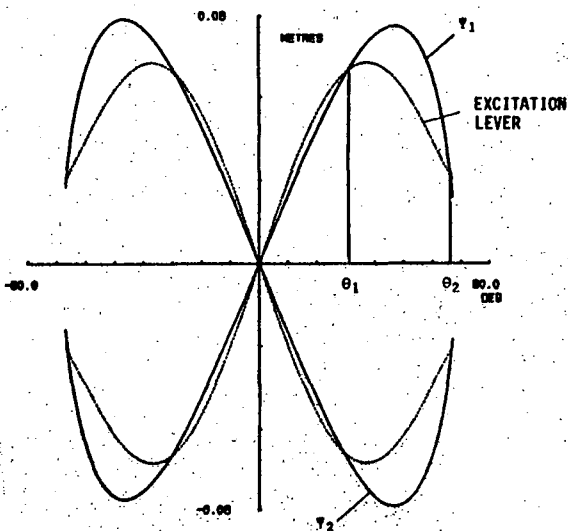
Figure 13 Following Sea Lyapunov Diagram

THE BOUNDEDNESS OF ROLLING MOTION OF A SHIP
BY LYAPUNOV'S METHOD

F. Caldeira-Saraiva

ABSTRACT

In the present paper, Lyapunov Theory is used to obtain stability bounds for the non-linear equation of pure-roll of a ship under the action of wind and waves. Examples of application are given, that show that the results obtained do not seem unduly conservative.

1 INTRODUCTION

As a preliminary step in the study of the rolling motion of a ship, this paper will consider the determination of bounds for the following second-order equation which describes under certain simplifying assumptions the pure rolling motion under the excitation of wind and waves:

$$\ddot{\theta} + f_1(\theta)\,\dot{\theta} + f_2(\theta)\,\dot{\theta}|\dot{\theta}| + f_3(\theta)\,\dot{\theta}^3 +$$
$$+ g(\theta) = e(t) \qquad (1)$$

This is a generalization, to include non-linear damping, of the simpler Liénard equation

$$\ddot{\theta} + f(\theta)\,\dot{\theta} + g(\theta) = e(t) \qquad (2)$$

The stability and boundedness of the trajectories that satisfy Eqn(2) have been studied extensively using Lyapunov methods. Early examples can be seen in Refs.[1,7], while extensive surveys of more up-to-date results can be found for instance in Refs.[8,9]. The assumptions usually made are that $\theta.g(\theta)>0$ for all $\theta \neq 0$ and $\int_0^\theta g(s)\,ds \to \infty$ as $\theta \to \infty$. In the case of the rolling motion of a ship, however, these assumptions are not valid. In fact $g(\theta)$ will change change sign at values of θ different from 0; moreover the interest is not so much in stability or boundedness per se but in boundedness within specified limits (lower than the first vanishing point of $g(\theta)$ different from zero)[10]. We shall therefore have to devise a different approach.

The approach followed in this paper will be similar to that of Ref.[11] which studied Eqn(2), though of course some of the simpler results that could be derived for the linear-damping case are now lost. The basic result, the establishing of Lyapunov bounds, can however still be obtained. Examples of application to the rolling motion of ships will be presented at the end.

2 AN AUXILIARY FUNCTION

Let us assume that g, f_1, f_2 and f_3 satisfy the following conditions:

(A) $g(\theta)$ continuously differentiable and odd in $I = [-a, a]$, with $g(\theta) > 0$ for $\theta \in (0,a)$ and $g(a) = 0$.

(B) $f_1(\theta)$, $f_2(\theta)$ and $f_3(\theta)$ even and continuous in I. Also $f_1(\theta)$ positive in that interval and $f_2(\theta)$ and $f_3(\theta)$ non-negative.

From these assumptions it follows immediately that $g(0) = g(-a) = 0$, that $G(\theta) \equiv \int_0^\theta g(s)ds$ exists and is continuously differentiable and also that $f_1(\theta)$ is bounded away from 0 and ∞ in the closed interval I.

For every continuous and differentiable function $\eta(\theta)$ defined in I, we can construct a Lyapunov function $V(\theta,\dot{\theta})$ as follows:

$$V(\theta,\dot{\theta}) = \frac{1}{2}[\dot{\theta} + \eta(\theta)]^2 + G(\theta)$$

The substantial derivative will then be

$$\dot{V}(\theta,\dot{\theta};e) = -f_3\dot{\theta}^4 - (\eta f_3 + f_2 s)\dot{\theta}^3 +$$
$$+ (\eta' - f_1 - f_2 s\eta)\dot{\theta}^2 +$$
$$+ [e + \eta(\eta' - f_1)]\dot{\theta} + \eta(e-g)$$

where the dependency on θ has been dropped, to lighten the notation, and $s \equiv \text{sign}(\dot{\theta})$. In the continuation we shall also at times use V_t and $\dot{V}_t$ for $V(\theta(t),\dot{\theta}(t))$ and $\dot{V}(\theta(t),\dot{\theta}(t);e(t))$ when we are particularly interested in the dependence on time. We can now prove the following.

Lemma 1 For any $\theta^* \in (0,a)$ we can select an odd continuously differentiable function $\eta(\theta)$ and a positive δ^* such that:

(a) $\eta'(\theta) < f_1(\theta)$ in I
(b) $|e| < \delta^*$ implies $\dot{V}(\pm\theta^*,\dot{\theta};e) < 0$
(c) $|\theta| < \theta^*$ and $\dot{V}(\theta,\dot{\theta};0) > 0$ imply $\theta = \dot{\theta} = 0$

Proof Let us put

$$\dot{V} = X_1 + X_2 + X_3$$

where $X_1 = - f_2 \, \mathrm{s} \, \dot{\theta}^3$

$X_2 = - f_3 \, \dot{\theta}^4 - \eta f_3 \, \dot{\theta}^3 - \alpha \, f_3 \, \eta^4$

$X_3 = (\eta' - f_1 - \mathrm{s} f_2 \eta)\dot{\theta}^2 + [e + \eta(\eta' - f_1)]\dot{\theta} + (e - g)\eta + \alpha f_3 \eta^4$

and $\alpha = 3^3/4^4$.

It follows immediately that, for any θ and $\dot{\theta}$

$X_1 = - f_2(\theta) \, |\dot{\theta}|^3 \leqslant 0$

Also

$$\frac{\partial X_2}{\partial \dot{\theta}} = - f_3 \dot{\theta}^2 \, (4\dot{\theta} + 3\eta)$$

and so for any given θ, X_2 reaches its maximum for $\dot{\theta} = -\frac{3}{4}\eta$, i.e.

$X_2(\theta,\dot{\theta}) \leqslant - f_3 \, (\frac{3^4}{4^4} \eta^4 - \frac{3^3}{4^3} \eta^4 + \frac{3^3}{4} \eta^4) = 0$

Let us finally consider X_3. Seen as a function of $\dot{\theta}$, it consists of two second-order polynomials, one for $\dot{\theta} > 0$ and one for $\dot{\theta} < 0$. The discriminant is

$\Delta = e^2 - e \, 2[\eta(\eta' - f_1) - 2 \, \mathrm{s} \, \eta^2 f_2] +$

$+ \eta^2(\eta' - f_1)^2 +$

$+ 4\eta \, (g - \alpha \, \eta^3 f_3)(\eta' - f_1 - \mathrm{s} \, f_2 \eta)$

Δ is itself a second-order polynomial in e whose two roots e_1 and e_2 satisfy

$e_1 e_2 = P(\eta) = \eta^2(\eta' - f_1)^2 + 4\eta(g - \alpha \, \eta^3 f_3)(\eta' - f_1 - \mathrm{s} f_2 \eta)$

We shall now show that we can choose $\eta(\theta)$ odd and continuously differentiable such that $\eta'(\theta) < f_1(\theta)$ in I and $P(\eta)$ negative in $[-\theta^*, \theta^*]\backslash\{0\}$. Since f_1 is positive in I, it is clear that we can choose $\eta(\theta)$ odd, continuously differentiable and increasing, such that $\eta'(\theta) < f_1(\theta)$ in I. Then, if $\eta(\theta)$ is chosen sufficiently small, the dominating term in $P(\eta)$ will be $4\eta g(\eta' - f_1)$ which is negative in $[-\theta^*, \theta^*]\backslash\{0\}$.

Then the two roots of Δ will be real and of opposite signs. We can therefore choose $\delta^* < \mathrm{Min}\{|e_1|, |e_2|\}$ and if $|e| < \delta^*$, then $\Delta < 0$, so $X_3 < 0$ and therefore $\dot{V}(\pm \theta^*, \dot{\theta}; e) < 0$.

For future use we shall note at this stage that if we select $\theta' \in (\theta^*, a)$ for η sufficiently small we can also have $P(\eta) < 0$ for all $\theta \in (-\theta', -\theta^*) \cup (\theta^*, \theta')$ and $\frac{1}{2} \eta^2(\theta^*) + G(\theta^*) < G(\theta')$. Then for some $\delta^* > 0$ sufficiently small, all $\dot{\theta}$ and all e of absolute value at most δ^* we will also have $\dot{V}(\pm \theta'; \dot{\theta}; e) < 0$.

If $e = 0$, then $\Delta = P(\eta) < 0$ except at $\theta = 0$. So if $\theta \neq 0$, $\dot{V}(\theta, \dot{\theta}; 0) < 0$. $\dot{V}(\theta, \dot{\theta}; 0) > 0$ implies therefore $\theta = 0$. But then

$X_3 = (\eta' - f_1) \, \dot{\theta}^2$

and so we must have $\dot{\theta} = \theta = 0$.

For any $\theta^* \in (0, a)$, $\delta < \delta^*$ as defined in Lemma 1 and V defined using the corresponding $\eta(\theta)$, we can now define the correspondences

$\Theta(\delta) = \{(\theta, \dot{\theta}) : |\theta| < \theta^*$ and, for some e, $|e| < \delta$ and $\dot{V}(\theta, \dot{\theta}; e) > 0\}$

$\Theta'(\delta) = \{(\theta, \dot{\theta}) : \theta^* < |\theta| < a$ and, for some e, $|e| < \delta$ and $\dot{V}(\theta, \dot{\theta}; e) > 0\}$

and we can prove the following.

Lemma 2 For $\delta \in [0, \delta^*]$, Θ and Θ' are upper-semi-continuous and $\Theta(\delta)$ and $\Theta'(\delta)$ are compact and non-void.

Proof The proof is similar for the two correspondences, so we shall just consider Θ. Suppose $\delta_i \to \delta_0$, $\delta_i < \delta^*$, $(\theta_i, \dot{\theta}_i) \in \Theta(\delta_i)$ and $(\theta_i, \dot{\theta}_i) \to (\theta_0, \dot{\theta}_0)$. Then $\delta_0 < \delta^*$. For each i there is e_i such that $\dot{V}(\theta_i, \dot{\theta}_i; e_i) > 0$ and $|e_i| < \delta_i < \delta^*$, so there is a subsequence of e_i tending to a limit e_0. Then $|e_0| < \delta^*$ and $\dot{V}(\theta_0, \dot{\theta}_0; e_0) > 0$. Also $|\theta_0| < \theta^*$ and, from Lemma 1, $\theta_0 \neq \pm \theta^*$, so $|\theta_0| < \theta^*$ i.e. $(\theta_0, \dot{\theta}_0) \in \Theta(\delta_0)$. This establishes upper-semi-continuity. Closedness of $\Theta(\delta)$ follows from the same argument.

The sets $\Theta(\delta)$ and $\Theta'(\delta)$ are non-void for any $\delta \in [0, \delta^*]$, since $(0,0) \in \Theta(\delta)$ and $(\pm a, 0) \in \Theta'(\delta)$. The sets are also bounded in θ, by definition, so all that remains is to show that $\dot{\theta}$ is bounded.

It is clear from the expression of $\dot{V}$ that if $f_3(\theta) \neq 0$, the term $-f_3 \, \dot{\theta}^4$ dominates for $\dot{\theta}$ large in absolute value. It follows then that $\dot{V} < 0$ for high $|\dot{\theta}|$. If $f_3 = 0$ but $f_2 \neq 0$ then the term $-f_2 \, \mathrm{s} \, \dot{\theta}^3 = -f_2|\dot{\theta}|^3$ dominates and the same argument applies. Finally, if $f_3 = f_2 = 0$ the highest-order term is $(\eta' - f_1) \, \dot{\theta}^2$ which again is negative

for $\overset{\bullet}{\theta}$ large in absolute value. For any $\theta \varepsilon I$ and $e \varepsilon [-\delta^*,\delta^*]$ let us define $\overset{\bullet}{\theta}_M > 0$ as either 0 if $V(\theta,\overset{\bullet}{\theta};e) < 0$ for all $\overset{\bullet}{\theta}$ or the modulus of the root of highest absolute value if $V(\theta,\overset{\bullet}{\theta};e) = 0$ has a real $\overset{\bullet}{\theta}$ root. From what we said above it follows that $\overset{\bullet}{\theta}_M$ exists always and is finite. Since roots are continuous functions of the coefficents and θ and e belong to compact intervals, it follows that there is $\overset{\bullet}{\theta}_{MM}$ such that for all $\theta \varepsilon I$ and all $e \varepsilon [-\delta^*,\delta^*]$, if $|\overset{\bullet}{\theta}| > \overset{\bullet}{\theta}_{MM}$ $\overset{\bullet}{V}(\theta,\overset{\bullet}{\theta};e) > 0$. So, for any $(\theta,\overset{\bullet}{\theta}) \varepsilon \theta(\delta) \cup \theta'(\delta)$, $|\overset{\bullet}{\theta}| < \overset{\bullet}{\theta}_{MM}$.

Since $\theta(\delta)$ and $\theta'(\delta)$ are non-void and compact for $\delta \varepsilon [0,\delta^*]$ and V is a continuous function, we can define

$$W(\delta) = \text{Max}\{V(\theta,\overset{\bullet}{\theta}) : (\theta,\overset{\bullet}{\theta}) \varepsilon \theta(\delta)\}$$
$$W'(\delta) = \text{Min}\{V(\theta,\overset{\bullet}{\theta}) : (\theta,\overset{\bullet}{\theta}) \varepsilon \theta'(\delta)\}$$

and we can prove the following.

Lemma 3 $W(\delta)$ is continuous at $\delta = 0$.

Proof   Suppose $\delta_1 \to 0$ and $(\theta_1,\overset{\bullet}{\theta}_1) \varepsilon \theta(\delta_1)$ are such that $W(\delta_1) = V(\theta_1,\overset{\bullet}{\theta}_1)$. Since $|\theta_1| < \theta^*$ and $|\overset{\bullet}{\theta}_1| < \overset{\bullet}{\theta}_{MM}$ it follows that the sequence $(\theta_1,\overset{\bullet}{\theta}_1)$ is bounded and therefore has limit points. But from Lemma 2 and Lemma 1 condition (c) it follows that all such limit points are $(0,0)$, thus $(\theta_1,\overset{\bullet}{\theta}_1) \to (0,0)$ and continuity of V implies $W(\delta_1) \to W(0)$.

3   THE BOUNDEDNESS OF TRAJECTORIES

We shall now prove two theorems that answer the following questions:

1   Given a certain maximum desirable motion $|\theta^*|$, is there a bound in the excitations and a set of initial conditions that guarantee that $|\theta^*|$ will never be exceeded?

2   Given any initial position in the (open) interval I, is there a bound on the excitation that guarantees that the motion will never leave I?

Theorem 1   For any $\theta^* \varepsilon (0,a)$ there is $\delta > 0$ and a neighbourhood of the origin Q such that if $(\theta(t_0),\overset{\bullet}{\theta}(t_0) \varepsilon Q$ and $|e(t)| < \delta$ for all $t > t_0$, then $(\theta(t),\theta(t)) \varepsilon Q$ and $|\theta(t)| < \theta^*$ for all $t > t_0$.

Proof   Using Lemma 1, we can obtain δ^* and a function $\eta(\theta)$ which will give rise to a Lyapunov function $V(\theta,\overset{\bullet}{\theta})$. From Lemma 3 it follows that there will be $\delta \varepsilon (0,\delta^*]$ such that $W(\delta) < G(\theta^*)$.

Define the neighbourhood of the origin $Q = \{(\theta,\overset{\bullet}{\theta}): |\theta| < \theta^* \text{ and } V(\theta,\overset{\bullet}{\theta}) < W(\delta)\}$. Suppose that $(\theta(t_0),\overset{\bullet}{\theta}(t_0)) \varepsilon \theta$, $|e(t)| < \delta$ for all $t > t_0$ and, for some $t^* > t_0$ we had $(\theta(t^*),\overset{\bullet}{\theta}(t^*)) \notin Q$. Because Q is closed and the trajectory continuous, there will be t_1 in $[t_0,t^*)$ such that $(\theta(t_1),\overset{\bullet}{\theta}(t_1))$ belongs to the boundary of Q, while $(\theta(t),\overset{\bullet}{\theta}(t)) \notin Q$ for all $t \varepsilon (t_1,t^*]$. If $\theta(t_1)$ equalled θ^* we would have $V_{t_1} > G(\theta^*) > W(\delta)$, so it must be $\theta(t_1) < \theta^*$ and therefore $V_{t_1} = W(\delta)$. For some $t_2 \varepsilon (t_1,t^*]$ and all $t \varepsilon (t_1,t_2]$ we must then have $\theta(t) < \theta^*$ and $V_t > V_{t_1} = W(\delta)$. It follows then from the definitions of $W(\delta)$ and $\theta(\delta)$ that $\overset{\bullet}{V}_t < 0$ in $(t_1,t_2]$, and we reach a contradiction.

Theorem 2   Given any $\theta^* \varepsilon (0,a)$, there will be $\delta > 0$ and $\overset{\bullet}{\theta}^*$ such that if $(\theta(t_0),\overset{\bullet}{\theta}(t_0)) = (\theta^*,\overset{\bullet}{\theta}^*)$ and $|e(t)| < \delta$ for all $t > 0$ then $|\theta(t)| < a-\varepsilon$ for some $\varepsilon > 0$ and all $t > t_0$.

Proof   As stated in the proof of Lemma 1, there is $\theta' \varepsilon (\theta^*,a)$ and V such that $V(\theta^*,0) < G(\theta')$ and $\overset{\bullet}{V}(\pm \overset{\bullet}{\theta}',\overset{\bullet}{\theta};e) > 0$ for some $\delta^* > 0$, all $\overset{\bullet}{\theta}$, $\theta^* < |\theta| < \theta'$ and $|e| < \delta^*$. From Lemma 3 it follows that there is $\delta \varepsilon (0,\delta^*]$ such that $W(\delta) < V(\theta^*,0)$. For such δ there will be $(\theta,\overset{\bullet}{\theta}) \varepsilon \theta'(\delta)$ such that

$$W'(\delta) = \frac{1}{2} [\overset{\bullet}{\theta} + \eta(\theta)]^2 + G(\theta) > G(\theta)$$

$$> G(\theta') > V(\theta^*,0)$$

There is therefore $\overset{\bullet}{\theta}^*$ such that

$$W'(\delta) > G(\theta') > V(\theta^*,\overset{\bullet}{\theta}^*) > W(\delta)$$

Define

$$Q < \{(\theta,\overset{\bullet}{\theta}) : |\theta| < \theta' \text{ and } V(\theta,\theta') < V(\theta^*,\overset{\bullet}{\theta}^*)\}$$

Suppose that $(\theta(t_0),\overset{\bullet}{\theta}(t_0)) = (\theta^*,\overset{\bullet}{\theta}^*) \varepsilon Q$, $|e(t)| < \delta$ for all $t > t_0$ and for some $t^* > t_0$, $(\theta(t),\overset{\bullet}{\theta}(t)) \notin Q$. Then, as in the proof of Theorem 1, it follows that there will be t_1 in $[t_0,t^*)$ such that $|\theta(t_1)| < \theta'$ and $V_{t_1} = V(\theta^*,\overset{\bullet}{\theta}^*)$. There will be therefore a non-empty interval $(t_1,t_2]$ such that for t in such interval $V_t > V(\theta^*,\overset{\bullet}{\theta}^*)$ while at the same time $W'(\delta) > V_t > W(\delta)$ which implies $\overset{\bullet}{V}_t < 0$. We reach therefore a contradiction.

4   APPLICATION

The rolling motion of a trawler can be described by an equation of the form of eqn.(1) with

$$f_1(\theta) = .0267 \ s^{-1}$$

$$f_2(\theta) = .00655 \ degree^{-1} \ s^{-1}$$

$$f_3(\theta) = 0.$$

and

$$g(\theta) = .279 \ \theta - .750 \times 10^{-2} \ \theta|\theta| +$$

$$+ .542 \times 10^{-3} \ \theta^3 -$$

$$- .136 \times 10^{-4} \ \theta^3|\theta| +$$

$$+ .132 \times 10^{-6} \ \theta^5 -$$

$$- .466 \times 10^{-9}\theta^5|\theta| \ deg \ s^{-2}$$

where θ is in degrees. The excitation satisfies $|e(t)| < \delta = 1.98$ deg s^{-2}, which corresponds to wave slopes of 8 degrees. Then in Fig.1 we see the corresponding regions $\theta(\delta)$ and $\theta'(\delta)$ (whose boundaries are defined by crosses) and the Lyapunov bound $V(\theta,\dot{\theta}) = W(\delta)$ (defined by the pointed line) which intersects the θ-axis for $|\theta| = 40$ degrees. We see also the result of a simulation starting from the origin and driven by an excitation of absolute value always δ, which reached values of θ of about 39 degrees, i.e. within 2% of the Lyapunov bound.

In Fig.2 we see a Lyapunov bound $V(\theta,\dot{\theta}) = W'(\delta)$ (for a different V though) and a simulation that, starting outside the bound (but under the vanishing angle of $g(\theta)$ which is 94 degrees) rapidly left the interval I.

These applications of Theorems 1 and 2 show us that the bounds obtained are not necessarily conservative.
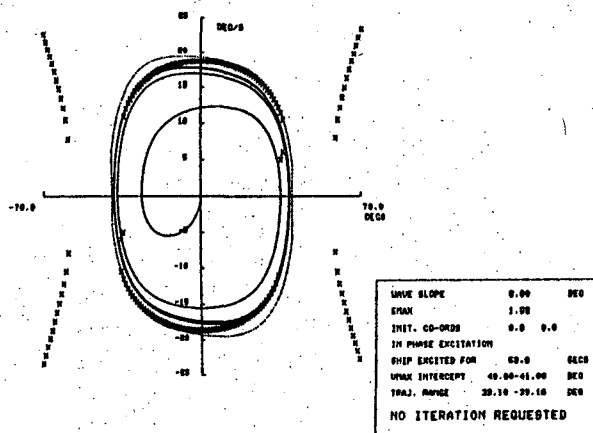
Fig.1
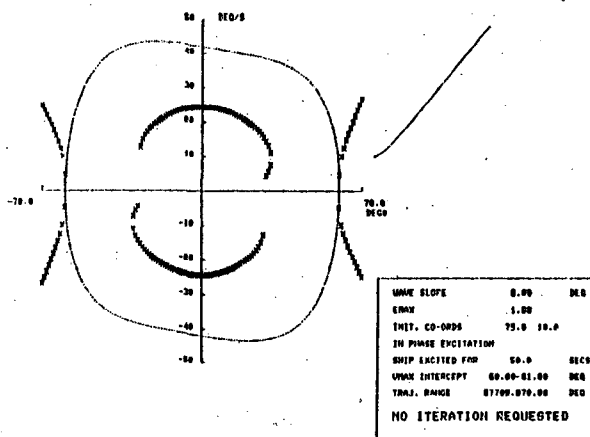
Fig.2

5   CONCLUSIONS AND EXTENSIONS

In this paper we have addressed the question of finding a Lyapunov envelope for the motion of a system described by a second-order equation, when the restoring coefficient can change its sign at points different from the origin. We have presented a method for constructing a Lyapunov function and a bound to the trajectories. We have also found on application of the method to the rolling motion of a trawler that the bound looked efficient.

Further studies are at present being concluded which generalize Eqn(1) to encompass parametric excitation and coupling with other modes of motion.

6   ACKNOWLEDGEMENTS

REFERENCES

1   CARTWRIGHT, M.L.   Forced Oscillations in Non-linear Systems in LEFSCHETZ, S. (Ed.). Contributions to the Theory of Non-linear Oscillations. (Princeton University Press, 1950). Vol.1, pp.149-241.

2   REUTER, G.E.H.   A Boundedness Theorem for Non-linear Differential Equations of the Second Order. Proc. Camb. Philos. Soc., 1951, 47, pp.49-54.

3   MIZOHATA, S. and YAMAGUTI, M. On the Existence of Periodic Solutions of the Non-linear Differential Equation $\ddot{x} + a(x)\,\dot{x} + \theta(x) = p(t)$, Mem. Coll. Sci. Univ. Kyoto, 1952, A27, pp.109-113.

4   ANTOSIEWICZ, H.A. On Non-linear Differential Equation of the Second Order with Integrable Forcing Term, J. London Math. Soc., 1955, 30, pp.64-67.

5   LEVIN, J.J. and NOHEL, J.A. Global Asymptotic Stability for Non-linear Systems of Differential Equations and Applications to Reactor Dynamics. Arch. Rational Mech. Anal., 1960, 5, pp.194-211.

6   LaSALLE, J.P. and LEFSCHETZ, S. Stability by Lyapunov's Direct Method with Applications. (Academic Press, 1961).

7   YOSHIZAWA, T. Stability Theory by Lyapunov's Second Method. (The Mathematical Society of Japan, 1966).

8   KNOWLES, I. On Stability Conditions for Second Order Linear Differential Equations. Journal of Differential Equations, 1979, 34, pp.179-203.

9   STAUDE, U. Uniqueness of Periodic Solutions of the Liénard Equation in Recent Advances in Differential Equations. (Ed. R. Conti) Academic Press, 1981, pp.421-429.

10 ODABASI, A.Y. Conceptual Understanding of the Stability Theory of Ships. Schiffstechnik, 1978, 25, pp.1-18.

11 CALDEIRA-SARAIVA, F. The Boundedness of Solutions of Liénard Equation with a Vanishing Restoring Term. IMA Journal of Applied Math. (Forthcoming).

NUMERICAL CALCULATION OF FORCES AND MOMENTS DUE TO FLUID
MOTIONS IN TANKS AND DAMAGED COMPARTMENTS

F. Petey

Abstract

In view of simulating the ship motions in a seaway
the liquid flow in tanks with a free surface is nu-
merically simulated. For the low fill depth case
the shallow water equations are employed. The
appearance of hydraulic jumps causes the ordinary
difference-schemes to fail. Therefore Glimm's method
is used. For the deep fill case the free surface
of the liquid remains essentially flat, since the
greatest natural period of the tanks is much smaller
than the period of the main excitation due to the
rolling motions. A very simple equation of motion
is thus derived which can be easily integrated nu-
merically. The results obtained from numerical flow
simulations are compared to experimental results
and to analytical solutions.

1.Introduction

If we are interested in solving the ship equa-
tions of motion in the time domain, we have to take
account of the dynamic forces exerted on the ship
by the liquid in the tanks, in flooded compartments
and also on the ship deck, if it happens to become
totally or partially awash.

Since we are interested in computing ship motions
for several ship geometries, seaway conditions and
for relatively long periods of time, it is of para-
mount importance to use a model which, being accu-
rate enough, requires a relatively small computa-
tional effort. As a result of this consideration, this
model represents a compromise of the conflicting
requirements for accuracy versus computer demand.

The method is used as a subroutine in ship motion
programs. It is suitable for simulation of large-am-
plitude motions of the ship which is considered to
be a six-degree-of-freedom system.

In the simulation, time is advanced in increments.
The forces due to the liquid motions inside the ship
at each time step can be added to other external
forces (such as wave exciting forces, wind forces
etc.), so that we obtain a complete time domain
solution for both ship motion and internal fluid
motion. The rate of flow of water through orifices in
the ship hull and through scuppers is estimated by
straightforward equations, so that the volume of
water inside the ship can be corrected at each time
step /1/.

2.Low fill depth case

For the case in which the liquid fill depths are small
compared to the tank width, the velocity vector of
a fluid particle is almost parallel to the tank bottom.
We may thus neglect the velocity component perpen-
dicular to the tank bottom and assume that the par-
ticle velocity is independent of the vertical coordi-
nate.

We investigate first the case in which the movement
of the fluid particles is restricted to the yz-plane
(fig.1). The liquid in the tank is allowed to slosh
freely back and forth between the tank walls in
response to a prescribed rolling motion. We com-
pute an one-dimensional flow described by the ve-
locity v(y) in the y-direction of a fluid particle
relative to the moving frame attached to the tank
and the liquid depth h(y) (measured in z-direction).
We can write the so called shallow water equations
for this case (2) as

a) Conservation of momentum in y-direction

$$\frac{\partial v}{\partial t} + v \frac{\partial v}{\partial y} + f_z \frac{\partial h}{\partial y} = f_y \qquad (1)$$

Fig.3 Hydraulic jump in a rectangular tank oscillating about the midpoint of the tank bottom. Roll angle PHI in deg. and time T in s.

T=2.56 PHI=-0.05

T=3.21 PHI=-2.00

T=3.84 PHI=0.04

T=4.49 PHI=-2.00

T=0.02 PHI=0.00

T=0.65 PHI=2.00

T=1.29 PHI=0.04

T=1.93 PHI=-2.00

Fig.1.
Roll motion about fixed axis.

Fig.2 Forced harmonic oscillation of fluid in a rectangular container. Comparison of results from simulation with experiment. Surface elevation measured at right side of tank (in mm).

b = tank width = 1.20 m

h_0 = still fill depth = 0.09 m

ω = forcing frequency = 2.45 1/s

ϕ_0 = roll amplitude = 2 deg

R = distance to roll axis = 0.0

experiment

simulation

$\omega t + \pi/2$

Fig.6. Dam-breaking problem. Water surface just after the removal of the dam.

Fig.4. Forced harmonic oscillations of a rectangular tank. Comparison of results from simulation with analytical solution.

simulation

analytical solution

t (in s)

b = tank width = 7.90 m

h_0 = still fill depth = b/5

T = forcing period = 9.7 s

T_0 = natural period = 4.0 s

R = distance to roll axis = 0.0

ϕ_0 = roll amplitude = 5.0 deg

Transverse force (in y-direction)

dam at t=0

h = 50 mm

h = 10 mm

bottom
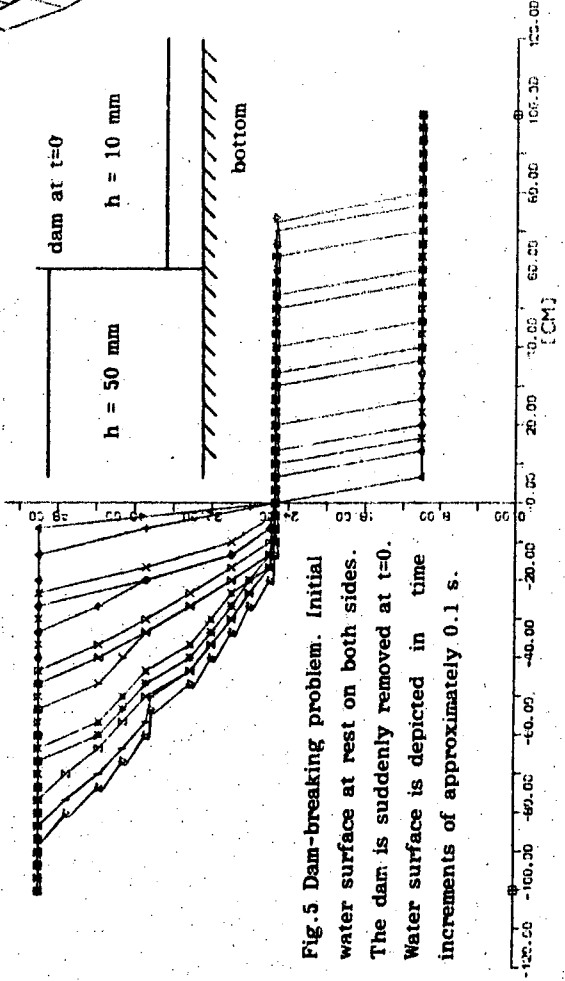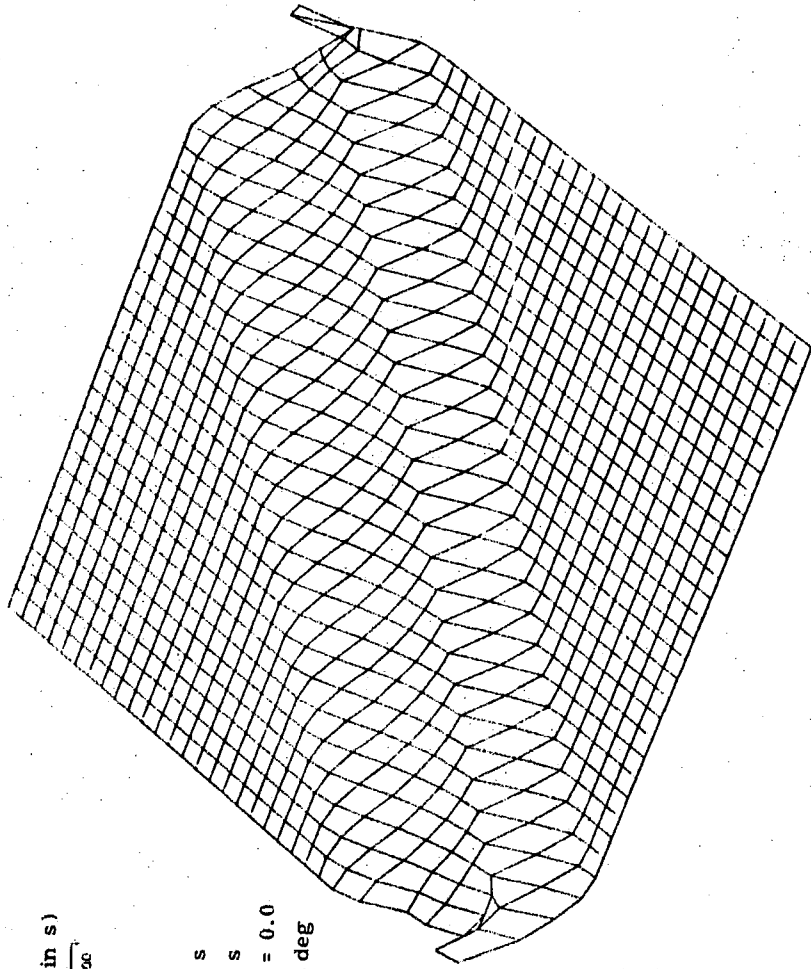
Fig.5 Dam-breaking problem. Initial water surface at rest on both sides. The dam is suddenly removed at t=0. Water surface is depicted in time increments of approximately 0.1 s.

b) Conservation of mass

$$\frac{\partial h}{\partial t} + v \frac{\partial h}{\partial y} + h \frac{\partial v}{\partial y} = 0 \qquad (2)$$

where

$$f_z = g \cos\phi - \dot\phi^2 R + \ddot\phi y + 2\dot\phi v$$

$$f_y = -g \sin\phi + \dot\phi^2 y + \ddot\phi R$$

and g is the gravitational acceleration. At a first stage we solved equations (1) and (2) by using a traditional finite-difference integration scheme. The simulation did not remain stable, if the tank bottom becomes partially dry, or if, in the case where the tank oscillates harmonically, the forcing rolling period and the natural tank period closely match (resonance). Experiments show that in the resonance case a hydraulic jump is formed which travels periodically back and forth between the tank walls. The energy of the fluid particles crossing the jump is not conserved. As a consequence of the discontinuity in the liquid surface at the travelling jump the derivatives of h(y) and v(y) with respect to y in (1) and (2) become infinite and the solution diverges.

We use therefore Glimm's method /2 or 5/ to solve the above nonlinear hyperbolic system of equations. Both h(y) and v(y) are computed at points on a grid across the tank by "randomly" sampling explicit wave solutions obtained from Riemann (also known as dam-breaking) problems at each location on the grid at each time step. This sampling is performed so that momentum and mass are conserved in the mean. The mechanism by which Glimm's method propagates the solution to the equation is rather different from that of finite-difference schemes, as it requires many time steps for the cumulative effect of the sampling to give correct wave speeds. One feature of the results is that they contain a certain fluctuation due to the randomness of the method. Results are correct on the average only. No special handling is required of hydraulic jumps or for the case in which the tank bottom becomes partially dry. Interaction of the fluid with the tank top cannot be dealt with. The method requires a computational effort equivalent to that of classical finite-difference schemes.

If in addition to rolling the other 5 degrees of freedom are to be taken in account, we have to consider the flow both in x- and in y-direction. We introduce thus a third variable (velocity of a fluid particle in x-direction) for the description of the flow and use,

in addition to equations (1) and (2), the conservation of momentum law in x-direction /5/. Chorin /4/ has shown how Glimm's method can be used to compute complicated two-dimensional flow problems by using a so called splitting technique. The approximate solution to the 2-dimensional flow is constructed at each time step from a combination of solutions to several one-dimensional flows in x- and in y-direction. The method conserves both momentum and mass in the mean and exhibits a certain degree of randomness too. A detailed discussion is given in reference /6/.

Fig.2 shows a comparison between experiment /3/ and simulation for the forced harmonic oscillation of an open rectangular container (resonance case). Fig.3 is the flow visualization.

For very slow forced harmonic small-amplitude oscillations of an open rectangular container an explicit solution /3/ can be obtained from the linearized approximation of equations (1) and (2). The numerical results (fig.4, sway force) seem correct, on the average. The deviations are due to the randomness of the method.

Fig.5 is the numerical simulation of a dam-breaking problem. According to the analytical solution /2/ a single shock, which travels with constant speed (approximately 664 mm/s) to the right, and a single rarefraction, which propagates with constant speed 700 mm/s to the left, are formed. The free surface of the liquid is depicted with a time increment of approximately 0.1 s. The mean speeds are correct. We notice that the shock remains perfectly sharp.

Next we compute the following two-dimensional problem to check the validity of Chorin's scheme: a watertight bulkhead joins diagonally two corners of a square open tank dividing it in two equal regions filled with the same liquid but with different fill depths (50 and 10 mm respectively) on each side. The tank is at rest. The bulkhead (the dam) is suddenly removed at time t=0, so that, in the central region of the tank, the previous one-dimensional dam-breaking problem is repeated. Fig.6 shows the free surface of the liquid just after the removal of the bulkhead. Fig.7 is a vertical section A-A across the tank, perpendicular to the removed bulkhead. The mean speeds are correct. A comparison between fig.7 and fig.5 shows however that the two-dimensional shock is not perfectly sharp.

Boundary conditions are treated by reflection technique. If the tank boundary is parallel to one of

Fig.7. Section A-A across the tank of figure 6 perpendicular to the removed dam. Water surface depicted in time increments of approximately 0.2 s.

[M]

ϕ_0= roll amplitude = 5 deg

deep fill depth method

Glimm's method

ϕ_0= 25 deg

* l = tank length = 5 m
  b = tank width = 8 m
  h_0= still fill depth = b/5
  T_0= natural period = 4.0 s
  R = distance to roll axis = 0.0

ϕ_0= 25 deg

MOMENT ABOUT X-AXIS

FORCE IN Y-DIRECTION

MOMENT ABOUT X-AXIS

Fig.8. Propagation of a small disturbance in a cylindrical tank with low fill depth. The disturbance propagates out of the origin and is reflected at the tank wall.
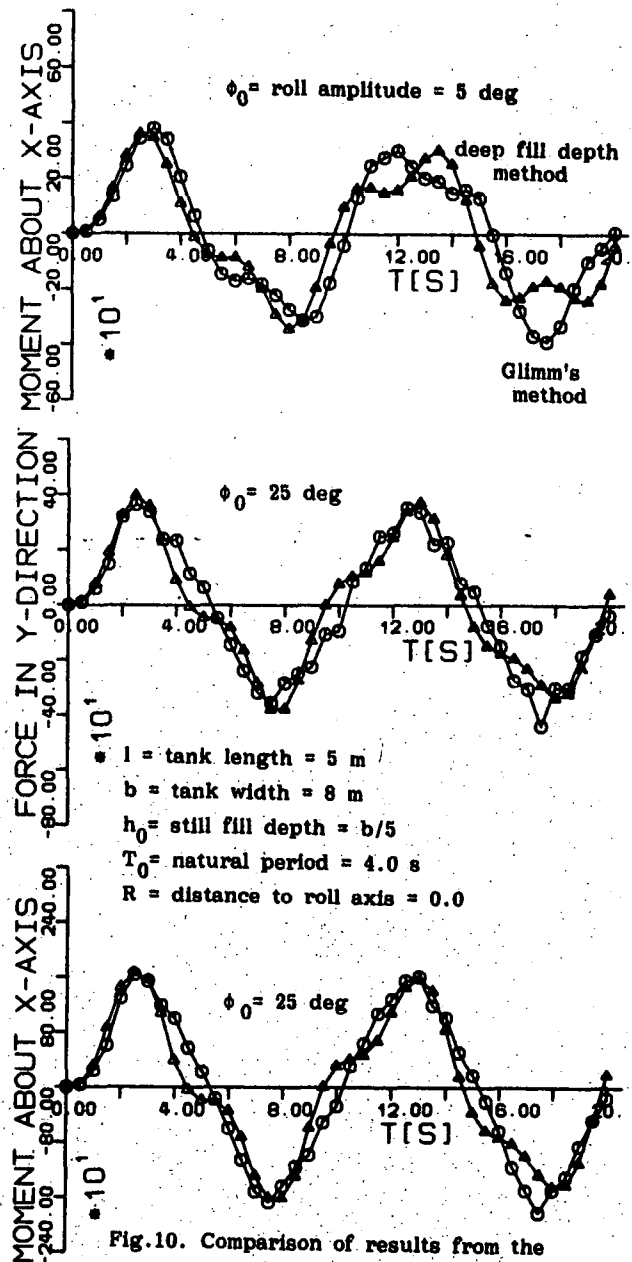
Fig.10. Comparison of results from the deep fill depth method with Glimm's method. The rectangular tank, initially at rest, begins oscillating harmonically with forcing period 10 s.

the mesh directions no problem arises. If it lies obliquely on the grid, it can be treated by a technique introduced by Chorin /4/. We can however obtain reliable results , if we simply decompose the oblique boundary stepwise in the two mesh directions. To check the validity of this approximation we picked a problem which is by no means tailored to the mesh geometry: an open circular cylindrical container (vertical orientation) filled with liquid. The initial circular free surface was at rest, when we introduced a small disturbance at its center. This small disturbance is propagated out of the origin in form of a ring with constant speed, is reflected at the cylindrical tank wall and returns to the origin. The numerical results are depicted in fig.8. The propagation speed is correct, on the average. The shape of the ring however is somewhat sharper in the mesh directions.

3. Deep fill depth case

For tanks with deep fill depth the greatest natural period and the period of the main excitation due to the rolling motions do not closely match, since the former is much smaller than the latter (fig.9). As a result the liquid free surface may be oblique but remains essentially flat. Moreover, the ship motions are relatively slow, so that only the gravitational force is expected to play an important role.

The influence of trim could be easily accounted for, but this would introduce undue complication in the present case. If the volume of liquid inside the tank remains constant during the simulation, the position of the liquid free surface can thus be described by only one parameter, the transversal surface slope σ. We determine the position of the center of gravity of the liquid mass in the tank for several surface slopes. The curve so obtained represents the path along which this center of gravity, at which all the liquid mass is assumed to be concentrated, is allowed to move as σ changes during the simulation. The equation of motion of the liquid free surface can be obtained from Lagrange's equation /1/:

$$\ddot{\sigma} = \frac{g}{\partial y'/\partial \sigma} \sin(\phi + \sigma) \cos(\sigma) \cos(\theta) \qquad (3)$$

where y' is the position of the center of gravity of the liquid in y-direction and θ is the pitch angle. If the tank shape is rectangular, spherical, cylindrical etc., all terms in equation (3) can be computed explicitly in the program. For more

complicated tank shapes y' has to be computed prior to the simulation and stored. During the simulation this value is interpolated and the derivative of y' with respect to σ computed numerically. A damping term could be easily introduced in (3).

Fig.10 shows several comparisons between this deep fill method and the low fill depth one for an open rectangular tank. The filling $h_0/b = 0.2$ represents the upper limit of the range of validity of the shallow water method /5/. The tank, initially at rest begins oscillating harmonically with a forcing period of 10 s.

4. References

/1/ H. Soeding, Damage Stability in a Seaway, (in German), Report No.429 Institut für Schiffbau, 1982

/2/ J. Dillingham, Motion Studies of a Vessel with Water on Deck, Marine Technology, Vol.18, No.1, 1981

/3/ Verhagen and Wijngaarden, Non-linear Oscillations of Fluid in a Container, Journal of Fluid Mechanics, 1965

/4/ A.J. Chorin, Random Choice Solution of Hyperbolic Systems, Journal of Computational Physics 22, 1976

/5/ F.J. Petey, Calculation of Liquid Motions in Partially Filled Tanks and Flooded Compartments (in German), Schiffstechnik, Vol. 32, No. 2, 1985

/6/ P. Colella, Glimm's method for Gas Dynamics, SIAM J. SCI. STAT. COMPUT., Vol.3, 1982

5. Author

Fernando Petey, Institut für Schiffbau der Universität Hamburg, Federal Republic of Germany
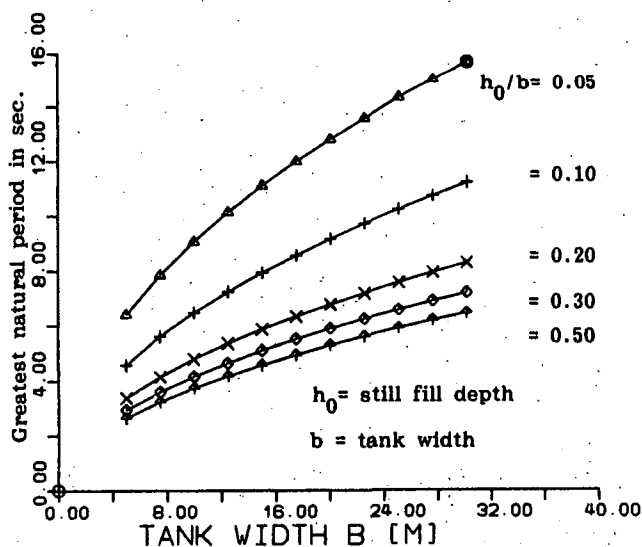
Fig.9. Rectangular tank

THE SAFETY AGAINST CAPSIZING IN RELATION TO SEAWAY PROPERTIES IN MODEL TESTS

P. Blume

ABSTRACT

Significant wave height and peak period are not sufficient for the description of the severity of a seaway with respect to capsizing tests. Therefore tests with 2 models were performed in different seaways with regard to spectral shape, significant wave height and peak period. In following waves the height of the center of gravity was varied in order to find the limit between safe and unsafe.

As expected the correlation between significant wave height and stability parameters derived from the righting lever curve in smooth water for the limiting KG is not good. Heights of the individual wave group which hit the model are more suitable but in general it is difficult to determine them. However the correlation with statistical seaway data also can be improved taking into account the mean wave length and one grouping parameter beside the wave height.

1. INTRODUCTION

There is a growing interest in the development of new stability criteria which are suitable also for modern ship designs in a better way than the traditional requirements. It seems to us that up to now model tests are still the best approach to solve the problem with the smallest limitations in the modelling of the real physical event. But the results of such tests cannot be seen as absolute values (due to a lot of influences and arbitrary chosen conditions); they must be compared with results from corresponding tests with ships of known behaviour. Therefore it is desirable to develop some standards for future capsizing tests.

To guarantee the comparability of test results it is necessary to control the conditions at these tests very carefully. Thereby the seaway properties play an important role. Significant wave height and peak period alone are not sufficient for the description of the seaway with respect to capsizing. The investigation reported here was planned with the

aim to get some insight into the problem. It was sponsored by the German Ministry of Research and Technology. Possibly the results can be taken as a first step to a standardization of capsizing model tests in irregular seas.

In an earlier investigation four different ship models (named A,B,C and D) were tested. First results were presented at the Stability 82 - Conference [1]. As a result of further work a proposal for stability criteria valid for a distinct group of ships was derived which takes care of individual geometrical parameters of the ships [2]. The first experiences with this proposal will be reported during this conference by Hormann und Wagner. For the present investigation the models A and C were used. Model A was tested in 12 additional seaways whereas the program for model C was kept shorter with 5 seaways. Both models were tested at one draught on desired relative courses of 0 and 30 degrees. The test procedure was the same as in the earlier investigation, all tests were repeated several times up to at least 10 tests at the same conditions.

2. SELECTION AND ANALYSIS OF THE MODEL SEAWAYS

The model seaways were selected with regard to the spectral shape, the significant wave height and the peak period. There are one group of sharply peaked spectra with JONSWAP-shape, peak enhancement factor $\gamma = 5$, another group of Pearson-Moskowitz-type and one spectrum as wide as possible. These spectra are named J, P and B respectively with two numbers which indicate increasing wave height and peak period with increasing number.

The control signals for these seaways were computed using 560 harmonic components. Thereby for the seaways with different heights but the same peak period in both groups only the amplitudes of the control signal were changed. A comparsion of the analysed data for the J-seaways with the

corresponding data of the similar seaways I, II and III of the ealier investigation shows differences which possibly can be attributed to the different number of components. The control signal for the seaway I, II and III was composed of 20 components only. So finally one additional seaway named J 2.2 - 100 with 100 components was investigated. Fig. 1 and 2 show the spectra of the model seaways. The curves are smoothed mean curves of 3 to 6 measurements.

All seaways were measured at two positions using sonic,resistance and capacitive probes. The distances from the wave maker were 54 m and 86 m. The time records were statistically analysed. Then spectra were calculated using a frequency resolution of 7.5% of the peak frequency and some spectra parameters were determined.

Beside these standard procedures the main analysis was done with regard to the grouping properties. The envelopes were analysed and the values J_1 and J_2 according to Goda [3] were
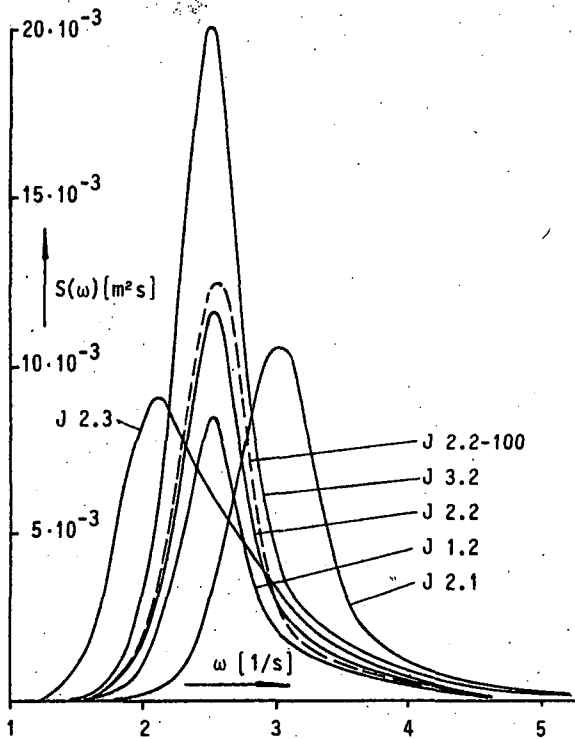
Fig. 1 Spectra of the J-seaways
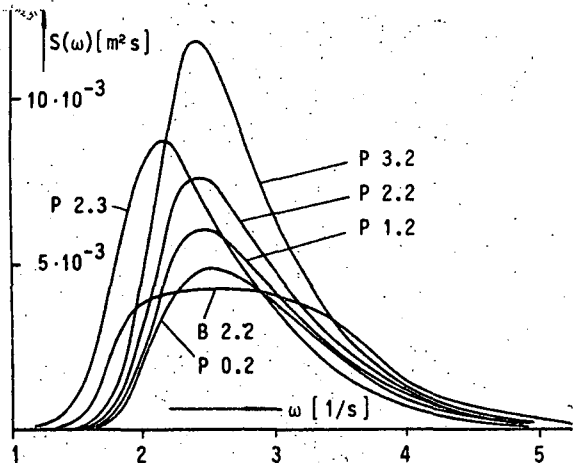
Fig. 2 Spectra of the P- and B-seaways

determined which give the mean number of successive waves in a group which are higher than a certain value and the mean number of waves from one group to the next. Further the SIWEH-function (Smoothed Instantaneous Wave Energy History) by Funke and Mansard [4] and a grouping factor GF were calculated. Also the correlation coefficients r_{HT} for wave height and period, ϕ_{HH1} for two successive wave heights and ϕ_{TT1} for two successive periods introduced by Rye [5] were determined. Finally data from the wave group which the models actually did meet in each test were determined from video recordings, mainly the wave heights H and the crest heights n' above the mean water level. These values then were averaged over three successive waves.

All results cannot be given here. Therefore all data for the same seaway from the measurements at the two positions and with different wave probes were averaged. The main data are compiled in Table 1 which also contains the results for the seaways I, II and III of the earlier investigation [1,2].

The mean wave height H̄ or the mean height n̄' of the crests of the wave group relative to the significant wave height $4\sqrt{m_0}$ depends on the type of the spectrum and on the wave height itself as it is shown in Figure 3. The wave groups become relative higher with increasing peakedness of the spectrum and decreasing significant wave height.

Rye is in favour of the not undisputed opinion that the grouping properties only depend on the spectral shape [3] with increasing tendency at increasing peakedness of the spectrum. He explains different conclusions from other authors as well as the large scatter of the analysis results which can lead to this other view with shortcomings of measurements or simulations and analysis methods as
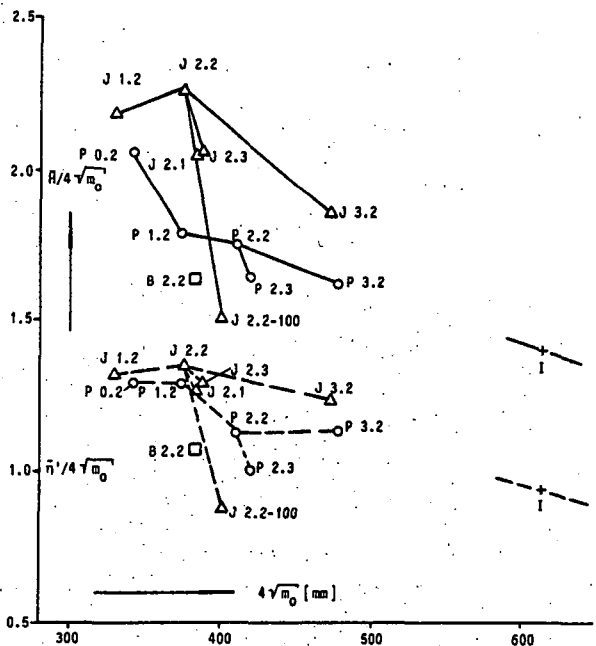

Fig. 3 Relative mean wave height H̄ and crest height n̄' of the wave groups as function of the significant wave height

Table 1 Averaged data of the test seaways

seaway	J 1.2	J 2.1	J 2.2	J 2.3	J 3.2	J 2.2 -100	P 0.2	P 1.2	P 2.2	P 2.3	P 3.2	B 2.2	III	II	I
$4\sqrt{m_0}$ [m]	0.330	0.384	0.376	0.387	0.472	0.401	0.342	0.374	0.410	0.419	0.477	0.383	0.413	0.549	0.613
T_p [s]	2.50	2.09	2.49	2.92	2.52	2.48	2.57	2.58	2.58	2.97	2.60	< 2.62 >	2.16	2.35	2.49
$\zeta_{w\,sig}$ [m]	0.328	0.399	0.370	0.380	0.471	0.393	0.338	0.375	0.412	0.412	0.482	0.366	0.418	0.499	0.601
$\zeta_{w\cdot max}$ [m]	0.551	0.622	0.631	0.630	0.675	0.555	0.669	0.728	0.638	0.701	0.840	0.554	0.599	0.681	0.814
H [m]	0.720	0.787	0.850	0.797	0.873	0.603	0.703	0.667	0.717	0.687	0.773	0.625	-	-	0.860
$\bar{n}'$ [m]	0.433	0.487	0.507	0.500	0.583	0.350	0.443	0.483	0.463	0.420	0.540	0.413	-	-	0.579
h [-]	0.0433	0.0703	0.0489	0.0411	0.0603	0.0550	0.0537	0.0559	0.0601	0.0519	0.0676	0.0601	0.0726	0.0744	0.0824
$\lambda/L_{pp\,A}$ [-]	1.347	0.938	1.315	1.576	1.310	1.045	1.029	1.113	1.125	1.306	1.168	1.027	0.954	1.194	1.250
Q_p [-]	3.80	4.24	3.82	3.42	4.05	4.14	2.32	2.43	2.52	2.17	2.69	1.98	4.84	4.81	4.58
GF [-]	0.881	0.823	0.906	0.879	0.884	0.716	0.856	0.940	0.904	0.739	0.850	0.663	0.721	0.676	0.716
Φ_{HH1} [-]	0.529	0.497	0.532	0.531	0.529	0.531	0.278	0.281	0.332	0.238	0.349	0.131	0.233	0.222	0.209
J_1 [-]	1.86	1.81	1.61	1.53	1.85	1.37	1.38	1.33	1.43	1.34	1.46	1.20	1.30	1.17	1.44

there are limited length of records, insufficient digitalization frequency and too small number of components. The shape of the spectrum can be described by the peakedness parameter Q_p introduced by Goda. This value as well as some grouping parameters now were averaged over all measurements within the three groups of spectral shape J, P and B. Thereby only the seaways composed of 560 components were used. The mean values and their standard deviations are given in Table 2 whereas in Figure 4 the mean values are drawn as function of Q_p in comparision to the results of Rye derived from numerical simulations. With the exception of r_{HT} the results of the tests and simulations are more or less similar and of the same tendency; thereby one has to keep in mind the wide scatter expressed by the standard deviations. The best agreement can be recognized for the correlation factor Φ_{HH1} for two successive wave heights.
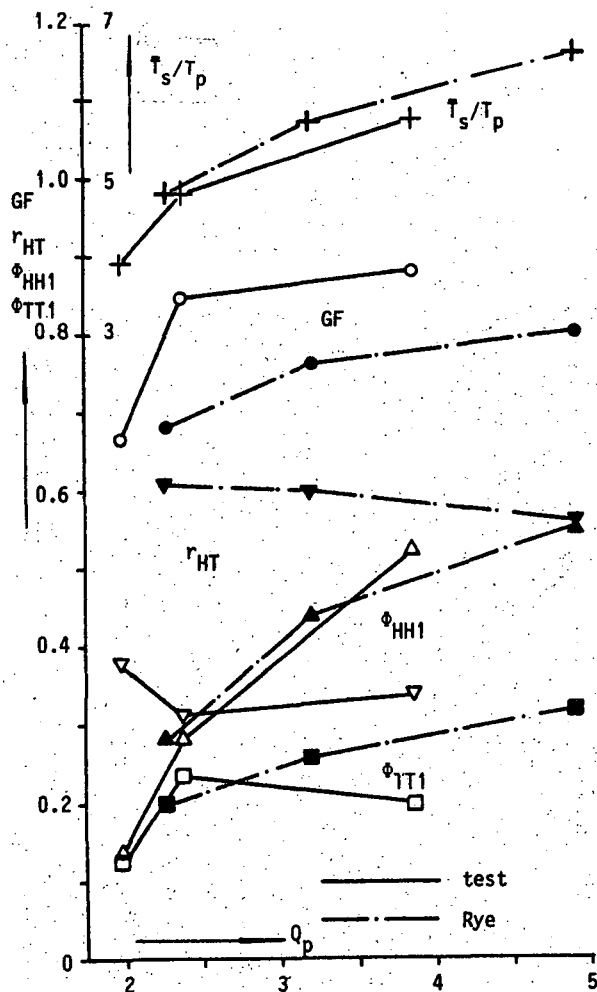
Fig. 4 Grouping parameters as function of the peakedness parameter

Tab. 2 Averaged grouping parameters and their standard deviations

Spectr.	JONSWAP, $\gamma = 5$ mean	S	Pears.-M.-Sp mean	S	wide spec mean	S
GF	0.878	0.0539	0.847	0.0860	0.663	-
$\bar{T}_s/T_p$	5.78	0.579	4.80	0.504	3.90	-
r_{HT}	0.333	0.0969	0.314	0.0984	0.378	-
Φ_{HH1}	0.525	0.0576	0.284	0.0575	0.131	-
Φ_{TT1}	0.192	0.0883	0.236	0.0756	0.126	-
Q_p	3.86	0.262	2.37	0.209	1.98	-

In Figure 5 the dependency of the grouping parameters from the number n of the harmonic components within the control signal for the wave maker is shown. Here the values have been averaged over 6 measurements of the seaways I, II and III with only 20 components, 4 measurements of seaway J 2.2-100 with 100 components and 21 measurements of all J - seaways with 560 components. In spite of an decreasing Q_p - value the grouping parameters and the ratio of maximum to significant wave height increases with increasing number of components.
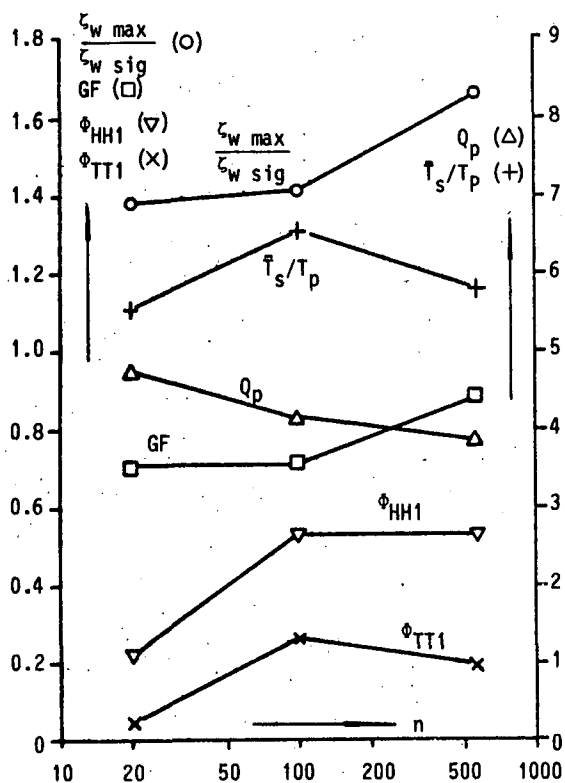
Fig. 5 Grouping parameters and maximum wave height
        as function of number of components

ship A

ship C
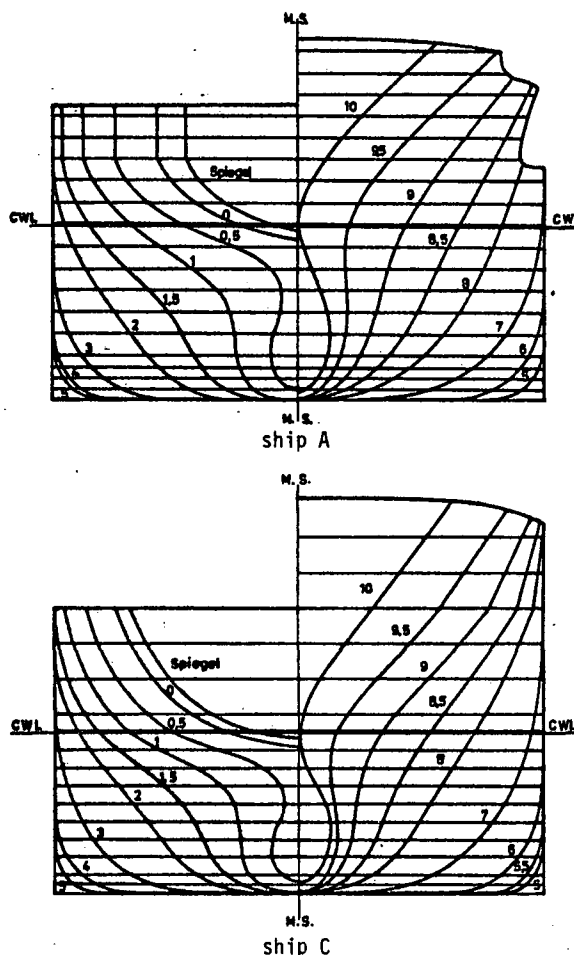
Fig. 6 Cross sections

3. MODELS AND TEST PROCEDURE

As already mentioned two models named A and C
from an earlier investigation have been used again.
The main dimensions of the models are compiled in
Table 3 and the Figure 6 shows their cross sections.

Tab.3   Main dimensions of the models

	model A	model C
LPP [m]	4.821	4.938
LOA [m]	5.180	5.272
B [m]	0.821	0.875
T [m]	0.293	0.344
D [m]	0.382	0.503
V [m³]	0.783	0.985
CB	0.675	0.663
CWP	0.816	0.849
LPP/B	5.87	5.64
B/D	2.15	1.74
B/T	2.80	1.74
D/T	1.30	1.46

The models were tested at one draught only on
desired courses of 0 and 30 degree relative to the
waves (0 degree means following waves). During all
tests a static heeling moment was acting on the
model producing a heeling angle of 2 degrees. The
free running model was hand operated by a helmsman
being accommodated on a subcarriage in front of the
main carriage. The model was connected to this
subcarriage by flexible cables for energy supply and

data transmitting. Carriage and subcarriage followed
the model so that no considerable forces acted onto
the model. Due to the restricted width of the tank
(18 m) the model had to be steered on
zig-zag-courses at the tests with 30 degree relative
course.

For each seaway a starting delay relative to
the start of the wave maker was determined at the
first trials and then kept constant so that the
model always met the same wave group. During the
tests these wave groups were recorded by a video
camera which was directed at the opposite tank wall.
The same wave shape was recorded at all tests in a
particular seaway but the position of the model
relative to the crests differed from test to test a
little bit due to unavoidable changes in speed and
course. So the main wave crests were met in
different phases of their development. This fact
contributes essentially to the scatter of the
measured data and is the reason that a large number
of runs is needed for the same condition with
respect to seaway, desired course and load
condition.

From these video recordings also the wave
heights $\bar{H}$ and heights $\bar{\eta}'$ of the crests above the
mean water level mentioned in the section before
were determined. Of course one cannot expect the
same accuracy as for direct measurements. Thereby

the height $\bar{\eta}'$ of the crests turned out to be more reliable and more important.

The tests were performed in the different seaways and at both courses for two to four different heights of the center of gravity in order to find the limit between safe and unsafe. For a better statistical reliability at least 10, partly up to 23 runs were conducted at the same conditions. So altogether nearly 1000 single runs were necessary during this investigation.

For the judgement of the safety against capsizing the remaining area E_R under the smooth water righting lever curve beyond the measured maximum heeling angle ϕ_{max} was used. From the E_R-values of each run the mean value $\bar{E}_R$ and the standard deviation s were calculated from all tests at the same condition. For a safe ship it is required that the mean value diminished by three times the standard deviation is equal or larger than zero:

$$(\bar{E}_R - 3\ s) \geq 0$$

Figure 7 shows an example where $\bar{E}_R$ and $\bar{E}_R - 3\ s$ are drawn as function of the metacentric height. From these graphs the limiting values of GM_0 can easily be found. In the Figures 8 and 9 the righting lever curves at the limit between safe and unsafe for the different test seaways are shown for both models.

From these curves stability parameters can be derived which are compiled in the Tables 4 and 5. Here also the results from the earlier investigation with seaway I, II and III are included.

4. CONCLUSIONS FROM THE TEST RESULTS

From the earlier investigation it was learned that from the considered stability parameters the maximum rightimg lever GZ_m and the total area E_0 under the righting lever curve seems to be most appropriate for the discrimination between safe and unsafe. Therefore the following considerations are restricted to these two parameters. Certainly the wave height is the most important seaway parameter. In the Figures 10 and 11 the lever GZ_m and the area E_0 are shown in dependency of the significant wave height $4\sqrt{m_0}$. The large scatter clearly indicates that the significant wave height alone is not sufficient to describe the severity of a seaway with regard to the safety against capsizing. For example the necessary lever GZ_m in a JONSWAP-seaway is about 1.5 times larger than in seaway B 2.2 at the same wave height. For the area E_0 this ratio is even about 2. This is true for both models, but the values for the model C are much lower than for model A due to the more favourable form of this model.

The stability parameters of both ships can be made comparable by multiplying them with the hull form factor C which has been introduced in [2]. The factor is defined by the equation

$$C = \frac{T \cdot D'}{B^2} \sqrt{\frac{T}{KG}} \ \frac{CB}{CWP} \sqrt{\frac{L_0}{L}}$$

Further details can be found in [2] or in the contribution by Hormann and Wagner. For the base length L_0 here a model value $L_0' = 100\ m\ /28 = 3.57\ m$ was used (28 is the original scale of model A). Depending on the height of the center of gravity the hull form factors differ at the same model as the case may be, but the factors for model C are much higher than for model A:

model A: $\quad C = 0.1274 \sqrt{\frac{T}{KG}}$

model C: $\quad C = 0.1761 \sqrt{\frac{T}{KG}}$ with KG/T $\geq$ 1

After the multiplication with the hull form factor the stability parameters of both models don't show a significant difference for the same seaway. This is supported by the t-test on differences [6]. The t-value can be calculated easily from the differences d, their standard deviations s and the number n of tests (here 8 pairs):

$$t = \frac{\bar{d}}{s_d/\sqrt{n}}$$

Here the values t = 0.500 and t = 0.886 were determined for the differences of $C*GZ_m$ and $C*E_0$ respectively which both are to be compared with the values t_α = 2.365 and 3.499 for a level of significance of 5% and 1% respectively. The smaller values of t clearly indicate that there is no significant difference between the weighted stability parameters of both models contrary to the unweighted parameters (for which t = 8.073 and t = 5.912 were determined). That means the hull form factor works very well and the relative order of both models with respect to the safety against capsizing is always the same indepent from the used seaway.

Now correlations between the weighted stability parameters and a set of seaway parameters were calculated by linear regression. The finally selected set of seaway parameters x can be taken from Table 6 which contains the results of the regression. There are given the mean value $\bar{y}$ and the standard deviation S_y of the stability parameters, the coefficients a and b of the regression line y = ax + b, the standard deviation S_{xy} relative to the regression line and the correlation coefficient

$$r = \sqrt{\frac{S_y^2 - S_{xy}^2}{S_y^2}}$$

As expected the best correlation coefficients at the single seaway parameters in the upper part of the table can be found for the crest height $\bar{\eta}'$. By adding the mean wave length ratio and mainly the

Table 4 Stability parameters at the limit between safe and unsafe for model A

seaway	KG [mm]	GM_0 [mm]	GZ_{30} [mm]	GZ_{40} [mm]	GZ_m [mm]	ϕ_m [Grad]	ϕ_0 [Grad]	E_{30} [mm rad]	E_{40} [mm rad]	E_{30}-E_{40} [mm rad]	E_m [mm rad]	E_0 [mm rad]
J 1.2	306	45	19.4	18.7	19.9	34	56.8	5.83	9.26	3.43	7.31	12.35
J 2.2	294	57	24.3	26.4	26.8	37	63.7	7.40	12.01	4.26	10.49	18.57
J 2.3	299	52	22.8	23.3	23.9	37	61.0	6.77	10.90	4.13	9.45	15.87
J 3.2	283	68	30.8	33.5	33.7	38	71.0	8.90	14.66	5.76	13.22	25.37
P 0.2	301	50	21.8	22.0	22.7	36	60.0	6.49	10.41	3.92	8.84	14.88
P 1.2 P 2.3 J 2.2 -100	296	55	25.3	25.1	25.4	37	62.7	7.174	11.58	4.41	7.84	17.51
P 2.2 J 2.1	292	59	26.3	27.7	28.1	37	65.0	7.71	12.53	4.83	11.23	19.68
P 3.2	286	65	29.3	31.6	31.9	38	69.2	8.41	13.88	5.46	12.51	23.29
B 2.2	308	43	18.3	17.5	18.8	34	55.5	5.49	8.70	3.22	6.77	11.39
I, II	291	61	26.8	28.6	28.9	38	66.5	7.86	12.86	5.00	11.96	20.71
III	300	52	22.5	23	23.9	37	61.0	6.79	10.86	4.07	9.57	15.75

Table 5 Stability parameters at the limit between safe and unsafe for model C

seaway	KG [mm]	GM_0 [mm]	GZ_{30} [mm]	GZ_{40} [mm]	GZ_m [mm]	ϕ_m [Grad]	ϕ_0 [Grad]	E_{30} [mm rad]	E_{40} [mm rad]	E_{30}-E_{40} [mm rad]	E_m [mm rad]	E_0 [mm rad]
J 2.2	363	25	17.6	21.8	23.8	48	71.8	4.25	7.61	3.36	10.84	17.11
J 2.3	371	17	12.7	16.7	17.8	47	66.8	3.21	5.79	2.58	7.93	11.81
J 3.2	361	27	17.7	23.1	25.2	49	73.6	4.51	8.09	3.58	11.76	18.38
P 2.2	368	20	14.2	18.6	20.0	47	70.0	3.60	6.47	2.87	8.85	13.81
B 2.2	376	12	10.2	13.4	14.4	46	63.4	2.56	4.62	2.06	6.10	8.98
I	369	19	13.4	17.8	19.7	47	68.0	3.47	6.16	2.72	8.50	12.84
II	371	17	12.8	16.9	18.4	47	67.0	3.25	5.81	2.56	8.00	11.94
III	374	14	11.3	14.7	16.3	46	64.5	2.81	5.09	2.28	6.72	10.06
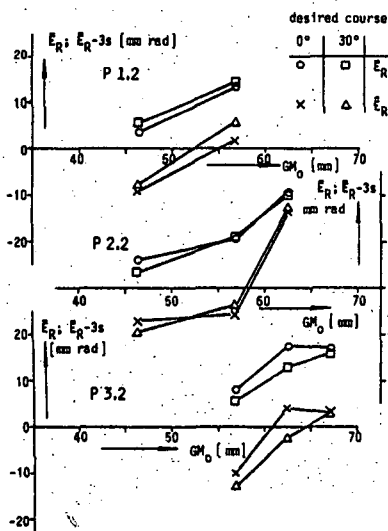
Fig. 7 Determination of GM_0 at the limit between safe and unsafe
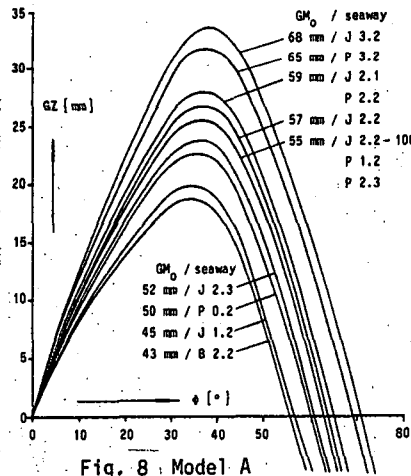
Fig. 8 Model A
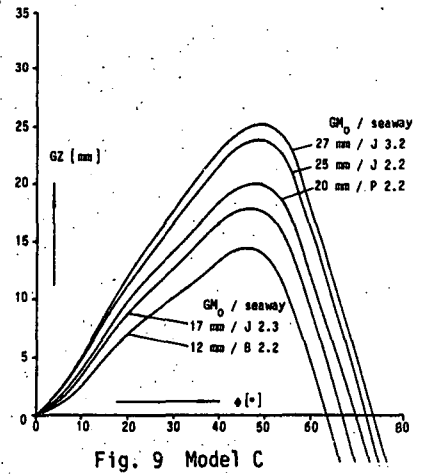
Fig. 9 Model C

Righting lever curves in calm water at the limit between safe and unsafe

Table 6 Results of the regression analysis

	stability parameter							
	C·GZm				C·E₀			
	for $4\sqrt{m_0}$, $\zeta_{w\,sig}$, $\zeta_{w\,max}$		for R, n̄'		for $4\sqrt{m_0}$, $\zeta_{w\,sig}$, $\zeta_{w\,max}$		for R, n̄'	
N	23		19		23		19	
ȳ	3.309 mm		3.345 mm		2.269 mm rad		2.307 mm rad	
Sy	0.559 mm		0.591 mm		0.508 mm rad		0.529 mm rad	
seaway parameter (x)	a [-]	b [mm]	S_{xy} [mm]	r [-]	a [rad]	b [mm rad]	S_{xy} [mm rad]	r [-]
$4\sqrt{m_0}$	0.002917	2.050	0.508	0.416	0.002462	1.206	0.468	0.387
$\zeta_{w\,sig}$	0.003627	1.770	0.491	0.478	0.003082	0.961	0.454	0.447
$\zeta_{w\,max}$	0.004319	0.438	0.413	0.674	0.003843	-0.286	0.381	0.660
R	0.004482	-0.048	0.428	0.690	0.003866	-0.620	0.395	0.665
n̄'	0.006197	0.329	0.423	0.697	0.005385	-0.313	0.390	0.667
$4\sqrt{m_0} \cdot GF \cdot f(\lambda/L)$	0.007974	0.650	0.360	0.766	0.007007	-0.068	0.341	0.741
$4\sqrt{m_0} \cdot \Phi_{HH1}^{1/2} \cdot f(\lambda/L)$	0.009174	1.115	0.314	0.827	0.008178	0.313	0.296	0.812
$n̄' \cdot f(\lambda/L)$	0.006804	0.153	0.405	0.727	0.005929	-0.475	0.374	0.708
$n̄' \cdot \Phi_{HH1}^{1/4} \cdot f(\lambda/L)$	0.007682	0.562	0.319	0.842	0.006782	-0.149	0.295	0.830
$\zeta_{w\,max} \cdot f(\lambda/L)$	0.004039	0.706	0.430	0.639	0.003587	-0.044	0.396	0.625
$\zeta_{w\,max} \cdot \Phi_{HH1}^{1/4}$	0.005559	0.511	0.311	0.832	0.005015	-0.256	0.286	0.826
$\zeta_{w\,max} \cdot \Phi_{HH1}^{1/4} \cdot f(\lambda/L)$	0.006310	0.236	0.270	0.875	0.005686	-0.501	0.251	0.869

$$f(\lambda/L) = exp(-0.5\,(\bar{\lambda}/L - 1)^2)$$

grouping parameter Φ_{HH1} the correlation could be improved as shown in the lower part of the table.

The mean crest height n̄' of the actual encountered waves can be determined only with a larger effort. Therefore the crest height is not a good choice for the comparison of routine tests. Instead of n' the wave height $\zeta_{w\,max}$ measured at one (ore more) stationary positon(s) can be used with about the same results.

The ratio $\zeta_{w\,max}/\zeta_{w\,sig}$ and Φ_{HH1} are dependent from spectral shape and number of components with a similar tendency. So the maximum wave height in the seaway parameter also can be replaced by $4\sqrt{m_0}$ and the ratio can be included in the dependency from Φ_{HH1}. For the practical use therefore the following parameters offered themselves for the description of the severity of an irregular seaway with regard to the safety against capsizing:

$$P_{mo} = 4\sqrt{m_0}\ \Phi_{HH1}^{1/2}\ exp(-0.5(\bar{\lambda}/L - 1)^2)$$

$$P_{max} = \zeta_{w\,max}\ \Phi_{HH1}^{1/4}\ exp(-0.5(\bar{\lambda}/L - 1)^2)$$

The Figures 12 to 15 show $C*GZ_m$ and $C*E_0$ as function of these both seaway parameters. Different symbols indicate the different types of spectrum, open and solid symbols distinguish between model A and C. Additionally the regression lines and the range plus/minus 10 % are drawn. At the weighted lever $C*GZ_m$ nearly all measured points are within the plus/minus 10 %. At the weighted area $C*E_0$ the scatter is somewhat larger. But certainly the still existing scatter can be reduced scarcely because the

accuracy of the single measurements also is not higher and cannot be increased in a simple way due to the plurality of influences which are not under control.

Summarizing one can state the following from this investigation:

- with regard to the seaway the height and length or shape of the actual encountered wave crests are of importance, but these data can be measured only with larger effort.

- two succeeding high waves raise the danger of capsizing considerably, but from a higher number of waves doesn't follow a significant additional increase.

- herewith the grouping properties become important. An irregular seaway for capsizing tests should contain sufficient high and continous wave groups. Therefore the spectrum should be not to wide. For the classification of different seaways with regard to their severity two parameters are proposed which are composed from wave height, mean wave length ratio and a grouping parameter.

- with regard to the test procedure it is recommendable for tanks with their restricted length to start with the tests always at the same position with a fixed time delay relative to the start of the wave maker. So the model always meets the same wave train as good as possible, the seaway becomes deterministic. Is this not possible, e.g. at open air tests on a lake one needs very long test runs to meet the desired dangerous situations. In every case repetitions of tests are necessary as much as
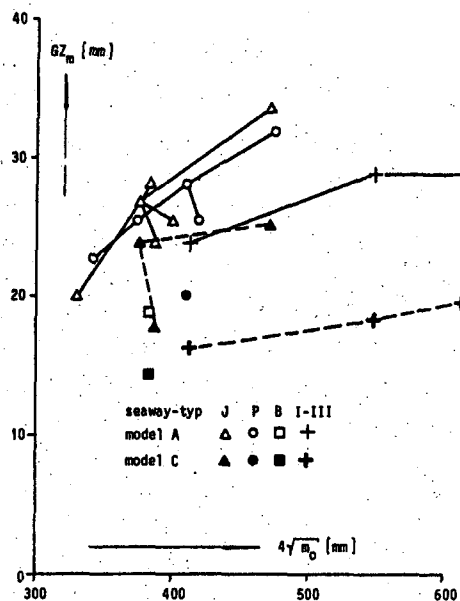
Fig. 10 Righting lever GZ_m at the limit between safe and unsafe
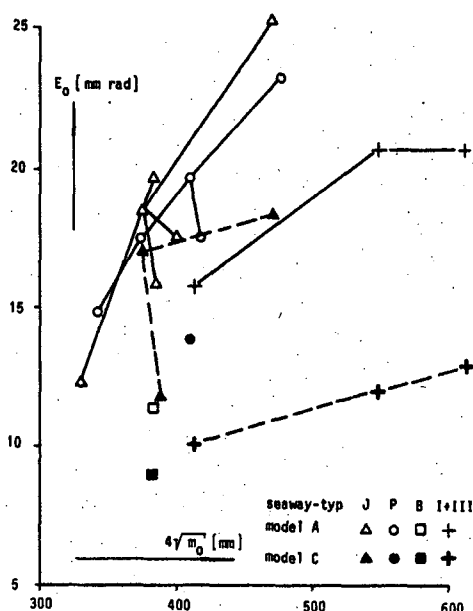
Fig. 11 Area E_0 at the limit between safe and unsafe
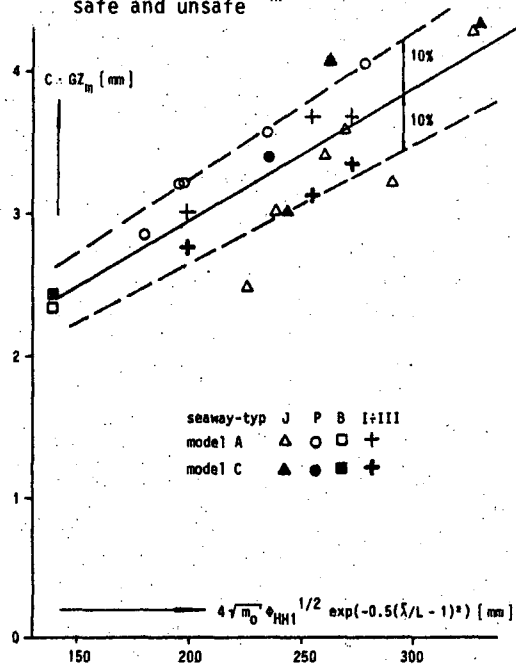
Fig. 12 Weighted lever GZ_m as function of the seaway parameter P_{mo}
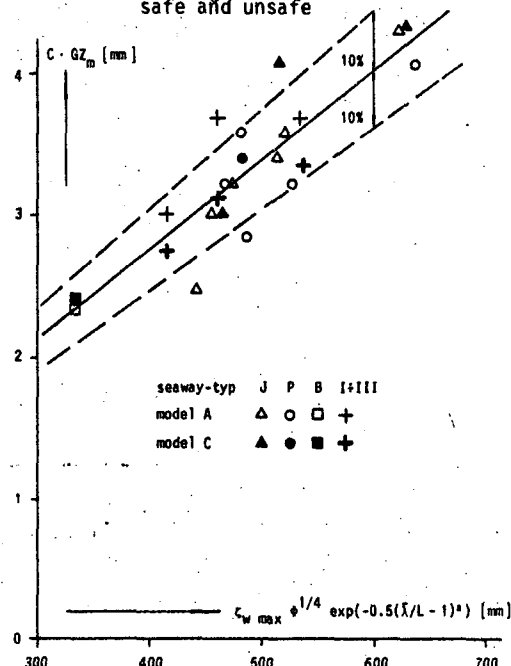

Fig. 13 Weighted lever GZ_m as function of the seaway parameter P_{max}
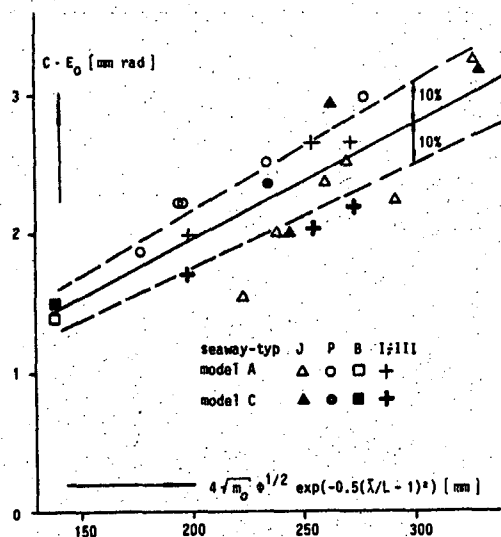
Fig. 14 Weighted area E_0 as function of the seaway parameter P_{mo}
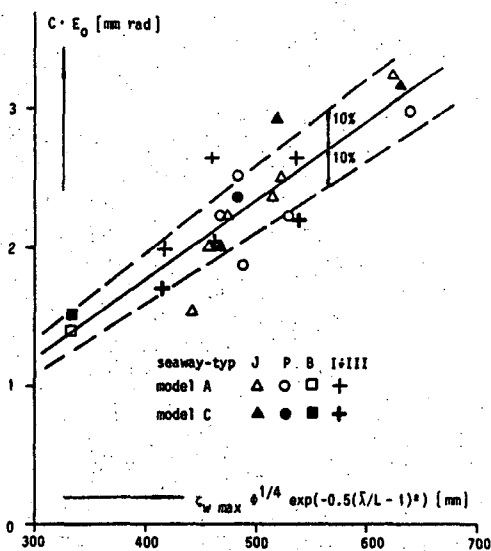
Fig. 15 Weighted area E_0 as function of the seaway parameter P_{max}

possible due to the stochastic nature of many influence factors.

ACKNOWLEDGEMENT

NOMENCLATURE

B	beam
C	hull form factor
CB	block coefficient
CWP	waterplane coefficient
E_{30}, E_{40}, E_m	area under the righting lever curve up to 30, 40 deg. and the maximum
E_o	total area under the lever curve
E_R	area beyond ϕ_{max}
GF	grouping factor
GM_o	metacentric height
GZ	righting lever
GZ_m	maximum righting lever
$h = \dfrac{2 \, m_o}{g \, \pi \sqrt{m_o}}$	significant steepness
$\mathcal{H}$	wave height in a wave group
J_1	mean number of waves in a group
KG	height of center of gravity above base
L, LPP	length between perpendiculars
LOA	length over all
m_o	variance of the seaway
P_{mo}, P_{max}	seaway parameter
Q_p	peakedness parameter
r	correlation coefficient
η_{HT}	correlation coefficient for wave height and period
S, s	standard deviation
$S(\omega)$	spectral density
T	draught
T_p	peak period
T_s	mean period of SIWEH
V	volume displacement
γ	enhancement factor
$\zeta_{w \, sig}$	mean of the upper 1/3 of wave heights
$\zeta_{w \, max}$	maximum wave height
λ	mean wave length
ϕ_{max}	maximum heeling angle
ϕ_{HH1}, ϕ_{TT1}	correl. coefficient for 2 successive wave heights and periods respectively
ω	circular frequency

REFERENCES

1. P. Blume, H.G. Hattendorff, An Investigation on Intact Stability of Fast Cargo Liners, II. International Conference on Stability of Ships and Ocean Vehicles, Tokyo, October 1982

2. Report on Stability and Safety against Capsizing of Modern Ship Designs, International Maritime Organization, Paper SLF/34, submitted by the Federal Republic of Germany

3. Y. Goda, On Wave Groups, Conference on Behaviour of Offshore Structures (BOSS), Trondheim, 1976

4. E.R. Funke, E.P.D. Mansard, On the Synthesis of Realistic Sea States in a Laboratory Flume, National Research Council, Hydraulics Laboratory, Canada, Report LTR-HY-66, 1979

5. H. Rye, Ocean Wave Groups, The Norwegian Institute of Technology, Univ. Trondheim, Report No. UR-82-18, 1981

6. E.L. Crow, F.A. Davis, M.W. Maxfield, Statistics Manual, Dover Publications, New York, 1960

EXPERIMENTAL STUDY ON PURE LOSS OF STABILITY
IN REGULAR AND IRREGULAR FOLLOWING SEAS

N. Umeda, Y. Yamakoshi

ABSTRACT

The authors undertook to study the pure loss of stability of a ship travelling in following seas. We measured the stability of a model ship towed with a heel angle in regular waves. The results were then compared with hydrostatic computations which to some extent were able to predict such measured values. Further, We confirmed that the relation between wave and stability is non-linear. Thus one cannot easily predict stability in irregular waves.

To bypass this difficulty, we made a stochastic representation based on the concept of Grim's effective wave: an irregular wave profile is approximated by a regular wave which is called "the effective wave." Moreover, we carried out our model experiments in irregular waves. The measured values of stability were similar to those predicted by using the hydrostatic computation and the concept of the effective wave. However, there are some difficulties in utilizing this method of prediction for practical purposes.

1 INTRODUCTION

The pure loss of stability in following seas is an important factor of the capsizing of ships. The transverse stability of a ship is drastically reduced when a wave crest moves into the amidship position.

Many studies on stability in regular following seas have been made.[1]-[4] They show that hydrostatic computations can predict experimental values to a certain degree. If stability variation are linear phenomena, stability variation in irregular seas can easily be predicted with a linear superposed method. However, the relation between stability and wave does not have any linearity. Therefore it is difficult to predict stability in irregular following seas.

Grim[5] proposed the concept of an effective wave to predict safety in irregular following seas. However, he did not make a stochastic presentation of stability itself. The capsizing depends on the successive time of stability loss. Thus Grim also proposed to use the time mean of the effective wave. However, this notion is not directly connected with the actual occurrence of capsizing. Krappinger[6] computed the probability of capsizing by making use of Grim's effective wave concept. Further, he compared this results with the results of model experiments. Nonetheless he was unable to clarify the validity of the effective wave concept because of the difficulty of carrying out capsizing experiments. On the other hand, Kastner[7] carried out time domain simulation based on hydrostatic theory. Further he discussed the spectra and probability distribution of stability variation. His results were not unfruitful; however, the procedure cannot easily be employed for practical purposes. Recently Helas [8] proposed a stability criterion based on the effective wave concept.

We the authors think that Grim's effective wave concept is an excellent one because stability variation are non-linear phenomena. Thus we attempted to apply this concept by making model experiments on stability variation. In this regard, it is easier to record many peaks of stability variation than to observe many capsizing; which is why we only measured stability variation in our model experiments. These results should prove helpful whenever the effective wave concept is utilized for stability criteria.

2 EXPERIMENTAL TECHNIQUE

In order to evaluate stability variation in waves, we carried out a captive model tests with heeled model in both regular waves and in irregular waves. The model tested was a coastal small trawler whose particulars are shown in Table 1

and whose body plan is shown in Fig.1.

Fig.2 shows a picture of the set-up for these experiments. The model was free with regard only to pitch and heave, which were measured by potentiometer. The heel angle φ of 10 degrees was fixed. A rigthing moment and a ship resistance acting on the heeled model were measured by a dynamometer. The encounter wave heights were recorded by a servo-operated type of wave probe attached the towing carriage. The heeled model was towed with constant velocity in following waves generated by a flap-type wavemaker with constant velocity. The irregular waves generated in the basin had a significant wave height of about 0.0655 meters and a mean wave period of about 1.39 seconds in model scale. The spectrum of waves was defined by the ITTC spectrum. There are some difficulties in the experiments in irregular following waves because a length of record per one run is restricted on the length of towing tank. To reach the sufficient number of cycles multiple runs were made in irregular following waves.

3 STABILITY IN REGULAR FOLLOWING SEAS

We computed the stability variation in regular waves by integrating the water pressure around the form of the model hull. The disturbances caused by the ship model were assumed to be negligible as higher order values; the sinkage and trim were assumed to be balanced in the waves. We carried out our computations in a two fold manner, both with the effect on the wave orbital velocity (Smith's effect) taken into account and with the same effect neglected.

Further, we compared our computed results with the results of experiments described in section 2. These values were expanded in Fourier series. The phase lag ($\epsilon/2\pi$) corresponds to the relative position of the model to the wave where the stability is the largest. When the center of gravity of a model is situated in any of four positions -- the wave trough, up slope, crest and down slope--, then its relative position is 0.0, 0.0-0.25-0.5, 0.5 and 0.5-0.75-1.0 respectively.

Figs.3 - 6 show the first-order varying component $GM(\omega)$ of stability in regular waves. According to computations and experiments, the amplitude of response has a peak at the situation (λ/L =1.0 ; λ is the wave length); roughly speaking, the amplitude of stability is proportional to wave amplitude. The values computed without the Smith's effect coincided with the values measured for Fn = 0.0. However, some discrepancy occurred because the measured values

decreased with the increasing Froude number. Both the measured values and the computed values show that the stability is larger when a wave trough moves into the center of a model; stability is smaller when a wave crest moves into its center.

Fig. 7 shows the steady component GM(0) and the second order varying component GM(2ω) of stability in waves. Since these components are not smaller than first order components, stability in waves is concluded to possess non-linear properties. Further, some similarity was found between computed values and measured values. On the other hand, there was some discrepancy in steady component in waves whose height was low.

In general, our hydrostatic computations accounted for the stability variation. However, the any dependence on the Froude number cannot be interpreted by such computations. Moreover, though the Smith's effect is not small, it too cannot explicate speed dependence. We believe that one must take into account the disturbance engendered by a ship itself in order to obtain adequate agreement between empirical experiment and abstract computation.

4 STOCHASTIC THEORY ON THE STABILITY

4.1 Grim's effective wave[5]

We consider that a ship runs in irregular following waves which have the spectrum $S(\omega)$. Grim proposed the concept of the effective waves. An irregular wave profile around the ship is replaced with a regular wave by a least square method. The length of the regular wave is equal to the ship length (between perpendiculars) L . The crest or the trough of the wave is situated at the center of gravity. The stability variation has an apparent peak under this condition ,which was examined in section 3. Grim called this regular wave " the effective wave",of which ζeff is the amplitude.

The spectrum of the effective wave Seff(ω) is derived from the least square method.

$$S_{eff}(\omega) = S(\omega)$$
$$\cdot [\frac{(\omega^2 L/g)\sin(\omega^2 L/2g)}{\pi^2 - (\omega^2 L/2g)^2}]^2 \quad (1)$$

Furthermore, Grim discussed the stochastic properties of the effective wave. However the goal which we set out to achieve was to get the stochastic properties of stability itself. We derived these properties of stability as indicated in the following sections.

4.2 Stability in the effective wave

One can compute stability in the effective wave GZw by making use of the hydrostatic method described in section 3. Fig.8 shows a computational result concerning the model ship used in our experiments. This computation does not consider the Smith's effect. The relation between stability and the effective wave are expressed as follows:

$$GZ_w = F(\zeta_{eff}) \qquad \zeta_{eff} = G(GZ_w) \qquad (2)$$

This relation is not only non-linear but also non-memory. The concept of the effective wave can simplify the memory effect, that is, the frequency dependence. In referring to double amplitude, this relation is also expressed as follows;

$$GZ_w{}^d = f(2\zeta_{eff}) = f(\zeta_{eff}{}^d) = F(\zeta_{eff}) + F(-\zeta_{eff}) \qquad (3)$$

To simplify the following formula, we assumed that $F(\zeta eff)$ is a monotonic increase function.

4.3 Significant amplitude

We can regard the effective wave as a narrow-band Gaussian process of which the mean is zero. Therefore the double amplitude distribution p is similar to Rayleigh distribution:

$$p(\zeta_{eff}{}^d) = \frac{\zeta_{eff}{}^d}{m_0} \exp\left[-\frac{\zeta_{eff}{}^{d2}}{2m_0}\right] \qquad (4)$$

Here, m_0 is the variance of the effective wave. Concerning the relation between the effective wave and the stability, namely,

$$p(GZ_w) \, dGZ_w = p(\zeta_{eff}{}^d) \, d\zeta_{eff}{}^d \qquad (5)$$

the significant double amplitude of the stability $(GZ)_{1/3}$ is proved as follows:

$$(GZ)_{1/3} = 3\int_{\sqrt{2m_0 \ln 3}}^{\infty} f(\zeta_{eff}{}^d)$$

$$\cdot \frac{\zeta_{eff}{}^d}{m_0} \exp\left[-\frac{\zeta_{eff}{}^{d2}}{2m_0}\right] d\zeta_{eff}{}^d \qquad (6)$$

4.4 Zero crossing mean period

The number of up-crossing per unit time of stability variation is given by

$$E[N_+(k_0)] = \frac{1}{2}\int_{-\infty}^{\infty} |\dot{k}| f_{k\dot{k}}(k_0, \dot{k}) \, d\dot{k} \qquad (7)$$

where k is GZw; k_0 is the threshold of GZw. The

probability density function of the stability variation $f_{k\dot{k}}$ is given by

$$f_{k\dot{k}}(k, \dot{k}) = f_{\zeta\dot{\zeta}}(G(k), \dot{k}\dot{G}(k)) \frac{\partial(\zeta, \dot{\zeta})}{\partial(k, \dot{k})} \qquad (8)$$

$f_{k\dot{k}}$ is the probability density function of the effective wave which one can evaluate as the Gaussian process.

Therefore we can give the average time between successive zero up-crossing as follows:

$$T_z = \frac{1}{E[N_+(0)]} = 2\pi\sqrt{\frac{m_0}{m_2}} \qquad (9)$$

As a result, the zero crossing mean period of the stability variation is equal to that of the effective wave.

4.5 The expected number of stability loss intervals

Stability in following seas is assumed to be

$$GZ(t) = GZ_0 + GZ_w(t) \qquad (10)$$

where GZ_0 is stability in still water; GZw is stability variation which is treated as a stationary random process.

One can regard the situation at which GZ is negative as the loss of stability. Thus the conditions of stability loss intervals are given by

$$\frac{d}{dt}(GZ_w(t)) < 0$$

$$\frac{d}{dt}(GZ_w(t+\tau)) > 0 \qquad (11)$$

$$GZ_w(t) = GZ_w(t+\tau) = -GZ_0$$

Therefore, the expected number of stability loss intervals is given by

$$E[N_k(\tau)] = -\int_{-\infty}^{\infty}\int_{-\infty}^{\infty}\int_{-\infty}^{\infty}\int_{-\infty}^{\infty}$$

$$\cdot \dot{k}\dot{k}_\tau\delta(k+k_0)1(-\dot{k}-0)\delta(k_\tau+k_0)$$

$$\cdot 1(\dot{k}_\tau-0) f_{k\dot{k}k\dot{k}}(k, \dot{k}_\tau, k, \dot{k}_\tau) \, d\dot{k}d\dot{k}_\tau d\dot{k}d\dot{k}_\tau$$

$$= -\int_0^{\infty}\int_{-\infty}^0 \dot{k}\dot{k}_\tau f_{k\dot{k}k\dot{k}}(-k_0, -k_0, \dot{k}, \dot{k}_\tau) \, d\dot{k}d\dot{k}_\tau \qquad (12)$$

where k, k_τ and k_0 are GZw(t), GZw(t+τ) and GZ_0 respectively.

$f_{k\dot{k}k\dot{k}}$ is the four variable probability density function of stability. Considering the relation

between stability and the effective wave, it is proved that

$$f_{kkkk} (k, k_\tau, \dot{k}, \dot{k}_\tau) = f_{\zeta\zeta\dot{\zeta}\dot{\zeta}} (\zeta, \zeta_\tau, \dot{\zeta}, \dot{\zeta}_\tau)$$

$$\cdot \frac{\partial (\zeta, \zeta_\tau, \dot{\zeta}, \dot{\zeta}_\tau)}{\partial (k, k_\tau, \dot{k}, \dot{k}_\tau)} = f_{\zeta\zeta\dot{\zeta}\dot{\zeta}} (G (k), G (k_\tau),$$

$$\dot{k}\dot{G} (k), \dot{k}\dot{G} (k_\tau), (\dot{G} (k)\dot{G} (k_\tau))^2 \qquad (13)$$

$f_{\zeta\zeta\dot{\zeta}\dot{\zeta}}$ is the four variable probability density function of the effective wave. Since the effective wave is regarded as a zero mean valued Gaussian process, one can give $f_{\zeta\zeta\dot{\zeta}\dot{\zeta}}$ by

$$f_{\zeta\zeta\dot{\zeta}\dot{\zeta}} (\zeta_0, \zeta_0, \dot{\zeta}, \dot{\zeta}_\tau)$$

$$= \frac{1}{4\pi^2 |\Delta|^{1/2}} exp [-\frac{1}{|\Delta|} (a \zeta_0^2 + b \zeta_0 (\dot{\zeta} - \dot{\zeta}_\tau)$$

$$+ d \dot{\zeta} \dot{\zeta}_\tau + 1/2 e (\dot{\zeta}^2 + \dot{\zeta}_\tau^2))] \qquad (14)$$

where the coefficients are:

$$a = (m_2 - m_2 (\tau)) [(m_0 - m_0 (\tau))$$

$$\cdot (m_2 + m_2 (\tau)) - m_1^2 (\tau)]$$

$$b = m_1 (\tau) [(m_0 - m_0 (\tau))$$

$$\cdot (m_2 + m_2 (\tau)) - m_1^2 (\tau)]$$

$$d = -m_2 (\tau) (m_0^2 - m_0^2 (\tau)) + m_0 (\tau) m_1^2 (\tau)$$

$$e = m_2 (m_0^2 - m_0^2 (\tau)) - m_0 m_1^2 (\tau)$$

$$|\Delta| = \frac{e^2 - d^2}{m_0^2 - m_0^2 (\tau)} > 0$$

$$m_0 = \int_0^{\omega_{max}} S_{eff} (\omega_e) d\omega_e$$

$$m_2 = \int_0^{\omega_{max}} \omega_e^2 S_{eff} (\omega_e) d\omega_e$$

$$m_0 (\tau) = \int_0^{\omega_{max}} S_{eff} (\omega_e) cos \omega_e \tau d\omega_e$$

$$m_1 (\tau) = -\int_0^{\omega_{max}} \omega_e S_{eff} (\omega_e) sin \omega_e \tau d\omega_e$$

$$m_2 (\tau) = \int_0^{\omega_{max}} \omega_e^2 S_{eff} (\omega_e) cos \omega_e \tau d\omega_e$$

If ω max takes the value of infinity, our computation involves case which have more than two peaks in a concerned interval. Some conventional methods have been presented to avoid such problem as this.[10] However, we adopt another method, in which ω max is $2\pi\alpha /t$ (1/2< α <1). In this method, the periodic behaviour of the component waves does not contribute to the final value. Further the final value did not depend on the arbitrary value of α with the restricted range (1/2< α <1). In addition, we used the wave-

length rather than the frequency as a variable to carry out our computations accurately.

4.6 Probability of capsizing

According to Krappinger [7] and Hirayama [11], the probability of capsizing is defined as the probability that a ship will have capsized in a stationary random sea before time tc. We assumed that an act of capsizing could be described by a Poisson process. Further, the case that stability loss interval exceeds the time interval τ_C is regarded as capsizing. Therefore the expected capsizing rate v is given by

$$v = \int_{\tau_0}^{\infty} E [N_k (\tau)] d\tau \qquad (15)$$

Moreover one can derive the probability of capsizing as follows:

$$p (t_c) = 1 - exp (-v t_c) \qquad (16)$$

5 STABILITY IN IRREGULAR FOLLOWING SEAS

The authors compared their experimental results with the computational prediction described in section 4.

The significant amplitude of stability $(H 1/3)' = (GZ)_{1/3} / (\zeta_W)_{1/3}$ is shown in Fig.9. The measured values decrease with the increasing Froude number. This tendency is similar to that in regular waves. The measured values for Fn=0.0 are much larger than the computed values . The component wave length corresponding to the critical frequency $\Omega = U \omega_e / g = 1/4$ where Fn=0.2 is equal to the ship length; U is the ship speed. In this case, the effective wave concept gives us a good approximation, because the encounter spectrum has a recognizable peak where $\Omega = 1/4$. The measured values for Fn=0.2 coincides with the computed values. However, hydrostatic computation in regular waves does not accurately estimate measured values at such a speed. Thus we conjectured that any errors of the hydrostatic computation, or any errors inherent in the effective wave concept ,or any errors in our experiment cancelled one another out.

In Fig.10, the zero up-crossing mean periods $T_z \sqrt{g/L}$ are shown. At the high speed situation Fn>0.2, some discrepancy between the measured values and calculated values occurred. This seemed to be caused by the fact that the analyzed time history was actually the sum of short time histories measured in each separated experiment.

Fig.11 shows the expected number of stability loss intervals. According to the measured

values and the computed values, the long stability loss intervals occur at high speed situations. The computed values are smaller than the measured values. In particular, this tendency is evident in a high speed situation. To obtain a satisfactory agreement, we must satisfactorily predict amplitude, time period, mean value and so on. We also carried out computations in which the experimental mean values corrected the threshold of stability. The dotted lines in Fig.11 show these results, which are much larger than the original computational results. Hydrostatic computation in regular waves does not well predict the steady component of stability. This component possibly involves higher order hydrodynamic forces. Therefore,in order to predict the expected number of stability loss intervals, we must correctly compute the mean value in irregular waves.

Fig.12 shows the computed probability of capsizing. In these computations, we used the computed values of E[N] with the correction mentioned above. We assumed that the initial stability GM_0/B was 0.338; the time of capsizing τc was 0.4. This diagram shows that the probability of capsizing is strongly dependent on the Froude number.

In general, the results of the stochastic prediction based on the effective wave concept are similar to the experimental results. However, we cannot conclude that this method can be used for a practical purpose as long as the authors discussed.

6 CONCLUSION

The authors believed they have confirmed that hydrostatic computation can to some extent predict stability variation measured in regular following seas. Our stochastic prediction method made use of hydrostatic computation and the effective wave concept, and was verified by the stability measurement of a model in irregular following waves.

REFERENCES
1. Watanabe,Y., "On the Dynamic Properties of the Transverse Instability of a ship due to Pitching," Journal of the Society of Naval Architects of Japan (J.S.N.A.),Vol.53,1934.
2. Paulling,J.R., "The Transverse Stability of a Ship in a Longitudinal Seaway," J.S.R., Vol.4,No.4,1961.
3. Upahl,E., "Ermittlung der Schiffsstabilität von Hecktrawlern in regelmässigem längslaufendem Seegang," Schiffbauforschung, 18,3/4,1979.
4. Hamamoto M. and Nomoto,K., "Transverse Stability of Ships in a Following Sea," Proceeding of 2nd International Conference on Stability of ships and Ocean Vehicles (STAB'82),1982.
5. Grim,O., "Beitrag zu dem Problem der Sicherheit des Schiffes im Seegang," Schiff und Hafen, Heft 6,1961.
6. Krappinger,O., "Über Kenterkriterion,"Schiffstechnik,Heft 48,1962.
7. Kastner,S., "Hebelkurven in unregelmässigem Seegang," Schiffstechnik,Bd 17,Heft 88,1970.
8. Helas,G., "Intact Stability of Ships in Following Waves," STAB'82,1982.
9. Price,W.G. and Bishop,R.E.D., "Probabilistic Theory of Ship Dynamics," Chapman and Hall,1974.
10. Takeuchi,S. and Yamamoto,Y., "Approximate Distribution and Simulation of Successive Extremes for Gaussian Random Process," J.S.N.A., Vol.131,1972.
11. Hirayama,T., "Experimental Study on the Probability of Capsizing of a Fishing Vessel in Beam Irregular Waves," J.S.N.A.,Vol.154,1983.

Table 1 principal particulars of ship

|		Ship	Model
Length B.P.	Lpp[m]	14.40	2.25
Breadth	B [m]	3.05	0.477
Draft Fore	df[m]	0.35	0.055
Aft	da[m]	1.396	0.2181
Displacement Volume	▽ [m³]	27.56	0.1051
C.G. from midship	lcb[m]	1.28	0.201
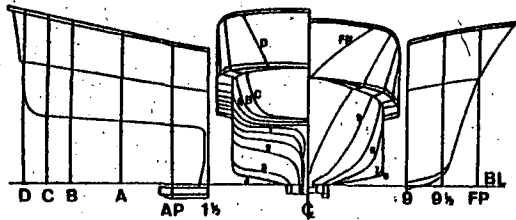
Fig.1 Lines of ship
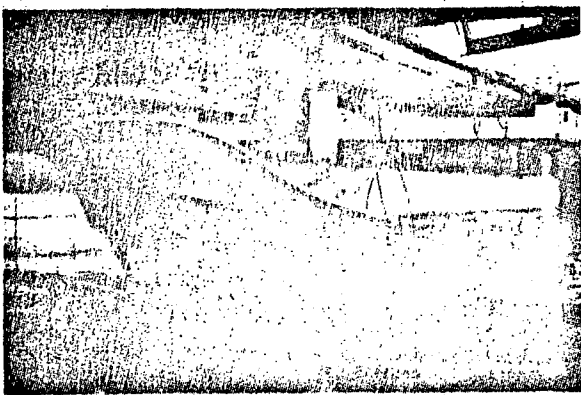
Fig.2 Photograph of experiment
in irregular waves

Fig.3 Stability variation in regular waves
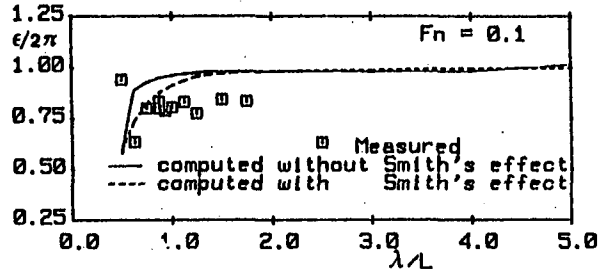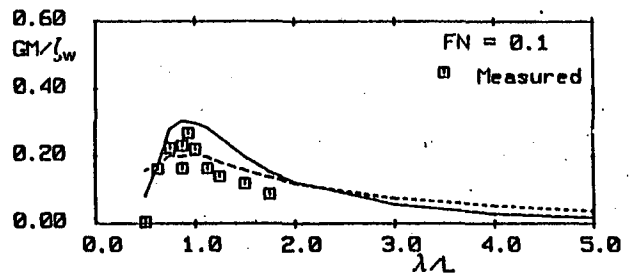
Fig.4 Stability variation in regular waves

Fig.5 Stability variation in regular waves
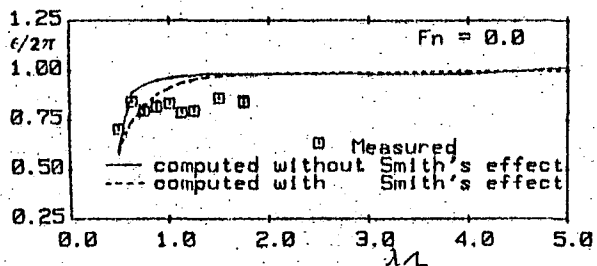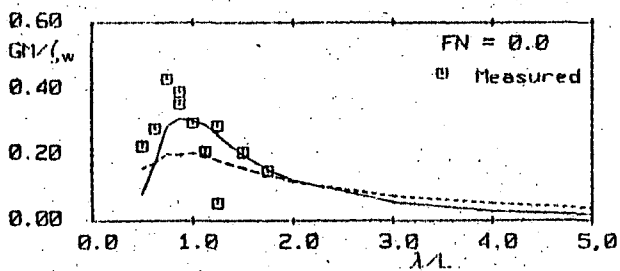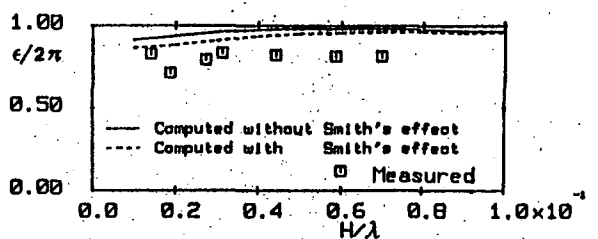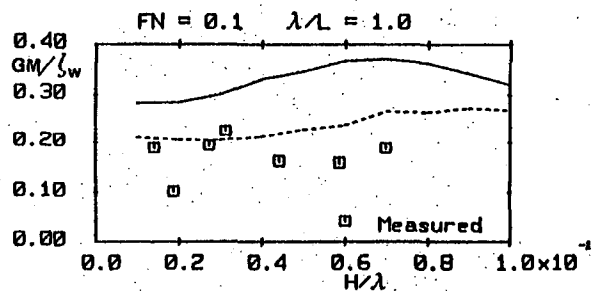
Fig.6 Stability variation in regular waves
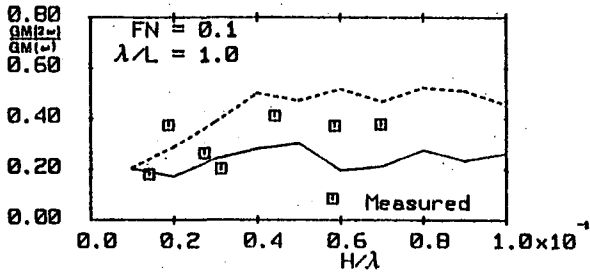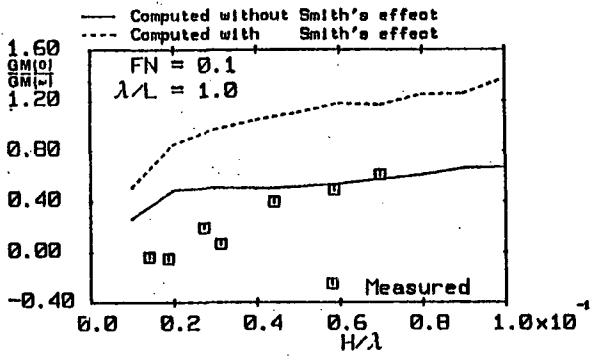
Fig.7 Higher order components of
stability variation
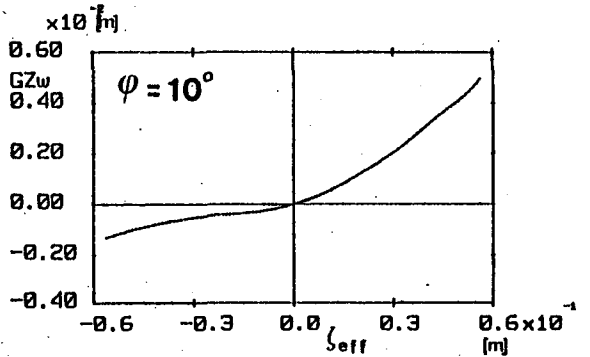
Fig.8 Computed stability
in effective wave (model scale)
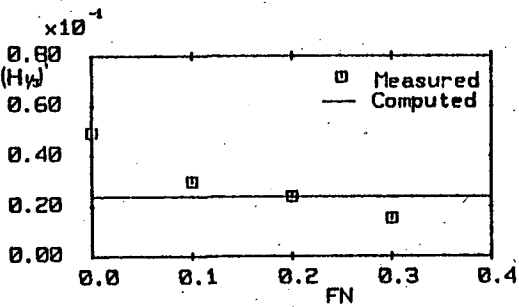
Fig.9 Significant amplitude of
stability variation
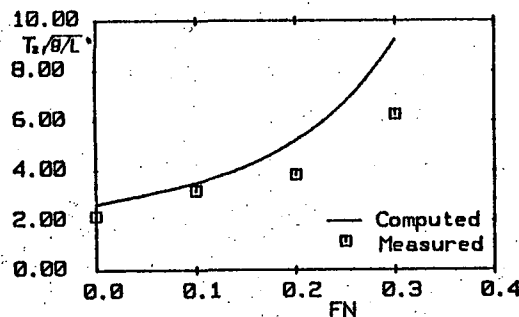

Fig.10 Zero crossing periods
of stability variation
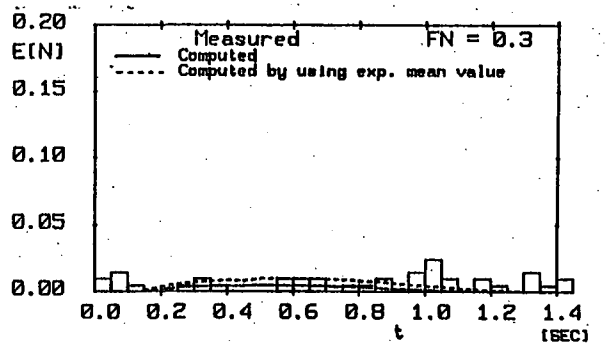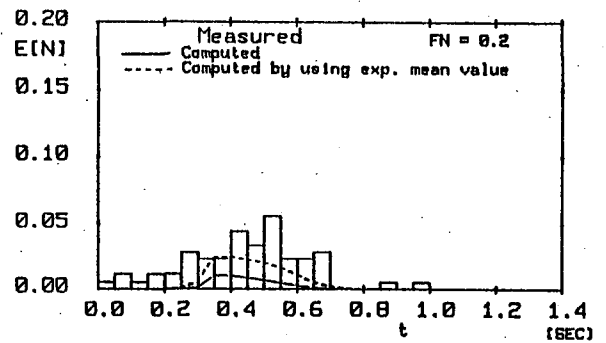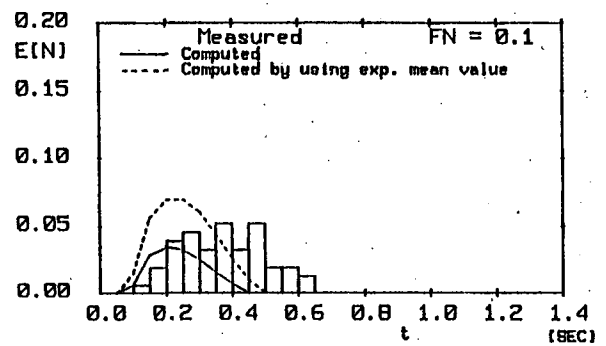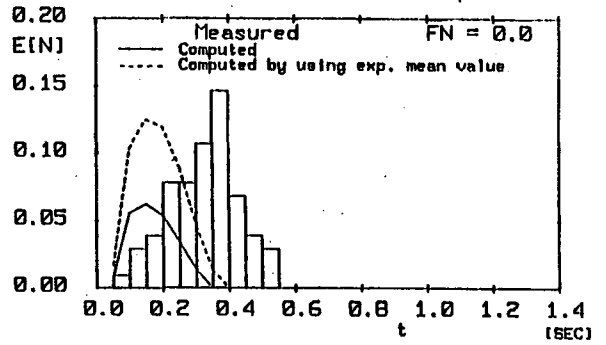
Fig.11 Expected numbers
of stability loss intervals
(model scale; GMo/B=0.338)
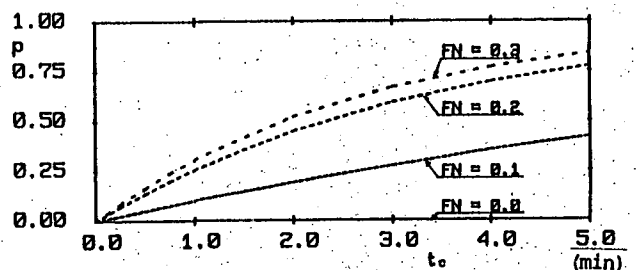
Fig.12 Computed probability of capsizing
(model scale; GMo/B=0.338; $\mathcal{T}$c=0.4 sec)

N. Umeda graduated from Osaka University, Japan, in 1980. Now he works at National Research Institute of Fisheries Engineering, Japan. He has been engaged in researches on the safety of fishing boats for seven years.

Y. Yamakoshi graduated from the Yokohama National University, Japan, in 1972. He has been a chief of Ship Performance Section at National Research Institute of Fisheries Engineering, since 1984. He is interested in ship motion and stability of fishing boats.

MODEL EXPERIMENTS ON INCLINED SHIP IN WAVES

Cao, Zhen-Hai; Li, Jun-Xing

ABSTRACT

The characteristics of an inclined ship in waves is an important aspect of investigation from the point of view of stability and safety. The angle of inclination of a ship can arise from the steady beam wind, shifts of cargo and partly flooding. A project of model experiments on inclined ship in waves has been carried out in the seakeeping model basin of CSSRC. The ship form under test is a wide shallow hull form. All of these model experiments were carried out at zero speed in regular waves. Various angles of inclination of the model in its mean position and various vertical heights of center of gravity of the model were adopted in the experiments. The comparison with the experimental results of the up-right condition of the model in regular beam sea is also included, and the detailed discussion of the investigation is made.

1.INTRODUCTION

The stability of a ship is a prior aspect to be considered by Naval Architect in the design stage. The designers always make their new design have adequate restoring moment to ensure the safety in navigation. Besides, international classification societies and govermental regulatory bodies of maritime nations have their own stringent requirements and regulations. They all stipulate the minimum stability critera for various category of ships. Nevertheless, despite the precautionary measure present in the ship design process, loss of life and ships due to capsizing is still occuring. On the basis of statistic investigations of accidents in the past, the causes of capsizing of various category of ships are very different. The most capsizing accidents of cargo ship are due to shifts of cargo /1/. According to the amount and bias of cargo to be shift, the ship capsizes immediately or has a steady angle of inclination. The inclination angle of a ship can also arise from the presence of the steady beam wind, partly flooding, shipping of water or ice trapped on deck, etc. If a ship in inclined condition has an asymmetric athwartship underwater geometry, the hydrodynamic properties and the characteristics of motion response should be different from the up-right condition. The coupling effects of six modes of inclined ship motions in waves are more complex than the usual case in upright condition.

To investigate the characteristics of an inclined ship in waves is an important aspect for ship safety and survivability of a damged vessel. A few authors have developed theoretical methods to predict the characteristics of inclined ship in waves/2//3/. They used the source sink distribution technique to compute the hydrodynamic coefficients of two dimensional, asymmetrical underwater cross section and strip theory to evaluate the five modes of motion except the surge. From their study it was revealed that a ship in its inclined condition can be excited to higher roll motion than the up-right condition under certain circumstances. Undoubtedly, it is an unfavourable factor for stability of inclined ship if it has higher roll response in waves.

This paper describes the results of model experiments on inclined ship in regular waves which were carried out in the seakeeping model basin of CSSRC. The ship form under test is a wide shallow hull with two different vertical heights of

C.G. and two different inclination angles. For the sake of comparison, the model in up-right condition is also tested. The present paper describes the model experiment results, and some relevant discussions is also given.

2.MODEL EXPERIMENTS

The ship form under test is a wide shallow hull with the parallel middle body extending to about fourty percent of the ship length. No appendages were attached except the bilge keels. The principal characteristics of the model are presented in Table 1 and the body plan is shown in Fig.1.

The principal dimensions of the seakeeping basin in which the model experiments were carried out is 69 meters in length, 46 meters in breadth and 4 meters in depth. Pneumatic type wave-maker is equipped. All of these model experiments were carried out at zero speed in regular waves without restraint on any mode of motion. The measure of three translations and three angular displacements were picked up by six degree of freedom instrument which was developed by CSSRC. The wave parameters were measured by capacity type

wave probe. The up-right condition has two different vertical heights of C.G. as shown in Table1.By translating the ballast iron to the portboard in these two heights of C.G.,we could make the model reach the predetermined inclination angles, i.e.ϕ_0=5 degree,ϕ_0=10 degree,to simulate the shifts of cargo. Thus, the inclined model has lower freeboard at port side and higher freeboard at starboard side. The displacements of the model in inclined condition and in up-right condition are the same. We specify here that the heading angle of incident wave is 180 degree for head wave; 90 degree for beam wave which incidence is from higher freeboard to lower freeboard. The wave length was varied from 1.4 m to 6.5 m and the wave height was approximately kept in the range from 50 mm to 60 mm. Before the experiments were carried out in waves, the roll decay tests for various situation were carried out in calm water to measure the roll damping coefficients and roll periods of the model with various heights of C.G. and various angles of inclination. The immersed midship cross sections at ϕ_0=5 degree and ϕ_0=10 degree together with the locations of the center of buoyancy and gravity are shown in

Table 1 Principal Characteristics of Model in up-right condition

|	
Length, L	2.80 m
Breadth at midship, B	0.512 m
Draft, T	0.096 m
B/T	5.33
Displacement Volume	0.108 m^3
Block Coefficient, C_b	0.783
L.C.B.	0.0915 m fore of 10th station
L.C.G.	0.0915 m fore of 10th station
Vertical height of C.B.	0.0496 m above the keel
Vertical height of C.G.	0.107 m; 0.188 m above the keel
Pitch radius of gyration	0.28 L
Transverse radius of gyration	0.34B
Metacentric height, GM	0.17 m; 0.09 m
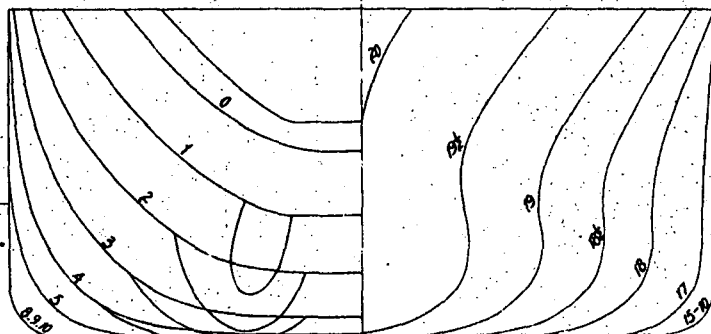
Fig. 1 Body Plan
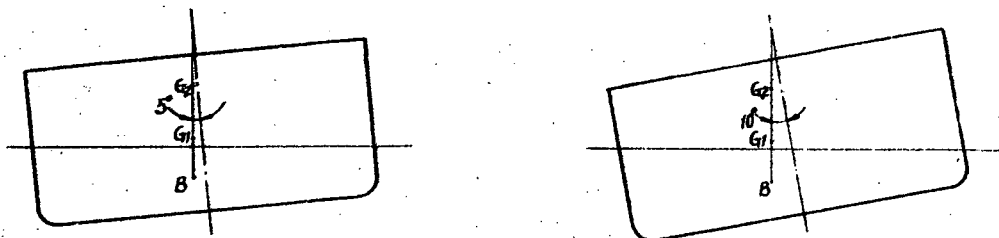
Fig. 2 Midship sections at various inclination angles
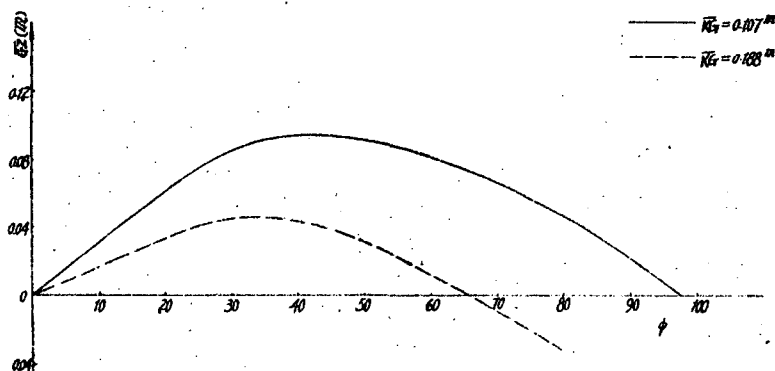
Fig. 3 Righting moment arm versus inclination angle

Fig.2.The static stability charateristics of the model with two different vertical heights of C.G. is present in Fig.3 by the curve of righting moment arm GZ versus heel angle ϕ. All of the model experiment results were described in the form of non-dimensional amplitude Z_A/S_A, ϕ_A/KS_A, etc, and non-dimensional wave length λ/L.

As far as the safety of inclined ship in waves is concered, the roll and heave motions always play an important role. Besides, the roll and heave are the main modes of motion of a ship in beam seas, so they are the only topics we shall discuss. Of course, the pitch of inclined model should be taken into account in head seas. The responses of roll and heave against the non-dimensional wave length λ/L are described in Fig.4 to Fig.7. The roll periods in various situations obtained from decay test in calm water are shown in Table 2.

Table 2 The roll periods of the model in various situation

T_ϕ \ ϕ KG	0 degree	5 degree	10 degree
0.107m	1.014 sec	0.932 sec	0.923 sec
0.188m	1.69 sec	1.62 sec	1.57 sec

3.RESULTS AND DISCUSSIONS

Two different vertical heights of C.G. of the model under tests are all above the water line. The ratios of KG/T are 1.11 and 1.96 respectively. For the condition of lower vertical height of C.G., KG=0.107m, the peak value of roll response is lower in up-right condition and nearly no peak exists in inclined condition at ϕ_0=10 degree. The roll responses are nearly the same in inclined condition for various wave lengthes in the range of experiment. For inclined condition at ϕ=5 degree, the roll response for wave heading μ=90 degree is higher than for wave heading μ=270 degree. For inclined condition at ϕ=10 degree, the roll responses are almost the same, and smaller than those in up-right condition at both μ=90 degree and μ=270 degree.The heave response in inclined condition is slightly higher than in up-right condition. The differences of heave responses among various inclined conditions are not distinct.

For the condition of higher vertical height of C.G., KG=0.188m, the roll response has a remarkable peak in both up-right condition and inclined condition. But the locations of the peak in abscissa
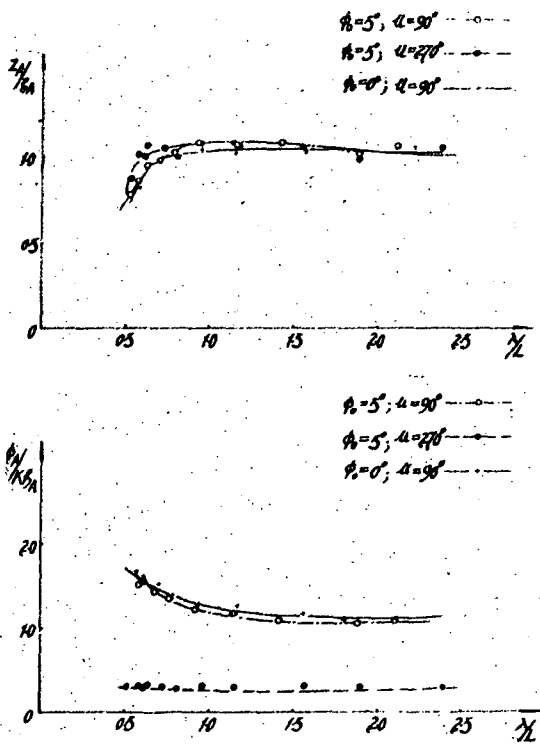
Fig.4 Roll and heave responses for lower vertical height of C.G. (KG=0.107m) in beam waves at up-right condition and inclined condition (φ=5 degree)
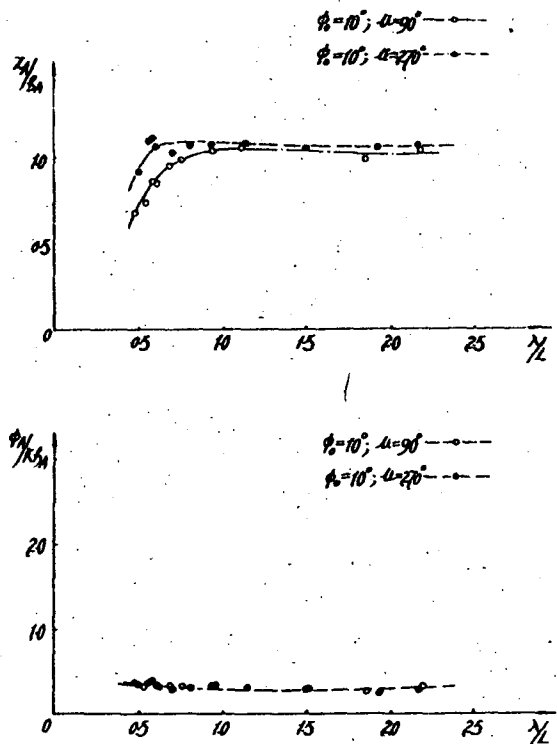

Fig.5 Roll and heave responses for lower vertical height of C.G. (KG=0.107m) in beam waves at inclined condition (φ=10 degree)
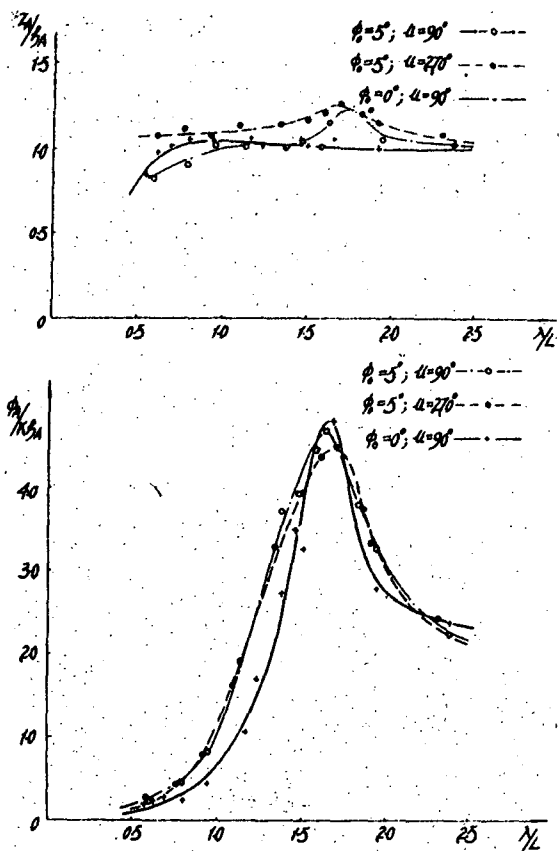

Fig.6 Roll and heave responses for higher vertical height of C.G.(KG=0.188m) in beam waves at up-right condition and inclined condition (φ=5 degree)
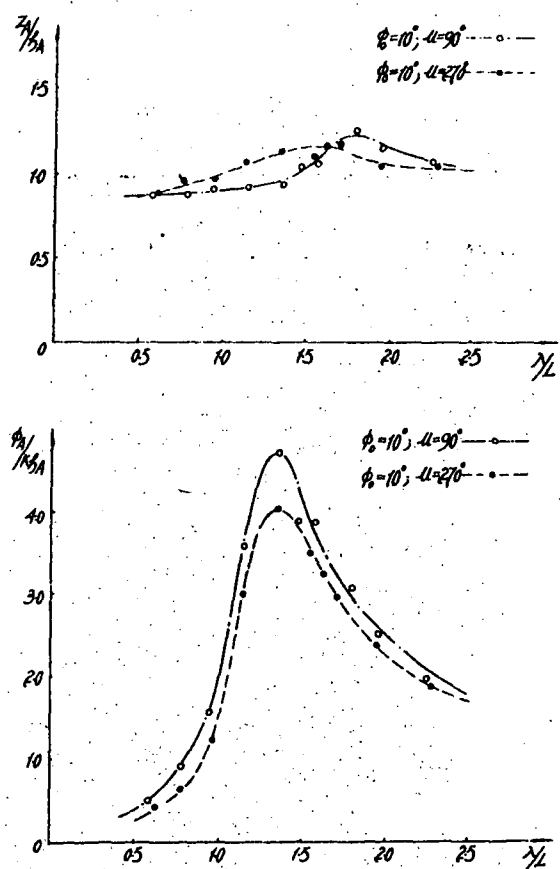
Fig.7 Roll and heave responses for higher vertical height of C.G. (KG=0.188m) in beam waves at inclined condition (φ=10 degree)

are different and the range of significant response is wider in inclined condition than in up-right condition, that is to say that the inclined ship can be excited easily by waves of various lengthes. There is no remarkable difference of peak value between the up-right condition and the inclined condition at ϕ =5 degree. But for inclined condition at ϕ =10 degree, the peak value of roll response for wave heading μ =90 degree is higher than that of roll response for wave heading μ =270 degree. The heave response for inclined model is higher than for up-right model. This is of the same tendency as in the condition of lower vertical height of C.G. But there is an evident characteristics existing in inclined model, i.e. the location of the peak of the heave response in abscissa is close to the peak of roll response. This phenomenom does not exist in up-right condition. From the comparision of heave responses between the conditions of two different vertical heights of C.G., it is observed that the difference is not evident between two up-right conditions. The heave response for the higher vertical height of C.G. is obviously higher than that for the lower vertical height of C.G. in inclined condition. All of these phenomena are due to the coupling effect between heave and roll in inclined condition.

For a symmetric up-right model in regular head waves, the occurrance of roll motion would not be expected. However, if the model in inclined condition, the roll motion would occur in head waves because the model no longer has the symmetric hydrostatic and hydrodynamic properties. The experimental results of an inclined model in head waves with higher vertical height of C.G. at inclination angle ϕ =10 degree are shown in Fig.8. From this figure it can be observed that the location of the peak of roll response in abscissa is close to those of peaks of heave and pitch. That is to say the coupling effect between vertical and horizontal plane motions of an inclined ship is important.

4.CONCLUDING REMARKS

From the model experiments, the following findings could be made:

1. The difference in roll response between inclined condition and up-right condition depends on both of the vertical

height of C.G. and the angle of inclination. Generally speaking, the peak value of roll response of inclined model is not higher than that of up-right condition. But the range of significant response nearby the peak of roll response of the inclined model is wider than that of the up-right model.

2. Under certain circumstance the roll responses of inclined model at wave heading μ = 90 degree could be higher than those at wave heading μ =270 degree.

3. The heave responses of inclined model are higher than those of up-right model. Particularly, there is a peak of heave response nearby the peak of roll response in inclined condition.

4. The inclined model can be excited to a large roll motion by head waves. Under this circumstance the peak of roll response at the location in abscissa is in correspondance with the peaks of heave and pitch.
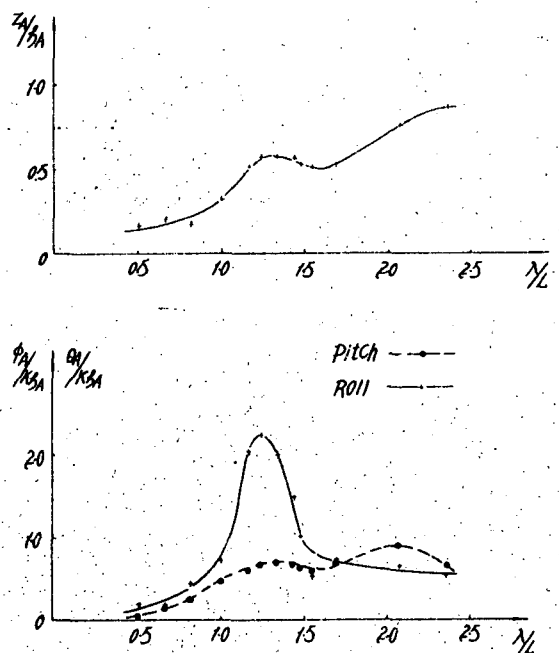

Fig.8 Roll, pitch and heave responses for higher vertical height of C.G. (KG=0.188m) in head waves at inclined condition (ϕ=10 degree)

NOMENCLATURE

L	Ship model length
B	Breadth at midship of the model
T	Draft of the model
C_b	Block coefficient
ς_A	Wave amplitude
Z_A	Heave amplitude
θ_A	Pitch amplitude
ϕ_A	Roll amplitude
ϕ_o	Initial angle of inclination
T_ϕ	Roll period
KG	Vertical height of C.G. above the keel
K	Wave number $(=2\pi/\lambda)$
λ	Wave length
GM	Metacentric height
μ	Wave heading angle; head wave $(\mu = 180$ degree $)$, and beam wave from higher freeboard to lower freeboard $(\mu = 90$ degree$)$

REFERENCES

1. Takaishi,T.,"consideration on the Dangerous Situations leading to capsize of Ships in Waves", Proceedings of Stability '82.

2. Lee, C.M. et al, "Prediction of motion of Ships in Damaged condition in Waves", Proceedings of Stability '82.

3. Kobayashi,M.,"Hydrodynamic forces and moments acting on two-dimensional asymmetrical bodies" Proceedings of Stability '75.

Cao, Zhen-Hai

Graduated from Dept. of N.A.,Shanghai Jiao-Tung University in 1955. He has been working for China Ship Scientific Research Center as a research Engineer since then. In the past,he worked in the field of ship performance, seakeeping and model testing technique, including the design and supervision of the construction of seakeeping basin. He was a member of the committee for revising the rules on Stability for the China Classification Society in 1973.

In recent years he has been working in the field of stability of ships,and was invited to be a committee member of the Stability and Load Line Technical Sub-Committee of Register of Shipping of the People's Republic of China.

Li, Jun-Xing

Graduated from Dept. of N.A., south China Engineering Institute in 1964. He has served China Ship Scientific Research Center as a research engineer ever since. He has been working in the field of seakeeping and performance of high speed vessels.

MODEL EXPERIMENTS ON CAPSIZING
OF A LARGE STERN TRAWLER

M. Kan, T. Saruta, T. Okuyama

ABSTRACT

Results are presented of model tests performed to investigate into the accident of a large stern trawler, which capsized and foundered at the Bering Sea with 32 victims except only one survivor.

Model experiments on ship motions in her various intact and flooded conditions did not show any evidence of poor seakeeping qualities . Measurements of the intact stability showed a good agreement with the calculation which met the criteria with a substantial margin. Stabilities with the free water in the factory and in process of flooding through the garbage shoots were also measured, and besides capsizing tests of the initially heeled model with open garbage shoots were performed. From these results and other examinations including the testimony of the survivor, it was concluded that the capsize had been caused by water flooding through the unclosed garbage shoots into the factory and then probably into the fish hold.

1. INTRODUCTION

On 6th January 1982 at about 16:00, a large stern trawler of 549 gross tonnage, similar to the GAUL [1], capsized and foundered during hauling net in the Bering Sea at a position 54°05' North 178° 25' West, 140 miles north of the Tanaga Island in Aleutian Islands (Fig.1). Out of 33 crews on board, 32 members lost their lives and only third officer was saved by her friend ship.

The wind speed was reported as about 15 m/sec from the east, and the significant wave height as about 5 m, which was consistent with the estimation by the Meteorological Agency. The wave period was also estimated as about 9 seconds. From the wind speed of 15 m/sec and the air temperature of about 1 °c, the possibility of icing on the ship was considered very little.

She had two decks between which there was a large fish processing factory and there were two openings called garbage shoots with the size of 50cm x 40cm on her starboard side, and one on the port side in the factory (Fig.2). There was no testimony concerning whether those garbage shoots were closed or left open. It was reported that it had taken about 17 minutes from beginning of the heel to the capsize.

The Ministry of Transport organized the committee to examine the cause of the accident and to study the safety of a fishing ship in an operation condition. The model experiments described here were performed as a work of the committee [2].


Fig.1 Spot of Accident and Weather Chart
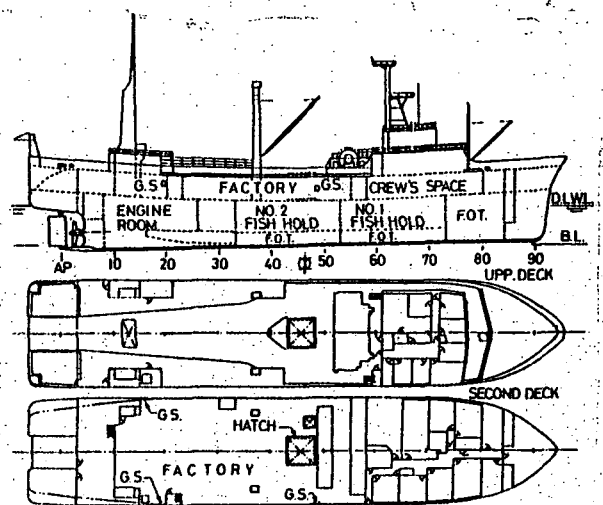
Fig.2 General Arrangement

2. Model

The principal items and the load condition of
the model are shown in Table 1. As a result of an
inquiry of the committee, the load condition of the
ship at the time of an accident was estimated as
shown in the table. The drafts of the model are
slightly different from the corresponding values of
the estimation, perhaps due to the problem of the
accuracy of the model and/or the accuracy of the
hydrostatic calculations of the ship.

Table 1 Principal Items

ITEMS	MODEL	SHIP
DISPLACEMENT (ton)	0.172	1477
LENGTH L_{pp} (m)	2.50	50.8
BREADTH B (m)	0.531	10.8
DRAFT d_f (m)*	0.104 (0.097)**	2.11
d_a (m)	0.318 (0.318)	6.46
d_m (m)	0.211 (0.207)	4.29
TRIM BY STERN (m)	0.214 (0.221)	4.35
KG (m)	0.231	4.69
GM (m)	0.0394	0.80

* drafts are measured from bottom of box keel
** values in brackets are estimated by the committee
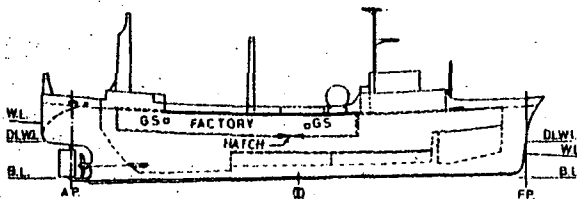

Fig.3 Arrangement of Model

Photo.1 View of Model
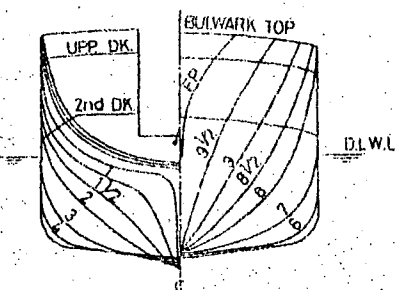
Fig.4 Body Plan

Fig.3 shows the arrangement of the model and
Photo.1 shows its view. The body plan is shown in
Fig.4. To examine the effects of the flooding water
in the factory, the compartment of the factory, the
hatch in the factory and three garbage shoots
were made as similar to the ship as possible.
However, since the thickness of the model was about

3cm, the inner breadth or volume of the factory
space and other compartments was decreased to that
extent. Though the sheer of deck was similar to the
ship, the camber was neglected. In order to avoid
flooding into the inside when the model was
capsized, or to avoid the leak of the water in some
compartment to another one, the openings on the
deck had the water tight lids using rubber packings
and spring clasps. The lids were made by the
transparent materials to observe the inside of the
model. The main superstructures above the upper
deck were also made as similar as possible in order
to examine the effects of the wind. Physical values
described after here are given in full scale
according to the Froude's similarity law.

3. Rolling in Beam Sea

Model tests on the rolling characteristics in
beam seas were carried out to examine the effects
of GM, flooded water, heel and wave steepness.

Fig.5 shows the effect of GM. Since the
natural rolling period of the model was confirmed
to be reasonable by comparison with the full scale
test of the sister ship "No.27 Akebono Maru", it
could be said that GM less than 0.8 m had an effect
of decreasing the rolling amplitude for the
presumed wave length $\lambda/L=2.5$.
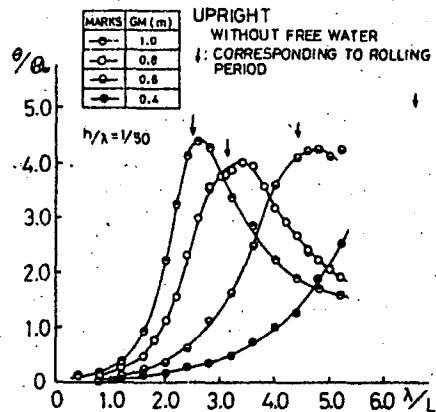
Fig.5 Effect of GM on Roll
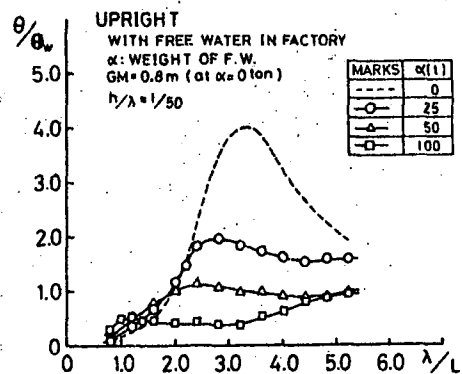
Fig.6 Effect of Flooded Water on Roll

Fig.6 shows the effects of the flooded water
in the factory. For $\lambda/L=2.5$ the free water

decreases the rolling response. Fig.7 is another example of the effects of the free water and GM.

Effects of the heel is shown in Fig.8. Since the heel of the ship has an effect of shifting the natural rolling period to the shorter range, the rolling amplitude increases for λ/L=2.5. But this may not be the case of the final situation of the accident because of the possible existence of the flooded water. It can be considered that the flooded water in the factory even in the listed condition will decrease the roll response, which is consistent with the survivor's testimony that there was little roll motion after listing to the starboard. In the same figure the effect of the wave steepness is shown as expected.
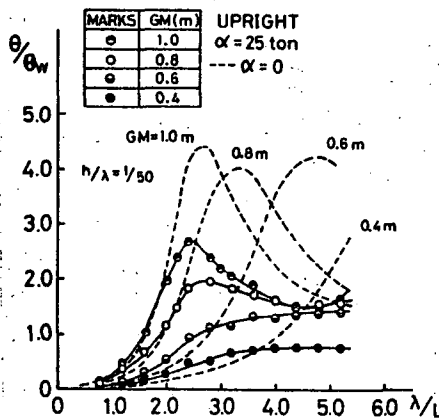

Fig.7 Effect of Flooded water and GM on Roll
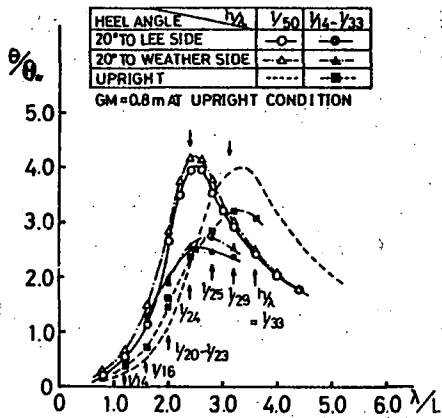
Fig.8 Effect of Heel and Wave Steepness on Roll

These results on the roll motion in various conditions do not show any evidence of poor characteristics connected with the capsize.

4. Measurement of Stability

Static stability was measured in various conditions. Fig.9 shows an apparatus for measuring the righting moment under the trim free condition. Measured moment was corrected by subtracting the moment acting on the load cell after removing the model. Fig.10 is an example of the measured intact stability by using the above apparatus and by means of the weight shift. Good agreement among both

methods and calculation shows a sufficient accuracy of the experiment as well as the calculation program of the intact stability.
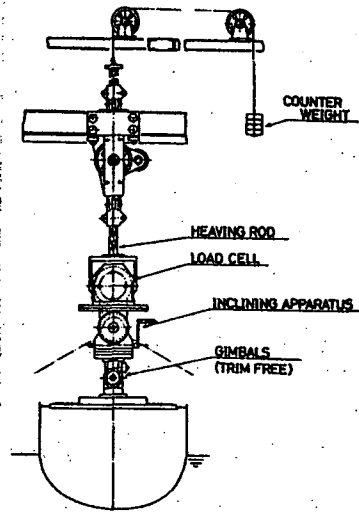
Fig.9 Apparatus for Measurement of Stability
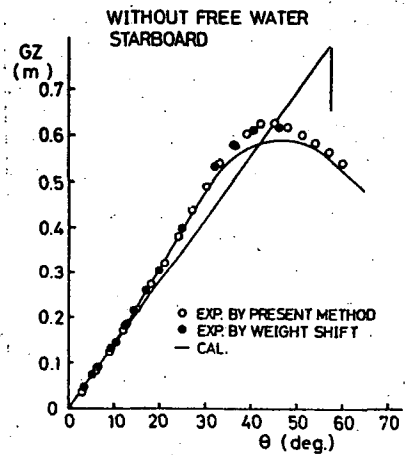
Fig.10 Intact Stability
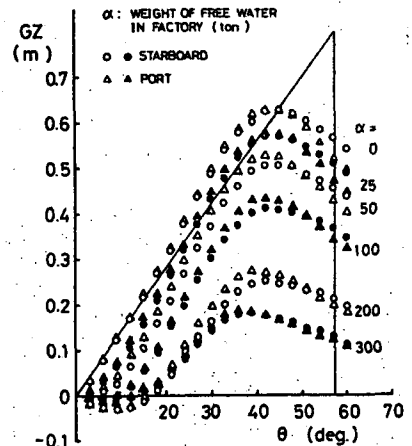
Fig.11 Stability with Free Water in Factory

Fig.11 is an example of the measured righting arm of the flooded condition. Since there is not a complete similarity of the factory between the model and the ship, quantitative agreement with the calculation is not so good. An example of the

calculation of the flooded condition which was performed for the actual ship, is shown in Fig.12.

The righting moments in case of the open garbage shoots and the opened or closed hatch in the factory were measured as shown in Fig.13. The heel angle of about $\theta=13°$ corresponds to one of the beginning of the flooding through the garbage shoot, which are not exactly similar to the actual ship because of the thickness of the model. At about $\theta=24°$ the water accumulated in the factory begins to spill into the fish hold through the hatch .
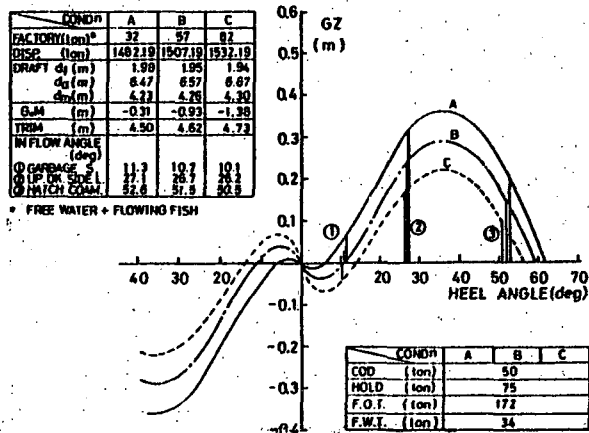
Fig.12 Calculation of Stability in Flooded Condition for Actual Ship

This figure suggests that if the water in the factory does not fall into the fish hold, then there is a possibility of prevention of the capsize provided that the heeling lever is less than the maximum GZ of about 0.3 m, but that once flooding through the garbage shoots begins under the condition of unclosed hatch, then the capsize occurs inevitably.
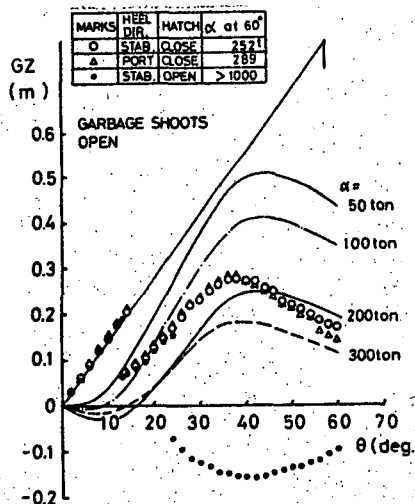
Fig.13 Stability with Openings

5. CAPSIZING EXPERIMENTS

Allowing the flooding through the garbage chutes and giving the initial heel angle by means of the weight shift, the capsizing experiment was carried out. Fig.14 shows an example in still water, which shows the effects of GM, number of the opening, and the initial heel angle on the elapse time to the capsize and the final ballance angle of the model in case of the closed hatch in the factory. As expected from the mentioned above, there exist some cases where the capsize does not occur even if the flooding is allowed. Photo.2 is an example of a seriese of shot.
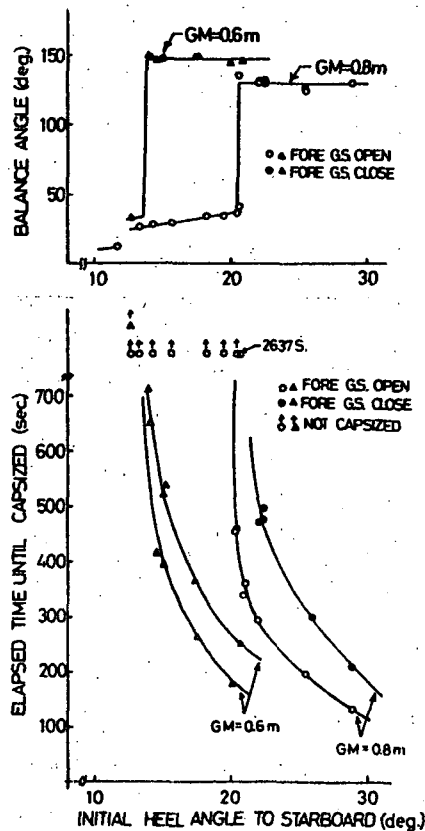
Fig.14 Capsizing Tests in Still Water
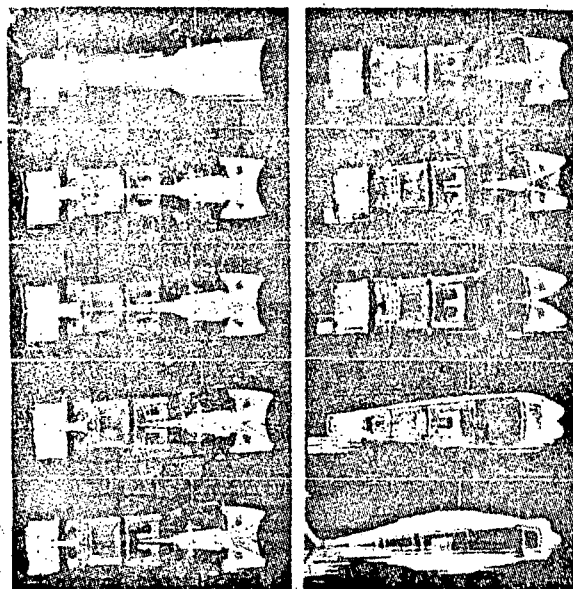
Photo.2 Example of Capsizing Tests in Still Water (every 45 seconds shot, initial heel 21°)

Fig.15 shows the effect of waves and hatch opening on the ellapse time to the capsize. It shows that the capsize occurs faster in waves than in still water, and that the capsize occurs inevitably for the given load condition with the unclosed hatch. Fig.16 is an example of the record of heel in waves.
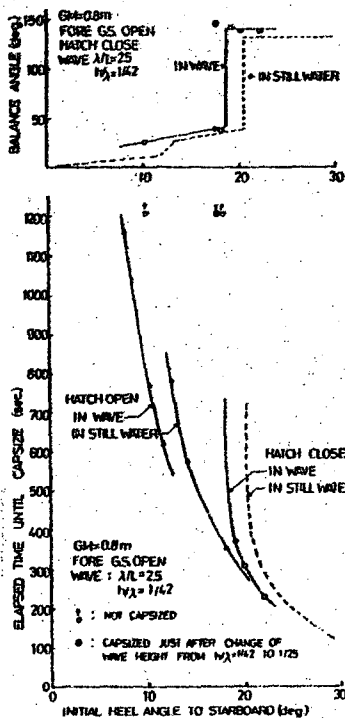
Fig.15 Capsizing Tests (effect of wave and hatch)
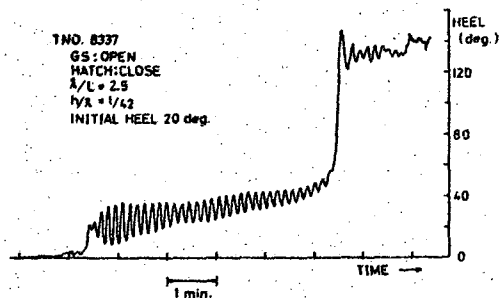
Fig.16 Example of Capsizing Tests in Wave

6. OTHER EXPERIMENTS

Besides above mentioned tests, the heel moment by the rudder action, and by the wind force was measured. The attitude of the model drifting in the waves and wind was also measured. It was made clear that although the attitude of the model was unstable in beam waves only, it became stable in wind or in coexistence of wind and waves and drifted with stable drifting angle from 0 to 20 degrees depending on the heel angle.

The relation between the quantity of flooded water in the factory and the water level in various heel conditions was also observed to examine the possibility of falling of the water into the fish hold or the engine room (Fig.17).
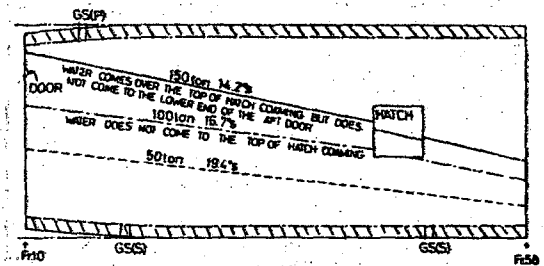
Fig.17 Example of Water Level

7. Conclusions

Results of experiments and stability calculations confirmed that if the garbage shoots had been closed, then the capsize had never occured under the presumed weather and load conditions. It was concluded that although there were some uncertainties about the causes of the occurrence of the initial heel and it's increase, which were supposed to be partly due to the wind forces from the port side, flowing of fishes in the factory caused by the break of wooden partition plates, and consequently due to the one-sided hauling net toward the starboard, in which there had been reportedly more than 30 tons of pollack, or due to the steering action, the conclusive cause of the capsize after the occurence of the heel to some extent was undoubtedly water flooding through the unclosed garbage shoots into the factory. According to the experiments, it was also suggested that even if the flooding into the factory through the garbage shoots began, there was a possibility of prevention of the capsize provided that the flooded water was confined in the factory. This should be taken into consideration in an emergency like the present case.

After the investigation of the committee, the Ministry of Transport presented a recommendation on the opening like the garbage shoot that it should be closed in principle, especially in rough seas and at the time of hauling net, and that it should be equipped with the remote controllable closing unit or moved up above the upper deck.

REFERENCES

1. Morrall,A., "The GAUL Disaster: An Investigation into the Loss of a Large Stern Trawler",Trans.RINA, Vol.123, 1981
2. Ship Bureau, Ministry of Transport, "Report on Inquiry Committee of Accident of No.28 Akebono Maru", 1982.11

EXPERIMENTAL RESULTS OF COEFFICIENTS OF ADDED MASSES OF A SUBMERSIBLE VEHICLE FLOATING UNDER THE WATER SURFACE

J. Gniewszew

ABSTRACT

In order to estimate the coefficients of added masses of a submersible vehicle with influence of free water surface model tests have been carried out in the experimental tank of the Ship Research Institute of the Technical University of Gdańsk. In this connection linear accelerations measurements for 13 relative submersions have been performed. The linear accelerations have been measured for the movements along all three axes of the coordinate system.

1. INTRODUCTION

There are several reasons of tactical and technical nature why submersible vehicles float close to water surface /especially in the Baltic Sea area, where the mean depth is 50m/. That is why the problem of the influence of free water surface on hydrodynamic forces is of great importance [1], [2], [3]. The absence of allowance for the influence of free water surface on hydrodynamic forces in operating submersible vehicles and submarines may lead to loss of motion stability and other related undesirable consequences.

The primary aim of this work has been to determine experimentally the coefficients of added masses of a submersible vehicle being in motion under water surface at various submersion depths. The aim has been achieved by measuring linear accelerations for 13 relative submersions. The linear accelerations have been measured for motion along all three axes of the coordinate system. Model tests have been conducted in the experimental tank of the Ship Research Institute of the Technical University of Gdańsk.

As the results of the tests have shown free water surface leads to changes in added masses in comparison with the values of added masses of a submersible vehicle floating in unbounded liquid. In this case the quantities of added masses are dependent on the distance between a submersible vehicle and free water surface as well as on the direction of a submersible vehicle's motion with respect to free water surface.

2. RESEARCH PROCEDURES

The experimental determination of the coefficients of added masses of a hull of a submersible vehicle was based on the fundamental dependence

$$F_i = m_i \cdot a_i \qquad /1/$$

where F_i - external force acting on a submersible vehicle;

m_i - total of vehicle's mass and of vehicle's added mass, λ_{ii};

a_i - acceleration of vessel's mass.

Thus equation /1/ may be written as

$$F_i = \left(m + \lambda_{ii} \right) \cdot a_i$$

hence the coefficient of added mass

$$K_{ii} = \frac{\lambda_{ii}}{m}$$

For the purpose of accurate estimation of the values of added masses of a vehicle the force making the vehicle move was being changed. A coordinate system bound with the center of the vehicle's mass /fig.1/ was assumed here.
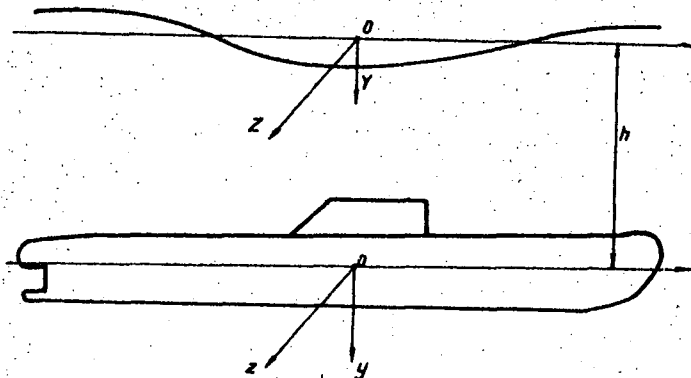
Fig.1 Coordinate axes system of a submersible vehicle in determining added masses.

The tests consisted in measuring acceleration values of a submersible vehicle.

The model tests were conducted in the experimental tank of the Ship Research Institute of the Technical University of Gdańsk. In order to conduct the tests a special measuring device had been designed to measure accurately linear accelerations in the case of linear movements of the model vehicle. The following scheme /fig.2/ was applied to determine linear accelerations.
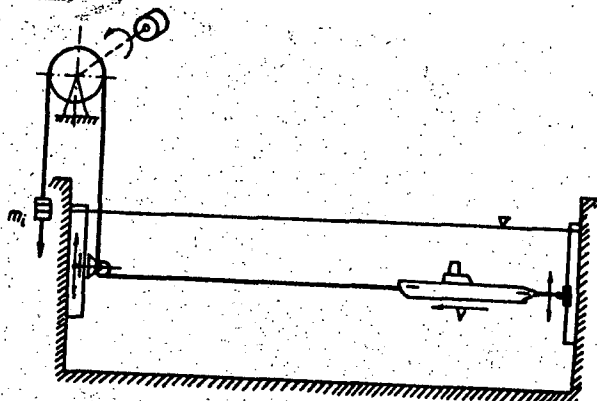
Fig.2 Scheme of the measuring device for determining linear accelerations.

A simplified gravitation device is presented in the scheme. Accelerated linear motion of the model is made by the falling of a weight of an appropriate mass caused by gravitation. In this case the resistance of the device was determined. It was below the acceptable limit of error, that is below 1% with respect to the smallest load. The device had been graduated for determining acceleration values at specified parameters and time.

A set of amplifiers along with the UV 2006 SE recorder were used to record the parameters.

Parameters of the tested model:

$$L = 0.760m$$
$$B = 0.063m$$
$$H = 0.063m$$
$$M_a = 1.572kg$$
$$J_o = 0.04571 \text{ kg m}^2$$

scale $\lambda = 100$

The model was made of wood and covered with polyurethane paint. Its buoyancy was neutral.

Symbols used in the paper

a	$[m/s^2]$	– acceleration
B	$[m]$	– width of the model
F	$[N]$	– towing force
H	$[m]$	– height of the model
L	$[m]$	– length of the model
K_{ii}		– coefficient of added mass
M_a	$[kg]$	– mass
V	$[m/s]$	– velocity of the model
λ_{ii}	$[kg]$	– added mass
λ		– scale of the model
$\bar{f} = \frac{Y}{L}$		– relative submersion
Y	$[m]$	– submersion of the model

3. ANALYSIS OF THE RESULTS

Linear accelerations were measured for 13 relative submersions of the model vehicle. They were measured for motion along all three axes of the coordinate system. Since the direct effect of each of the measurements mentioned above was measurement of the distance travelled by the model of the vehicle in function of time the first stage in computing procedure was determination of the velocity of the model in function of time, that is $V_M = f$ (t). It was that curve determined on the basis of regressive analysis which became the basis for determining the acceleration at the initial point. Since the regressive analysis made with the HP-9830A computer has shown that the curve is described by quadratic polynominal, that is

$$V/t/ = at^2 + bt + c$$

thus differentiating V/t/ with respect to time at point 0 initial acceleration

$$\frac{dV}{dt}_o = 2 at + b = b$$

is obtained. Thus coefficient b determines the acceleration value at the initial point.
Regressive analysis of each velocity curve /in other words of each load/ was made with the HP-9830A computer.

The results are presented in tabular form as values of coefficients of added mass in function of relative submersion, that is $K_{ii} = f/t/$ for each of the loads /tables 1,2,3/.

The mean values of the coefficients of added masses obtained from the model tests are presented in tables /4,5,6/ and in diagrams /fig.3,4,5/.
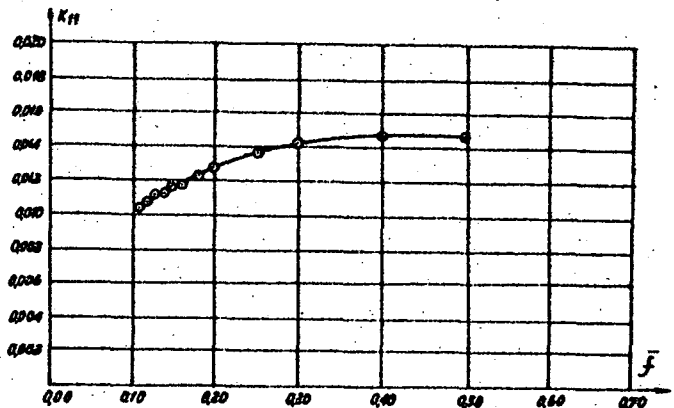
Fig.3 Values of the coefficients of added mass of the submersible vehicle floating along OX axis at different submersion depths obtained from the model tests.
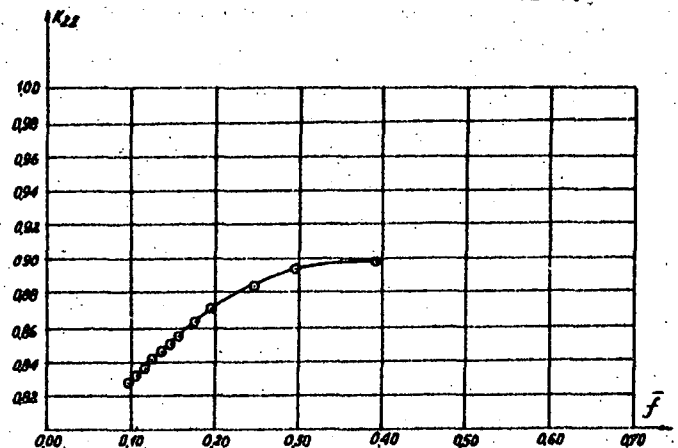
Fig.4 Values of the coefficients of added mass of the submersible vehicle floating along OY axis at different submersion depths obtained from the model tests.
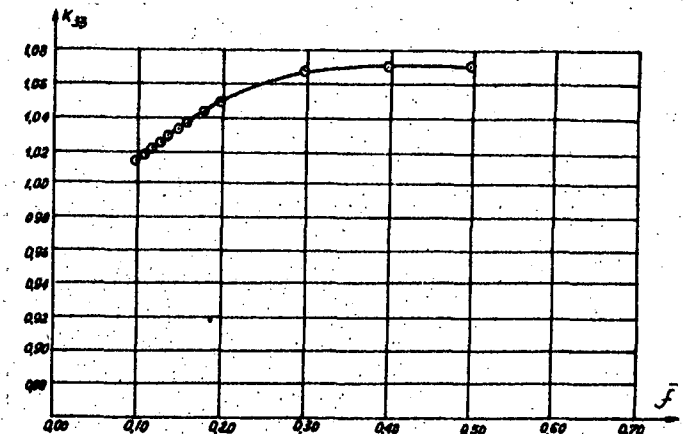
Fig.5 Values of the coefficients of added mass of the submersible vehicle floating along OZ axis at different submersion depths obtained from the model tests.

TABLE 1

F_1 [N]	0.196			0.490			0.686		
$\bar{f}$	a_1	$m+\lambda_{11}$	λ_{11}	a_2	$m+\lambda_{11}$	λ_{11}	a_3	$m+\lambda_{11}$	λ_{11}
0.10	0.1233	1.5895	0.0175	0.3086	1.5877	0.0157	0.4323	1.5868	0.0148
0.11	0.1233	1.5899	0.0179	0.3085	1.5882	0.0162	0.4322	1.5873	0.0153
0.12	0.1232	1.5904	0.0184	0.3084	1.5887	0.0167	0.4321	1.5877	0.0157
0.13	0.1232	1.5908	0.0188	0.3083	1.5891	0.0171	0.4320	1.5881	0.0161
0.14	0.1232	1.5912	0.0192	0.3083	1.5895	0.0175	0.4318	1.5886	0.0166
0.15	0.1232	1.5916	0.0196	0.3082	1.5899	0.0179	0.4317	1.5890	0.0170
0.16	0.1231	1.5920	0.0200	0.3081	1.5903	0.0183	0.4316	1.5893	0.0173
0.18	0.1231	1.5927	0.0207	0.3080	1.5910	0.0190	0.4331	1.5901	0.0181
0.20	0.1230	1.5934	0.0214	0.3079	1.5917	0.0197	0.4312	1.5907	0.0187
0.25	0.1229	1.5948	0.0228	0.3076	1.5931	0.0211	0.4309	1.5921	0.0201
0.30	0.1229	1.5958	0.0238	0.3074	1.5941	0.0221	0.4306	1.5931	0.0211
0.40	0.1228	1.5966	0.0246	0.3072	1.5949	0.0229	0.4304	1.5939	0.0219
0.50	0.1228	1.5968	0.0248	0.3073	1.5946	0.0226	0.4305	1.5934	0.0214

TABLE 2

F_1 N	0.490			0.981			1.471		
$\bar{f}$	a_1	$m+\lambda_{22}$	λ_{22}	a_2	$m+\lambda_{22}$	λ_{22}	a_3	$m+\lambda_{22}$	λ_{22}
0.10	0.1696	2.8893	1.3173	0.3416	2.8719	1.2999	0.5154	2.8541	1.2821
0.11	0.1691	2.8974	1.3254	0.3406	2.8800	1.3080	0.5139	2.8622	1.2902
0.12	0.1687	2.9052	1.3332	0.3397	2.8878	1.3158	0.5125	2.8700	1.2980
0.13	0.1682	2.9127	1.3407	0.3388	2.8953	1.3233	0.5112	2.8775	1.3055
0.14	0.1678	2.9199	1.3479	0.3380	2.9024	1.3304	0.5099	2.8847	1.3127
0.15	0.1674	2.9268	1.3548	0.3372	2.9093	1.3373	0.5087	2.8916	1.3196
0.16	0.1670	2.9334	1.3614	0.3364	2.9160	1.3440	0.5076	2.8982	1.3262
0.18	0.1663	2.9457	1.3737	0.3350	2.9283	1.3563	0.5054	2.9105	1.3385
0.20	0.1652	2.9668	1.3948	0.3337	2.9394	1.3674	0.5035	2.9216	1.3496
0.25	0.1645	2.9794	1.4074	0.3312	2.9620	1.3900	0.4996	2.9442	1.3722
0.30	0.1636	2.9946	1.4226	0.3295	2.9771	1.4051	0.4971	2.9593	1.3873
0.40	0.1632	3.0025	1.4305	0.3286	2.9851	1.4131	0.4957	2.9673	1.3953
0.50	0.1644	2.9807	1.4087	0.3311	2.9632	1.3912	0.4977	2.9555	1.3835

TABLE 3

F_1 [N]	0.490			0.981			1.471		
$\bar{f}$	a_1	$m+\lambda_{33}$	λ_{33}	a_2	$m+\lambda_{33}$	λ_{33}	a_3	$m+\lambda_{33}$	λ_{33}
0.10	0.1507	3.2513	1.6793	0.3156	3.1086	1.5366	0.4683	3.1410	1.5690
0.11	0.1504	3.2578	1.6858	0.3149	3.1151	1.5431	0.4674	3.1475	1.5755
0.12	0.1501	3.2640	1.6920	0.3143	3.1213	1.5493	0.4664	3.1537	1.5817
0.13	0.1499	3.2700	1.6980	0.3137	3.1273	1.5553	0.4656	3.1597	1.5877
0.14	0.1496	3.2758	1.7038	0.3131	3.1330	1.5610	0.4647	3.1654	1.5934
0.15	0.1493	3.2812	1.7092	0.3126	3.1385	1.5665	0.4639	3.1709	1.5989
0.16	0.1491	3.2865	1.7145	0.3120	3.1438	1.5718	0.4631	3.1762	1.6042
0.18	0.1487	3.2963	1.7243	0.3111	3.1535	1.5815	0.4617	3.1859	1.6139
0.20	0.1483	3.3050	1.7330	0.3102	3.1623	1.5903	0.4605	3.1947	1.6227
0.25	0.1475	3.3227	1.7507	0.3085	3.1800	1.6080	0.4579	3.2124	1.6404
0.30	0.1470	3.3343	1.7623	0.3074	3.1916	1.6196	0.4563	3.2240	1.6520
0.40	0.1467	3.3392	1.7672	0.3069	3.1965	1.6245	0.4556	3.2289	1.6569
0.50	0.1467	3.3397	1.7677	0.3059	3.2070	1.6350	0.4569	3.2194	1.6474

TABLE 4

F_1 [N]	0.196		0.490		0.686		
$\bar{f}$	λ_{11}	K_{11}	λ_{11}	K_{11}	λ_{11}	K_{11}	K_{11} średn.
0.10	0.0175	0.0111	0.0157	0.0100	0.0148	0.0094	0.0102
0.11	0.0179	0.0114	0.0162	0.0103	0.0153	0.0097	0.0105
0.12	0.0184	0.0117	0.0167	0.0106	0.0157	0.0100	0.0108
0.13	0.0188	0.0120	0.0171	0.0109	0.0161	0.0103	0.0111
0.14	0.0192	0.0122	0.0175	0.0111	0.0166	0.0105	0.0113
0.15	0.0196	0.0125	0.0179	0.0114	0.0170	0.0108	0.0116
0.16	0.0200	0.0127	0.0183	0.0116	0.0173	0.0110	0.0118
0.18	0.0207	0.0132	0.0190	0.0121	0.0181	0.0115	0.0123
0.20	0.0214	0.0136	0.0197	0.0125	0.0187	0.0119	0.0127
0.25	0.0228	0.0145	0.0211	0.0134	0.0201	0.0128	0.0136
0.30	0.0238	0.0151	0.0221	0.0141	0.0211	0.0134	0.0142
0.40	0.0246	0.0156	0.0229	0.0146	0.0219	0.0139	0.0147
0.50	0.0248	0.0158	0.0226	0.0144	0.0214	0.0136	0.0146

TABLE 5

$\frac{F_1}{[N]}$	0.490		0.981		1.471		
$\bar{r}$	λ_{22}	K_{22}	λ_{22}	K_{22}	λ_{22}	K_{22}	K_{22} średn.
0.10	1.3173	0.8380	1.2999	0.8269	1.2821	0.8156	0.8268
0.11	1.3254	0.8431	1.3080	0.8321	1.2902	0.8207	0.8320
0.12	1.3332	0.8481	1.3158	0.8370	1.2980	0.8257	0.8369
0.13	1.3407	0.8529	1.3233	0.8418	1.3055	0.8305	0.8417
0.14	1.3479	0.8574	1.3304	0.8463	1.3127	0.8351	0.8463
0.15	1.3548	0.8618	1.3373	0.8507	1.3196	0.8394	0.8506
0.16	1.3614	0.8660	1.3440	0.8550	1.3262	0.8436	0.8549
0.18	1.3737	0.8739	1.3563	0.8628	1.3385	0.8515	0.8627
0.20	1.3948	0.8873	1.3674	0.8698	1.3496	0.8585	0.8719
0.25	1.4074	0.8953	1.3900	0.8842	1.3722	0.8729	0.8841
0.30	1.4226	0.9050	1.4051	0.8938	1.3873	0.8825	0.8938
0.40	1.4305	0.9100	1.4131	0.8989	1.3953	0.8876	0.8988
0.50	1.4087	0.8961	1.3912	0.8850	1.3835	0.8801	0.8871

TABLE 6

$\frac{F_1}{[N]}$	0.490		0.981		1.471		
$\bar{r}$	λ_{33}	K_{33}	λ_{33}	K_{33}	λ_{33}	K_{33}	K_{33} średn.
0.10	1.6793	1.0683	1.5366	0.9775	1.5690	0.9981	1.0146
0.11	1.6858	1.0724	1.5431	0.9816	1.5755	1.0022	1.0187
0.12	1.6920	1.0763	1.5493	0.9856	1.5817	1.0062	1.0227
0.13	1.6980	1.0802	1.5553	0.9894	1.5877	1.0100	1.0265
0.14	1.7038	1.0838	1.5610	0.9930	1.5934	1.0136	1.0301
0.15	1.7092	1.0873	1.5665	0.9965	1.5989	1.0171	1.0336
0.16	1.7145	1.0906	1.5718	0.9999	1.6042	1.0205	1.0370
0.18	1.7243	1.0969	1.5815	1.0060	1.6139	1.0267	1.0432
0.20	1.7330	1.1024	1.5903	1.0116	1.6227	1.0323	1.0488
0.25	1.7507	1.1137	1.6080	1.0229	1.6404	1.0435	1.0600
0.30	1.7623	1.1211	1.6196	1.0303	1.6520	1.0509	1.0674
0.40	1.7672	1.1242	1.6245	1.0334	1.6569	1.0540	1.0705
0.50	1.7677	1.1245	1.6350	1.0401	1.6474	1.0480	1.0709

4.CONCLUSIONS

A few general conclusions based on the tables and diagrams obtained from the model tests have been formulated below:

1.Free water surface leads to changes in added masses in comparison with the values of added masses of a submersible vehicle floating in unbounded liquid.

2.The quantities of added masses are dependent on the distance between a submersible vehicle and free water surface /on the submersion depth/,as well as on the direction of a submersible vehicle's motion with respect to free water surface,and is not dependent on the velocity of a vehicle.

3.The values of all coefficients of added masses of a submersible vehicle decrease with the decrease of the relative submersion depth $\bar{T}$,thus free water surface leads to a decrease of the values of added masses of a submersible vehicle.

4.The influence of free water surface on added masses of a submersible vehicle decreases with the increase of the relative submersion depth $\bar{T}$ and is practically nonexistent at the relative submersion depth $\bar{T} > 0.5$.

5.A considerable influence of free water surface on added masses occurs at the relative submersion depth $\bar{T} = 0.10$.This influence causes the values of coefficients of added masses of a submersible vehicle to decrease approximately by 50 % of the values of coefficients of a vehicle floating at a large submersion depth /in unbounded liquid/.

REFERENCES

1.GNIEWSZEW J.:Wpływ swobodnej powierzchni wody na siłę nośną okrętu podwodnego przy pływaniu w położeniu podwodnym.Zbiór Prac WSMW.Gdynia 1972;no.36,105-124.

2.GNIEWSZEW J.:Opór okrętu podwodnego poruszającego się w stanie zanurzonym w pobliżu swobodnej powierzchni wody. Studia i materiały oceanologiczne no.20.Oceanotechnika/2/,PAN,Sopot 1977.

3.GNIEWSZEW J.:Wpływ swobodnej powierzchni wody na wzdłużny moment hydrodynamiczny okrętu podwodnego przy pływaniu w położeniu podwodnym.Zeszyty Naukowe WSMW,Gdynia 1975;no.1/44, 37-55.

4.JAROSZ A.:Przegląd i ocena stanowisk badawczych stosowanych do badań modelowych ciał zanurzonych.Instytut Okrętowy PG,Gdańsk 1976;no.52.

A CRITERION FOR SHIP CAPSIZE IN BEAME SEAS

H. Sadakane

ABSTRACT

This paper deals with a ship capsize in beam waves during one swing from weather side to lee side. A formula for a critical capsize condition is found on the basis of an unsteady-roll analysis using an apploximate solution technique of simplified roll equation. The condition can be applied and extended to the effect of the wave period, the shape of GZ-curve, the roll damping etc. on the ship capsize.

1. INTRODUCTION

It has been recognized that ship capsize is caused by many factors and by their combination, like wind , shipping of water on deck, breaking of cargo, breaking waves, an abrupt change of current, coupling of ship motion, and so on. However, the capsize itself does not seem to have been clarified enough in view of its dynamics, since the capsize can be considered as an unsteady dynamical process of the extreme roll. It would be therefore necessary make consideration the extreme roll process by using analitycal and/or numerical treatment.

If the capsizing phenomenon, represented by a single equation of roll motion, is defined as a situation that, during a process of increasing roll amplitude, the roll angle exceeds the vanishing point of stability, then the capsize condition and associating factors may be found by analysing the process in detail. Such a deterministic process probably affected by three factors, namely the ship properties like stability, inertia and damping, the wave properties like period and steepness, and finally the initial condition of the roll motion.

In early time, theoretical analyses on the concept of increasing roll amplitude

were made by Froude [1], Watanabe [2] and Kato [3]. They clarified the basic characteristics of linear roll in unsteady process. Subsequently, Krappinger [4] calculated a capsize condition by taking into account the variation of ship restoring moment in following waves. Recently Blocki [5] has made interesting works with respect to the ship capsize due to the variation of ship restoring moment.

In this paper, a theoretical analysis is made on a critical capsizing roll during one swing from weather side to lee side, using a simple roll equation with nonlinear restoring term and an approximate solution method. As a result, a formula for a clitical capsize condition is found, which is expressed in terms of the three factors mentioned above. Secondly as an application of the critical line, discussions are made on the critical value of the wave period as a most probable period for capsize and the effectiveness of the ship stability factors against the capsize.

2. EQUATION OF ROLL MOTION AND SOLUTION PROCEDURE

The following equation of apparent roll motion with nonlinear restoring moment is used to study the present ship-capsize problem.

$$\ddot{\theta}_a + 2K_e \dot{\theta}_a + \omega_0^2 f(\theta_a) = (\gamma \pi H / \lambda) \omega^2 \sin \omega t \qquad (1)$$

where $f(\theta_a) = \theta_a + \beta_3 \theta_a^3 + \beta_5 \theta_a^5 + \beta_7 \theta_a^7 + \text{-----}$ (2)

In the above, θ_a represents the apparent roll angle, K_e the linearized damping coefficient, ω_0 the natural frequency, γ the coefficient of effective wave slope, H the wave height, λ the wave length, ω the wave frequency and t the time. The superscript dot " $\cdot$ " stands for the differenciation

with respect to t, and β_n (n=3,5,$\cdots$) the coefficients for the nonlinear restoring moment. Supose the roll amplitude and the roll period vary with time in an unsteady capsizing process. Then a phase plane analysis may be appropriate for examining the amplitude change [6]. For variables on phase plane, we adopt here the roll ampli- tude A and the phase difference ϕ between the exciting moment and the roll angle. In order to compose the phase plane expressed by the terms A and ϕ, eq.(1) should be transformed into a set of simultaneous ordi- nary differential equations of first order.

2.1 Averaged equation of roll motion

An approximate solution of eq.(1) can be derived by assuming

$$\theta_a = A \sin(\omega t - \phi) \qquad (3)$$

where A and ϕ are also assumed to be slowly varing functions of time t, i.e. $\dot{A} \ll A\omega$ and $A\dot{\phi} \ll A\omega$. Then the differenciation of eq.(3) with respect to t can be expressed as

$$\dot{\theta}_a \doteqdot A\omega \cos(\omega t - \phi) \qquad (4)$$

Denoting $\dot{\theta}_a$ as θ_a, eq.(1) becomes the following set of first-order equations.

$$\left. \begin{array}{l} \theta_a = \dot{\theta}_a \\ \dot{\theta}_a = -2K_e\dot{\theta}_a - \omega_0{}^2 f(\theta_a) + (\gamma\pi H/\lambda)\,\omega^2 \sin\,\omega t \end{array} \right\} \quad (5)$$

From eqs. (3) and (4), the following equations can be obtained.

$$\left. \begin{array}{l} A^2 = \theta_a{}^2 + (\theta_a/\omega)^2 \\ \mathrm{Tan}(\omega t - \phi) = (\theta_a/\theta_a)\omega \end{array} \right\} \quad (6)$$

Differentiating eq.(6) with respect to t and rewriting it using eq.(5), we can obtain the following equations.

$$\left. \begin{array}{l} \dot{A} = (1/\omega)[\omega^2\theta_a - 2K_e\dot{\theta}_a - \omega_0{}^2 f(\theta_a) \\ \qquad + (\gamma\pi H/\lambda)\omega^2 \sin\,\omega t]\cos(\omega t - \phi) \\ \dot{\phi} = (1/\omega)[\omega^2 \sin(\omega t - \phi) + \frac{1}{A}(-2K_e\dot{\theta}_a - \omega_0{}^2 f(\theta_a) \\ \qquad + (\gamma\pi H/\lambda)\omega^2 \sin\,\omega t)]\sin(\omega t - \phi) \end{array} \right\} \quad (7)$$

Taking the average of eq.(7) over the peri- od $2\pi/\omega$, and considering the roll amplitude A and the phase difference ϕ to be constant during the period,performing the averaging, we obtain the so-called averaged equations of roll motion in the following form.

$$\dot{A} = -K_e A + \frac{1}{2}(\gamma\pi H/\lambda)\omega\sin\,\phi \qquad (8)$$

$$\dot{\phi} = \frac{1}{2\omega}\{\omega^2 - \omega_0{}^2 g(A) + \frac{1}{2}\frac{\gamma\pi H/\lambda}{A}\omega^2 \cos\,\phi\} \qquad (9)$$

where $g(A) = 1 + \frac{3}{4}\beta_3 A^2 + \cdots 2\frac{(2n+1)!!}{(2n+2)!!}\beta_{2n+1}A^{2n}$ (10)

$$n = 1, 2, 3 \cdots$$

2.2 Backborn curve

In a extreme roll, since the natural roll period of a ship changes with the roll amplitude , the relation between the amplitude and the period plays a important role to the roll of the ship in waves. In this section, the backborn curve describing the above relation will be derived.

Substituting $\dot{A} = 0$ and $\dot{\phi} = 0$ into eq.(5) and (6) and eliminating ϕ, we obtain the steady-roll solution

$$(2K_e A_0)^2 + A_0{}^2 (-\omega^2 + \omega_0{}^2 g(A_0))^2 = (\gamma\pi H/\lambda)^2\omega^4 \quad (11)$$

where A_0 is the steady-roll amplitude. Eq.(11) gives the frequency-response curve. Substituting $(\gamma\pi H/\lambda)\omega^2 = 0$, $K_e = 0$ and $\omega = \omega_s$ into eq.(11), we obtain the backborn curves

$$T_s = T_0/\sqrt{g(A_0)} \qquad (12)$$

where T_s ($= 2\pi/\omega_s$) is the roll period for A_0, and T_0 ($= 2\pi/\omega_0$) the roll period for an infinitesimal roll amplitude, i.e., for the linearized motion.

2.3 Unsteady roll and phase plane

For the preparation of the analysis on the ship capsize, the characteristics of the unsteady roll is discussed by the use of the phase plane.

Fig.1 shows an example of trajectories of motion (ϕ, A) on the phase plane during unsteady roll. Condition for the ship stability is prescribed as $\beta_3 < 0, \beta_5 = \beta_7 \cdots = 0$. The trajectories of thin solid lines with an arrow converge to a stable forcus with time. During the converging process, the roll is in an unsteady state which means the roll amplitude and the period change in every one swing. Conversely, if the change of such trajectories is prescribed, we can derive the variation of the roll amplitude.

Since the direction of the trajectories reverses the course at the position satisfying $\dot{A} = 0$ and $\dot{\phi} = 0$ on the phase plane, a contour linked through these points gives an information on the behavior of the trajectories, i.e., the unsteady roll. Such contours are calculated by the following equation.

$$A = (\gamma\pi H/\lambda)(\omega/2K_e)\sin\,\phi \qquad (13)$$

$$\phi = \cos^{-1}\{A(\omega_0{}^2 g(A) - \omega^2)/(\gamma\pi H/\lambda)\omega^2\} \quad (14)$$

Eq.(13) gives the contour of $\dot{A} = 0$ as shown in Fig.1 The inside domain of this contour corresponds to $\dot{A} > 0$. Eq.(14) also gives

the contour of $\phi=0$ as shown in Fig.1. The domain of $\phi>0$ is the upper side of this contour.

Accodingly if the contours on the phase plane are prepared, we can approximately predict the course of the trajectories, i.e. the subsequent roll motion.

3. CRITICAL CONDITION FOR CAPSIZE

For the criteria of ship capsize, the lee-side heel angle for judging ship capsize has usually been calculated using the energy conservation concept in unresisted roll in still water. However,the roll damping and the exciting moment do act on a ship hull while it swings the weather side to lee side. These moments will rationally be taken into account in the present analysis by considering the nonlinearity of the restoring moment and the unsteady roll in waves.

In this chapter, as the first step of considering the above problems, the capsize due to waves will be analyzed by using the preceding approximate solution technique, and a critical condition for capsize will be stated.

Capsize is defined here as the condition that the roll angle of ship exceeds to the vanishing point of stability and the waves are assumed to be sinusoidal during one swing of the ship roll.

3.1 Factors of capsize

To describe an equation of capsizing roll motion and its critical condition, it is necessary to find out basic factors in the unsteady roll process using a simplified roll equation. The factors will be found in the condition of increasing roll amplitude and in the initial condition of weather side roll, as follows:

(1) Condition of increasing roll amplitude

In order for the roll amplitude to increase during one swing, it is necessary that $(\gamma\pi H/\lambda)\omega/2$ representing the exciting moment is large and ϕ becomes about $\pi/2$ during one swing, which can be understood from eq.(8). At the same time, the condition $\phi>0$ also makes the roll amplitude increase. Since the condition $\phi>0$ makes the phase velocity $\omega-\dot\phi$ of the roll angle θ_a decrease, the roll period $2\pi/(\omega-\dot\phi)$ becomes large. The prolonged time brings the increase of the roll amplitude because the condition $\dot A>0$ during one swing.

(2) Initial condition of weather -side roll angle

Considering the one swing capsize from weather side to lee side, the capsize process should be initiated by the weather-side roll angle θ_{aw} and the phase difference ϕ_w. Therefore, if we plot the points (ϕ_w,θ_{aw}) in extreme rolls, we can get a diagram dividing these points into two region, i.e., a set of points which lead to capsize, and the other uncapsized, as shown in Fig.2. The hatched domain in Fig.2 corresponds to the group of capsized points, in which the lowest point θ_{awm} should represent a critical situation for capsize to occur at a least possibility. In other words, if the roll angle of a ship in a wave exceeds the θ_{awm}, depending on ϕ_w , there is a possibility that the ship may capsize after one swing to the lee side. Accordingly, the θ_{awm} can be considered as a factor for the capsize. And the phase angle ϕ_w can be taken as $2/\pi$ approximately.

From the above discussion, two kinds of factors for the capsize can be proposed, namely one is $(\gamma\pi H/\lambda)\omega$, the other is θ_{awm}.

3.2 Determination of capsize condition

Studies on the capsize in waves have so far been carried out through experiments and numerical simulations. Considering the complicated mechanism of the capsizing phenomena, these direct methods are still necessary. To understand the phenomena physically, however, theoretical approach should be needed. In order to derive an expression for capsize condition, the capsize is assumed here, as usual, that the roll angle exceeds the vanishing point of the ship stability θ_v .

The condition for capsize is expressed as the following inequality.

$$|\theta_{awm}|+\Delta A > \theta_v \qquad (15)$$

where $|\theta_{awm}|$ represents the amplitude for θ_{awm}, and ΔA the increment of A during one swing from weather side to lee side, which can be approximated to be the form.

$$\Delta A \doteqdot \dot A T \qquad (16)$$

As shown in Fig.3, the time derivative $\dot A$ is calculated at the time when $A=(|\theta_{awm}|+\theta_v)/2$ and T is the one swing period. T is estimated from the phase velocity mentioned in the section 3.1(1).

$$T \doteqdot \pi/(\omega-\dot\phi) \qquad (17)$$

When the roll period in nonlinear and in unsteady roll is concerned, $\dot\phi$ should not be neglected against ω, although we assum-

ed $\dot{A} \ll A\omega$ and $A\dot{\phi} \ll A\omega$ to obtain the first approximate solution in the section 2.1. Eq. (17) is approximated to the follow form.

$$T \fallingdotseq (T_w/2)(1+\dot\phi/\omega) \qquad (18)$$

where T_w the wave period. For $\dot{A}$ and $\dot\phi$ in eqs. (16) and (18), the following equation can be used which is derived by substituting $\phi = \pi/2$ into eqs.(8) and (9).

$$\dot{A} = -K_e A + \frac{1}{2}(\gamma\pi H/\lambda)\omega \qquad (19)$$

$$\dot\phi = \{\omega^2 - \omega_0^2 \, g(A)\}/2\omega \qquad (20)$$

where $\qquad A = (|\theta_{awm}| + \theta_v)/2 \qquad (21)$

Rearranging eq.(15) using eqs.(16) through (20), and dividing by $\omega_0\theta_v$, the condition for least possible capsize becomes the form,

$$\frac{\gamma\pi H/\lambda}{\theta_v}\nu > 2K_e A/(\omega_0\theta_v) + \frac{4\nu}{\pi}\{3-g(A)/\nu^2\}^{-1}$$
$$(1-|\theta_{awm}|/\theta_v) \qquad (22)$$

where ν denotes the tuning factor. The right hand side of the expression (22) includes the roll damping, the stability of the ship, and the initial roll angle in the weather side. If the exciting moment in the left hand side exceeds the terms of restoring moment, damping moment etc. in the right hand side, there must be a possibility for the ship to capsize.

The nonlinear roll damping can also be considered for an extreme roll. When the roll damping term in eq.(1) is expressed as

$$2(K_1\dot\theta_a + K_2|\dot\theta_a|\dot\theta_a + K_3\dot\theta_a^3)$$

the equivalent damping coefficient K_e in the 2nd term of the right hand side in eq.(22) should be replaced to the following form.

$$K_e = K_1 + \frac{8}{3\pi}K_2 A + \frac{3}{4}K_3\omega_0^2 A^2 \qquad (23)$$

3.3 Critical line for capsize

From eq.(22) we can define a critical capsize line which separates a non-capsize domain and the domain of possible capsize, in the following form.

$$\frac{\gamma\pi H/\lambda}{\theta_v}\nu = 2K_e A/(\omega_0\theta_v) + \frac{4\nu}{\pi}\{3-g(A)/\nu^2\}^{-1}$$
$$(1-|\theta_{awm}|/\theta_v) \qquad (24)$$

For instance, as shown in Fig.4 , the critical line can be drawn by taking the ordinate and abscissa as $|\theta_{awm}|/\theta_v$ and $(\gamma\pi H/\lambda)\nu/\theta_v$ respectively. When the wave height is small enough to satisfy the condition,

$$\frac{\gamma\pi H/\lambda}{\theta_v}\nu < 2K_e/\omega_0 \qquad (25)$$

one can see that no capsize happens. Conversely, for a wave height exceeding a point P as shown in Fig.4, namely

$$\frac{\gamma\pi H/\lambda}{\theta_v}\nu > K_e/\omega_0 + \frac{4\nu}{\pi}\{3-g(A)/\nu^2\}^{-1} \qquad (26)$$

capsize happens immediately, since the roll angle can not recover again to the upright position because $\theta_{awm} \geq 0$. Such a value of the point P may play a simple index to estimate the ship stability against capsize.

4. APPLICATION OF CRITICAL CAPSIZE CONDITION

The preceding discussion on the critical capsize condition can also be extended to other aspects of ship stability.

4.1 Tuning factor and capsize

The peak amplitude in steady roll motion of a ship takes place at the resonance wave period on the frequency-responce diagram. However, the resonance wave period in unsteady process like capsizing can not be defined clearly, since the roll period of changes with the roll amplitude as seen in the preceding chapter. However, we can find a particular value of the wave period concerning capsize. The right hand side of eq.(22) can be regarded as a function of the tuning factor ν, and becomes a minimum at a certain value of ν, i.e. ν_c. The value corresponds to a critical period which induces a capsize at the smallest wave steepness. From eq.(22) the value of such a critical tuning factor can be obtained in the form.

$$\nu_c = \sqrt{g(A)} \qquad (27)$$

where $\qquad A = (|\theta_{awm}| + \theta_v)/2$

Considering the right hand side of eq.(27) is the same as eq.(12) giving the backborn curve, the wave period $\nu_c T_0$ corresponds to the ship roll period with the mean roll amplitude $(|\theta_{awm}| + \theta_v)/2$. Thus eq.(27) gives a critical wave period for a ship to have the most possible occurrence of capsize. By comparing the critical capsize line for the ν_c value, we may discuss the effect of, for example, shape of GZ-curve on capsize, which will be stated in the next section (2).

4.2 Critical capsize condition and ship stability

The present critical condition is

affected by the ship stability.

(1) GZ_{max} and the stability

GZ_{max}, i.e., the maximum value of GZ, is an important factor related to the ship stability. It is said that higher GZ_{max} brings better stability. Let us examine this from the point of the critical capsize condition calculated by eq.(24). Suppose three kinds of GZ-curves GZ_{A-1}, GZ_{A-2} and GZ_{A-3} respectively, as shown in tht left in Fig.5. The ratio of GZ_{max} values is 3:2:1. The corresponding critical lines are clearly influenced by the difference of GZ_{max}. We can interprete this difference as the likelyhood of capsizing in waves. For example, taking the wave of $(\gamma\pi H/\lambda)\nu/\theta_v$ =0.8, we can read the value of $|\theta_{awm}|/\theta_v$ in Fig.5 as follows.

For GZ-curve A-2 $|\theta_{awm}|/\theta_v = 0.4$ (28)
For GZ-curve A-3   "   = 0

The ship having GZ-curve A-3 will capsize even from upright, while the ship having GZ-curve A-2 is not the possibility of capsize within about 40 % inclination of the stability range to the weather side. The signs ■ , ● and ▲ in Fig.5 represent the points calculated by a numerical simulation using Runge-Kutta method. The fact that the agreement between them is quite well indicates a validity of the present critical line.

(2) Shape of GZ-curve and critical capsize condition

The effect of shape of GZ-curve on capsize has so far been examined only in view of dynamical stability. However, this effect can also be studied by using the present critical line method.

In order to compare the critical lines corresponding to three kinds of GZ-curves as shown in the left in Fig.6, in which the the values of dynamical stability at θ_v are all the same, we can find that a round GZ-curve like C-1 has poor stability against capsize, as shown in Fig.6. In the figure, the tuning factor is prescribed to be the severest value, i.e., ν_c in eq.(27).

5. EXPERIMENT

To confirm the results obtained in the preceding chapters, capsize experiment is carried out in a water tank. Two kinds of cylindrical models are used of which the cross sections are ellipse and square, called elliptic model and box model respectively, as shown in the right part of Fig.7. GZ-curves for these models are

considerably different in form and GZ_{max}, so that the stability of the box model is very poor. Experimental conditions are listed in Table 1.

In the experiment, regular beam waves are generated. The model is set in the water tank making its lateral motions free. To establish the initial condition ϕ_w and θ_{aw} the model's roll is restricted at the beginning to keep heel in certain angle, and then at the prescrived wave phase angle,the model is made free from the restriction.

Experimental results are shown in Fig.8. The marks ■ and ● are the experimental points of the box model and of the elliptic model respectively. It is shown that the experimental points for the box model , having even poorer stability,lie in safty side for capsize rather than those for the elliptic model. Calculated results by eq.(24) agrees qualitatively well with the measured data.

6. CONCLUSIONS

A critical condition for ship capsize in beam waves is proposed on the basis of the unsteady-roll analysis using an approximate solution techniqe of simplified roll equation. The critical capsize condition can be expressed in terms of GZ-curve, roll damping coefficient, tuning factor, wave steepness, and initial roll angle in weather side. The present critical condition will also provide an useful criterion for the ship stability against capsize.

NOMENCLATURE

A   Roll amplitude
A   Steady-roll amplitude
GZ   Righting arm
H   Wave hight
T   One swing period
T   Roll period in small amplitude
T   Roll period in finite amplitude
t   Time
β   Coefficients for nonlinear righting arm
γ   Coefficient of effective wave slope
θ_a Apparent roll angle

θ_{aw} Initial roll angle in weather side

θ_{awm} Critical roll angle of θ_a

θ_v Vanishing point of stability

K_e Equivalent damping coefficient

K_i Nonlinear damping coefficients (i=1,2,3)

λ Wave length

ν Tuning factor

ν_c Critical tuning factor

ϕ Phase difference

ϕ_w Initial phase difference in weather side

ω_0 Natural frequency in small amplitude

ω_s Frequency in finit amplitude

REFERENCE

[1] W. Froude:The Non-uniform Rolling of Ship, Trans.R.I.N.A., 1896.

[2] Y. Watanabe:On the Limiting Angle of Roll on Irregular Waves, Jour.S.N.A.J., No.50, 1932.

[3] H. Kato:ON the Rolling of Ships among Irregular Waves, Jour.S.N.A.J., No.65, 1940.

[4] O. Krappinger:Uber Kenterkriterien, Schiffstechnik 9-H. 48, 1962.

[5] W. Blocki:Ship Safty in Connection with Parametric Resonance of the Roll,I.S.P. ,No.306, 1980.

[6] A. Y. Odabasi:A Morphology of Mathematical Stability Theory and its Application to Intact Ship Stability Assessment, Second Int. Conf. on Stability of Ships and Ocean Vehicles, Tokyo, 1982.

Table 1 Experimental condition

| Model	T_0 (sec)	K_e (1/sec)	ν_e	H/λ
Elliptic model	0.785	0.43	0.7~0.9	1/10~1/15
Box model	2.50	0.32	2.0,2.5	1/18,1/10
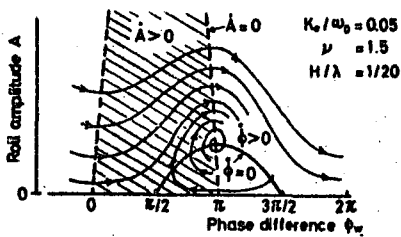
Fig. 1. Example of phase plane diagram
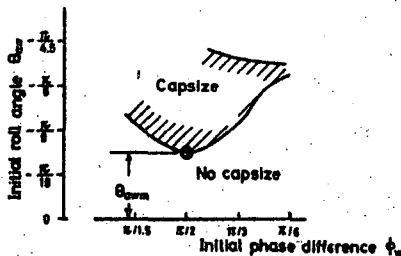

Fig. 2. Effect of initial condition for capsize
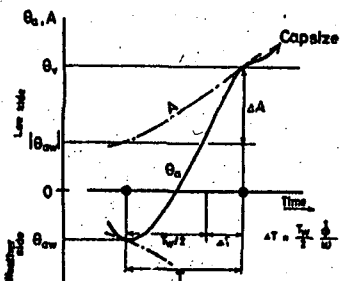

Fig. 3. Roll angle during one swing
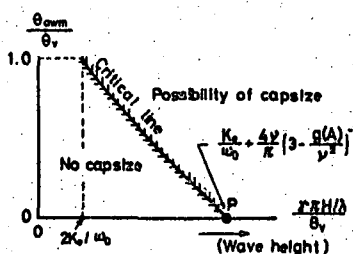
Fig. 4. Critical capsize line
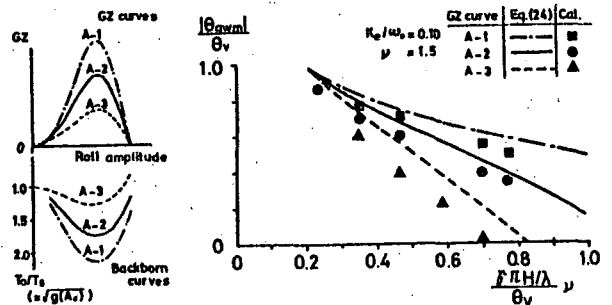

Fig. 5. Effect of GZmax on critical capsize condition
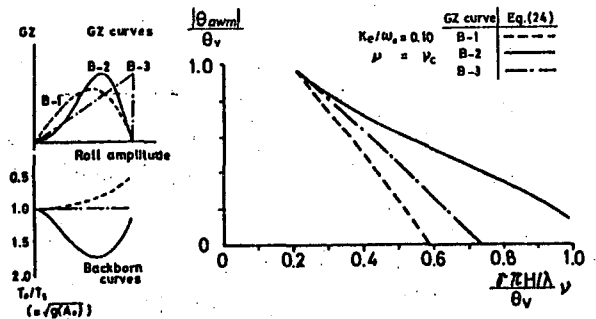
Fig. 6. Effect of shape of GZ-curve on critical capsize condition
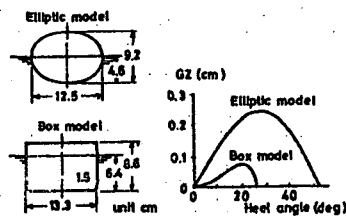

Fig. 7 Model sections and their GZ-curves
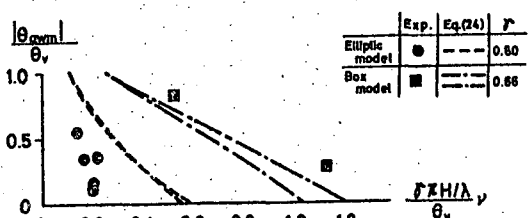
Fig. 8 Critical capsize condition for cylindrical model

STABILITY CRITERIA FOR PRESENT DAY SHIPS DESIGNS

H. Hormann, D. Wagner

ABSTRACT

During the past twenty years a dramatic change has taken place in the design of dry cargo ships, which has a bearing upon their seaway behaviour and thereby upon their stability characteristics. The traditional methods for assessment of the stability of ships take these changes into account to a limited extent only and may entail misjudgements of stability, as has been proved by tank tests. The introduction of a form factor "c" has made it possible to assess stability in such a way as to take into account individually and in line with their significance the parameters determined by tank tests, such as principal dimensions, KG and ship's form. The application of this new method of stability assessment has a bearing upon the minimum stability values required. For instance, with an increasing B/D ratio these increase as against the requirements of IMO Res. A 167. However, adherence to these more stringent "weighted criteria" only leads to a safety level equivalent to that of "traditional" ships, but not to a higher one. At the example of three ships with widely differing B/D ratios the effect of this new method upon the stability requirements is demonstrated and compared with the requirements having existed so far.

1. INTRODUCTION

In the early seventies, the container was introduced into shipping as a means of transport. At that time, sceptics predicted not much life expectancy for this trend. Compared with conventional general cargo traffic, the investments and extra organizational efforts required appeared to be extraordinary so that it was deemed doubtful that this novel transport system would prove to be an economic success. Today, we know that, in fact, the development was completely different. The container has revolutionized shipbuilding and shipping and led to ships being constructed that are capable of carrying deck loads which would have been inconceivable 15 years ago.

2. CHANGE IN THE RANK, WHICH STABILITY HAS

Parallel to this brisk change in the transportation system, the determination and assessment of intact stability have become continuously more important. In former days, particularly with big ships, stability was a natural side product, so to speak, generally not requiring any particular attention in the design phase. Nowadays, however, the proper determination of stability has become one of the most important design parameters on which a vessel's economic success or failure essentially depend.

It is evident that previously existing stability reserves are nowadays being utilized and that ships are loaded up to their stability limits. Now, where is this limit ?

3: DEVELOPMENT IN PARAMETERS OF HULL FORMS

Up to this date stability is assessed according to the conventional method by applying the experience gained with other ships. This is correct, as long as the ships' form parameters are similar. This could still be taken for granted, when IMO Resolution A 167 was introduced twenty years ago. Sufficient knowledge was available respecting the stability limits, at least of the majority of ships then existing.

However, with progressing containerisation the principal dimensions of dry cargo ships have changed fundamentally. In the diagrams Figs. 1 and 2 the mean values of the B/D and L/B ratios of all dry cargo ships at present classed with Germanischer Lloyd have been plotted over their respective years of construction. For the period from 1960 to 1985 the diagrams show a continuous increase in the B/D ratio from 1.69 to 1.96 and a decrease in the L/B ratio from 6.9 to approx. 6.2. This means that on an average in the course of the past few years the breadths of ships have increased continuously. (The remarkable increase of the ratio L/B in 1985 may be incidental. This ratio varies between 1980 and 1985 as follows: 1980: 6.19; 1981: 6.45; 1982: 6.26; 1983: 6.03; 1984: 6.13; 1985: 6.35, as plotted in Fig. 2 with dotted lines.)
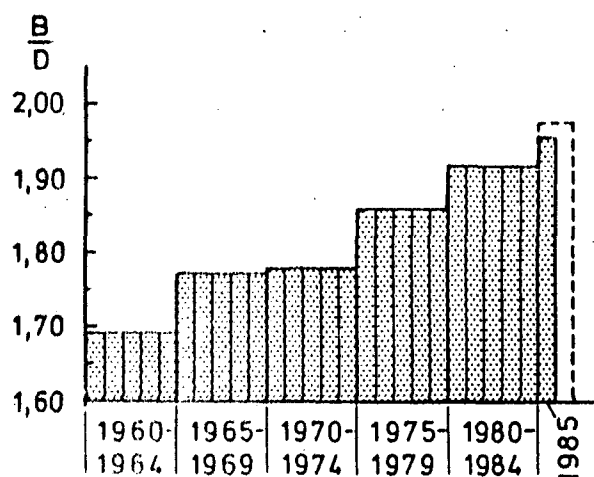
Fig. 1 Development of the medium ratio B/D of all dry cargo ships classified with GL, depending on their date of completion
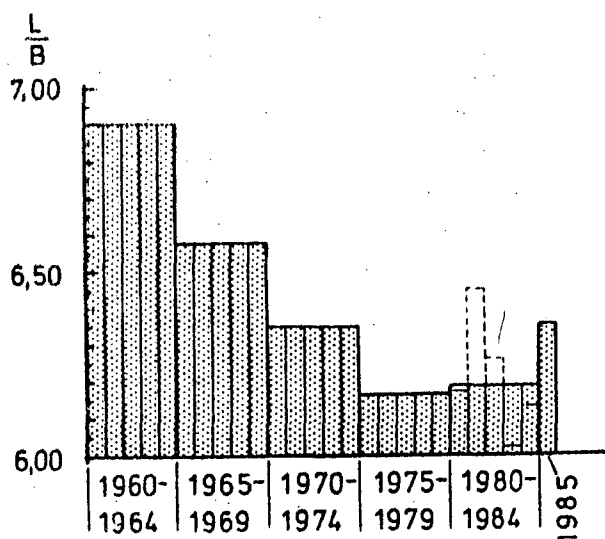

Fig. 2 Development of the medium ratio L/B of all dry cargo ships classified with GL, depending on their date of completion

4. REPERCUSSION ON STABILITY

As a result the stability characteristics of numerous ships have changed as against older designs; this can be demonstrated particularly well at the range of stability. During the early sixties in general the stability range of dry cargo ships by far exceeded 60°, while modern container ships in many instances hardly reach a range of stability of e.g. 50°. Even though no reliable experience is available on the connection between this decrease in the range of stability and a resultant effect upon the ships' safety against capsizing, still to-day stability is assessed according to the criteria employed so far, which, however, almost entirely ignore the range of stability, simply because this had never been a problem.

Thus, as before, stability is judged on the basis of collective empirical values, which owing to changed ship designs have meanwhile to be regarded as being questionable or at least incomplete. However, as on the other hand optimum utilization of stability is one of the decisive aspects for the profitability a container ship, it is logical that not sufficiently reliable dimensioning criteria today constitute a greater risk to stability than was the case previously at the time of introduction of Resolution A 167.

Against this background in the Federal Republic of Germany for the first time in 1979 systematic attempts were made of the development of stability criteria, which are specific for defined ships, i.e. for their different dimensions and shapes, thus better taking into account their stability characteristics than has been possible with the criteria available so far, which are essentially those of IMO Resolution A 167, is being applied worldwide up to the present day to all sizes, shapes and types of ships, although originally having been provided for a certain category of ships only. Later, the so-called IMO weather criterion was introduced, the development of which was completed recently. However, this weather criterion (Res. A 562 (14)) must, subject to the wording of that Resolution, be applied to ships of up to 100 m in length only supplementary to the criteria of A 167 and to larger ships supplementary to other criteria recognized by the Administration; these are, however, not defined or rather not existing. The disadvantage of both methods is that they do not adequately take into account the existing differences in stability characteristics and - as proved during tank tests - the resultant different stability requirements.

5. "DYNAMIC" OR "STATIC" METHODS ?

It is an ongoing argument that stability criteria using the still water righting arm curve do not take dynamic effects into account. This is a misconception from the onset. Of course, the still water curve shows the physical ability of a ship in calm water to counteract heeling moments, but already Rahola's findings did indirectly cater for the ship in a seaway - simply by setting the "safe limit" for this curve so that a ship complying with these limits very likely could sustain all forces to be expected. Surely, all attempts to directly calculate the dynamic behaviour of a ship in a seaway tell us a lot, but even if we suppose that we were able to exactly calculate the intact stability level for a particular ship to just successfully meet a given irregular seaway, we would always have to process

the result in order to cover also all other possible irregular seaway conditions, combinations with wind forces, etc. This means adding a margin or multiplying by a safety factor. Looking at this, one easily realizes that again the physically exact calculation stops at a certain point and the "safe values" are only established by doing a further step which has to be characterized as one of estimation and summarizing.- The differences in all the approaches tried out in recent years in substance consist in this generalizing estimation step done at different points.

All methods proposed up to now - and certainly also in future - stop the true physical approach sooner or later but at any rate before the final applicable value is formulated.

These thoughts automatically make it evident, that there is no justification for dividing the various methods of assessing safe intact stability values into dynamic and static ones. Starting from this point one can easily see that a stability criterion developed on the basis of model tests in an irregular seaway is as good as any theoretical calculation approach - it even is believed to be a superior way, because in model tests almost all dynamic influences acting on a ship in the seaway chosen are implicitly covered, a degree of correctness which will hardly even be achieved by calculation. The estimation steps in the model test approach is the establishment of a correlation between the exact safe intact stability values for one seaway (or at best a limited number of seaways) to all the possible seaways a ship might encounter in its life. How this correlation is done is explained in another context.

6. FORMFACTOR "C"

Idea, approach and course of action of the German series of tank tests and their evaluation was introduced and commented upon on other occasions (see bibliography). At this time only certain aspects are spoken to which are of particular interest for the considerations here offered.

In a formula proposed by Dr. Blume (Hamburg Ship Model Basin) for a form factor "c" the form parameters essentially determining a vessel's stability, as has been observed and proved by measurements during the tanks tests conducted in irregular seaways, have been compiled in accordance with their respective significance. The formula reads as follows:

$$c = \frac{d \cdot D'}{B^2} \cdot \sqrt{\frac{d}{KG}} \cdot \frac{C_B}{C_W} \cdot \sqrt{\frac{100}{L}} \; ;$$

$KG \geq d$ and $L \geq 100 \, m$

where L = length according to LLC 66 [m]
B = moulded breadth [m]
D' = moulded depth, corrected for hatches or trunks [m]
KG = vertical centre of gravity [m]
C_B = block coefficient
C_W = waterplane coefficient

The imaginary moulded depth D' is determined in accordance with the following formula:

$$D' = D + h \cdot \frac{2b-B}{B} \cdot \frac{2 \cdot \Sigma l_H}{L} \; ; \qquad b \geq \frac{B}{2}$$

where D = moulded depth [m]
h = height of hatches [m]
b = breadth of hatches [m]
Σl_H = sum of length of hatches within a range of L/4 from ⊠ [m] (see sketch Fig. 3)
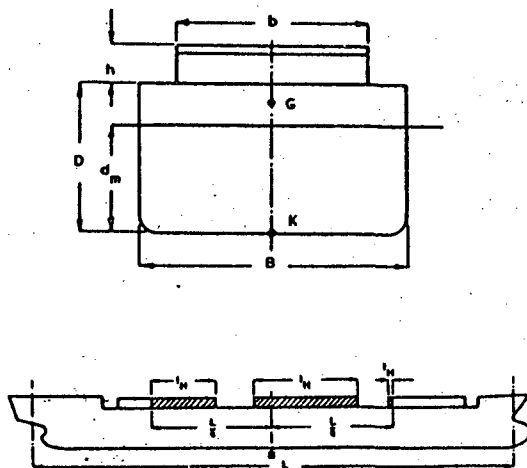
Fig. 3 Symbols, used in the formula for Formfactor "c"

The new stability requirements using this "c"-factor for a particular ship and its actual loading condition result from the following formulae:

GZ_{30^o}	$\geq \dfrac{0.04}{c}$ [m]
GZ_{max}	$\geq \dfrac{0.05}{c}$ [m]
E_{30^o}	$\geq \dfrac{0.012}{c}$ [m · rad]
E_{40^o}	$\geq \dfrac{0.02}{c}$ [m · rad]
E_0	$\geq \dfrac{0.035}{c}$ [m · rad]
$E_{30^o-40^o}$	$\geq \dfrac{0.007}{c}$ [m · rad]

where GZ_{30^0} = righting lever at 30^0 inclination

GZ_{max} = maximum righting lever

E_{30^0} = area under GZ-curve up to 30^0

E_{40^0} = area under GZ-curve up to 40^0

E_0 = total area under GZ-curve

$E_{30^0-40^0}$ = area under GZ-curve between 30^0 and 40^0

Except for the criteria E_0 and GZ_{max}, these are the assessment criteria known from Resolution A 167, however, with "weighted" and thereby variable minimum values.

7. TRANSFORMATION OF TANK TEST RESULTS INTO LIMITING VALUES

Now, how did these criteria come about? On the basis of the tank experiments it was possible to fairly accurately ascertain for the individual ships investigated the limit betwenn "safe" and "unsafe" - namely, in following or quartering seas. However, as the resultant stability requirements appeared to be unrealistically stringent, - a natural result of the extreme characteristic of the seaway chosen, - a way had to be found for reasonably harmonizing the results obtained by experiments and practical experience. To this effect, the stability particulars of nearly 150 container ships were analyzed and the most unfavourable loading condition listed in the individual stability booklets was categorized into three grades of stability, i.e. excellent, normal and limiting condition. The statistical analysis of the values thus obtained led to the criteria already mentioned, which so to speak represent the category "limiting condition of stability" i.e. just acceptable cases. As already mentioned previously, these values are markedly below the requirements directly deduced from the experiments. This will be surprising to unprejudiced readers. However, it has to be considered that the tank tests were carried out under comparatively extremely severe seaway conditions, and it is easy to understand that in view of a different, less severe seaway less stringent stability requirements would have been imposed with regard to safety against capsizing. Even more important, during the tank test

the most critical situation was intentionally, searched for while in practice, as a rule exactly the opposite will occur, furthermore, no "nauticals" counteraction against dangerous situations were taken.

When dimensioning a vessel's stability, it will hardly be possible or at least extremely difficult to determine the seaway to be assumed, the probability of occurrence of this seaway under unfavourable loading conditions, and the practical qualifications of the crew, to logically relate these aspects to each other and to draw conclusions as to a vessel's required stability. However, when relying upon the statistics of a small fleet sailing successfully, the parameters mentioned are considered almost exhaustively, so that the stability criteria, as weighted by form factor "c" may be regarded as a good combination of scientific research, practical experiments and experience acquired.

8. PHILOSOPHY OF THE NEW METHOD

Stability criteria presently used - be they internationally accepted or set forth by national Administrations in addition to or in lieu of those recommended by IMO - distinguish the ships by length and sometimes by types. This tacitly implies that the hull forms and all other features affecting stability (superstructures, hatch coaming, etc.) only have an influence on the safety against capsizing to an extent as reflected in the static righting arm curve. This simplification is certainly acceptable as long as the general parameters of the hull forms, such as L/B, B/D ratios etc. vary within certain limits so that the dynamic behaviour of the hulls in a seaway can be taken as having similar characteristics.

Looking at the evolution of hull parameters as mentioned within the last 20 years, i.e. since the mid-sixties, when the traditional general dry cargo ship started to gradually turn into a "wrapper for containers", one has to admit that the above assumption regarding the physical similarity of the dynamic behaviour cannot be upheld. This is already obvious at least in its tendency, by comparing only the curves of static stability of a modern cargo (container) ship with its prodecessors. (Fig. 4)
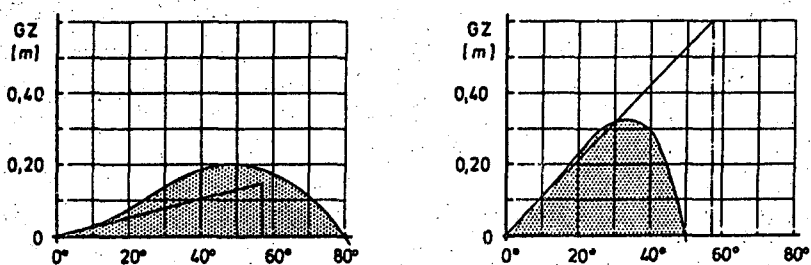

Fig. 4   Comparison of GZ-curves of a traditional dry cargo ship (left) and a modern container ship (right) with identical areas under the GZ-curves.

All considerations of such complicated physical phenomena like the motions of a shaped volume in a seaway necessitate mathematical simplifications or practical condensation into formulae or diagrams one can work with. After having closely followed up the attempts for decades to adequately cover ships' movements by mathematical models, we came to the conclusion that a promising alternative was to use series of model tests, in which the models in real service conditions are subjected to irregular seaways. Here, in an all-embracing way the dynamics including all major and minor effects of the form of a ship are covered, even those which do not result from buoyant but from two-dimensional parts like bilge heels and bulwarks. - It can certainly be stated that such trials are almost true copies of reality. The problem at this stage is now to condense all the influences into a number of parameters, by which the variation in form between ships are described. This number of parameters expressed in a formula can be related to the description of the stability we are all familiar with - the static righting arm curve in still water. If we now have two ships of different form characteristics, we can "weight" the curves of static stability with the factor compiled using certain form characteristics and thus compare their safety against capsizing in a certainly much better fashion than by using just the usual static stability curves (see Figs. 5 to 10).

This is the basic philosophy behind the proposed "form-factor c". (In Ref. 1. and 2. a different presentation was used to explain the idea of the form factor; it might be beneficial for the indepth understanding of the approach to read the relevant parts of the previous papers again.)

9. APPLICATION OF THE METHOD

As already mentioned, application of the stability criteria weighted by form factor "c", derived for the respective ship, leads to greatly varying stability requirements. The D'/B ratio has a particularly strong effect, as the square of the ship's breadth is used in the form factor formula. According thereto great breadth, low depth ships require a higher stability than ships of equal breadth, but greater moulded depth. This tendency is clearly proved by the results of the tests conducted in the Hamburg Ship Model Basin.

In order to offer an idea of the effect of application of the proposed stability criteria on ships in service, for three ships with different B/D ratios still water righting arm curves were calculated, which just about come up to these crite-

ria. The ships chosen have B/D ratios of 1.64, 2.0 and 2.45 respectively, i.e. a relatively narrow ship, an extremely broad ship and one in between, all of them are modern container ships. The form factors "c" range between 0.186 and 0.083. Presumably the "c" values of most of the ships nowadays in service will range within these limits, so that the examples selected offer a clear idea of the possible effects of application of the weighted stability criteria. In order to enable a direct comparison to be made, the still water righting arm curves required according to Res. A 167 were included in the GZ-diagrams.

For each of the three ships taken as examples two draughts were investigated. The results are shown in Figs. 5 to 10.

10. MINIMUM GZ-CURVES ACCORDING TO GERMAN APPROACH (———) AND RES. A 167 (----).

Vessel I:

L = 161.70 m   B = 25.40 m   D = 15.50 m
B/D = 1.64   L/B = 6.37
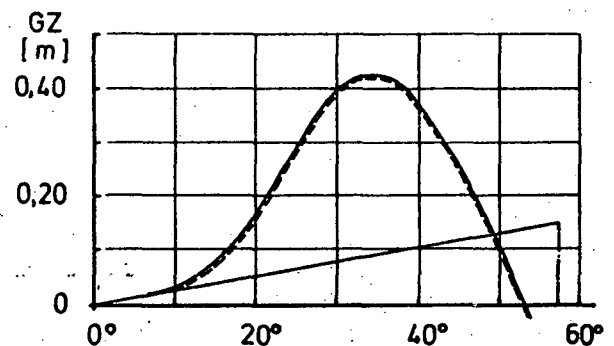
Fig. 5   Vessel I
d = 9.95 m form factor "c" = 0.1861
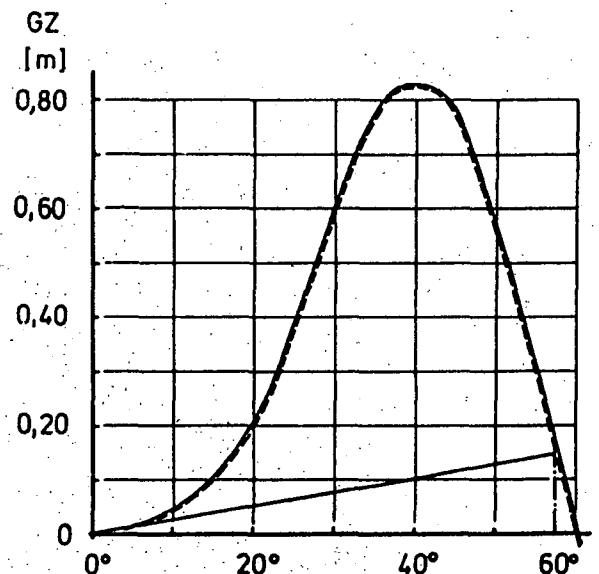
Fig. 6   Vessel I
d = 8.50 m form factor "c" = 0.1507
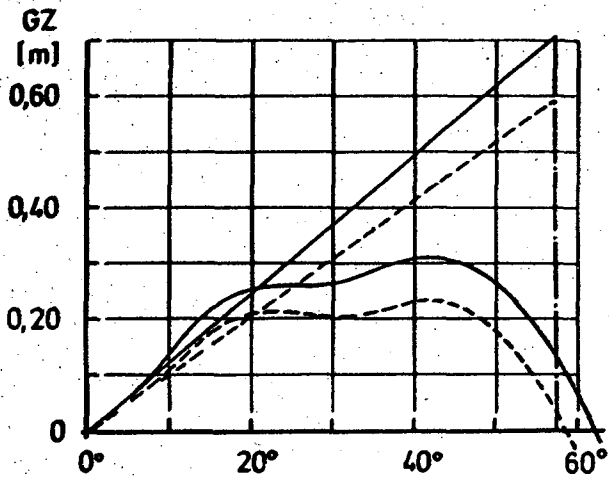
Fig. 7   Vessel II
d = 7.00 m   form factor "c" = 0.1573
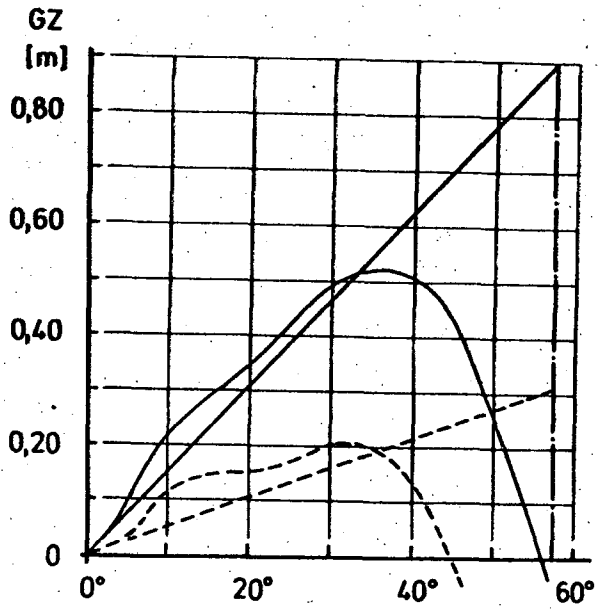
Fig. 9   Vessel III
d = 6.15 m   form factor "c" = 0.1092
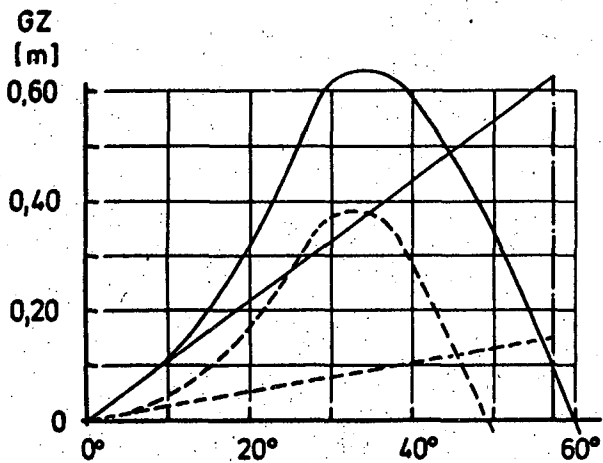
Fig. 8   Vessel II
d = 5.00 m   form factor "c" = 0.0949
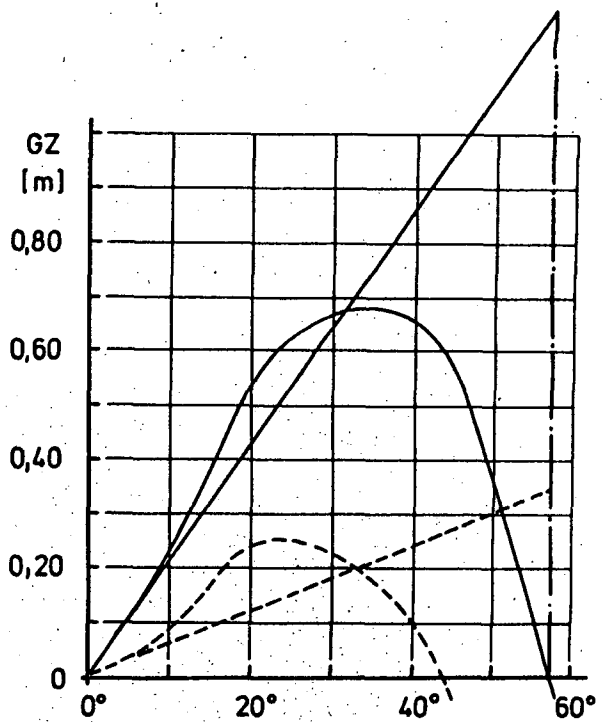
Fig. 10   Vessel III
d = 5.00 m   form factor "c" = 0.0827

When comparing these still water righting arm curves, it will be noted that for ship No. I application of the proposed weighted criteria does not lead to more stringent requirements than those based on the criteria of Res. A 167. On the contrary, with the smaller draught even lower stability values would have been possible, which would, however, have resulted in a lesser initial stability. It may be interesting to note in this context that as an individual criterion the initial metacentric height GMo does not permit any conclusion to be drawn as to a vessel's safety against capsizing. Therefore, the proposed set of weighted criteria does not contain any GMo requirement. On the other hand, it is of course evident that for operational reasons GMo must not be too small, so that it appears to be reasonable to at least adhere to GMo $\geq$ 0.15 m as required in Res. A 167, even when applying the new criteria.

With ship No. II at a draught of 7.0 m the still water righting arm curve weighted with the "c" factor is only slightly above the curve required according to Res. A 167. In the weighted curve the criteria GZ_{30o}, GZ_{max}, E_{40o}, $E_{30o-40o}$, and E_0 all are determining at the same time.

At the draught of 5.0 m the weighted lever arm curve is markedly above the A 167 curve. It is determined by the criteria E_{30o} and E_0.

With ship No. III the still water righting arm curves required according to the weighted criteria are most noticeably above the curves required according to Res.A 167. In this case the weighted curves are determined by the criterion E_0 exclusively.

As a result of this, on ships having traditional maindimensions, as were common at the time of introduction of Res. A 167, even in the event of application of the weighted criteria no more stringent stability requirements are imposed than previously. It is hereby proved that for such ships the value of Res. A 167 is undisputed. This aspect is very important when considering the introduction of such a new method, which is supplementary to the set of criteria used so far.

For ships having principal dimensions deviating from these traditional ones, i.e. essentially for ships with an increasing B/D ratio, when applying the critera weighted with the form factor "c", more stringent stability requirements will result. In the light of the experience gained by the tank test this is indeed necessary. If these new criteria are observed, the safety standard of such ships is approximately equal to that of "traditional" ships, or vice versa: if such ships are assessed in accordance with the criteria of Res. A 167, their safety standard can be considerably lower. For ship

No. III it has e.g. to be taken for granted that with lever arm curves corresponding to the minimum requirements of Res. A 167 a considerable risk of capsizing would exist in heavy following or quartering seas.

11. WHY NO ACCIDENTS SO FAR

It can be argued that up to this date hardly any capsizing accidents of container ships have been reported on. This is true also for extremely broad ships, although surely in many instances their stability is definitely considerably inferior to that required according to the weighted criteria. Thus, practice appears to disprove the risk of stability of such ships, as reckoned with in the preceding statements. In this context it should be mentioned that the tank tests were carried out with models **not** carrying deck containers. Had this been the case, in many of the runs performed capsizing would definitely not have occured. During the indifferent phase, which could often be observed prior to capsizing or to uprighting, the stability behaviour of the models would have been essentially improved by additional buoyancy (= containers) in the midship area.

It is logical to presume that the same applies to the full scale ships, i.e. that with their buoyancy the deck containers contribute to stability in critical moments, thus frequently preventing capsizing. On the other hand, it would be more than dubious in considering safety against capsizing to make the survival chances of ships dependent on thin-walled, possibly inadequately lashed and perhaps slightly rotten tin boxes. The risk implied would become incalculable, so that the supporting effect of the containers should be kept as a silent reserve only.

12. FINAL REMARKS

As compared with previous methods, the method described above for assessment of the stability of modern container ships means a considerable progress, as it enables stability to be assessed from case to case, so that the different behaviour at sea of different ship designs is taken into account properly.

So far, the applicability of this method is confined to a certain category of ships, which should have the following characteristics:

- continuous deck with hatches and normal-type forecastle.
- Deckhouse arranged aft on a poop or directly on the weather deck.
- Vertical shell in midship area above the waterline.

If these characteristics prevail, we now have a tool "ready to use" - a feature which compares favourably with all other approaches to reach improved stability criteria. The difference is that those others - might they be as complete in their theoretical consideration as they will - as a final step to practical use still require the fixing of actual limiting values in a very global way. This final step normally has no direct link to the method offered, but is done relying on "experience" or very general considerations.

It is not the intention of this paper to downrate any of the other approaches, previously and presently proposed. It is beyond doubts that eventually comprehensive calculation and assessment methods will result, which give the future naval architect the possibility of calculating ships' behaviour in a seaway as others can calculate the effect of laminar flow of air on a foil. But until this stage is reached, the "c"-factor method can be used successfully.

REFERENCES

1. Report on Stability and Safety against Capsizing of Modern Ship Design, International Maritime Organization, Paper SLF 34, submitted by the Federal Republic of Germany

2. P. Blume, H.G. Hattendorff; An Investigation on Intactstability of Fast Cargo Liners, Second International Conference on Stability of Ships and Ocean Vehicles, Tokyo, October, 1982

3. H. Hormann; Judgement of Stability - Questions to be Solved - A Contribution from the Point of View of an Approving Authority, Second International Conference on Stability of Ships and Ocean Vehicles, Tokyo, October, 1982

4. O. Krappinger, H. Hormann; Kentersicherheit, Problemstellung und Lösungsansätze, Yearbook of "Schiffbautechnische Gesellschaft", 78th Volume 1984

THE APPLICATION OF SHIP STABILITY CRITERIA BASED ON ENERGY BALANCE

C. Kuo, D. Vassalos, J.G. Alexander, D. Barrie

ABSTRACT

This paper gives a brief description of the
Strathclyde approach to developing intact stability
criteria for ships and outlines the progress made
since the International Conference on the Stability
of Ships and Ocean Vehicles in Tokyo in 1982. The
practical application of the criteria is highligh-
ted, along with the assessment of their applicabi-
lity through comparisons with available stability
data and experience.

1. INTRODUCTION

A number of basic requirements must be met
when designing a ship for operation in various sea-
ways, but one of the most fundamental is undoubted-
ly satisfactory stability.

It is generally acknowledged that a ship must
be "stable" in order to perform its function effec-
tively, but an accurate definition of this concept
has yet to appear. Furthermore, once a criterion
for judging stability has been developed, questions
arise about how far it is valid for all loading
conditions and seaways; how its requirements can
be met in practice; whether its application will
inhibit a vessel's performance, and so on.

The real crux of the problem is the need to
quantify the "stability" of a ship in a way that
represents reality acceptably and is, at the same
time, in a form that designers can use. The prob-
lem is not new. It has been receiving attention
for over a hundred years. However, despite its
being the focus of considerable attention in recent
years progress has been very limited. There are
many reasons for this state of affairs, key ones
including the difficulty of the problem and an
incorrect emphasis of research efforts.

This paper will summarise the lessons learned
during the past thirteen years of research into
ship stability, outline the key steps involved in
the development of Strathclyde's practical ship
stability criteria and highlight the effort expen-
ded in developing confidence in the proposed cri-
teria.

2. LESSONS LEARNED

A number of research teams at the University
of Strathclyde have worked on ship stability since
1973 and it would be helpful to make a brief exami-
nation of the lessons learnt during these thirteen
years.

The initial research work, from 1973 to 1976,
concentrated on an entirely theoretical approach
because it offered solutions "superior" to the sta-
bility criteria based on empirical methods, see
Ref.(1). Many of the research techniques proposed
for assessing ship stability initiated during that
period, such as Lyapunov methods, are still being
used. The main lesson, however, has been that the
development of stability criteria which take full
account of vessel dynamics in a realistic environ-
ment is a long-term process. It was suggested at
the first International Conference or Ship Stabi-
lity in 1975 that the task would need "another hun-
dred years!". That estimate may not be accurate
but it does reflect the magnitude of the problem.
Consequently, during the period 1976-79 the empha-
sis was placed on developing sound and usable cri-
teria which could be applied at as many stages of
the ship design process as possible. This revealed
that for a complex subject like ship stability it
is essential to devise a strategy for tackling the
problem in carefully-planned stages. The resulting
"levels of stability" approach was directed at re-
lating the reliability of a stability assessment to
the quality and quantity of input information avai-
lable and the current state of knowledge, see Ref.
(2). In addition, some of the elementary levels of
stability were developed to demonstrate the appli-
cability of the approach.

During the period 1981-85, as part of the
SAFESHIP project sponsored by the UK Department of
Transport, a method was developed for assessing
ship stability criteria that takes explicit account
of the effects of wind, waves and vessel motions.
Criteria were proposed, based on an energy balance
approach, and refinements have been sought and
introduced in the light of experience gained from
practical applications.

The key lesson to be borne in mind is that
success in proposing a new criterion depends on
progress in the co-ordination of sound theory with
model experiments, full scale data and practical
experience, together with the good fortune every
researcher needs. Concentrating on any single one
of the above areas is unlikely to lead to the
desired answer.

3. INTACT STABILITY CRITERIA BASED ON ENERGY BALANCE

For a long time now strong support has been voiced at IMO for a physical approach to the development of ship stability assessment, that is, an approach taking explicit cognisance of the influence of such physical phenomena as wind and waves. Over the past ten years or so several proposals for modifications to the still-water regulations have been made, culminating in the recent proposal by IMO (3) of what is commonly referred to as a "weather criterion". However, despite the fact that there is some evidence of success in the application of weather criteria in several countries, doubts have been expressed about their suitability for wider application. This is principally because the weather criteria are based on a static treatment and the effect of waves is not explicitly modelled. In addition, the criterion is strictly applicable only to relatively small vessels.

But the need for a physical approach was never in question. In particular, several submissions have been made to IMO in relation to the effect of waves on stability assessment and IMO has confirmed this to be one of the priority topics for attention (4).

The stability criteria developed at the University of Strathclyde during PHASE I and PHASE II of the SAFESHIP project follow the physical approach in that they explicitly model the effect of wind, waves and vessels motions. They are also, as will be demonstrated in the following sections, applicable to all ship types and sizes. A brief explanation of the Strathclyde criteria is given next. For further details, see (5).

The Basic Approach of the Strathclyde Criteria

To derive a quantitative measure of ship stability on the basis of a physical approach, it is necessary to start from a physically realisable and potentially dangerous situation, then model the vessel's behaviour in the said situation mathematically, and finally develop criteria by rationally simplifying the mathematical model. These key steps will now be elaborated in relation to the stability criteria developed at Strathclyde University.

a) Potential Capsize Situation

The three generally-recognised capsizing modes are:

   i) low cycle resonance (dynamic mode)
  ii) pure loss of stability (quasi-dynamic mode)
 iii) broaching (dynamic mode).

Since the first mode of capsize can be avoided through proper handling by the crew, and broaching

can be largely avoided by following certain design and operational guidelines, it was decided to confine research work to the establishment of stability criteria on the basis of the second capsizing mode. This mode pertains to a vessel steaming in following/quartering seas, getting caught on a wave crest, and "flopping" over with little or no preliminary rolling. In addition, it is widely accepted that following/quartering seas constitute the most dangerous situation for all vessel with the exception of very small vessels, which can be overwhelmed by severe beam seas.

The element of beam wind has also been incorporated in the situation described above, which - as indicated by Arndt et al (6) - is by no means uncommon, even though it seems to be a contradiction in physical terms.

b) Mathematical Model

A general form of rolling equation may be used to describe the dangerous situation referred to above, which includes all possible known effects. However, in view of the severe limitations on accuracy in measuring even such simple parameters as the position of the centre of gravity, there is no virtue in seeking a very precise mathematical model. This is the reasoning behind the adoption of the "levels of stability" approach. There is, undoubtedly, a need to agree on a roll equation for use in stability research but an equation that can accurately predict vessel behaviour right up to the instant of capsize does not exist.

On the basis of the above, and in order to maximise the interim benefits at the earliest possible stage, research attention was focussed on the following equation of ship roll motion which contains terms that can be readily computed and are considered to be important for theoretical reasons and as a result of experience (7).

$$I_v \ddot{\phi} + C_e \dot{\phi} + g \Delta GZ(\phi,t) = W(\phi) \qquad (1)$$

where $\dot{\phi}$ is the roll velocity
      $\ddot{\phi}$ is the roll acceleration
      t is the time
      ϕ is the roll angle
      I_v is the virtual roll inertia
      C_e is the equivalent linear damping coefficient
      g is the acceleration due to gravity
      Δ is the displacement
      $GZ(\phi,t)$ is the time-varying roll restoring lever computed in regular waves under the free trim condition, see (7)
      $W(\phi)$ is the wind heeling moment.

c) Proposing Stability Criteria (Energy Balance Method)

By analogy with the weather criteria, a generalisation of Moseley's dynamical stability theory is used to derive a quantitative measure of stability. Such a generalisation is necessitated by the fact that moments now in the equation of motion depend on t and $\dot{\phi}$ as well as on ϕ.

Moseley's theory involves the balance of energy between exciting and restoring moments and can be established only for autonomous roll equations such as that pertaining to the weather criteria.

For Equation (1) the first integral over a half roll cycle beginning at ϕ_1 will take the form

$$\frac{1}{2}\dot{\phi}^2 + \int_{\phi_1}^{\phi}[g\Delta GZ(\phi,t)+C_e\dot{\phi}-W(\phi)]d\phi = 0 \quad (2)$$

In this integral it is implicit that t and $\dot{\phi}$ are related to ϕ via the actual motion record determined by the differential equation and initial conditions as well as the time t_1 at which the half roll cycle begins. One possible way to proceed is by numerical evaluation but this is precisely what stability theories seek to avoid. Instead, the following plausible approach has been adopted on the basis that the shape of a representative extreme half roll can be closely approximated by a sinusoidal curve.

Since the important parameters to know in each case are the extreme angles, ϕ_1 and ϕ_2, the frequency of oscillation, ω, and t_1, the chosen function is:

$$\phi(t) = \frac{1}{2}(\phi_1+\phi_2) + \frac{1}{2}(\phi_1-\phi_2)\cos\omega(t-t_1)$$
$$t_1 \leq t \leq t_1+\frac{\pi}{\omega} \quad (3)$$

Using this function, Equation (2) yields

$$F(\phi_1,\phi_2) = \int_{t_1}^{t_1+\frac{\pi}{\omega}}[g\Delta GZ(\phi,t)+C_e\dot{\phi}-W(\phi)]\dot{\phi}\,dt \quad (4)$$

Three different quantitative measures of stability have been proposed based on Equation (4), see (5). The easiest to compute is the net area analogy of the weather criteria which is equivalent to saying that $F(\phi_1,\phi_2) > 0$ for ϕ_2 being the least of 50°, the angle of second intercept, or the down flooding angle. The pictorial presentation may also be presented in a similar form as illustrated in Fig. 1.

Input Information

The integral in Equation (4) represents the net work done by all the moments considered as acting on the ship, which in turn depends on the parameters used to define the ship, the environment, and the ship's roll motion.

The strategy adopted in searching for possible capsize situation has been to choose each parameter, where appropriate, in such a way as to give the most stringent case. On this basis the following input information is used:

i) **Ship Parameters:** For the critical loading condition, the roll restoring lever GZ(,t) is calculated in regular waves of given length, height and direction. This represents the restoring capability of the vessel at an arbitrary moment in time as she rolls in following/quartering seas.

ii) **Dynamic Properties of the Ship:** The dynamic properties of the ship are represented through the parameters defining the potential ultimate half roll cycle, i.e.,

ϕ_1 : The extreme windward roll angle represents the rolling behaviour of ships and is calculated according to the weather criteria.

t_1 : The starting time of the extreme half roll is chosen iteratively such that the most unfavourable combination between exciting and restoring roll moments is ensured.

ω : The frequency of oscillation of the extreme half roll is taken to be equal to the encounter frequency using the vessel's service speed.

Roll damping: calculated according to Ikeda's method (8)

iii) **Environmental Parameters**

The environment is modelled explicitly by a steady beam wind and regular waves, as follows:

Wind heeling: calculated according to weather criteria (without gusting) with a modification to take into account the variation in the projected area with angle of heel.

Wave Direction: following or quartering

Wave Length: the projected wave length on the ship's centreplane is taken to be equal to the ship's length.

Wave Height: calculated from empirical formulae, see Fig. 2.

4. APPLICATIONS OF STRATHCLYDE CRITERIA IN PRACTICE

The evaluation and interpretation of theoretically-derived stability criteria, at whatever level of sophistication, inevitably pose the problem of how to develop confidence in these criteria. During the past five years considerable effort has been directed towards achieving such confidence in the criteria proposed by Strathclyde, and the methods used are summarised as follows.

a) Assessment of a Large Number of Ships

The Strathclyde criteria have now been applied to thirty-five ships from a wide variety of types varying in length from ten to two hundred metres. It should be noted that so far results have been in agreement with operational experience and casualty records. Furthermore, the application of the criteria has been found to reveal discriminative features between ships not revealed by the simpler IMO weather and statistical criteria. This is due to the fact that the Strathclyde criteria explicitly consider the effects of the environment and the vessel dynamics. This point is elaborated in the next section.

b) Comparison with Existing Criteria

In relation to the search for improved stability standards it is relatively easy to propose a new criterion, based on a limited number of applications, that would appear to meet the need. It is, however, a quite different and altogether more difficult task to demonstrate conclusively that any new criterion is an improvement on its predecessors, in that it gives a better description of the factors that are important for stability.

Recent research work at Strathclyde has focussed on comparing the developed Strathclyde criteria with the IMO A.167 and IMO weather criteria (13). The features present in these three methods of assessment have been identified and their influence on the assessment results has been investigated. This has been done by systematically varying the ship design parameters and environmental conditions that influence the effect of each assessment feature, using the following data:

A: Fishing Vessel (L = 21.40 m)

B: Tug/Supply Boat (L = 52.60 m)

C: Fishing vessel (L = 56.85 m)

D: Fishery Protection Vessel (L = 64.00)

HSVA-A: Container Vessel (L = 135 m).

The relative influence of each parameter on assessment results was then considered. Table I illustrates the way in which the parameters that were investigated arose from the various assessment features and Table II gives the details of the first four test vessels. The details of HSVA-A are given in Table III. ((13) for further details).

The investigation demonstrated very clearly that the Strathclyde assessment method is, in general, no more restrictive than either the IMO A.167 or IMO weather criterion. In all the cases where differences have been observed, however, they have been due to the fact that the simpler IMO methods did not model features that are known to have a strong influence on stability. A sample of results from this investigation, illustrating the above observations, is presented in Figs. 5 and 6.

c) Correlation Studies with Model Experiments

A good opportunity to test the Strathclyde criteria with container vessels of lengths from approximately 135 to 200 metres arose through collaboration with the Federal Republic of Germany. The Strathclyde research team was asked to compare its criteria with the FRG-proposed criterion, which is experimentally derived (14). Recognising this as a further test for consolidating the effectiveness of the Strathclyde criteria, the team agreed to carry out these correlation studies using twenty different test cases.

The FRG team have approached the development of their criteria by carrying out systematic model tests in extreme seas - to establish limits against capsizing and measures of safety (limiting values) and by calibrating the latter through comparison with experience. Recognising that the Strathclyde criteria are not based on a fully dynamic model of vessel behaviour, it was thought that correlation studies should be aimed at achieving the following objectives:

i)   To compare the trends of the limiting values established through the model experiments with the corresponding trends established using the Strathclyde method.

ii)   To compare the levels of safety indicated by the two approaches.

The relevant information for the test vessels is given in Table III. (See (14) for more information). It will be noted from Table III that a range of seaways was used. This was employed as a ready alternative to varying the size of the test vessels.

A sample of the results pertaining to the minimum requirements (limiting values) for the Strathclyde, FRG, and IMO A.167 criteria and to Seaway I, is given in graphical form in Figure 7, where comparisons can be made of both the trends and the levels of safety revealed by the various criteria and the model experiments.

From these results it will be noted that the experimentally-derived FRG criteria and the theo-

retically-based Strathclyde criteria are in close agreement in all cases as regards the level of safety and in most cases they indicate similar trends. Disagreement in trends has been observed in cases with extreme breadth/draught ratios and this has been attributed to overestimation of damping in the Strathclyde criteria for high breadth/draught ratios and large roll amplitudes. It will also be noted that the results of both the Strathclyde and the FRG criteria are markedly different from those of the IMO A.167 criterion.

d) Parametric Studies

Once sufficient effort has been expended on developing confidence in any newly-proposed criteria, there remains one further task. For regulatory purposes it is important to link stability assessment to design if new ships are to benefit fully. If a design fails to satisfy the regulations the designer will be asked to improve its stability characteristics while maintaining the competitiveness of the design. For this to be possible, knowledge is needed of how, and by how much, design and other related paramaters affect stability. In other words, a systematic parametric investigation is warranted. On the basis of the information described in Section (b), the following groups of parameters were investigated:

    i) Ship design parameters

    ii) Dynamic properties of the ship

    iii) Environmental parameters.

This investigation has identified the most influential parameters from the point of view of stability assessment as well as the sensitivity of stability to changes in these parameters.

Of the ship design parameters investigated, KG (height of centre of gravity), L/B (length-to-breadth ratio) and absolute size were found to have the most influence on stability assessment. Changes in any of these could affect this assessment far more than specific changes in form. The parameter to which stability is most sensitive is KG, a fact which highlights the importance of estimating this parameter as accurately as possible. The research findings have also demonstrated very clearly the importance of selecting suitable values for the environmental parameters. A sample of summary results for a small vessel (vessel A) and a large vessel (vessel HSVA-A) is given in Figs. 8 and 9.

The investigations described above underline the amount of effort needed to validate any newly proposed criterion, although there are, and always will be, disagreements regarding the conclusiveness of such tests.

5. CONCLUDING REMARKS

On the basis of the foregoing, the following remarks can be made:

a) Over the past five years, in association with the SAFESHIP Project, Strathclyde University has developed a procedure for assessing the intact stability of ships, that explicitly incorporates the effects of wind, waves asnd vessel motions and is based on energy balance. The proposed stability criteria have now been applied to thirty-five vessels and comparisons have been made with empirical data, other stability criteria, and model experimental data. In all cases the results derived from the proposed criteria agree closely with the evidence at hand. On the basis of these applications, refinements have been sought and introduced in the criteria.

b) A systematic parametric investigation has been undertaken, the results of which have indicated that despite the large number of parameters that affect the stability assessment of a vessel, the same qualitative trends can be attained by considering only a limited number of such parameters.

c) The stage has been reached in the stability research at Strathclyde University at which a practical "tool" has been developed that offers a significant improvement over existing methods for judging the intact stability of ships.

d) As long as ships continue to be lost at sea, the need will exist for a constant reviewing of stability standards and increased effort to provide more effective criteria. As regards the Strathclyde criteria, however, it is felt that the stage has now been reached at which an improved ship stability criterion - inspired by the UK Department of Transport - could be put forward at an international level as a practical contribution towards greater ship safety.

REFERENCES

1. KUO, C and ODABASI, A Y: "Application of Dynamic Systems Approach to Ship and Ocean Vehicle Stability". Proceedings Int. Conf. on Stab. of Ships & Ocean Vehicles, Glasgow, 1975.

2. - - - Intact Stability Research, Ninth Workshop: Ross Priory. Dept of Ship & Marine Technology, Univ. of Strathclyde, September 1979.

3. - - - IMO RESOLUTION A.562(14) Recommendation on a Severe Wind and Rolling Criterion (Weather Criterion) for the Intact Stability of Passenger and Cargo Ships of 24 metres in Length and Over. A 14/Res.562. 16th January 1986.

4. - - - IMO Publication SLF 30/WP/7, Report of the ad hoc Working Group on Ship Stability, February 1985.

5. VASSALOS, D: "A Critical Look into the Development of Ship Stability Criteria Based on Work/Energy Balance". RINA W4(1985), issued for written discussion.

6. ARNDT, B, et al: "Twenty Years of Experience - Stability Regulations of the West German Navy". 2nd Int. Conf. on the Stability of Ships and Ocean Vehicles, Tokyo, 1982.

7. MARTIN, J, KUO, C WELAYA, Y: "Ship Stability Criteria Based on Time-varying Roll Restoring Moments", 2nd Int. Conf. on the Stability of Ships and Ocean Vehicles, Tokyo, 1982.

8. IKEDA, U, et al: "A Prediction Method for Ship Roll Damping", Dept of N. Architecture, Univ. of Osaka Prefecture, December 1978

9. BARRIE, D: "Incorporating Wind Heeling Moments in Stability Criteria", Internal Report, Dept of Ship and Marine Technology, Univ. of Strathclyde, February 1985

10. YAMAGATA, M: "Standard of Stability Adopted in Japan", Trans. INA, Spring Meeting, 1959.

11. ALEXANDER, J G: "Equivalent 'Design Waves' for Stability Assessment", Int. Report, Dept of Ship & Marine Technology, May 1985.

12. ANDREWS, K S. DACUNHA, N M C and HOGBEN, N: "SAFESHIP: Environmental Aspects", NMI Report No. 185.

13. BARRIE, D: "The Influences of Ship and Environmental Parameters on Stability Assessment", Ph.D. Thesis, 1986.

14. - - - IMO Publication SLF/34: "Report on Stability and Safety Against Capsizing of Modern Ship Design", September 1984.

AUTHORS' DETAILS

Prof Chengi Kuo, BSc, PhD: Head of The Department of Ship & Marine Technology University of Strathclyde GLASGOW, Scotland, UK

D Vassalos, BSc, PhD: Lecturer in the Department of Ship & Marine Techology University of Strathclyde GLASGOW, Scotland, UK

J G Alexander, BSc: Research Assistant in the Department of Ship & Marine Technology University of Strathclyde, GLASGOW, Scotland, UK

D A Barrie BSc: Consultant (JG) Y-ARD Limited Charing Cross Tower GLASGOW, Scotland, UK

TABLE I : ASSESSMENT FEATURES AND ASSOCIATED PARAMETERS

FEATURE	SUB - FEATURES	PARAMETERS	ASSESSMENT METHOD
Roll Restoring		Design parameters (Size, Dimensions Lines, Loading)	Statistical Criteria IMO Weather Criterion Strathclyde Criteria
Roll Damping		Design Parameters	Strathclyde Criteria
Windward Roll Angle	Position Measured From (upright, intersection)	Design Parameters	IMO Weather Criterion Strathclyde Criteria
Roll Cycle		Phasing of Wave and Roll Motion Roll period Encounter Period Ship Speed	Strathclyde Criteria
Wind Heeling	Presence of gusts Velocity - height profile Variation in windage area with heeling angle	Wind Speed Above Water Profile Design Parameters	IMO Weather Criterion - Strathclyde Criteria
Waves	Regular / Irregular Undiffracted / Diffracted	Waveheight Wavelength Direction	Strathclyde Criteria

TABLE II : DETAILS OF SHIPS IN BASIS CONDITION

	Vessel			
	A	B	C	D
Length/m	21.40	52.60	56.85	64.00
Breadth/m	6.71	12.20	12.19	11.60
Depth/m	3.35	5.50	7.77	7.32
Draught/m	2.37	3.40	4.25	4.49
Displacement /tonnes	160	1299	1500	1532
L/B	3.20	4.31	4.66	5.52
D/T	1.34	1.62	1.83	1.63
C_B	0.472	0.575	0.498	0.448
C_{VP}	0.761	0.743	0.772	0.708
C_W	0.760	0.955	0.828	0.836
C_P	0.621	0.602	0.602	0.536
C_{VP}	0.620	0.773	-0.646	0.634
GM/m	0.768	1.160	0.525	0.926
KG/m	2.58	4.66	5.57	4.63
KG_B/m	2.45	5.26	5.37	4.86
LCG/m	-0.77	0.08	-1.11	-1.53

TABLE III : TEST VESSEL LOADING CONDITIONS

| Ship	Sea-way	Code No.	Vel. (ms^{-1})	B/T	L (m)	B (m)	D (m)	LCG (m)	Disp (tonnes)	T (m)	Wave Height (m)	GM (m)
	I	A1	9.2	2.8	135.0	23.0	10.7	-1.108	17620	8.2	5.86	1.7
HSVA-A	I	A2	"	3.43	135.0	23.0	10.7	-0.743	13879	6.7	5.86	1.7
	I	A3	"	4.42	135.0	23.0	10.7	-0.717	10439	5.2	5.86	2.35
	II	A4	"	2.8	154.3	26.3	12.2	-1.265	26301	9.4	5.99	1.94
	III	A5	"	2.8	192.9	32.9	15.3	-1.577	51370	11.7	6.19	2.07
	III	B1	"	3.58	202.4	32.2	18.85	-5.218	35552	9.0	6.23	1.10
HSVA-B	I	B2	"	3.58	141.7	22.5	13.2	-4.251	12194	6.3	5.91	1.37
	I	B3	"	2.93	141.7	22.5	13.2	-3.652	15873	7.7	5.91	1.09
	I	B4	"	4.54	141.7	22.5	13.2	-3.278	9007	4.97	5.91	2.07
	II	C1	"	2.55	158.0	28.0	16.1	-3.793	33087	11.0	6.02	0.55
HSVA-C	I	C2	"	2.55	138.3	24.5	14.1	-3.319	22166	9.63	5.38	0.53
	I	C3	"	3.11	138.3	24.5	14.1	-2.611	17189	7.88	5.88	0.48
	I	C4	"	4.0	138.3	24.5	14.1	-2.066	12681	6.13	5.88	0.70
	III	C5	"	2.55	197.5	35.0	20.1	-4.741	64623	13.75	6.21	0.563
	III	C6	"	3.11	197.5	35.0	20.1	-3.730	50113	11.25	6.21	0.188
	II	D1	"	3.58	161.0	32.2	13.8	-0.934	28496	9.0	6.03	2.75
HSVA-D	I	D2	"	2.93	140.9	28.18	12.08	-1.521	24686	9.63	5.9	2.54
	I	D3	"	3.58	140.9	28.18	12.08	-0.750	19089	7.88	5.9	2.50
	I	D4	"	4.60	140.9	28.18	12.08	-0.398	14042	6.13	5.9	3.54
	III	D5	"	3.58	201.3	40.30	17.30	-1.073	55654	11.25	6.23	2.75
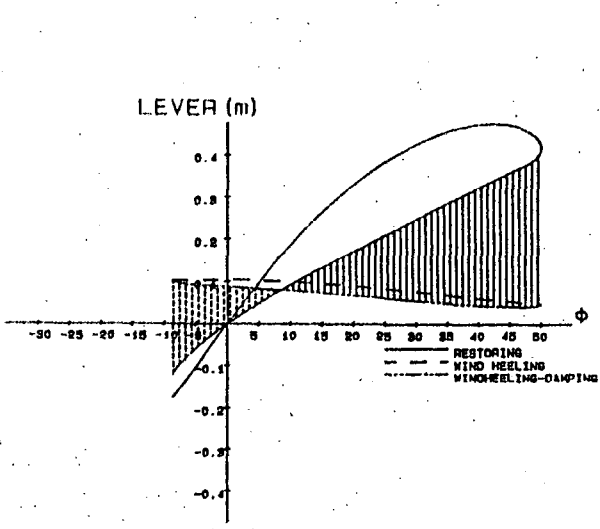
Fig. 1 Energy Balance Diagram of Strathclyde Criteria ("Butterfly Diagram").
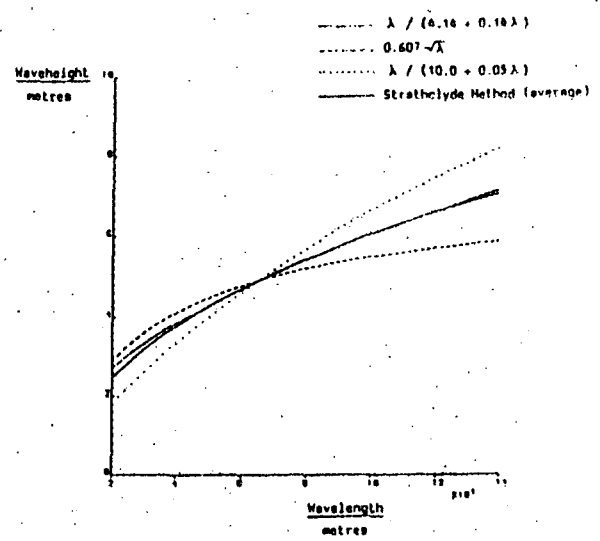
Fig. 2 Wave Height Determination in Strathclyde Method.
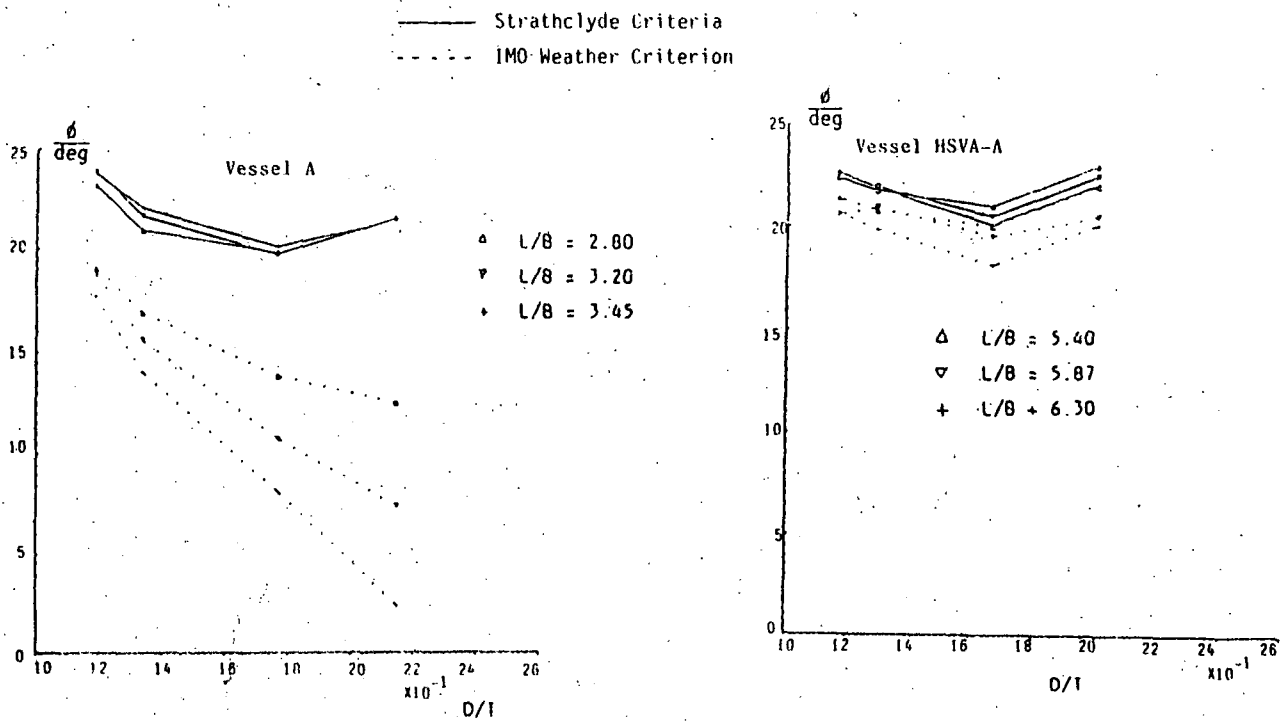
Fig.3 Variation in Windward Angle (ϕ_1) with L/B and D/T
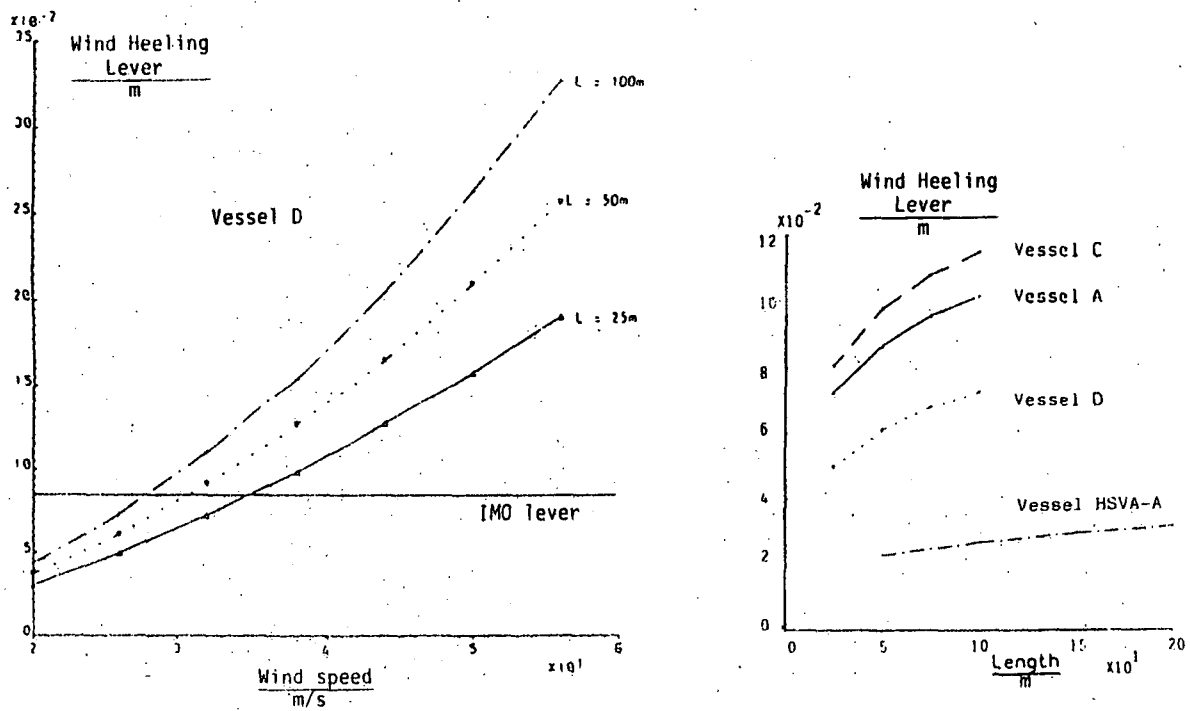
Fig.4 Variation of Wind Heeling Lever with Wind Speed and Size
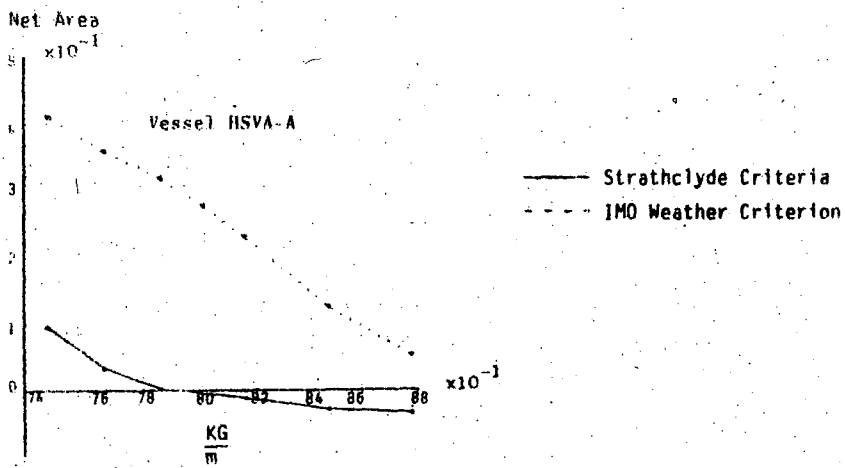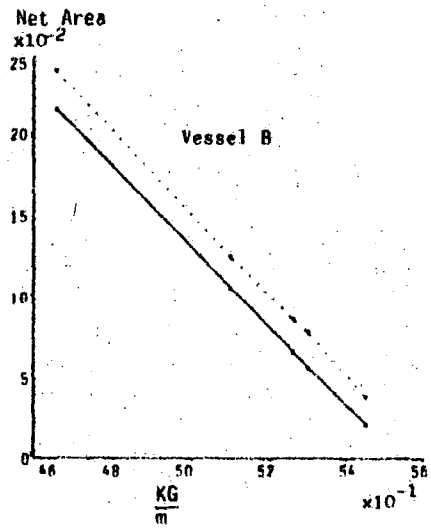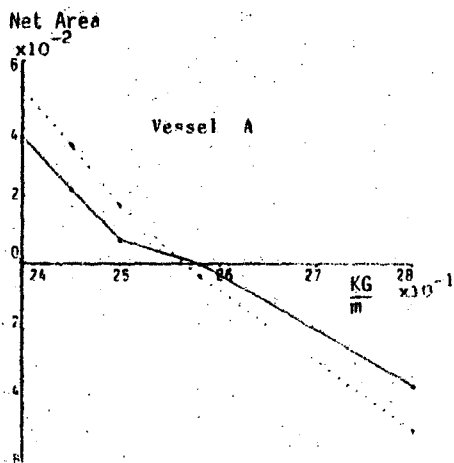
Fig. 5 Stability Assessment Versus KG

Variation in Stability Assessment with D/T and L/B - Vessel A

Net Area
$\times 10^{-2}$

Strathclyde Criteria

IMO Weather Criterion

Net Area
$\times 10^{-2}$

D/T

D/T

```
----  L/B = 2.80
- - -  L/B = 3.20
-..-  L/B = 3.45
```

○ Basis Form
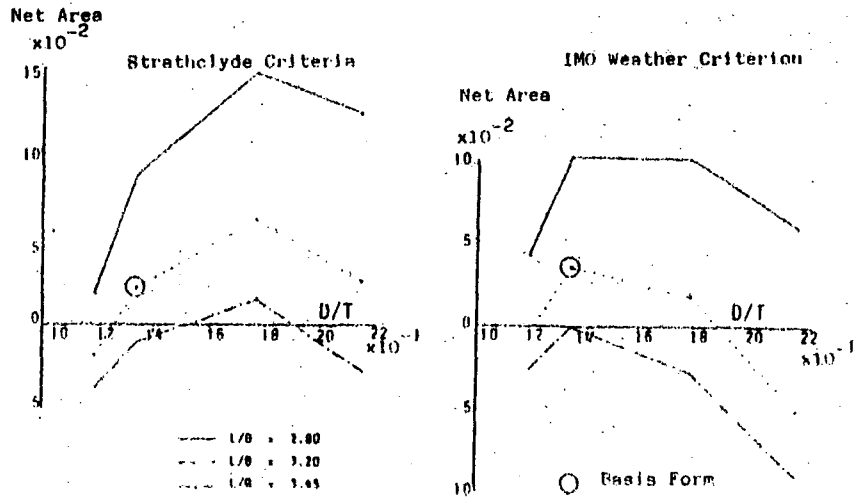
Variation in Stability Assessment with D/T and L/B - Vessel C

$\times 10^{-2}$

Strathclyde Criteria

IMO Weather Criterion

○ Basis Form

$\times 10^{-2}$

L/B = 4.30

L/B = 4.64

L/B = 5.00

D/T

D/T

Fig.6 Variation in Stability Assessment with D/T and L/B
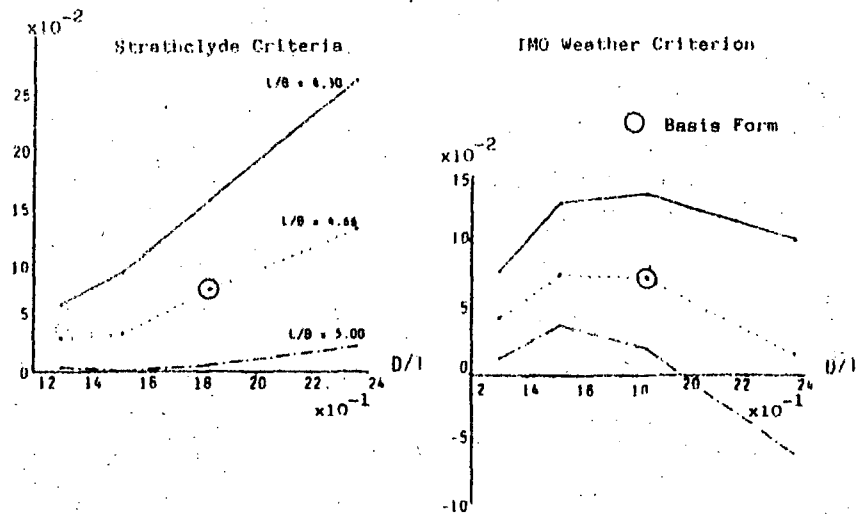
Fig.7 Variation of Minimum GZ_{max} with B/T
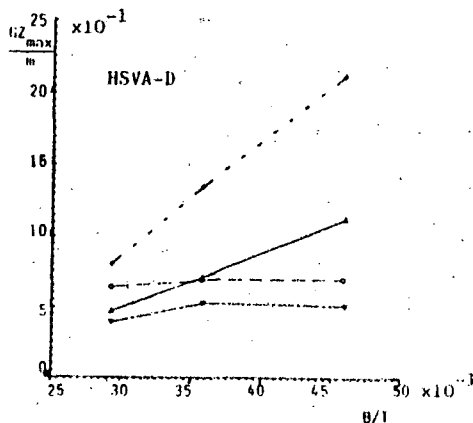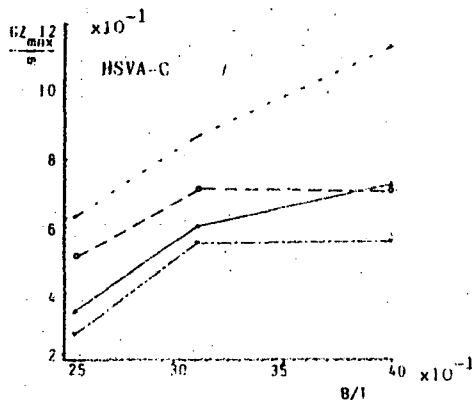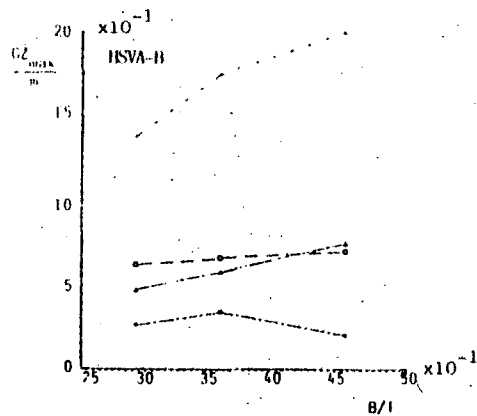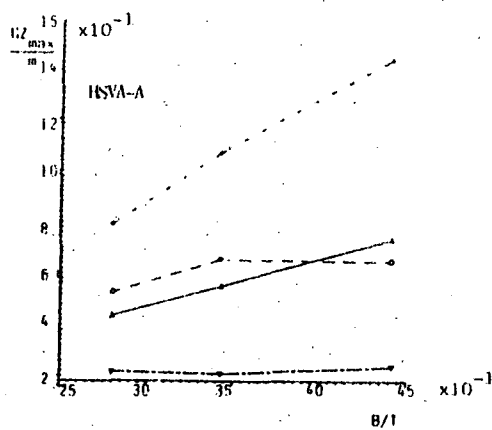
- - - ♦   HSVA Model Experiments

—·— o   Strathclyde Criteria

——— ▲   FRG Criterion

- - - ▼   A167 Criterion

Fig.8   Influence of Parameter Variation on
Stability Assessment - Vessel A

Fig. 9 Influence of Parameter Variation on
Stability Assessment - Vessel HSVA-A

THE NORWEGIAN RESEARCH PROJECT
STABILITY AND SAFETY FOR VESSELS IN ROUGH WEATHER

T. Nedrelid, E. Jullumstrø

ABSTRACT

This paper summarizes some of the work performed under the Norwegian research program "Stability and Safety for Vessels in Rough Weather". Future stability criteria should be built up around dangerous physical situations. We know that both design factors as well as human and weather factors are important when preventing capsizing in waves.

This means that we have tried to develope mathematical models that better describe the capsizing mechanisms and extreme responses of a vessel. Better environmental description are achieved through new analysis of wave statistics and new wave measurements given from offshore research work.

In the program we have concentrated on studying the capsizing mechanism in a following wave situation. Results from loss of stability when balanced on a wave crest are presented. Also theoretical models describing the "broaching to" situation supplied with model test results, are presented.

Theoretical stability is often poorly understood by people working at sea. We normally put restrictions on the vessel design, but often, to prevent capsizing, the actual operational stability is more important. We have therefore been studying if operational procedures can be put forward more precisely through operational manuals onboard a vessel. If this is accepted, operational stability should be more integrated into the process of assessing new criteria.

1. INTRODUCTION

In Norway we still experience that vessels dissappear or capsize in rough weather situations. For quite some time, stability work and investigations into earlier accidents have been performed.

In the seventies, several Norwegian cargo and fishing vessels were lost due to environmental loads. This initiated the research project "Ships in Rough Seas (SIS). In this project one focused on breaking waves and how to calculate extreme motions of vessels in waves, theoretically. The idea was that if one could calculate capsizing events, one might directly put forward rules of restrictions that would improve the design and the safety.

At the start of the eighties much effort was put into the research program called "Stability Criteria". The work was concentrated on model testing of vessels in so-called survival tests. From earlier experience and investigation one can define several dangerous wave/vessel situations that might lead to capsizing. The idea was to find the situation in which the vessel is most exposed and through the probability of the actual wave to occur, define the risk for capsizing.

As critical wave/vessel situations are defined through parameters as heading against the waves, speed and the actual loading conditions, human decision or seamanship influence much.

Accepting this, we built up this new research program (called "Stability and Safety for Vessels in Rough Weather") in three main subjects:

- Ship and cargo
- Environmental description
- Stability criteria

We still need to calculate extreme motions in waves to understand the nature of capsizing in order to improve the vessel design.

We still need better knowledge as to the nature of environmental loads (waves, current and wind) and their statistical occurence along the Norwegian coast.

We still need to define correct stability criteria that consider all important aspects when we are to accept or approve the design and/or the operation.

2. THE PROJECT ORGANISATION

The research program was started in 1981 as a cooperative project between several Norwegian institutions with MARINTEK being the responsible part. The project has been supervised by a committee with members from industry, authorities and the research institutions themselves. Also, representatives from UK have met in this Norwegian committee.

The program has been sponsored by:

- The Norwegian Council for Scientific Work (NTNF)

- The Norwegian Fishery Technology Council (NFFR)

- The Norwegian Maritime Directorate (NMD)

Over the years, plans and economy has changed. Several items being studied under the umbrella of this program have been worked on independently, sponsored separately.

The basic idea leading to the plans and the sub-project list, has its origin in earlier research work and the acceptance that future criteria should be built up of the three following parts:

1. Traditional design criteria based upon the physical understanding of stability in critical wave situation.

2. Risk analysis.

3. Operational procedures.

This leads to the following sub-projects where some are presented in the next sections (3, 4, 5 and 6).

- Developing better theoretical models to get a more precise understanding of the capsizing event. This particular program has concentrated on the following wave situation (see section 3).

- Ship motion and its influence on the shifting of cargo. This program initiated a study on the problem of shifting bulk cargoes. A more independent project has been working separately over the last years with comprehensive studies on the cargo properties as the angle of repose (see section 4).

- The original plans included studies on the environmental loads, concentrating on the waves. However, the program has not directly sponsored such studies due to a change in project economy. Some work being performed with separate financing, mostly from the oil industry, has been followed closely by this program (section 5).

- The problem of assessing future stability and safety criteria has been accepted as on of the most important goals of the project. During the work one has realized the complexity of stability. However, we have presented a criteria philosophy (see section 6) and put much effort into starting a discussion around operational procedures. Operational manuals and "practical operational stability" are vital key words.

3. THEORETICAL MODELS AND MODEL TEST RESULTS FROM FOLLOWING WAVE SITUATIONS

3.1 Stability for vessels balanced on a wavecrest in following waves.

It is an international understanding that future criteria should reflect physical situations and the "following waves" is one to be considered. This situation defines three wave/response phenomena which could be dangerous:

- Loss of stability when balanced on a wave crest.
- Parametric resonance rolling.
- "Broaching to".

"Loss of stability" were likely to be the first physical situation taken into consideration when proposing criteria. The influence of waves on transverse stability has been studied for years in the literature. It is well known that the righting levers (GZ) in general are reduced compared to the still water values when the vessel is balanced on the wave crest at position near amidship. The righting levers increase above the still water values when the vessel is balanced on a trough.

When assessing criteria for such a situation by hydrostatic calculations, this means that

- no relative speed between the wave and vessel is considered

- no ship responses are taken into account

- interaction between the ship wave and the actual wave is not considered

During the project work a reliability study was made. In this study we tested computer programs often used in Norway - some results are shown in fig. 1. Conclusions made:

- Most computer programs produce identical still water hydrostatics and righting moment curves (KY).

- When calculating hydrostatic and righting lever for a vessel balanced on a wave crest in following seas, differences occur from one program to another. This is mainly caused by deviation in each

program type of mathematical model: How the model does itterations for varying draughts and how it finds the vertical stable position and draught (volume and displacement). How a computer program adjusts for longitudinal position of buoyancy and corrects for trim in heeled conditions is also an important factor.

- The accuracy and the routines when reading hull data is also an important factor. As an example one program was parallel tested in UK and Norway for the same basic hullform. These results gave different answers.
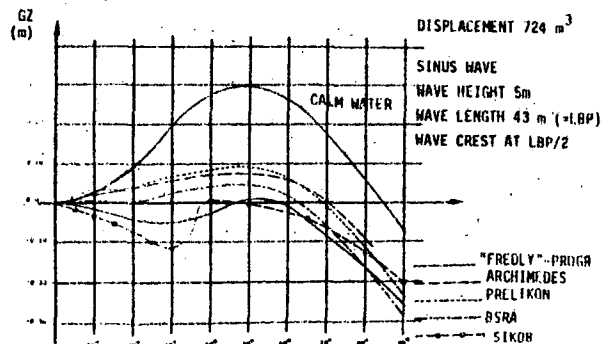

Fig. 1. GZ-curves for a basic model.

3.2 Model tests in following waves.

A model of a typical Norwegian coaster was chosen as the "basic ship". More than hundred vessels of similar size and arrangement are working in the North Sea and Norwegian waters.
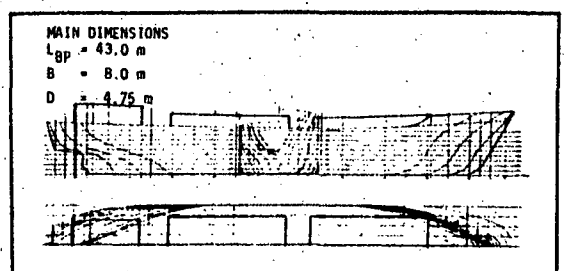

Fig. 2. Lines - basic hull form.

The model test was performed in the towing tank at MARINTEK. The experiment was arranged partly as a captive test and tests with the model free to roll, pitch and sway. The model was attached to a wagon and run from the end of the tank in direction following the waves. For each run the constant heeling angle was adjusted in steps of 3-5 degrees. Starting from upright position, tests were performed for heeling angles up to 60°.

Only regular waves were tested. They were traditionally referred to as regular sinusoidal. The correct length was achieved by tuning the period of the wave maker. Some results are shown in fig. 3.
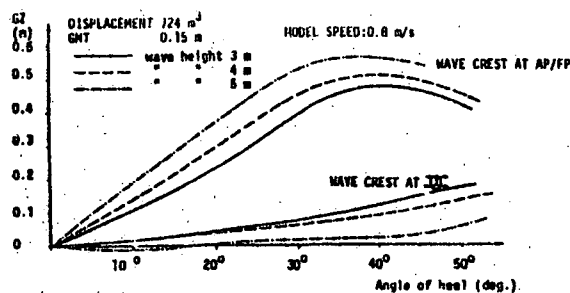

Fig. 3. GZ at low forward speed.

Non-captive tests were performed with the model running in upright position. All motions in six degrees of freedom were measured. The intention of the tests was to find if a negtive righting moment would lead to a capsizing. The stability was decreased to critical, according to previous computer calculations and the tests with the captive model.

The following main conclusions were made after analysing the results:

1) The interaction effects between the seawave and the actual diffraction waves are very important factors. These are unlinear and not well known and should be studied further in the future.

11) As the interaction effects dominate the resulting geometry situation, it is likely that certain types of vessels are more exposed to loss of stability in following sea than others, especially if

these effects occure on a hullform with flat aft end and great flare in the foreship. A hullform like this is initially more exposed to hydrostatic loss of stability. For others the "loss of stability situation" must be reconsidered as not being dangerous.

iii) Before assessing criteria for "loss of stability" in following waves, the above important facts should be considered and studied closer.
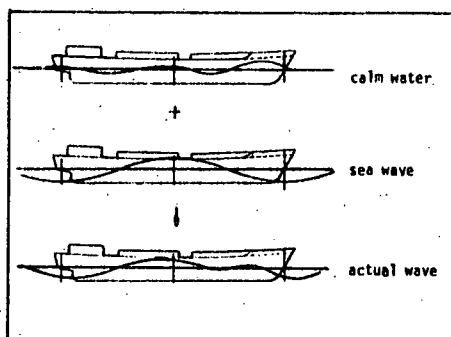
Fig. 4. Wave interaction.

3.3 Broaching to-situation - theoretical models

In following waves we often refer to a dangerous situation named as "broaching" or "broaching to". The situation is described as course instability. The vessel turns around in following waves and capsizes as a total transient event. To study this stability problem we have been working closely on the course instability problems of "broaching to", both through theoretical studies and model tests. Due to the combination of an external moment from the wave and a reduced rudder effect, an oscillating yaw-motion can occure, increase uncontrolled and turn the vessel around.

In the literature one can refer to several theoretical works trying to explain this situation. From these works we can conclude the following:

1. The probability of broaching is greater when the ship is running down into a wave trough.

2. The probability of broaching increases with increasing waves.

3. The wavelength must be greater than the ship length when broaching is likely to occure.

In principle, due to great motions and waves, this situation is complex to understand and analyse. We decided to attack the problem through theoretical analysis of ship manoeuvring in following waves. As we found it important to evaluate the transverse forces and yaw-moments on the hull, theoretical models were developed. The first was a generalized strip theory and the other a generalized bow-flow potential theory. The last one was developed for our situation in a computer program and used to calculate the forces and moments of a simplified hull (flat plate). [2]

In the actual "broaching" situation a vessel is running in the waves with speed close to the phase-velocity of the wave. The wave encounter frequency is low and the vessel is stabilized in the vertical plane. Making the assumption that non-viscous forces are dominating such a situation, the problem can be described by potential theory:

$$\phi(\underline{x}, t) = - UX + \psi(\underline{x}, t)$$

The potential $\psi(\underline{x}, t)$ describes the velocity field around the vessel and have to fulfil certain boundary conditions that reflect the free surface and the hull surface.

- UX : represents the free flow potential
ψ : represents the part that is caused by the hull itself and can be derived into
$\psi = \psi_w + \psi_s$

ψ_w : represents incoming waves

ψ_s : represents the vessels effect on the waves due to radiation and diffraction

As the actual motions refer to low frequencies only, the stationary generalized bow-flow problem is considered. The numerical method is then based upon a system of describing the potential by a dipole-distribution that copes with the given boundary conditions. The transverse force and the yaw-moment are presented in the form:

$Y = Y_v V + Y_{\dot{v}} \dot{V}$ transverse force

$N = N_v V + N_{\dot{v}} \dot{V}$ Yaw moment

where V and $\dot{V}$ represents the crossflow and acceleration.

The result of some calculations that refer to initial conditions of the model test described in the following, is shown in fig. 5. They refer to calculations in the yaw-modus and is taken from [2].
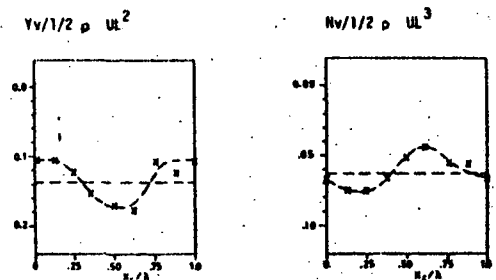
Fig. 5. Hydrodynamic coefficients numerically calculated for a flat plate in yaw-modi [2]

$T/L = 1:5$

$\lambda/L = 1.45$
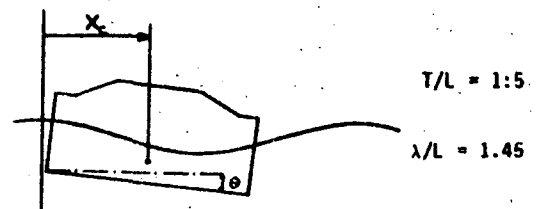
Fig. 6. Definitions.

The results refer to the plate floating stable in the wave, i.e. stable in vertical direction in different positions in the wave (see table below).

X_c	θ
0	0
$\lambda/4$	-0.079 rad
$\lambda/2$	0
$3/\lambda/4$	0.079 rad

3.4 Broaching to-situation, model tests

Model tests were being performed to verify computed values for the transverse horizontal force- and yaw-moment on a captive flat plate in varying yaw modi and following waves. Tests were also performed for an actual hull form with a comparable lateral area and aspect ratio as the plate.

The model tests were performed in the towing
tank at MARINTEK. The experiments were arranged
as a partly captive test. The models were made
free to heave and pitch. They were kept in the
roll, sway and surge mode and attached to the
tankwagon. Through a dynamometer the horizontal
force in surge and sway and the yaw moment were
measured (fig. 7).
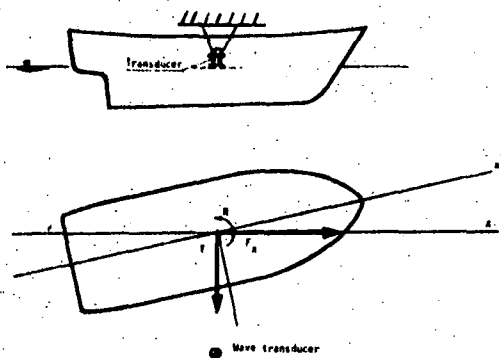
Fig. 7. Model test set up

The tests were made for varying forward speed.
The yaw-angle was varied from 0 to 15^0 in steps of
abt. 3^0.

The wave trains were produced as regular waves
for a given wave length. The wave length was espe-
cially chosen to fit the ratio $\lambda/L=1.0$ and
$\lambda/L=1.45$. The height was chosen to be well below
the critical steepness ratio, thus giving rather
regular sinusoidal waves. The correct length of
the wave was achieved by tuning the period of the
wave maker.

The tests in the wave train were performed by
running the model at varying speed. The measure-
ments were recorded in a time section of constant
forward speed after the acceleration period.
Referring to the theoretical calculations the
positions at the plate and the hull model were
defined as shown in fig. 8.

As a general conclusion, the model tests show
that the theoretical models calculate forces and
moments in correct range. There are, however, cer-
tain deviations in the values compared, that need
closer studies before the theoretical model can be
fully accepted. These deviations could probably be
caused by inaccurate measurement and defining of
the position in the waves.
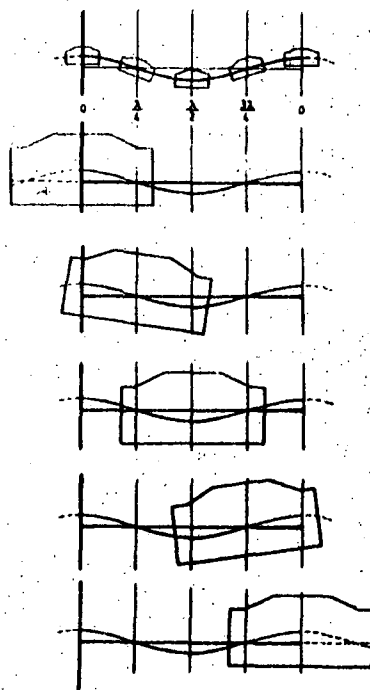
Fig. 8. Definitions of the position in the waves.
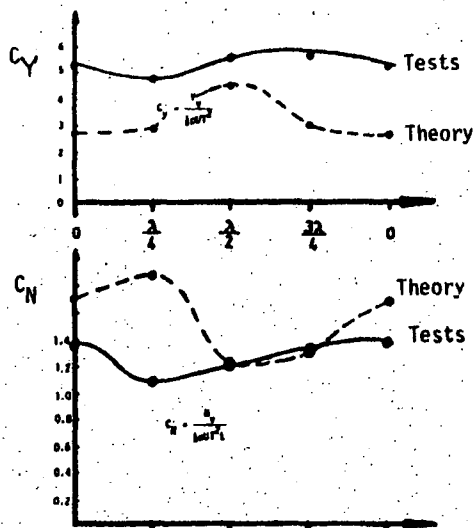
Fig. 9. Hydrodynamic coefficients as a function of
position in waves (flat plate.

The measured values for transverse horizontal
force, the yaw moment and also the longitudinal
force show that they are varying with the objects
(plate, vessel) position in the waves.

As seen from fig. 9, maximum yaw-moment occurs when the vessel is positioned in a trough in abt. 3° yaw angle. At an increased angle (6°) the situation has changed. The maximum transverse force has its maximum on the top of the wave crest, and the surfing force from the waves is also most pronounced at crest situations.
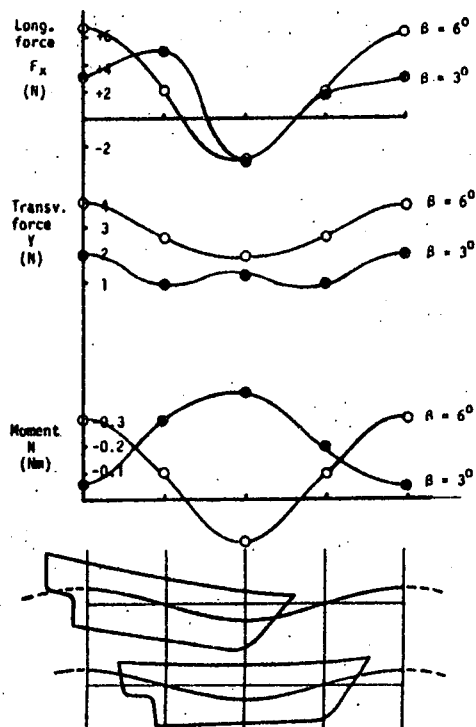
Fig. 10. Hydrodynamic forces acting on a captive hull model in following waves.

Based upon these measurements and also observations made from earlier model tests in similar following wave situations, we can describe the broaching event as follows:

1. When a vessel is balanced on a wave crest it looses upright stability and is pushed forward by the wave surfing forces.

2. Transverse disturbances easily occur as the control-force from the rudder decreases. At small yaw angles great transverse forces makes the vessel change direction.

3. Running down the wave the yaw moment increases and the vessel turns around easily, ends up in 90° against the waves.

4. As this transient event happens fast, the forward kinematic energy transfers to an inclining moment.

5. The vessel rolls heavily or capsizes.

4. SHIP MOTION AND SHIFTING OF CARGO.

An area that requires both stability rules and criteria reflecting physical situations is transportation of bulk cargoes onboard ships. The research programme performed have been looking into cohesive bulk cargoes in particular and the effect of ship motions upon cargoes in general.

The before mentioned basic ship is also tested in longcrested and shortcrested seas with different headings, speeds and stability. The motions pitch, heave and roll were measured, so also the accelerations in x-y-z directions at different locations in the cargo hold area.

A strip theory computer programme was used for calculating the same parameters in longcrested seaways and with similar wave height as in the model test. A comparison between the model test results and the computer calculations show a fairly good agreement. The conclusion is that for the actual (conventional) hull form the computer programme strip theory is well suited for a motion-acceleration calculation. Another important conclusion from the tests/calculations is the range of the accelerations in the cargo area. For relatively normal seastates the accelerations, especially in the transverse and vertical directions, are considerable.

New methods have been tested out for the determination of the slope stability of cohesive bulk cargoes. The methods are commonly used by soil engineers when determining the safety factors against rupture of different materials. For the cohesive cargoes, which are very complex to handle in the existing rules and recommendations, both cohesion and frictional angle have to be known together with moisture content and porosity of the cargo pile as loaded into the ship's hold. A testing method is used (triaxial apparatus) to find the cohesion and friction angle, when parameters like porosity and moisture content are varied. The testing apparatus does also give possibilities of investigating the change in cohesion and friction over time when the sample (i.e. the cargo pile) is exposed to several cyclic loads. Tests show that the cohesion will vary quite a lot over time for some materials.

The test-results from the triaxial tests have been used in connection with the motions and accelerations of the basic ship with a certain load configuration, stability and wave condition.

Applying D'Alembert's principle, the acceleration forces exerted to a particle within the cargo pile can be expressed as D'Alembert's force:

"A mass particle (m), will be in equilibrium when exposed to an acceleration (a*g) by a force (f) equal to (m*a*g) in the opposite direction".

Applying this principle, the methodology of a dynamic problem is reduced to a static one. In this way, the ship is turned a certain angle to a static angle which corresponds to the total force from accelerations in transverse and vertical direction and from roll motion. In this context, it should be mentioned that the pitch motion and the longitudinal acceleration is not taken into account. The reason for this is that these parameters are small compared to the others. Using D'Alembert's principle, the slope stability of a cargo pile in "rest" can be judged when set into motion during a sea voyage. The safety factor can be calculated for a given sea state and a given heading for the ship when the necessary motion parameters are known. Fig. 11 shows the roll motion, transverse and vertical acceleration as a function of phase angle for a certain wave condition of the "basic" ship. The motion and accelerations are given as significant values for a significant wave height of 5.0 m, heading 90 degrees. The parameters represent a time interval of 30 minutes in the actual seastate.

By making use of the motion and accelerations in fig. 11, the safety factor against sliding failure is calculated for a full scale cargo configuration of the "basic" vessel. Copper concentrate with high and low porosity is calculated. The friction angle and cohesion are decided out from triaxial tests, and the result from the calculation is presented in fig. 12. A rupture, or sliding failure will take place when the safety factor is lower than 1.0. It will be seen from the curves that the contributions from roll and accelerations are presented separately, and that the change in safety factor is rather high when one of the parameters are included/excluded.
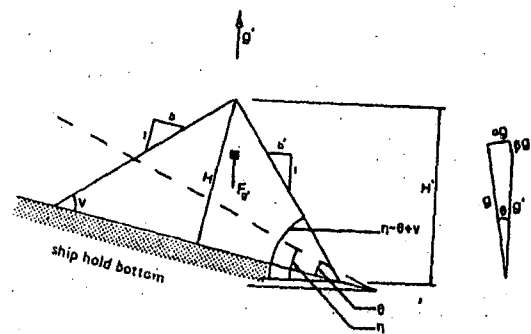
n - rotation of cargo pile from roll motion
θ - rotation of cargo pile from accelerations
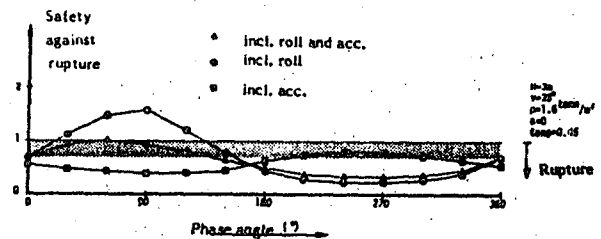
Varation of rupture safety as a function of phase angle, high porosity
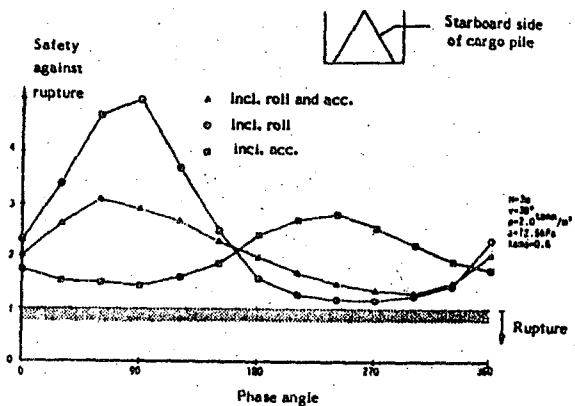
Varation of rupture safety as a function of phase angle, low porosity

Fig. 12. Safety factors against sliding failure for copper concentrate.

Fig. 11. Significant roll motions and acceleraions as function of phase angles.

Comparing the upper and lower diagram, one will observe the change in safety factor with the variation of porosity. With high porosity in the cargo pile, a sliding failure would take place during the 30 minutes voyage with beam seas, while the cargo with low porosity would not shift during the same time interval.

A computer program is developed to give the master of the ship the necessary knowledge about the cargo and the safety with respect to shifting in varying seastates.

Fig. 13 shows an example of some of the output from this programme. The ship master will have information e.g. about the variation in safety factors for different loading configurations. For the given example one will notice that the safety factor will be less than 1.0 for cargo pile height above 6.0 m. The computer programme also gives possibilities to judge variation in material parameters, seastates, cargo configurations etc.

Slope length   B = 8.00 m
Gamma   G = 20.00 kN/m3
Cohesion   C = 7.50 kN/m2
Friction Tanfi = .60
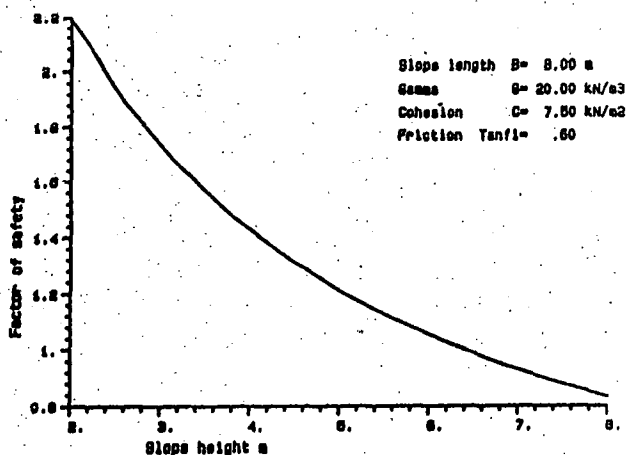
Fig. 13. Factor of sliding safety with respect to height of cargo pile.

As a conclusion, the following can be recognized:

Cargo shifting onboard vessels is causing a lot of accidents and the probability of such occurences should be better documented via methods as described or similar methods.

Most cargoes will shift if the weather conditions, i.e. the motions and accelerations acting upon the cargo are severe enough. However, in most cases the ship's master has poor knowledge of the limits when cargo starts shifting and the forces which is acting on the cargo.

New rules and criteria should be established in a way that gives the master of the ship optimum information about ship stability, cargo properties and dynamic behaviour of ship and cargo. This information should lead forward to a guide for the master on how to handle the ship in severe, dangerous sea conditions.

5. ENVIRONMENTAL - A BRIEF PRESENTATION OF NORWEGIAN WAVE RESEARCH WORK

The initial plans of the program on wave research have not been realized. Due to changes in the financing situation and the fact that parallel research work has actually been going on sponsored by the oil-industry, these plans were deleted.

Under this program umbrella we have kept a close watch on this research. Results have been presented in the steering committee and given moral support when needed. At MARINTEK breaking waves have been studied for several years. The statistics of breaking waves have been studied through re-analysis of wave signals from wave rider buoys positioned along the Norwegian coast.
[4]

In the laboratory new testing techniques for generating transient waves have been developed. The last generation of these is a non-linear experimental technique for deterministic generation of freak waves both in 2-dimensional (longcrested freak waves) and in a directional 3-dimensional short-crested wave field. This technique has also lead to a better understanding of the physics of non-linear gravity waves. It explains why the conventional statistics used to derive a "100-year" design wave from a limited amount of data obtained with waverider buoys, do not necessarily contain the event of the extreme freak wave.
[5]

When performing survival testing of vessels in waves to measure stability, this wave generating technique has lead from stochastic testing into deterministic testing of vessels using a design philosophy as shown on the fig. 14 below.

```
┌─────────────────┐  ┌─────────────────┐
│ Extreme freak   │  │ Probability for │
│ wave breaking   │  │ selected wave   │
└────────┬────────┘  └────────┬────────┘
         │                    │
         └──────────┬─────────┘
           ┌────────▼────────┐
           │ Extreme response│
           └────────┬────────┘
           ┏━━━━━━━━▼━━━━━━━━┓
           ┃  Critical event ? ┃
           ┗━━━━━━━━┳━━━━━━━━┛
           ┌────────▼────────────┐
           │ Probability for failure │
           └─────────────────────┘
```
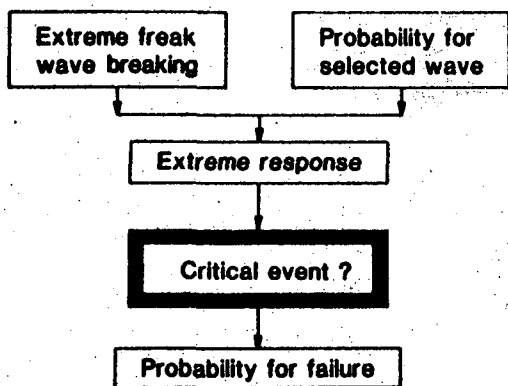
Fig. 14. Design philosophy.

On the subject of forcasting dangerous wave situations, work has been performed by MARINTEK in cooperation with the Norwegian Meteorological Institute. A practical operational forecasting model of dangerous wave situations along the Norwegian coast has been developed. 24 different areas along the coast were found to be more exposed than others (the Ship in Rough Seas Project). Examples from two of these areas have been chosen to be observed in detail in order to evaluate the forecasting model.   [6]

In one of the areas a capsizing of a coaster and the following inquiry lead to a closer study of that particular area. The meteorologists have, however, not yet finalized the evaluation of their model. When the time comes, a radio forecast will be developed especially suited for the coaster and the fishing vessel traffic.

6. OPERATIONAL PROCEDURES AND MANUALS

The basic stability philosophy behind the program idea mentioned earlier, consists of three main parts. One of them is operational procedures. We feel that this theme,

operational stability,

should be studied closer in the future and be integrated into criteria definitions. We have often asked if the general safety of a vessel will be increased if only new design requirements similar to the ones in force today but more sophisticated, are developed. Is it possible to plan and design vessels that never capsize without also setting operational criteria? Or is it possible through bad semanship to capsize any vessel?.

We know that for a vessel, an important part of the operational advice is given in the stability booklet, where advice is given on how to obtain a specified stability (expressed by Gx and Gm) under all loading conditions considered relevant.

However, this stability information is not related to environmental conditions. Furthermore, no advice is presently given as to how the probability of capsizing can be kept at a relatively low level.

We intend operational procedures or manuals to be the tool of the future in answering these questions and the one to combine both the human, environmental and design factors in a total stability and safety concept.

Examples of operational manuals have been developed during the program and discussed with people concerned [7]. Our latest version of a manual is built up of three chapters which are presented in individual booklets:

- One brief emergency part of 2-3 pages

- One operational part that describes the most important items in operational stability. These are:
  • a weathertight vessel
  • stability and loading conditions
  • practical control of the actual stability during a journey
  • how to judge a critical situation in waves
  • safety actions to control and improve the tightness and stability
  • damage stability
  • using working tools onboard (fishing gear i.e.)
  • cargo handling
  • evacuation plans

- One general part that presents general information to the master, such as:
  • the basic principles of stability
  • the vessel motion characteristics in waves
  • cargo handling
  • wave and weather information.

In principle the manual should contain the state of the art of stability knowledge expressed in a simple manner. In this way it also has an educational aspect that over time will improve safety.

LITERATURE

1. T. Nedrelid: "Stability for Vessels Balanced on a Wavecrest in Following Waves. Hydrostatical Calculations - Model Tests." NHL-report [1985].

2. T. Utnes, NHL/VHL: "Calculations of Hydrodynamic coefficients for Vessels in Following Waves (in Norwegian) [1985].

3. T. Nedrelid, O.E. Reitan: "Measuring of Hydrodynamical Coefficients for Vessels in Following Waves. Model tests." MARINTEK [Dec. 1985].

4. S.P. Kjeldsen, D. Myrhaug: "Parametric Modelling of Joint Probability Density, Distributions for Steepness and Asymmetry in Deep Water Waves." Applied Ocean Research [1984] Vol. 6, No. 4.

5. S.P. Kjeldsen: "Dangerous Wave Groups". Maritime Research No. 2 [1984] Vol. 12.

6. P. Schølberg, Meteorological Institute, S.P. Kjeldsen, MARINTEK: "Bølgevarsling - program for verifisering. Meteorologiske Institutt/ MARINTEK [1984].

7. Emil Aall Dahle, T. Nedrelid: "Operational Manuals for Improved Safety in a Seaway". Stab. [1986] Polen.

8. F. Fredriksen, E. Jullumstrø: "Sliding Failures of Bulk Cargoes During Sea Transportation". MARINTEK report no. 520021 [1985].

9. F. Fredriksen, A. Kavlie, E. Jullumstrø: "BULKCALC-A Computer Programme for Calculation of Safety Factors Against Rupture of Cohesive Bulk Cargoes". MARINTEK report no. 530094 [1986].

10. E. Jullumstrø: "Shifting of Cargo and Stability Criteria of Small Cargo Vessels". NHL-report no. 183225 [1983].

PROBABILITY OF CAPSIZING IN STEEP WAVES FROM THE SIDE IN DEEP WATER

by

E. Aa. Dahle [*] and D. Myrhaug [**]

ABSTRACT

A model for estimating the probability of capsize in steep and high waves from the side in deep water is presented. The main element of the model is the estimation of probability of occurrences of steep and high waves for given sea states by using the joint probability density distribution of crest front steepness and wave height.

The sea states are described by using a joint frequency distribution of significant wave height and mean zero-crossing period. The dominant wave direction is taken from wind statistics. Then, the operations of the vessel have to be investigated in order to assess when it is exposed to the waves, and its loading conditions and associated stability.

The stability has then to be associated with a critical wave height, using model experiment data.

Finally, the human element with regard to maintaining the stability (i.e. closing openings and securing cargo) should be assessed. An example from Norwegian waters has been chosen in order to illustrate the application of the model.

1. INTRODUCTION

In 1981, The Norwegian Petroleum Directorate issued its first Guidelines for safety evaluation of platform conceptual design [1].

In these guidelines, those responsible for the design "shall verify a sufficiently low probability of loss of human life, high material damage and unacceptable environmental pollution as a consequence of the accident".

The types of accidents should be relevant to the design under consideration and should have a probability of occurrence above 10^{-4} per year if their consequence is to be considered. In such cases, the accident is denoted a "Design Accidental Event" DAE.

The design must then be such that only personnel in the immediate vicinity of the accident are endangered. This requirement is considered as satisfied provided that the following 3 criteria are complied with;

1) at least one escape way from central positions which may be subjected to an accident, shall normally be intact for at least one hour during a DAE.

2) shelter areas shall be intact during a DAE until safe evacuation is possible.

3) depending on the platform type, function and location, when exposed to the DAE, the main support structure must maintain its load carrying capacity for a specified time.

In this paper this approach will be compared with the capsizing accident.

2. THE PROBABILISTIC MODEL

First, the definition of "capsize" used in this paper is illustrated in Fig. 1. Clearly, only the "stable side position" may comply with the 3 criteria listed above.
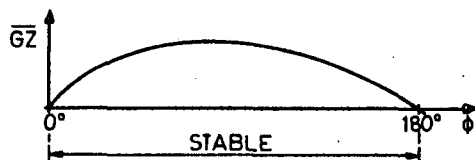
a. Self-righting.
Capsize not feasible
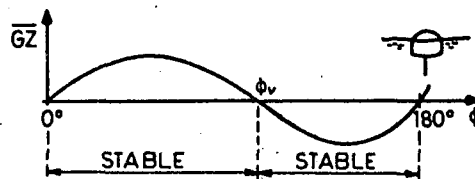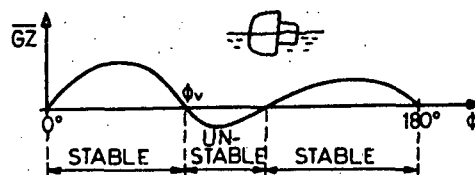
b. Capsize to 180°

c. Capsize to stable side position

Fig. 1. Definition of capsize.

A method for estimating probability of capsize was first presented by Sevastianov [2].

This paper follows the principles of [2] in estimation of the probability of capsize in steep, near-breaking waves from the side in deep waters. This event is considered to be relevant to smaller ships, i.e. with length below 45 m.

As for the estimation of the probability of this event, only an order of magnitude can be arrived at. Obviously, this is also the case for accidents in the oil industry. The aim of this paper is to compare the probability of capsize with the target value of 10^{-4} per year.

In the paper, the probabilities of the different elements of capsize in deep waters are dealt with in succession. First, the joint probability of encountering a steep and high wave in a given sea state is covered, and the probability of capsize after such an encounter is discussed. Then, operational aspects are briefly covered. Realistic estimates of probabilities of adherence to operational requirements, based on knowledge of the ship and its crew, should be included.

Finally, the total probability of capsize in deep waters is calculated.

3. PROBABILITY OF EXPOSURE TO BAD WEATHER

By investigating the operations of a ship, the period of time for which it is exposed can be determined. For a fishing vessel, for instance, three operational phases are of interest, i.e.

- in transit from the harbour to the fishing ground
- on the fishing ground
- in transit from the fishing ground back to the harbour.

Only a closer study can reveal the phases of interest as indicated by Dahle and Nedrelid [3].

The direction of the wind in the area under consideration may be important and may often be available as a direction frequency diagram. Assuming near correspondence between wind and wave direction, knowing the course of the vessel, and defining an exposed sector of 90 degrees width on each side of the ship, a probability of exposure can be arrived at.

Such "wind roses" for various areas may be given on a yearly or monthly bases. For Norwegian waters, the former data are given by Haaland [4].

An example is shown in Fig. 2. The probability of weather from the side, P_1, is then the integrated wind frequency distribution for 90 degrees, on each side of the ship.
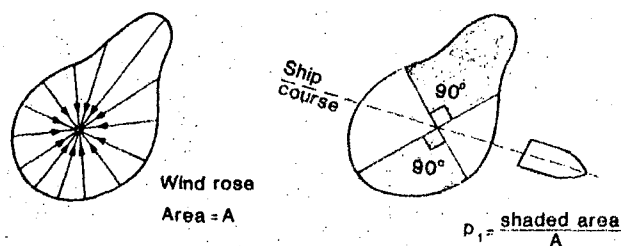
Fig. 2. "Wind rose" and P_1.

Table 1. Joint distribution of H_s and T_z (based on data from Krogstad [5]).

T_z(s) H_s(m)	3-4	4-5	5-6	6-7	7-8	8-9	9-10	10-11
1.5-2.5	0.0054	0.0963	0.1315	0.0738	0.0277	0.0081	0.0015	0
2.5-3.5		0.0015	0.0508	0.0612	0.0311	0.0106	0.0022	0.0003
3.5-4.5			0.0017	0.0325	0.0273	0.0085	0.0015	0.0001
4.5-5.5				0.0047	0.0206	0.0078	0.0013	0.0001
5.5-6.5					0.0066	0.0092	0.0015	0.0002
6.5-7.5					0.0005	0.0039	0.0019	0.0001
7.5-8.5						0.0010	0.0018	0.0001
8.5-9.5							0.0007	0.0002
> 9.5								0.0004

Then the level of "bad weather" must be defined. A natural choice will be the significant wave height H_s. The choice depends on vessel size. $H_s \geq 1.5$ m is chosen in this paper.

The joint probability distribution of significant wave height H_s and mean zero-crossing period T_z for $H_s \geq 1.5$ m is given in Table 1. This table is obtained from the joint frequency table of H_s and T_z given in Krogstad [5]. This data is obtained by a Waverider buoy covering the period 1974-80 at Halten on the Norwegian continental shelf.

Finally, the duration of various sea states is given in Kjeldsen [6] by a Weibull distribution. From this, the average duration of storms for winter conditions is obtained as ,(see Table 2)

$$\bar{\tau} (H_s) = 1.27 \cdot t_c \qquad (1)$$

Strictly, $\bar{\tau}$ is a function of both H_s and T_z, but to the authors knowledge this information is not yet available.

From this data, a weight function w is set to 1.0 if the duration of the exposed period (t) is exceeding the duration of the sea state. Otherwise, w is taken as the ratio $t/\bar{\tau}$.

Table 2. t_c and $\bar{\tau}$ as functions of H_s, from Kjeldsen [6].

H_s (m)	t_c (hours)	$\bar{\tau}$ (hours)
1.5-2.5	35	44.5
2.5-3.5	17	21.6
3.5-4.5	9.6	12.2
4.5-5.5	6.3	8.0
5.5-6.5	4.4	5.6
6.5-7.5	3.3	4.2
7.5-8.5	2.5	3.2
8.5-9.5	2.0	2.5
$\geq$ 9.5	1.7	2.2

Then the general expression for the probability of being in a situation S_i during a one-year operation of the ship is:

$$P(S_i) = \sum_j \sum_k P_{1jk} \cdot P_{2jk} \cdot w_{jk} \cdot P_{3jk} \cdot P_{4jk} \qquad (2)$$

where j and k denote summing over significant wave height and zero-crossing period, respectively. Further

P_{1jk} = see Fig. 2.

P_{2jk} = yearly fraction of time of exposure in sea state jk.

P_{3jk} = $P(\varepsilon_c, H_c | H_{sj}, T_{zk})$, i.e. the conditional probability of steep ($\varepsilon \geq \varepsilon_c$) and high ($H \geq H_c$) waves for a given sea state (H_{sj}, T_{zk}), see section 4.

P_{4jk} = joint probability of H_s, T_z, see section 4.

The probability of capsize caused by a steep near-breaking wave in deep water is then

$$P_c = P(S_i) \cdot P_5 \cdot P_6 \cdot P_7 \qquad (3)$$

where:

P_5 = probability of being hit by a steep near-breaking wave during the period of rolling when the vessel is most exposed. In this analysis, P_5 = 0.5.

P_6 = conditional probability of capsize, given an extreme wave situation. According to the discussion in section 5, P_6 is 0 for the "safe" regions of Fig. 5, and 1.0 for "unsafe" regions.

P_7 = conditional probability of compliance with the requirements that makes a ship "safe", i.e. the probability of important openings being closed properly, and cargo secured to sustain large heeling angles in the situations under study.

4. PREDICTION OF OCCURRENCES OF STEEP AND HIGH WAVES IN DEEP WATERS

4.1 Joint distribution of crest front steepness and wave height

A method for estimating encounter probabilities of occurrence of steep and high waves in deep water for given sea states will be described briefly in this section. The method is based on the idea given in Kjeldsen and Myrhaug [7] utilizing the advantages that are contained in a zero-downcross analysis by using the wave trough and the following wave crest in the definition of a single wave, and defining the wave height as the difference between these water levels, Fig. 3. The zero-downcross analysis is the only analysis which provides parameters that give a representation of the physical conditions with relevance to breaking waves, and thus, the only parameters which should be correlated with measurements of severe ship responses or wave forces in such waves. Further, a more accurate description of steepness and asymmetry in transient near-breaking waves were obtained by Kjeldsen and Myrhaug [7], when the three following parameters were introduced: crest front steepness ε, vertical asymmetry factor λ and horizontal asymmetry factor μ. The crest front steepness is defined by

$$\varepsilon = \frac{\eta'}{(g/2\pi)TT'} \qquad (4)$$

ASYMMETRIC WAVE OF FINITE HEIGHT
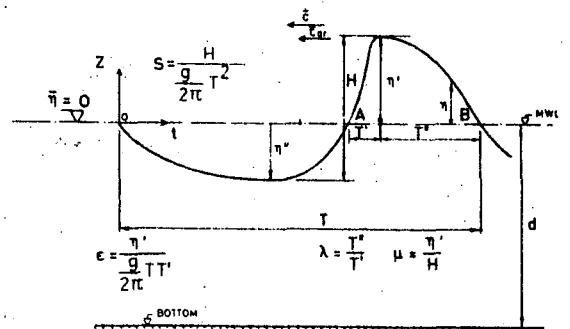
Fig. 3. Basic definitions for asymmetric waves of finite height (from Kjeldsen and Myrhaug [7]).

where η' is the crest elevation measured from the mean water level, T' the time defining the position of the wave crest relative to the zero-upcrossing point in the time domain, T the zero-downcross period and g the acceleration of gravity. The definitions in the time domain, also of λ and μ, are shown in Fig. 3. It is generally accepted that use of the crest elevation for design applications provides a basic parameter more relevant to finite amplitude wave geometry than the wave height. Observations of breaking waves show that these waves can be characterized by a very steep crest front and high asymmetry factors. The ε-parameter is thus a mean crest front inclination in the time domain.

However, it is not sufficient to describe the wave conditions by steepness and asymmetry parameters alone, but they should be combined with the wave height to give a much better description of the severeness of a given sea state. Joint probability density distributions for ε, H and λ, H are given in Myrhaug and Kjeldsen [8]. Myrhaug and Kjeldsen [9] discuss closer the ε-H distribution, see also Myrhaug and Kjeldsen [10].

The joint probability density destribution of crest front steepness and wave height, $p(\hat{\varepsilon}, \hat{h})$, is obtained as a best fit to field data records from the Norwegian continental shelf. Here $\hat{\varepsilon} = \varepsilon/\varepsilon_{rms}$ and $\hat{h} = H/H_{rms}$ are the normalized crest front steepness and wave height, respectively. ε_{rms} and H_{rms} are the rms-values used for normalisation. The joint probability density distribution is determined by

$$p(\hat{\varepsilon}, \hat{h}) = p(\hat{\varepsilon} | \hat{h}) \, p(\hat{h}) \qquad (5)$$

Here $p(\hat{h})$ denotes the marginal distribution of $\hat{h}$ and $p(\hat{\varepsilon} | \hat{h})$ denotes the conditional distribution of $\hat{\varepsilon}$ given $\hat{h}$. The joint probability distribution is fitted to the actual data by first fitting the conditional distribution of $\hat{\varepsilon}$ given $\hat{h}$ and then fitting the marginal distribution of $\hat{h}$.

The data represent 58 time series, each of 20 minutes duration, from measurements at sea on the Norwegian continental shelf including altogether 6353 individual zero-downcross waves. These data were taken from a larger data base, see Myrhaug and Kjeldsen [8], sampled in the period 1974-78 with three Waverider buoys located at Tromsøflaket, Halten and Utsira. The properties of the obtained probability density distributions show that data

obtained from the three locations can be regarded as belonging to the same statistical population. This means that common statistical distributions can be obtained, which are representative for the wave dynamics in the whole area (Kjeldsen and Myrhaug [11]).

Two different parametric models were fitted to the data. These two models are based on the fit by a Weibull and a log-normal distribution, respectively, to the conditional distribution histogram of $\hat{\varepsilon}$ given $\hat{h}$. In Myrhaug and Kjeldsen [9] is shown that the latter model is closer to the trend in the data for higher values of crest front steepness and wave height, and this model will therefore be used in this analysis. The marginal distribution histogram of $\hat{h}$ was fitted by a Weibull distribution.

The Weibull probability density distribution of $\hat{h}$ is given by

$$p(\hat{h}) = \frac{\beta \hat{h}^{\beta-1}}{\varphi^\beta} \exp\left[-\left(\frac{\hat{h}}{\varphi}\right)^\beta\right] \; ; \; \hat{h} \geq 0 \qquad (6)$$

with the Weibull-parameters

$$\varphi = 1.05 \text{ and } \beta = 2.39 \qquad (7)$$

The log-normal probability density of $\hat{\varepsilon}$ given $\hat{h}$ is given by

$$p(\hat{\varepsilon}|\hat{h}) = \frac{1}{\sqrt{2\pi} \, \gamma \hat{\varepsilon}} \exp\left[-\frac{(\ln \hat{\varepsilon} - \theta)^2}{2\gamma^2}\right] \; ; \; \hat{\varepsilon} \geq 0 \qquad (8)$$

where the mean value θ and the variance γ^2 of $\ln \hat{\varepsilon}$ are given by

$$\theta(\hat{h}) = \begin{cases} 0.024 - 1.065 \, \hat{h} + 0.585 \, \hat{h}^2 \text{ for } \hat{h} \leq 1.7 \\ 0.32 \arctan[3.14 \, (\hat{h}-1.7)] - 0.096 \text{ for } \hat{h} > 1.7 \end{cases} \qquad (9)$$

and

$$\gamma^2(\hat{h}) = -0.21 \arctan[2.0 \, (\hat{h}-1.4)] + 0.325 \qquad (10)$$

The rms-values used herein for normalisation, ε_{rms} and H_{rms}, are related to wave spectral parameters by

$$\varepsilon_{rms} = 0.0202 + 32.4 \, \mathcal{K} \; ; \; \mathcal{K} = \frac{m_2}{g \sqrt{m_0}} \qquad (11)$$

and

$$H_{rms} = 2.8582 \sqrt{m_0} \qquad (12)$$

respectively, obtained as the best fit to the data by linear regression analysis. m_0 and m_2 are the zeroth and second moment of the one-sided wave energy spectrum $S(f)$, respectively, defined by $m_n = \int_0^\infty f^n S(f) df$, $n = 0,2$, where f is the frequency. $\mathcal{K}$ is related to a steepness parameter based on the significant wave height estimated from the spectrum, $H_s = 4 \sqrt{m_0}$, and the average zero-crossing wave period estimated from the spectrum, $T_z = \sqrt{m_0/m_2}$, i.e. $\mathcal{K} = H_s/4gT_z^2$.

Fig. 4 a shows the joint distribution histogram and the corresponding isodensity curves of $\hat{\varepsilon}$ and $\hat{h}$. Fig. 4 b shows the fitted joint probability density distribution of $\hat{\varepsilon}$ and $\hat{h}$ as given by Equations (5) - (10).

4.2 Estimates for probabilities of occurrence of steep and high waves for a given sea state

Estimates for probabilities of occurrence of steep waves will now be calculated by using the joint distribution of $\hat{\varepsilon}$ and $\hat{h}$. The probability of occurrence of waves with $\varepsilon \geq \varepsilon_c$ and $H \geq H_c$ for given rms-values of ε and H are given by


(a)

(b)
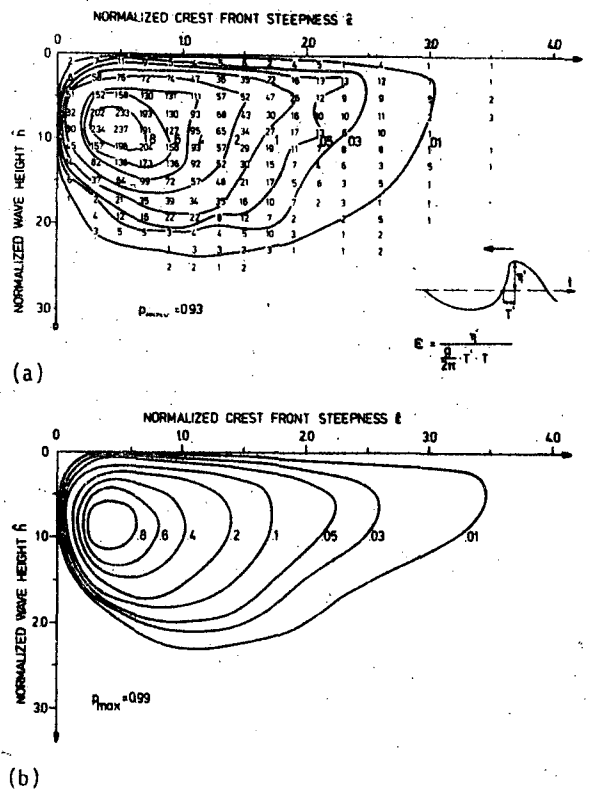
Fig. 4. Joint probability density distribution of $\hat{\varepsilon}$ and $\hat{h}$, (a) observed joint distribution; (b) fitted joint distribution based on log-normal model for $p(\hat{\varepsilon}|\hat{h})$.

$$P[(\varepsilon \geq \varepsilon_c) \cap (H \geq H_c) | \varepsilon_{rms}, H_{rms}]$$
$$= \int_{\varepsilon_c}^\infty \int_{H_c}^\infty p(\varepsilon, H) dH d\varepsilon = \int_{\hat{\varepsilon}_c}^\infty \int_{\hat{h}_c}^\infty p(\hat{\varepsilon}, \hat{h}) d\hat{h} d\hat{\varepsilon} \qquad (13)$$

Since ε_{rms} and H_{rms} are coupled to spectral parameters this is a conditional probability given a sea state. In Myrhaug and Kjeldsen [9], [10] the sea states are described by a JONSWAP spectrum.

In this analysis sea states with $H_s \geq 1.5$ m will be considered. Further, for a given sea state an "extreme wave" is defined by the following threshold values of crest front steepness and wave height

$$\varepsilon_c = 0.25 \text{ and } H_c = 4 \text{ m} \qquad (14)$$

The choice of H_c is in accordance with the example discussed in section 6. However, in a general case H_c has to be given in correspondence with the stability characteristics, for instance the energy E as discussed in section 5 and indicated in Fig. 5. The critical value ε_c is not too well known, but current research is aiming at resolving this matter. The asymmetry factors λ and μ are also important for a proper "extreme wave" description.

The sea state is described by H_s and T_z. Thus, the probability given in Equation (13) is a conditional probability given H_s and T_z, that is

$$P_3 = P[(\varepsilon \geq 0.25) \cap (H \geq 4 \text{ m}) | H_s, T_z] \qquad (15)$$

P_3 is given in Table 3 for the sea states in Table 1.

$T_0(s)$ / $H_s(m)$	3.5	4.5	5.5	6.5	7.5	8.5	9.5	10.5
2	$2.1 \cdot 10^{-6}$	$3.2 \cdot 10^{-7}$	$<10^{-8}$					
3		$2.6 \cdot 10^{-5}$	$4.2 \cdot 10^{-6}$	$6.8 \cdot 10^{-5}$	$1.1 \cdot 10^{-5}$	$2.1 \cdot 10^{-6}$	$5.0 \cdot 10^{-7}$	$1.3 \cdot 10^{-7}$
4			$7.2 \cdot 10^{-5}$	$1.9 \cdot 10^{-3}$	$5.2 \cdot 10^{-4}$	$1.6 \cdot 10^{-4}$	$5.7 \cdot 10^{-5}$	$2.2 \cdot 10^{-5}$
5				$1.0 \cdot 10^{-2}$	$3.8 \cdot 10^{-3}$	$1.5 \cdot 10^{-3}$	$6.3 \cdot 10^{-4}$	$2.9 \cdot 10^{-4}$
6					$1.2 \cdot 10^{-2}$	$5.1 \cdot 10^{-3}$	$2.0 \cdot 10^{-3}$	$1.2 \cdot 10^{-3}$
7					$2.5 \cdot 10^{-2}$	$1.2 \cdot 10^{-2}$	$5.8 \cdot 10^{-3}$	$3.0 \cdot 10^{-3}$
8						$2.1 \cdot 10^{-2}$	$1.1 \cdot 10^{-2}$	$5.9 \cdot 10^{-3}$
9							$1.8 \cdot 10^{-2}$	$9.9 \cdot 10^{-3}$
10								$1.5 \cdot 10^{-2}$

5. PROBABILITY OF CAPSIZE WHEN HIT BY A BREAKING WAVE FROM THE SIDE

I this section the probability of capsize when exposed to breaking waves from the side is discussed.

The problem is only relevant for smaller vessels, and published work is scarce. Notably, Dahle and Kjaerland [12], Kholodin and Tovstikh [13], Balitskaya [14], Sevastianov [2] and Hirayama and Yamashita [15] have given some data.

In Norway the results from extensive model tests with 3 different vessel types were published as part of the SIS-project in 1983 by Nedrelid et al. [16]. In the tests metasentric height, displacement and extent of super-structure were varied in breaking waves of different height H_c. Although not measured, it is assumed that E for the breaking waves in these experiments were above the lower limit of 0.25 used in the present analysis.

In Fig. 5, where capsize and some non-capsize cases are plotted, a tentative curve has been drawn. A distinction has been made between vessels with bulwark and vessels with rail, because a marked capsize difference has been observed with low values of stability. The "stability" is expressed by the internal work E ideally done by the vessel until $\overline{GZ}$ becomes zero, i.e.

$$E = \Delta \int_0^{\varphi_v} \overline{GZ} \, d\varphi \quad \text{(tons} \cdot \text{m} \cdot \text{degrees)} \tag{16}$$

Δ = displacement (tons)

$\overline{GZ}$ = righting arm (m)

φ_v = heeling angle (degrees)

φ_v should be taken as the angle where $\overline{GZ}$ physically becomes zero, and might be the flooding angle if considerable ingress of water can take place at the roll angle preceeding a breaking wave.

Fig. 5 indicates that capsize probability depends on E, i.e.:

- with corresponding $\overline{GZ}$-curves, a loaded vessel is more safe than one in ballast
- the area below the $\overline{GZ}$-curve is important, and may be provided by enclosed superstructures, by low $\overline{KG}$ or both
- for large φ_v and reasonable Δ and $\overline{GZ}$-values, capsize is very unlikely.

Furthermore, in the investigations the following observations were made:

- the capsize probability for vessels with low $\overline{GZ}$ and freeboards, and a small φ_v (40-50 degrees) depends on the amount of water on deck. A rail instead of a high bulwark is recommended by Sevastianov [2] and Dahle and Kjaerland [12] in such cases.
- As expected, models with positive $\overline{GZ}$-values extending beyond 90 degrees never capsized in waves of H = 10 m.
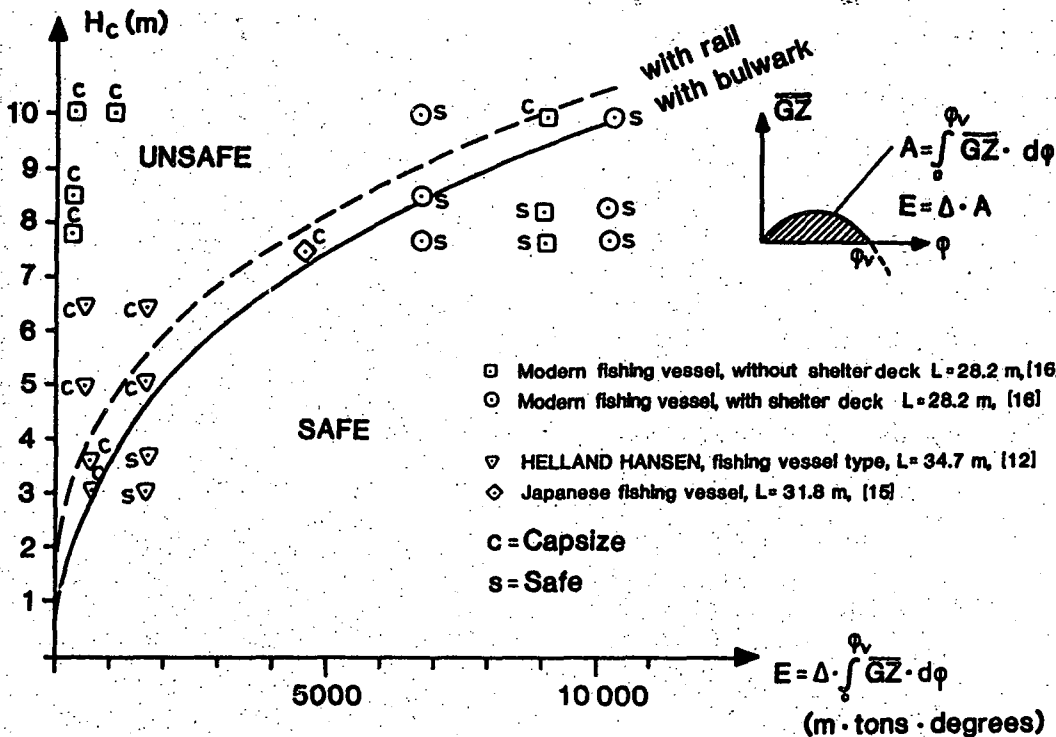

Fig. 5. Probability of capsize.
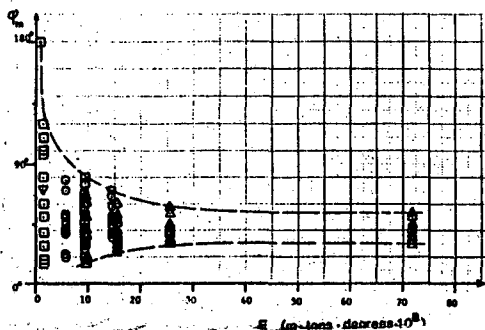
Fig. 6. Maximum roll angle vs. E for breaking waves with
H = 6-10 m, [16]. Symbols as in Fig. 5.

Another important matter is the behaviour of the
cargo when heeled. This matter depends on the operating
condition, and is an important matter for cargo ships.

Fig. 6 illustrates the problem. It shows rolling angle
against E for breaking waves between 6 and 10 m height for
models used, [16].

For vessel models, which were safe from capsizing,
the roll amplitude was between 30 and 50 degrees, which
may cause cargo shift onboard a ship.

If a breaking wave hits a ship, it is important to
consider the roll direction before the impact. If the roll is
against the wave, the probability of capsize is decreased. In
this study, the probability of capsize obtained from
stationary vessel models hit by a steep wave has therefore
been reduced.

Finally, the human aspect with regard to closing of
openings of considerable size (doors, cargo hold hatches)
must be considered. This aspect may decide φ_v, and
therefore has an important impact on the probability of
capsize. For the Norwegian fleet, it is an unfortunate fact
that the crew on fishing vessels in general is less concerned
with closing appliances than crew on merchant ships. This
matter might be improved by introduction of simple-to-read
operation manuals and better training of skippers.
Nevertheless, a probability of closing off important openings
in bad weather should be assigned in the determination of
capsize probability. Also, negligence with regard to securing
cargo should be considered, when relevant.

6. EXAMPLE OF APPLICATION OF THE MODEL

In this example, the intention is to arrive at the order
of magnitude of P_c. For this purpose the Norwegian vessel
M/S HELLAND-HANSEN shown in Fig. 7 has been chosen,
mainly because the H_c for compliance with the IMO's
stability recommendations was arrived at through model
tests, Dahle and Kjaerland [12].
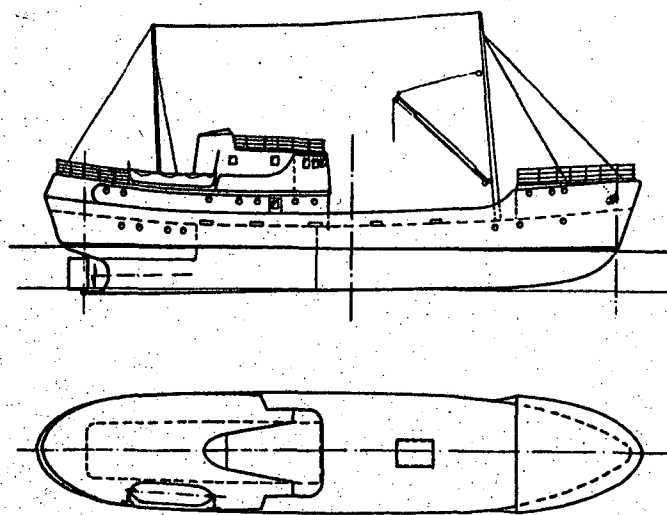
Principal dimensions:
LOA.........: 34.70m
L..........: 30.90m
B..........: 6.90m
D..........: 3.53m
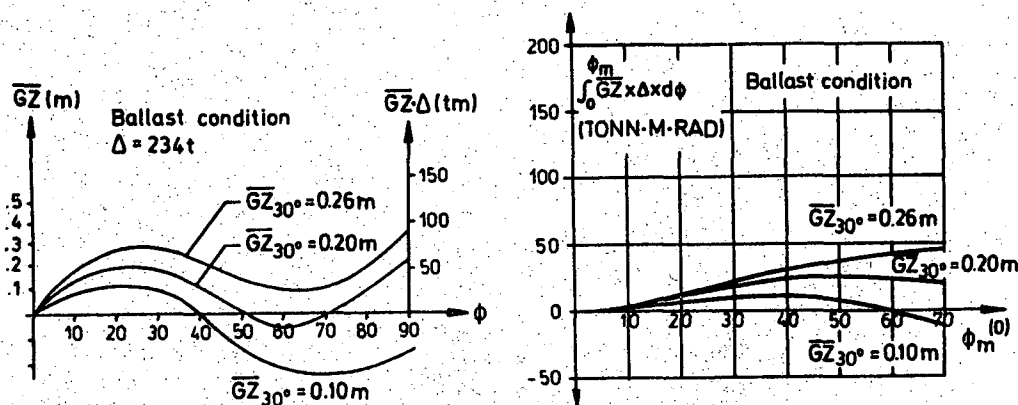

Fig. 7. M/S Helland-Hansen.
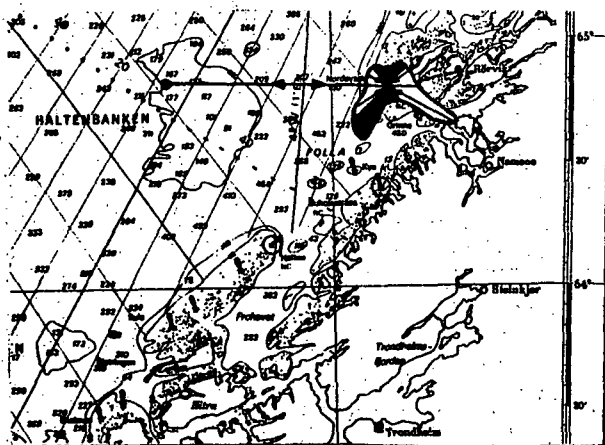
Fig. 8. Location and "wind rose" for the area.

The vessel is supposed to fish on the Halten bank, delivering its catch in Rørvik, see Fig. 8. The one-way trip lasts for about 8 hrs, and the number of trips per year is 40 in this example.

The ship is only supposed to be exposed when steaming to the ground in ballast conditions.

The different contributions to P_C are:

P_1 = probability of weather from the side

From the "wind rose" of Fig. 8, it can easily be calculated that $P_1 = 0.4$.

P_2 = yearly fraction of exposed time
$P_2 = 40 \cdot 8/8760 = 0.037$

w = weight function

For each sea state, w can be calculated as $w = t/\overline{t}$, see Table 2. The result is given in Table 4.

Table 4. Weight function w vs H_s.

H_s(m)	1.5 -2.5	2.5 -3.5	3.5 -4.5	4.5 -5.5	5.5 -6.5	6.5 -7.5	7.5 -8.5	8.5 -9.5	>9.5
w	1	1	1	1	0.7	0.5	0.4	0.3	0.3

P_3 = Conditional probability of steep and high waves for a given sea state
P_5 is given in Table 3.

P_4 = joint probability distribution of H_s and T_z
P_4 is given in Table 1.

According to Equation (2), the probability per year of being exposed to an "extreme wave" (H ≥ 4 m, ε ≥ 0.25) in sea states with H_s ≥ 1.5 m is

$P(S_i) = 0.6 \cdot 10^{-5}$

To obtain the final probability per year of capsize, the procedure is:

P_5 = probability of being hit within T/2, where T is the period of rolling
$P_5 = 0.5$

$P_6 \cdot P_7$ = conditional probability of capsize given an extreme wave situation (P_6), including the human element (P_7)

Choosing $\overline{GM}$ = 0.63 m, the ballast condition from Fig. 7 gives E = 1660 m · tons · degrees, corresponding to H_c = 4 m as used in this analysis. Then, P_6 = 1 for H_c ≥ 4 m.
P_7 is set at 0.8.
The probability of capsize per year is then:

$P_C = P(S_i) \cdot (P_5 \cdot P_6 \cdot P_7) = 0.6 \cdot 10^{-5} \cdot (0.40) = 0.24 \cdot 10^{-5}$

P_C is far below the target value of the Norwegian oil industry of 10^{-4}.

From data collected by the SIS project, the probability of capsize and disappearance for the relevant vessels in the Norwegian fishing fleet is about P_C = 6 · 10^{-4}. The data covers the period 1970-77.

Compared with the result from the example above, this indicates that capsizings in steep and high waves in deep waters only give a minor contribution to the accident statistics. Obviously, a much higher probability of occurrence of dangerous waves is needed to carter for the rather high historical accident frequency.

The explanation is that most of the vessel losses occurred in the so-called "exposed areas" along the coast, as reported by Dahle [17].

Furthermore, some of the vessels were inferior with regard to stability and closing appliances.

7. SUMMARY AND CONCLUSIONS

A model for estimating the probability of capsize in steep and high waves from the side in deep water has been presented. The main element of the model is the estimation of probability of occurrences of steep and high waves for given sea states by using the joint probability density distribution of crest front steepness and wave height.

The sea states are described by using a joint frequency distribution of significant wave height and mean zero-crossing period. The dominant wave direction is taken from wind statistics.

Then, the operations of the vessel have to be investigated in order to assess when it is exposed to the waves, and its loading conditions and associated stability under such conditions.

The stability then has to be associated with a critical wave height, using model experiment data.

Finally, the human element with regard to maintaining the stability (i.e. closing openings and securing cargo) should be assessed.

An example from Norwegian waters has been chosen in order to illustrate the application of the model. However, the critical wave height of 4 m which is used is only applicable for the corresponding stability characteristics, and cannot be generally used. It should also be noted that some of the elements in the model are in an early stage, and have to be updated and developed.

The example indicates that a vessel, complying with the IMO stability recommendations, has a probability of

capsize in steep and high waves from the side in deep waters which is far below the accident target value of the Norwegian oil industry.

However, the vessel accident rate in Norwegian waters is fairly high. The accidents happen mostly in exposed areas near the coast. In these areas, the probability of occurrence of dangerous waves is much higher than in deep waters.

A relevant extension of the model would be to develop it further for use in such exposed areas.

REFERENCES

1. Guidelines for Safety Evaluation of Platform Conceptual Design. Norwegian Petroleum Directorate 1981.

2. Sevastianov, N.B.: "Practical and Scientific Aspects of the Stability Problem for Small Fishing Vessels." Int. Conf. on Design Considerations for Small Craft. RINA, London 1984.

3. Dahle, E.Aa. and Nedrelid, T.: "Stability Criteria for Vessels operating in a Seaway". Proc. Second Int. Conf. on Stab. of Ships and Ocean Vehicles, Tokyo 1982.

4. Håland, L.: "Contribution to the description of the climate on the Norwegian Continental Shelf". Scientific report no. 18, Norwegian Meteor. Inst. Oslo 1978 (In Norwegian).

5. Krogstad, H.E.: "Height and period distributions of extreme waves". Applied Ocean Research, 1985, Vol. 7, No. 3, pp. 158-165.

6. Kjeldsen, S.P.: "Design waves." NHL report 1 81 008. Trondheim 1981.

7. Kjeldsen, S.P. and Myrhaug, D.: "Kinematics and dynamics of breaking waves". Report No. STF60 A78100, "Ships in Rough Seas", Part 4. Norwegian Hydrodynamic Laboratories, Trondheim, Norway, 1978.

8. Myrhaug, D. and Kjeldsen, S.P.: "Parametric modelling of joint probability density distributions for steepness and asymmetry in deep water waves". Applied Ocean Research, 1984, Vol. 6, No. 4, pp. 207-220.

9. Myrhaug, D. and Kjeldsen, S.P.: "On the prediction of occurrences of steep and high waves in deep waters". Submitted for publication, 1985.

10. Myrhaug, D. and Kjeldsen, S.P.: "On the occurrence of steep asymmetric waves in deep water". To be presented at STAB'86, Gdansk, Poland, September 1986.

11. Kjeldsen, S.P. and Myrhaug, D.: "Wave-wave and wave-current interactions in deep water". Proc. 5th POAC Conference, Trondheim Vol., III, 1979, pp.179-200.

12. Dahle, E.Aa. and Kjaerland, O.: "The capsizing of M/S HELLAND-HANSEN." TRINA, Vol. 122, London 1980.

13. Kholodin, A.N. and Tovstikh, E.V. "The model experiment for the stability of small ships on erupting waves". ITTC 1969.

14. Balitskaya, E.O.: "Results of experimental investigation for capsizing in breaking waves". U. of Michigan. 1970. (Translated)

15. Hirayama, T. and Yamashita, Y.: "On the Capsizing Process of Fishing Vessels in Breaking Waves." Journ. of Kansai. Soc. of Nav. Architects, Osaka 1985. (Summary in English)

16. Nedrelid, T., Reitan, O.E., Kjeldsen, S.P.: "Future Stability Criteria. Survival Tests of Ships in Dangerous Wave Situations - Model Test result." SIS-project, Trondheim 1983. (In Norwegian)

17. Dahle, L.A.: "Waves and climate on the Norwegian continental shelf. Mapping of exposed areas along the coast". SIS report. NHL, Trondheim 1979. (In Norwegian)

*) Professor, Dr.ing., Division of Marine Systems Design, Norwegian Institute of Technology, Trondheim, Norway.

**) Professor, Division of Marine Hydrodynamics, Norwegian Institute of Technology, Trondheim, Norway.

ANALYSIS OF A SELF - RIGHTING TEST OF A RESCUE BOAT

H. G. Goldhammer

ABSTRACT

Self-righting ability is nowadays a normal quality of rescue vessels, which are to be able to work and assist other vessels in rough weather circumstances.

Self-righting ability was also claimed for an almost new Danish rescue boat that capsized in Skagerak in 1981, with the loss of 6 men. Investigations proved that the stability was substantially less than desired. However, the accident was explained as being due to bad circumstances.

The appearance of an amateur film from the self-righting test renewed the question of responsibility.

The paper describes the analysis of the film which concluded, that the test as in fact carried out was no proof of stability.

1. INTRODUCTION

The capsize of the almost new-built rescue vessel RF2 shocked the entire Danish nation. At delivery the vessel was declared "unsinkable" and "capsize safe". From all sides, particularly from fishermen and technical circles there was heard claims of explanations of how this could happen.

The vessel left station at Hirtshals a late evening on December 1st. 1981, to search for survivers from a cutter. The conditions were very rough. Even if the wind was about 20 m/sec only, a combination with an exceptionally strong current along the coast, i.e. across the harbour entrance and across the wind, made the conditions very special.

About two hours later, i.e. about 01 a.m. it was decided to call off the rescue, but before RF2 managed to terminate action and return safely to the harbour, she was

PRINCIPAL DATA

Loa	15 m
B	4,4 m
D	2,1 m
Power	368 kW
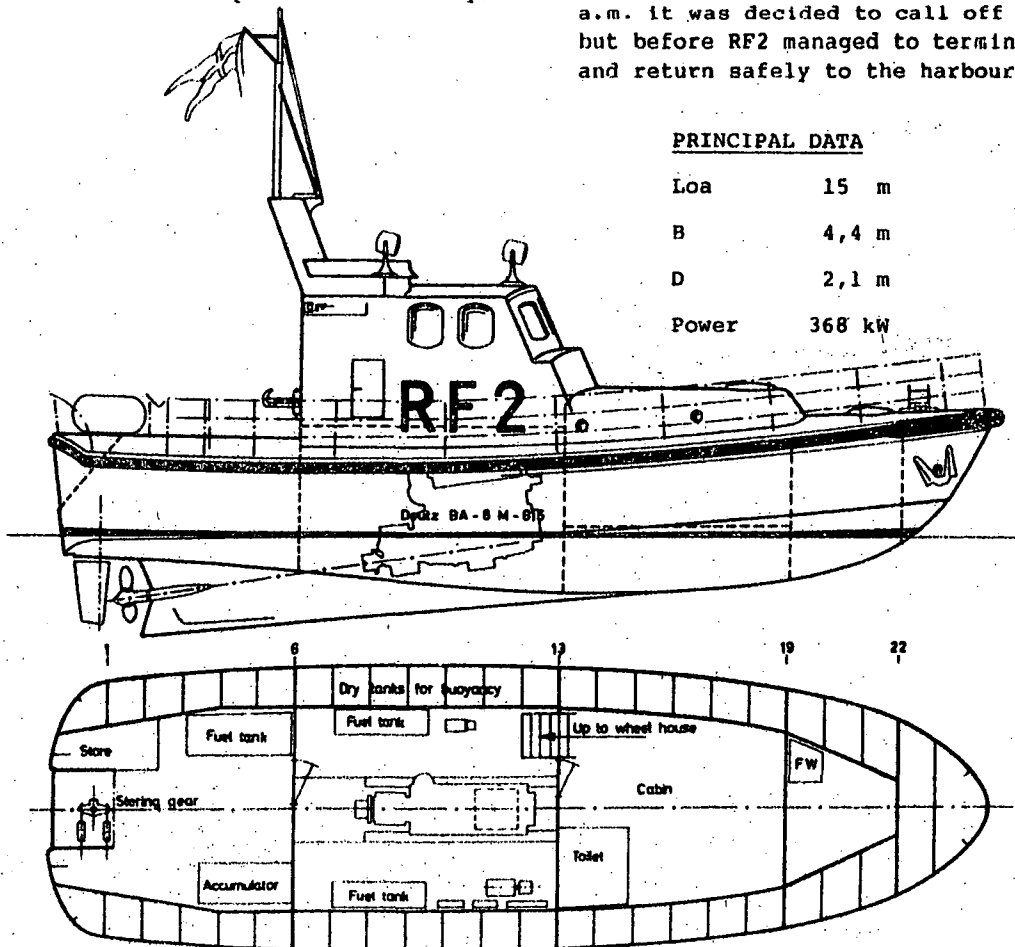
Fig.1. General arrangement and main data of rescue vessel RF2.

struck just outside the harbour by a
breaking wave, lifted on the wave crest only
to fall down in the trough at the same time
heeling 90° to the port side.

The vessel was not able to right her-
self and some seconds later turned upside
down. A few hours later RF2 was found and
salvaged a few kilometres down the coast.

When the vessel was turned to even keel
it was discovered that the entire top of the
wheel house was torn away and the two win-
dows in the port side plus a few more blown
in. The hull, however, was almost intact.

The whole crew, six men all wearing
survival suits, were found drowned either on
board RF2 or in the water.

1.2 The Salvage Commissions

The accident was investigated by a sal-
vage commission, whose report focused on
some weaknesses of the design, especially
the stability of the vessel which was
substantially less than desired. The direct
cause of the capsize, however, was the

failing of the two windows in the port side
of the wheel house, as large angle stability
was quite depending on the intactness of the
wheel house.

Even if the wheel house had remained
intact, the stability near 90° heel was in-
sufficient and the vessel would have kept a
stable position at about 100° heel.

The question of responsibility for the
accident was explained away as a case of bad
circumstances. However, the question of re-
sponsibility was according to the public
opinion never clarified, when a Danish TV-
programme presented a film of the self-
righting test of the RF2. The film was an
amateur film and hitherto unknown to the
commission.

The film caused the investigations to
be resumed by the same commission. The task
was to clear up whether the test, which was
the main control on the boat's stability,
ought to have forced the authority to real-
ize, that the stability of the vessel was
substantially less than requested by them-
selves, and to investigate into im-
provements.

2. THE SELF-RIGHTING TEST

Throughout the last hundred years or so
self-righting tests have been used to test
the stability of rescue- or life boats. In
the days when stability calculation was a
time-consuming and not very accurate pro-
cess, practical tests were popular.

When making the test straps are passed
around the bottom part of the boat and
fastened to one side of the deck, while the
other end is hauled by a crane. Thus an
inclining moment is forced upon the boat and
the boat will heel gradually following the
crane hoist. When upside down, if self-
righting, the boat will right herself.

If the hauling of the crane and there-

fore the inclining of the boat is suffi-
ciently slow (see Appendix), the quality of
stability is tested at all angles during the
turn. If the straps become slack then the
righting moment of the boat is negative. The
heeling of the boat will then continue with-
out any further hoisting until the moment
becomes positive again. At this point of
heeling the boat will have a stable equilib-
rium and the boat is thus not self-righting.

However, it can not be denied that the
primary sense of such a test nowadays is as
a public demonstration of the safety of the
vessel. Stability is much better stated by
calculation. In the present case the test,
dubious as it was carried out, made the job
of PR very well, even unjustly. The public
and especially the rescue men fully trusted
the safety of the RF2.
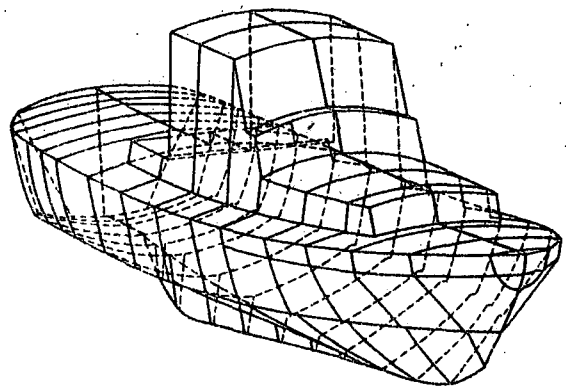
Fig.2.
Lines of RF 2 in axonometric projection.

3. THE STABILITY OF RF2

The hydrostatical calculations i.e. the
statement of the values of Δ, KB, KM
etc. were done by the designer himself by
means of a planimeter and equivalent
methods. At the inclination test a rough
calculation of weights brought about a meta-
centric height of the light condition of
1,000 m (observe the three dicimals!).

The stability curve of the vessel was
brought about by estimating GZ at the
heeling when the wheel house side was im-
mersed and by estimating GM with the
vessel upside down (180°). No real stability
calculations were carried out. As stated by
the commission the GZ at 90° heeling was
at least 0,4 m too high.

The displacement at DWL was about 16
tons. The designer had found the loaded dis-
placement to be 18,5 tons, but the very
accurate calculation of the commission
stated that in the condition of the accident
the displacement was about 22 tons.

The metacentric hight GM as cal-
culated by the designer was 1,0 m at the
loaded displacement, but the commision found
that at the accident GM had only been
about 0,8 m.

It should be mentioned that previous to the building the authority let carry out expensive model seakeeping tests to check the stability. These tests were carried out at a displacement of 18,5 tons, but at a metacentric hight of GM = 1,29 m. It is thus not at all remarkable that the tests appear to indicate good seakeeping abilities, but considering the much diverging data which were the fact, these tests must be said to be of no value at all.

The values of the commission, must be very nearly exact, as calculated on electronic computers by two independent institutions and methods, and with very high agreement. At the values valid for the conditions of the accident these calculations fulfilled the stability requirements of IMCO, but with a very narrow margin only.
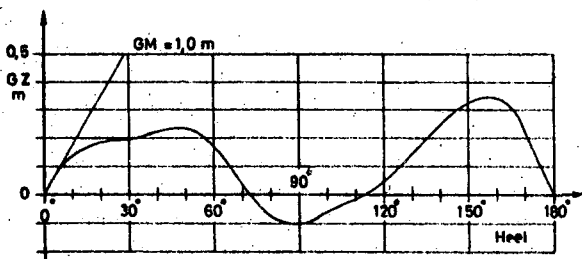

Fig.3. Stability curve of RF 2.
$\Delta = 16$ t and GM = 1,0 m.

The inclination test and the self-righting test were thus the only real check on the stability. They were carried out in the harbour of Nyborg where the building yard is situated. If these tests had been properly and professionally carried out, and if the results had been satisfactory, then the stability might have been satisfactory too.

The inclination test may have been adequate, but is not properly documented. The results were not safe because of the missing hydrostatic data. The self-righting tests, however, was non-professionally carried out. The test demonstrated nothing at all directly. The analysis of the inofficial film as described below gives results in accordance with the calculations of the commission, and demonstrates thus the insufficient stability.

4. THE SECOND COMMISSION

In May 1983 the commission was reestablished. The film which was hitherto unknown to the commission appeared directly to indicate, that the self-righting test ought to have drawn the authority's attention to the fact that the stability of the boat was insufficient.

The task of the second commission was to analyse the film and if possible, state whether the immediate impression was correct.

4.2 The Measuring on the Film

To analyse an event like the turning around of a boat thus stating angles of heel as a function of time, on the base of an amateur film, taken from a moving position (the after deck of a tug) with a hand held camera in non-professional size (Super-8) by a non-professional photographer, requires super professional measuring equipment and operating staff.

The measuring on the original film was executed at the ILF (Institute of Surveying and Photogrammetry) at the Technical University of Denmark. The pictures of the Super-8 film were measured in a Zeiss Jena Stecometer, allowing the stating of the coordinates of a point on the film picture within 0,001 mm.

a. A system of coordinates called "local" is fixed relative to the earth. Points in the harbour visible on the film are measured on the spot and fixed in this coordinate system.

b. A system of coordinates called "boat coordinates" is fixed in the vessel. Characteristic points in the vessel visible on the film, are measured on the vessel and fixed in this system.

c. On every single one of the film pictures are those of the points from a. and b. which are visible on the actual picture, measured in the stecometer. The number of points visible varies from picture to picture. These "machine-coordinates" are input in a computer.

d. The computer program (PASCAL) now run determines on the base of the data from a., b. and c. the 12 unknown: 3 coordinates and 3 angles of both the camera and, more interesting to us, the boat coordinate system, all in relation to the local coordinate system.

The six degrees of freedom of the boat will be determined with a high degree of accuracy: about 1 cm on the coordinates and 0,3° on the angles. The accuracy deteriorates a little with the boat upside down, as many of the points of the boat system are invisible on the pictures. However, this means nothing as far as the conclusions of the investigations concern, as they are based mainly on the heeling up to 160°.

5. THE ANALYSIS OF THE MEASUREMENTS

The film was taken with a Super-8 camera EUMIG ELECTRONIC, which was not at hand at the time of analysis. It was therefore impossible to make any tests on the camera. As the Danish importer of the camera specified the film speed to be within 18 ± 0,5 pictures per second, 18 pictures per second was suggested to be the actual film speed.

The analysis requires a comparison of
the hoisting speed of the crane with the
speed of unrolling of the straps, which may
be determined from the angle of heel. In-
itially this was done by suggesting the
midship section being circular. This ap-
peared to be too inaccurate. Therefore a
more correct calculation was established
using the enveloping polygon of the midship
section, and taking into account that the
displacement of the boat would be reduced by
the strap force, and the position of the
boat in the water would change due to the
heeling. See Fig. 4 .

5.2 The Unrolling of the Straps and the
    Hoisting of the Crane

In the analysis-diagram Fig. 5   the
unrolling of the straps is plotted over the
picture number of the film (curve Ⓑ). The
curve starts at zero at zero time. Zero time
is unknown, however, as the film starts at
19° heel, the zero time is estimated to be 2
seconds or 36 pictures before film start
(picture 0).

The unrolling is calculated by com-
bining the values found in Fig. 4   with the
heeling angles measured on the film. It is
plotted picture by picture.

The unrolling is compared with the
hoisting curve of the crane Ⓐ . If this
curve is correct then the vertical distance
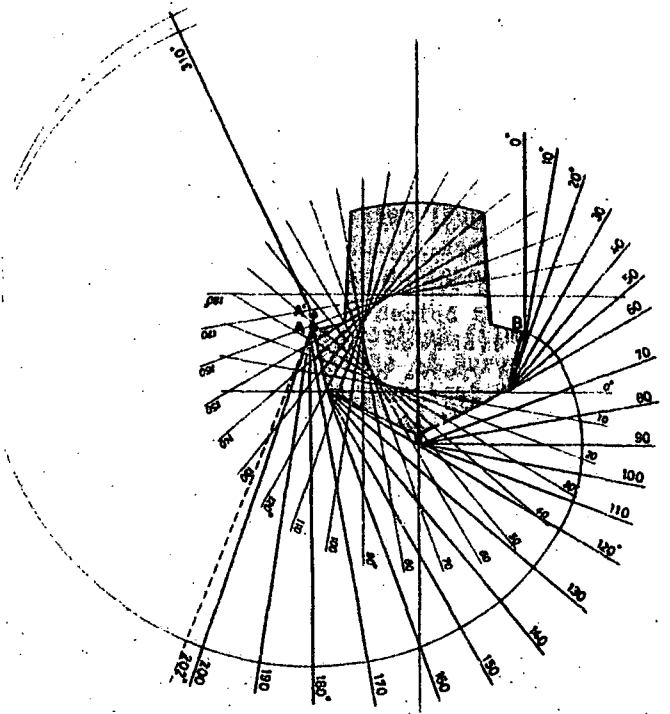
Fig.4.

The diagram shows the unrolling of a strap
secured at point A , passed under the bottom
of the vessel and touching the fender list
at point B. The curve shows the movement of
point B on the strap relative to the vessel.
The unrolling curve Ⓑ on Fig.5 is determi-
ned by measuring on this diagram.
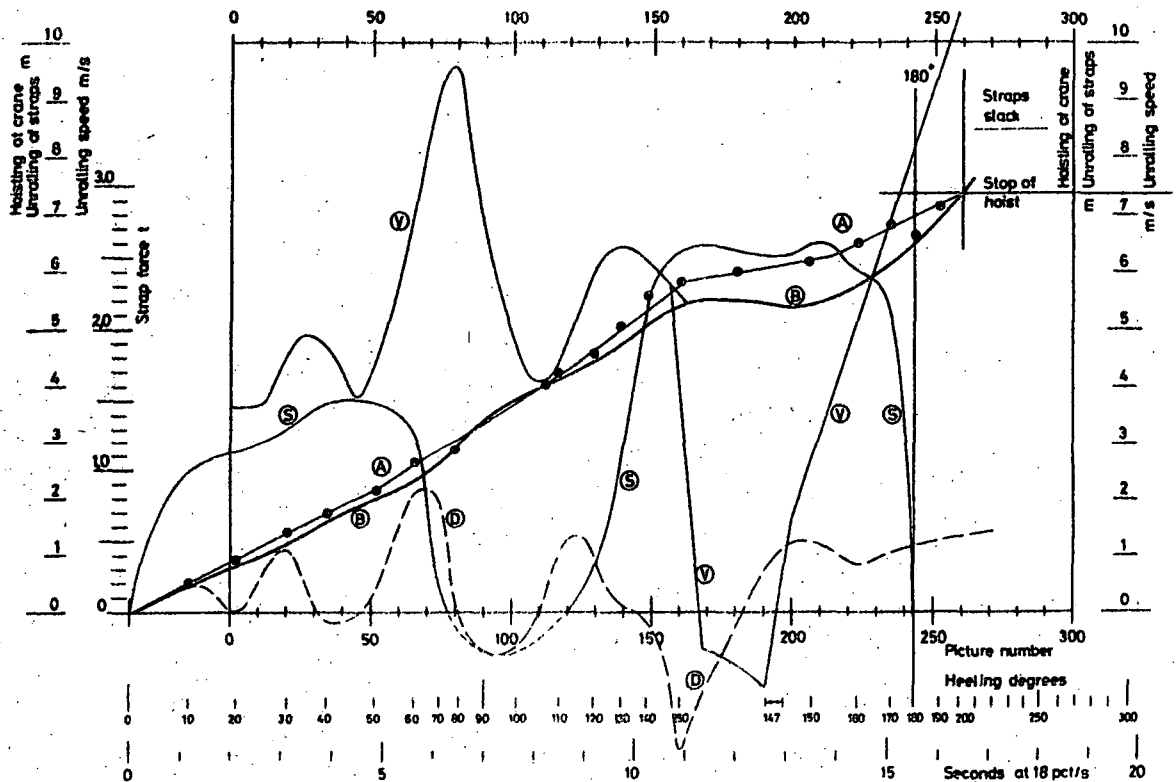
Fig.5. Analysis.

Main parameter is picture number. Start of test correspond to 2 seconds before
picture 0. Additional scale gives heeling in degrees.
Curve Ⓐ is the hoisting of the crane, curve Ⓑ is the unrolling of the straps
determined as the elevation of point B in Fig.4. Curve Ⓥ is the velocity
corresponding to curve Ⓑ . Curve Ⓢ is the necessary strap-force to overcome
ste statical stability moment and curve Ⓓ is the additional dynamic strap-
force calculated by means of eq. II.

of curve Ⓐ above curve Ⓑ will at any time represent the stretching of the straps. If curve Ⓑ is above curve Ⓐ then the straps are slack.

Curve Ⓑ was calculated under the assumption that only the straps were deformed during the test, and the remaining system crane/wire was completely stiff. This is surely not correct, but the elasticity of the straps, which were plastic ropes, must have been totally dominating.

However, curve Ⓐ had to be estimated. It is known that the highest hoisting speed of the crane is 0,6 m/sec, and the crane operator believed he had used the highest speed throughout. This can in fact not be correct. The problem of the analysis is to find the most probable curve Ⓐ.

We know that curve Ⓐ must start at Origo as curve Ⓑ. By direct visual inspection on the film pictures it was observed that from picture 261 (about 200° heel) the straps were slack, and observing the splicings on the straps, it was stated that the hoisting had stopped. Thus we have one point of curve Ⓐ at picture 261, as Ⓐ and Ⓑ must intersect there.

5.3 The Strap-force and the Speed of Unrolling

The unrolling diagram has been used to calculate the strape-force. It was possible to include in the calculations the variable reduction of the displacement caused by the strap-force itself. The calculations were iterative. The necessary static strap-force is plotted in the diagram, Fig. 5 as curve Ⓢ. As the stability has a "hole" (negative stability lever) at an interval near 90°, the strap-force of course has the same. We now have to analyse the equation of the movement:

$$M_S = g \cdot \Delta \cdot GZ + M_H + M_F + I \cdot \frac{d^2\phi}{dt^2} \qquad (I)$$

M_S is the inclining moment originating from the strap-force, $g \cdot \Delta \cdot GZ$ is the static stability moment, where Δ (displacement mass) as well as GZ are variables. M_H is the hydrodynamic and M_F is the frictional damping of the movement.

The last term $I \cdot \frac{d^2\phi}{dt^2}$ represents the inertial forces. I is the moment of inertia of the vessel including added mass. It is here determined as by roll calculations $I = k^2 \cdot \Delta$, where k is the radius of gyration. This is estimated as $k = 0,4 \cdot B$.

We may now simplify by letting $M_S = M_{nec} + M_{dyn}$, where M_{nec} is the inclining moment corresponding to necessary strap-force, i.e. equal to the static stability moment. M_{dyn} is the corresponding inclining moment caused by the dynamics. We get as $\frac{d^2\phi}{dt^2} = \frac{d\omega}{dt}$

$$M_{dyn} = M_H + M_F + I \cdot \frac{d\omega}{dt} \qquad (II)$$

where ω is the angular speed of turning.

5.4 The Influence of the Damping

The damping by hydrodynamical forces come mostly from the side of the wheel house being driven through the water nearly perpendicular to the movement, and the keel doing the same, however not simultaneously. The hydrodynamic damping moment may be determinated as:

$$M_H = c \cdot \tfrac{1}{2} \cdot \rho \cdot (b \cdot \omega)^2 \cdot A \cdot b$$
$$= c \cdot \tfrac{1}{2} \cdot \rho \cdot \omega^2 \cdot A \cdot b^3 \qquad (III)$$

where A is the actual active submerged surface, b is the estimated arm from the centre of pressure of A to the centre of rotation and ρ is the specific mass of the water. At such a movement the coefficient c may be estimated to 1,0.

The completely different damping by friction is calculated by:

$$M_F = C_F \cdot \tfrac{1}{2} \cdot \rho \cdot (R \cdot \omega)^2 \cdot S \cdot R \qquad (IV)$$

valid as long as the deck-edge is not submerged. S is the "wetted surface" of the vessel and R is the mean radius of the hull surface. No values were known for the coefficient C_F valid for cases like this. Therefore the ITTC-57 formula was used for C_F, even if this must be very rough as both the definition of Reynolds' number and the movement itself are quite different from the condition of ship propulsion. The contribution from the friction is small however. The above formula may be used from 0° to about 40°, above which heeling the value is reduced to zero at about 130°.

A lot of elements of damping of other kind are neglected.

5.5 The Oscillations of the System

To get the unrolling we used the measured heelings. By differentiating the heelings ϕ over the time we get the angular speed ω, and differentiating again gives us $\frac{d\omega}{dt}$. Differentiations were executed by calculation directly on the measured heelings, i.e. on any of the film pictures, but mean values were used carrying out the entire calculation for each 10° heeling.

Having investigated the damping, i.e. calculated M_H and M_F, the M_{dyn} may now be found from equation (II). It was found that the term of inertial forces was numerically much larger than the other terms. The result is plotted as curve Ⓓ in the diagram Fig. 5, giving M_{dyn} converted into additional (dynamical) strap-force, S_{dyn}.

Curve Ⓓ is obviously oscillating, the period being 2 increasing to 4 seconds. This result clearly displays the effect of the elasticity of the system.

To investigate these oscillations the case is modelled by a system with polar (mass) moment of inertia I (as above), being turned by a tangential (strap) force having the arm a. Such a system will have the period:

$$T = 2\pi\sqrt{\frac{I}{C \cdot a^2}} \qquad (V)$$

where C is the strap-constant i.e. the force per unit of elongation. This strap-constant may be deduced from Fig. 6 , and is variable with the strap length, which increases with the unrolling.

Angle of heel	30	60	120	deg.
Period calc. by eq.V	1,93	2,86	3,64	sec.
Measured on curve Ⓓ	2,1	3,3	4,4	sec.

The differences may be due to the damping and to errors in the moment of inertia or added mass. However, the agreement may be said to be astonishing, and may be taken as a confirmation of the method.

The period of the ship rolling freely as calculated by

$$T = \frac{2 \cdot \pi \cdot k}{\sqrt{g \cdot GM}}$$

is $T_R = 3,5$ seconds.

Some elements of elasticity are neglected above: the hoisting wire, the crane arm, the mounting of the crane on the quay. These members are of course not perfectly stiff and may, however small, contribute to the differences above.

5.6 The Hoisting of the Crane

As mentioned earlier it is the relation between the two curves Ⓐ and Ⓑ which is interesting in this analysis. Except for the two points origo and the point at picture 261, where the straps became slack, we still do not know the track of curve Ⓐ.

We know generally that the straps become slack when curve Ⓑ is over curve Ⓐ. We know that the claimed "high speed throughout" cannot be true (Fig. 5), but we also know that the turning moment M_S + M_D become below zero theoretically in the region near 90° heel.

By direct visual inspection of the film pictures in this region it was attempted to state if the straps became slack, but with negative result. The straps are almost vertical, and minor slackness will thus not be visible.

After a lot of considerations help was found by investigation of the strap-force, given in Fig. 5 as the sum Ⓢ + Ⓓ. Knowing this force as a function of heeling angle and picture number, it is possible by using the Figs. 4 and 6 to calculate the lengthening of the straps as function of the heeling. This lengthening becomes of course meaningless when Ⓢ + Ⓓ is negative, i.e. the straps are slack. Elsewhere the
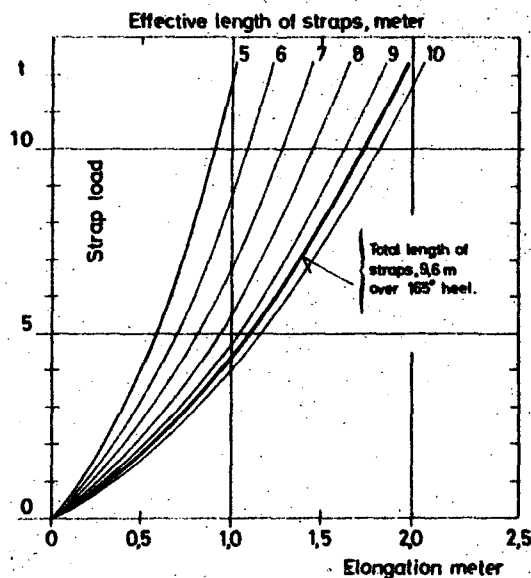

Fig.6. Strap diagram.

Connexion between elongation of and force on a strap, consisting of 2 parts 28 mm plastic ropes, given for different effective strap lengths.

calculated lengthening may be added to the value of unrolling, curve Ⓑ.

In this way a series of points is determined for every 10 degrees of heeling, the black dots in Fig. 5 , which must indicate the track of curve Ⓐ. The curve chosen might have followed the dots all the way, but this would require the assupmtion of a lot of regulation of the crane, which was not considered probably, especially knowing that the determination of the points must be less safe with the boat upside down.

The now fixed curve Ⓐ intersects the curve Ⓑ at abt. picture 75 where the straps thus become slack. There is a fine agreement between this fact, and the increasing slope of the unrolling curve Ⓑ : the boat overtakes the crane hoisting.

The curves Ⓐ and Ⓑ intersect again at about picture 112, thus the straps tighten again. In the region of slackness this reaches a magnitude of 20 cm.

5.7 The Unexpected Stopping and the Final Turning

The turning of the boat continues with relatively high speed until it comes to a sudden stop at picture 160. The turning rests for about two seconds, during which a creeping in the opposite direction of about two degrees is visible. About picture 200 the turning is resumed continuing now at high speed until upright.

The diagram Fig. 5 gives the answer why: During the time of slack straps and a little while thereafter the unrolling speed keeps nearly constant at a high level. The curves Ⓐ and Ⓑ are almost parallel with small vertical distance in this region. This means that the strap-force is very small. Almost suddenly the stability moment at a very small increase of heel rises to high

values at picture 150 where the stability has its absolute maximum.

As seen on picture 150 the crane driver manages to react to the very high speed by lowering the hoisting speed (the slope of curve Ⓐ gets smaller) nearly simultaneously to the steep rise of the uprighting moment. The turning can not continue before the crane has built up a sufficiently high value of the strap-force to overcome the uprighting moment.

The strap-force reaches very soon its highest level and the strap-lengthening, becomes nearly 1,0 meter. Subsequently the movement continues at very high speed until upright.

The hoisting is controlled at least once during this interval before it is stopped at picture 260 at 200° heel, where the straps become slack.

The final uprighting of the vessel goes on without any visible influence from the region with negative stability (the "hole"), obviously by the help of the high speed.

6. CONCLUSIONS OF THE ANALYSIS

Did the analysis bring any knowledge about the stability which we did not have in advance? In spite of the extended investigation and efforts the answer must be: Not directly!

However, the analysis has confirmed very clearly what the hydrostatical and stability calculations had brought about earlier: The stability was far from being sufficient especially in the region about 90° heel. Beyond this the test and the film of the test is to be a lesson on how such a test should NOT be executed.

Several faults and shortcomings of the test may be mentioned:

There was no real check on missing weights at the test.

No releasing mechanism in the crane hoist at the test. That was contrary to the building specification.

There was very bad communication, if any, between the crane driver and the leader of the test, who was the consultative engineer of the yard. The only order to the crane driver in advance was: "High speed".

Above all, the turning was far too fast. The whole turn round takes about 20 seconds. As seen in the Appendix the British RNLI Institution of Lifeboats requires the test from upright to 180° to take about 90 seconds, and the now official Danish procedure, see the Appendix, will last even longer. As in fact carried out all significant stability qualities are blurred by the high speed. Only the unexpected stopping would make probable that things were not normal.

As conclusion of the analysis it may be said, that the test was at least of no value at all, but even worse: because of the shortcomings not being recognized the test

gave the owner/authority and the crew a false feeling of security about the stability.

7. CONCLUDING REMARKS

We have already answered the question whether the visitors of the test should have been able to observe the slackening straps during the passage through the "hole" in the stability.

Even if the answer is NO, the test ought to have given the spectators occasion to be very doubtful about the stability. It must have been visible, at the very test as it in fact is on the film, that the wheel house caused a remarkable wave in the harbour basin when clashing in the water, and it ought to have been visible too that the movement accelerated about that time.

It was at least without any doubt visible to anybody, that the movement stopped at 150° and hesitated two seconds before continuing. And it must have been astonishing to all the spectators that the whole affair could be over in so short a time.

Did the authority not at all react to the doubtful execution of the test, on which they had based a lot of the control of the stability? At the test the authority was represented by one person only. It was a foreman having no knowledge about such tests at all, and no insight in stability. He got no instructions in advance. How could he alone supervise such an important test?

The men higher in the hierarchy seemed not at all to have been interested in the stability of the vessel. Afterwards the supervising foreman was only asked whether the vessel righted herself after she had been turned upside down. As this was the case then everything was OK.

Nobody at all realized that stability is a problem, which may not be neglected unpunished. Only tragic that the punishment in this case hit a totally innocent crew.

REFERENCES

1. Betænkning om "RF.2"s forlis. (Report on the loss of "RF.2", submittet by the Commission appointed by the Minister of Industry). Betænkning nr. 956, Copenhagen 1982. In Danish.

2. Betænkning II om "RF.2"s forlis. Betænkning nr. 1005, Copenhagen 1984. In Danish.

The Technical University of Denmark
Department of Ocean Engineering
Building 101 E
DK-2800 Lyngby, Denmark
Telephone: +45 2 88 48 22 ext. 4067
Telex: 37529 DTHDIA DK

H. E. GULDHAMMER
Associate Professor, M.Sc.

APPENDIX

On the request from the Danish Author-
ity of Lifeboats the British RNLI described
their method of carrying out self-righting
tests, by sending a telex from which we
quote:

during design of the self righting craft cross curves of
stability should be calculated to determine that the range
of stability is 180 degrees. after construction an
inclining experiment is undertaken to determine the position
of the vertical centre of gravity which in conjunction
with the cross curves of stability will indicate whether or
not the craft has a self righting capability.

during the self righting test the craft is turned slowly
within 1 and 1/2 minutes of time through 180 degrees and
then released from the crane hoist. the craft should then
turn in either direction to upright.

It will be observed that the turning
movement in this method is so slow, that no
"holes" in the stability can escape the
attention of the supervisor.

The Danish Government Ship Inspection
Service (Statens Skibstilsyn) which is now
the responsible controlling authority of all
Danish rescue boats, is practising a pro-
cedure of self-righting tests. The method
has been in use for approval of totally
closed plastic life boats etc. for several
years.

According to this procedure the boat is
heeled by a crane as by other methods, but
the hoisting is interrupted at suitable
heelings. At each stop the crane force is
eased off, and now the boat shall right
correspondingly. The hoisting is continued
until next stop, 6-8 stops until the heeling
is 180°. Then the boat shall right herself
when released.

This procedure may be explained as a
further development of the RNLI-method. At
each stop the supervisor of the test may
state if the stability is positive, and by
watching the willingness of the boat to
recover he will get a feeling of the quality
of the stability, but of course no numeric
values.

Another advantage of the procedure is
that during the slackening of the straps the
boat will regain at least partially her
original displacement, which is reduced by
the influence of the hoisting force. The
influence on the stability of this re-
duction, which may at some heelings be
substantial, is thereby eliminated to some
extend. The value of the test may thus be
improved remarkably.

It should be mentioned that measuring
the crane hoisting force during the test
will increase the amount of information
obtained considerably, especially if a cali-
brated crane hook dynamometer is used.

BSRA TRAWLER SERIES STABILITY IN LONGITUDINAL WAVES

A. Campanile, P. Cassella

ABSTRACT

As pointed out in the literature, a ship experiences a stability reduction when travelling in a following sea; as crest is amidship and wave and ship lengths are nearly the same, the effect is substantial with small wave heights also; this unfavourable effect due mainly to the change in the geometry of the immersed volume.

It has been shown in previous papers that the characteristics of the immersed volume of an actual ship in a longitudinal wave can be obtained by a proper transformation of corresponding data of a similar hull. Because of the usual practice to design the ship form according to a standard series, then a viable procedure is obtained to predict the transverse stability reduction among waves on the basis of an appropriate tabulation of geometrical properties of parent forms.

The method is herein applied to BSRA trawler series and the computational routine is illustrated by a worked example. Besides, the influence of wave height and relevant ship parameters on significant stability indices is investigated; the existence of geometrical ratio limiting values to fulfill stability requirements, in relation to ship size and vertical centre of gravity, is evinced.

1. FOREWORD

The problem of the safety against ship capsizing continues to be very important, especially in the case of small vessels, as dramatically pointed out by casualties, with loss of life, recorded in recent years; in respect to this accident, more rigorous reccomendations and regulations have been issued by intergovernmental and national authorities and a great effort has been produced to get a better understanding of the phenomenon. Unfortunately, it is almost impossible to consider all of the factors affecting the ship stability; moreover, a comprehensive description of the dynamic behaviour of a vessel subjected to extreme conditions is recognized as a very difficult task. However, it is conceivable that the safety at sea can be effectively improved adopting, on the basis of the up to date knowledge, rational and practicable stability criteria and adequate computational procedures in the assessment of the transverse stability.

The definition of more adequate stability indices in relation to typical ship forms, expected marine environment and operational aspects is extensively being pursued by many researchers and specific organizations. The authors by no means intend herein to suggest new stability criteria: the transverse stability reduction of a ship travelling in a following seaway is as well established as the increased risk of capsizing under the action of a heeling moment when a crest is nearly amidship for a sufficiently long time period, [1], [2], [10], [14], [15], [18]. It is the intent here to give a quite simple procedure to evaluate the transverse stability curve, both in still water and in longitudinal wave, of a fishing vessel derived according to a standard series. It has been considered that most small fishing vessels are still being built by shipyards equipped with reduced technical and computing facilities, while face, on the other hand, critical stability conditions frequently during their life.

The present investigation has been carried out within a general program, [6], [8], [9], [16], having the purpose of producing the charts of geometrical elements involved in the stability calculations for the parent forms of the most used standard series; these data, given in a suitable non dimensional form, will apply as well to any series hull derived on the basis of geometrical similitude. The proposed presentation will provide, in addition to resistance charts, a practical means to deduce quickly stability characteristics in the preliminary design and consequently the possibility of judging soundly of the effect on the stability of varying some form parameters, where applicable.

The paper deals with the BSRA trawler series; at this stage, the variations in block coefficient and depth to draught ratio have been examined, while the variations in beam to draught and length to displacement ratios are taken into account by the proposed method as a direct consequence of geometrical similitude connecting concerned forms; however, it is planned to extend the analysis to other variations in order to cover systematically all the parameter ranges investigated by the series. Moreover, the data available at the moment have been processed to analyse the influence of

main form parameters on some statical and dynamical stability indices.

2. HULL SIMILITUDE IN LONGITUDINAL WAVE

The theoretical background of hull geometrical similitude is discussed in [7] and the generalized formulation in the case of a ship statically poised on a longitudinal sinusoidal wave is fully reported in [4] and [5]; some definitions and results are now reported as far as they are involved in the present application.

Two hulls are here defined similar if their geometries are obtained, each from the other, by a linear change in the offset co-ordinates:

$$x/L = x'/L'; \quad y/B = y'/B'; \quad z/D = z'/D' \qquad (1)$$

where x,y,z are the current longitudinal, tansverse and vertical co-ordinates and L, B, D are the length between the perpendiculars, the moulded breadth and the moulded depth, respectively. In such a transformation the form coefficients, in particular the block coefficient and the depth to design draught ratio, do not change.

The transformation (1) applies as well inside the immersed volumes of inclined hulls in presence of sinusoidal waves with the crest amidship, provided the following non dimensional coefficients, indicative of the free surface geometry respect to ship frame, assume the same values for both similar hulls:

$$C_\Delta = \nabla/(C_B L B T) = \nabla'/(C_B L' B' T')$$

$$C_\phi = (B/T) \tan\phi = (B'/T') \tan\phi' \qquad (2)$$

$$C_k = H/(T \cos\phi) = H'/(T' \cos\phi')$$

where ∇ is the actual immersed volume, T is the design draught, C_B is the block coefficient, ϕ is the heel angle, H is the wave height and the wave lenght is set equal to the ship length. Then, the co-ordinates of the centres of immersed portions of the two hulls are related according to relations (1) or, in other terms, their ratios to proper main dimensions are the same for both ships, say:

$$x_B/L = x'_B/L'; \quad 2y_B/B = 2y'_B/B'; \quad z_B/T = z'_B/T' \qquad (3)$$

Therefore, assuming an hydrostatic type pressure distribution, the buoyancy arm curve of an actual ship can be obtained from the data relative to a similar hull by:

$$KZ = (2y_B/B) B/2 \cos\phi + (z_B/T) T \sin\phi \qquad (4)$$

The procedure will be particularly useful in designing the ship form according to the offset tables of a standard series.

## 3. APPLICATION TO B.S.R.A. TRAWLER SERIES

The method briefly described above has been applied to BSRA trawler series because it has been felt, by the authors, particularly effective in the assessment of stability of fishing vessels because of its computational easiness. The BSRA series resistance and propulsion tests, [12], [13], [17], are relative to variations in breadth to draught ratio, trim, length to displacement ratio, block coefficient, longitudinal position of the centre of buoyancy, load condition, bow and stern profiles; therefore the availability of a large group of systematically varied forms will allow the authors to examine methodically the influence of main parameters affecting the fishing vessel stability.

At the moment, they have been considered three parent forms, models ZP, XF, ZQ, characterized by the block coefficient values of .522, .565 and .596 respectively. Three different values of moulded depth to design draught ratio, namely 1.2, 1.4 and 1.6, have been associated to each parent form obtaining a group of 9 hulls which are different from hydrostatic point of view according to (1); the deck has been assumed to have no camber or sheer. An extensive set of hydrostatic calculations has been performed to scan adequately the domain of coefficients in (2); only the level trim has been considered throughout.

In particular, for each of the 9 hulls, there are considered: a) 10 different values of the immersed volume, and consequently of the C_Δ coefficient, about equally spaced between zero and maximum values; b) 10 different heel angles corresponding to the C_ϕ coefficient values of .0, .025, 0.25, 0.50, 0.75, 1.00, 1.25, 1.50, 1.75 and 2.00; c) 5 different wave heights corresponding to the C_k coefficient values of 0, .5, 1., 1.5 and 2. In each case the co-ordinates of the centre of buoyancy have been calculated; the transverse and vertical co-ordinates have been normalized according to expressions (3) and have been graphically reported in 45 pairs of graphs, one of them is given for example in figures 1 and 2; each pair of graphs is referred to given values of the block coefficient, the depth to draught ratio and the wave height coefficient C_k, and contains the curves, vs. load coefficient C_Δ, of non dimensional quantities $(2y_B/B)$ and (z_B/T); each curve is relative to a given value of the heel angle coefficient C_ϕ.

The charts, not reported here because of lack of room, provide a quite simple presentation of obtained numerical data; they allow to calculate, on the basis of formula (4), the stability curve, at any assigned load condition, of an actual ship derived from one of the selected parent forms, as well as the buoyancy arm deduction due to a longitudinal wave with a given height, the crest amid-

ship and the length equal to the ship length, i.e. likely in the most dangerous conditions.

FIG.1

FIG. 2
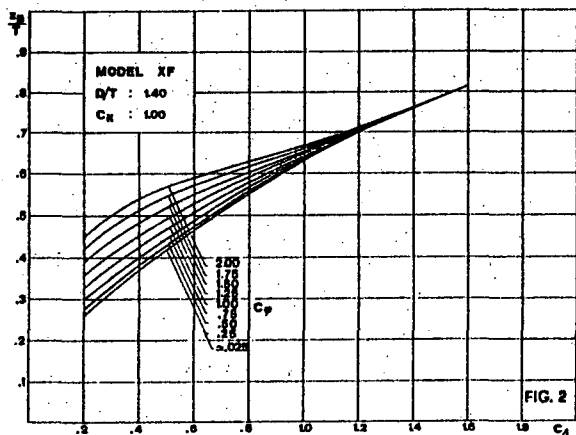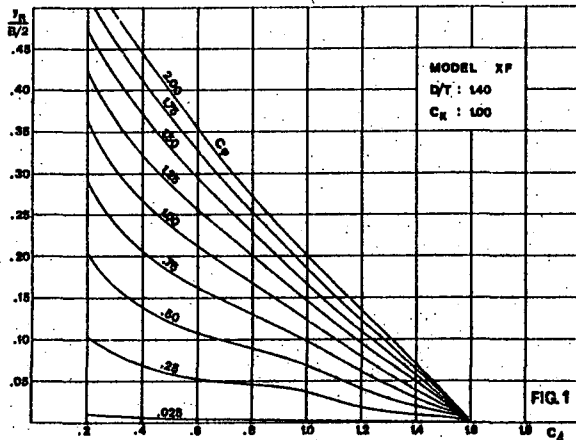
At a given load condition, it is possible to draw out the curves of non dimensional co-ordinates of the centre of buoyancy as function of C_k coefficient, pointing out in such a way the influence of the wave height. This has been accomplished with reference to the design load and resulting charts, as those typical ones in figures 3 and 4 relative to model XF with D/T = 1.4, will be applied in the next sections to illustrate the practical application of the proposed procedure and to analyse methodically the influences of some form parameters.

FIG. 3

FIG.4
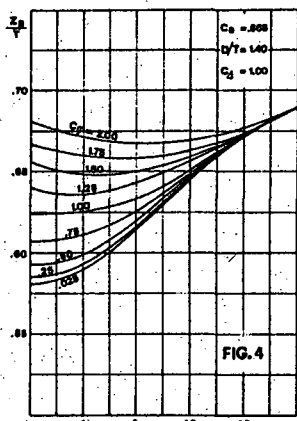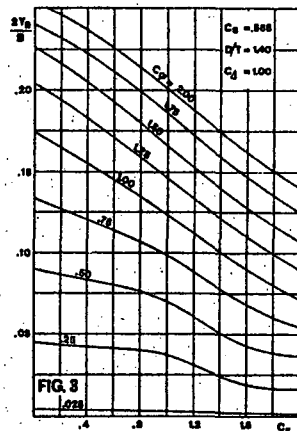
4. EVALUATION OF AN ACTUAL RIGHTING CURVE

A sample application is developed hereafter to illustrate the computational procedure; it is assumed that the actual ship is obtained by a linear expansion of the table of the offsets of the parent form having a block coefficient of .565 and a D/T ratio of 1.4. In the specific case, they are considered a beam to draught ratio of 3, a length to displacement ratio of 4.85 and a displacement volume, at the design draught, of 100 c.m.; as a consequence, the length b.p. is 22.512 m, the breadth is 4.856 m, the depth is 2.267 m and the design draught is 1.619 m. Moreover, it is assumed $KG = .8 D = 1.813$ m and $H = .05 L = 1.126$ m.

To derive the righting arm values, the readings must be made in figures 3 and 4, for each constant C_ϕ curve, at abscissa values given by:

$$C_k = H/(T \cos\phi) \qquad \text{where: } \tan\phi = C_\phi/(B/T)$$

In such a way, a series of $(2y_B/B)$ and (z_B/T) ratios values is obtained and correspondingly righting arms are given by:

$$GZ = y_B \cos\phi + (z_B - KG) \sin\phi$$

The resulting values are summarized in table 1 and the righting arm curve is given in fig.5.

TABLE 1

C_ϕ	$\phi(°)$	C_k	$y_B(m)$	$z_B(m)$	$GZ(m)$
.025	.48	.695	.010	.983	.003
.25	4.76	.698	.099	.987	.030
.50	9.46	.705	.190	.994	.053
.75	14.04	.717	.267	1.008	.063
1.00	18.43	.733	.335	1.023	.068
1.25	22.62	.753	.392	1.040	.065
1.50	26.56	.777	.440	1.052	.053
1.75	30.26	.805	.482	1.066	.040
2.00	33.69	.836	.513	1.081	.021

In fig.5 it is also given the curve relative to still water condition; besides, there are plotted 3 curves relative to a different position of the centre of gravity, characterized by the KB/D value of .7, and to H/L ratio values of .0, .05, .10; obviously, the additional curves have been obtained repeating the procedure illustrated above; it must be noted that the curve relative to KB/D=.8 and H/L=.1, not reported in fig.5, has negative values.

FIG.5
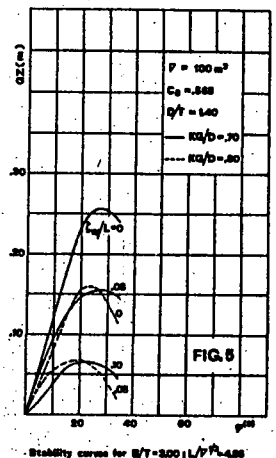
5. WAVE HEIGHT AND FORM COEFFICIENT INFLUENCES

In order to study, at the design load condition, the influences on the stability of wave height, some form coefficients and vertical position of the centre of gravity, the charts like those in figures 3 and 4 have been processed to derive the righting arm curves in the cases listed in the table 2. In each case two different positions of the centre of gravity have been considered, i.e. KB/D values of .7 and .8, in combination with still water condition and wave slope H/L values of 0.05 and 0.10.

TABLE 2

change in	# model	C_B	$L/\nabla^{1/3}$	D/T	B/T
reference	1 XF	.565	4.85	1.4	3.00
B/T	2 XF	.565	4.85	1.4	2.00
	3				2.25
	4				2.50
	5				2.75
	6				3.25
	7				3.50
D/T	8 XF	.565	4.85	1.2	3.00
	9			1.6	
$L/\nabla^{1/3}$	10 XF	.565	4.35	1.4	3.00
	11		4.60		
	12		5.10		
C_B	13 ZP	.522	4.85	1.4	3.00
	14 ZQ	.596			

In order to compare results, each curve of stability has been represented by three stability indices, namely the initial metacentric height $GM = [d(GZ)/d\phi]_{\phi=0}$, the maximum righting arm GZmax and the area Emax under the righting arm curve up to angle at which the maximum arm occurs; these indices, calculated with reference to 100 c.m. displacement volume, have been divided by corresponding ship breadth because, as the ship dimensions are scaled by a constant factor, the righting arms are equally scaled and consequently considered ratios are independent of the actual size.

The non dimensional values of considered stability indices are graphically given in figures from 6 to 17; in detail, figures 6, 7, 8 refer to B/T variation, figures 9, 10, 11 to freeboard variation, figures 12, 13, 14 to length to displacement ratio variation and figures 15, 16, 17 to block coefficient variation.

The inspection of indices graphs reveals the stability trends respect to examined variables, some of which well known by technical literature.

As regards the main concern of the paper, it is evinced that the ship stability in presence of wave, with crest amidship, is markedly reduced, as compared to still water condition, in all the examined cases; for example, in the reference case

no.1 of table 2 with KG/D=.8 the righting energy index is cancelled out for H/L=.1, while Emax/B is .008 in still water, i.e. Emax = .084 m.rad for 1000 t displacement. As expected, the reduction in stability indices increases as the wave height increases.

As regards the beam to draught ratio, its substantial influence on stability is clearly confirmed. In particular, GM/B ratio increases as B/T increases, the relation being approximately linear both in still water and in presence of wave; the previous behaviour is more or less preserved in the case of maximum righting arm and righting energy indices.

As regards the freeboard, it affects markedly the stability indices, quite differently in various cases. The metacentric height to beam ratio reduces in still water as D/T increases because of raising of the centre of gravity; in presence of wave the previous behaviour changes: GM/B at first increases, then decreases in relation to D/T ratio, the initial trend due likely to the increase in the emersed portion of the deck. Dynamic stability indices, i.e. GZmax/B and Emax/B, are augmented by a greater freeboard, but this trend is limited to certain values after which they decline; it must be considered that the well known favourable effect on dynamic stability of an increased freeboard is partly balanced by the contemporary raising of the centre of gravity; this second effect is prevailing for great D/T values. As a consequence, freeboard cannot be indefinitely augmented in order to improve dynamic stability, the limiting value depending on how the centre of gravity raises in relation to deck position; of course, it is not conceivable, generally, that KB/D ratio will be constant whichever value would be assumed by deck height above keel.

Righting arms are not affected by a linear change of longitudinal dimensions because immersed volume and its transverse statical moments are all proportional to longitudinal scale factor. Consequently, the ratios of selected stability indices to beam, normalized by a transverse dimension, do not depend in still water on length to displacement ratio, as shown by figures 12, 13 and 14; in presence of wave they reduce as length to displacement ratio increases simply because H/T ratio becomes larger as far as wave slope H/L is kept constant. It is worth to note that, in still water also, the indices absolute values reduce, at a given displacement, as the length to displacement ratio increases because the ship breadth reduces according to:

$$B = [(\nabla^{2/3} B/T)/(C_B L/\nabla^{1/3})]^{1/2}$$

The variation in block coefficient affects moderately the stability indices; in detail, the ma-

ximum righting arm to breadth ratio is almost constant in relation to considered block coefficient range both in still water and in presence of wave; the curves of other two indices, as non dimensional quantities, are approximately rectilinear in still water, while in presence of wave the curves corresponding to different wave heights are shaped with different curvatures, behaviour that does not seem easily predictable without further investigation.

6. INFLUENCE OF DISPLACEMENT

The previous analysis has been performed in a non dimensional form; actual values of stability indices are easily obtained by preceding non dimensional values once main dimensions are given. In order to point out the influence of ship size, the metacentric height, the maximum righting arm and the reference righting energy have been calculated in the range of the displacement volume, assumed as representative of ship dimensions, from 100 to 1000 c.m. It has been made reference to model XF with D/T 1.4 and length to displacement ratio 4.85; the examined cases are subdivided into two groups: in the first one it has been considered the still water condition and the B/T range from 3 to 3.5; in the second one they have been considered the H/L values of .05 and .1 for B/T equal to 3; in all cases calculations have been carried out for both KB/D values of 0.7 and 0.8. The obtained results are shown in figures 18, 19 and 20.

The figures point out again that, at a given displacement, the stability is markedly reduced by the raising of the centre of gravity and the presence of wave, while is improved by higher values of B/T ratio.

On the other hand, at given values of KB/D, B/T and H/L ratios, stability indices reduce in such a way that stability requirements are hardly met for low values of displacement. For example, with reference to still water condition, the minimum value of 0.08 m.rad requested by Rahola criteria is reached, in the case of KB/D equal to .7, only at 850 c.m. displacement volume for B/T equal to 2.5, the corresponding figures for B/T equal to 3 and 3.5 being about 160 and 70 c.m. respectively; if KB/D is equal to .8, the .08 m.rad righting energy requirement cannot be fulfilled in all the examined range of displacement by B/T equal to 2.5 and is met by B/T values of 3 and 3.5 only at 850 and 200 c.m. displacement volumes respectively.

7. CONCLUDING REMARKS

In the present paper it has been shown that the stability of an actual ship, both in still water and in a following sea, can be predicted by a proper transformation of corresponding data of a similar hull. If the ship form is selected according to the charts of a standard series, then a simple procedure, based on geometrical similitude, is obtained to consider adequately stability requirements even, in the preliminary design, before producing the lines plan. Consequently, as the involved geometrical quantities have been systematically produced for series parent forms, it is possible to optimize ship dimensions from the point of view of stability, likewise it is usual to do from the point of view of hydrodynamic resistance.

It must be considered that the theoretical background of the proposed procedure is strictly valid in the case of two hulls derived, each from the other, by a linear change in the offset co-ordinates and consequently the method will provide accurate results only for those sets of relevant ship parameters, that in the present case are block coefficient and D/T ratio, directly considered by the available centre of buoyancy co-ordinates charts. It is felt that an interpolating procedure can be adopted with an accuracy sufficient for practical purposes, this assumption being confirmed by fair curves obtained along with the development of the present work, some of them are reported.

The method has been purposely applied to BSRA trawler series because fishing vessels are frequently subjected to critical stability conditions. Resulting charts allow to evaluate statical and dynamical stability in a following sea as easily as in still water, providing a relatively simple means to judge of this unfavourable occurence.

The analysis of some stability indices in relation to main form coefficients suggests the possibility of determining the limiting ship proportions to fulfill stability requirements for predictable operational conditions; to this purpose, it seems appropriate a preliminary investigation to take into account, approximately at least, the incidence of typical camber, sheer, superstructures.

REFERENCES

1. Arndt B.; Systematische Berechnungen der Seegangsstabilität; Hansa, 1964

2. Arndt B. and Roden S.; Stabilität bei vor-und achterlichem Seegang; Schiffstechnik, 1958

3. Campanile A.; Gli elementi geometrici delle carene mediante la rappresentazione delle sezioni trasversali con segmenti di polinomio; Istituto di Macchine Marine, Napoli, Report No.16, 1983

4. Campanile A. and Cassella P.; L'affinità geo-
   metrica delle carene su onde longitudinali;
   NAV82, Napoli, 1982

5. Campanile A. e Cassella P.; Affinité géométri-
   que des carènes sur houles longitudinales; Bul-
   letin de l'ATMA, 1983

6. Campanile A. and Cassella P.; Series 60 hull
   characteristics of stability among waves;
   IMAEM, Athens, 1984

7. Cassella P.; Sulla affinità geometrica delle
   carene; Tecnica Italiana, Vol.XLIV, No.1, 1979

8. Cassella P. and Russo Krauss G.; Stability dia-
   grams for Series 60; IMAEM, Istambul, 1978

9. Cassella P. and Russo Krauss G.; Caratteristi-
   che geometriche e di stabilità delle carene
   della serie N.P.L.; Tecnica Italiana, Vol.XLVI,
   No.3, 1981

10. Brix O.; Rollschwingungen, Stabilität und
    Sicherheit im Seegang; Schiffstechnik, 1952

11. IMCO; Reccomendation on intact stability of fi-
    shing vessels; 1968

12. Pattullo R.N.M.; The B.S.R.A. trawler series
    (part II). Block coefficient and longitudinal
    centre of buoyancy variation series. Resistance
    and propulsion tests; Trans.RINA, Vol.110, 1968

13. Pattullo R.N.M. and Thomson G.R.; The B.S.R.A.
    trawler series (Part I). Beam-draught and
    length-displacement ratio series resistance and
    propulsion tests; Trans.RINA, Vol.107, 1965

14. Paulling J.R.; Transverse stability of tuna
    clippers; Fishing Boats of the World: 2;
    Fishing News (Books) Ltd, 1960

15. Paulling J.R.; The transverse stability of a
    ship in a longitudinal seaway; Journal of Ship
    Research, 1961

16. Russo Krauss G.; Metodo per il rapido traccia-
    mento del diagramma di stabilità di una qualun-
    que carena da carico appartenente alla Serie
    B.S.R.A.; Tecnica Italiana, Vol.XLVIII, No.5,
    1983

17. Thomson G.R. and Pattullo R.N.M.; The B.S.R.A.
    trawler series (part III). Resistance and pro-
    pulsion tests with bow and stern variations;
    Trans.RINA, Vol.111, 1969

18. Wendel K.; Stabilitätseinbussen im Seegang und
    durch Koksdeckslast; Hansa, 1954

Authors

Campanile A., professor of Special Ships, De-
   partment of Naval Engineering, University of
   Naples, Naples, Italy

Cassella P., professor of Ship Hydrostatics, Di-
   rector of the Department of Naval Engineering,
   University of Naples, Naples, Italy
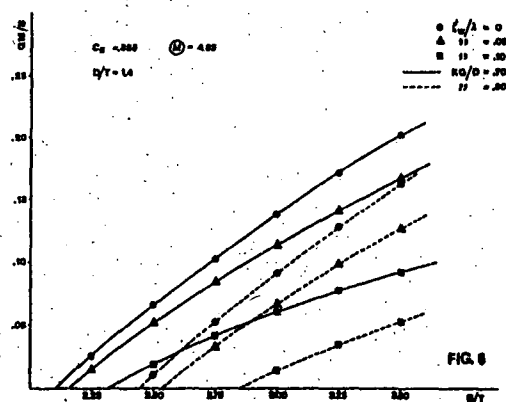
FIG. 6
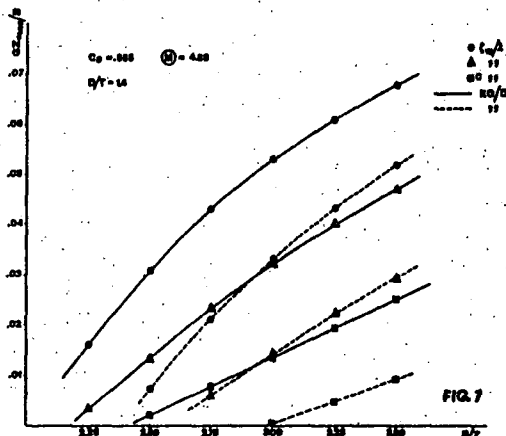
FIG. 7
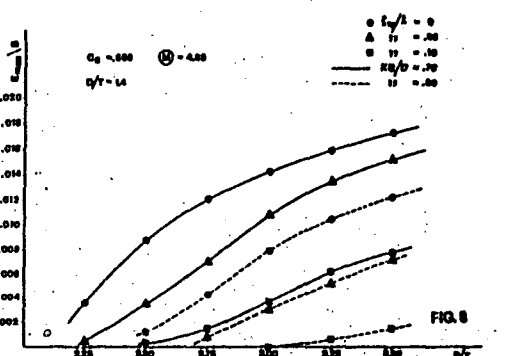
FIG. 8
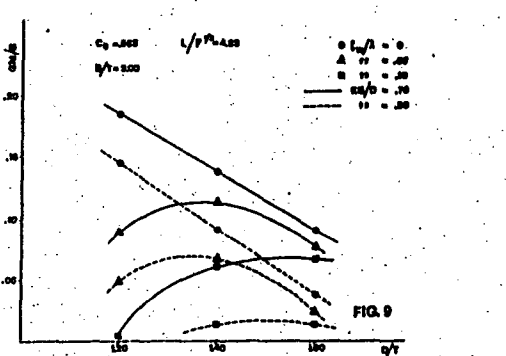
FIG. 9
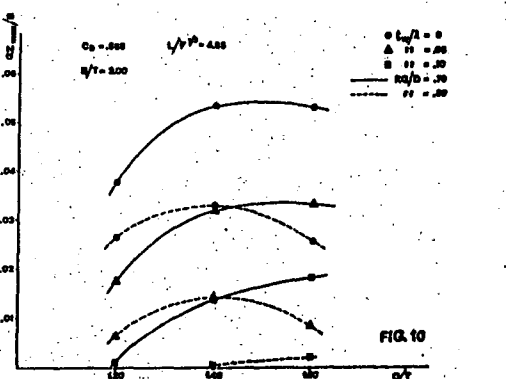
FIG. 10
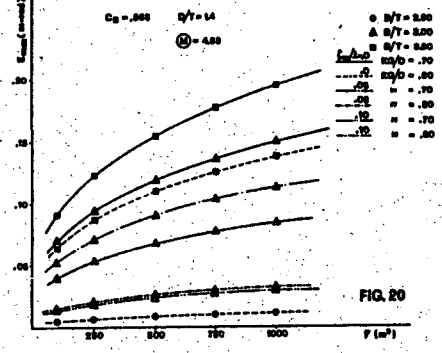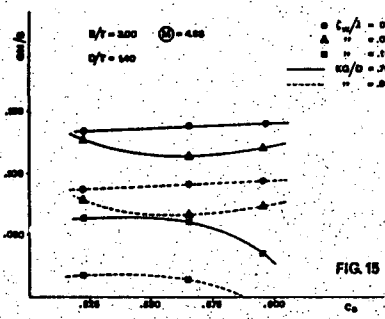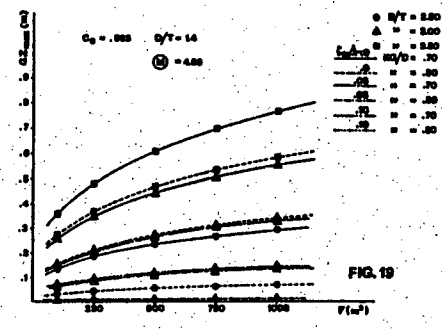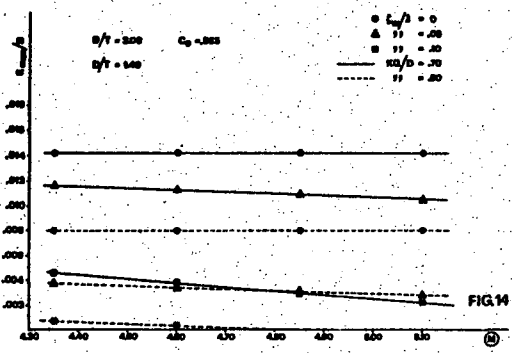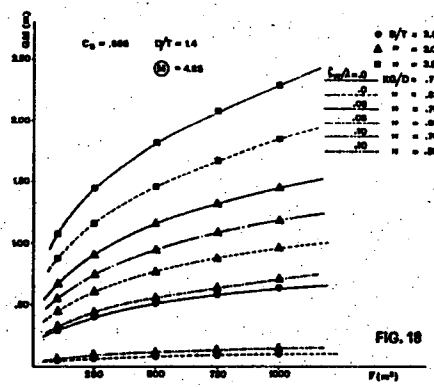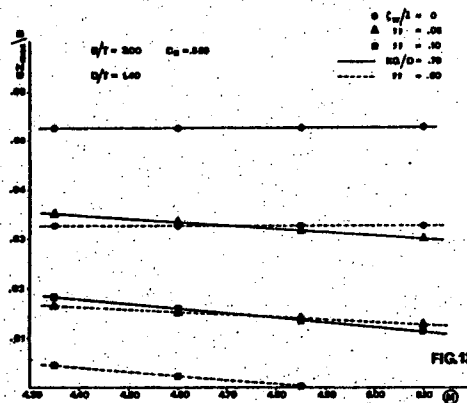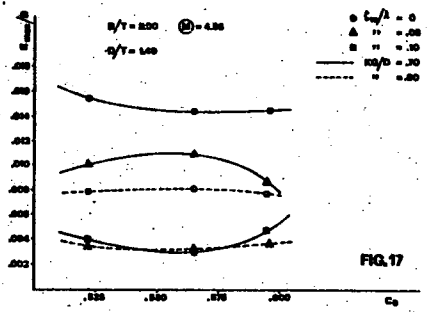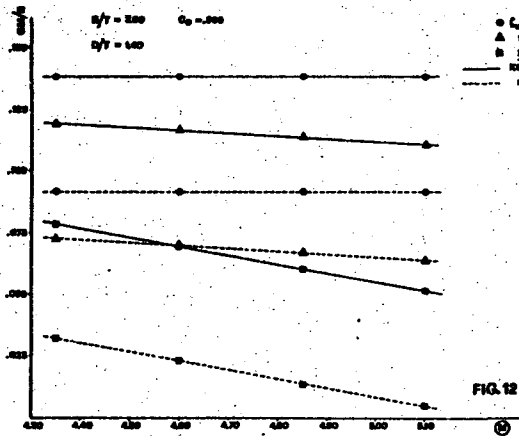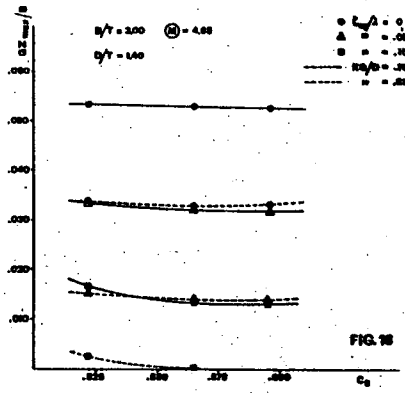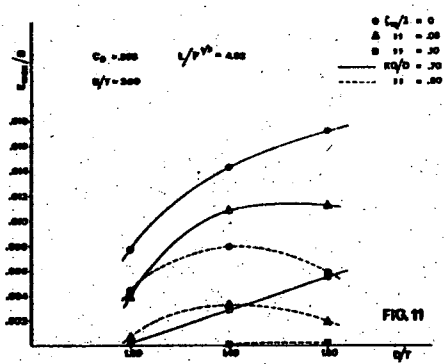
DETERMINATIONS OF HEELING MOMENT DUE TO BULK CARGO MOVEMENT UNDER HARMONIC COMPARTMENT'S OSCILLATIONS

L. Dykhta, E. Klimenko, Yu. Remez

ABSTRACT

While in shipment of loose bulk cargo, having a free surface the shifting due to inclinations of the ship creates an additional heeling moment. This phenomenon leads to the decrease of stability sometimes up to its full loss. The complete solution of the problem of determination of additional heeling moment is connected with considerable mathematical difficulties. Therefore, a great number of important, in applied aspects, problems of bulk carriers' seakeeping is solved in the first approximation using Sizov's hypothesis about quasi-static behaviour of bulk cargo, due to ship's inclinations [2]. At the same time the problem of estimation of dynamic effects connected with the real behaviour of bulk cargo shifting remains one of actual problems of seakeeping. In the paper an attempt of determination of dynamic components of heeling moment due to bulk cargo shifting (e.g. grain) under harmonic oscillations of rectangular compartment is made.

INTRODUCTION

The magnitude of additional heeling moment depends considerably on the quantity of moving cargo and the form of its free surface. Their determination calls for the mathematical description of movement and stressed state of cargo. In other words, it calls for the boundary value problem solving for the system of quasi-linear partial differential equations to solve for the tensor components of stresses and vector components of cargo particles' velocity.

1. STATEMENT OF THE BOUNDARY VALUE PROBLEM

The problem is considered in an approximate statement under the following simplifying assumptions:

- the compartment is a rigid body having only one degree of freedom and performing the harmonic rotary oscillations with frequency ω and amplitude θ_m; which fulfil to such conditions

$$\varphi < \theta_m < \varphi + \theta; \qquad \omega \ll (2g/\theta_m B)^{1/2};$$

$$\theta = \min\left\{ \text{arc tg } 2\frac{H-T}{B}, \text{arc tg}\frac{2T}{B} \right\}, (1)$$

where B and H - breadth and height of the compartment, φ and T - angle of internal friction and depth of bulk cargo in the compartment, g - free fall acceleration;

- the compartment oscillates relatively to horizontal axis of rotation, representing the line of intersection of the compartment principal plane and undisturbed free surface of cargo (without loss of generality, this assumption gives a possibility of considerable simplification of terminal formulas);

- the cargo is an incompressible homogeneous continuous ideal (without coalescense of particles) bulk medium under gravity;

- the movement of cargo is two-dimensional;

- the undisturbed free surface is a horizontal plane;

- deviations of the free surface from any inclined plane, as well as velocities and accelerations of particles are small

values of the first order, the squares and products of them are neglected.

Three rectangular Cartesian coordinate systems are introduced for mathematical formulation and solution of the problem. The origins of all the systems are placed on the rotation axis of compartment. Those systems are as follows:

- the system Oxy fixed in space; positive direction of vertical axis Ox - downwards;

- the system Ox_1y_1 fixed in the compartment; when the compartment is in straight position, the systems $Ox_1y_1z_1$ and $Oxyz$ coincide;

- the system $O\xi\eta$ moving together with cargo; axis $O\eta$ coincides with its level, obtained in quasi-static approximation, axis $O\xi$ is directed along the internal normal to the above mentioned level of free surface.

Let ρ be the density of cargo, σ_x and σ_y - the normal components of stress, τ_{xy} - its tangent component, v_x and v_y - vector components of cargo particles velocity.

The description of movement and stressed state is reduced to the solving of the following boundary value problem for the above-mentioned functions in the domain occupied by bulk cargo.

$$\frac{dv_x}{dt} + \frac{1}{\rho}\left(\frac{\partial\sigma_x}{\partial x} + \frac{\partial\tau_{xy}}{\partial y}\right) = g;$$

$$\frac{dv_y}{dt} + \frac{1}{\rho}\left(\frac{\partial\tau_{xy}}{\partial x} + \frac{\partial\sigma_x}{\partial y}\right) = 0;$$

$$\frac{\partial v_x}{\partial x} + \frac{\partial v_y}{\partial y} = 0; \tag{2}$$

$$(\sigma_x - \sigma_y)^2 + 4\tau_{xy}^2 = \\ = \sin^2\varphi\,(\sigma_x + \sigma_y)^2;$$

$$\frac{2\tau_{xy}}{\sigma_x - \sigma_y} = \frac{\frac{1}{2}\left(\frac{\partial v_x}{\partial y} + \frac{\partial v_y}{\partial x}\right) \pm \frac{\partial v_x}{\partial x}\,tg\,\varphi}{\frac{\partial v_x}{\partial x} \pm \frac{1}{2}\left(\frac{\partial v_x}{\partial y} + \frac{\partial v_y}{\partial x}\right)tg\,\varphi},$$

where $\frac{d}{dt}$ - differential operator equals

$$\frac{d}{dt} = \frac{\partial}{\partial t} + \vec{v}\,\nabla \tag{3}$$

and ∇ - Hamilton's operator.

Double sign $\pm$ in the latter equation

of the system (2) due to the following reason. It is possible to draw two families of slip lines in bulk medium. By the solving of the problem of its movement the active family of slip lines should be chosen. Active family is understood to be the family of lines along which the shearing deformations are arisen by the disturbance of utmost equilibrium state [1].

For the provision of an uniqueness of the solution of differential equations (2) it is necessary to submit the obtained values to boundary conditions:

- on the free surface of cargo, determined by equation

$$F = y\sin\theta_1 + x\cos\theta_1 - \zeta = 0,$$

where θ_1 - the angle of the $O\eta$ - axis inclination to horizontal plane and ζ - the elevation of free surface, two conditions must be fulfiled

$$\frac{dF}{dt} = 0; \quad \sigma_\xi - \tau_{\xi\eta} = 0. \tag{4}$$

Here σ_ξ and $\tau_{\xi\eta}$ are normal and tangent components of stress in the $O\xi\eta$ coordinate system;

- on the compartment surface contacted with cargo and determined by the equation

$$F_1(x, y, t) = 0$$

two conditions must also be fulfiled

$$\frac{dF_1}{dt} = 0, \quad \sigma_n = |\tau_n|\,ctg\,\delta, \tag{5}$$

where σ_n and τ_n are normal and tangent components of stress on the compartment surface, $\vec{n}$ - unit vector of normal to this surface, δ - angle of friction between this surface and the cargo.

2. QUASI-STATIC APPROXIMATION

The assumptions introduced allow to reduce the non-linear non-stationary boundary value problem (2)-(5) to two more simple problems. One of them determines the cargo stressed state in the scope of quasi-static approximation, while another one gives the possibility

to determine the dynamic additions to the stresses, as well as the components of cargo particles velocity vector and the form of free surface. For this aim in the known bulk medium mechanics expressions for stresses [1,4]

$$\left.\begin{array}{c}\sigma_x\\\sigma_y\end{array}\right\} = \rho\sigma(1 \pm \sin\varphi \cos 2\beta);$$

$$\tau_{xy} = \rho\sigma \sin\varphi \sin 2\beta \qquad (6)$$

it is advisable to represent the both functions σ and β as follows:

$$\sigma = \sigma^{(0)} + \sigma^{(1)}; \quad \beta = \beta^{(0)} + \beta^{(1)}. \qquad (7)$$

Here the superscript nought relates to the values obtained in quasi-static approximation while superscript one denotes the dynamic additions to those values.

The functions $\sigma^{(0)}$ and $\beta^{(0)}$ are determined by solving the following non-linear boundary value problem (for simplification of writing the superscript nought is omitted):

$$(1 + \sin\varphi \cos 2\beta)\frac{\partial\sigma}{\partial x} + \sin\varphi \sin 2\beta \frac{\partial\sigma}{\partial y} -$$
$$- 2\sigma\sin\varphi\left(\sin 2\beta \frac{\partial\beta}{\partial x} - \cos 2\beta \frac{\partial\beta}{\partial y}\right) = g;$$

$$\sin\varphi \sin 2\beta \frac{\partial\sigma}{\partial x} + (1 - \sin\varphi \cos 2\beta) \times$$
$$\times \frac{\partial\sigma}{\partial y} + 2\sigma\sin\varphi\left(\cos 2\beta \frac{\partial\beta}{\partial x} + \sin 2\beta \frac{\partial\beta}{\partial y}\right) = 0. \qquad (8)$$

The solution of this problem must fulfil to boundary conditions on the free surface of cargo

$$\sigma_\xi = \tau_{\xi\eta} = 0 ; \quad \zeta = 0, \qquad (9)$$

and on the compartment surface $F_1 = 0$ contacted with cargo

$$\sigma_n = |\tau_n| ctg \delta. \qquad (10)$$

For the aims of this work the boundary condition (10) is not considerable and may be ignored. In this case the solution of the problem (8) obtained by Sokolovsky [3] has the form

$$\sigma = \frac{x + y tg\theta_1}{\cos^2\varphi}(1 - \lambda);$$

$$2\beta = \theta_1 + (\mathscr{x} - 1)\frac{\pi}{2} - \mathscr{x} \arcsin \frac{\sin\theta_1}{\sin\varphi};$$

$$\lambda = \sin^2\varphi + \mathscr{x}\cos\varphi(\sin^2\varphi - \sin^2\theta_1)^{1/2}; \qquad (11)$$

$$\mathscr{x} = \pm 1,$$

and allows to write the expressions for stresses arisen in bulk medium

$$\left.\begin{array}{c}\sigma_x\\\sigma_y\end{array}\right\} = \rho g(x + y tg\theta_1)(1 + \sin^2\varphi);$$

$$\tau_{xy} = -\rho g(x + y tg\theta_1)\sin\varphi \cos\varphi. \qquad (12)$$

Two magnitudes of value $\mathscr{x} = \pm 1$ conform to two forms of medium's stressed state [3].

3. ADDITIONAL HEELING MOMENT

While determination of the both dynamic additions $\sigma^{(1)}$ and $\beta^{(1)}$, as well as the elevation of cargo free surface above the plane $\zeta = 0$ and the components V_x and V_y of cargo particles velocity vector, one should take into consideration the discontinuity of bulk movement in the oscillating compartment. When the amplitude $\theta_m > \varphi$, the phases of movement relatively to the compartment alternate with phases of relative unit.

In the phases of relative movement the magnitudes of values mentioned are obtained as a solution of the following linearized boundary value problem (superscript one is omitted):

$$\dot{V}_x + (1 + \sin^2\varphi)\frac{\partial\sigma}{\partial x} - \frac{1}{2}\sin 2\varphi\left(\frac{\partial\sigma}{\partial y} - \frac{\partial\mathcal{X}}{\partial x}\right) +$$
$$+ \sin^2\varphi \frac{\partial\mathcal{X}}{\partial y} = 0;$$

$$\dot{V}_y - \frac{1}{2}\sin 2\varphi\left(\frac{\partial\sigma}{\partial x} + \frac{\partial\mathcal{X}}{\partial y}\right) + \qquad (13)$$
$$+ \cos^2\varphi \frac{\partial\sigma}{\partial y} + \sin^2\varphi \frac{\partial\mathcal{X}}{\partial x} = 0;$$

$$\frac{\partial V_x}{\partial x} + \frac{\partial V_y}{\partial y} = 0;$$

$$\frac{\partial V_x}{\partial y} + \frac{\partial V_x}{\partial x} - 2 \operatorname{ctg} 2\varphi \frac{\partial V_y}{\partial y} = 0 ;$$

$$\gamma = 2\sigma^{(0)} \beta^{(1)} ,$$

where the point above the letter denotes the time derivative. This solution fulfils to the boundary conditions (4) on the free surface of cargo and to conditions (5) on the compartment surface contacted with cargo.

As it follows from great number of experiments with oscillating compartments, the deviations of bulk cargo free surface from its position in quasi-static approximation are small. These deviations are due to the movement of relatively thin layer of cargo placed immediately near the plane $\zeta = 0$. This special feature of phenomenon allows considerably simplify the solving of boundary value problem by introduction of assumption on one-dimensional movement of bulk cargo in the thin layer mentioned. According to this assumption we have obtained the terminal expressions for the unknowns of the problem

$$\begin{Bmatrix} V_x \\ V_y \end{Bmatrix} = \frac{\dot{\zeta}}{\cos(\varphi-\theta)} \begin{Bmatrix} \sin \\ \cos \end{Bmatrix} (2\varphi-\theta) \mp$$

$$\mp \dot{\theta} \frac{B}{2} \frac{\operatorname{tg}(\varphi-\theta)}{\cos(\varphi-\theta)} \begin{Bmatrix} \sin\varphi \\ \cos\varphi \end{Bmatrix} ;$$

$$\sigma = -\rho g \zeta \sec\varphi ; \quad \gamma = \sigma \operatorname{ctg}\varphi ; \quad (14)$$

$$\zeta = \sum_{m=-\infty}^{\infty} f_m \left(\frac{B \exp(\lambda_m \eta)}{2 \operatorname{sh} \lambda_m B/2} - \lambda_m^{-1} \right) e^{im\omega t} ;$$

$$\lambda_m = \frac{1}{2} \operatorname{ctg}\varphi \, m^2 \omega^2 / g .$$

where θ is the heel angle and are the Fourier's coefficients of expansion of the function $f(t)$ into series

$$f(t) = -\sec(\varphi-\theta) = \sum_{-\infty}^{\infty} f_m e^{im\omega t} \quad (15)$$

If the function $\zeta(\eta,t)$ is known, it is easy to determine the additional dynamic heeling moment M, due to cargo shifting.

$$M = \sec(\varphi-\theta) \sum_{-\infty}^{\infty} M_m e^{im\omega t} ;$$

$$M_m = B f_m \left(\frac{B}{2} \operatorname{cth} \lambda_m \frac{B}{2} - \frac{1}{\lambda_m} \right) . \quad (16)$$

The value M is to be added to the heeling moment determined in quasi-static approximation.

NOMENCLATURE

B — breadth of compartment;

g — free fall acceleration;

H — height of compartment;

F — function defined the cargo free surface;

F_1 — function defined the compartment's surface;

f, f_m — a function and its -th coefficient in Fourier expansion (15);

M, M_m — additional dynamic heeling moment due to cargo shifting and its m-th coefficient in Fourier expansion (16);

n — unit normal vector;

T — depth of cargo in the compartment;

t — time;

x, y — coordinate system fixed in space;

x_1, y_1 — coordinate system fixed in the compartment;

V_x, V_y — velocity vector components in (x, y)-system;

β — angle between the main stress and Ox-axis;

γ — auxiliary quantity $(\gamma = 2\sigma^{(0)}\beta^{(1)})$

δ — angle of friction between the bulk cargo and the compartment surface;

ζ — elevation of cargo free surface;

$\mathrm{æ}$ — symbol of sign;

θ, θ_m — rolling displacement and its amplitude;

θ_1 — angle between $O\eta$ and Oy-axis;

φ — auxiliary quantity defined in (1);

λ_m — parameter defined in (14);

ξ, η — coordinate system moving together with cargo;

ρ — cargo density;

$$\sigma = \frac{\sigma_x + \sigma_y}{2\rho}$$

σ_n, τ_n - normal and tangent stress com-
            nents on the compartment
            surface;

σ_x, σ_y, τ_{xy} - two normal and tangent
            stresses in (X, Y)-system;

σ_ξ, σ_η, $\tau_{\xi,\eta}$ - the same quantities in
            (ξ, η)-system;

φ - angle of internal friction;

ω - circular frequency.

REFERENCES

1. Geniyev G.A. Some questions on dynamics
   of bulk medium. M. Gosudarstvennoye iz-
   datelstvo po stroitelstvu i arkhitektu-
   re, 1958,
2. Sizov V.G. On stability of ships trans-
   porting bulk cargoes. Sudostroyeniye,
   1958, No.6, pp.7-11.
3. Sokolovsky V.V. On utmost equilibrium
   state of bulk medium. Prikladnaya mate-
   matika i mekhanika, vol.15, No.6, pp.
   689-708.
4. Sokolovsky V.V. The statics of bulk me-
   dium. M. Fizmatgiz, 1960.

- N. Klimenko, Dipl. Eng.
L. Dykhta, Dr.
Yu. Remez, Prof., Sc.Dr.
Nikolayev Shipbuilding Institute,
Prospect Geroev Stalingrada, 9,
327001, Nikolayev, USSR.

COMPUTER AIDED STABILITY CALCULATIONS

E. Kogan

ABSTRACT

To determine parameters of stability computer programs have been worked up to make the next calculations:

1. cross curves of stability;

2. stability curves for intact and damaged ships;

3. allowable verticals of center of gravity in accordance with the criteria of the Register of Shipping of the USSR.

The programs have clearance of the Register of Shipping of the USSR.

The initial information for calculations consists in ship's lines, watertight compartments and ship's load. The programs can be used for ships of different shapes (single-hull ships,docks, catamarans,floating facilities,etc.) While calculating the stability curves it is taken into account the fact of variation of the trim,caused by changing of heeling angle. It is essentially important for small ships with developed superstructures.

INTRODUCTION

The calculations of stability are time-consuming at the design stage. Therefore the algorithms and programs were worked up soon after the first computers were created. Although matematic formalization of problem is relatively simple, the programs have been improved so far. It is caused by the necessity to provide the adequate accuracy of the calculations by using minimum information on ship's lines as well as by the desire to provide the universal programs for ships and other floating facilities with different forms of under- and above-water parts.

The information on ship's lines consists in unequal standing cross-sections while each section is described by train of points irregularly distributed on its contour.The distribution of the sections and points on their contours must guarantee the necessary accuracy of linear interpolation between any adjacent points. More complicated methods of interpolation do not guarantee the necessary accuracy because of variety ship's shapes.Besides, the instructions in preparation of the information are complicated greatly. The additional information on ship's form consists in description of the stem, sternpost,draft marks and projecting parts.

The description of the moulded surface by unequal standing points has led to the rejection of the traditional formulas of numerical integration which were replaced by summation of characteristics of trapeziums in which the curve of sectional areas,waterline and cross-sections were divided by set sections and points. Nevertheless even in the cases of linear shapes the distances between the cross-sections must not exceed 1/3-1/4 of station spacing in ship's ends and one station spacing in midships because of nonlinearity of displacement characteristics Deficient sections are calculated by linear interpolation.Thus it is possible to provide the necessary accuracy in calculations of stability of floating docks, scows,floating facilities and ships with large parallel middlebody using minimum of input information.It is worth mentioning that sections are usually represented by their right branchs, nevertheless there is the possibility to describe

non-symmetrical to centreplane sections.

1.CALCULATIONS OF STABILITY

The form stability arms are calculated by the formulas:

$$l_f = y_c \cos\theta + z_c \sin\theta.$$

$$d_f = y_c \sin\theta - z_c \cos\theta + z_{co}.$$

Cross curves of stability are calculated for some values of displacement in the range of heeling angles from $5°$ to $85°$ in $5°$ step. To not accumulate miscalculations the draught is computed with the accuracy no less than $0,1\%$ at any values of displacement and heeling angle.The time of computation is minimized by means of using the results of the previous calculations. The trim of the ship remains constant while listing(it is usually zero in according to the Register of Shipping of the USSR. The statical and dynamical arms are obtained by formulas:

$$l_{st} = l_f - z_g \sin\theta,$$

$$d = d_f - z_g(1 - \cos\theta).$$

The program for calculation of the trim and stability of ships under concrete load has been worked out too. Statical and dynamical stability arms are calculated for some values of heeling angle. The trim is changed and it is calculated for every heeling angle so that the trim moment(the moment to the line of intersection the waterplane and midstation plane) remains equal to nought.

As to the calculation results the influence of the initial trim and its change during listing is small if ship's displacement exceeds some thousand tons. But the influence is essential and must be taken into account when stability curves for small ships with large superstructures in their ends are calculated.

2.CALCULATIONS OF UNSINKABILITY

The calculations of unsinkability consist in determination of the trim and stability of the damaged ships for the range of heeling angles from $0°$ to $50°$. The amount of damage water,trim,mean draught and stability arms are calculated for eve-

ry heeling angle. The compartments are divided in some groups:

1.bilged compartments where solid cargo was kept before the damage(or was no cargo);

2.bilged compartments where liquid cargo was kept before the damage;

3.compartments to which filtering water penetrates from the adjacent compartments;

4.ballast tanks which are used to right the ship.

At the beginning of the calculation it is analysed what group the compartment belongs to and the displacement and the coordinates of the center of gravity are recounted by adding the filtering and ballast waters and by substracting the flowed-out liquid cargo.Then the influence of the filtering and ballast waters on the stability is accounted by increasing the heeling moment due to loose water. The calculations of the compartments of the first and the second groups are carried out by the method of constant displacement.The heeling angle after damage, minimum freeboard and distance to water - plane from restrictive ports are calculated too.

An important problem is to decrease the amount of the information which is necessary to describe the compartments.Sticking to the general principle of the description of any compartment by means of some typical cross-sections which enable to use linear interpolation, it is necessary to take into account the information on snip's lines. Fig. 1 shows the principle of the description of the compartment's sections when their contours coincide partly with ship's shape. The part of the compartment within the ship is calculated by the program.The sections symmetrical to centreplane are represented by their right parts, the left parts are formed by the program too.To decrease the amount of information the notion of a cylindrical compartment or its part is used when two adjacent sections are identical. In this case the first section is only described.

The coefficients of permeability of different parts of any compartments may be sometimes different. Therefore the compartments are divided into some spaces. Every space has its own coefficient of
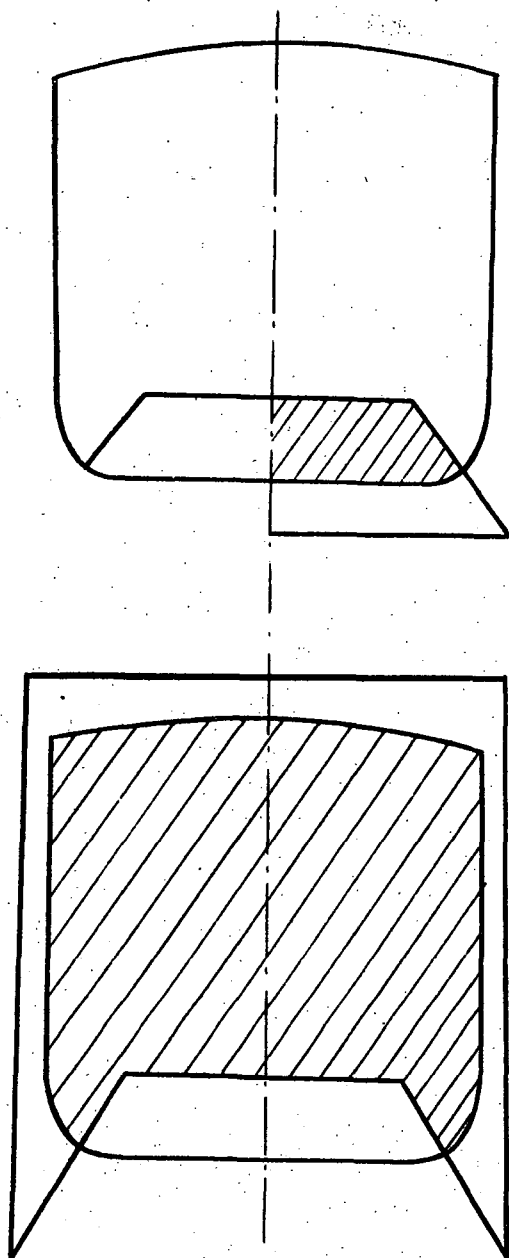
Fig.1 The representation of
some compartments.

permeability which may be different for
volume and surface of flooding water.

This form of the description of
ship's compartments is a result of un-
sinkability computation experience during
20 years. It enables to take into account
the peculiarity of different types of
ships and floating facilities at the same
time providing vividness and minimum of
input information.

3. CALCULATIONS OF THE ALLOWABLE Z_g.

The stability control in operation
is convenient to fulfil by means of al-
lowable verticals of center of gravity
which are calculated in accordance with

the rules of the Register of Shipping of
the USSR:
  1. the metacentric height $h=h_0$;
  2. the maximum righting arm $l_{st\,max} = l_0$;
  3. the angle of maximum righting arm $\theta = \theta_0$;
  4. the angle of vanishing stability $\theta = \theta_1$;
  5. the weather criterion $k=k_0$.

Some of the problems may be solved
quite simply. For example the first con-
dition leads to formula:

$$z_g = r + z_c - h_0 ,$$

the third condition-to

$$z_g = z_c + r\sec\theta_0 - y_c \,tg\,\theta_0 ,$$

the fourth condition-to

$$z_g = z_c + y_c \,tg\,\theta_1 .$$

To solve the equation $l_{st\,max} = l_0$ the
curve of maximum righting arms for some
heeling angles is computed:

$$l_{st\,max} = y_c \sec\theta_0 - r\,tg\,\theta_0 .$$

The heeling angle which is the so-
lution of this equation is obtained by
interpolation. To increase the accuracy
of the calculations the $5°$ step for
heeling angle and Lagrangian interpola-
tion formula are used. If the angle of
maximum righting is known the value of
z_g is computed by formula (1).

The scheme of the solution of the
equation $k=k_0$ depends on the fact whe-
ther the angle of wetness is set or no.
Being known it is taken as the angle of
the stability curves breaking off, and Z_g
is obtained by the equation:

$$\frac{d(\theta_w) - d(\theta_r)}{\theta_w + \theta_r} = l .$$

When the angle of wetness is not set the
weather criterion and Z_g are calculated
for some values of critical dynamic
angle of heel by the equations:

$$l_{st}(\theta_d) = \frac{d(\theta_d) - d(\theta_r)}{\theta_d + \theta_r} ,$$

$$k = \frac{l_{st}(\theta_d)}{l} .$$

The value of Z_g is obtained by interpo-
lation using the curve $k=f(Z_g)$.

Because the trim of the intact ship is usually small the results of calculations of buoyance and cross stability curves are used to compute allowable values of Z_g in accordance with the stability criteria for intact ships. The calculations of Z_g in accordance with the stability criteria for damaged ships are carried out by direct using ship's lines and compartments because the trim may be essential after flooding the compartments. Besides, the trim's change during listing is taken into account. The scheme of the problem solution coincides practically with the above described scheme for intact ships.

The programs for stability computations have been agreed with the Register of Shipping of the USSR(clearance No. 2.37, 23.06.83).

NOMENCLATURE

l_f - statical form arm,
d_f - dynamical form arm,
l_{st} - statical arm,
d - dynamical arm,
$l_{st\,max}$ - maximum righting arm,
y_0 -transverse center of buoyance,
Z_0 -vertical center of buoyance,
Z_g -vertical center of gravity,
h - metacentric height,
r - metacentric radius,
k - weather criterion,
l - arm of dynamic heeling moment,
θ - heeling angle,
θ_d - critical dynamic angle of heel,
θ_0 - angle of maximum righting arm,
θ_1 - angle of vanishing stability,
θ_w - angle of wetness,
θ_r - amplitude of roll,
$Z_{oo} = Z_o \big|_{\theta=0}$.

E.Kogan,Dr
Nikolayev Shipbuilding Institute
Prospect Geroev Stalingrada,9
327001, Nikolayev USSR

STABILITY ASSESMENT OF USCG BARQUE EAGLE

E.C. Haciski, N.T. Tsai

ABSTRACT

The U.S. Coast Guard training barque EAGLE (WIX 327), built in 1936, with the original name HORST WESSEL, by Blohm & Voss in Germany, has recently been renovated to improve her performance. As part of the renovation, the stability of large sailing vessels in general and EAGLE in particular were studied. Changes in the subdivision, ballast and tankanges were made to satisfy the criteria of two-compartment damage stability. The technical background of this stability assessment and the structural modifications are presented here.

1. INTRODUCTION

The 1800-ton, 70-meter barque EAGLE was built in 1936 by Blohm & Voss shipyard in Hamburg, Germany, under the auspices of the German Navy and Germanischer Lloyd. After World War II, in January 1946, the U.S. Coast Guard acquired her as a war reparation and renamed her EAGLE. Two other sister ships, the GORCH FOCK* (renamed TOVARISTSCH) and ALBERT LEO SCHLAGETER (renamed SAGRES II) are now with the Soviet Union and Portugal, respectively.

Throughout EAGLE's service in the Coast Guard, several arrangement and machniery modifications have been made. However, no significant structural improvement had been made since construction. After more than 40 years of sailing, it was apparent that major renovations were needed to upgrade her equipment and structure. At the request of Coast Guard, the Germanischer Lloyd conducted an independent survey in 1980 and confirmed such needs. Germanischer Lloyd also expressed its concern as to whether the stability would be satisfactory.

The stability of large sailing vessels is a more difficult technical area than the stability of other kind of ships because of the strong influence of the sails on the rolling motions of the vessels. There were few design guidelines in the area of stability of large sailing vessels in the literature. As a sailing vessel built in the early 1930's, EAGLE was not designed with specific stability criteria as used today.

After more than 40 years in service, the structure of the EAGLE had deteriorated to the point that many deck areas and bulkheads were no longer watertight. To improve her seaworthiness, it was decided in the beginning that the structure conditions of EAGLE should be restored to enable her to meet the original status of a "100-A4 MC" class vessel as classified by Germanischer Lloyd and that the damage stability of EAGLE should be upgraded to the current practices of Coast Guard vessels.

Since she was built in 1936, EAGLE predates and is technically exempt from the current regulations of the Coast Guard. On the other hand, since such stability requirements were developed with the data

* A similar ship named GORCH FOCK was built later by Blohm & Voss in 1956.

from many successful sailing vessels in the past, it would be a significant bench mark if she could satisfy such regulations. Therefore analyses were conducted to evaluate the stability of EAGLE in terms of the Coast Guard criteria for sailing passenger vessels on exposed waters [1] as well as the stability criteria of U.S. Navy[2]. In addition, the stability characteristics of the EAGLE were also compared with the guidelines provided by Germanischer Lloyd [3]. The results were presented in [4] and [5]. Only a brief description of the stability assessment of EAGLE is presented here.

2. SHIP OFFSET AND HYDROSTATICS CHARACTERISTICS.

Two different ship offsets were digitized for our analysis. One offset describes the ship up to the main deck and the other describes the ship up to the poop and forecastle decks (01 level). The body plan of EAGLE with 01 level are shown in Figure 1. The draft diagram and functions of form at even trim condition is shown in Figure 2. For stability analysis, the ship is considered to be watertight up to the forecastle and poop decks. Also included in the analysis are the appendages and the teak covering on the main weather decks.
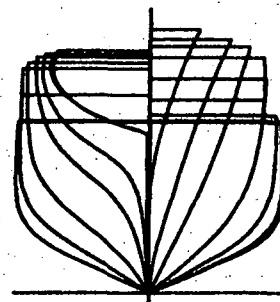
Fig. 1 Body plan

2.1 Loading Conditions

The full load and minimum operating conditions of EAGLE before and after renovation are listed in Table 1.

Table 1 Summary of Loading Conditions

Conditions	Disp.	VCG	LCG
A.Before Renovation			
Full Load	1766.t	4.90m ABL	0.46m
Min. Op.	1651.	5.06	0.11
Light Ship	1514.	5.28	-0.14
B.After Renovation			
Full Load	1763.	4.91	0.64
Min Op	1607.	5.11	-0.04
Light Ship	1461.	5.34	0.15

DRAFT DIAGRAM AND FUNCTIONS OF FORM
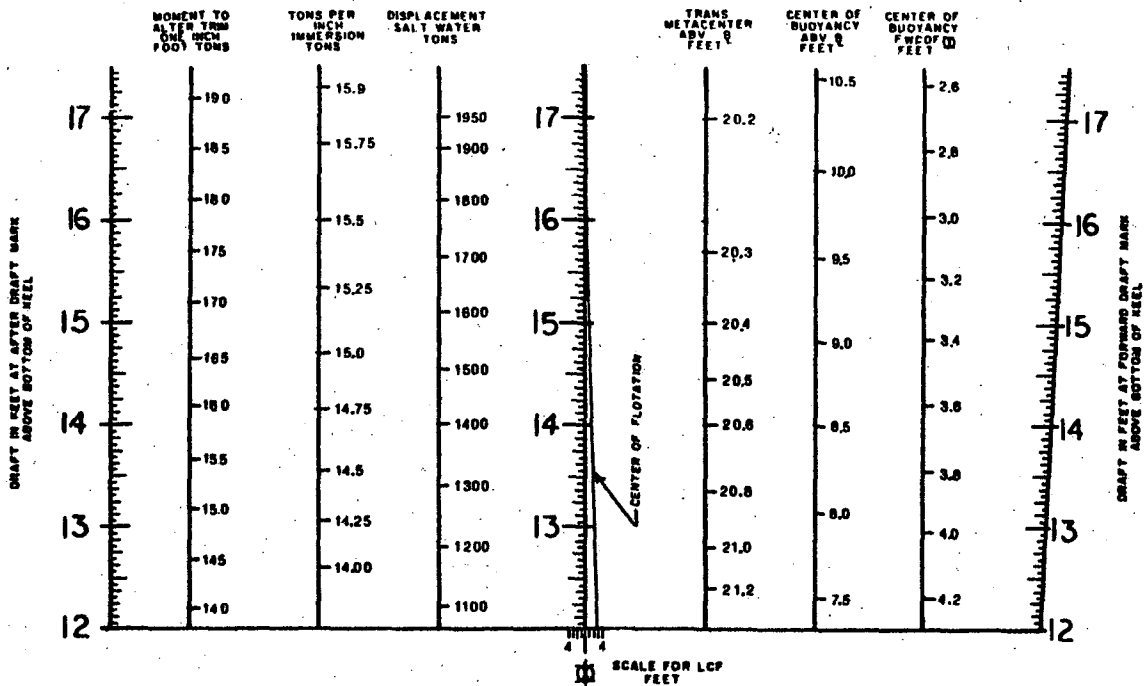
Fig. 2 Draft diagram and functions of form

NOTE:

1. In the stability analysis, correction factors due to free surface effect and inclining experiment margins should be added to the values of VCG above.

2. The decrease of light ship weight is due to the removal of the oregon pine covering on second deck and the modernization of deck equipment such as the windlass and other machinery.

3. The increased dead weight is due to the increased fresh water capacity and the inclusion of full fore- and aft peak tanks. Those peak tanks are normally full on departure but are assumed to be empty at the minimum operating conditions.

4. In the convention used here, the LCG in m forward of amidships is positive.

3. WIND HEELING MOMENTS

Projected sail areas are calculated in separate groups for the sails, rigging, spars and hull above the waterline for both the full load and minimum operating conditions. Fig. 3 shows the configuration and name of the sails of EAGLE. Table 2 lists the total sail areas of various loading conditions. Sail condition I is when all the sails are trimmed fore and aft. In sail condition II the top two square sails of the fore and main masts are set at 45 degrees to the beam wind; and the lower three square sails of the fore and main masts are set at 30 degrees to the beam wind. In sail condition III all the square sails of the fore and main masts are set at 45 degrees to the beam wind.

Table 2 Summary of sail areas and levels

A. Sail Set	I	II	III
Full load	2850	2597	2446 sq.m
level ABL	23.89	23.14	23.2 m
Min. op.	2862	2614	2459 sq.m
level ABL	23.82	23.05	23.12 m

B. Sail furled conditions

Full load	494 sq.m	
level ABL	13.73 m	
Min op.	507 sq.m	
level ABL	13.59 m	

The general form of beam wind heeling arm equation as recommended by the U.S. Navy practice is adopted here:

$$HA = \frac{0.0035 A L U^2 \cos^2\theta}{2240 \times \text{Displacement}}$$

where U is wind speed in knots
A is projected sail area in sq.ft
L is level of A above half draft in ft
Angle is in degrees
Displacement in long tons

With the loading conditions and sail areas determined, the wind heeling moments and arms are calculated from the above equation in terms of wind speeds and angle of heel. The other wind heeling moment calculation method using wind gradient profile and with a drag coefficient 0.004 instead of 0.0035 would have give similiar results.

4. INTACT STABILITY

The statical stability curves of EAGLE are calculated using the Ship Hull Characteristics Program (SHCP) as developed by the U.S. Navy and are shown in Figure 4 for different ship offsets. The condition with upper (poop and forecastle) decks provides much needed reserve bouyancy as the ship heeled beyond 40 degrees. The condition with upper decks and teak deck covering includes also the effect of deck camber. The contribution of teak covering and deck camber toward intact stabilty is very significant at heeling angles exceeding 40 degrees. The condition with upper decks, teak deck covering and galley deck house provides the ship with the largest righting moment at heeling angles exceeding 80 degrees. The condition considered most appropriate and, thus, used in this stability analysis is the one with water tight up to 01 decks and with teak deck covering but without the galley deck house on the main deck. The statical stability curves of the ship in intact condition before and after renovation are about the same.

In the sail set conditions, we have followed the requirements of the U.S. Coast Guard for sailing vessels and the guidelines of the Germanischer Lloyd. The results are presented as follows.
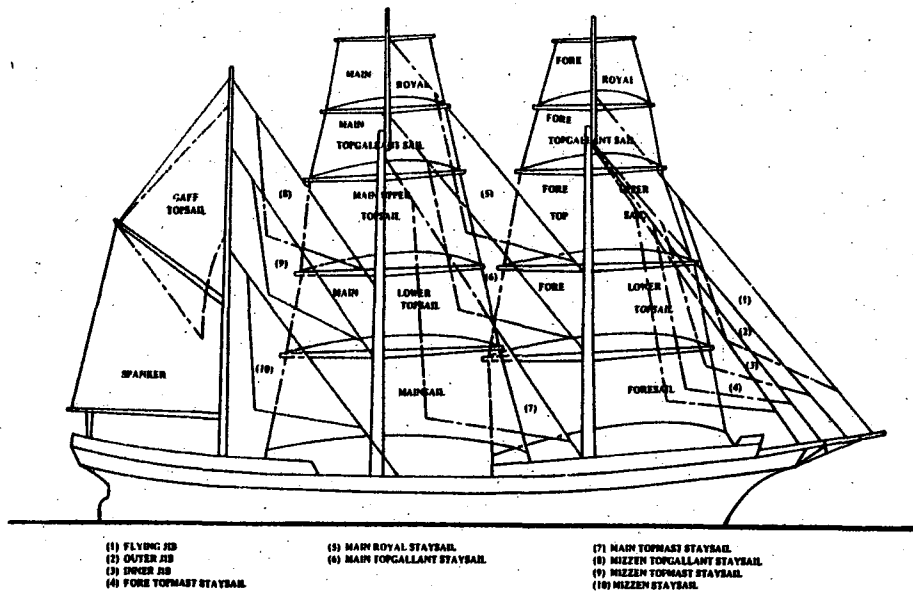
Fig. 3 Sail plan—USCGC *Eagle*

(1) FLYING JIB   (5) MAIN ROYAL STAYSAIL   (7) MAIN TOPMAST STAYSAIL
(2) OUTER JIB   (6) MAIN TOPGALLANT STAYSAIL   (8) MIZZEN TOPGALLANT STAYSAIL
(3) INNER JIB   (9) MIZZEN TOPMAST STAYSAIL
(4) FORE TOPMAST STAYSAIL   (10) MIZZEN STAYSAIL

4.1 Criteria of U.S. Coast Guard Office of Merchant Marine Safety

According to the requirement of the Criteria of U.S. Coast Guard Office of Merchant Marine Safety CFR-46 Section 171.055, the sailing vessel must have positive righting arms in each conditon of loading and operation from zero to 90 degrees of heel for service on exposed waters. Each vessel must be designed to satisfy the following equation where the stability numeral S_n is designed to be 16.4, 18.6 and 20.8 tons/sq.m or larger for the three conditions explained later.

$$Sn = \frac{Hz \times \Delta}{A \times H} \times 10^3$$

where $S_n =$ Stability numeral with n equal to 1,2, 3.

Δ = displacement in metric tons

A = projected lateral area in sqaure meters of the portion of the vessel above water line computed with all sail set and trimmed flat, except that 100% of the fore triangle area may be used in lieu of the area of the individual headsails when determining A if the total area of the headsails exceeds the fore triangle area.

H = The vertical distance in meter between the geometric center of the projected area A and the center of underwater lateral area of the ship

HZ= Wind heeling arm at zero degree for each criteria.

The numeral S1 is determined when the angle of heel caused by the beam wind, as represented by the heeling arm HZ, equals to that at which deck edge immersion first occurs. S2 is determined when the area under the assumed heeling arm curve between zero degree and the downflooding angle or 60 degrees, whichever is less, is equal to the area under the righting arm curve between the same range of heel angles. S3 is determined when the area under the assumed heeling arm curve between the angles of zero and 90 degrees is equal to the area under the righting arm curve between zero degree and (a) 90 degrees if the range of stability is less than 90 degrees; or (b) the largest angle corresponding to a positive righting arm but not more than 120 degrees if the range of stability is greater than 90 degrees.

The deck edge immersion angle at full load condition of EAGLE is determined to be 25 degrees.
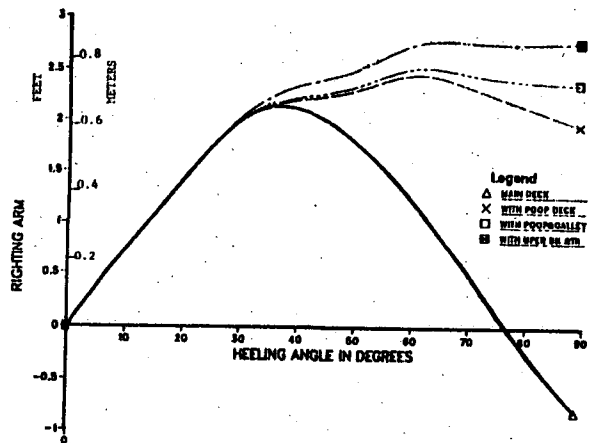
Fig. 4   USCG barque Eagle statical stability curves for various deck configurations.

The righting arm at this angle and loading condition is 0.49 m. Because of the different sail areas listed in Table 2, three different values of S1 are determined as: 17.1, 19.35 and 20.5 tons/sq.m for conditons I, II, and III, respectively.

The dynamic balance to downflooded condition for full loading condition is determined at the down flooding angle of 67.25 degrees. Since this angle is larger then 60 degrees, we use 60 degrees for this criteria. The limiting beam wind speed and then the stability numeral S2 are calculated. The three numerals for the different sail conditions are: 20.8, 23.7 and 25.2 tons/sq.m respectively.

The dynamic balance throughout the range of stability at full load was calculated for the range of 0 to 120 degrees of heel. The righting arm curve was extended to cover the whole range in this case. The limiting beam wind and then the stability numeral S3 are determined. The values of S3 are 50.9, 57.8 and 61.2 tons/sq.m respectively for the three sail conditions. Figures 5,6 and 7 show the righting and heeling arms curves for these three conditions.

Using similar equation, the different values of stability numerals for minimum operating conditions are calculated. The results are summarized in Table 3.

Table 3
Summary of stability numerals Sn(tons/sq.m)
Sail set conditions

CONDITIONS	I	II	III
Full Load			
S1 static (deck immersion)	17.1	19.4	20.5
S2 dynamic (Downflooding)	20.8	23.7	25.2
S3 dynamic balance through range of stability	50.9	57.8	61.2
Minimum operating condition			
S1	14.0	16.0	16.9
S2	15.8	17.9	19.0
S3	33.1	37.7	39.9

The stability numerals required for a sailing vessel on exposed waters are S1=16.4, S2=18.6 and S3=20.8 tons/sq.m. Among the numerals in Table 4, only sail condition III meets the requirement for both the full load and minimum operating conditons. This condition of least sail area specifies that the square sails on the fore and main masts be kept not more than 45 degrees from the direction of the beam wind. On the other hand, the U. S. Coast Guard regulation specifies that the sail should be trimmed fore and aft as listed in condition I. Because of the interferance of the riggings and practical consideration, the square sails of the EAGLE could not be braced beyond 50 degrees. Under the sail condition III, the largest beam wind as determined by the stability numerals is 31.37 knots. The general practice of the EAGLE is to shorten sails when wind exceeds 25 knots.

Fig. 5 Eagle sail set, stability criteria
USCG - S1 and Germanischer Lloyd guideline

In a recent regulation for sailing school vessel [6], a numeral multiplier related to the displacement of the vessel was developed. Because this new multiplier was developed for sailing vessels up to 500 tons, it is not utilized here. However, based on the technical information therein, the stability numerals S1, S2 and S3 for vessels like EAGLE would be 9.8, 10.5 and 9.5 t/sq.m approximately.

4.2 Criteria of Germanischer Lloyd.
When the EAGLE was built in 1936, she was certified by the Germanischer Lloyd as a "100 A-4 MC" class sailing vessel. It was recently learned that the stability conditions of EAGLE at that time were:

Fig. 6 Eagle intact stability, sail set, US Coast Guard stability criterion S2

Fig. 7 Eagle intact stability, sail set, US Coast Guard stability criterion S3, knockdown range

Metacentric height GM equals to 1.06 meter
Maximum righting arm GZ is 0.55 meter at 50 degrees of heel
GZ equals to 0.5 meter at 90 degrees of heel

Further discussion with Germanischer Lloyd resulted in the following recommended stability criteria for the renovated EAGLE.

GM	0.6 m
GZ	0.1 m at 90 degrees of heel
Maximum GZ	0.3 m

In addition, the area under the righting arm curve from upright condition to 90 degrees of heel should be 1.4 times or greater than the corresponding area under the heeling arm curve in all sailing conditions. The sails should all be braced fore and aft in all calculations.

In this study, three set of sail conditions were evaluated; full sail, storm sail and sail furled conditions. The storm sail condition includes the spanker, the main lower topsail, the fore lower topsail and the fore topmast staysail. We also included in our study the case of terminating the righting arm curves at the downflooding angle instead of 90 degrees of heel. This would be more realistic and provide us with more safety margin inasmuch as the ship is a training vessel. The results of this evaluation are summarized in Table 4.

Table 4

CONDITIONS	Maximum safe beam wind speed in knots with righting arm curve up to	
	90 degrees	Downflooding angle
Full load		
Full sail	38.1	31.5
Storm Sail	76.0	62.8
Sail furled		105.5
Min. operating condition		
Full Sail	33.3	28.1
Storm Sail	66.0	55.8
Sail furled		92.8

OUTPUT INFORMATION

ASSUMED KG   17.050
AI AREA   5.373
AI/A2 RATIO   2.426
RA @ 5 DEG   0.300
      15 DEG   0.899
      20 DEG   1.179
ARM RATIO   0.601
GM - FEET   3.438
RANGE   46.000
RAMAX - HA   1.969
INPUT INFORMATION

POLE HEIGHT   17.050
FS SMALL   0.000
THETA R DEG   25.000
WIND 0 DEG   1.600
DOWN FLOOD   69.150
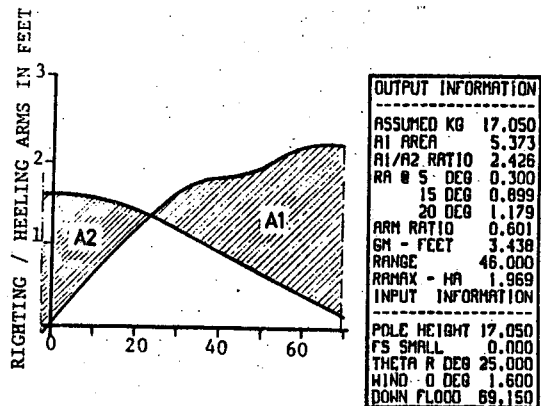
Fig. 8   US Navy intact stability criteria, sail furled, min. operating condition

The general practice of EAGLE is to shorten the sails beginning at wind speed about 25 knots or when the deck edge is close to the water surface. For the full load and full sail condition, the ship heeling angle under the beam wind speed of 31.5 knots is about 25 degrees. The deck edge immersion angle at that loading condition is about 25 degrees. Therefore, the dynamic reserve stability meets the requirements of Germanischer Lloyd.

4.3 Intact Stability, Sail Furled Conditions

For this condition, the ship is considered as any other monohull vessel and the stability criteria of the U.S. Navy applies. The beam wind speed required of this ship is 90 knots. The stability requirements of the U.S. Navy Design Data Sheet DDS-079-1 are satisfied as shown in Figure 8.

5. DAMAGE STABILITY

5.1 Floodable length calculations

The vessel was originally designed with water tight boundary up to the main deck and with major transverse bulkhead at frames 10, 25, 37, 63, 90 and 107. Using the results calculated from SHCP, the floodable length curve with permeability of 0.95 is shown in Figure 9. As it is, the EAGLE can only satisfy one-compartment flooding conditions. Considering physical extent of damage of underwater shell plating one compartment standard can not be considered as a realistic conditions of flooding after collision damage. In the case when damage occurs in the area of any watertight main transverse bulkhead, the ship will have two compartment flooding. Therefore, only a two-compartment standard can ensure a minimum surviviability after hull damage.
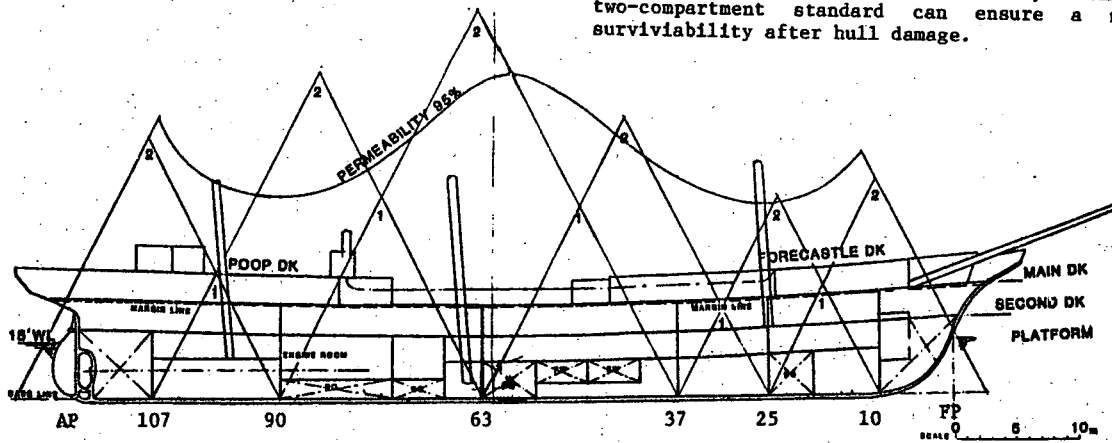
Fig. 9   Watertight subdivision and floodable length curve, before renovation
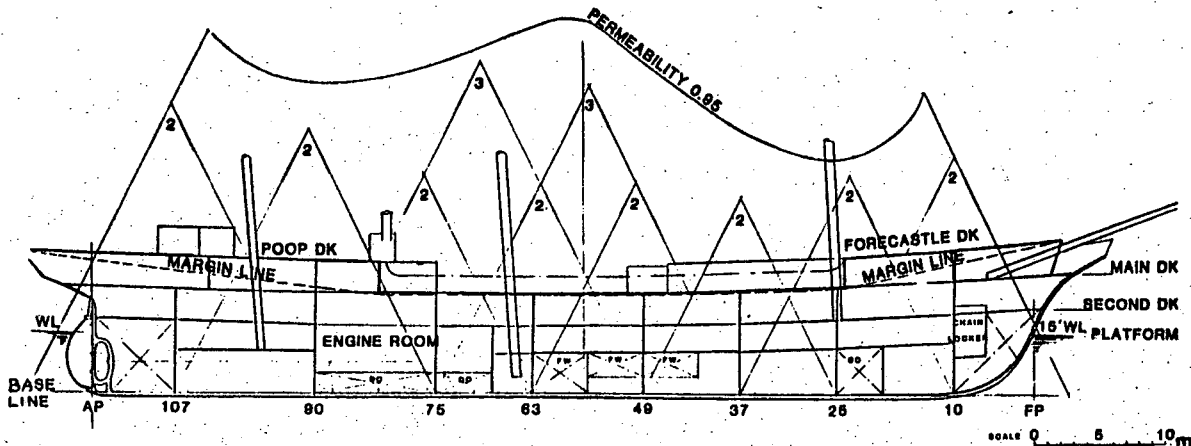
Fig. 10   Watertight subdivision and floodable length curve, after renovation

To improve this condition, transverse bulkhead were added and strengthened in the ship to extend water-tight subdivision up to the poop and forecastle decks. The floodable length curve of the renovated vessel is shown in Figure 10. It shows that as renovated, she will survive the two-compartment flooding conditions.

5.2 Limiting draft of EAGLE

The limiting draft diagram of EAGLE in the case of two-compartment flooding is shown in Fig. 11. The permeability of each compartment in full load and minimum operating conditions is listed in Table 5. The normal full load and minimum operating conditons are within the limiting draft region.

Table 5 Permeability of Compartments

Compartment	Loading conditions F.L.	M.O
To FR 10,forepeak tank,chain locker	0.94	0.94
FR 10-25,Stores,D.O.tanks ,living	0.83	0.92
FR 25-37,berth, stores	0.89	0.92
FR 37-49,stores, fresh water tanks	0.88	0.89
FR 49-63,shops,living area,F.W. tanks	0.81	0.81
FR 63-75,gen. rm,stores,D.O. tank	0.88	0.88
FR 75-90,engine rm,living area, D.O.	0.88	0.91
FR 90-107,shops,living area	0.94	0.94
FR 107-,stores,living area,aft P.T.	0.95	0.95

5.3 Damage stability in sail furled conditions.

It should be noted that the loading condition of the vessel used in the analysis is modified according to the DDS-079-1 in that the full load condition consists of one pair of empty fuel tanks and only two-third of its fresh water capacity. The minimum operating condition, however, remains the same as listed in the stability test data or inclining experiment report.

With loading conditions modified, we have:

ITEM	Displacement	KGV
Full load	1692 tones	5.09 m
Minimum operating	1606	5.17

Another major modification to improve the damage stability was the cross-connection of the three pairs of fresh water tanks between frames 37 and 63 (as shown in Figure 12). These deep wing tanks contributed to large asymmetric heeling moment when damaged. As shown in Figure 13, the static heeling angle of the vessel was about 20 degrees when area of the three pairs of water tanks is damaged. This exceeded the maximum heeling of 15 degrees as specified in the U.S. Navy stability criteria. Cross-connection of the three pairs of water tanks eliminated much of the asymmetric heeling moment as shown by the rigting arm curve in Figure 13 also. Thus, after renovation, EAGLE can survive all two-compartment flooding conditions.
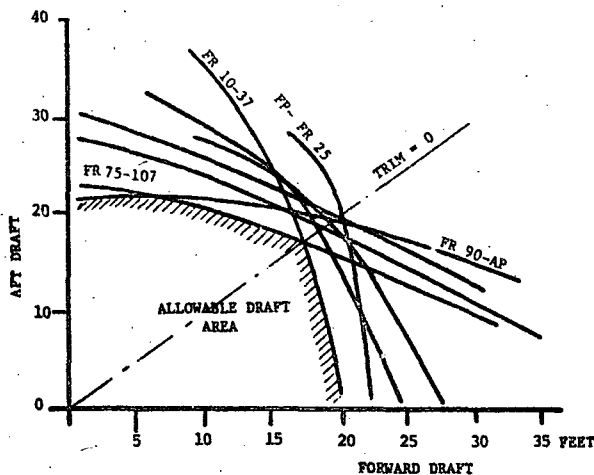
5.4 Damage stability in sail set conditions.

The same damaged condition but with sail set conditions were studied to determine the beam wind speed she could safely survive. The criteria used in this case is that the beam wind speeds should not be greater than that when deck edge immersion first occurs. For the most critical damaged condition, EAGLE could withstand beam wind up to 14 knots in full sail and 28 knots in the storm sail conditions before the main deck edge is immmersed. It is expected that the crew would shorten the sail when the wind velocity exceeds those speeds.
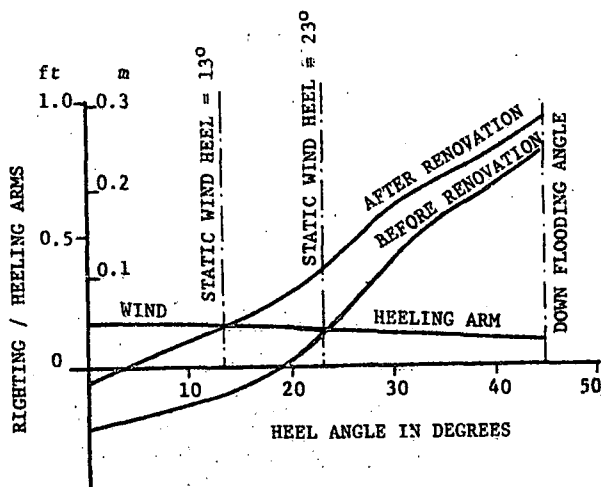

Fig. 13   Damage stability curves
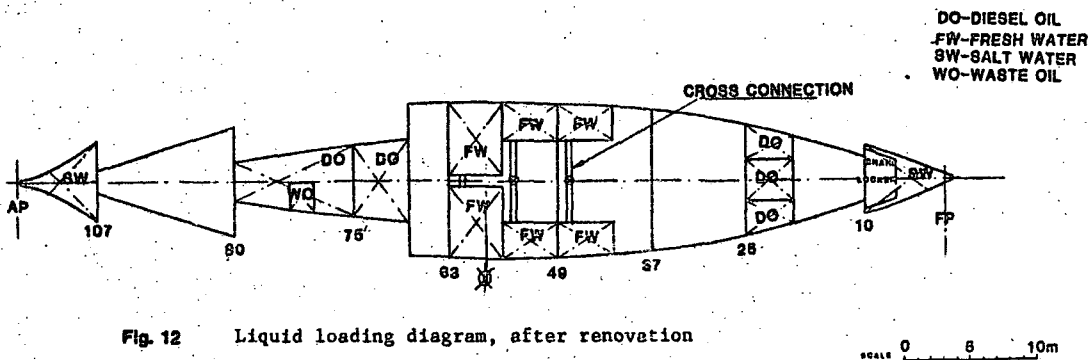
Fig. 12   Liquid loading diagram, after renovation

DO-DIESEL OIL
FW-FRESH WATER
SW-SALT WATER
WO-WASTE OIL

6. DISCUSSION AND CONCLUSIONS

Because the large sails the sailing vessels carry, the stability characteristics of sailing vessels is different from those of other ships. The roll damping of sail equipped ships has been found to be very much important in the determination of the stability of sailing vessels [7]. The aerodynamic effect on roll damping for sailing vessel can not be ignored. As for large sailing vessel which has large sails, masts and riggings, the aerodynamic effect is remarkable even in no wind condition. Because the roll amplitude of sailing vessel is less in wind than in no wind, the total dynamic stability does not necessarily become worse in wind in spite of a large heeling angle. The damping effect of sails also reduces the rolling angles induced by waves.

The stability of large sailing vessels is far from an engineering science at this time. Continued research in the area of ship motion and sail interaction is needed before we can be sure of all the possible conditions of stability. Although the existing stability criteria may have their own built-in margin of safety, one should aware that the sailing of a large sailing vessel is in itself a very important factor in the assessment of the stability of this class of ships. A well trained crew headed by experienced officers will enable the sailing vessel survive many possible dangers beyond the current understandings of naval architects. The advances in weather forcasting and communication would also reduce many of the risks associated with the past sailing voyages. With continued research about the science of sailing and ship motion in waves, we should be able to upgrade the method and criteria of stability assessment of large sailing vessels in the future.

To improve the safety and performance of EAGLE, extensive work was performed to upgrade the hull structure, propulsion, and auxiliary systems. EAGLE has been divided into nine main watertight subdivisions making her a two-compartment ship; her power and control were improved by installing a 1000-horsepower Caterpillar D-399 diesel engine and Caterpillar 7271 transmission. The list of improvement is seemingly endless; new air compressors and receivers, new fuel oil service and transfer systems, etc. From 1979 to 1983, over 230 thousand man-hours of work was spent to restore EAGLE to essentially new ship conditions.

The opinions presented in this paper are the views of the authors and not necessarily those of the U.S. Coast Guard.

REFERENCES

1. "Subdivision and Stability Regulations; Final Rules", Code of Federal Regulations Volume 46, published in Federal Register Vol.48 No. 215, November 1983
2. "Stability and Buoyancy of U.S. Naval Surface Ships," Design Data Sheet 079-1, U.S. Navy, August 1975
3. "Intact Stability of Ships with Propulsion by Sail," letter from Germanischer Lloyd to U.S. Coast Guard, October 8, 1984.
4. Tsai, N.T., Haciski, E.C. and Kucinski, J.J., "Modernization of the Barque Eagle", J. of Naval Engineering, ASNE, May 1985.
5. Tsai, N. T. and Haciski, E.C., "Stability of Large Sailing Vessels: A Case Study," Marine Technology, SNAME, Jan 1986.
6. "Sailing School Vessel Regulations", 46 CFR Parts 169, 170, 171 and 173, U.S. Coast Guard, January 1986
7. Takarada, N. and Obokata, J., "An Experimental Study on The Roll Damping of Sail Equipped Ships", Sumitomo Heavy Industries, LTD, August 1983

The Authors

EUGENE C. HACISKI received his B.S. degree in mechanics from the Warsaw University of Technology in 1946, and his M.S. degree in naval architecture from the Technical University of Gdansk, Poland, in 1950. Prior to joining the U.S. Coast Guard in 1967, he served as a project engineer in the Gdansk Ship Design Center and in the Shipyard Maua in Rio de Janeiro, Brazil. After serving 7 years in the U.S. Coast Guard Yard in Curtis Bay, Maryland, as a supervisory naval architect and 3 years in the Merchant Marine Technical Division, USCG, he was assigned in 1976 to his current position of Chief, Hull Section, Naval Engineering Division, USCG Headquarters. He is a member of SNAME, ASNI KORAB-INT. and SAWE.

NIEN-TSZR TSAI is formerly a naval architect with the Hull Section, Naval Engineering Division U.S. Coast Guard Headquarters. He received his B.S. and M.S. in mechanical engineering from Cheng-Kung University in Taiwan, China, and his Ph.D. in mechanical engineering from the University of Rochester, Rochester, New York, USA in 1969. Prior to joining the Coast Guard, he worked at General Dynamics, Litton Ship Systems and the David Taylor Ship Research and Development Center in the area of ship dynamics, moored and towed ocean systems evaluation and development. He is member of ASME and ASNE.

STABILITY OF HYDROFOIL SAILING BOAT IN CALM WATER
AND REGULAR WAVE CONDITION

Y. Masuyama

ABSTRACT

A performance of hydrofoil sailing boat
has been analyzed from aspect of dynamic
stability in calm water in conjunction with
numerical simulation in regular wave condi-
tion. The dynamic stability analysis
was carried out by applying the small-
disturbance theory. It was clarified that
the stability of the boat was affected
sensitively by the change of equilibrium
sailing state as a function of sail trim
angle. While the influence of the wave
motion on the sailing performance was numer-
ically simulated using non-linear equations
of motion, with indicating that the maximum
attainable sailing velocity decreased by
shortening of the wave period.

1 INTRODUCTION

To attain high velocity on sailing,
many research works concerning with the
hydrofoil sailing boat have been conducted
on various points of view such as theoreti-
cal prediction of sailing performance [1,2]
and proposal of new conception of hydrofoil
craft with higher performance [3,4]. In
such works, however, the sailing performance
have merely been presented as the solution
of equilibrium equations and the dynamic
stability analysis which is necessary for
the hydrofoil craft being lifted dynamically
by the foil, has not been conducted. In the
case of a powered hydrofoil craft the
dynamic stability analysis has already been
conducted by Kaplan et al [5]. Decomposing
motions of the craft into two groups of
longitudinal and lateral directions, they
have indicated the results of analysis for
each direction separately. Since the
motions in both directions affect each other
for the case of sailing boat, it is required

to analyze the stability with considering
their interaction.

In the present study, the dynamic
stability in calm water is examined with
accounting for the above described interac-
tion. Including the obtained results of the
dynamic stability analysis, the influence of
wave motion on the sailing performance of
the hydrofoil boat is also analyzed through
the numerical simulation.

2 DETERMINATION OF EQUILIBRIUM SAILING STATE

The boat for analysis is equipped with
two surface-piercing dihedral front foils
declining 40° and an inverted "T" rear foil
functioning as a rudder. Type of a hull is a
catamaran, and the boat is supposed to be
operated by one crew (helmsman) with car-
rying just an ordinary cloth mainsail. The
configuration and principal dimensions of
the boat are shown in Fig. 1 and Table 1,
respectively.

Before carrying out the dynamic stabi-
lity analysis, we must determine the equi-
librium sailing state of the boat. Since
the boat has a six-degree-of-freedom, the
equilibrium state can be expressed by the
solution of six simultaneous equations using
the state parameters such as U, V, W, Φ, Θ
and Ψ. Each velocity (U, V and W) and angle
(Φ, Θ and Ψ) with respect to the hull are
defined in Fig. 2. The force and moment on
the boat are generated from the combination
of hydrodynamic force on foils, aerodynamic
forces on both sail and hull, and gravita-
tional force. The point of application of
hydrodynamic force is assumed to be the cen-
ter of submerged area of the foil. Applying
the method of Wadlin et al [6], the hydro-
dynamic coefficients were calculated. The
aerodynamic coefficients of sail and hull
are determined by wind tunnel test [7], and
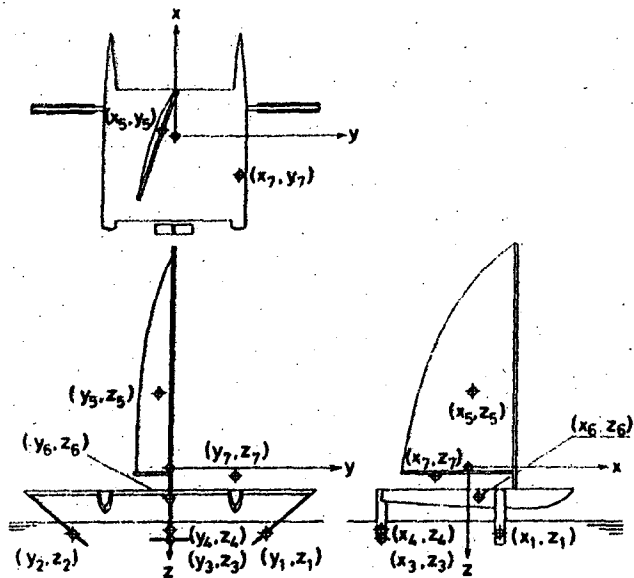
Fig. 1 Arrangement of the boat for analysis and applying point of related forces

Table 1 Principal dimensions and coordinates of the boat for analysis

DIMENSIONS				
LOA (m)	5.08		I_{xx} (kg·m²)	1800
sail area (m²)	16.0		I_{yy} (kg·m²)	1270
mass (kg)	255		I_{zz} (kg·m²)	1500
crew mass (kg)	70		I_{zx} (kg·m²)	-120
COORDINATES				
i	x_i(m)	y_i(m)	z_i(m)	
1	0.81	(2.18)[1]	(2.00)[1]	A.P. of front foil (st.)[3]
2	0.81	(-2.18)[1]	(2.00)[1]	A.P. of front foil (port)
3	-2.32	0.	(1.87)[1]	A.P. of rear foil
4	-2.32	0.	1.87	A.P. of rudder
5	(0.09)[2]	(0.)[2]	-1.90	C.E. of sail [4]
6	0.15	0.	0.88	C.E. of hull
7	-1.02	1.90	0.20	C.G. of crew [5]

1) coordinates at zero submergence of the foil;
   to be varied with depth of submergence
2) coordinates at zero sail trim angle;
   to be varied with magnitude of sail trim angle
3) A.P.; application point of hydrodynamic force
4) C.E.; center of effort of aerodynamic force
5) C.G.; center of gravity
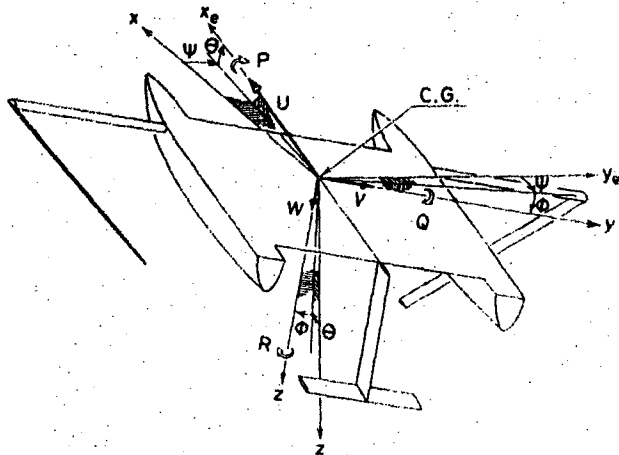
Fig. 2 Coordinate systems and positive directions of velocity components, angular velocities and angles

their points of application are the center of effort of the mainsail and the centroid of the hull, respectively.

The equilibrium equations are solved with constant wind and sail conditions including wind velocity, U_{ST}, wind direction, γ_T, and trim angle of mainsail, ε (see Fig. 3). In order to keep the γ_T constant, the yaw angle, Ψ, is required to be zero through the perfect control of the rudder. Thus, instead of the Ψ, rudder angle, δ, comes into unknown quantity. In the steady cruising condition, since the center of gravity (C.G.) of the boat moves horizontally, we should use the height of C.G. from water surface level, H, instead of the velocity W for the calculation. Consequently, the equilibrium equations are made up of six unknown quantities such as U, V, Φ, Θ, δ and H. The equations can be solved using the Powell method. Details of the calculation and the results have already described [8].

3 DYNAMIC STABILITY ANALYSIS

3.1 Linearized Equations of Motion and Characteristic Equation

The motion of hydrofoil sailing boat referring to the body axes is described by the Euler's equation. From the results of equilibrium sailing state analysis [8], it was indicated that the angles of pitch, heel and leeway were relatively small, especially in pitch. Thus the perturbed equations of motion can be reduced from the Euler's equation as follows:

$$
\begin{aligned}
m(\dot{u} + qw_0 - rv_0) &= \Delta X - mg\theta \\
m(\dot{v} + ru_0 - pw_0) &= \Delta Y + mg\phi\cos\phi_0 \\
m(\dot{w} + pv_0 - qu_0) &= \Delta Z - mg\phi\sin\phi_0 \\
I_{xx}\dot{p} - I_{zx}\dot{r} &= \Delta K \\
I_{yy}\dot{q} &= \Delta M \\
I_{zz}\dot{r} - I_{zx}\dot{p} &= \Delta N
\end{aligned}
\qquad (1)
$$

In the equation the symbols with zero suffix indicate each value in equilibrium state, and the symbols without suffix for velocities (u,v and w), angular velocities (p,q and r) and angles (ϕ,θ and ψ) indicate the each deviation from their equilibrium values. The $\Delta X \sim \Delta Z$ and $\Delta k \sim \Delta N$ are perturbed forces and moments, respectively.

Since the sailing boat runs usually accomodating with side-slip and heel and the aerodynamic force on sail directs differently to the advancing course, the deviations in any directions affect simultaneously on

Fig. 3 Velocities and angles with respect to the wind

Now we have the stability determinant as,

$$
\begin{vmatrix}
m\lambda & -X_{\dot{v}}\lambda-X_v & -X_{\dot{w}}\lambda-X_w & -X_{\dot{p}}\lambda^2-X_p\lambda-X_\phi & -X_{\dot{q}}\lambda^2+(mw_0-X_q)\lambda & -X_h \\
-X_u & & & & +(mg-X_\theta) & \\
-Y_u & (m-Y_{\dot{v}})\lambda & -Y_{\dot{w}}\lambda-Y_w & -Y_{\dot{p}}\lambda^2-(mw_0+Y_p)\lambda & -Y_{\dot{q}}\lambda^2-Y_q\lambda-Y_\theta & -Y_h \\
& -Y_v & & -(mg+Y_\phi) & & \\
-Z_u & -Z_{\dot{v}}\lambda-Z_v & (m-Z_{\dot{w}})\lambda & -Z_{\dot{p}}\lambda^2+(mv_0-Z_p)\lambda & -Z_{\dot{q}}\lambda^2-(mu_0+Z_q)\lambda & -Z_h \\
& & -Z_w & +(mg\phi_0-Z_\phi) & -Z_\theta & \\
-K_u & -K_{\dot{v}}\lambda-K_v & -K_{\dot{w}}\lambda-K_w & (I_{xx}-K_{\dot{p}})\lambda^2-K_p\lambda-K_\phi & -K_{\dot{q}}\lambda^2-K_q\lambda-K_\theta & -K_h \\
-M_u & -M_{\dot{v}}\lambda-M_v & -M_{\dot{w}}\lambda-M_w & -M_{\dot{p}}\lambda^2-M_p\lambda-M_\phi & (I_{yy}-M_{\dot{q}})\lambda^2-M_q\lambda-M_\theta & -M_h \\
0 & 0 & -1 & -v_0 & u_0 & \lambda
\end{vmatrix}=0
$$

(5)

The characteristic equation is then obtained by expanding the above equation.

$$
f_8\lambda^8+f_7\lambda^7+f_6\lambda^6+f_5\lambda^5+f_4\lambda^4 \\
+f_3\lambda^3+f_2\lambda^2+f_1\lambda+f_0 = 0 \qquad (6)
$$

The necessary and sufficient condition to make the solutions of eq.(6) stable is determined by either applying the Routh's discriminant method to the coefficients, or finding the roots without positive real parts.

3.2 Stability Derivatives

Although we may follow the calculation procedure by Kaplan et al [5] to determine the stability derivatives for each hydro-foil, those for sail are determined using the method previously developed by the author [9]. Summing up all the derivatives and substituting them into eq.(6), we can examine the dynamic stability of the hydro-foil sailing boat.

3.3 Results of Stability Analysis in Calm Water

The dynamic stability analysis was performed in all of the possible equilibrium sailing state as a function of ε. Figure 4 shows the variation of sailing state parameters with ε for the wind velocity of 10 m/s. Illustration by the root locus diagram of the characteristic equation for the same condition is shown in Fig. 5, where the simultaneous movements of the eight roots are represented. For large ε which makes boat velocity low, the real parts of all roots are negative and the movements of them are relatively small. With decreasing ε the movements of the roots become large gradually, and then one of them on the real axis becomes positive at 20°. This means that the boat falls into static instability or divergence at small ε which yields high boat

both motions in longitudinal and lateral directions. From this aspect, it is required to carry out the stability analysis using all of the formulae in eq.(1). However, the motion around z axis would be neglected for the dynamic stability analysis, although it should be treated in the course stability analysis. Thus the last formula in eq.(1) and the terms of ψ, r and $\dot{r}$ are eliminated. As consequence, the linearized equations of motion can be reduced to the following eq.(2).

$$
\left.\begin{array}{rl}
m(\dot{u}+qw_0) & = \Delta X -mg\theta \\
m(\dot{v}-pw_0) & = \Delta Y +mg\phi \\
m(\dot{w}+pv_0-qu_0) & = \Delta Z -mg\phi\phi_0 \\
I_{xx}\dot{p} & = \Delta K \\
I_{yy}\dot{q} & = \Delta M
\end{array}\right\} \quad (2)
$$

From the definition of angular velocity, it is apparent that $\dot{\phi}=p$ and $\dot{\theta}=q$. The velocity of the C.G. to the true vertical direction is then expressed as follows:

$$
\dot{h} = w - u_0\theta + v_0\phi . \qquad (3)
$$

Thus, the linearized equations of motion are rewritten by using stability derivatives as,

$$
\left.\begin{array}{l}
m\dot{u}+mw_0\dot{\theta}+mg\theta-X_uu-X_vv-X_{\dot{v}}\dot{v}-X_ww-X_{\dot{w}}\dot{w} \\
\quad -X_\phi\phi-X_p\dot{\phi}-X_{\dot{p}}\ddot{\phi}-X_\theta\theta-X_q\dot{\theta}-X_{\dot{q}}\ddot{\theta}-X_hh= 0 \\
m\dot{v}-mw_0\dot{\phi}-mg\phi-Y_uu-Y_vv-Y_{\dot{v}}\dot{v}-Y_ww-Y_{\dot{w}}\dot{w} \\
\quad -Y_\phi\phi-Y_p\dot{\phi}-Y_{\dot{p}}\ddot{\phi}-Y_\theta\theta-Y_q\dot{\theta}-Y_{\dot{q}}\ddot{\theta}-Y_hh= 0 \\
m\dot{w}+mv_0\dot{\phi}-mu_0\dot{\theta}+mg\phi_0\phi-Z_uu-Z_vv-Z_{\dot{v}}\dot{v}-Z_ww \\
\quad -Z_{\dot{w}}\dot{w}-Z_\phi\phi-Z_p\dot{\phi}-Z_{\dot{p}}\ddot{\phi}-Z_\theta\theta-Z_q\dot{\theta}-Z_{\dot{q}}\ddot{\theta}-Z_hh= 0 \\
I_{xx}\ddot{\phi}-K_uu-K_vv-K_{\dot{v}}\dot{v}-K_ww-K_{\dot{w}}\dot{w} \\
\quad -K_\phi\phi-K_p\dot{\phi}-K_{\dot{p}}\ddot{\phi}-K_\theta\theta-K_q\dot{\theta}-K_{\dot{q}}\ddot{\theta}-K_hh= 0 \\
I_{yy}\ddot{\theta}-M_uu-M_vv-M_{\dot{v}}\dot{v}-M_ww-M_{\dot{w}}\dot{w} \\
\quad -M_\phi\phi-M_p\dot{\phi}-M_{\dot{p}}\ddot{\phi}-M_\theta\theta-M_q\dot{\theta}-M_{\dot{q}}\ddot{\theta}-M_hh= 0 \\
\dot{h}-w+u_0\theta-v_0\phi= 0 .
\end{array}\right\} (4)
$$

Fig. 4 Variation of sailing state parameters with sail trim angle, ε
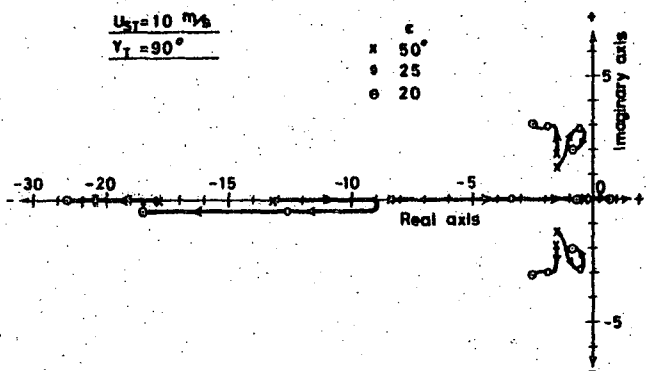

Fig. 5 Root locus diagram of stability characteristic equation

velocity. Such an unstable region is indicated as a shaded zone in Fig. 4. From the figure it should be noted that the boat becomes unstable when the submerged length of starboard (windward) foil, l_{F1}, becomes smaller than 0.1m prior to apart from water surface, although the solutions of the equilibrium equations can be obtained until l_{F1} becomes to zero, i.e. taking off from water surface.

As a result of dynamic stability analysis, it was clarified that there was a critical sailing state which was defined by the value of ε and the conventional performance prediction neglecting the stability analysis gave the over-estimated value for the maximum velocity.

4 NUMERICAL SIMULATION IN REGULAR WAVES

4.1 Calculation of Hydrodynamic Forces Acting on Foil in Regular Waves

Defining the angle between x_e axis in the space-fixed coordinate system and the direction of wave as χ in Fig. 6, the profile of wave observed at point (x_{ei}, y_{ei}) can be expressed as,

$$\zeta = - \frac{\zeta_w}{2}\sin k(ct - x_{ei}\cos\chi - y_{ei}\sin\chi), \quad (7)$$

where $k = 2\pi/L_w$ and $c = \sqrt{g/k}$.

Using the coordinate of C.G. of the boat (x_{eG}, y_{eG}, z_{eG}) and transforming from the body axes (x_i, y_i, z_i), we can determine the coordinate of each foil (x_{ei}, y_{ei}, z_{ei}) as follows:

$$\begin{bmatrix} x'_{ei} \\ y'_{ei} \\ z'_{ei} \end{bmatrix} = S \begin{bmatrix} x_i \\ y_i \\ z_i \end{bmatrix}, \quad (8)$$

and

$$\left. \begin{array}{l} x_{ei} = x'_{ei} + x_{eG} \\ y_{ei} = y'_{ei} + y_{eG} \\ z_{ei} = z'_{ei} + z_{eG} \end{array} \right\} \quad (9)$$

where,

$$S = \begin{bmatrix} \cos\Psi\cos\Theta & \cos\Psi\sin\Theta\sin\Phi & \cos\Psi\sin\Theta\cos\Phi \\ & -\sin\Psi\cos\Phi & +\sin\Psi\sin\Phi \\ \sin\Psi\cos\Theta & \sin\Psi\sin\Theta\sin\Phi & \sin\Psi\sin\Theta\cos\Phi \\ & +\cos\Psi\cos\Phi & -\cos\Psi\sin\Phi \\ -\sin\Theta & \cos\Theta\sin\Phi & \cos\Theta\cos\Phi \end{bmatrix}.$$

Thus we can determine the wave profile at each foil using eq.(7). The wave profile calculation throughout the whole length of the foil makes it possible to decide both submerged length of each foil and depth of the center of the foil, d_i. At the depth of d_i, the tangential velocity of orbital motion of water particle can be expressed as

$$U_{twi} = \frac{\zeta_w \pi c}{L_w} e^{-kd_i}. \quad (10)$$
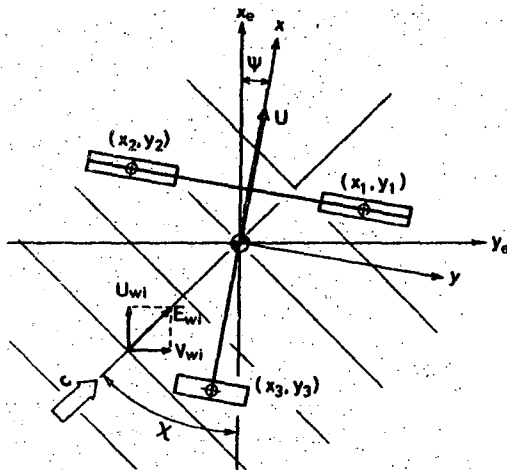
Fig. 6 Correlation between wave direction and space-fixed coordinate system

The horizontal and vertical velocities are represented respectively as follows:

$$E_{wi} = U_{twi}\sin k(ct-x_{ei}\cos\chi-y_{ei}\sin\chi)$$
$$W_{wi} = -U_{twi}\cos k(ct-x_{ei}\cos\chi-y_{ei}\sin\chi).$$ (11)

These velocity components of water particle are transformed in the body axes as

$$\begin{bmatrix} U_{wbi} \\ V_{wbi} \\ W_{wbi} \end{bmatrix} = S^T \begin{bmatrix} E_{wi}\cos\chi \\ E_{wi}\sin\chi \\ W_{wi} \end{bmatrix}, \quad (12)$$

where S^T is the transposed matrix of S.

Finally, substituting these values into the Euler's equation, we may analyze the motion of the boat in regular waves. The applicability of the calculation method was confirmed through towing tank test [10].

4.2 Condition of Simulation

In order to analyze the motion of six-degree-of-freedom, the motion around z axis represented by ψ, r and $\dot{r}$ must be considered although it was not considered in the stability analysis. The value of ψ can make nil by correcting the rudder angle through the calculation of the following relationship:

$$\delta = -C_1\psi - C_2\dot{\psi}, \quad (13)$$

where the C_1 and C_2 would be selected to take the value from 0 to 2 to minimize ψ with maximizing boat velocity.

The calculation was performed under the constant wind velocity of 10m/s for various wave conditions. The direction of wave propagation was considered to correspond with that of wind. The wave height, ζ_w, was chosen as 1, 2 and 3m referring to the relationship between wind velocity and significant wave height, $H_{1/3}$, recommended by WMO [11]. While, the wave period, T, was chosen in the range of $3.6\sqrt{H_{1/3}} < T < 5.48\sqrt{H_{1/3}}$ which was proposed by ISSC [12]. Consequently, the wave conditions used for the simulation are summarized in Table 2 for long and short wave periods.

Table 2 Wave conditions for numerical simulation

wave height (m)	1	2	3
long wave period T= $5.48\sqrt{\zeta_w}$ (s)	5.48	7.75	9.49
short wave period T= $3.6\sqrt{\zeta_w}$ (s)	3.60	5.09	6.24

4.3 Numerical Simulation Results·

An example of the numerical simulation results in regular wave is shown in Fig. 7 for the case of U_{ST}=10m/s and γ_T=90°. In the early stage of the sailing, the boat runs in calm water with equilibrium condition. After 5 seconds the wave motion starts and within two wave periods the wave height becomes to some values specified in Table 2. The height and period of the wave in this case are 3m and 6.24s respectively for ε equals 22°. Although the stability analysis has resulted in the stable sailing at the velocity of 13.50m/s (see Fig. 4), the boat capsizes at 25s in the present simulation. Namely at 25s the height of C.G. becomes lower than the wave profile, ζ, exhibiting large negative value of the pitch angle, θ. Thus the boat starts to dive into the water from bow and sinks within short seconds.

The influence of wave motion on the sailing performance of the hydrofoil boat can be summarized as follows; i) increased resistance to thrust motion due to rudder control, ii) lowering of the critical highest sailing velocity due to capsize, iii) thrust reduction due to stall of sail for quartering wind, and iv) surfriding effect for following wind. Each item will be quoted in the following explanation.

The critical sailing velocity for various wind directions in three regular wave conditions is illustrated in polar diagram as shown in Figs. 8 and 9 for long and short wave periods, respectively. In these figures, the critical sailing states determined through the dynamic stability analysis in calm water are indicated with heavy curves.

In Fig. 8 for T=$5.48\sqrt{\zeta_w}$ s, in spite of relatively small effect of wave on the critical velocity, the decreases in velocity caused by the above items i), ii) and iii)
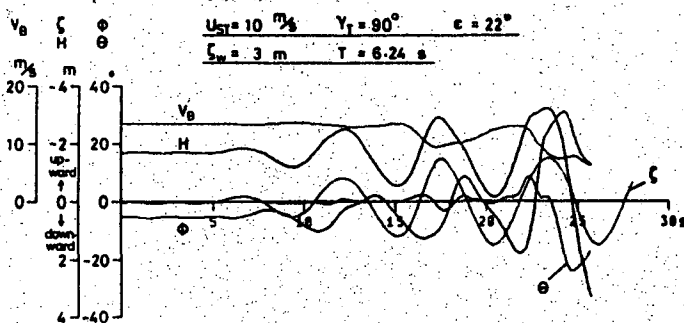

Fig. 7 Numerical simulation results indicating the motion of the boat in regular wave
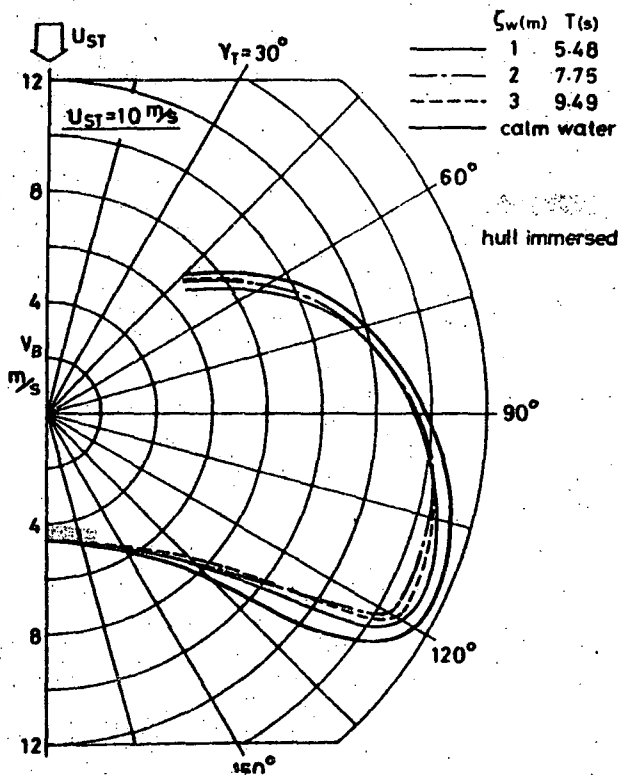
Fig. 8 Variations of the critical sailing velocity with both wind and wave directions for long wave period
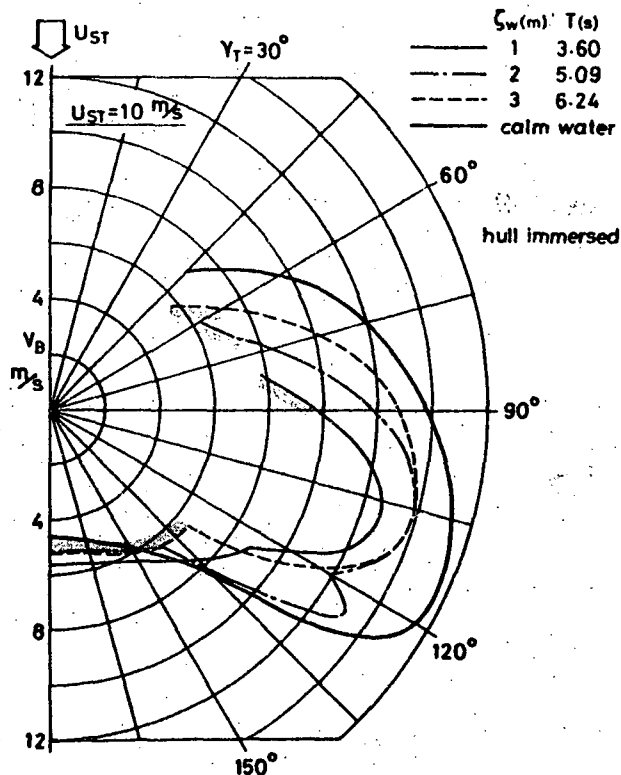

Fig. 9 Variations of the critical sailing velocity with both wind and wave directions for short wave period

are observed in the ranges of $50° \sim 90°$, $90° \sim 120°$, and $120° \sim 140°$, respectively. Exceeding $140°$, it becomes impossible to sail in foil-born mode because of being outstripped by wave and immersing the hull in the water.

For $T = 3.6\sqrt{\zeta_w}$ s, a considerably large effect of wave on the performance can be observed as shown in Fig. 9. In the range of $50° \sim 90°$, the boat velocity decreases drastically because of the above item i). Especially, in the case of $\zeta_w = 1m$, the hull immerses with making impossible to sail. For $90° \sim 110°$, reduction of the velocity is also large by referring to the item ii). Such reduction in the velocity brings on a serious problem to the hydrofoil sailing boat, because it occurs in the higher sailing velocity region with lowering the attainable maximum velocity through capsizing. The item iii) occurs in the range of $110° \sim 130°$. For the case of $\zeta_w = 2m$, the abnormal velocity increase is observed in the range of $125° \sim 130°$. This velocity increase is due to the activated sail work through the surfriding effect described as the item iv). However, exceeding $130°$ the sail stalls entirely, and the boat loses the velocity with outstripping by wave. While for the case of $\zeta_w = 1m$, with exceeding $120°$, the value of $c/\cos(2\pi - \chi)$ approaches to the

velocity of the boat with stalling the sail. Therefore the boat can be maintain the surf-riding condition. In such condition the boat velocity becomes sometimes higher than that in calm water.

Through the simulation works conducted here it was indicated that the performance of hydrofoil sailing boat was influenced stronger by the wave period rather than the wave height. At the short wave period, the boat velocity decreased considerably compared to that predicted by the dynamic stability analysis in calm water even though the wave height is low.

5 CONCLUSION

The results of dynamic stability analysis indicated that, at higher velocity the boat fell into static instability or divergence with limiting the attainable maximum velocity. Since the equilibrium equations were solved with including unstable solutions, the results gave an over-estimated maximum velocity unless the dynamic stability analysis were conducted.

Among the influences of the wave motion on the performance of hydrofoil sailing boat, the accelerated capsizing due to wave motion was serious problem because it lowered significantly the maximum attainable

boat velocity in the critical sailing state. In the wave motion the wave period affected stronger than the wave height. The boat velocity at short wave period, decreased considerably compared to that predicted by the dynamic stability analysis in calm water even though the wave height was low. Finally it was noted that the numerical simulation including the wave conditions as the parameters should be conducted as well as the dynamic stability analysis for the performance prediction of hydrofoil sailing boat.

ACKNOWLEDGEMENT

The author would like to acknowledge the continuing guidance and encouragement of Professor K. Nomoto of the World Maritime University and Osaka University. The author also wishes to thank Professor M. Hamamoto of Osaka University for helpful suggestions about the calculation and experiment of hydrofoil.

NOMENCLATURE

c   wave celerity
d_i depth of submergence of hydrofoil
g   acceleration due to gravity
H   height of C.G. from water surface level
I_{xx}, I_{yy}, I_{zz} moments of inertia about x, y and z axes
I_{zx} product of inertia about z and x axes
K,M,N   moments of roll, pitch and yaw
L_w wave length
l_{Fi} length of submerged part of hydrofoil
m   mass of boat and crew
P,Q,R   angular velocities in roll, pitch and yaw
T   wave period
U,V,W   velocity components along x, y and z axes
U_{ST} true wind velocity
U_{twi} tangential velocity of orbital motion of water particle
V_B boat velocity ($=\sqrt{U^2+V^2+W^2}$)
X,Y,Z   force components along x, y and z axes
α_s attack angle of sail (in Figs. 3 and 4)
β angle of leeway (in Figs. 3 and 4)
γ_T angle between true wind velocity and centerline of boat
δ angle of rudder
ϵ trim angle of sail
ζ_w wave height
λ root of characteristic equation

Φ, Θ, Ψ angles of heel, pitch and yaw (Euler angles)
χ angle between x_e axis and wave direction

REFERENCES

1) Bose,N. and McGregor,R.C.: A Record of Progress Made on a Purpose Built Hydrofoil Supported Sailing Trimaran, The 3rd High-Speed Surface Craft Conference, 1980, London.

2) Smitt,L.W.: Design Features of the One-Way Hydrofoil Proa "The Ugly Duckling", International Conference on Sailing Hydrofoils, R.I.N.A., 1982, London.

3) Wynne,J.B.: Possibilities for Higher Speeds Under Sail, Trans. N.E.C.I.E.S., Vol.96, 1979.

4) Bradfield,W.S.: On the Design and performance of Radical High-Speed Sailing Vehicles, Marine Technology, Vol.17, No.1, 1980.

5) Kaplan,P., Hu,P.N. and Tsakonas,S.: Methods for Estimating the Longitudinal and Lateral Dynamic Stability of Hydrofoil Craft, Stevens Institute of Technology E.T.T. Report No.691, 1958.

6) Wadlin,K.L., Shuford,C.L. and McGehee,J. R.: A Theoretical and Experimental Investigation of the Lift and Drag Characteristics of Hydrofoils at Subcritical and Supercritical Speeds, NACA Report 1232,1955.

7) Masuyama,Y. and Tatano,H.: Hydrodynamic Analysis on Sailing (4th Report) Wind Tunnel Experiments on Yacht Sails, Jour. of the Kansai Soc. of Naval Architects, Japan, No.185, 1982. (in Japanese)

8) Masuyama,Y.: Stability Analysis and Prediction of Performance for a Hydrofoil Sailing Boat (Part 1) Equilibrium Sailing State Analysis, to be published in the International Shipbuilding Progress.

9) Masuyama,Y.: Stability Analysis and Prediction of Performance for a Hydrofoil Sailing Boat (Part 2) Dynamic Stability Analysis, to be submitted to the International Shipbuilding Progress.

10) Masuyama,Y.: Motion of a Hydrofoil System in Waves, Jour. of the Kansai Soc. of Naval Architects, Japan, No.196, 1985. (in Japanese)

11) World Meteorological Organization (WMO) Code 1100.

12) 7th ISSC Committee Report, Committee I.1 Environmental Conditions: Design Waves and Extreme Spectra, 1979, Paris.

The Author

Yutaka Masuyama graduated from Toyama University, Department of Mechanical Engineering in 1969. After this he obtained a Master's degree in fluid dynamics in 1971. Then he worked in a yacht designing office, Kumazawa Craft Laboratory, Yokohama, as a yacht designing staff. In 1975 he joined the staff of the Department of Mechanical Engineering at Kanazawa Institute of Technology. He was awarded a Dr. Eng. from Osaka University for a thesis on 'the Performance of Hydrofoil Sailing Boat' in 1983. Since 1984 he has been an Associate Professor in the Department of Mechanical Engineering at Kanazawa Institute of Technology.

He built three test boats for research on hydrofoil sailing and ,with the last one "Hi-Trot III", he participated in the World Sailing Speed Record Week held at Portland, England, in 1978.

OPERATIONAL STABILITY OF SHIPS AND SAFE TRANSPORT OF CARGO

S. Kastner

ABSTRACT

Safe sea transportation of cargo is not just a matter of safe stowage and securing of cargo, solely, but is strongly related with the design and construction of the ship, and her outfit, as well as with the way the ship is being operated at sea in different environmental conditions.

This paper points at the four-fold interaction of
- type and preparation of cargo
- vessel design and outfit
- environment
- ship operation.

Minimum stability requirements by authorities cannot include any risk possible, but do not show clearly on which operational conditions they have been based upon. Still, they are seen as guide-lines for the ship operator too.

The ship master needs further information on the actual ship behaviour to be expected in extreme conditions, and on measures for prevention and survival. With respect to ship stability, he is concerned about safety from capsizing, and about low motion accelerations on the cargo. Cargo constitutes the most part of the total ship mass, and its feedback to ship behaviour is paramount. Results of modern ship motion and sea-keeping theory should be transferred aboard the ship to the operator in a comprehensible fashion.

Due to the above mentioned interaction, information must include measures on cargo stowage and securing, but also on operational measures to reduce ship motion. The quest of naval architects for designing ships with good motion behaviour should be revived.

In a pilot-study for the German Federal Ministry of Transport, the underlying problem areas have been looked at, and work is underway within IMO to develop a Code of Safe Practice for stowage and securing of cargo to be given aboard ships.

1. INTERACTION PROCESSES

Safe sea transportation of cargo depends on the design of the ship, and on the way the ship is being operated.
It seems obvious that safer sea transportation requires collaboration of all related parties such as Naval Architects, Ship Masters, and Shipping Agents.

Looking into the physical and operational background of sea transportation, we find a four-fold interaction of

- cargo (its type, preparation, stowage, securing)
- vessel (design, outfit)
- environment (wind, waves)
- operation (load distribution, navigation),

as being illustrated by the Venn diagramm in Fig. 1.
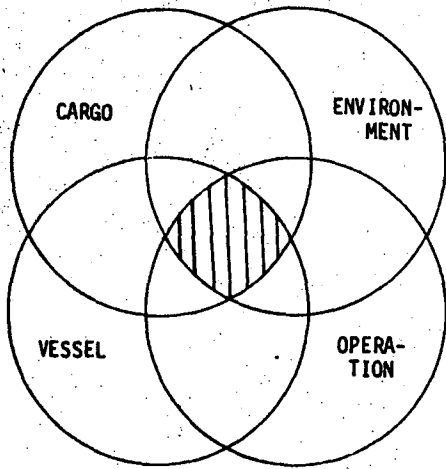
Fig. 1: Four-fold Interaction of Cargo and
         Vessel, Environment and Ship
         Operation

In this context, I want to stress the importance of including "cargo" into the consideration, since it constitutes the major part of the total ship mass, and its behaviour is paramount to the safe transport aboard a ship. The type of cargo generally defines the type of ship to be designed. This is still true for e.g. Multi-Purpose-Carriers.

Measures to ensure safe transport, without damage to ship and cargo, fall into two categories:

(i)   reducing loads acting on the cargo, accomplished by ship design, operation, stowage, ballasting

(ii)   dealing with the inevitable loads acting on the cargo whilst at sea from the environment, by cargo securing.

Within IMO (International Maritime Organisation) in London at the BC-Subcommittee, work is presently underway to develop a "Code of Safe Practice" to be given aboard ships. It centers on a standardisation and internationally accepted recommendations of good stowage and securing measures, in particular for non-bulk cargo. This new Code presents also an opportunity to include guide-lines on how to handle and operate a ship in a seaway safely, in order to reduce loads on the cargo /1,2/.

Furthermore, ship design must consider a good ship behaviour in a seaway, and should account more for a feedback from the practical experience of the ship operator.

2. OPERATIONAL STABILITY

Operational stability defines the actual stability status of the ship during her voyage, which varies in time due to changes in cargo and ballast of the ship, and due to the changing environmental conditions at sea.

The actual stability status must be compared with the minimum stability requirements set by authorities, in order to ensure safety of the ship from capsizing /3/. We might call this the "regulatory" stability.

Naturally, the ship motions, and the resulting acting loads on the cargo, depend on the actual operational stability. In fact, what I therefore am proposing is to distinct very clearly between the operational stability of a ship and minimum stability requirements set by authorities. The letter are often seen as guide-lines for the operational stability by the ship masters too. However, minimum stability alone lacks the needed information on its background, such as at which severe conditions the ship will survive. Thus, with the prevailing lack of specific information on the background of the requirements, the navigator finds himself left alone, although he has to make decisions in the daily life operations, very often at the border-line of safety.

Those minimum requirements for stability constitute the minimum set standard, in order to allow the ship to sail, but they cannot include all possible risks from any extreme severe but very rare event. Minimum stability must allow the ship to overcome regularly encountered situations. If minimum levels are set too high, in order to cope with very rare extreme events too, transportation may feel drawbacks such as

- reduced economy
- worse ship behaviour in a seaway

- cargo experiences unnecessarily higher motion accelerations, which requires more securing and lashing.

If at the current situation minimum stability levels are set too low, this might dangerously be misunderstood by operators. The ship allowed to sail at this condition, might not be able to resist a severe environment. Fig. 2 compares the probability densities of righting levers existing and in demand.
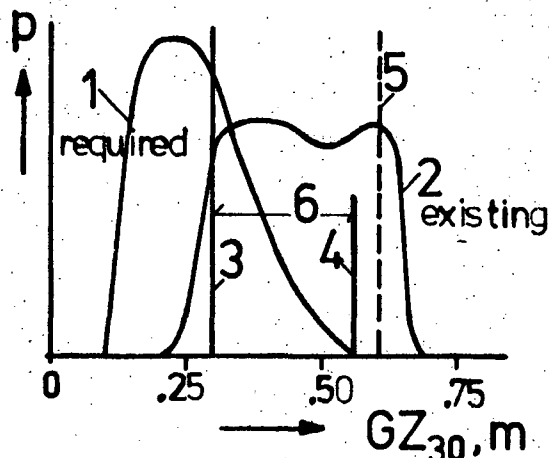

FIG. 2: Required and Existing Righting Lever at 30 deg Heel (schematic).

Legend:
1 minimum required in operation
2 existing in loaded condition
3 minimum for design (regulatory)
4 maximum required in operation for safety from capsizing
5 maximum allowed for roll acceleration
6 Master's range of judgement (operation according to the environment)

As long as we do not give further information aboard on the probability of safety from capsizing, and on the conditions related with the minimum stability, we leave it up to the judgement of the ship master to operate safely at extreme environmental conditions. We may call the range between the minimum righting arm levers set by authorities for ship design and certification and the actual levers needed at rare extreme seaway the "range of judgement" for the ship master, see No.6 in Fig. 2 /4/.

This leads us to the following conclusions:
- Stability requirements should indicate clearly the underlying conditions in order to inform the master on the operational limits of his ship
- Further information to the master should be given aboard on the ship motion behaviour in a seaway, on the danger from damage of cargo and loss of ship in extreme conditions, and on measures for prevention and survival.

Since extreme situations will need higher requirements than the minimum set stability standard, they should be listed and given aboard. Further information to the master has become more important than ever, because experience alone has become less helpful due to frequent changing of officers, new types of ships, and types of ship and cargo where not enough experience is available at all. However, increased information must be compiled in an easy accessible and least complicated way in order to be used effectively in the shipping practice.

3. LARGE MOTION ACCELERATIONS

The inevitable roll motion of a ship at sea can in its extremes result in either one of the following effects:

- capsizing at extreme roll with insufficient righting lever capability

- large roll amplitudes in a quick time sequence, i.e. at a high roll motion frequency, leading to high motion accelerations acting on the cargo, which might end up with danger from capsizing due to shifting of cargo.

It is well known, that measures to reduce the danger from capsizing by increasing the uprighting moment leads to larger roll accelerations, according to the simple formula (for the linear range)

$$\ddot{\phi}_{max} = \omega_{\phi}^2 \, \phi_{max} = \frac{g\overline{GM}}{i_T^{'2}} \phi_{max}$$

Thus, in Fig. 2, we have drawn a maximum admissible righting lever in still water to limit roll acceleration (no.5 in Fig. 2).

Within the thus defined and shown minimum and maximum righting levers in still water, the ship must operate, taking into account environmental conditions on her route, and appropriate stowage of cargo and ballasting of the ship.

Fig. 3 shows the definition of GM and GZ, with resulting local motion acceleration at the mass centre of a cargo unit, which has contributions from all degrees of freedom /1/, in vertical and transverse component with respect to the ship body (and a longitudinal component too).
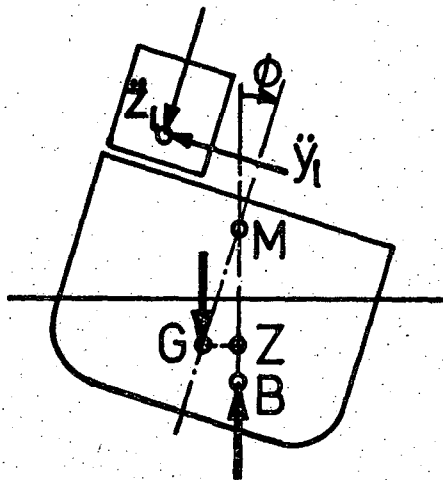
Fig. 3: Hydrostatic Righting Lever and Acting Motion Acceleration Components on Cargo

Although authorities set minimum requirements for the righting levers for safety from capsizing, there have been no upper limits set to reduce accelerations acting on the cargo. It is up to a good ship design and operation to limit motion accelerations, but ships with good motion behaviour have sometimes been asked for to cope with certain shipping demands.

4. BASIC PATTERN OF STABILITY MOMENTS

As shown in Fig. 3, the uprighting lever GZ always constitutes the uprighting moment from the weight of the ship (FG = gm) and the buoyancy force (FB = g$\rho\nabla$). The uprighting moment only

comes into effect under the action of any exiting heeling moment Mexc in order to compensate and to restore equilibrium of moments.

The position of both action centres B and G for the forces may vary in time during ship operation at sea, resulting in a time varying restoring moment.

Naval Architects now try to define limiting conditions for the variations of the B and G positions of the ship, in order to allow for a judgement on the remaining resultant uprighting moment.

We may set up the following matrix of possible variations of B and G, see Table 1.

Table 1: Variation of Forces Acting in B and G

	column no.	1	2
line	G	G	G'
no.	B	fixed	variable
1	B fixed	(11) B G	(12) B G'
2	B' variable	(21) B'G	(22) B'G'

Case (11) B G : Both B and G fixed

This is the ship condition sought for. In operational stability, we find this condition only for the ship in still water (fixed B), and for proper ship loading without any change in the resulting mass centre of the ship, i.e. at totally fixed mass distribution within the ship (fixed G).

Case (22) B'G': Both B and G variable

This is the worst condition for the ship to think of, where both the centres of buoyancy B' and of weight force G' vary in time during ship operation. Variation of B must be limited by proper ship design, i.e. is determined by ship dimensions and their relations, and ship hull form, whereas G can be influenced by the mass distribution within the ship, by stowage and securing of cargo to keep it in a fixed position even

```
I----------------------I----------------------I
I (11) B G             I (12) B G'            I
I STILL WATER          I CARGO SHIFTING       I
I                      I                      I
```
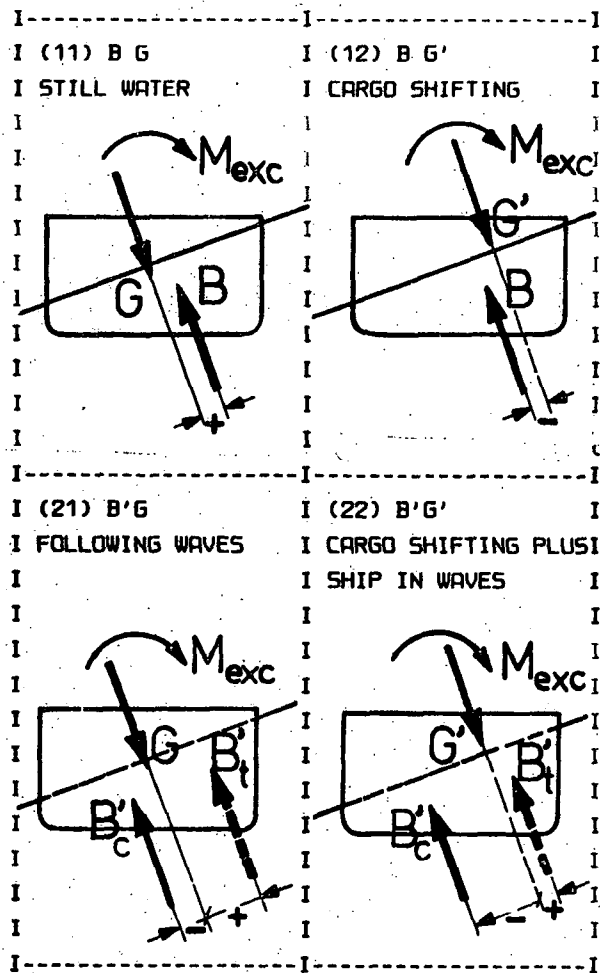
Fig. 4: Schematics of Basic Moment Patterns for Ship Stability, according to Table 1

(+ uprighting, - heeling,
 c crest, t trough)

under the action of exciting motion forces, and by ballasting. The two remaining intermediate cases are

Case (12) B G': Shifting of cargo

Here the buoyancy position B does not vary, which is the case in still water. Due to preceding ship motions, and resulting accelerations on the cargo, the cargo may have changed its position within the ship. Thus the resultant mass centre G' is changed from "shifting of cargo". This dangerous condition must be prevented at all circumstances.

Case (21) B'G : Ship with fixed cargo in a longitudinal seaway

Here we take into account the time variations of the righting levers of the ship in a seaway, but with no shift of cargo whatsoever. This is the most likely condition the ship is in at operation in severe aft longitudinal or quartering seas.

Fig. 4 illustrates the four different cases of variations of B and G as described above.

The first case(11) is not very realistic with respect to the operational stability conditions of the ship. However, for design and regulatory stability, requirements are often based on this condition, taking any variation of B and G into account implicitely, i.e. including a required margin for the righting lever GZ from experience, calculation and measurement.

For the operational stability, i.e. for actual conditions of the ship out in the Ocean, we may be confronted with the worst condition, case(22), B'G'. In order to avoid the inherent dangers, ship designers and operators have a lot of measures to overcome dangers to ship and cargo.

Thus, in practice, case(12), shifting of cargo, must be prevented at any rate. This is generally accomplished by stowage and securing of cargo. Any shifting of cargo can cause such a large change of the G-position, which cannot be overcome by a correspondingly varied position B of the buoyancy force, in order to result in sufficient positive righting lever GZ.

Based on the assumption, that cargo is prevented from shifting by specific measures, we end up with the above case(21), B'G ship with fixed cargo, but with time variation of the centre of the buoyancy force. Since for a ship operating in the sea we cannot prevent the acting of the seaway, the latter case(21) is usually the real one in practice, i.e. for the operational stability.

The Naval architect can design for ship with little variation of righting levers in a seaway, and for ballast possibilities to cope with the remaining changes in B. Therefore, the Naval architect must design ships with sufficient

variation capabilities in ballasting.
Furthermore, he should give information on
the seaway behaviour aboard the ship.

Finally, and very important, the ship
master has the power to change actual
operational stability by his navigation,
his search for the best route, and by
changing ship speed and heading of ship to
the waves. Ship masters can learn on the
effect of any measures in advance. By
long-term and short-term computer aided
weather routeing, he could know on the
conditions he will encounter at his voyage.

In any of the four cited conditions, a
capsizing of the ship may occur.
Generally, we try to avoid shifting of
cargo, and stability curves given aboard
are calculated for the intact ship with
fixed position of G. Thus, reducing loads
on the cargo, and proper stowage and
securing, is not only important for
preventing damage to the cargo, but for the
safety of the total ship too.

Damping and hydrodynamic mass effects
come into the equations of forces and
moments acting on the ship. Here mass
distribution and ship hull form, plus
special damping devices can help to improve
the motion behaviour of the ship.

Although the above case consideration
seems obvious, it might be worthwhile to
think of the physical origin for regulatory
work on safe sea transportation, and to
compare measures with the above scheme.

5. DISTRIBUTIONS OF OPERATIONAL STABILITY

Actual probability distributions of
the operational stability can be found from
evaluation of ship log books. However, it
is not mandatory to take notes on the
actual stability status of the ship. Thus
operational stability remains within the
practical experience of the ship master,
but regular notes and evaluation according
to an agreed upon scheme are highly
recommended. The operational stability
distribution has been roughly estimated
from stability booklets. For Container
ships, RoRo vessels and Multi-Purpose-
Carriers, about the type of distribution as
shown in Fig. 5 has been found.
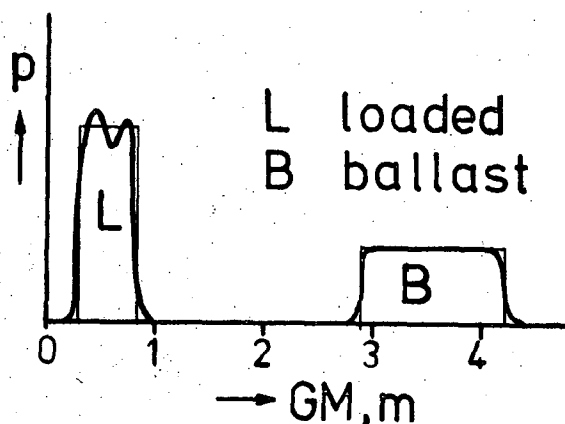
Fig. 5: Probability Density for Operatio-
nal GM

In Fig. 5, only the distribution of GM
has been shown. Remarkable is the
pronounced dif- ference between the loaded
and the ballast conditions.

Fig. 6 shows the corresponding opera-
tional range of the still water righting
levers.
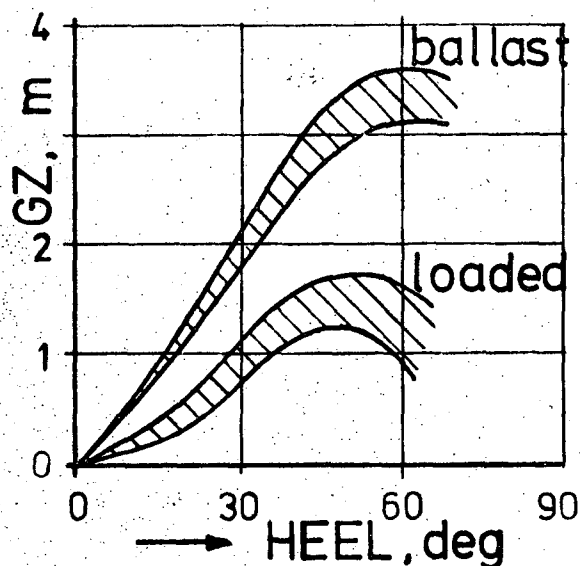
Fig. 6: Operational Righting Levers

The corresponding distribution of the
natural roll period, according to the
equation (Weiss' formula)

$$T\emptyset = \frac{f \cdot B}{\sqrt{GM}}$$

has been depicted in Fig. 7.

Resonance can be checked according to the condition:

TØ = TE for Mathieu and external excitation

and additionally the Mathieu condition:

TØ = 2 TE

The shown TØ - distribution in Fig. 7 is a long-term-distribution, i.e. the occurrence rate of the natural period TØ over a long period of time, for a certain route of the ship, or for her life-time. It must be compared with a corresponding long-term distribution of the encounter periods of ship and waves.

Such encounter distributions could be found from installing gaugés and automatic samplers, or could be derived by calculation from ship routes, speed and wave distributions. In /5/ two samples for different ship speeds of 14 kn and 26 kn are given, see Fig. 7.
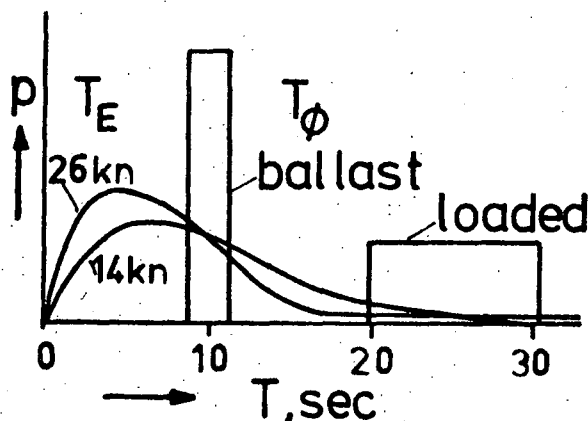
Fig. 7: Long-Term Resonance Probability from Comparing TE- and TØ- Distributions.

For the larger ship speed, a longer tail of the distribution reaches into the large period range of the loaded ship condition. That means, although compared with the life-time of the ship, this resonance tail only constitutes a small percentage of all encounter conditions ship-waves, they are only rare events which can cause large roll amplitudes and danger from resonance. Reduction of ship speed and change of heading are measures for the ship master to prevent resonance. Simple resonance diagrams can prove advantageous

aboard the ship to avoid resonance in advance /1,2/.

Short-term weather-routeing, i.e. optimizing the route, speed and heading with using on-line information at sea, has been developed by Soeding /6/. It reduces the effect of uncertainties which still exist in the long-term weather fore-casts.

According to Fig. 7, there is a larger probability to come into resonance with waves for the ship in ballast condition. However, this is not a dangerous condition for the ship, because it is related with large righting levers, and cargo is not affected. In order to alleviate ship operation at sea, ballast possibilities to increase the natural period TØ would be helpful, i.e. with ballast tanks in higher ship positions. They might also be helpful for certain loaded ship conditions to avoid resonance, by making the ship roll motion softer.

From evaluation of a few ships (container, Ro/Ro, MPC, Special cargo), the total water ballast is in the range of 2Ø to 4Ø p.c. of the deadweight. As a rule, with more need to adjust for special cargo, more ballast is required.

Contrary to the long-term evaluation of ship operation, for an actual seaway encounter, we must look into the short-term behaviour of the ship, i.e. compare the distributions of the natural period TØ of the ship with the encounter period TE within minutes or hours, see Fig. 8.
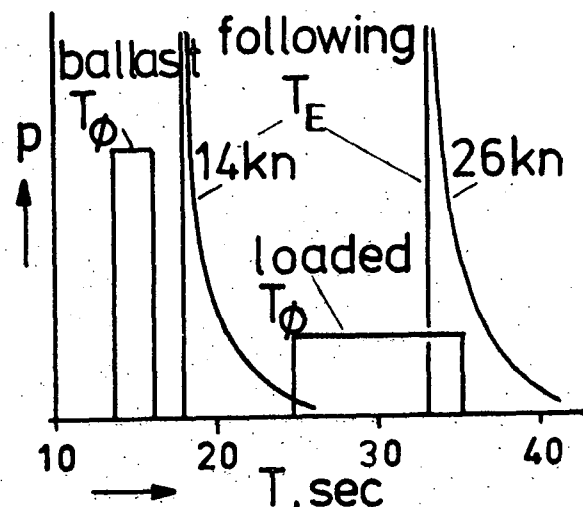
Fig. 8: Short-Term Resonance Probability

6. MEASURES TO IMPROVE OPERATIONAL STABILITY

We want to stress the need to review the current measures for a safe sea transportation, with the hope to gain and to improve, in the light of new ship types, which in extreme situations often operate at the border-line of safety.

The fact is, that some modern ship designs actually have resulted in a worse motion behaviour of ships, since mainly viewpoints of large stowage place have been considered.

Although often operating at the limits of the minimum stability set by authorities, the ship master does not receive more information on the ship behaviour at extreme conditions. He must judge and decide very much on his own experience.

Thus, there is a need for furnishing improved information to the master. Ship theory and model testing is now at a stage, where specific data for any ship type can be given. The practical set-up of information data aboard must be developed /7,8,9/. We list a few points to be looked at to improve operational stability of ships:

1) rethinking in the design of ships with respect to the seaway behaviour
2) develope information to the master given aboard the ship on ship motions
3) standardize the securing measures for the large variety of non-bulk cargo
4) stowage of cargo
5) actual size of stability parameters for ship in operation, its estimation and accuracy, and improved testing procedures
6) ballasting of ship
7) damping of roll motion
8) long-term operations
   - weather routeing, operational analysis
9) short-term operations by the ship master
   - speed reduction and change of heading
   - short-term weather routeing

10) support of ship motion gauges and processors, data reduction and indication of action parameters on operational ship stability
11) improved training of masters on ship motions and safety of cargo, and on prevention of extremes
12) sample and evaluate experience and accidents internationally
13) agree on observation chart on severe ship motion and extreme lashing forces /9/
14) develop international "Code of Safe Practice" by IMO to include the above general pattern.

7. ACKNOWLEDGEMENT

8. NOMENCLATURE

$\emptyset$	roll angle
$\ddot{\emptyset}$	roll angular acceleration
ω_ϕ	natural roll frequency
GM	metacentric height
g	gravity acceleration
$i'T$	roll radius of gyration
FB	buoyancy force
FG	weight force of total ship mass
∇	ship displacement volume
m	ship mass
M	moment
exc	exciting
rest	restoring
$\ddot{z}$	heave acceleration of ship
t	time
$T\emptyset$	natural roll period
TE	encounter period ship-wave
χ	heading ship-wave
GZ	righting lever
B	center of buoyancy in still water
B'c	B' in wave crest
B't	B' in wave trough

G   center of total mass of ship

B',G'   variable position of B or G, res-
            pectively

p   probability density

9. REFERENCES

/1/ Kaps, H. and S. Kastner: On the Phy-
sical and Operational Background of
Cargo Securing aboard Ships.
IMO working Paper BC26/4/7, London,
November 1984

/2/ Kaps, H. and S. Kastner: Pilot Study:
"Safe Transport of Cargo aboard Sea-
going Vessels".
Final Report to the Federal Ministry
of Transport, (in German), shortened
in HANSA, Vol.123, 1986, No.5, p.397/
398, Hamburg

/3/ Blume, Hattendorf, Hormann, Krappinger:
Kentersicherheit.
Transactions of Schiffbautechnische
Gesellschaft, Vol.78, 1984, Springer-
Verlag Berlin

/4/ Kastner, S.: Dynamische Einflüsse auf
die Kentersicherheit.
Symposium on "Safety at Sea", Bremen
Polytechnic 1984

/5/ N.N.: Handbuch des Atlantischen
Ozeans.
Deutsches Hydrographisches Institut,
Hamburg 1981

/6/ Soeding, H.: Einfluss des Seegangs
auf den Schiffsbetrieb.
Working Report SFB98, Project I5,
p.293/327, Hannover and Hamburg
Universities, 1983

/7/ Hutchison, B.L.: Risk and Operability
Analysis in the Marine Environment.
Transactions, SNAME, Vol.89, New York
1981

/8/ Cleary, W.A. Jr. and F. Perrini:
Improvement of Information to the
Master.
Transactions, International Conference
STAB'82, Tokyo

/9/ Kastner, S.: Proposed Framework for
the calculation of Lashing Forces for
Practical Use aboard Ships, and on
Actions to be taken in Heavy Seas.
Working paper for the Federal Ministry
of Transport, Bremen, July 1985

ON THE AUTHOR

Dr.-Ing. Sigismund Kastner is Pro-
fessor of Naval Architecture at Bremen
Polytechnic, F.R. Germany, where he is lec-
turing Ship Hydrodynamics and Ocean
Engineering.

OPERATION MANUALS FOR IMPROVED SAFETY IN A SEAWAY

E.Aa. Dahle, T. Nedrelid

ABSTRACT

The paper outlines a new stability evaluation with three main elements:

1. The traditional minimum stability regulations, which are based on calculations of hydrostatics and weights. In the future, more advanced methods of calculating the dynamic behaviour of vessels in wind and waves may also become available.

2. A risk analysis. In this case an approximate calculation of capsizing probability. The calculation should be based on a study of the intended operations of the vessel, especially with regard to environmental forces.

3. An operation manual. The intention of the manual is to maintain the risk of capsizing on an acceptable level through operational restrictions and/or stability requirements above the minimum given in traditional regulations. An outline example is presented in Appendix 1.

1   VESSEL STABILITY

1.1 Principles of stability

In the following the emphasis will be on maintaining vessel capsizing probability on a low, acceptable level for small vessels (i.e. L<100m). "Capsize" implies that the vessel has been the subject of external forces which has turned the vessel over to a large angle, where the vessel remains stable, The outcome may be:

- the vessel remains in a stable side position (Fig. 1c). Water ingress will often start, and the vessel will turn over 180°, or sink

- the vessel turns directly over to 180° (Fig. 1b)

- the vessel turns over to a large angle (60 - 90°) and returns to an upright position (Fig. 1a). If cargo shifts due to the large heel, the outcome may be:

- the vessel obtains a list, or possibly a more critical stable side position

- the vessel (which may otherwise have GZ-curves of the type shown in Fig. 1a. or 1c.) turns over to 180°.
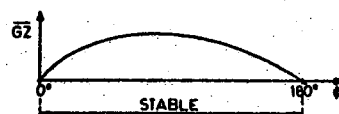
a. Self-righting.
   Capsize not feasible
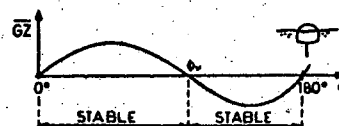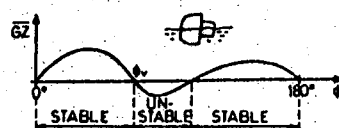
b. Capsize to 180°

c. Capsize to stable side position

Fig. 1. Definition of capsize.

The present IMO stability recommendations are based upon the curves for the vessels righting lever (GZ). These criteria are first applied in the concept and design phase of a ship. They are not always appropriate in operational situations, especially because they are independent of the loading condition. The understanding of stability through such curves is often poor.

Some questions to be asked are: Will the safety of small vessels be improved by new requirements similar to the ones in force today, only more sophisticated? Is it possible to plan and design safer vessels without also giving operational guidance? Is it possible through bad seamanship or ignorance to capsize any vessel?

1.2 The importance of "operational stability"

During investigations of capsizing questions often arise, such as:

- Did the vessel capsize due to wave action only?

- What was the stability condition in the capsizing situation?

- Did shifting of cargo or flooding occur?

- Was the vessel professionally operated with regard to external forces?

Questions like these are often difficult to answer due to insufficient attention to the operational aspects of stability. No precise guidance on appropriate operation is elaborated. Future studies could therefore be aimed at defining operational aspects of stability and to develope tools helping the operator to control and maintain a low probability of capsizing in practical life onboard a vessel.

2 EXTENDED STABILITY ASSESSMENT

Stability regulations should apply to:

- Vessel designers during the design process.

- Authorities as criteria for approval.

- The vessel operator as a tool for control of the vessel safety (risk of capsizing)

To achieve this, future stability regulations should contain three main elements as shown in Fig. 2.
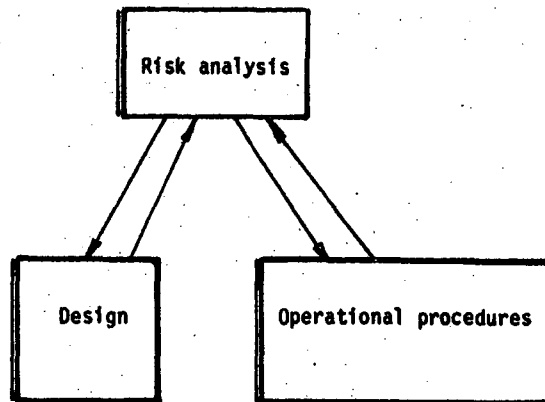
Fig. 2. Main elements in stability assessment.

2.1 Risk analysis

Risk analysis is the main tool to control the safety against capsizing.

The risk analysis can be based on experience, on a more thorough system analysis, or on a combination of both, Dahle and Myrhaug [3].

With notations used in strength considerations based on statistics, capsizing is the outcome of an event where the load or demand D (later described by the term "environment") has exceeded the capability of the vessels C (characterized by its "stability"). If environment and stability is described by probability densities, the capsizing event can be illustrated as shown in Fig. 3.
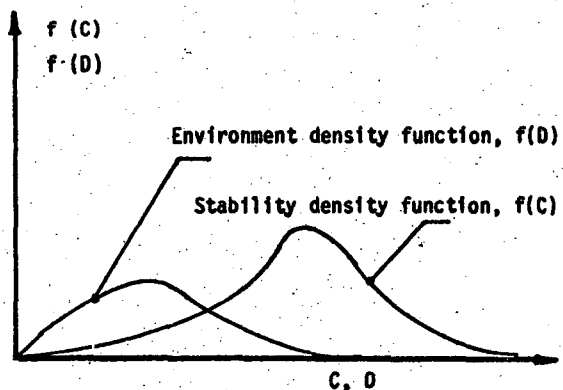

Fig. 3. Environment (D) and Stability (C) density functions.

The probability that D will exceed C, is expressed by:

$$P \ (C<D) = \int_0^{\infty} f(C) \cdot (\int_0^{D} f(D)dD) \cdot dC \qquad [1]$$

In Dahle and Myrhaug [3], Eq. [1] has been used with a simplified f(C)-function for a vessel in steep waves from the side. f(C) has been described in a deterministic manner with direct relation to wave height and steepness.

However, environment may act on the vessel in different ways, depending on how the vessel is operated, mainly through heading and speed. Also the stability characteristics may be influenced by the operator. This is illustrated in Fig. 4.
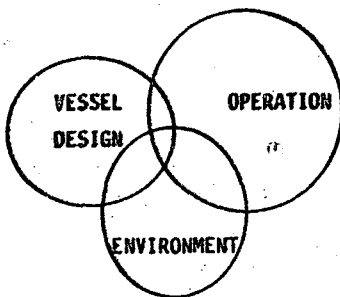
Figure 4 - Factors of safety.

Risk analysis has been carried out to some extent, e.g. assigning operational restrictions in the form of geographical limitations for smaller vessels. Hazards due to human factors (unreliability) have not yet been subject to extensive analysis.

Such hazards may be caused by:
- carelessness, negligence, use of intoxicants
- incomplete knowledge
- underestimation of own influence
- errors, mistakes
- relying upon others

The background factors can be:
- lack of motivation
- lack of education
- inadequate working environment
- deficient management system

The factors vary from one vessel to another. This is one of the reasons why probabilities are difficult to adopt for the human system.

3.2 Acceptance of a design

Minimum requirements should still be based upon traditional stability criteria. Such criteria are generally accepted and are based upon hydrostatics and weight calculations.

As indicated in Fig. 5, these minimum criteria should be connected to operational procedures in order to obtain an acceptable low risk of capsizing in the environment of the vessel.

This may result in more severe stability requirements if operational restrictions are not wanted. On the other hand, more relaxed stability requirements may apply if operational restrictions are acceptable for the intended service. However, human reliability must be taken into account in any case.
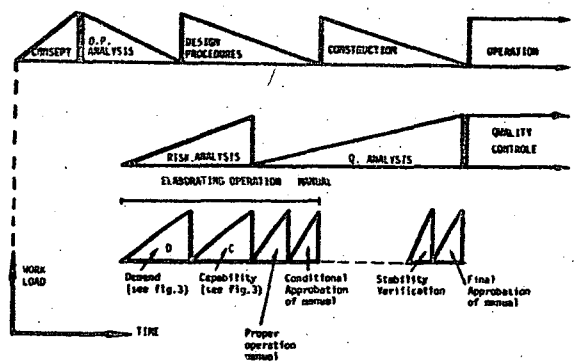
Fig. 5. Steps in elaborating an operational manual

3.3 Operation manuals

Operation manuals should be the future tool that combines the human-, the environmental- and the design factors in a total stability concept.

Systems of various kinds are often delivered with an operation manual where advice for safe operation is given.

For a vessel, an important part of the operational advice is today already given in the stability booklet. It can be considered a guide for acceptable loading conditions in regard to the traditional stability criteria.

However, this information is not related to environmental conditions. Furthermore, no advice is presently given as to how the probability of capsizing can be kept at a relatively low level.

The intention of an operation manual would therefore be:

A. To express the capability (C) of the vessel. The capability depends on the loading condition.

   In beam seas:
   - GZ-curves for different loading conditions.
   - The critical angle with regard to capsize, i.e. angle of vanishing stability ϕ_v (See Fig. 1b), or the angle of flooding, ϕ_f where large ingress of water takes place.
   - The intergral $E = \Delta \int_{0}^{\phi \ or \ \phi_f} GZ \cdot d\phi$, expressing the energy of the vessel to withstand wave impulse forces.
   - Influence of water on deck

   In following seas:
   - As for beam seas.
   - GZ-variations with a wave crest midships.
   - Wave speed and its relation to vessel speed.

B. To describe the environmental forces on the vessel (D) in
   - Beam seas
   - Following seas

C. To describe how the probability of capsizing can be minimized by correct operation, by
   - Improving the stability (C).
   - Operating the vessel in a way that minimize the environmental forces (D).
   - Combination of both.

D. To contain the contingency plan with regard to stability, including evacuation.

The operation manual should be:

- A most important document onboard a ship.

- A document that defines good seamanship in exposed situations.

- A document that incorporates all traditional stability information onboard a smaller vessel.

- A document that implicitly defines improper action possibly leading to accidents or capsizing and as such might be used by insurance companies or authorities.

Example of an operation manual outline is shown in Appendix 1.

3 CONLUSIONS

The stability assessment presented is based upon the following three elements:

a. Traditional codes and regulations.

b. Risk analysis.

c. Procedures and operation manuals.

The factor to be considered most important in future stability work is defined as "operational stability", expressed in operation manuals intended for the operator of the vessel.

An operation manual shall contain a description of

- the ability of the vessel to withstand environmental forces

- the environmental forces

- proper operation to minimize the probability of capsizing.

The manual should be simple and easy to read.

The manual should contain three parts, i.e:

Part 1. Mini-manual, an extract to be exhibited in the wheelhouse and in the messroom.

Part 2. The main manual, to be kept by the skipper/operator.

Part 3. Background material, on which the operating instructions are based, to be kept by the skipper.

Outline of the content is given in Appendix 1.

REFERENCES

1. "Mobile Platform Stability, Project Synthesis". MOPS Report no. 21. MARINTEK A/S 1985.

2. T. Nedrelid, Note on "Operational Manual Onboard a ship", An Introduction to a Discussion. MARINTEK A/S 1985.

3. E. Dahle, O. Myrhaug "Probability of Capsizing in Steep Waves from the Side in Deep Water". 3. Int. Conf. on Stab. and Ocean Vehicles. Gdansk, Sept. 1986.

4. E. Dahle and T. Nedrelid "Stability Criteria for Vessels Operating in a Seaway". 2. Int. Conf. on Stab. and Ocean Vehicles. Tokyo oct. 1982.

5. T. Nedrelid and E. Jullumstrø "The Norwegian Research Project "Stability and Safety for Vessels in Rough Weather". 3. Int. Conf. on Stab. and Ocean Vehicles Gdansk, Sept. 1986.

*) Dr.ing., Senior Principal Surveyor, DnV, Oslo, Norway.
**) Senior Research Engineer, MARINTEK, Trondheim, Norway.

APPENDIX 1.

Operation Manual.

1 MINI-MANUAL, A BRIEF EMERGENCY PART OF 2 - 3 PAGES.

- The mini-manual is meant to summarize in the form of checklists, important aspects of operational stability to prepare for an emergency situation. The first important action is to check the tightness of the vessel. All openings, doors and hatches must be checked to ensure that they are closed according to the tightness definition in the stability calculations.

- At full alert the mini-manual shall instruct on manoeuvres that minimize the risk of capsizing, actions to control the stability and to increase the stability.

- If the vessel is laying in stable side position, with accute danger of capsizing or flooding, special procedures should be followed. They will neccessarily depend on the reason for the inclination. If the situation does not improve rapidly, evacuation must be initiated.

- It should include instructions on how to operate and also on how to use the lifesaving equipment. Specified procedures should be followed when evacuating the vessel. No one should jump overboard in lifesaving suits except in extreme emergency situations.

- Corrective actions when exposed to shift of cargo, leakage or hull damage shall be described.

2. THE MAIN PART OF THE OPERATION MANUAL

- A technical specification of the vessel should be presented first in the manual. This should include all the main dimensions and drawings showing all compartments and openings. A weather tight vessel is the basic factor for all stability. The drawings and technical instructions should therefore define the weathertight compartments accounted for in the stability calculations. All openings leading into these compartments should be kept closed at sea.

- Traditional stability calculations should be incorporated in the manual. The manual should contain examples on how to calculate the vertical center of gravity (KG), the metacentric height (GM) and the righting lever curve (GZ).

- Traditional stability calculations should be incorporated in the manual. The manual should contain examples on how to calculate the vertical center of gravity (KG), the metacentric height (GM) and the righting lever curve (GZ).

- Control of the actual stability through GM should be presented by the Weiss formula

$$GM = (\frac{C \cdot B}{T})^2$$

where:

C = rolling coeffisient (values for different loading conditions given)

B = breadth of the vessel

T = rolling periode

- To judge the situation and make descisions for safety precautions is important. To decide the "degree of danger" one must observe or measure the motions, observe the weather, get weather forcast and information about exposed areas around the coast. The manual gives certain levels for critial parameters that define the situation as:

i   Normal operation.
    The vessel continues on course without any special action being taken.

ii Limited alert.
    The vessel continues the voyage eventually with reduced speed or change in heading. Control of all openings must be undertaken.

iii Full alert.
    The vessel shall be manoeuvered according to recommendations/instructions, giving a low risk of capsizing. Instructions/recommendations on how to improve the stability is given.

- Damage stability is an important aspect in a capsizing situation. Consequences of the most likely flooding situations should be calculated. These calculations should give guidance for action.

For the damaged vessel it is important to identify the compartments where leakage takes place. If the leakage cannot be controlled, the information in the manual giving ultimate draught, trim and stability should be consulted. This information must be seen in conjunction with the weather to try to assess if the vessel can survive with the damage (strength, stability etc.). Several actions can be taken, i.e. by closing openings, ballasting, remove heavy weights onboard, lower the speed and adjust the course to decrease rolling. Such relevant actions may be described.

- Use of certain devices and also some operations onboard should be adressed in the manual if they adversly might affect the stability. For a fishing vessel an example is the trawl, while crane operationes is an example for other vessels.

- Cargo handling is in general an important stability aspect. Shifting of cargo is often in focus when a cargo vessel capsizes. The manual should briefly present the principles for proper stowing and lashing for intended cargo. Special attention should be paid to dangerous cargo and cargo on deck.

- Alarm plans are normally exhibited onboard all vessels. In the manual, more detailed information on how to behave in an emergency situation should be given.

3 THE GENERAL INFORMATION PART OF THE OPERATION MANUAL.

Presenting the basic principles of stability in a simple way is an important chapter in the manual. The following main subjects should be presented:

- Definition of the righting lever

- Vertical center of gravity and the meta-centric height

- Compartments assumed tight in the stability calculations

- Free surface corrections

- The principles of how to improve the stability.

The vessel motion characteristics in waves and the dependence on the stability should be presented.

Experience from testing of similar types of vessels should be presented and dangerous situations should be pointed out. Advice on how to keep out of such situations should be given.

Cargo handling, should be presented. Advice on how to stow and lash cargo based upon experience should be listed. The possible consequence of shifting of cargo and dangerous near to capsizing situations should be described.

Wave and weather information is always important when making decisions on how to operate the vessel. This chapter will present the latest environmental data of interest to the operation of the vessel. Special attention will be paid to the occurence of breaking waves in certain coast areas.

In Norway, most of these areas are located. Dangerous waves only occure for certain wave heights and directions, and relevant information will be given in the manual for each area.

Third International Conference on Stability of Ships and Ocean Vehicles. Gdańsk, Sept. 1986

STAB'86

Paper 6.1

A PHENOMENON OF LARGE STEADY TILT OF A SEMI-SUBMERSIBLE PLATFORM IN COMBINED ENVIRONMENTAL LOADINGS

N. Takarada, T. Nakajima, R. Inoue

ABSTRACT

The authors make theoretical and experimental investigations on the stability of the moored semi-submersible platforms and point out that the existing intact stability criteria considering only unmoored platforms have not been sufficient to prevent the dangerous situations of the platforms in violent sea states.

Furthermore, a new computational approach for determining the required minimum $\overline{GM}$ ($\overline{GM}_r$) is proposed to avoid the significant larger inclination. This $\overline{GM}_r$ consists of the standard $\overline{GM}$ ($\overline{GM}_0$) and the several correction terms ($\Delta\overline{GM}$) which come from the effects of various kinds of environmental loadings and mooring tensions. The present approach is believed to be useful for designers as it is easily applied to many semi-submersible platforms for determining the adequate $\overline{GM}$.

1. INTRODUCTION

Many semi-submersible platforms have been built for the sake of their minimum motion characteristics in waves along with the ocean development represented by drilling of offshore oil. Stability of these platforms has been investigated for long, and the stability criteria have been established and improved by governmental organs and classification societies. However, most of them are based on the concept of the unmoored usual ships.

At Stability '82 Tokyo[1], the authors made clear that the influences of the mooring lines are to be taken into consideration and pointed out that the stability of semi-submersible platform should be investigated at moored condition by means of

experimental study.

In this paper, the authors attempt to discuss the above mentioned problems under single environmental load and various combined environmental loadings by means of simulation and experimental studies.

As a result of the investigation, the most important factor is keeping a small inclination angle in any cases to avoid the dangerous state of the platform. The $\overline{GM}$ value is stated by rules and regulations for the above purpose under single environmental load which is recognized as the most severe load. The authors approached to obtain required minimum $\overline{GM}$ value based on overturning moments and/or energies due to not only wind load but also wave exiting force and current force while keeping the degree of freedom of the design. The principal parameters such as dimentions, shapes and mooring points should be accounted as a correction of required minimum $\overline{GM}$ value.

2. WAVE-INDUCED HEELING MOMENTS

It has been already mentioned at Stability '82[1] that the wave-induced vertical steady force acting on the lower hulls is important for the stability of semi-submersible platforms in regular waves. In this chapter, the experimental results of the steady heeling moment due to waves are demonstrated with the theoretical ones.

2.1 The Model and the Outline of Experiment

The model of the semi-submersible platform is composed of the twin rectangular lower hulls and eight circular columns. The configuration and the princi-

Table 1 Principal particulars of the
semi-submersible platform

ITEMS		MODEL	FULL SCALE
LENGTH (overall)		1.700 m	102.0 m
BREADTH (overall)		1.160 m	69.6 m
HEIGHT to UP. DECK		0.670 m	40.2 m
LOWER HULL	LENGTH	1.700 m	102.0 m
	READTH	0.260 m	15.6 m
	HEIGHT	0.130 m	7.8 m
COLUMN No. - DIA.		4 - 0.20 m	4 - 12 m
		4 - 0.10 m	4 - 6 m
DRAFT		0.400 m	24.0 m
DISPLACEMENT		161.4 kg	35,730 ton
AIR GAP		0.200 m	12.0 m
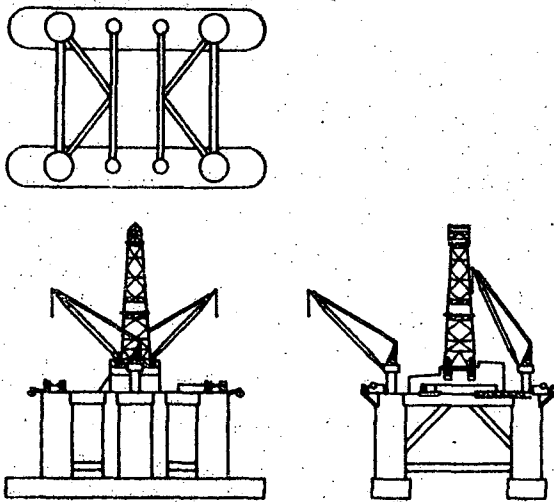
Fig. 1 Configuration of semi-
submersible platform

pal particulars of the model are shown in
Fig. 1 and Table 1, respectively.

The wave-induced heeling moment
is directly obtained from the balancing
of the righting moment assuming the follow-
ing matters.

1) The time averaged righting moment
   in waves is same as that in
   calm water and the wave-induced heel-
   ing moment and the righting moment are
   balanced at the steady tilt angle.

2) Since the magnitude of the wave-
   induced vertical steady force is some-
   what smaller, the change in draft due
   to this force is ignored.

The arrangement of the model test is
illustrated in Fig. 2.

2.2 Experimental Results of Wave-
Induced Heeling Moments
Fig. 3 shows an example of the steady

heeling moment as a function of steady tilt
angle with constant wave frequency. As
far as the steady tilt is in a range of
approximately ±12°, the steady heeling
moment varies nearly linearly. When the
steady tilt is in a range from the lee side
to about 5° on the weather side, it is the
moment to tilt to the lee side, while in
the case the steady tilt is over 5° on the
weather side, the moment to tilt to the
weather side is induced. The dominant
cause is considered to be the effect of the
wave-induced vertical steady force acting on
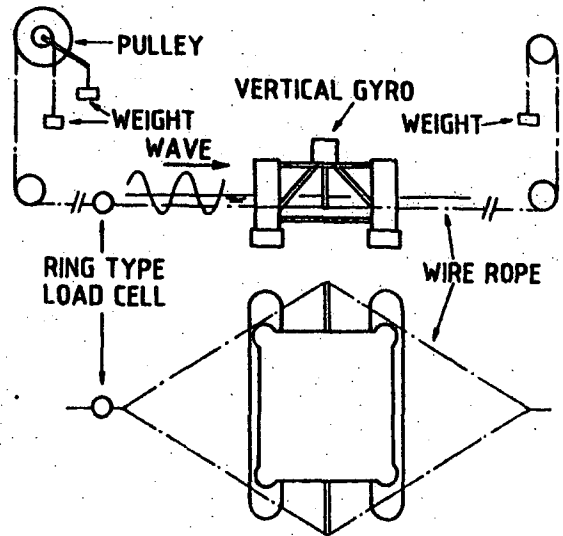
Fig. 2 Arrangement of the model test
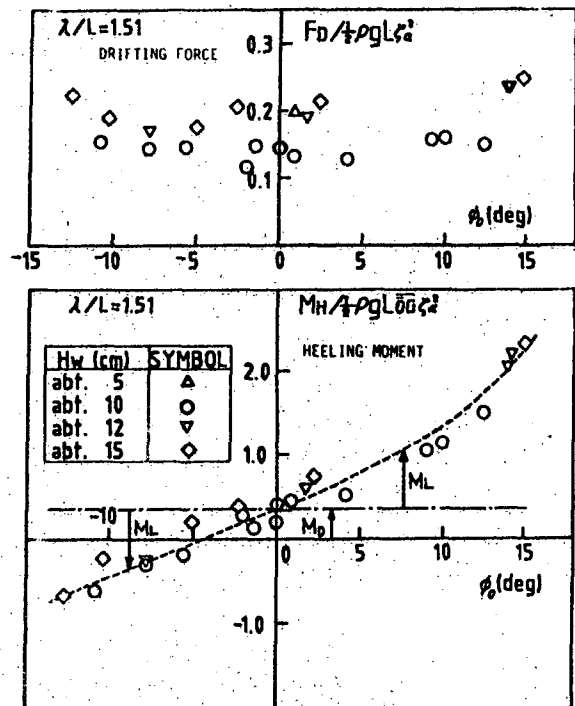
Fig. 3 Wave-induced steady heeling
moment influenced by steady
tilt angle

the lower hull and the hydrodynamic interaction.

In Fig. 3, the total steady heeling moment (M_H) of the waves acting on the semi-submersible platform is shown. Here, assuming the steady heeling moment in upright state to be M_D and that M_D may not be changed by the inclination of the platform since the wave drift force is nearly constant regardless of the steady tilt angle. The steady heeling moment due to the vertical steady force acting on the lower hulls (M_L) is obtained from the equation $M_L = M_H - M_D$. The rate of M_D and M_L is shown for reference in Fig. 3.
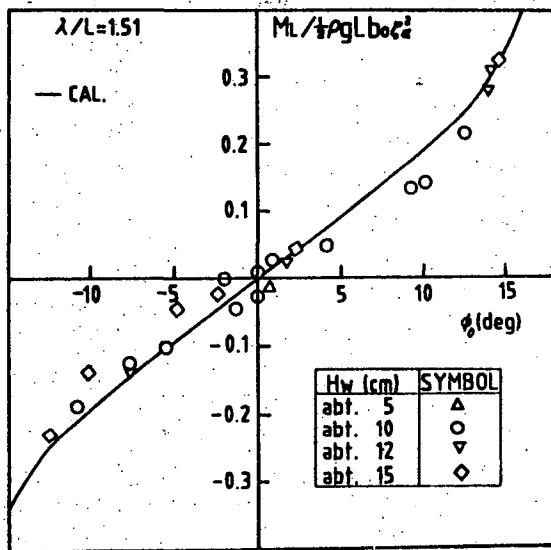
Fig. 4 Steady heeling moment induced by vertical steady force on lower hulls
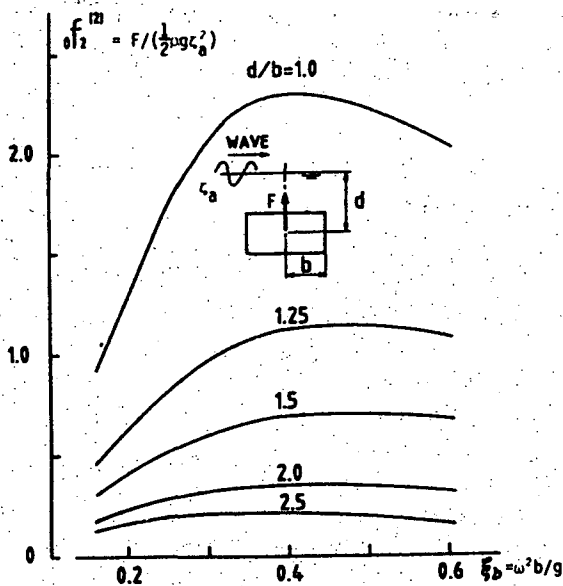
Fig. 5 Calculated results of wave-induced vertical steady force on lower hull section

The comparison between the value of M_L thus assumed and the calculated value is shown in Fig. 4. The calculated results of the wave-induced vertical steady forces on the rectangular section which are obtained from Ref. 6 are used for the estimation of the steady heeling moment (M_L) (See Fig. 5). Here, the calculated value in the fixed condition is obtained, by subtracting the connecting portions of the columns from the overall length of the lower hulls. The calculated values and experimental results coincided with each other fairly well.

2.3 Mechanism of Larger Steady Tilt

Since the steady heeling moment has been confirmed to be a dominant factor for steady tilt as a result of experiment, it is now attempted to interpret larger tilt in waves by this factor. The graphical illustrations of larger tilt are shown in Fig. 6.

Fig. 6(a) shows the case that the platform in the upright state in calm water tilts about 12° on the lee side due to the steady heeling moment in regular waves of $\lambda/L = 1.21$ and 15 cm height. When same waves approach in the state of initial tilt of about 5° on the weather side, the platform is restored to the upright state.

In Fig. 6(b), it is shown that when the changing rate of righting moment and steady heeling moment with respect to the tilt angle become close to each other, the balanced steady tilt angle varies significantly by a small difference in the initial tilt. Accordingly, to reduce the steady tilt by counter moment, a delicate adjustment is necessary, and any small misoperation will not be allowed. In Fig. 6(c), it is shown that the steady tilt increases with wave height and also that the steady tilt angle varies with the change in the wave height.

Fig. 6(d) shows the case that the platform is unstable at the small tilt angle when the changing rate of the steady heeling moment is greater than that of the righting moment. In such case, the platform tilts largely until the righting moment exceeds the steady heeling moment and may capsize unless the changing rate of the righting moment increases more. Therefore, the spare buoyancy of the upper deck might be important in this case.
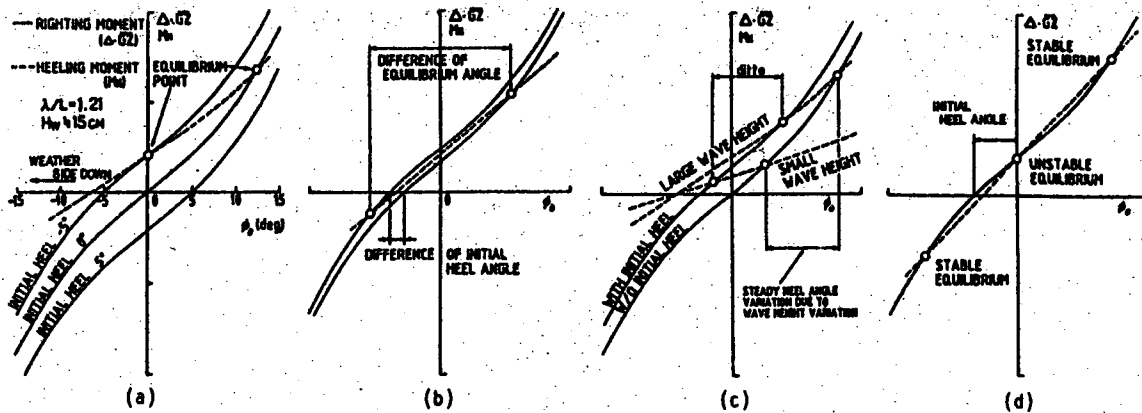
Fig. 6 Graphical illustrations explaining phenomena of large tilt angle
and unstable behavior due to wave action

2.4 Steady Tilt in Regular Waves

Fig. 7 illustrates both experimental and simulated results of the steady tilts due to the differences in height of the moored point presented at Stability '82[1]. In the figure, Cal (A) indicates the simulated results including the steady heeling moment in the upright condition (M_D) and the steady heeling moment due to the vertical steady force acting on the lower hulls (M_L), while the latter is omitted in Cal (B). From this figure, it is found that the results ignoring the steady heeling moment due to the vertical steady force on lower hulls cannot estimate the observed steady tilt in the experiment.

In the same figure, the experimental results using the model with skeletal structure of the upper deck are also plotted in blank marks. In this case, the effects of greenwater could be minimized. No apparent difference was found in the steady tilt even in the greenwater range.

Thus, from the comparison between experimental and simulated results, whether the greenwater is present or not, it is concluded that the steady heeling moment due to the vertical steady force acting on the lower hulls cannot be disregarded to estimate the steady tilt in waves.

3. DYNAMIC BEHAVIORS OF THE MOORED PLATFORM BY THE NUMERICAL SIMULATION

The mathematical expression of the numerical simulation and some simulated results with experimental records are demonstrated in this chapter. The present simulation is used in this paper as the computational tool for estimating the dynamic behaviors of the semi-submersible platform.

3.1 Equations of Motion

The motions of the platform treated here are the non-linear motions of three degrees of freedom in beam waves (sway, heave and roll). The finite difference method (Newmark-β method) is used to solve the coupled equations of motion in time domain. The principal assumptions are made as follows:

1) Although relatively higher wave is considered, only linear wave with the effect of water depth is treated and the wave breaking is ignored.

2) Although the larger steady tilt angle is taken into consideration in the equations, it is assumed that the lower hulls do not come out from the water and/or the upper deck does not touch the wave.

The frame of reference for platform behaviors is a right-handed Cartesian coordinate system originating at the center


Fig. 7 Steady tilt under mooring condition (Wave height = 25 cm)
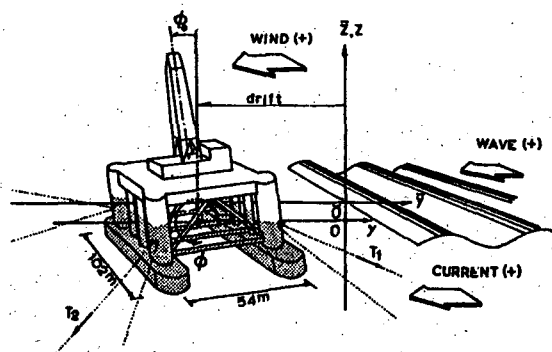
Fig. 8 Coordinate systems of the platform

of gravity of the platform (See Fig. 8).
The equations of platform motion are as
follows:

$$(M+A_{yy})\ddot{y}(t)+A_{yz}\cdot\ddot{z}(t)+A_{y\phi}\cdot\ddot{\phi}(t)+\kappa_{yy}(\dot{y},t)$$

$$+\kappa_{yz}(\dot{z},t)+\kappa_{y\phi}(\dot{\phi},t)+\frac{1}{2}\rho\sum_m C_{dym}\cdot\bar{A}_{ym}\cdot|\dot{y}(t)$$

$$-\bar{z}_m\cdot\dot{\phi}(t)-\dot{\xi}_m(t)-V_c\,|\cdot\{\dot{y}(t)-\bar{z}_m\cdot\dot{\phi}(t)-\dot{\xi}_m(t)-V_c\}$$

$$+\sum_k T_{yk}$$

$$=F_y(t)+\bar{F}_{yD}+F_{wy} \qquad (1)$$

$$(M+A_{zz})\ddot{z}(t)+A_{zy}\cdot\ddot{y}(t)+A_{z\phi}\cdot\ddot{\phi}(t)+\kappa_{zz}(\dot{z},t)$$

$$+\kappa_{zy}(\dot{y},t)+\kappa_{z\phi}(\dot{\phi},t)+\frac{1}{2}\rho\sum_m C_{dzm}\cdot\bar{A}_{zm}|\dot{z}(t)$$

$$+\bar{y}_m\cdot\dot{\phi}(t)-\dot{\zeta}_m(t)\,|\cdot\{\dot{z}(t)+\bar{y}_m\cdot\dot{\phi}(t)-\dot{\zeta}_m(t)\}$$

$$+C_{zz}\cdot z(t)+C_{z\phi}\cdot\phi(t)-\sum_k T_{zk}$$

$$=F_z(t)+\sum_m\bar{F}_{zDm}+F_{wz} \qquad (2)$$

$$(I_\phi+A_{\phi\phi})\ddot{\phi}(t)+A_{\phi y}\cdot\ddot{y}(t)+A_{\phi z}\cdot\ddot{z}(t)+\kappa_{\phi\phi}(\dot{\phi},t)$$

$$+\kappa_{\phi y}(\dot{y},t)+\kappa_{\phi z}(\dot{z},t)-\frac{1}{2}\rho\sum_m C_{dym}\cdot\bar{A}_{ym}\cdot\bar{z}_m$$

$$\cdot|\dot{y}(t)-\bar{z}_m\cdot\dot{\phi}(t)-\dot{\xi}_m(t)-V_c|\cdot\{\dot{y}(t)-\bar{z}_m\cdot\dot{\phi}(t)-\dot{\xi}_m(t)$$

$$-V_c\}+\frac{1}{2}\rho\sum_m C_{dzm}\cdot\bar{A}_{zm}\cdot\bar{y}_m\cdot|\dot{z}(t)+\bar{y}_m\cdot\dot{\phi}(t)-\dot{\zeta}_m(t)\,|$$

$$\cdot\{\dot{z}(t)+\bar{y}_m\cdot\dot{\phi}(t)-\dot{\zeta}_m(t)\}+\ell_{GZ}\cdot M\cdot\rho\cdot g$$

$$+C_{\phi z}\cdot z(t)-\sum_k(T_{yk}\cdot\bar{z}_k+T_{zk}\cdot\bar{y}_k)$$

$$=F_\phi(t)+\bar{F}_{\phi D}+\sum_m\bar{F}_{zDm}\cdot\bar{y}_m+F_{w\phi} \qquad (3)$$

where

M,I_ϕ: basic mass and moment of iner-
tia of the platform

A_{rs},C_{rs}: added mass and restoring
coefficient in r direction
due to the motion s

ρ : density of water

C_{dym},C_{dzm}: drag coefficients in y and z
directions

$\dot{\xi}_m(t)$,$\dot{\zeta}_m(t)$: wave particle velocities at the
element m in y and z directions

$\bar{A}_{ym}$,$\bar{A}_{zm}$: projected areas of the element
m in y and z directions

T_{yk},T_{zk}: mooring tensions in y and z
directions

$\bar{y}_m$,$\bar{z}_m$: moment lever arms for the
element m in y and z directions

ℓ_{GZ}: horizontal distance between CB
and CG

$\kappa_{rs}(\dot{s},t)$: term including the memory
effect function $K_{rsm}(t)$ in
r direction

$$(=\sum_m\int_0^t K_{rsm}(t-\tau)\dot{s}(\tau)d\tau)$$

(See Ref. 13)

$F_r(t)$,$\bar{F}_{rD}$: first and second order wave
force or moment in r direction

F_{wr}: wind force or moment in
r direction

V_c: current velocity

The hydrodynamic coefficients and the
wave excitation used in the equations above
are calculated by the singularity method,
while the second order forces and moments
due to wave are obtained from the experi-
ment. The drag and lift forces on the model
due to wind and current are estimated by
using the results of wind tunnel test and
towing test in the basin[7]. The catenary
equation is used to estimate the mooring
force in time domain.

3.2 Time Domain Simulation of the Platform Behaviors in Current and Wave

To verify the numerical simulation, some
calculated results of the platform behaviors
and the mooring tensions are compared with
the experimental records in time domain. In
the tank test the model of the semi-submersi-
ble platform which is described in the previ-
ous chapter is positioned by eight spread
mooring lines (each length is about 11.2 m
and the pre-tension is about 0.4 kgf) at
the 2.5 m water depth.

First, the horizontal excursion, steady
tilt and the mooring tension are simulated
in current and are shown in Fig. 9. In the
simulation, the current velocity obtained
in the experimental record is approximated
by a straight line for the sake of simplic-
ity of calculation. From this comparison,
the simulated results coincide fairly well
with the experimental ones. Another com-
parison between the experimental record in
current with regular wave and its time-
history obtained by the numerical simula-
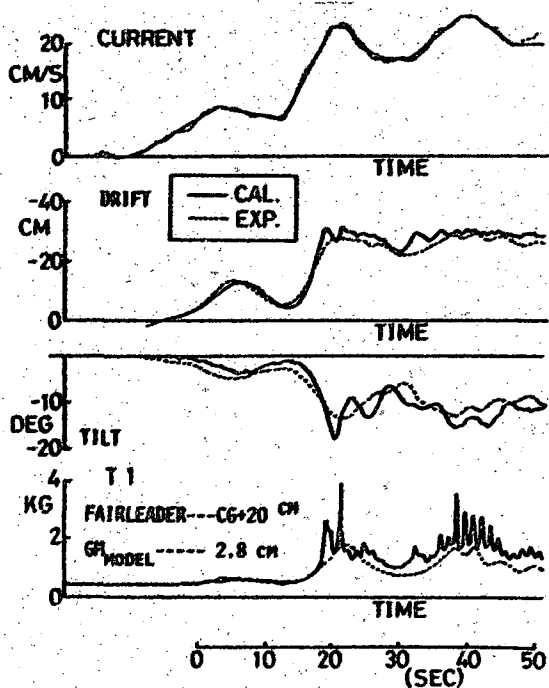
Fig. 9 Comparison of the semi-submersible
platform motions in current
between experiment and simulation

tion is shown in Fig. 10. Here, the moored
position on the model is 20 cm above the
height of the center of gravity and the wave
height is about 25 cm. Again, the behavior
of the semi-submersible platform can be
estimated fairly satisfactorily by the
numerical simulation.

4. SIMULATION ON THE STABILITY OF THE
SEMI-SUBMERSIBLE PLATFORM

In this chapter, it is shown that the
semi-submersible platform satisfying the
stability rules involves a possibility of
leading the dangerous state by means of the
numerical simulation.

4.1 Platform Configuration and the
Requirements of the Existing Rules

The semi-submersible platform discussed
here is a structure composed of twin lower
hulls and eight columns, of which configura-
tion and principal particulars are shown in
Fig. 1 and Table 1, respectively.

First, let us set the minimum $\overline{GM}$ value
of the platform to satisfy the existing
rules. The existing rules relating to in-
tact stability of semi-submersible platforms
are roughly classified into two categories
as shown in Table 2 according to the requi-
rements. One is the rule represented by
ABS and NK, which defined the $\overline{GM}$ value and
safety factor of righting energy with
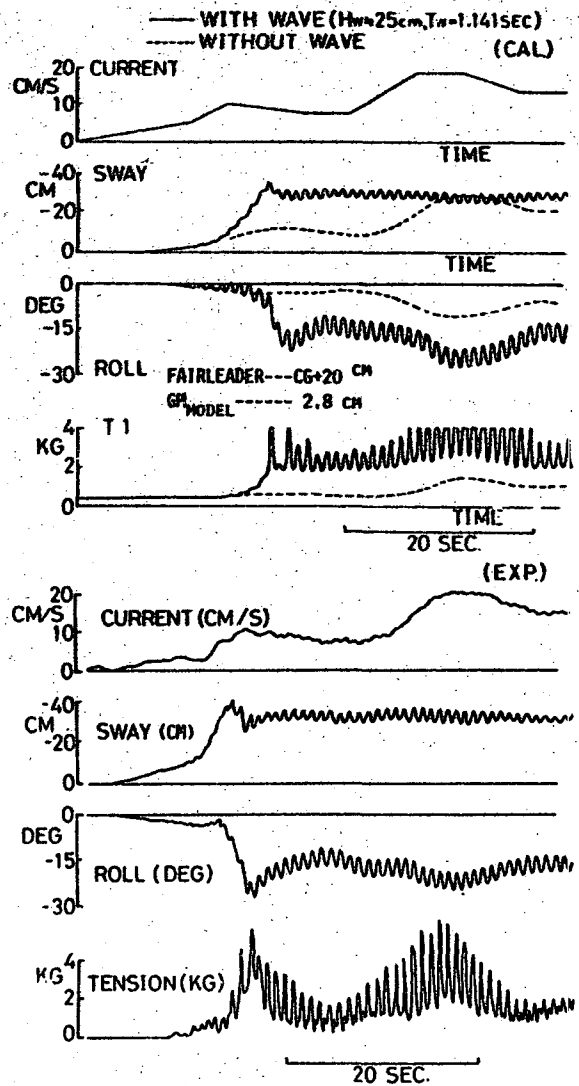
Fig. 10 Comparison of the semi-submersible
platform motions in current
with/without wave between experi-
ment and simulation

Table 2 Intact stability for semi-
submersible platforms required
by classification societies

Fig. 11 Intact stability of assumed semi-
submersible platform

respect to the wind heeling energy. The
other is the rule by DnV(or NMD), which
defines, besides the above, the first and
second interception angle of the heeling
moment and righting moment. Furthermore,
between the above two rules, the handling
of righting moment at the inclination angle
exceeding the flooding angle is different.

Next, the wind heeling moment curve,
the righting moment curve and the flooding
angle are necessary to establish the state
which satisfies both stability rules
mentioned above. The wind heeling moment
curve is estimated from the results of the
wind tunnel test shown in the report of the
panel SR-192[7]. The righting moment curve
of the platform is determined by the calcu-
lation. The flooding angle is assumed to
be the angle at which the upper deck end of
the platform comes to the calm water level
(approx. 25°). These results are shown in
Fig. 11. Hence, the minimum $\overline{GM}$ in which
the safety factor of righting energy satis-
fies the rule is 1.4 m. This value is found
to satisfy the ABS rule of $\overline{GM} \geq 0$, DnV rule of
$\overline{GM} \geq 1.0$ m and the first interception angle
$\theta_1 \leq 15°$. However, whether it satisfies the
DnV rule relating to the safety factor of
righting energy considering the loss of
buoyancy due to the flooding water from the
opening up to the second interception angle
θ_2 and $\theta_2 \geq 30°$ or not cannot be evaluated
unless the subdivisions in the upper
structure are known. Here, it is assumed
that these rules be also satisfied in the
state of $\overline{GM} = 1.4$ m.

4.2 Simulations of the Platform Behaviors

When the same platform in the basic

state as set above is moored with a pre-
tension of about 90 tons in the 150 m water
depth, whether dangerous state leading to
capsizing is induced or not is studied by
the numerical simulation of the platform's
behaviors. Here, dangerous states are de-
fined as follows.

(1) Time averaged tilting angle (steady
tilt angle) exceeds 15°.

(2) Wave crest reaches the bottom of the
upper deck.

Relating to state (1), as the DnV rule
limits the static balance angle of the
heeling moment and the righting moment under
15°, it is defined dangerous when the steady
tilt is greater than a certain angle. Here,
the "certain angle" is defined as 15° after
the DnV rule.

The state (2) is also dangerous for the
platform, because the wave crest hits
the bottom of the upper deck directly.
If this condition is further intensified,
the sea water begins to ride on the upper
deck, and wave may invade from the openings,
or the upper main structure, fittings and
materials aboard may be damaged. Two possi-
bilities may be considered as such dangerous
state of (2):

(a) Large relative vertical motion occurs
in the long wave period region; or

(b) Large steady tilt occurs in the short
wave period region with the relative
vertical motion.

In the case of (a), the waves having
long period close to the heave reasonance of
the semi-submersible platform are not consi-
dered to be serious, because the period of
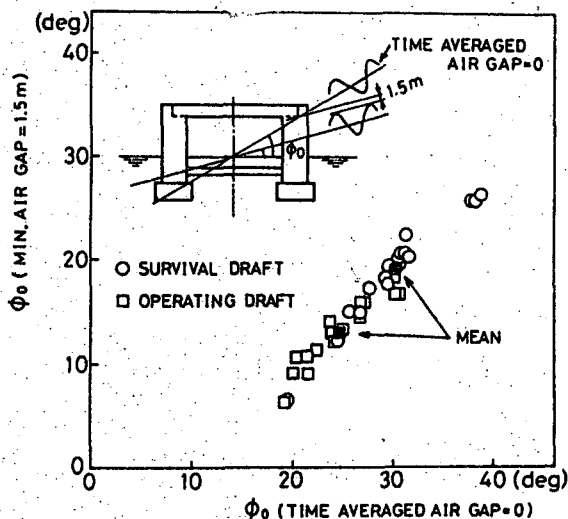
Fig. 12 Steady tilt angle where minimum
air gap is equal to 1.5 m
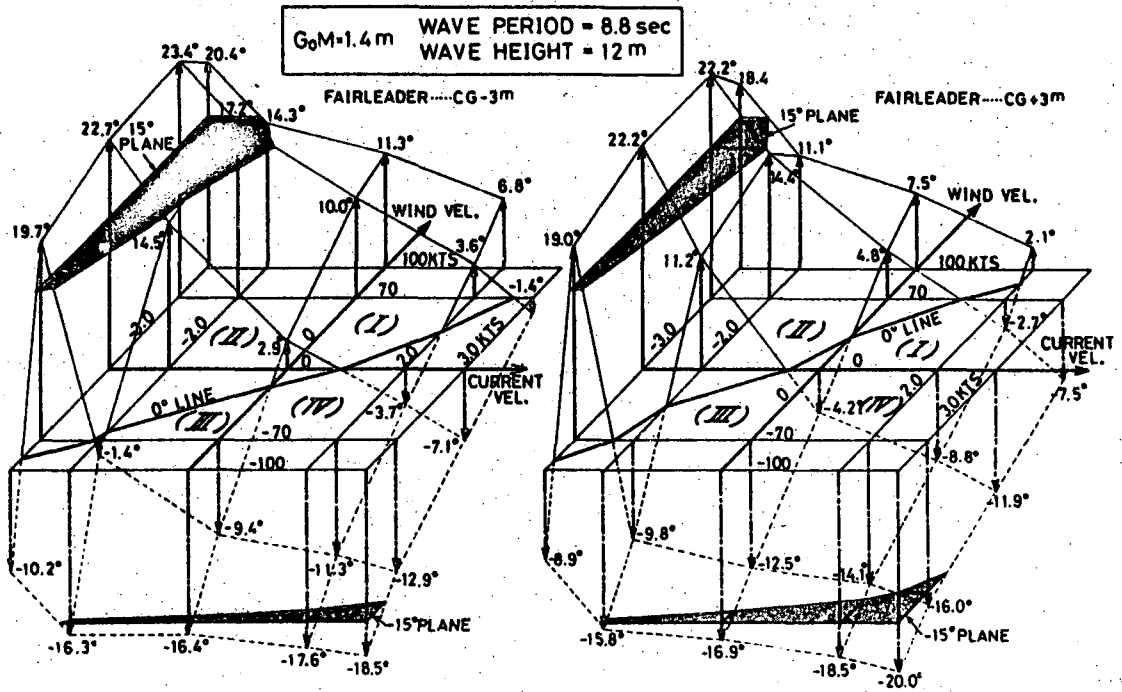
Fig. 13 Simulated results of steady tilt in wave, winds and currents

the heave reasonance is usually over 20 sec. and the waves over 20 sec. period are not considered in the DnV rule.

Fig. 12 shows the inclinations of the existing semi-submersible platform which airgap become 1.5 m at the edge of the deck in the regular wave having 10 sec. period ($H_w/\lambda = 1/10$). The abscissa indicates the angle where the time averaged airgap becomes zero. According to the figure, the average of the steady tilt angle between operating and survival conditions is approximately 16° which is somewhat larger than that in the state (1). Consequently, the state (1) comes first rather than the state (2) in the condition of short period waves in general.

In order to verify the safety of the platform, steady tilts in the basic condition are simulated under a combined loadings of wind (0, 70 and 100 knots), current (0, 2 and 3 knots) and the regular wave (height = 12 m, period = 8.8 sec.).

In Fig. 13, the positive direction of wind or current is defined same as that of wave while the inclination of the platform to the lee side is positive. When the plane which contains the axes of wind and current velocities is divided into four quadrants as shown in the figure, the dangerous state in which the steady tilt exceeds ±15° is found in the quadrants II, III and IV. In the quadrant III (in which both wind and current are reverse to wave direction),
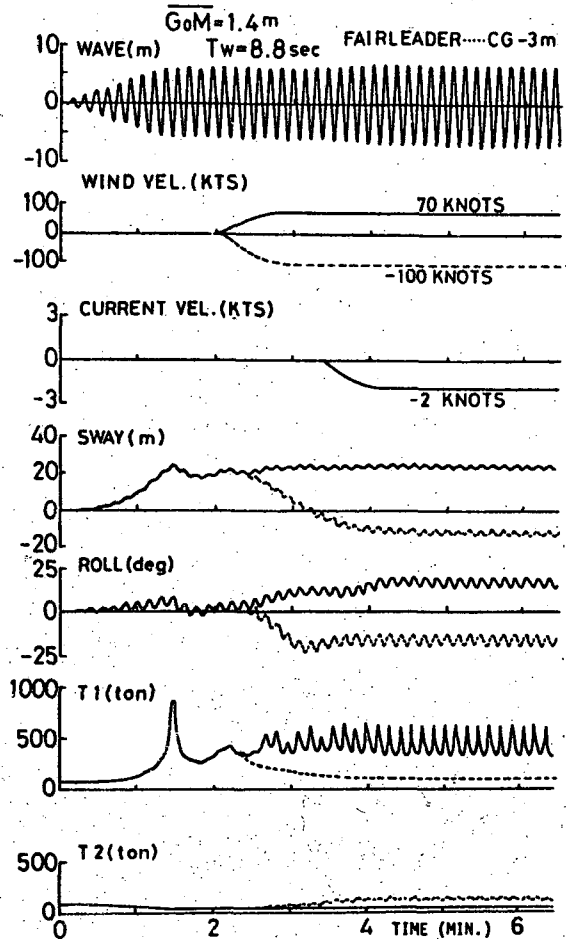

Fig. 14 Examples of records of simulation

the curved surface showing the steady tilt is extremely sharp, which indicates that the magnitude and direction of steady tilt are changed drastically by a slight difference in the wind and current velocities. On the other hand, although the steady tilt is somewhat smaller in the quadrant I (in which both wind and current are in the same direction as waves), it may give rise to the risk of breaking of the mooring line since all forces act in the same direction.

Fig. 14 shows examples of the simulated records in time domain in the quadrants II and III.

5. SOME PROBLEMS ON THE EXISTING RULES

It is now found that even the state satisfying the existing rules involves a possibility of leading to capsizing of the semi-submersible platform. This is because, as the authors have reported previously [1], the existing rules are based on the concept of the stability criteria for usual ships, assuming a free floating state considering only the wind effect as the external force.

In the existing rules, current is not treated while the dynamic effects on the stability due to wave action and platform motions are considered to be involved in the safety factor of the righting energy. However, in the case of a semi-submersible platform, it is usually moored for the purpose of its work, and the horizontal excursion is restricted by the mooring lines, so that the current and steady wave forces and the mooring force as its reaction must be taken into consideration in addition to the wind force.

Concerning with the steady wave force, importance of the heeling moment due to the vertical steady force acting on the lower hulls has been pointed out for long by authors[1] and et al.[4][5]. It has been also pointed out that the moored position (fairleader position) on the platform also takes important part in the overturning moment due to the mooring reaction.

In the moored condition, the short period wave (even though the height is not so high) might be serious rather than the long period and highest wave which is generally used for the design storm wave.

6. DESIGN APPROACH OF THE REQUIRED MINIMUM $\overline{GM}$ METHOD

6.1 The Required Minimum $\overline{GM}$ Value

In order to avoid the dangerous state of the platform, it is useful to be able to determine the required minimum $\overline{GM}$ ($\overline{GM}_r$) value to keep the steady tilt within a permissible limit angle in the simultaneous existence of all possible environmental forces. Based on this concept, a new practical method of estimating the $\overline{GM}$ value is presented.

In addition to the assumption as wall sided vessel (in the case of a semi-submersible platform, the column is vertical to the water surface), the following assumptions are made.
1) The steady forces in the vertical direction are small, and there is no draft change.
2) The time averaged righting moment in waves is same as that in calm water.
3) The lower hull does not come out from the water level in inclined state and/ or airgap does not become zero.

The required minimum $\overline{GM}$ value is determined in the following equations from Appendix A. Here, $\overline{KG}$ contains elevation of the center of gravity due to snowfall and/or icing on the upper deck.

$$\overline{GM}_r(\emptyset_0)=\overline{GM}_0(\emptyset_0)+\sum_{i=1}^{k}\Delta\overline{GM}_i(\emptyset_0) \qquad (4)$$

where

$$\overline{GM}_0(\emptyset_0)=\{\overline{M}_0(\emptyset_0)/W\}F(\emptyset_0)-(\overline{BM}/2)G(\emptyset_0) \qquad (5)$$

$$\Delta\overline{GM}_i(\emptyset_0)=\{\overline{M}_i(\emptyset_0)/W\}F(\emptyset_0) \qquad (6)$$

W : displacement

The $\overline{GM}_r$ value is determined by the static righting lever from the equilibrium of the heeling moment and the righting moment, or by the dynamic righting lever from the equilibrium of the heeling energy and the righting energy. $\overline{M}_i(\emptyset_0)$, $F(\emptyset_0)$ and $G(\emptyset_0)$ are expressed as follows:

	[Static righting lever] Heeling moment	[Dynamic righting lever] Heeling energy
$\overline{M}_i(\emptyset_0)$:	$M_i(\emptyset_0)$	$\int_0^{\emptyset_0}M_i(\emptyset)d\emptyset$
$F(\emptyset_0)$:	$1/\sin\emptyset_0$	$1/(1-\cos\emptyset_0)$
$G(\emptyset_0)$:	$\tan^2\emptyset_0$	$(1-\cos\emptyset_0)/\cos\emptyset_0$

$$(7)$$

Accordingly, the $\overline{GM}_r$ value may be considered as the sum of $\overline{GM}_0$ corresponding to

the reference heeling moment (or heeling energy) and the corrected value $\Delta\overline{GM}_i$ corresponding to the other heeling moment (or heeling energy).

(1) Minimum $\overline{GM}$ value with respect to wind

Practically, it is convenient to select the reference force and its direction, first. Here, the wind force is considered as the reference force since it has been generally regarded to be the most important and has been treated as the main force in the rules of classification societies. Therefore, the first term of the right side of Eq. (4) becomes as follows:

$$\overline{GM}_0(\emptyset_0)=\overline{GM}_{wind}(\emptyset_0)$$
$$=\{\overline{M}_w(\emptyset_0)/W\}F(\emptyset_0)-(\overline{BM}/2)G(\emptyset_0) \qquad (8)$$

where $\overline{M}_w(\emptyset_0)$ is the heeling moment or energy due to wind. Besides, the safety factor (C_w) used in the rules can be taken into consideration by the multiplication of the wind heeling energy by 1.3.

(2) The corrected value ΔGM_i

Since the wind force is selected as the reference force according to the $\overline{GM}_0$ value, the corrected value $\Delta\overline{GM}_i$ must be obtained from the other external forces. The corrected value $\Delta\overline{GM}_i$ is determined in Eq. (6) and the following items are considered as the other forces.

i	$\overline{M}_i(\emptyset_0)$	item
1	$\overline{M}_1(\emptyset_0)$:	due to current
2	$\overline{M}_2(\emptyset_0)$:	due to wave-induced steady heeling moment in upright state
3	$\overline{M}_3(\emptyset_0)$:	due to wave-induced vertical steady force acting on lower hulls
4	$\overline{M}_4(\emptyset_0)$:	due to mooring reaction

If there are other items to be considered, they may be added as required.

(a) $\overline{M}_1(\emptyset_0)$

To estimate $M_1(\emptyset)$ due to current, it is necessary to include the hydrodynamic interference effects of wave.

(b) $\overline{M}_2(\emptyset_0)$

Also as for the steady heeling moments $M_2(\emptyset)$ and $M_3(\emptyset)$ due to waves, interference effects of current must be taken into consideration.

It seems reasonable to consider $M_2(\emptyset)$ as the product of the wave drifting force and the distance of its point of action from the center of gravity.

(c) $\overline{M}_3(\emptyset_0)$

As mentioned in the second chapter, $M_3(\emptyset)$ is an indispensable item when the steady tilt of semi-submersible platform is concerned. Strict computation of the wave-induced steady force F_L is introduced in Ref. 6. When the submergence of the lower hull is relatively deep, the approximate value may be obtained by the formula for the circular cylinder given by Ogilvie[2]

$$F_L=4\pi e^{-2kz_0}(ka)I_1(2ka)\cdot f_0 \qquad (9)$$

or the approximate formula for the cylinder of arbitrary section given by Lee-Newman[3]

$$F_L=k^2e^{-2kz_0}S_A(2+m_{11}+m_{22})\cdot f_0 \qquad (10)$$

where $f_0 = \rho gL\zeta_a^2/2$
I_1: modified Bessel function
k : wave number
ζ_a: wave amplitude
L : length of lower hull
z_0: submerged depth of lower hull
a : radius of circular cylinder
S_A: sectional area of lower hull
m_{11},m_{22}: added mass coefficients in sway and heave in unbounded fluid

Whence, referring to Fig. 15, $M_3(\emptyset)$ is obtained from the following equation.

$$M_3(\emptyset)=(F_{L_1}-F_{L_2})b_0\cos\emptyset+(F_{L_1}+F_{L_2})h_0\sin\emptyset$$
$$(11)$$

The effect of submerged depth on F_L is given as $\exp(-2kz_0)$ as shown in Eqs. (9) and (10), and when the steady tilt angle is small, the corrected value $\Delta\overline{GM}_3$ corresponding to static righting lever may be approximated from Appendix B and Eq. (6) as follows:
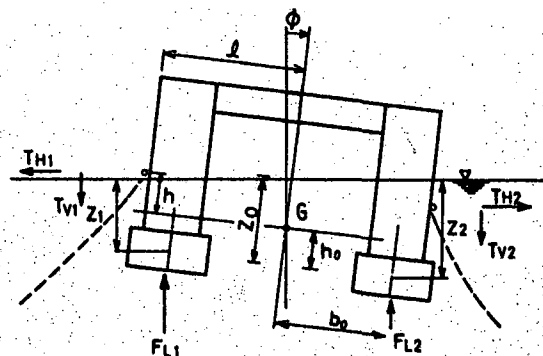

Fig. 15 Wave-induced vertical steady force on lower hulls and resultant mooring forces

$$\Delta \overline{GM}_3 = F_L \cdot (4kb_0{}^2 + 2h_0)/W \qquad (12)$$

This coincides with the $\overline{GM}$ computational formula by Numata et al[4].

(d) $\overline{M}_4 (\emptyset_0)$

The heeling moment due to mooring reaction $M_4 (\emptyset)$ is determined in the following equation (see Fig. 15).

$$M_4 (\emptyset) = (T_{H_2} - T_{H_1}) h \cos\emptyset - (T_{H_1} + T_{H_2}) \ell \sin\emptyset$$
$$+ (T_{V_1} + T_{V_2}) h \sin\emptyset - (T_{V_1} - T_{V_2}) \ell \cos\emptyset$$
$$(13)$$

6.2 Application of the Required Minimum $\overline{GM}$ Method

In Chapter 4, it was shown by the numerical simulation that the semi-submersible platform satisfying the requirements of the existing rules may tilt more than 15° and may fall into the dangerous state in the combined environmental loadings. Here, the present Required Minimum $\overline{GM}$ Method is applied to the same platform to find the minimum $\overline{GM}$ value from the aspect of the safety of the platform in the combined environmental loadings. The dangerous environmental condition is assumed to be the sum of 70 knots wind, -2 knots current and regular wave having 12 m in height and 8.8 sec. in period while the moored position on the platform is assumed to be 3 m lower than the height of center of gravity (CG - 3 m).

From Fig. 13 the steady tilt angle results as 17.2° in the above environmental condition.
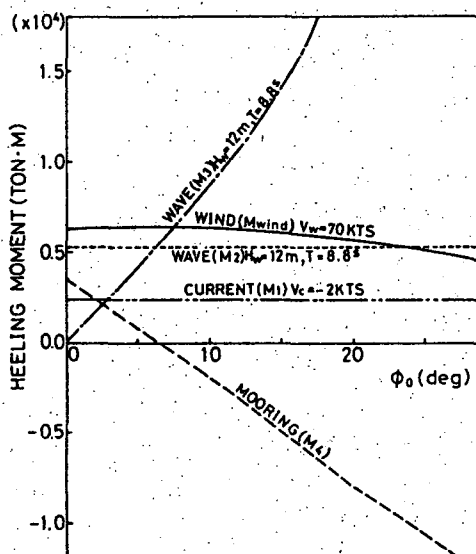
Fig. 16 Heeling moments due to various kinds of loadings
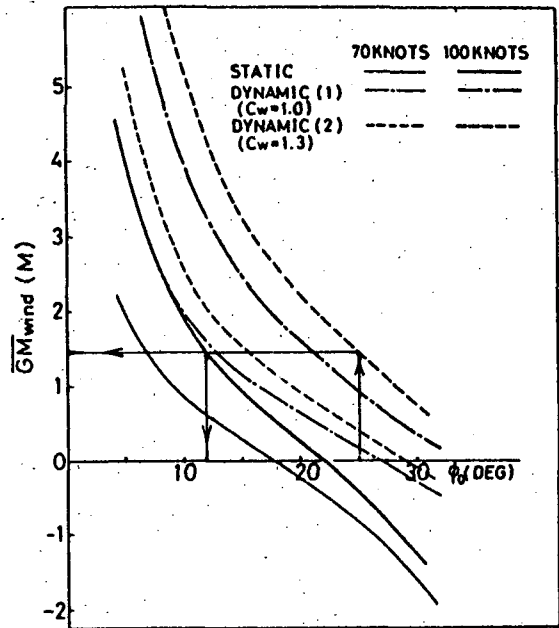
Fig. 17 Standard $\overline{GM}$ ($\overline{GM}_{wind}$) distributions against platform's steady tilt

First of all, the steady heeling moments acting on the platform under the above condition are calculated against the allowable tilt angle and are shown in Fig. 16. In Fig. 17, the minimum $\overline{GM}$ values ($\overline{GM}_{wind}$) corresponding to both static and dynamic righting levers regarding the wind heeling moment are plotted against the allowable tilt angle. In this figure, the broken lines refer to the results of the safety factor C_w of 1.3 which indicate the minimum $\overline{GM}$ value to safisfy the existing rules. Taking the allowable tile angle is 25° and the safety factor Cw is 1.3, the minimum $\overline{GM}$ value is found to be 1.4 m in survival condition (100 knots wind) from Fig. 17. According to the solid line in the same figure, the corresponding static balancing angle results as approximately 12°, which coincides with the results in Fig. 11.

The values of $\overline{GM}_r$ corresponding to static and dynamic righting levers under the same combined environmental loadings are shown in Figs. 18 and 19, respectively. However, the safety factor Cw of dynamic righting lever is defined as 1.0. When the allowable tilt angle is selected as 15°, after Chapter 2, the values of $\overline{GM}_r$ corresponding to the static and the dynamic righting levers results as about 1.9 m and 4.2 m, respectively. Among the corrected value $\Delta\overline{GM}_i$, $\Delta\overline{GM}_3$ keeps nearly constant regardless of changes in the tilt angle, and its value is also somewhat large
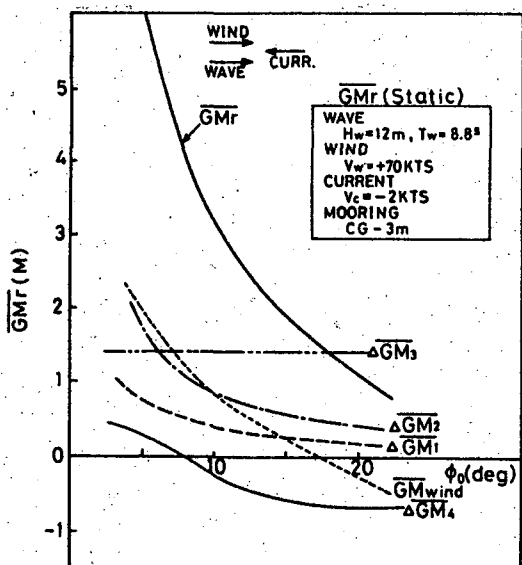
Fig. 18 Required minimum $\overline{GM}$ ($\overline{GM}_r$) obtained
by various kinds of loadings
(STATIC)
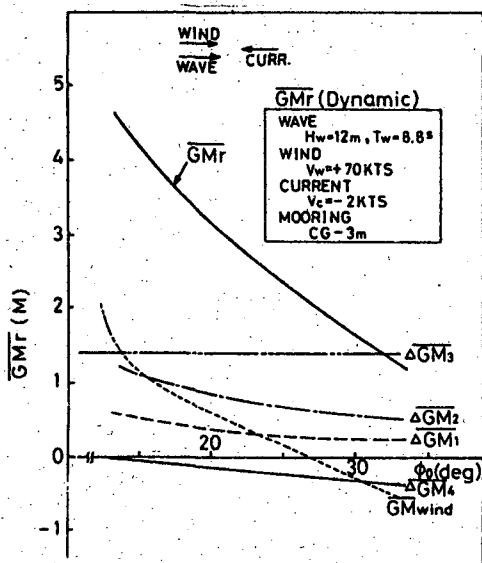
Fig. 19 Required minimum $\overline{GM}$ ($\overline{GM}_r$) obtained
by various kinds of loadings
(DYNAMIC)

at the larger tilt angles. Therefore, Eq. (12) which should be applied in a range of small tilt angle seems to be applicable also to the relatively larger angles.

Incidentally, as the authors pointed out the importance of the heeling moment due to wave-induced vertical steady force acting on lower hulls, it is confirmed from this figure that the contribution of $\Delta\overline{GM}_3$ to $\overline{GM}_r$ is significant.

Fig. 20 shows changes in $\Delta\overline{GM}_3$ corresponding to the static righting lever at various sectional shapes, intervals, and submergence of lower hulls. They are calculated according to Eq. (12) with

the assumption that the displacement and $\overline{BM}$ are unchanged. From this figure, it is found advantageous for $\Delta\overline{GM}_3$ to design the lower hull section in circular form, the interval in a smaller value and the submerged depth in a greater value. However, it is questionable whether Eq. (12) may be applicable or not in the state that the lower hulls come up closer to the water level. And also the other $\Delta\overline{GM}_i$ values might be changed. Therefore, it is difficult to make conclusion here.

As one of the other items contributing greatly to $\overline{GM}_r$, the mooring position on the platform is to be considered. Figs. 21 and 22 show the $\overline{GM}_r$ values corresponding to the static righting lever of the same platform having different mooring positions. These are examples in the quadrants II and IV of Fig. 13, respectively. In this case, under the combined environmental loadings of both quadrants, the value of $\overline{GM}_r$ can be minimized
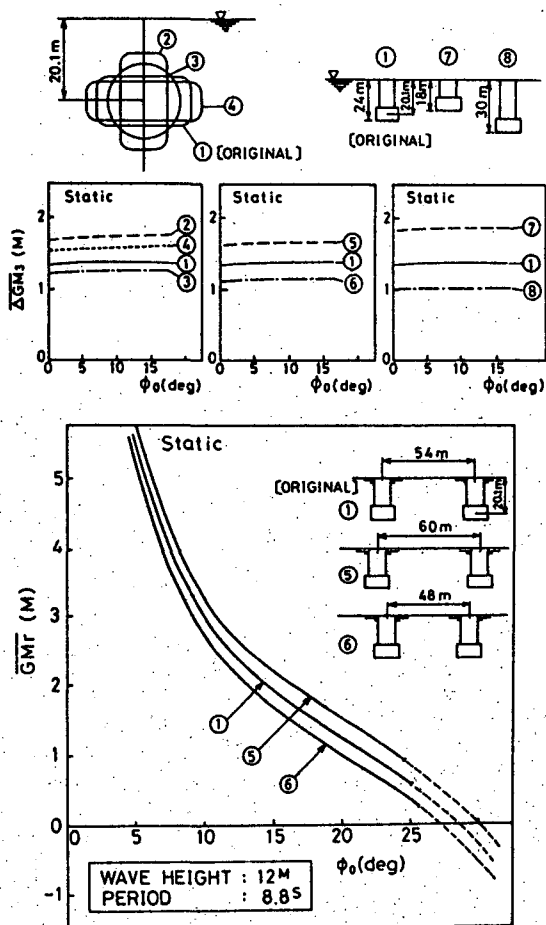

Fig. 20 Correction term $\Delta\overline{GM}_3$ due to wave-
induced vertical steady forces
on platform's lower hulls required
minimum $\overline{GM}$ for three structures
having different length of span
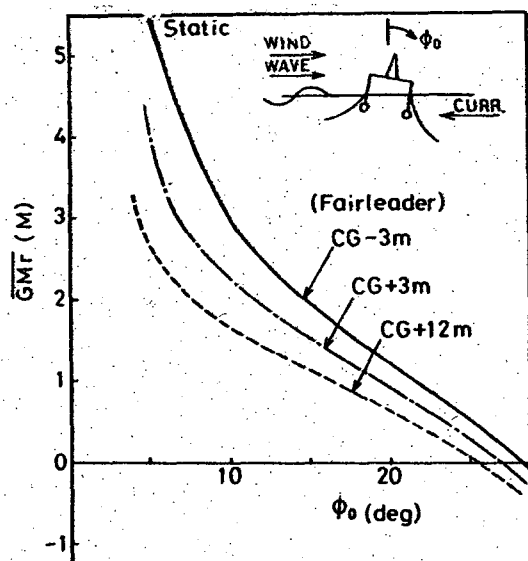
Fig. 21   Required minimum $\overline{GM}$ ($\overline{GM}_r$) by chang-
   ing fairleader heights (2nd
         quardrant)
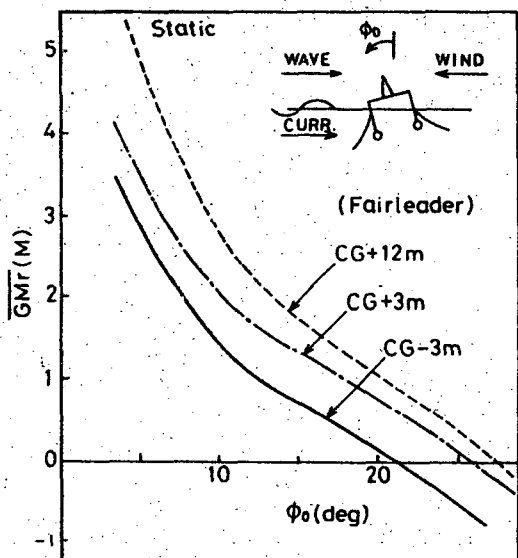
Fig. 22   Required minimum $\overline{GM}$ ($\overline{GM}_r$) by chang-
         ing fairleader heights (4th
         quardrant)

when the moored position on the platform is
3 m higher than the height of the center of
gravity.

7.   CONCLUSION

In the present paper, first of all, the
wave-induced steady heeling moment, in
particular, the steady heeling moment due to
the vertical steady force acting on lower
hulls, is experimentally determined, and
the results of simulation considering this
effect are found to simulate the experimental
results well, and it is concluded that this
effect cannot be ignored. At the same time,
large tilt phenomenon in waves is schemati-
cally explained.

In the next step, the mathematical
expression of the numerical simulation is
introduced. The behaviors under the combin-
ed environmental loadings are obtained by
the present simulation and are compared
with the experimental results for its
validity.

In the third step, it is demonstrated
that a moored semi-submersible platform
composed by twin lower hulls and eight
columns satisfying the requirements of the
existing rules may fall into dangerous state
which may lead to capsizing under the
combined environmental loadings by the
numerical simulation. It is thus pointed
out that the estimation of the stability in
the free floating condition as defined in
the existing rules is not sufficient to
guarantee safety of a semi-submersible
platform, and that it is necessary to
investigate together with the various
related factors in moored condition.

Finally, a new Required Minimum $\overline{GM}$
Method which evaluates and compensates
various heeling moments and/or heeling
energies by the $\overline{GM}$ value under the combined
environmental loadings is proposed.

REFERENCES

1) Takarada, N., Obokata, J., Inoue, R.,
   Nakajima, T. and Kobayashi, K.: The
   Stability on Semi-submersible Platform
   in Waves (On the Capsizing of Moored
   Semi-submersible Platform), The 2nd
   International Conference on Stability
   of Ships and Ocean Vehicles (Oct. 1982).

2) Ogilvie, T.F.: First-and second-order
   forces on a cylinder submerged under a
   free surface, J.F.M., Vol. 16 (1963).

3) Lee, C.M. and Newman, J.N.: The Vertical
   Mean Force and Moment of Submerged
   Bodies under Waves, J.S.R., Vol. 15, No.
   3 (1971).

4) Numata, E., Michel, W.H., and McClure,
   A.C.: Assessment of Stability Require-
   ments for Semi-submersible Unit, TSNAME
   (Nov. 1976).

5) Martin, J. and Kuo, C.: Calculation for
   the Steady Tilt of Semi-submersibles in
   Regular Waves, RINA (1978).

6) Inoue, R. and Kyozuka, Y.: ON the Non-linear Wave Forces Acting on Submerged Cylinders, J.S.N.A.J., Vol. 156 (1984).

7) Shipbuilding Research Association of Japan: A Study of the Design Forces and Stability of Offshore Structures, Panel SR-192 (1984).

8) Takarada, N., Nakajima, T., and Inoue, R. : A Study on the Capsizing Mechanism of Semi-submersible Platforms (1st Report), J.S.N.A.J., Vol. 155 (1984).

9) Takarada, N., Nakajima, T., and Inoue, R. : A Study on the Capsizing Mechanism of Semi-submersible Platforms (2nd Report), J.S.N.A.J., Vol. 156 (1984).

10) Takarada, N., Nakajima, T. and Inoue, R. : A Study on the Capsizing Mechanism of Semi-submersible Platforms (3rd Report), J.S.N.A.J., Vol. 157 (1985).

11) Motora, S, Koyama, T., Fujino, M. and Maeda, H.: Motions of Ships and Floating Structures, Seizando-Shoten.

12) Okawa, Y.: Deformation of Ocean Waves, B.S.N.A.J., No. 609 (1980).

13) Takagi, M. and Saito, K.: On the Description of Non-Harmonic Wave Problems in the Frequency Domain (3rd Report), J.K.S.N.A., No. 187 (1982).

Naonosuke Takarada, Ph. D

Professor, Yokohama National University,

Yokohama, Japan

Toshio Nakajima, Ph. D

Senior Researcher, Hiratsuka Research

Laboratory, Sumitomo Heavy Industries, Ltd.,

Hiratsuka, Japan

Ryuichi Inoue

Senior Researcher, Hiratsuka Research

Laboratory, Sumitomo Heavy Industries, Ltd.,

Hiratsuka, Japan

APPENDIX A

According to Reference 11), the static righting lever $\overline{GZ}(\phi)$ and dynamic righting lever (the righting energy divided by the displacement W) $\overline{GZ}_{(d)}(\phi)$ at the tilt angle ϕ of wall sided vessel are expressed as follows.

$$\overline{GZ}(\phi)=\sin\phi[\overline{GM}+(\overline{BM}/2)\tan^2\phi]$$

$$\overline{GZ}_{(d)}(\phi)=\int_0^\phi \overline{GZ}(\phi)d\phi$$

$$= (1-\cos\phi)[\overline{GM}+(\overline{BM}/2)$$

$$\cdot(1-\cos\phi)/\cos\phi] \qquad (A.1)$$

At the tilt angle ϕ, supposing the heeling moment or heeling energy due to the sum of various components and the righting moment or righting energy are balanced, the following expressions are established.

$$\overline{GZ}(\phi)\cdot W=M_t(\phi)=\sum_{i=0}^{k}M_i(\phi)$$

$$\overline{GZ}_{(d)}(\phi)\cdot W=\int_0^\phi M_t(\phi)d\phi=\sum_{i=0}^{k}\int_0^\phi M_i(\phi)d\phi$$

$$(A.2)$$

where $M_i(\phi)$ refers to various heeling moments.

Therefore, when heeling moment (heeling energy) is given, the minimum $\overline{GM}$ required to prevent from tilting over the tilt angle ϕ is given as follows.

$$\overline{GM}(\phi)=(F(\phi)/W)\sum_{i=0}^{k}\overline{M}_i(\phi)-(\overline{BM}/2)G(\phi)$$

$$=\overline{GM}_0(\phi)+\sum_{i=1}^{k}\Delta\overline{GM}_i(\phi) \qquad (A.3)$$

where

$$\overline{GM}_0(\phi)=\{\overline{M}_0(\phi)/W\}F(\phi)-(\overline{BM}/2)G(\phi)$$

$$\overline{GM}_i(\phi)=\{\overline{M}_i(\phi)/W\}F(\phi) \qquad (A.4)$$

provided

	[Balance of moment]	[Balance of energy]
$\overline{M}_i(\phi)$:	$M_i(\phi)$	$\int_0^\phi M(\phi)d\phi$
$F(\phi)$:	$1/\sin\phi$	$1/(1-\cos\phi)$
$G(\phi)$:	$\tan^2\phi$	$(1-\cos\phi)/\cos\phi$

APPENDIX B

Supposing the effect of submerged depth of wave-induced vertical steady force acting on lower hulls to be $\exp(-2kz_0)$, terms F_{L_1}, F_{L_2} in Eq. (11) may be rewritten as

$$F_{L_1}(z_1)=F_0\exp(-2kz_1) \qquad (B.1)$$

$$F_{L_2}(z_2)=F_0\exp(-2kz_2)$$

Where F_0 is the portion not related with the submerged depth in the formula of wave-induced vertical steady force. Next, referring to Fig. 15, it follows that

$$z_1=z_0\cos\phi-b_0\sin\phi \qquad (B.2)$$

$$z_2=z_0\cos\phi+b_0\sin\phi$$

and putting it into eq. (11), the following equation is obtained.

$$M_3(\phi)=[2b_0\cos\phi\sinh x+2h_0\sin\phi\cosh x]\cdot F_0\exp(-2kz_0) \qquad (B.3)$$

where $x=2kb_0\sin\phi$. Supposing the tilt angle ϕ to be small, we obtain

$$M_3(\phi)=(4kb_0^2+2h_0)\sin\phi\cdot F_0\exp(-2kz_0)$$

$$=(4kb_0^2+2h_0)\sin\phi\cdot F_L(z_0) \qquad (B.4)$$

STABILITY ANALYSIS OF TENSION LEG PLATFORMS

P. K. Muhuri

ABSTRACT

A moment method for analysing the stochastic stability of the surge motion of a tension leg platform (TLP) in a random sea is examined. In the differential equation describing the surge motion the variation of tether tension caused by the vertical component of the wave forces is random-time dependent in form. The asymptotic moment behaviour of the solution is determined and approximated in terms of an integral equation. Under the assumption of a narrow band process imposed upon the random coefficient, the stability results are obtained with the aid of deterministic stability theory. The mean square stability is studied and criteria for stability are obtained in terms of the damping coefficient and the autocorrelation function of the random sea.

INTRODUCTION

The problem of designing a cheap and reliable offshore platform for extraction of petroleum depends crucially on the conditions of the sea. Under favourable sea conditions free-floating drillships or semi-submersible platforms are quite adequate for the purpose. But such structures are quite unsteady in bad weather and have to be frequently dismantled and pipelines disconnected resulting in suspension of oil production. On the other hand rigid gravity structures resting on the sea bed allow continuous production but become very expensive for sea depths exceeding 100m or so.

To overcome these difficulties associated with erection of structures in deep seas, the possibility of designing a platform based on the principle of excess buoyancy is being explored in recent years. This design seeks to achieve a measure of steadiness of the platform by pulling vertically upwards on mooring cables attached to the seabed. Such structures which consist of a buoyancy tank attached to the seabed are known as tethered buoyant platforms (TBP) or tension leg platforms (TLP) (Fig. 1). They have great stability because the buoyancy holds the cable taut and being submerged they are subject to reduced wave disturbances. For such a vertically-moored TBP the platform is restrained vertically but free to move or rotate in a horizontal plane so that the effects of environmental loads are minimized. The natural frequencies of these motions are arranged to have values well below wave frequencies. This means that the horizontal motion of the platform remains small as a wave passes it. Recently the dynamics of a TBP subject to linear wave forces was discussed at length by Rainey [1]. Using the small wave theory, Rainey studied the horizontal motion of a vertically-moored TBP in a fluid of constant density taking into account the horizontal and vertical loads on fixed platforms arising out of water velocities caused by the passage of a wave. He also studied the inherent or complementary function instability of this motion associated with the vertical component of the forces assuming that the contribution due to the surge-force function vanishes. However in his instability analysis which predicted Mathieu instability at critical wave frequencies, the vertical force function was assumed to be deterministic. It is conceivable that under conditions prevailing in the sea, the above force function is a random

function of time.

The purpose of the present paper is to study the instability of the horizontal motion of a vertically moored TLP mentioned above subject to a random vertical force function. In particular we shall assume that this random function is characterized by a narrow band process and an white noise process.

PHYSICAL MODEL

Rainey [1] considered the following model of a TLP (Fig. 2). A spherical buoyant section (volume ∇ and mass M) is restrained by the tension T in the mooring cable and is exposed to waves giving rise to water velocity whose vertical and horizontal components are V and H. Ignoring the free surface, the fluid force on the sphere in an infinite inviscid fluid is due to buoyancy, dynamic buoyancy and added mass force. Buoyancy is given by the product of displacement and acceleration due to gravity, dynamic buoyancy by the product of displacement and fluid acceleration. Further the added mass force on a sphere is given by
0.5 (displacement) X
(fluid acceleration relative to sphere).

Applying Newton's second law and collecting the horizontal force components we can write
$$M \ddot{x} = -T \frac{x}{l} + \rho \nabla \dot{H}$$
$$+ \frac{1}{2} \rho \nabla \left[\dot{H} - \ddot{x} \right] \quad (1)$$
where x is the displacement of the platform due to surge motion, T the cable tension, l the length of the cable and ρ is the fluid density. An overdot denotes differentiation with respect to time. The cable tension T is determined from platform excess buoyancy (static vertical force) and vertical component of wave force. This is given by

$$T = (\rho \nabla - M) g + \rho \nabla \dot{V} + \frac{1}{2} \rho \nabla \dot{v} \quad (2)$$

where g is the acceleration due to gravity.
Substituting Equation (2) in Equation (1), we get the platform surge motion as

$$\left(M + \frac{1}{2} \rho \nabla \right) \ddot{x} + (1/l) \left[(\rho \nabla - M) g \right.$$

$$\left. + \frac{3}{2} \rho \nabla \dot{V} \right] x = (\frac{3}{2}) \rho \nabla \dot{H} \quad (3)$$

Rainey [1] expressed the above equation as
$$\ddot{x} + 2c \dot{x} + (1 + G(t)) x = f(t) \quad (4)$$

The damping coefficient term $2c\dot{x}$ is introduced to account for viscosity of fluid in the case when the platform oscillations are small. In fact under these conditions, viscosity will merely give rise to a thin boundary layer in phase with the platform velocity $\dot{x}$ (see Batchelor [2]). Further f(t) and G(t) denote the surge force function and the vertical force function, respectively. In writing (4), units are chosen so as to make the platform mass + added mass, cable length and the platform excess buoyancy, all unity.

Since the inherent or complementary function instability of the system (4) associated with the vertical random force function G(t) is independent of the surge function f(t), we consider the basic homogeneous equation

$$\ddot{x} + 2c \dot{x} + (1 + G(t)) x = 0 \quad (5)$$

for studying such an instability. If such instability exists then it will be in the form of a parasitic motion superimposed on the platform's normal movement. Since large oscillations may build up as a result of the growth of amplitude of the parasitic motion, avoiding such instability is, therefore, a primary design objective.

STABILITY ANALYSIS

Rosenbloom [3] initiated the stability study of moments associated with the solution of random differential equations. He studied the asymptotic moment behaviour of the solution of a first order random differential equation. Introducing the concept of mean square stability, the study of higher order random differential equations was made by Samuels and Eringen [4] in which the solutions of differential equations were

successively approximated in terms of
integral equations. The mean square
(m.s.) stability implies that every
m.s. bounded input leads to a m.s.
bounded output. Otherwise the system
is m.s. unstable.

In the present problem we will
closely follow the analysis as given
in the monograph by Soong [5]. We
assume that the random force function
G(t) in Equation (5) is given by a
zero—mean narrow band process or a
zero—mean white noise process.
Following Soong [5] we introduce
the operator L(t) defined by

$$L(t)x(t) = \ddot{x} + 2c\dot{x} + (1 + G(t))x = 0. \quad (6)$$

This is written as

$$\left[L_o(t) + L_1(t) \right] x(t) = 0 \quad (7)$$

where $L_o(t)$ represents the determinis-
tic part of the differential operator
L(t) and $L_1(t)$ represents the stocha-
stic part whose expected value is zero.
Equation (7) can be put in the form

$$L_o(t)x(t) = -L_1(t)x(t) \quad (8)$$

The solution of Equation (8) is obtai-
ned as an integral equation

$$x(t) = -L_o^{-1}(t)L_1(t)x(t) + c_1\phi_1(t) + c_2\phi_2(t), \quad (9)$$

where $L_o^{-1}(t)$ is the deterministic inte-
gral operator having the weighting
function associated with $L_o(t)$ as ker-
nel. $\phi_1(t)$ and $\phi_2(t)$ are independent
solutions of $L_o(t)\phi(t) = 0$. c_1 and c_2
are deterministic constants which can
be found from initial conditions.
Letting $F(t) = c_1\phi_1(t) + c_2\phi_2(t)$ and
multiplying Equation (9) by itself at
two points t_1 and t_2 and taking ex-
pectation of the resulting equation,
we have

$$\langle x(t_1)x(t_2)\rangle = \langle F(t_1)F(t_2)\rangle$$
$$- L_o^{-1}(t_1)\langle L_1(t_1)x(t_1)F(t_2)\rangle$$
$$- L_o^{-1}(t_2)\langle L_1(t_2)x(t_2)F(t_1)\rangle$$
$$+ L_o^{-1}(t_1)L_o^{-1}(t_2)\langle L_1(t_1)L_1(t_2)x(t_1)x(t_2)\rangle \quad (10)$$

where the symbol $\langle \rangle$ stands for mathe-
matical expectation. It is pointed
out by Soong [5] that when the ran-
dom process G(t) and the solution pro-
cess x(t) have widely separated spect-
ra, the following relations will app-
roximately hold :

$$\langle L_1(t_1)x(t_1)F(t_2)\rangle \simeq \langle L_1(t_1)\rangle\langle x(t_1)F(t_2)\rangle,$$
$$\langle L_1(t_2)x(t_2)F(t_1)\rangle \simeq \langle L_1(t_2)\rangle\langle x(t_2)F(t_1)\rangle,$$
$$\langle L_1(t_1)L_1(t_2)x(t_1)x(t_2)\rangle \simeq \langle L_1(t_1)L_1(t_2)\rangle\langle x(t_1)x(t_2)\rangle$$

Using (11) and noting that $\langle L_1(t)\rangle = 0$,
Equation (10) reduces to

$$\langle x(t_1)x(t_2)\rangle = \langle F(t_1)F(t_2)\rangle$$
$$+ L_o^{-1}(t_1)L_o^{-1}(t_2)\langle L_1(t_1)L_1(t_2)\rangle\langle x(t_1)x(t_2)\rangle.$$

In terms of the original quantities in
the basic differential Equation (6),
Equation (12) has the explicit form

$$\Gamma_{xx}(t_1,t_2) = \Gamma_{FF}(t_1,t_2)$$
$$+ \int_{-\infty}^{\infty}\int_{-\infty}^{\infty}\langle k(t_1,s_1)k(t_2,s_2)\rangle \Gamma_{xx}(s_1,s_2)ds_1ds_2 \quad (13)$$

where Γ_{xx} is the autocorrelation fun-
ction and

$$\langle k(t_1,s_1)k(t_2,s_2)\rangle = \Gamma_{GG}(s_1,s_2)h(t_1,s_1)h(t_2,s_2) \quad (14)$$

In the above h(t,s) is the weighting
function associated with the deter-
ministic differential operator $L_o(t)$
and

$$\Gamma_{GG}(s_1,s_2) = \langle G(s_1)G(s_2)\rangle. \quad (15)$$

Equation (13) defines an integral
equation satisfied by the autocorre-
lation function of the solution pro-
cess x(t). Taking the double Fourier
transform of Equation (13) we have

$$\hat{\Gamma}_{xx}(\omega_1,\omega_2) = \hat{\Gamma}_{FF}(\omega_1,\omega_2)$$
$$+ (1/4)\pi^2\int_{-\infty}^{\infty}\int_{-\infty}^{\infty}\hat{h}(\omega_1)\hat{h}(\omega_2)\hat{\Gamma}_{GG}(\omega_1-\nu_1,\omega_2-\nu_2)$$
$$\times \hat{\Gamma}_{xx}(\nu_1,\nu_2)d\nu_1 d\nu_2 \quad (16)$$

where the double Fourier transform of
a function is denoted by a circumflex.
Equation (13) and (16) provide the
basis for investigating the mean
square stability of Equation (5).

We now consider the following
two cases.
Case I. G(t) is given by a narrow
band process and its power spectral
density is approximated by a delta
function.

$$\hat{\Gamma}_{GG}(\omega_1-\nu_1,\omega_2-\nu_2) = 4\pi^2\Gamma_{GG}(0)$$
$$\times \delta(\omega_2-\nu_2)\delta(\omega_1-\nu_1+\omega_2-\nu_2) \quad (17)$$

Substituting Equation (17) in Equa-
tion (16) and carrying out the inte-
gration we get

$$\hat{\Gamma}_{xx}(\omega_1,\omega_2) = \hat{\Gamma}_{FF}(\omega_1,\omega_2) +$$

$$\Gamma_{GG}(0)\hat{h}(\omega_1)\hat{h}(\omega_2)\hat{\Gamma}_{XX}(\omega_1,\omega_2) \qquad (18)$$

Thus
$$\hat{\Gamma}_{XX}(\omega_1,\omega_2) = \hat{\Gamma}_{FF}(\omega_1,\omega_2)$$
$$\times[1 - \Gamma_{GG}(0)\hat{h}(\omega_1)\hat{h}(\omega_2)]^{-1} \qquad (19)$$

Taking inverse Fourier transform, the solution for $\langle x^2(t)\rangle$ is then given by

$$\langle x^2(t)\rangle = (1/4)\pi^2$$

$$\cdot \int_{-\infty}^{\infty}\int_{-\infty}^{\infty} \frac{\hat{\Gamma}_{FF}(\omega_1,\omega_2)\exp\{-it(\omega_1+\omega_2)\}\,d\omega_1 d\omega_2}{1 - \Gamma_{GG}(0)\hat{h}(\omega_1)\hat{h}(\omega_2)}$$

$$+ \oint\oint \frac{g(\omega_1,\omega_2)\exp\{-it(\omega_1+\omega_2)\}\,d\omega_1 d\omega_2}{1 - \Gamma_{GG}(0)\hat{h}(\omega_1)\hat{h}(\omega_2)} \qquad (20)$$

Instead of attempting to find the explicit value of $\langle x^2(t)\rangle$, we shall seek the mean square stability criterion form the complementary solution of (20). Following Soong [5], we write the second term of Equation (20) in the form

$$\alpha_1\exp\{-it(\omega_{11}+\omega_{21})\}$$
$$+ \alpha_2\exp\{-it(\omega_{12}+\omega_{22})\} \qquad (21)$$

where ω_{1r}, ω_{2r} $(r=1,2)$ are the roots of

$$1 - \Gamma_{GG}(0)\hat{h}(\omega_1)\hat{h}(\omega_2) = 0$$
$$(d/d\omega_1)\hat{h}(\omega_1) = 0 \qquad (22)$$

The criterion for mean square stability can now be stated as follows : the system is m.s. unstable if

$\omega_{1r} + \omega_{2r}$ $(r=1,2)$ has a positive imaginary part. Otherwise the system is m.s. stable.

In our present problem the weighting function $h(t)$ associated with Equation (5) is

$$h(t) = i(\lambda_1-\lambda_2)^{-1}[\exp(-i\lambda_1 t) - \exp(-i\lambda_2 t)] \qquad (23)$$

where,
$$\lambda_{1,2} = -ic \pm (1-c^2)^{1/2} \qquad (24)$$

The Fourier transform of $h(t)$ is given by
$$\hat{h}(\omega) = -(\omega-\lambda_1)^{-1}(\omega-\lambda_2)^{-1} \qquad (25)$$

Equations (22) then give on using (24) and (25)

$$1 - \frac{\Gamma_{GG}(0)}{(\omega_1-\lambda_1)(\omega_1-\lambda_2)(\omega_2-\lambda_1)(\omega_2-\lambda_2)} = 0 \qquad (26)$$

$$\frac{2(\omega_1+ic)}{(\omega_1-\lambda_1)^2(\omega_1-\lambda_2)^2} = 0$$

Solving for ω_1 and ω_2 we get
$$\omega_1 = -ic \qquad (27)$$

$$\omega_2 = -ic \pm \{(1-c^2) - \Gamma_{GG}(0)/(1-c^2)\}^{1/2} \qquad (28)$$

Equations (27) and (28) now give

$$\nu_{1,2} = -2ic \pm \{(1-c^2) - \Gamma_{GG}(0)/(1-c^2)\}^{1/2}$$

where
$$\nu_1 = \omega_{11} + \omega_{21}, \quad \nu_2 = \omega_{12} + \omega_{22}$$

It therefore follows that the platform surge motion given by Equation (5) is mean square unstable if ν_1 or ν_2 has a positive imaginary part. Otherwise the motion is mean square stable. Figure 3 shows the stability plot in the $\Gamma_{GG}(0)$-c plane.

Case II. G(t) is given by a white noise process with zero mean and autocorrelation function $\Gamma_{GG} = S_0\delta(s_1-s_2)$

where S_0 is a constant. For this case Equation (14) becomes
$$\langle K(t_1,s_1)K(t_2,s_2)\rangle = S_0\delta(s_1-s_2)$$
$$\cdot h(t_1-s_1)h(t_2-s_2). \qquad (29)$$

Substituting the above Equation into Equation (13) and upon setting $t_1=t_2=t$, we get

$$\langle x^2(t)\rangle = \langle F^2(t)\rangle$$
$$+ S_0\int_{-\infty}^{\infty} h^2(t-s)\langle x^2(s)\rangle ds \qquad (30)$$

The above integral Equation (30) can be solved with the use of Fourier transform theory.
The solution is [6]

$$\langle x^2(t)\rangle = \int_{-\infty}^{\infty} F^2(s)w(t-s)\,ds$$

$$+ \oint \frac{g(s)\exp(ist)}{1 - S_0 F.T(h^2(t))}\,ds \qquad (31)$$

where F.T denotes Fourier's transform and $w(t-s)$ is the inverse transform of
$$[1 - S_0 F.T\, h^2(t)]^{-1},$$
$g(s)$ is an analytic function in the domain of analyticity of F.T. $h^2(t)$, $\oint$ being a closed contour integral in that domain.

Assuming that the m.s. input is bounded, the m.s. output $\langle x^2(t)\rangle$ is a bounded function of t only if the roots of the Equation
$$1 - S_0 F.T\, h^2(t) = 0 \qquad (32)$$
have negative real parts.

In the present problem, the weighting function $h(t)$ associated with

Equation (5) is

$$h(t) = i(\lambda_1 - \lambda_2)^{-1} \left[\exp(i\lambda_1 t) - \exp(i\lambda_2 t) \right] \quad (33)$$

where

$$\lambda_1 = ic + (1-c^2)^{1/2}, \quad \lambda_2 = ic - (1-c^2)^{1/2}$$

The Fourier transform of $h^2(t)$ is given by

$$F.T\, h^2(t) = -i(\lambda_1 - \lambda_2)^{-1} \left[(\omega - 2\lambda_1)^{-1} + (\omega_1 - 2\lambda_2)^{-1} - 2(\omega - \lambda_1 - \lambda_2)^{-1} \right] \quad (34)$$

Equation (32) then gives on using (34) and writing $\xi = i\omega$,

$$\xi^3 + 6c\xi^2 + 4(1+2c^2)\xi + (S_0 + 8c) = 0 \quad (35)$$

Applying Routh-Hurwitz criterion we find that the system is m.s. stable if and only if (i) all the coefficients are positive and

(ii)
$$24c(1+2c^2) > S_0 + 8c. \quad (36)$$

The first condition is always satisfied for positive values of S_0 and c. The second leads to

$$16c^3(3 + 1/c^2) > S_0. \quad (37)$$

The m.s. stability region is shown in Fig 4.

DISCUSSION

(a) It is interesting to note from Figure 3 that a vertically-moored TLP would be mean square stable if the damping coefficient c exceeds unity.

(b) However if the damping is not large such that $0 < c < 1$, there are regions of both stability and instability in the $\Gamma_{GG}(0)$-c plane (see Fig. 3). This result is to be expected physically since if the damping is not large, parametric excitation of instability by random modulation of the vertical force is possible. In fact a random fluctuating vertical force superimposed on the static vertical load (excess buoyancy) increases the mean square value of the vertical load and so makes disturbances to the system grow more rapidly.

(c) Since the above stability analysis is independent of the surge force function f(t), the instability

phenomenon is not restricted to surge oscillations only but could equally well occur in the sway or yaw degrees of freedom provided G(t) has suitable features.

(d) In the case of white noise excitation, the platform is mean square stable for high damping while there is a region of instability for low values of damping (Fig. 4).

REFERENCES

[1] Batchelor, G.K. 1967. An Introduction to Fluid Dynamics. Cambridge University Press, Cambridge.

[2] Rainey, R.C.T. 1978. The dynamics of tethered platforms. Nav. Architect 2, 59.

[3] Rosenbloom, A. 1954. Analysis of linear systems with randomly time-varying parameters. Proc. Symp. Information Networks, Polytech. Inst. of Brooklyn., p. 145.

[4] Samuels, J.C. and Eringen, A.C. 1959. On stochastic linear systems. J. Math. Phys. 38, 93.

[5] Soong, T.T. 1973. Random Differential Equations in Science and Engineering. Academic Press, New York.

[6] Titchmarsh, E.C. 1948. Introduction to the theory of Fourier Integrals. Oxford University Press, Second Edition, Chapter IX.
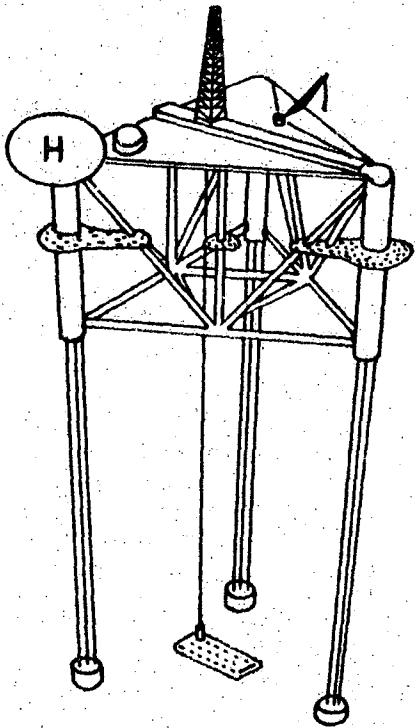
FIG.1. DEEP OIL TECHNOLOGY (D.O.T)
TENSION LEG PLATFORM

COMPONENTS OF WATER
VELOCITY
WATER DENSITY = ρ

FIG.2. ELEMENTAL TETHERED BUOYANT
STRUCTURE

FIG.3. STABILITY PLOT OF TLP WITH
NARROW BANDED VERTICAL
FORCE FUNCTION
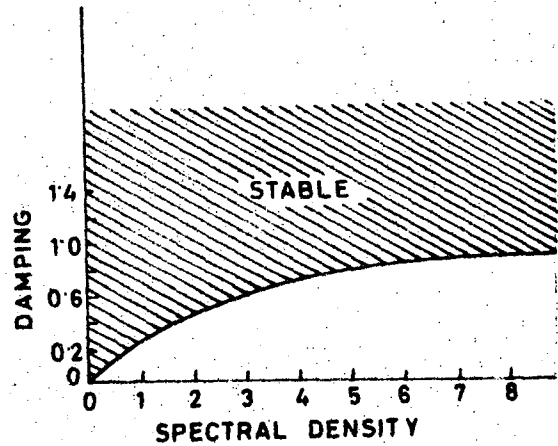
FIG.4. STABILITY PLOT TLP WITH
RANDOM VERTICAL FORCE
VARIATION

DEPARTMENT OF NAVAL ARCHITECTURE
INDIAN INSTITUTE OF TECHNOLOGY
KHARAGPUR — 721 302 (INDIA)

ON THE DANGEROUS COMPLEX ENVIRONMENTAL CONDITIONS
TO THE SAFETY OF A MOORED SEMI-SUBMERSIBLE
PLATFORM

BY

S. TAKEZAWA

T. HIRAYAMA

1.ABSTRACT

There are many external forces relating to the safety of moored semi-submersible platforms under survival conditions, for example, wind force, wave force and current forces. Induced phenomena such as heeling angle or mooring tensions by those forces directly affect the design of platform or its operation, but still today, the prediction of those complicated, non-linear and interfering phenomena is difficult by experiments to say nothing of theory. So, in this study, for making realistic experiments in a towing tank without wind blower and current generator, adding to the own long crested irregular wave maker we develop a mechanical and electrical experimental apparatus generating irregular pseudo wind force and steady pseudo current speed following to the specified values precisely. By detecting model motions in such a precisely reproduced environmental conditions by remote measuring systems, we can evaluate the combinations of dangerous complex environmental conditions against the safety of a moored intact semi-submersible platform in beam seas. Especially the role of mooring line under survival condition is made clear. In this connection, the relation between stability criteria and effect of mooring line which is not considered in current stability rules is already pointed out by Takarada et al.[2].

2.RESEARCH ASPECT

2.1 Design conditions and design loads

In this experimental study we use our towing tank, so we consider only about the safety in beam sea, beam current and beam wind. The adopted model is illustrated in Fig.1, and this is the same one used in the ship research panel 192(SR192) in Japan and ITTC's comparative study.

Principal dimensions are shown in Table1. Supposed design conditions and further the induced design loads are shown in Table 2 (here after, full scaled data are shown mainly). Operating condition is shown for references. For the estimation

Table 1.

PRINCIPAL DIMENSIONS

ITEM		MODEL 1/64	ACTUAL
Length	(m)	1.797	115.0
Breadth	(m)	1.172	75.0
Depth (to Main Deck)	(m)	0.594	38.0
Draught	(m)*	0.313	20.0
Displacement (in fresh water)	*	131.8 kg	34551ton
KG**	(m)	0.273	17.5
GM_T	(m)	0.045	2.87
GM_L	(m)	0.037	2.37
Gyradius of Roll	(m)	0.515	33.0

* corresponds to survival condition
** corresponds to condition (A) and (B)

Table 2.

(a) DESIGN CONDITION

	OPERATING	SURVIVAL
WATER DEPTH	160m	
WAVE HEIGHT	8 m	30 m
WAVE PERIODS	10 sec	15 sec
WAVE SLOPE	1/19.5	1/11.7
WIND VELOCITY	70 knot	100 knot
CURRENT VELOCITY	1.95*knot	2.36*knot

* Included wind induced current by the DNV rule (1983) (basic current = 1 knot)

(b) DESIGN LOAD (UNIT : ton)

	OPERATING	SURVIVAL
WIND FORCE	198.1	369.9
CURRENT FORCE	69.9	98.5
WAVE DRIFT FORCE	217.6	285.1**
*TOTAL FORCE	485.6	753.5

* Direction is supposed to be all the same.
** Corresponds to T=9.6sec H=9.91m (at maximum Wave drift force period)

of drag forces by current, the DNV Rule(1983) is referenced and for the drag forces by wind the wind tunnel results by MHI[5] is quoted. It should be noticed that for the estimation of wave drift forces, the coefficient at the frequency showing maximum drift force obtained by experiments in regular waves is used and it dose not necessarily corresponds to the wave shown in the design condition.

2.2 Stability curves.

Calculated stability curves against pure heeling moment are shown in Fig.2. These curves are needed for checking the intact stability. Even when the effect of mooring lines described later are
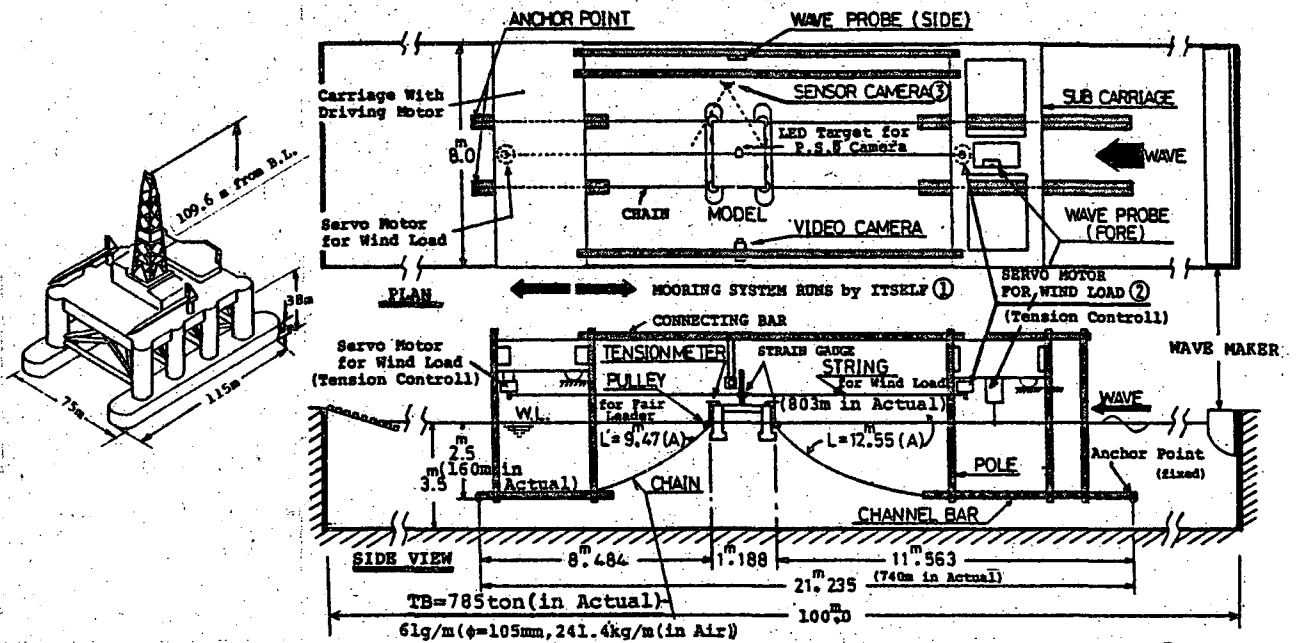
Fig.1   Sketch of adopted platform, mooring lines, and newly developed experimental instrument for ① current ② irregular wind load and ③ remote measuring of motion

taken into account, the apparent GM value is increased only by 8% from 2.87m to 3.12m (here the height of fair leader for mooring lines is 1.28m under the center of gravity) and this change will result in about 4% reduction of natural period of roll. Furthermore the change of stability curve itself is also very little even when the mooring height is altered up to the deck height [4] and so the curves including the effect of mooring lines are neglected in Fig.2. Of course the mooring height affects the steady heel through moment lever by horizontal external loads. In this connection, the most important change by mooring lines appears in the sway motion which have no natural period without mooring.

In Fig.2, the wind heeling moments calculated by referencing the wind tunnel experiments [1] are drawn and the resulting K values, namely safety factor or residual dynamical stability rate are also shown. Common requirements by rules are such that ① K>1.3, ② Minimum GM>1.0m, and it will be seen that our model clear No. ① requirements even at the minimum GM.

2.3 Mooring system

Considering that the experiments are conducted in the towing tank and in beam sea condition the four parallel mooring lines system is adopted. Decided mooring chain system under survival condition is shown in Fig.1 with the dimensions of adopted chain. This mooring system is decided by following requirement. (a) Even when the total horizontal force (shown in Table 2) act on the platform, mooring lines must be long enough not to stand up anchors. (b) The safety factor of about 2 must be kept against the breaking of mooring lines under the total horizontal force.
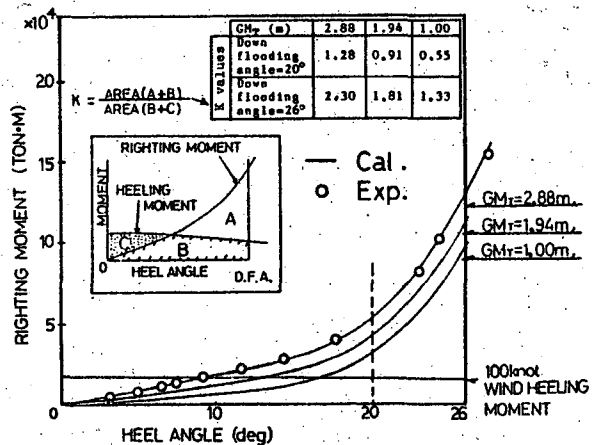

Fig.2   Estimated stability curves, heeling moment curve by wind and K values

In this mooring system, for the survival total steady force, the horizontal shift is estimated as about 27% of water depth and the safety factor to the breaking load becomes about 1.8. (For the operating condition, about the 5% winding up of the mooring chain length can suppress the horizontal shift of platform within ±5% of water depth.) Under such a situation, the main aspect of our research is that whether our model is really safe or not under various combination of specified design condition or loads described in table 2.

3. NEWLY DEVELOPED EXPERIMENTAL TECHNIQUES

In order to realize various combination of specified design condition or loads precisely, various experimental techniques are newly developed as follows.

3.1 Pseudo current adding system

Current speed is added relatively by moving the whole mooring system including four anchor

points with constant speed as shown by arrows in Fig.1. Therefore, precise uniform current is realized but the shear flow and the current-wave interaction can not be simulated.

3.2 Pseudo dynamic wind force loading system

Instead of air blowing, dynamic wind force is simulated as follows. At first the time histories of wind speed U(t) is synthesized from the wind speed spectrum. Here, as the wind spectrum, so called Dvenport's spectrum is adopted. Then the time histories of wind drag force $F_D(t)$ are obtained using the drag coefficient (C_{Di}) of each member with projected area Ai.

$$F_D(t) = \frac{1}{2} \rho \{u(t) + \bar{U}_{10}\}^2 \cdot \sum_i C_{Di} A_i \qquad (1)$$

Here, $\bar{U}_{10}$ means wind speed at the height of 10m from sea level. This drag force is loaded on the estimated drag force center by controlling the difference of left and right hand side string tensions shown in Fig.1. Tension control is made by rotating a pair of pulleys connected directly with electric servo motors. Tensions are detected by a pair of ring gauges at the connecting point of string with the tree, and of course such a control that these strings give no obstacle to the motion by waves is made.

This system does not include the vertical shear, vertical correlation, the relative wind speed to the moving platform and lift force. In spite of these defects this system has advantages that loaded wind force is very clear and desired arbitrary control is possible.

In Fig.3, the results obtained by using this loading system as a forced oscillation apparatus are shown. Time histories are forced transient [1] wind loads and other graphs are transfer functions of sway, roll and weather side tension. Left hand side figures correspond to the case without biased load, and the others correspond to biased load case of 100 knots wind. It will be seen that 100 knots steady wind load result large horizontal shift of platform and the sway natural period and as a matter of course related tension peak period show drastic alteration from about 200 to 100 second. This phenomenon is negligible for roll.

3.3 Opto-electrical remote measuring system

For detecting platform motions without mechanical interference, opto-electrical remote measuring system called Position Sensor Device (PSD) [3] is introduced. Rough arrangement of PSD is shown in Fig.1. A camera with a photo-electric sensor of semi conductor type can separately generate voltages corresponding to the ordinates of multi image of light-emission diode (LED) mounted on the
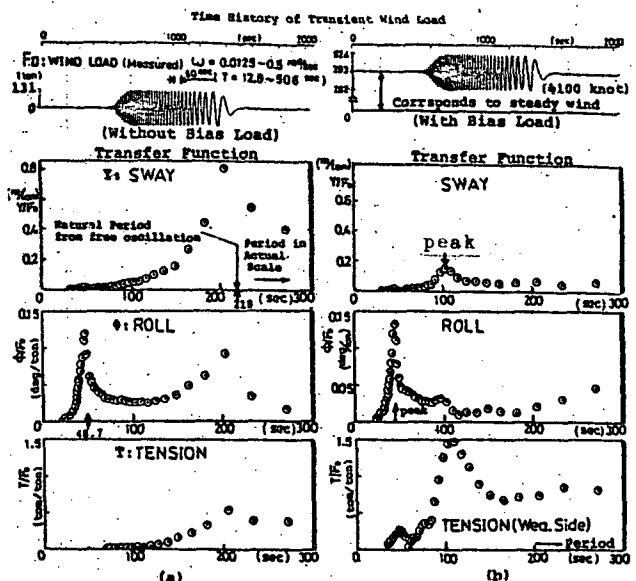

Fig.3 Transfer function between wind force and motion or tension by the forced transient experiment

model, and by the combination of this camera, six degrees of freedom motion can be also measured in real time. This system is made as calibration free system.

4. EXPERIMENTAL RESULTS AND DISCUSSIONS

4.1 Variation of platform conditions and combination of extreme external forces.

As for platform conditions, following cases are tried as shown in Fig.4. The first one is so called standard condition as described in Table 1 (condition A). The next one is extraordinary high mooring point condition but GM without mooring is the same as condition A (condition B). The last is low GM (1/2 of condition A and B) condition but height of mooring point is the same as condition A (condition C). In those cases initial tension of mooring chain is about 70ton.

Extreme external forces are generated to realize the design loads in model scale corresponding
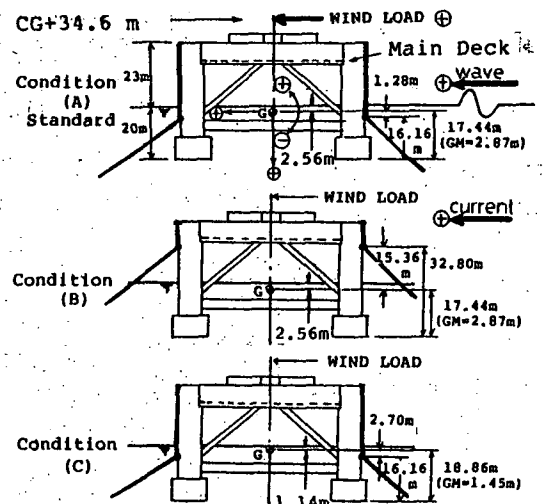

Fig.4 Variation of GM and the height of fairleader for mooring lines(Initial Tension is 70 ton)

to those estimated in Table 1. It must be noticed that in Table 2, considered wave drift force is estimated by regular wave (T=9.6sec, H=9.91m), and in this study we use JONSWAP type irregular wave with corresponding characteristic period and height (peak period of spectrum =10sec, max of significant wave height =10.8m) but mean drift force by this irregular wave becomes about the half of designed load. About the direction of external forces, arbitrary combination is tried even if some of it is rare in nature, and this arbitrariness is the superior point of our experimental apparatus.

4.2 Deviations by steady external loads

In order to examine the steady calculation (horizontal drift and heel) by steady forces, comparisons with experimental results are shown in Fig.5. Condition of platform is (A) with mooring chains. Both figures are drawn against current
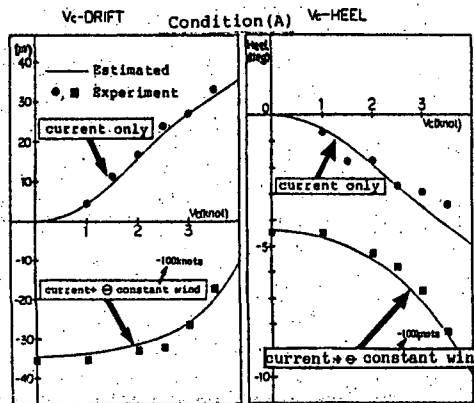

Fig.5 Comparison of experiment about drift and heel under constant current and wind with calculation

speed. Adding to current, the cases are also shown in which constant wind loads corresponding to 100knots wind speed are given. The direction of wind is opposite to the current and described as ⊖ constant wind. Estimated curves are calculated based on catenary curve theory and by using drag force coefficients described in the DNV rule. Drag coefficients by wind is quoted from the experimental results by MHI [5].

Comparison with experimental results show a good agreement, and this means that the drag coefficients are reliable and that the steady heeling moment by current is not so large as by mooring lines. Because, except up right condition, steady heeling moment obtained by captured model test is largely deviated from the one estimated from drag force coefficients without considering lift forces. From this figure it is known that designed current force and wind force (opposite direction to current) results in about 6 degrees heel. Furthermore, the total design load shown in Table 2 corresponds to 5.7 knots current, and this drag force results in 42.4m drift (=26.5% of water depth).
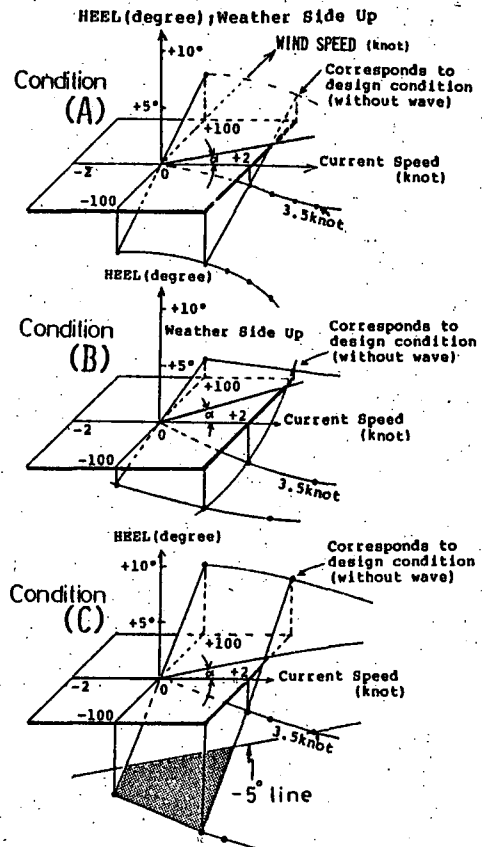

Fig.6 Heel by the combination of constant current and constant wind without waves. (by experiments). (A)(B) and (C) correspond to Fig.4.

Next, in Fig.6, we show figures of steady heel as the results of various combination of constant current and wind without wave. The positive or negative sign for direction is already shown in Fig.4. (A),(B) and (C) also correspond to that in Fig.4. These are experimental results and calculated results are neglected because good estimations are already examined. The larger angle (α) between current axis and the line defined as intersection of two planes, express the larger influence of current than wind, and condition (B) (high mooring point) shows this tendency. Small M condition (C) shows, as will be expected, about the twice as large face slope as that of condition (A) following to wind speed increase.

4.3 Extreme maxima by dynamic external loads

At first, we show an example of records in a survival condition. Time histories in Fig.7 corresponds to the case of ⊕ current (3.5 knot), ⊕ irregular wave ($H_{1/3}$=10.8m, T_{02}=8.85sec) and ⊖ wind (100 knots). ⊕, ⊖, means direction of progress. Measured wind load time history is shown in second column, and analyzed spectrum is also shown. The smooth curve in the raw spectrum is the given load spectrum calculated from the Davenport's spectrum. About this case, tensions do not become large, but slow drift and roll negative maxima (weather side down) becomes large. Platform condition is (A) and obtained extreme
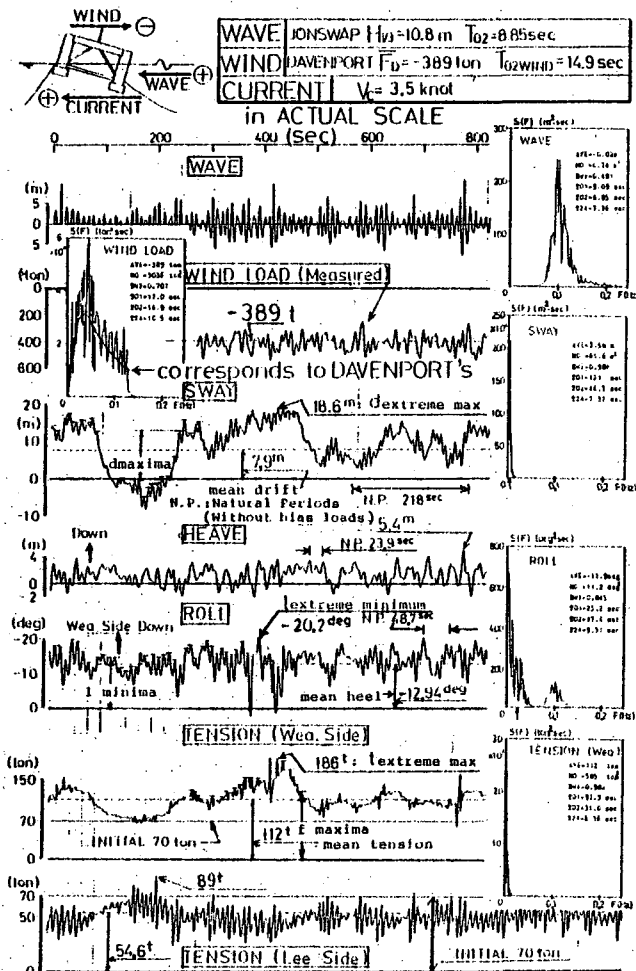
Fig.7 Example of record of motions and tensions under the extreme, complex and dynamic loads. (Encounter wave period is deviated according to relative current speed.)


Fig.8 Variation of extreme value of tension and heel and mean value of heel according to the combination of constant current and constant/irregular wind under the existence of irregular waves. (A)(B) and (C) correspond to Fig.4

maximum of -20.2 degrees dose not over the down flooding angle of 26 degrees, but water is poured upon the deck. So, even for condition (A) in which the K value (flooding angle is 26 degrees) is 2.3 (>1.3), the residual stability seems not so enough for this case. This will be also discussed later.

In the next according to condi'ions (A), (B) and (C), how the extreme maxima of tension and roll are changed is shown in Fig.8 by the change of external forces combination. Manner of expression is as the same as Fig.6, but the different point from Fig.6 is the existence of irregular wave. Characteristics of the variable wind loads and the irregular wave is the same as Fig.7. Used irregular wave is restricted to one kind, which have mean period showing maximum wave drift force and have maximum apparent wave steepness of about 1/10. Extreme maxima or minima are measured from absolute zero base and tension include initial tension. About roll, extreme maxima and minima out of about 200 peaks are expressed on the same plane, so the two curved faces are seen in each figure. Mean heels are also shown in the right hand side and they are very similar to Fig.6. On the other hand, he curved faces expressing extreme roll maxima or

minima show similar slope to that of mean, and differences between the extreme and the mean are considered to be introduced by the dynamic effect of waves. Of course, this effect include slow oscillations.

In order to see the difference between variable wind and constant wind effects, the results by constant wind loads are shown by solid circles (●). Considering this, the maximum difference of about 5 degrees in extreme roll occurs in the combination of (-2 knots current, -100 knots wind) at the condition (C), but the variable wind load effect seems small as for tensions. The combination of external forces which results in dangerous situation both in heel or tension is very clear in Fig.8 under the most severe waves concerning to wave drift force. Mooring lines becomes danger in the condition (A), and in this case the maximum tension reaches about 90% of breaking load. Condition (C) is most safety concerning to tension, but to heel angle it becomes worst especially when the wind

direction is inverse to that of current and wave. About this case (C), the extreme negative maximum roll (namely weather side down) becomes 25 degrees, but if the experiment is done in the strict design condition this angle will become larger than the down flooding angle, because mean drift force by irregular wave is about half of that designed load. Furthermore, K value of condition (C) is 1.74 and satisfies the stability requirement, but considering the lowest GM condition of 1.0m, extreme maximum in this time experiment obviously excess that down flooding angle even if the K value (=1.33 in actual) satisfy the requirement. Therefore, it must be noticed that there is possibility that some combination (even if appearance will be rare in nature) of external forces exist in which roll angle excess the down flooding angle even if the common stability requirement is fulfilled. It will be easily understood that the existence of mooring lines largely affects this result.

4.4 Combination of external forces dangerous to platform

Before considering dangerous extreme values, we will refer to the steady heel. In Fig.9 the combination of constant current and constant wind are shown by shadowed area in which weather side down heels excess 5 degrees. This figure is obtained from Fig.6. Experiments are made as far as 3.5 knot in current. Minus 5 degrees lines in condition (A) and (C) are parallel each other, and this means that the change of GM changes steady heel angle proportionally both in wind or current. Different tendency in condition (B) means that the effect of the height of mooring point is not the same either current or wind. In this case, the high mooring point decrease the moment lever by wind and increase the moment lever by current, and so the current effect on heel becomes large relatively.

In Fig.10, the similar expression for mean heel in constant current and constant wind, under the existence of irregular wave, is shown. Broken line correspond to Fig.9. Minus 7 degrees line are drawn for reference. The differences between solid line and broken line mean the effect of irregular wave. In this connection, the waves drift the platform and heel is generated by the mooring lines , and furthermore, the draft difference of two lower hulls add heeling moment based on lift force by wave and then the heel is increased further.

In Fig.11, regions expressing extreme heel over minus 20 degrees are shown. This angle is considered to be dangerous because water pouring on deck is seen. Broken lines correspond to the solid lines in Fig.10. Region in which the ex-
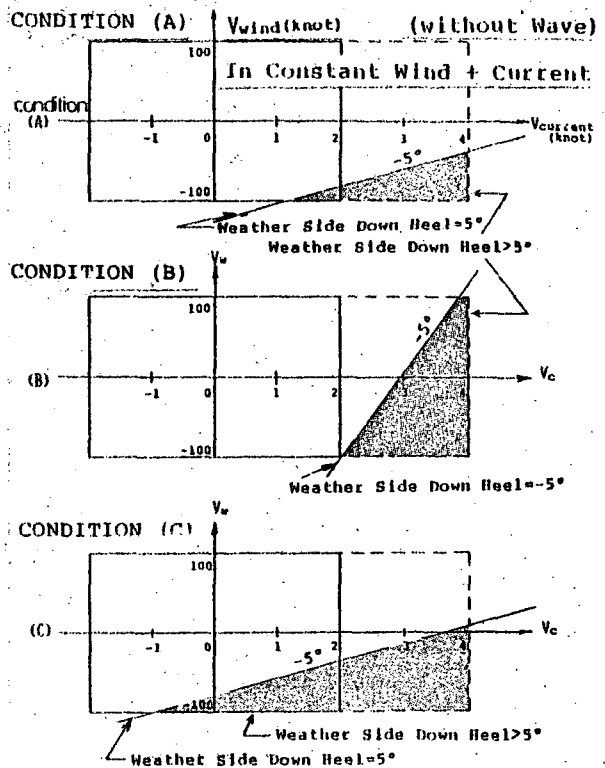

Fig.9 Region showing over 5 degrees weather side down heels are seen in the combination of constant current (Vc) and constant wind (Vw)
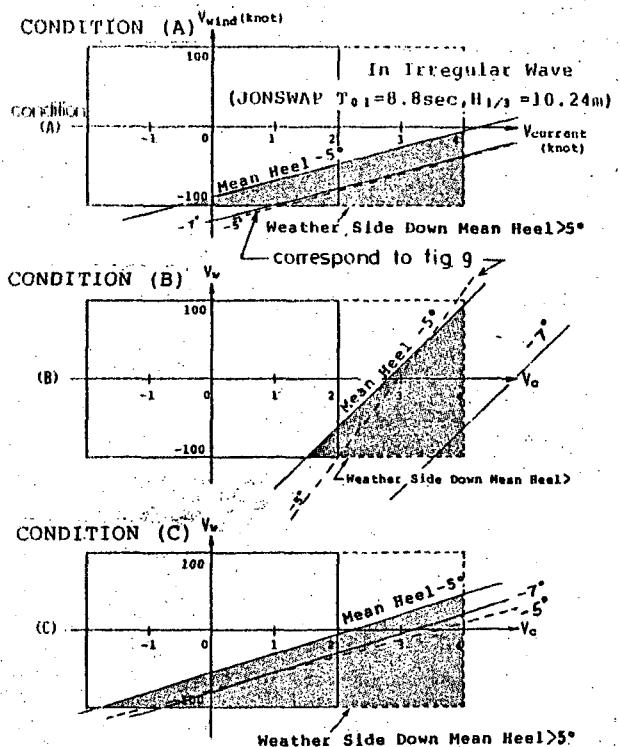

Fig.10 Region showing over 5 degrees weather side down mean heels are seen in the combination of constant current and constant wind under the existence of irregular waves shown in Fig.8

treme maximum tension exceed 80% of breaking load is also shown, but this region appears in condition (A) only.

From this figure, followings will be resulted.
(a) In each figure, the solid line and broken line is not parallel each other, and this means the

CONDITION (A) Vwind

In Irregular Wave
(JONSWAP T_0)=8.8sec,$H_{1/3}$=10.24m)

Weather Side Tension
=T_0(786t)=0.8=629ton

Danger in Tension
629 tan

(A)

Vcurrent (knot)

Danger in Heel
Weather Side Down Max Heel
=20 degrees

CONDITION (B) Vc(knot)

correspond to fig 10

(B)

Vc(knot)

Danger in Heel
Weather Side Down Max Heel=20°

CONDITION (C) Vc(knot)

(C)

Vc(knot)

Danger in Heel
Weather Side Down Max Heel=20°
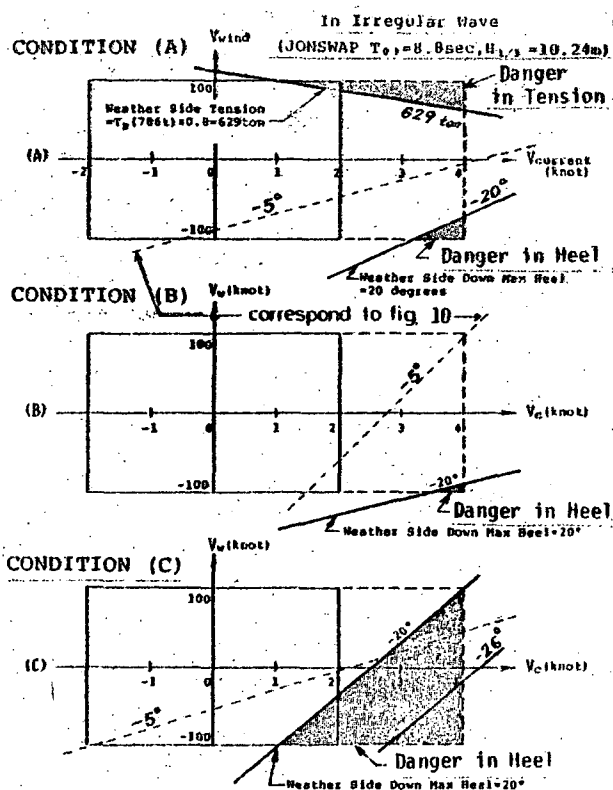
Fig.11 Region showing dangerous situations (over 20 degrees weather side down extreme heel and extreme tensions over 80% of the breaking load) are seen in the combination of constant current and constant wind under the existence of irregular waves shown in Fig.8. The effects of irregular winds will be estimated from empty circles in Fig.8

dynamic effect of irregular wave is not uniform over the combination of current and wind. (b) Small GM case of (C) expands the dangerous region, but reduce dangerous region for tension. (c) On the other hand, about large GM case of (A), dangerous region for tension appear within designed load region (Vcurrent < 2.4 knots, Vwind < 100knots) but dangerous heel does not appear within this region. So there exist optimum combination of GM and mooring lines. (d) On the contrary, the high mooring point of (B) seems not necessarily expand dangerous region for heel opposite to our estimation. (e) As already mentioned in section 4.3, for the case of opposite wind to current and wave, the dangerous situation which excess the down flooding angle can occur even if the common stability criteria is satisfied.

5. CONCLUSION

Following main point will be concluded from the beam sea experiments of moored semi-submersible platform under various kinds of combination of complex and survival external forces. But here, it must be noticed that the irregular wave used here was only one kind which have maximum mean wave drift force.

(1) The most dangerous combination of irregular wind, steady current and irregular wave was made

clear for tension or heel, and it was also shown that there is some possibility that the platform become dangerous in extreme roll angle even if the stability criteria is fulfilled and this is affected by GM and the extraordinary height of fair leader for mooring line.

(2) To avoid dangerous situation both in heel angle and mooring tension, there exist optimum GM, initial tension and the height of fair leader for mooring lines.

(3) Experimental results obtained here will be very reliable because non-contact type optical and electric measurement system is introduced, and because the added pseudo dynamic wind force and pseudo current speed is very clear by the newly developed experimental apparatus.

REFERENCES

[1] Hirayama,T. & Takezawa,S., "Transient and irregular experiments for predicting the large rolling in beam irregular waves" Second International Conference on Stability of Ship and Ocean Vehicles, Tokyo, Oct 1982.

[2] Takarada,N., Obokata,J., Nakajima,T. & Kobayashi,K., "The stability on semi-submersible platform in waves (on the capsizing of moored semi-submersible platform)" Second International Conference on Stability of Ship and Ocean Vehicles, Tokyo, Oct.1982.

[3] Takezawa,S., Hirayama,T. & Morooka,C.K., "A practical calculation method of a moored semi-submersible rig motion in waves (in Japanese, but english edition is under printing by JSNA JAPAN as SELECTED PAPERS)." Journal of The Society of Naval Architects of Japan, Vol.155, June 1984.

[4] Takezawa,S. & Hirayama,T., "Safety on a moored semi-submersible platform under extreme complex external loads." Fifth internal symposium on offshore mechanics and arctic engineering, April 1986.

[5] The 102nd Research Panel (SR192) "Studies on the design loads and the stability of ocean structures (in Japanese)" The Shipbuilding Research Association of Japan, No.379, March 1985.

DETAILS CONCERNING THE AUTHORS

Seiji TAKEZAWA

Professor / Doctor
Graduated from the University of Tokyo
(Faculty of Engineering),
Now the Professor of Yokohama National University(Department of the Naval Architecture and Ocean Engineering),

Majoring in ship and floating body performances in waves.

Tsugukiyo HIRAYAMA

Associate Professor / Doctor
Graduated from Yokohama National University
(Faculty of Engineering);
Now the Associate Professor of the same university and the same department of Professor TAKEZAWA,

Majoring in ship and floting body dynamics in waves.

Postal Address;

Yokohama National University, Faculty of Engineering

Tokiwadai-156,Hodogaya-ku,Yokohama,
JAPAN 240

Telex: 3822614 YNUENG J

COMPARISON OF WIND OVERTURNING MOMENTS ON A SEMISUBMERSIBLE OBTAINED BY CALCULATION AND MODEL TEST

B.K. Yu, Y.S. Won

ABSTRACT

One of the main disadvantages of a semisubmersible is its small payload capacity compared with that of a conventional ship type vessel. Stability during the transit condition is not a major factor of semisubmersibles due to their large water plane area (large restoring moment) in spite of its large wind overturning moment. Therefore the payload capacity in the transit condition is usually determined by its displacement regardless of its stability. But in the operating and survival conditions the stability limit is the crucial factor for the payload capacity because of its small water plane area. This stability limit depends on the wind overturning moment and the stability criteria to be applied.

This paper explains the wind tunnel test procedure in accordance with the Norwegian Maritime Directorate (NMD) guidelines and the wind overturning moment calculation methods according to American Bureau of Shipping (ABS) and Det norske Veritas (DnV) rules. These three results applied for a typical semisubmersible were compared and physically explained on their discrepancies. The payloads were also estimated in accordance with ABS and DnV stability criteria, and both results were compared with each other. As a calculation example, the Aker H4.2 model (a typical modern eight-column semisubmersible drilling platform) presently under construction at HHI shipyard, was used.

NOMENCLATURE

A : wind exposed area

Ap : projected area perpendicular to the wind direction

B : beam length of main deck

Cd : nondimensional drag coefficient $(= F/0.5\,\rho\,Lpp^2\,V_{10}^2)$

Ch : height coefficient as a function of the height above the water line

Cl : nondimensional lift coefficient $(= Lift/0.5\,\rho\,Lpp^2\,V_{10}^2)$

Cm : nondimensional moment coefficient $(= M/0.5\,\rho\,Lpp^3\,V_{10}^2)$

Cs : shape coefficient as a function of the geometry of the element

d : distance between the acting point and the center of the main deck

Da : drag force on the above-water part of a platform

Du : resultant force on the under-water part of a platform

F : drag force in the wind direction (ABS rule)

Fn : drag force normal to the elemental surface (DnV rule)

H : height above the sea level

Ha : distance of the center of the wind force above the water line

Hu : distance of the center of reaction below the water line

L : longitudinal length of main deck

Lpp : length between the perpendiculars (= 110 m)

M : wind overturning moment

Ma : overturning moment on the above-water part of a platform

Mu : overturning moment on the under-water part of a platform

Vh : mean wind speed at height H above sea level

V_{10} : mean wind speed at 10 m above sea level

α : power law wind profile exponent

β : angle between the longitudinal axis and the wind direction

κ : surface drag coefficient

ρ : density of air

σ_x^2 : RMS value of the longitudinal turbulent velocity component

1. INTRODUCTION

The wind drag force and overturning moment are very important factors in the design of a semisubmersible platform. The wind force is one of the main environmental forces critical in the design of an adequate mooring system or a dynamic positioning system in order to keep the platform on location during the drilling operation. The wind overturning moment is used to estimate the hydrostatic stability and to determine the payload of the platform at different drafts. In this regard, considerable effort has been made to estimate the wind force and overturning moment accurately in the proper design of platforms [1,2].

Through cumulative experiences, classification societies have suggested empirical calculation procedure to predict the wind force and moment. The basic and typical calculation procedure is adopted by ABS rules and regulations [3]. It assumes that the wind drag force is proportional to the shape coefficient, the height coefficient and the square of the mean wind velocity. The shape coefficient is given for the various shape of structures from cumulative experiences and the height coefficient is given as a step function of the elevation from the water surface to simulate the ocean wind. The ABS method gives practical estimate of wind forces but cannot consider other complicated flow effects due to lift, shielding and solidification. Such effects were taken into consideration by the DnV [4]. However the DnV method poses difficulties in design practice due to its complexity and sophistication.

To date, the most reliable method to obtain the wind force and moment appears to be by carrying out the wind tunnel test with a carefully scaled model. Most classification societies hence accept the wind forces obtained by either the calculation method or the wind tunnel test, with the NMD [5] mandatorily requiring wind tunnel test for all new buildings working in the Norwegian sector of the North Sea, and for other new buildings under the Norwegian Flag.

This paper presents the wind tunnel test procedure according to the NMD guideline and the empirical calculation methods used in ABS and DnV rules. The wind forces and moments have been calculated employing the lever arm approach as done in the analysis of the wind tunnel test results for the typical semisubmersible drilling platform under construction at HHI. The calculation results according to ABS and DnV methods are compared with the wind tunnel test results. In addition the deck payloads have been estimated based on the stability results from the three different methods.

2. WIND TUNNEL TEST

The model tests were performed at the Danish Maritime Institute wind tunnel in accordance with Norwegian Maritime Directorate (NMD) guidelines for the wind tunnel test procedure. According to these guidelines, the model should be tested for the above-water construction and the under-water body separately.

2.1 Wind Tunnel

Wind tunnel tests were carried out on a model of the Aker H4.2 drilling platform in the test section of the closed-circuit wind tunnel, with dimensions of 1.0 m height, 0.7 m width and 2.6 m length. The maximum wind speed is 80 m/sec and the grid of tubular rods were provided to simulate ocean wind profile. On the bottom of the test section a turntable was located to set and rotate the model. The forces on the model were measured by the 6-component strain gauge balancer while pressures were measured by the low-

pressure transducers.

2.2 Model

The model scale used in the tests was 1:285 which means a pontoon length of 0.386 m. The model materials were plastic, brass and wood. It contains all structural details and equipment fitted, which could affect the test result significantly. The respective photographs of the above- and under-water parts of the model are presented in Photos 1 and 2.

2.3 Simulation of Ocean Wind

The above-water part of the model has a smooth hull and it was tested in a simulated natural ocean wind of which the characteristics can be described by two parameters, i.e., the mean velocity profile and the turbulence intensity.

The mean velocity profile :

$$Vh / V_{10} = (H/10)^{\alpha}$$

The turbulence intensity :

$$\sigma_x / Vh = 2.45 \sqrt{\kappa} \ (H/10)^{-\alpha}$$

The ocean wind profile was simulated by means of a graded grid consisting of horizontally placed tubes mounted 2 meters upstream of the model. The velocity and turbulence intensity were measured by a hot-wire anemometer.

As the value of exponent, α , the NMD recommends the range of 0.11 to 0.14. As in Fig.1, values for α and κ in this model test were 0.115 and 0.001 respectively. For the under-water body the tests were performed in a uniform low turbulence flow.

2.4 Scale Effect

Flow around a body is a function of the Reynolds number. To precisely ensure the same flow in the model scale as in full scale, it is necessary to make model tests at a Reynolds number identical to that of the prototype structure.

As is inevitable for a large offshore structure designed for severe wind conditions, exact prototype Reynolds number cannot be attained in tests. However, for practical purposes, it is sufficient to require that the character of the flow in the model scale is the same as that of the full scale flow to obtain reliable results from model tests. This condition is satisfied at rather low Reynolds number for flow around models with sharp edges, where the separation always takes place at the edges almost regardless of the speed. Consequently for the above-water part most structures including deck structures, derrick, and even the cylindrical bodies in shield area may show little scale effect.

However, most structures underneath the main deck such as column, pontoons and bracing consist of cylindrical elements, loads upon which are subject to considerable Reynolds dependence. This is because the flow around them in model scale remains in the laminar region. On the contrary in full scale flow field, separation may take place at round body and the flow field becomes turbulent. Therefore the model underneath the main deck was tested with an artificial roughness on the body surface (See Photo 2) to simulate similar turbulent flow field to that of the prototype. The comprehensive investigation is elaborated in [6].

Before the main test program began, Reynolds dependence tests were performed to ensure that the Reynolds numbers applied during the tests would be sufficiently high to avoid severe scale effects. The results of these tests are shown in Fig.2 and Fig.3 for the above-water part and the under-water part, respectively, where the Reynolds number is based on Lpp. The wind speed for the subsequent tests were determined to be 40 m/sec free stream for the above water part and 50 m/sec for the under-water part.

2.5 Calculation of Overturning Moment

The center of reaction is important in the estimation of the wind overturning moment as the latter equals the wind force acting on the semisubmersible in the wind direction multiplied by the distance from the center of the force to the center of reaction [7]. Thus, wind overturning moment may be expressed as:

$$M = Da (Ha + Hu)$$

The wind force or drag, Da, and its center above waterline, Ha, were obtained from the model tests with the above-water part of the model, and the center of reaction, Hu, is normally obtained from tests with the under-water part.

Analysis was first performed for the above-water part of the semisubmersible. The center of action of the wind force is then obtained from the measured moment as :

$$Ha = Ma / Da$$

The measured overturning moment, Ma, contains the effect of aerodynamic drag and the effect of lift.

For the under-water part, the height of the center of reaction is calculated as :

$$Hu = Mu / Du$$

Here Mu is the measured overturning moment for the under-water part, which consists of both hydrodynamic drag and hydrodynamic lift. Du represents resultant force acting on the under-water part.

For the free floating condition, the hydrodynamic drag, Du, equals the wind drag force, Da. However Ha and Hu will not necessarily be the same as the distance to the geometrical centers of the above-water part and the under-water part. This approach is illustrated in Fig.4.

2.6 Test Program

In accordance with NMD guideline the model tests were performed at three different drafts, transit : 7.5 m, survival : 19.5 m and operation : 23.5 m. For each of the three loading conditions the wind direction was changed in steps of 10° from 0° to 360° to find the critical wind directions at which the wind overturning moment becomes maximum. These results showed that the critical wind directions are 90° for the transit draft, and 310° for the operational and survival drafts, respectively. The model was then inclined around these axes to measure the forces and moments at the inclining angles of 15° and 20°. The test results are reported in [8].

3. EMPIRICAL CALCULATIONS

3.1 Classification Rules

First consider ABS rules for mobile offshore drilling units to estimate the wind forces. According to the ABS/MODU method, the force due to the wind acting on a vessel is obtained by a summation of forces acting on each subdivided element. The force on each element is expressed by the following equation which has been developed through numerous model tests and full scale experiences.

$$F = 0.5 \rho \, Cs \, Ch \, Ap \, V_{10}^2$$

The Norwegian classification, DnV, established a general formula to estimate the wind loads on the offshore structures based on a rather sophisticated approach. This formula may be expressed as :

$$Fn = 0.5 \, \rho \, Cs \, A \, \cos^2 \beta \, Vh^2$$

The important differences between ABS and DnV methods can be categorized into three aspects. Firstly the respective methods calculate wind forces in different directions. Namely, in the DnV method the wind drag force normal to the elemental surface is calculated, whereas in the ABS method the drag force

in the wind direction is calculated. As an example, the drag force in the wind direction on the inclined element shows the discrepancy of $\cos^2 \beta$ between two methods if the same shape coefficient and the same wind velocity are assumed. For the wide rectangular cross sectional element such as the main deck of a semisubmersible platform, the DnV method requires assuming that the normal force to the elemental surface is acting at one-third point from the leading edge of the element to consider the lift effect.

The second aspect is that the classification societies adopt different values of shape coefficient. The DnV method gives in general larger shape coefficients than those of ABS. However these results from DnV methods were adjusted by taking into consideration of the geometry and arrangement of elements in more detail, such as the shielding effects, three dimensional effects, solidification effects and various shapes of the cross sections.

The third aspect is the wind velocity profile, which is defined as a step function in the ABS method by introducing the height coefficient, Ch. In the DnV method the wind velocity profile is defined as an exponent fuction of height.

3.2 Assumptions for Calculation

The projected area of the semisubmersible considered herein comprised 18 elements commensurating with configurations and locations. For each element, the element force was calculated individually and the summation of them resulted in the total wind force. For wind overturning moment calculation, the same procedure as used in wind tunnel test was also used i. i.e., the wind overturning moment can be obtained by multiplying the total wind force by the distance between the centers of the wind force and the reaction.

To simplify calculation during the inclination of the platform, several assumptions were made as long as they did not induce any significant errors. First,

the projected area is assumed to remain unchanged during inclination. This projected area is always located near the free surface boundary and does not induce significant change of the wind overturning moment in which we are interested. Secondly, the assumption is made that the elevations of the element acting points do not vary with any considerable significance. This assumption might compensate the increase of reaction arm and the decrease of wind force arm.

In application of the DnV method for the wide rectangular cross-sectional element the acting point of wind force is assumed to be located at one-third from the leading edge. In case of the diagonal wind direction the acting point on the maindeck of the semisubmersible is assumed to be described as follow :

$$d = L B / 6 (L \sin \beta + B \cos \beta)$$

4. RESULTS AND DISCUSSIONS

The results from the wind tunnel test and empirical calculation methods are plotted in Fig.5 through Fig.13 for transit, storm and operating drafts, respectively. Figs.5 through 7 show the comparison of the results along the wind directions at the even keel condition; Figs.8 through 13 for the inclining angles in the transverse and the critical wind directions.

The figure a) for each presents the drag and lift coefficients for the above-water part as defined in Nomenclature. The figure b) presents the above- and under-water lever arms as discussed in the previous section. Finally the wind overturning moment coefficients are plotted in the figure c). This gives the heeling levers for stability analysis.

4.1 Variations along the Wind Directions

Both calculation methods overpredict the drag forces on the above-water part. In the diagonal wind direction, the ABS method was determined to be more

conservative while alternately in the transverse direction, the DnV method was more conservative. From the wind tunnel test it is found that there are lift forces even at the upright condition. The lift forces are sensitive to the wind directions and may contribute significantly to the overturning moment, depending on the location of the center of lift.

The calculated lever arms remain almost constant because the overturning moment due to the lift effect is not included for the even keel condition in both calculation methods. The lever arms obtained from the wind tunnel test vary with the lift forces. Hence the lift forces contribute significantly to the overturning moment in even keel condition, particularly for the under-water part. In all wind directions, the under-water lever arms obtained from the wind tunnel test show much larger values than the calculated ones. These under-water lever arms are the most uncertain factor in determining the wind overturning moment. That is, in calculation methods the overturning moment due to the lift effect cannot be considered in even keel condition, whereas in the wind tunnel test the scale effect may overwhelm the test results for the under-water body composed of several cylindrical elements.

The wind overturning moments between the calculated values and model test results show sufficient correlation to determine the critical axis, except for the transit draft at which the lift force is dominant for the overturning moment.

In this example, the calculation methods as a whole overestimate the drag forces and underestimate the lever arms. This underestimation seems to come from the neglect of lift effects.

4.2 Variation along the Inclining Angle

Fig.8 through Fig.13 present the main results at each draft when the vessel inclines in the transverse and diagonal wind directions.

The calculation methods overpredicted the drag forces than the model test result. The calculated drag force according to the DnV method shows a similar trend to that of the model test result, whereas the ABS method results in linearly increasing drag force. As mentioned in the previous section, the ABS and DnV methods demonstrated more conservative results in the diagonal and transverse wind directions respectively.

The ABS method does not include the lift force, while the DnV method includes the lift force on the wide rectangular element, i.e., the main deck of the semisubmersible. The DnV method gives it the linearly increasing lift force but underestimates in comparison with the model test result.

The trends of the calculated lever arms and the model test results show large discrepancies. The calculated lever arms vary almost linearly, whereas the model test results vary sensitively to the inclination of the vessel. These discrepancies may be attributed to the lift effect, particularly for the under-water levr arms. The fact that the lever arms from the model test decrease as the inclining angle becomes large implies that the location of the lift center moves leewards and the lift force contributes to reduce the overturning moment at the large inclining angles.

The wind overturning moments obtained by the calculation methods illustrated serious discrepancies at the transit draft where the lift effects are so dominant that the calculation methods cannot predict the wind overturning moment properly. At the storm and the operating drafts, the calculation methods gave conservative results in the transverse wind direction, but not in the diagonal direction.

4.3 Payload and Maximum Allowable KG

The obtained wind overturning moments were used to estimate the hydrostatic stability and to determine the payload of a semisubmersible. This section provides

the summary for the difference of payloads for different wind overturning moments when adopted in stability calculations.

The payload calculation for the transit condition was not included as stability is not a major factor. For the survival condition, the payload with the platform unmoored was calculated for a wind speed of 100 knots. For the operating condition, only the intact stability was considered in this analysis to emphasize the effect of wind overturning moment on the payload calculation. However, the damaged stability should be included to determine the exact payload for the operating condition.

The maximum allowable KG values and the corresponding pure deck payloads were derived in accordance with the stability criteria of ABS and DnV rules. The ABS stability criteria were applied to the wind overturning moment obtained by the model test and the ABS method, whereas the DnV stability criteria were applied to the model test and the DnV method. The results are summarized as below in Table 1.

TABLE 1. PAYLOAD AND MAXIMUM ALLOWABLE KG

RULE	WIND	SURVIVAL	OPERATION
ABS	MODEL TEST	4341(18.98)*	6168(19.79)**
	ABS METHOD	4939(19.55)	6258(19.87)
DnV	MODEL TEST	4236(18.86)	6168(19.79)
	DnV METHOD	4740(19.36)	6461(20.05)

* denotes payload in tons.
** denotes maximum allowable KG in meters.

The magnitude of the wind overturning moments in the critical direction was in the order of model test results, ABS method and finally DnV method. Consequently, the payload of each method was in the direct opposite order. However, it was noted that in the survival condition, the payload according to DnV

criteria was smaller than that by ABS due to the additional requirement of the maximum static heeling angle of 15 in DnV rule.

5. CONCLUSIONS

In this example, the following conclusions were obtained :

- The ABS method is more conservative than the DnV method in the diagonal wind direction whereas the opposite was determined in the transverse direction.

- The calculation methods are always more conservative than the model test results as far as the drag force is concerned, but not necessarily for the wind overturning moment.

- The discrepancies between the calculation results and the model test results may be attributed to the lift effect. The lift effect is more significant for the underwater part, at the transit draft, and at the large inclination angles.

- One of the main difficulties in estimating the wind overturning moment was the determination of the center of reaction for the under-water lever arm.

- The payloads from the model test results were conservative than those from the calculation methods.

REFERENCES

1] Norton, D.J., "Mobile Offshore Platform Wind Loads", Offshore Technology Conference, Houston, Texas, 1981, OTC paper No. 4123.

2] Macha, J.M. and Reid, D.F., "Semisubmersible Wind Loads and Wind Effects", Transaction of the Society of Naval Architects and Marine Engineers, 1984, Paper No. 3.

3] American Bureau of Shipping, "Rules for Building and Classing Mobile Offshore Drilling Units", New York, 1985.

4] Det norske Veritas, "Rules for Classification of Mobile Offshore Units", Oslo, Norway, 1985.

5] Norwegian Maritime Directorate, "Mobile Drilling Platforms, Regulation laid down by Norwegian official control institutions", 1982.

6] Jacobsson, P. and Dyne, G., "Reynolds Number Effects in Model Tests with a Four-Column Semisubmersible", Second International Symposium on Ocean Engineering and Ship Handling, Gothenburg, Sweden, 1983, pp.343 - 362.

7] Bjerregaard, E.T.D. and Sorensen, E.G., "Wind Overturning Effect Obtained from Wind Tunnel Tests with Various Semisubmersible Models", Offshore Technology Conference, Houston, Texas, 1981, OTC paper No. 4124.

8] Wind Tunnel Test Report, "Wind Tunnel Tests with the Aker H-4.2 I Semisubmersible Drilling Platform", test performed at Danish Maritime Institute, 1985, proprietary of Hyundai Heavy Industries Co., Ltd.
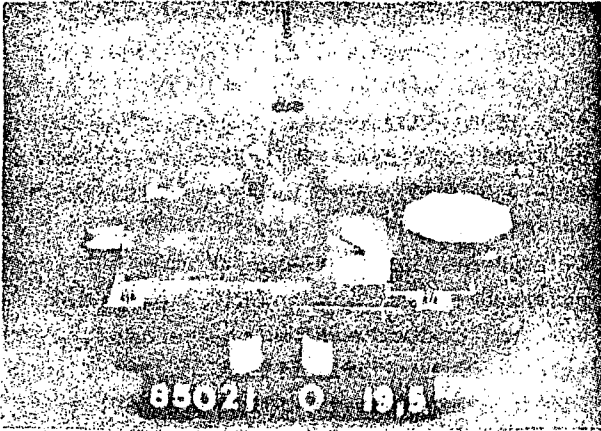
PHOTO.1 ABOVE-WATER MODEL

FIG.2 Re-TEST FOR ABOVEWATER MODEL

PHOTO.2 UNDER-WATER MODEL
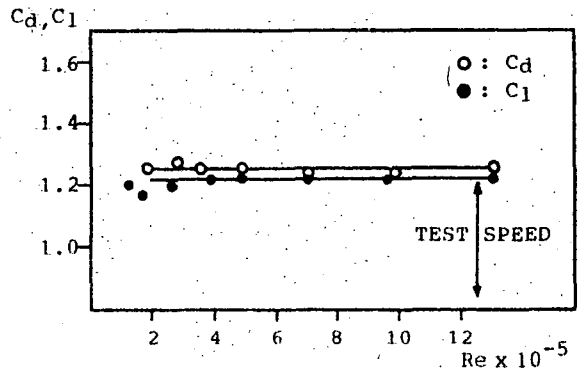
FIG.3 Re-TEST FOR UNDERWATER MODEL
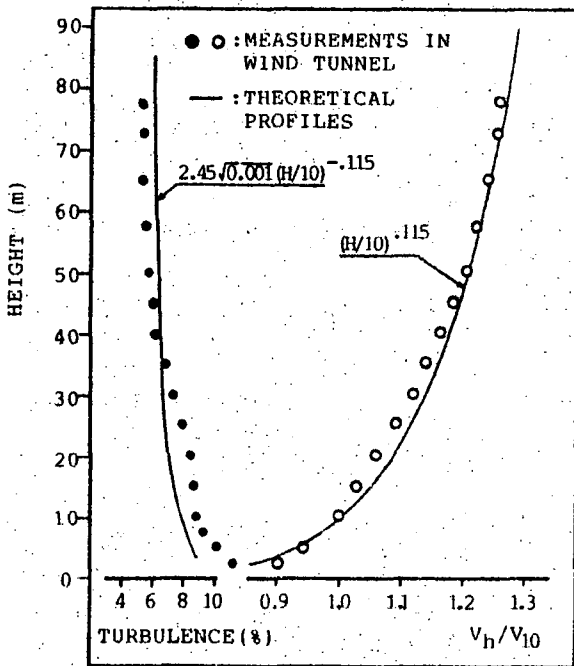

FIG.1 PROFILES OF WIND SPEED AND
TURBULENCE INTENSITY
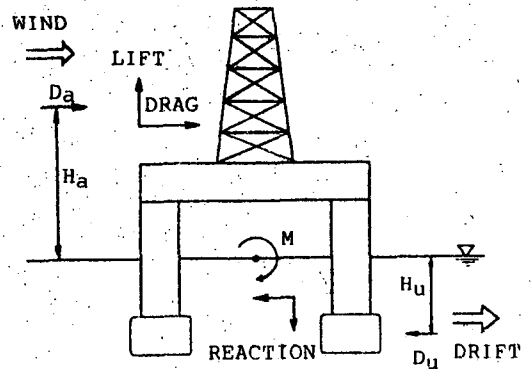
FIG.4 LEVER ARM APPROACH METHOD
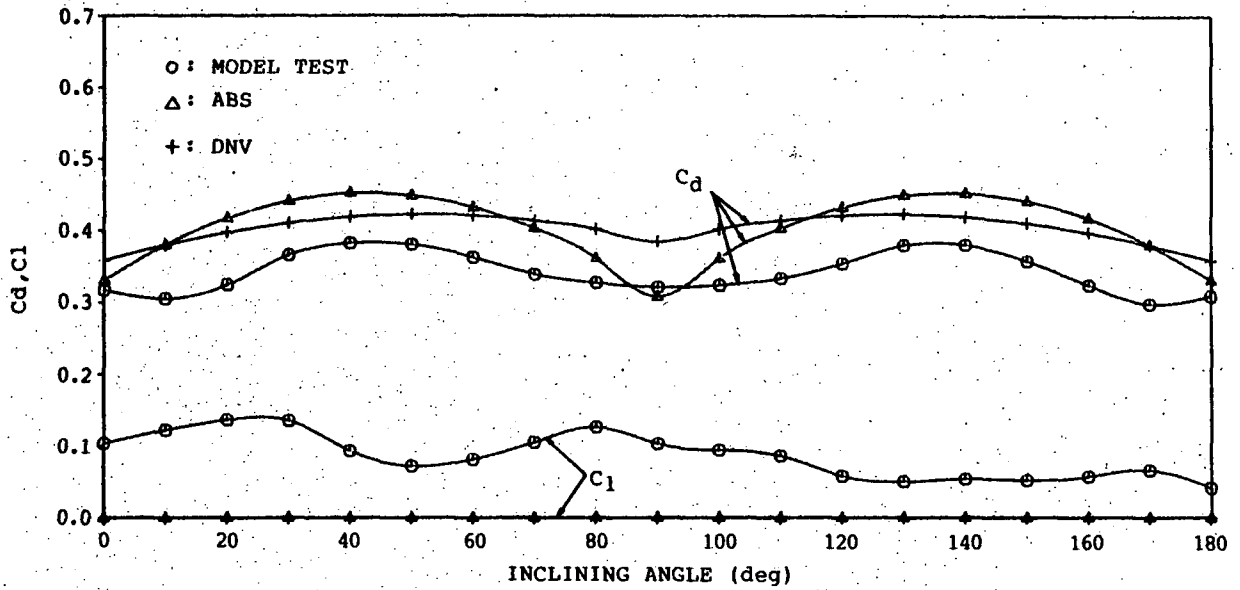
a) DRAG/LIFT COEFFICIENT
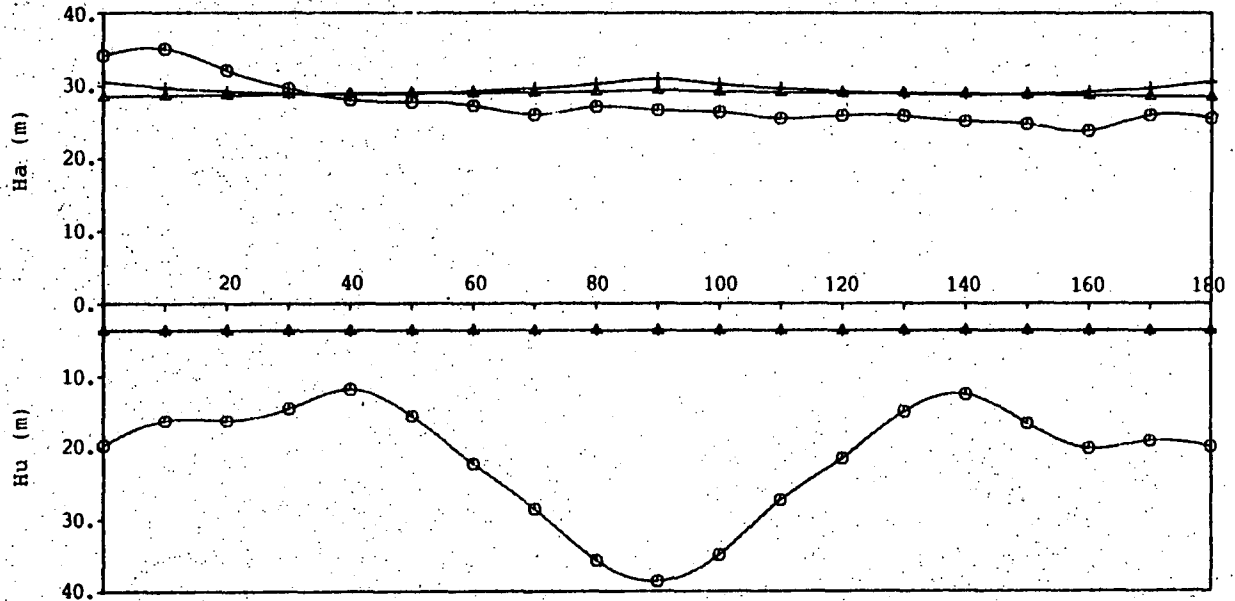
b) ABOVE-/UNDER-WATER LEVER ARM
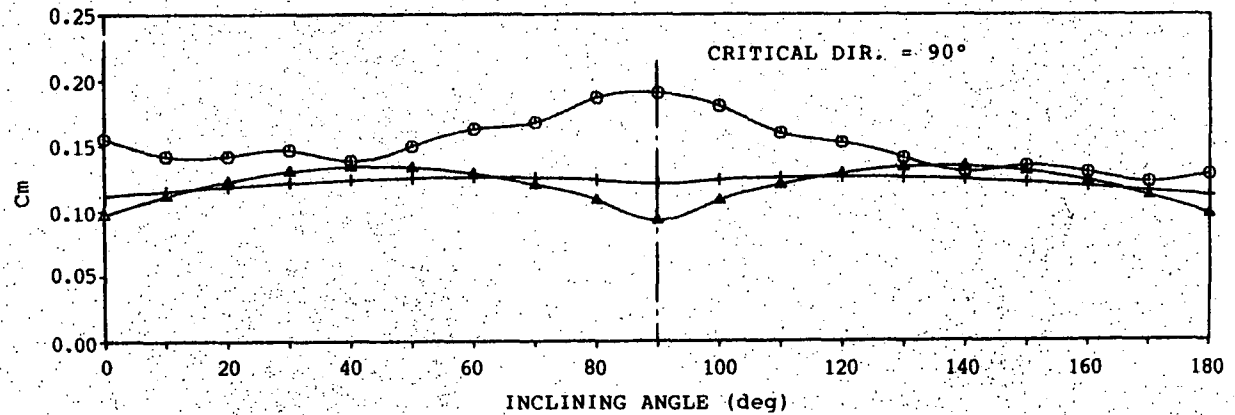
c) OVERTURNING MOMENT

FIG.5 CRITICAL WIND DIRECTION (TRANSIT DRAFT)

- 262 -
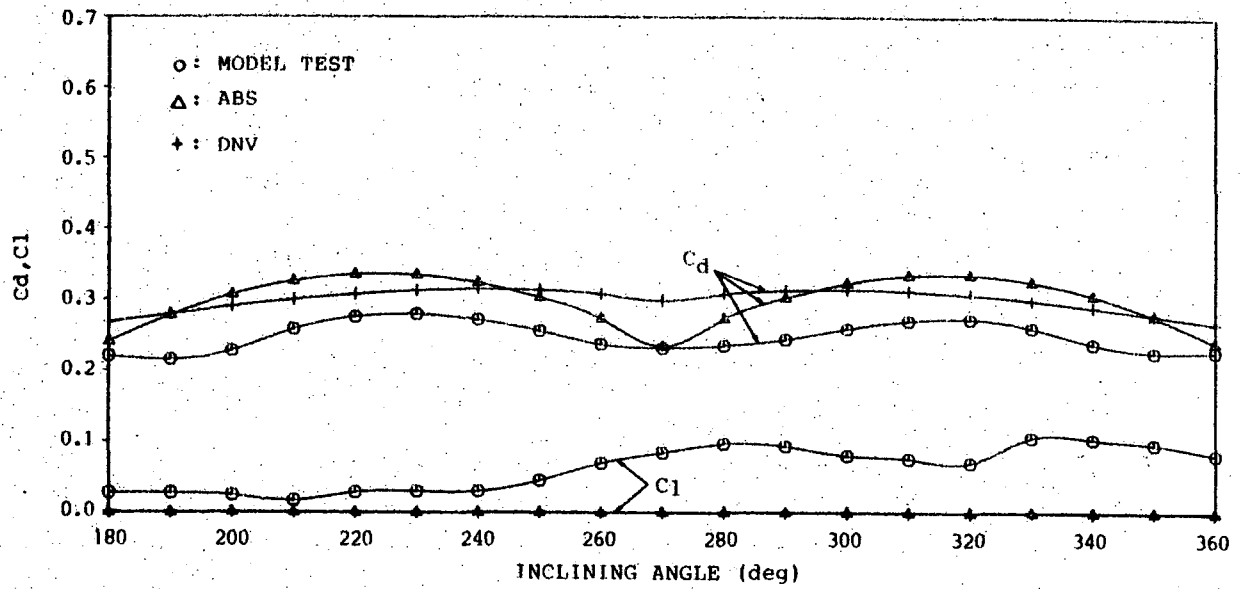
a) DRAG/LIFT COEFFICIENT
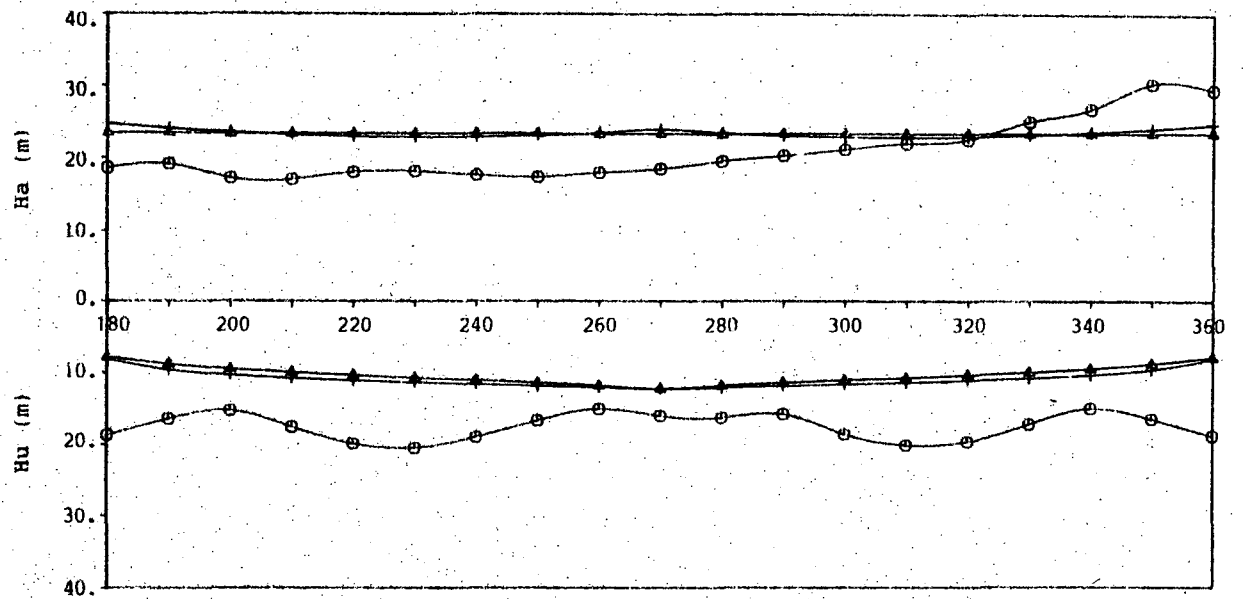

b) ABOVE-/UNDER-WATER LEVER ARM
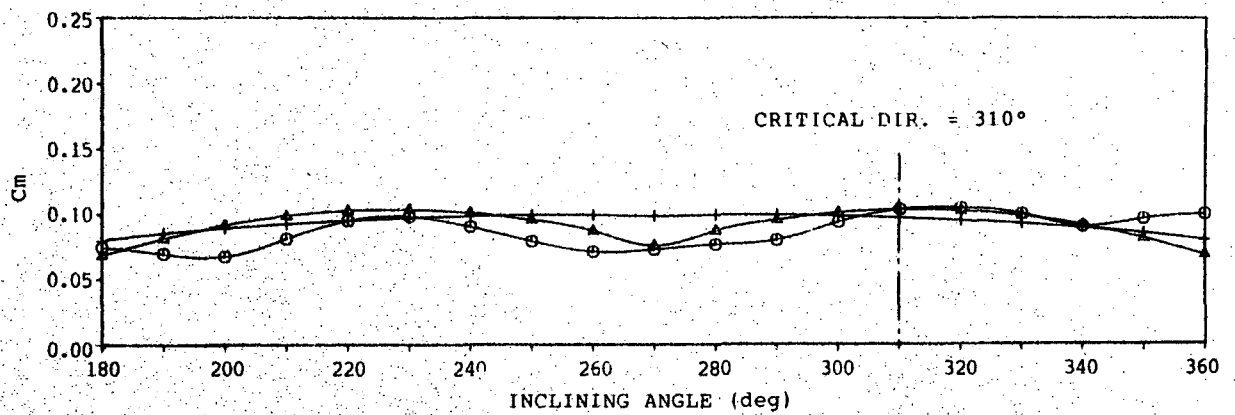

c) OVERTURNING MOMENT

FIG.6 CRITICAL WIND DIRECTION (SURVIVAL DRAFT)
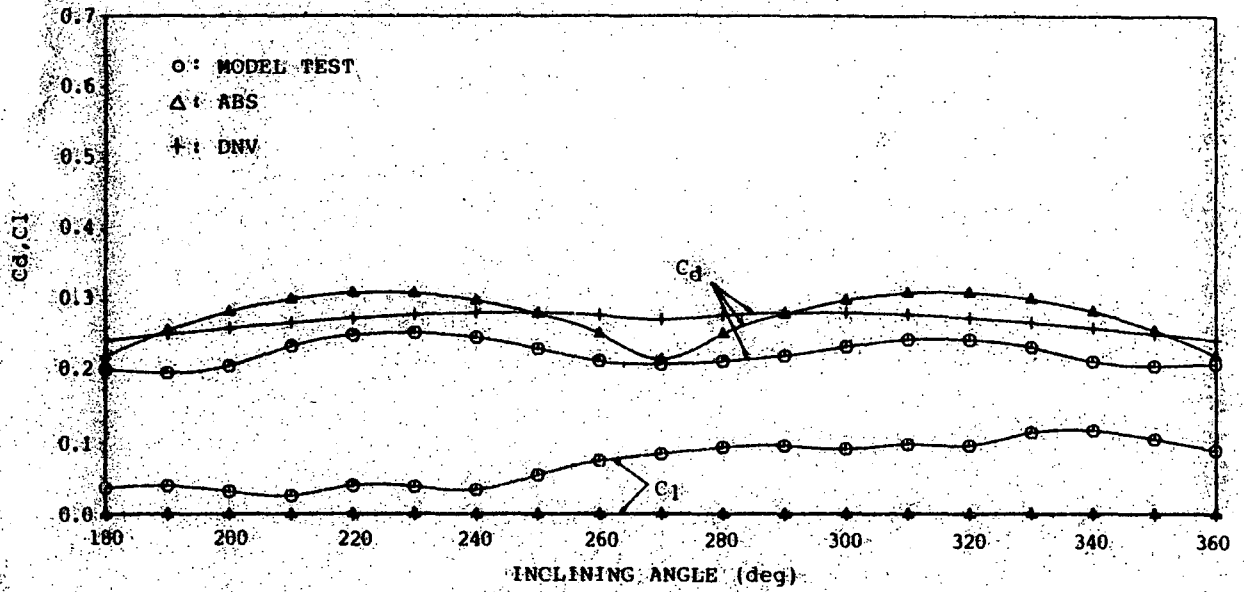
a) DRAG/LIFT COEFFICIENT
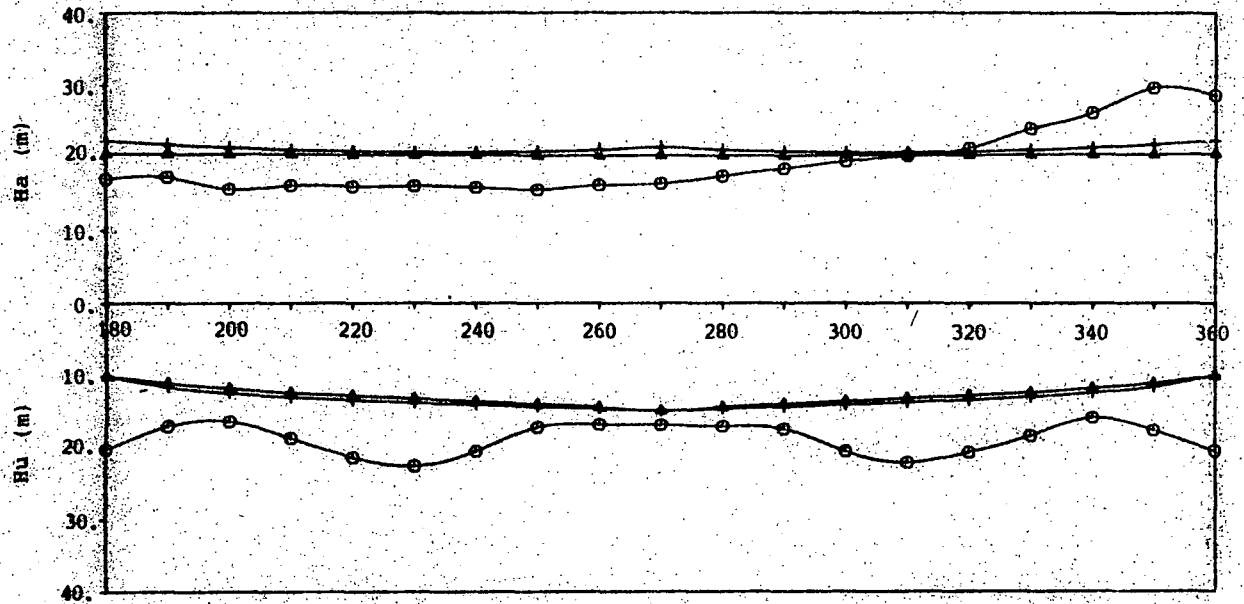
b) ABOVE-/UNDER-WATER LEVER ARM
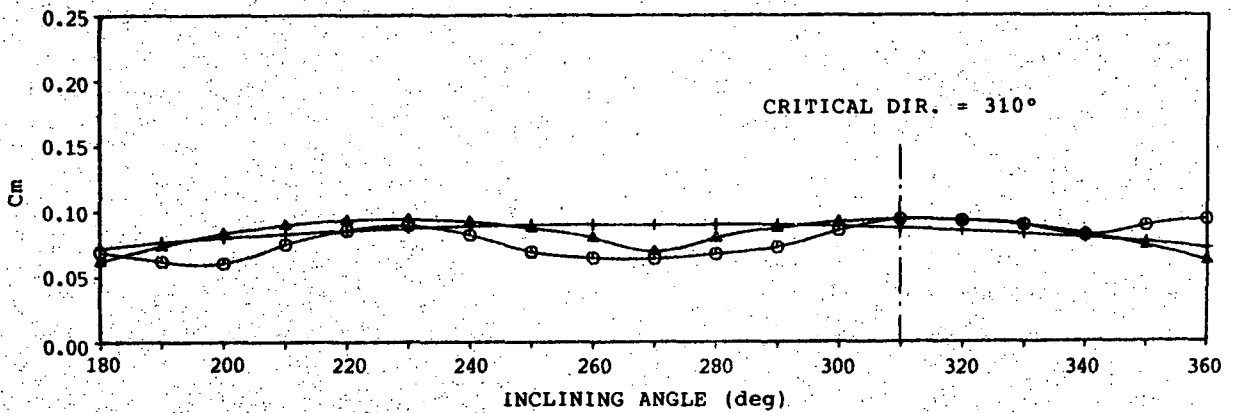
c) OVERTURNING MOMENT

FIG.7 CRITICAL WIND DIRECTION (OPERATING DRAFT)
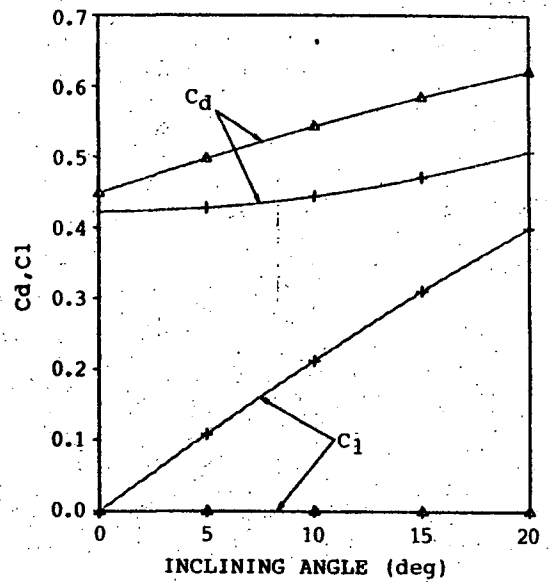
o: MODEL TEST
△: ABS
+: DNV

a) DRAFT/LIFT COEFFICIENT

b) ABOVE-/UNDER-WATER
LEVER ARM
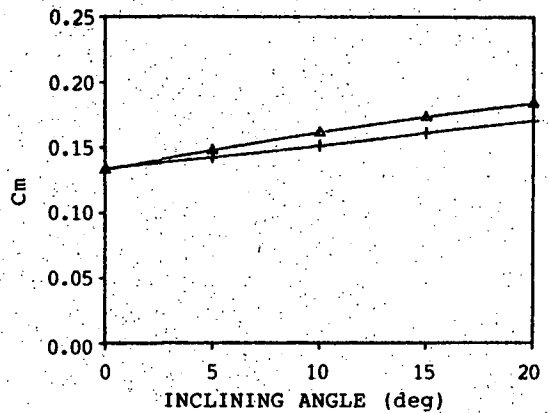
c) OVERTURNING MOMENT

FIG.8 RESULTS FOR INCLINATION
(TRANSVERSE WIND, TRANSIT)

a) DRAG/LIFT COEFFICIENT
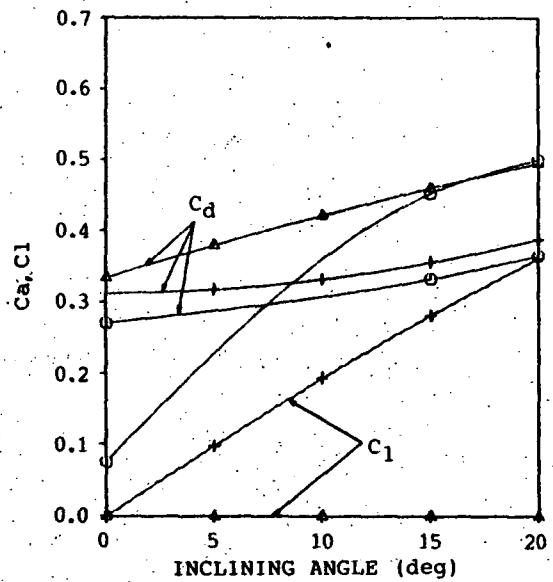
b) ABOVE-/UNDER-WATER
LEVER ARM

c) OVERTURNING MOMENT

FIG.9 RESULTS FOR INCLINATION
(DIAGONAL WIND, TRANSIT)

o: MODEL TEST
Δ: ABS
+: DNV

a) DRAG/LIFT COEFFICIENT

a) DRAFT/LIFT COEFFICIENT
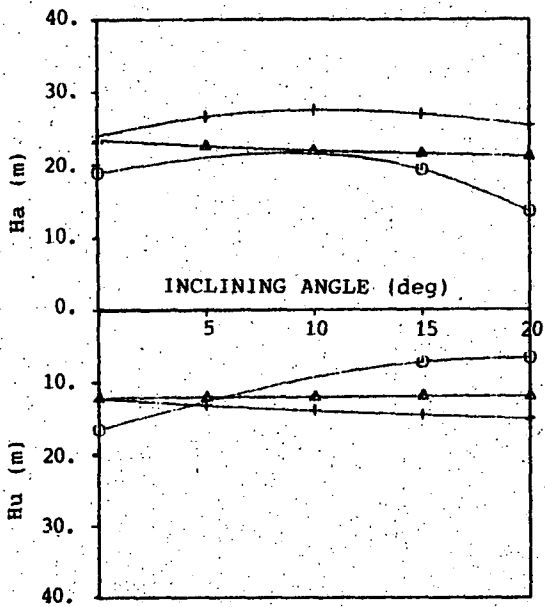
b) ABOVE-/UNDER-WATER LEVER ARM
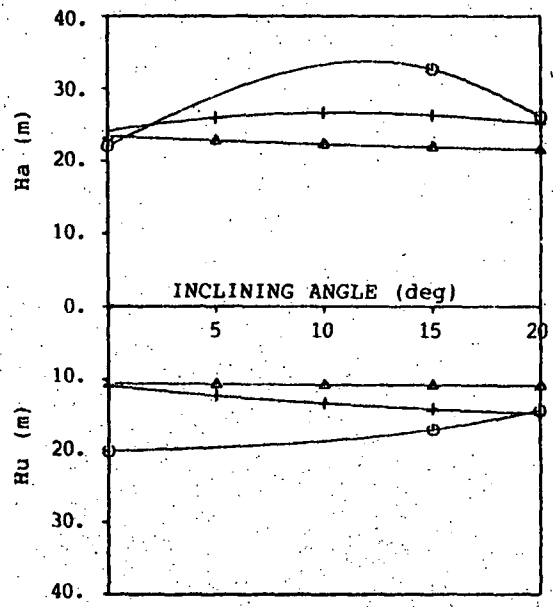
b) ABOVE-/UNDER-WATER LEVER ARM
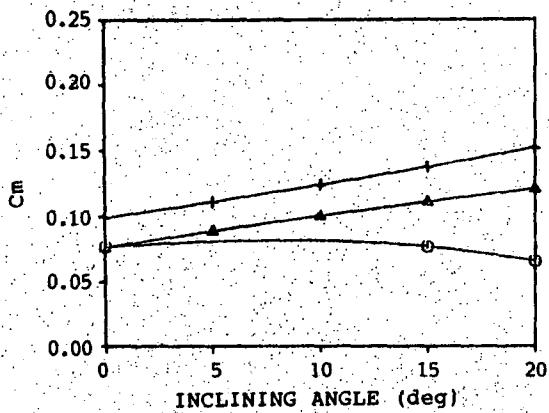
c) OVERTURNING MOMENT
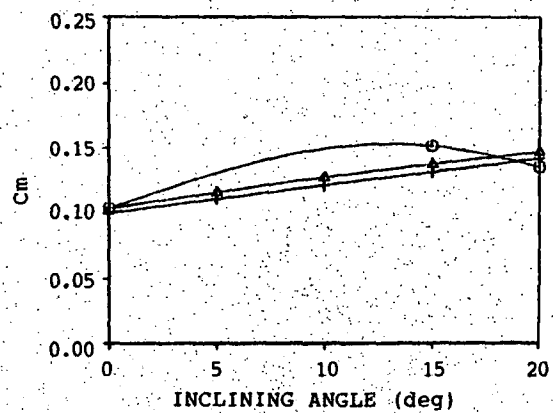
c) OVERTURNING MOMENT

FIG.10   RESULTS FOR INCLINATION (TRANSVERSE WIND, SURVIVAL)

FIG.11   RESULTS FOR INCLINATION (DIAGONAL WIND, SURVIVAL)

- 266 -

o: MODEL TEST
△: ABS
+: DNV

C_d

C_1

INCLINING ANGLE (deg)

a) DRAG/LIFT COEFFICIENT

C_d

C_1

INCLINING ANGLE (deg)

a) DRAFT/LIFT COEFFICIENT

b) ABOVE-/UNDER-WATER
LEVER ARM

b) ABOVE-/UNDER-WATER
LEVER ARM

INCLINING ANGLE (deg)

c) OVERTURNING MOMENT

INCLINING ANGLE (deg)
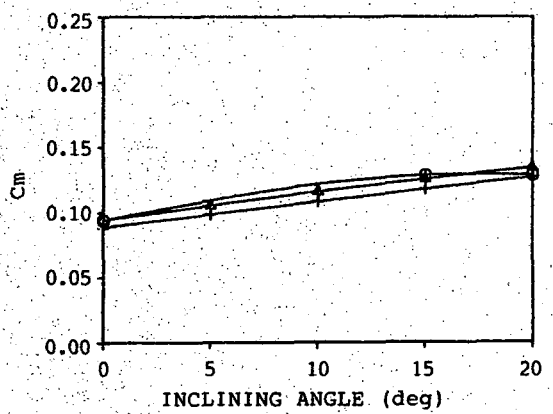
c) OVERTURNING MOMENT

FIG.12   RESULTS FOR INCLINATION
(TRANSVERSE WIND, OPERATING)

FIG.13   RESULTS FOR INCLINATION
(DIAGONAL WIND, OPERATING)

TITLE :

COMPARISON OF WIND OVERTURNING MOMENTS ON A SEMISUBMERSIBLE OBTAINED BY CALCULATION AND MODEL TEST

AUTHOR'S NAME : Y.S. WON and B.K. YU

COMPANY NAME   : HYUNDAI HEAVY INDUSTRIES CO., LTD.,
                  ULSAN, REPUBLIC OF KOREA

AUTHOR'S CAREERS

Y.S. WON

1] Ms., Naval Architect (1982), Seoul
   National University, Seoul, KOREA

2] 1/1982 - Present
    Researcher at Hyundai Maritime
    Research Institute, HHI, KOREA

B.K. YU

1] Ph.D., Naval Architect and Offshore
    Engineering (1979), University of
    California, Berkeley, U.S.A.

2] 2/1984 - Present
    Principal Researcher at Hyundai
    Maritime Research Institute, HHI,
    KOREA

3] 4/1982 - 1/1984
    Senior Naval Architect at Global
    Marine Development Inc., U.S.A.

4] 7/1979 - 4/1982
    Senior Researcher at the Offshore
    System Div., Lockheed Missiles &
    Space Co., U.S.A.

ON THE OCCURRENCE OF STEEP ASYMMETRIC WAVES IN DEEP WATER

by

D. Myrhaug[*] and S.P. Kjeldsen[**]

ABSTRACT

Traditional wave steepness s = H/L does not de-
fine steep asymmetric waves in a random sea uniquely.
Three additional parameters characterising single
zero-downcross waves in a time series are crest front
steepness, vertical asymmetry factor and horizontal
asymmetry factor. Results for steepness and asymmetry,
from zero-downcross analysis of wave data obtained
from full scale measurements in deep water on the
Norwegian continental shelf in 58 time series are
presented. The analysis demonstrates clearly the
asymmetry of both "extreme waves" and the highest
waves. Further, estimates for encounter probabili-
ties of occurrence of steep and high waves in deep
water for given sea states described by a JONSWAP
spectrum are presented by using the joint distri-
bution of crest front steepness and wave height.

1. INTRODUCTION

Experience both among naval architects and civil
engineers show that damages to marine structures in
many cases are found to be due to the combined simul-
taneous action of several environmental parameters.
Thus, encounter probabilities for engineering appli-
cations should be derived as multi-variate probabi-
lity density distributions for practical applica-
tions. Longuet-Higgins [1] derived joint probability
density distributions for wave heights and wave
periods, however, it is not possible to use such a
distribution for engineering applications, where
extreme loads are considered. This is due to the
fact that wave height and wave period are not suffi-
cient parameters to describe single waves in a ran-
dom sea, that contains a damaging potential. Many
different waves, some close to breaking, others not,
can exist in a random sea, all with the same values
for wave height and wave period. Therefore 3 new
parameters were introduced by Kjeldsen and Myrhaug
[2], and a new type of joint probability density dis-
tributions for evaluation of single waves leading to
extreme loads in a random sea was introduced,
Kjeldsen and Myrhaug [3].

The severeness of a rough sea state can only be
satisfactorily described as an event that contains
both high values for the wave heights and high values
for steepness and asymmetry parameters. The three
new parameters characterizing single zero-downcross
waves in a time series are: crest front steepness,
vertical asymmetry factor and horizontal asymmetry
factor, introduced by Kjeldsen and Myrhaug [2].
Myrhaug and Kjeldsen [4] presented parametric models
for joint probability density distributions for deep
water waves. Among these joint distributions were
crest front steepness - wave height and vertical
asymmetry factor - wave height distributions. The
parametric models were fitted to data obtained from
measurements at sea on the Norwegian continental
shelf. These joint distributions are useful to make
an approximation to the estimation for probabilities
of occurrence of steep asymmetric waves and breaking
waves in deep water. Due to relatively small number
of waves in the data for high values of both wave
height and crest front steepness and wave height and
vertical asymmetry factor these fitted joint distri-
bution models should be carefully applied for margi-
nal values.

This paper presents the crest front steepness
and asymmetry factors for extreme waves and the
highest waves which are present in the most severe
sea states in 22 gales. The analysis demonstrates
clearly the asymmetry for both "extreme waves"
and the highest waves. Further, estimates for pro-
babilities of occurrence of steep and high waves in
deep water for given sea states described by a
JONSWAP spectrum are given. These estimates are
made by using two different parametric models for
the joint distribution of crest front steepness and
wave height. The first model is based on the fit by
a Weibull distribution to the conditional distri-
bution for crest front steepness for given wave
height. The second model is based on the fit by a
log-normal distribution to the conditional distri-
bution for crest front steepness for given wave
height. Both these parametric models do an equally
well overall fitting to the data. However, the

latter model seems to be closer to the trend in the data for higher values of the crest front steepness for given wave heights. Results of a sensitivity analysis which is performed in order to investigate the sensitivity in the estimates for probabilities of occurrence of steep and high waves to which parametric model is used are presented.

2. BACKGROUND

Kjeldsen and Myrhaug [2] utilized the advantages that are contained in a zero-downcross analysis by using the wave trough and the following wave crest in the definition of a single wave, and defining the wave height as the difference between these water levels, Fig. 1. The zero-downcross analysis is the only analysis which provides parameters that give a representation of the physical conditions with relevance to breaking waves, and thus, the only parameters which should be correlated with measurements of severe ship responses or wave forces in such waves. Further, a more accurate description of steepness and asymmetry in transient near breaking waves were obtained by Kjeldsen and Myrhaug [2], when the three following parameters were introduced:

Crest front steepness:

$$\varepsilon \equiv \frac{\eta'}{(g/2\pi)T \cdot T'}$$

Vertical asymmetry factor:

$$\lambda \equiv \frac{T''}{T'} \qquad\qquad (1)$$

Horizontal asymmetry factor:

$$\mu \equiv \frac{\eta'}{H}$$

The definitions in the time domain are shown in Fig. 1. Here η' is the crest elevation measured from the mean water level, while T' and T'' are times defining the position of the wave crest relative to the zero-crossing points in the time domain. T is the zero-downcross period and g the acceleration of gravity. It is generally accepted that use of the crest elevation for design applications provides a basic parameter more relevant to finite amplitude wave geometry than the wave height. Observations of breaking waves in the laboratory show that these waves can be characterised by a very steep crest front and high asymmetry factors, see Kjeldsen [5]. The ε-parameter is thus a mean crest front inclination in the time domain.

In this study the mean water level, MWL, is defined as the arithmetic mean of a 20 min recording period of surface fluctuations, with proper correction for tide, if any. This means that a trend in the mean values has to be removed.

Thus, in the definition λ describes asymmetry with respect to the vertical axis in the crest, while

ASYMMETRIC WAVE OF FINITE HEIGHT
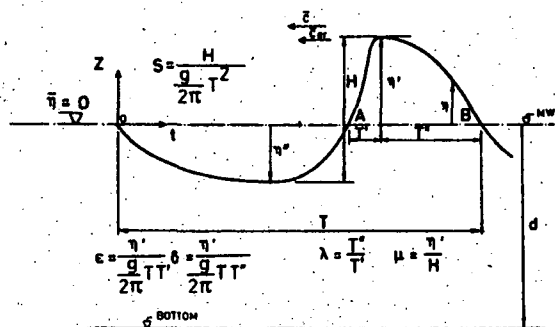
Fig. 1. Basic definitions for asymmetric waves of finite height (from Kjeldsen and Myrhaug [2]).

μ describes asymmetry with respect to a horizontal axis in the mean water level. It is now possible to obtain the crest rear steepness directly as:

$$\delta \equiv \varepsilon/\lambda = \frac{\eta'}{(g/2\pi)TT''}$$

The definitions of ε and λ refer to a simple counting technique in the time domain. No attempts should be made to interpret this as synoptic information. Such an interpretation would require full details regarding the directional wave spectra. However, that information was not available in the field data analysed here.

From available measurements at sea on the Norwegian continental shelf, nearly 25000 single storm waves in deep water were analysed statistically. An "extreme wave" was defined as follows (Kjeldsen and Myrhaug [6]):

$$H > H_c \quad \text{and} \quad \varepsilon > \varepsilon_c$$

or $\qquad\qquad\qquad\qquad\qquad\qquad (2)$

$$H > H_c \quad \text{and} \quad s > s_c$$

where the subscript c denotes specific threshold values of the wave parameters. In the present study dealing with smaller vessels, the following thresholds were used:

$$H_c = 5 \text{ m}, \quad \varepsilon_c = 0.25, \quad s_c = 0.10 \qquad (3)$$

However, other threshold values may be more relevant for other related problems depending on structure geometry.

Time records that contained at least one "extreme wave" according to the definition in (2) and (3) were then selected for a closer study. This was approximately 8% of the most severe sea states in 22 gales including 58 time series, each of 20 min duration. From this data, including altogether 6353 individual zero-downcross waves, joint probability density distributions as well as marginal density distributions for relevant parameters were obtained. The field data were sampled in the period 1974-78
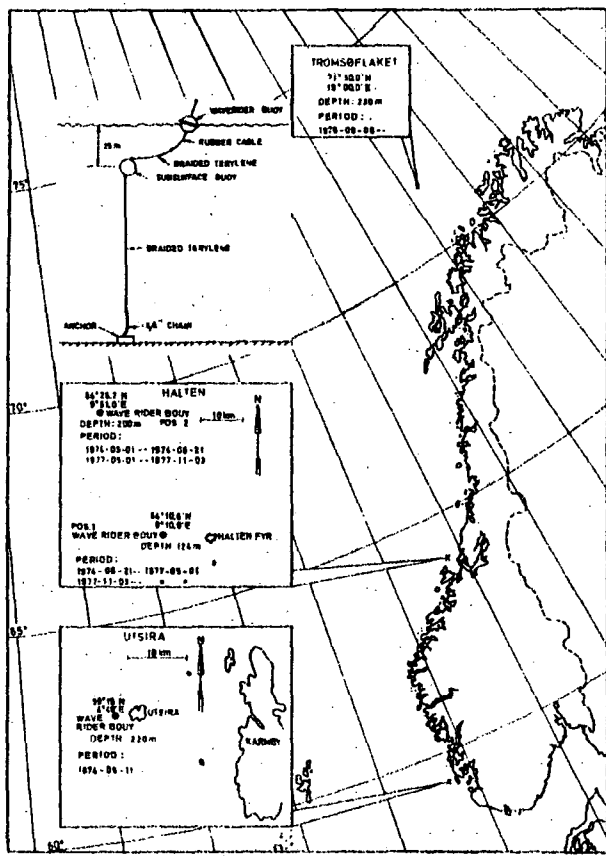
Fig. 2. Stations for wave measurements.

With three Waverider buoys, located at Tromsøflaket, Halten and Utsira on the Norwegian continental shelf, Fig. 2. Recording was obtained every 3 hours, starting 20 minutes before 0 time GMT. In the zero-downcross analysis waves having a distance from the mean water level to the wave crest less than 0.5 m were neglected.

The properties of the obtained probability density distributions show that data obtained from the three locations can be regarded as belonging to the same statistical population. This means that common statistical distributions can be obtained, which are representative for the wave dynamics in the whole area (Kjeldsen and Myrhaug [7]). Rms-values are used for normalisation, and dimensionless plots of probability density distributions are then obtained. The resulting data base provides a coupling to sea state, wind velocity and wave spectral parameters.

3. RESULTS OF MEASUREMENTS AT SEA

3.1. Steepness and asymmetry of random "extreme waves".

The steepness and asymmetry of random "extreme waves" according to the definition in (2) and (3) are now considered. Totally 60 "extreme waves" are considered herein.

The steepest monochromatic deep water Stokes wave approximated to an order of 120 Padé approximants are given by Cokelet [8]. For the steepest

wave given in his calculations the following values are derived

$$\epsilon = 0.421 \quad \text{and} \quad \mu = 0.679$$

calculated with reference to still water level and used for comparison with experimental values obtained in the laboratory, see Kjeldsen [5]. Calculated with respect to the mean water level these parameters become

$$\epsilon = 0.408 \quad \text{and} \quad \mu = 0.757$$

These latter values should be compared with the values obtained from the full scale measurements referred to herein.

For a monochromatic train of sinusoidal waves $\epsilon = 2s$ and the vertical and horizontal asymmetry factors λ and μ are 1 and 0.5, respectively. Keeping this in mind the results of the analysis as presented below will demonstrate clearly the asymmetry of "extreme waves".

Fig. 3 shows that ϵ is larger than $2s$ for most of the waves and these are represented by the dots. The crosses represent the waves for which $\epsilon < 2s$ and the line represents $\epsilon = 2s$.
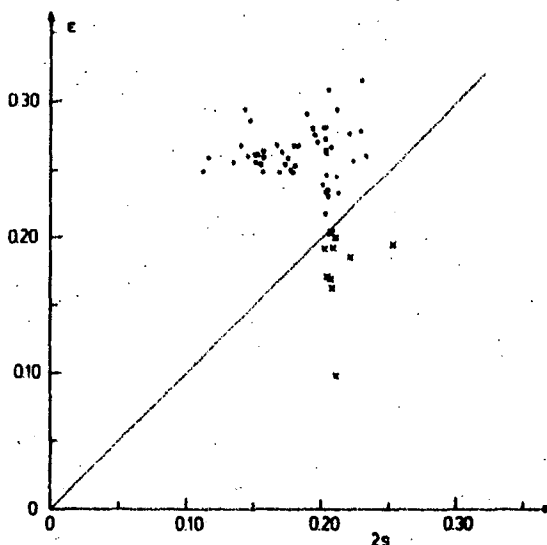
Fig. 3. ϵ vs $2s$ for "extreme waves".

Figs. 4 and 5 show ϵ versus λ and μ, respectively, where the dots and crosses have the same meaning as in Fig. 3. Figs. 4 and 5 show that $\lambda > 1$ and $\mu > 0.5$, respectively, for most of the waves of the waves where $\epsilon > 2s$. This is also demonstrated in Fig. 6 which shows μ versus λ. Thus Figs. 4-6 show that most of the steep waves, were the crest front steepness is used as a measure of the steepness, are characterised by an asymmetric wave crest. That is, the crest is asymmetric in the direction of the wave propagation considered in the time domain and the crest height is heigher than the corresponding trough level below the mean water surface. Considered in the time domain the shape of steep asymmetric waves are characterised by a shallow and relative long trough followed by a high and relative short crest, as indicated in Fig. 1.

Fig. 4. ϵ vs λ for "extreme waves".

other waves are represented by the crosses.

Fig. 8 shows $\epsilon_{H_{max}}$ versus $\lambda_{H_{max}}$ where the dots and crosses have the same meaning as in Fig. 7. The figure shows that $\lambda > 1$ for most of the highest waves where $\epsilon_{H_{max}} > 2s_{H_{max}}$. As shown in Fig. 9 only few of the waves are both the highest wave and the "extreme wave" in the time series. Thus Figs. 7 and 8 show that most of the highest waves in the time series have $\epsilon_{H_{max}} > 2s_{H_{max}}$ and among these waves $\lambda > 1$, except for only few of them. The horizontal asymmetry factor μ was not available for the highest waves. However, it seems clear from the data analysed here that also a large number of the highest waves, although they are generally not "extreme waves" according to the definition in (2) and (3), are characterised by a relative steep crest front ($\epsilon_{H_{max}} > 0.10$) and a crest which is asymmetric in the direction of wave propagation considered in the time domain.

Fig. 5. ϵ vs μ for "extreme waves".

Fig. 7. $\epsilon_{H_{max}}$ vs $2s_{H_{max}}$.

Fig. 6. μ vs λ for "extreme waves".

3.2. Steepness and asymmetry of the highest waves.

The steepness and asymmetry of the highest wave in each of the 58 time series are now considered.

Fig. 7 shows that $\epsilon_{H_{max}} > 2s_{H_{max}}$ for the most of the waves and these are represented by the dots. The
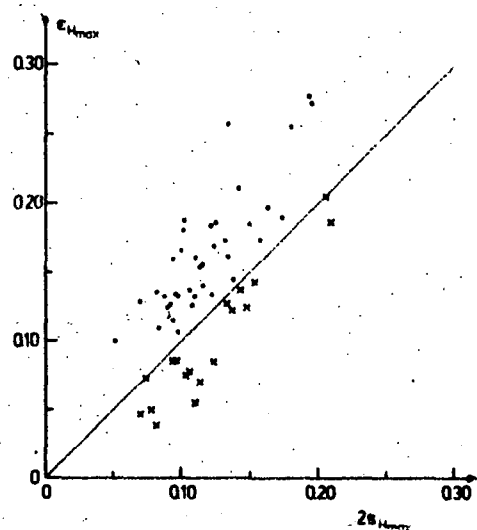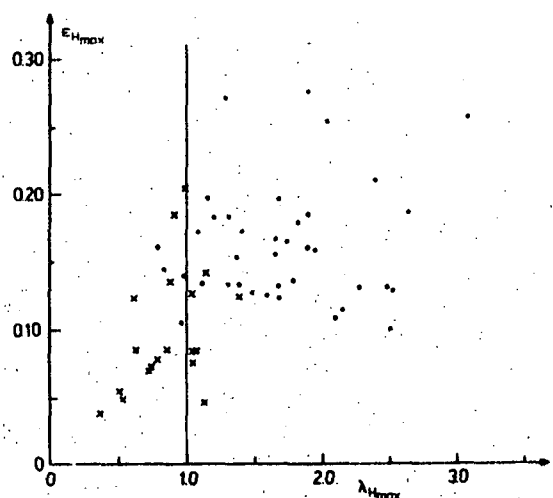
Fig. 8. $\epsilon_{H_{max}}$ vs $\lambda_{H_{max}}$.
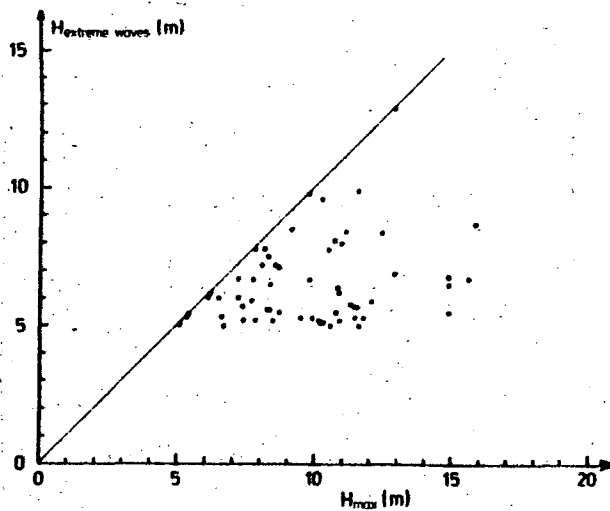
Fig. 9. $H_{extreme\ waves}$ vs H_{max}.

3.3. Joint probability density distribution of crest front steepness and wave height.

It is, however, not sufficient to describe the wave conditions by steepness and asymmetry parameters alone, but they should be combined with the wave height to give a much better description of the severeness of a given sea state. Joint probability density distributions for ε, H and λ, H are given in Myrhaug and Kjeldsen [4]. As a first approximation these joint distributions represent tools to estimate the probabilities of occurrence of steep and asymmetric waves in deep water. Myrhaug and Kjeldsen [9] discuss closer the ε-H distribution and use it to estimate probabilities of occurrence of three types of steep and high waves in deep water for given sea states described by a JONSWAP spectrum. These latter results will be summarized here and in the next section.

The joint probability density distribution, $p(\hat{\varepsilon}, \hat{h})$, which best fits to the field data records from the Norwegian continental shelf was determined. Here $\hat{\varepsilon} = \varepsilon/\varepsilon_{rms}$ and $\hat{h} = H/H_{rms}$ are the normalized crest front steepness and wave height, respectively. ε_{rms} and H_{rms} are the rms-values used for normalisation. The joint probability density distribution is determined by

$$p(\hat{\varepsilon},\hat{h}) = p(\hat{\varepsilon}|\hat{h})p(\hat{h}) \qquad (4)$$

Here $p(\hat{h})$ denotes the marginal distribution of $\hat{h}$ and $p(\hat{\varepsilon}|\hat{h})$ denotes the conditional distribution of $\hat{\varepsilon}$ given $\hat{h}$. The joint probability distribution was fitted to the actual data by first fitting the conditional distribution of $\hat{\varepsilon}$ given $\hat{h}$ and then fitting the marginal distribution of $\hat{h}$.

The following distributions were investigated to fit the conditional distribution histograms and the marginal distribution histograms: Weibull and log-normal.

Let x denote the wave parameter under consider-

ation. The Weibull probability density distribution is given by

$$p(x) = \frac{\beta_x\ x^{\beta_x-1}}{\rho_x^{\beta_x}}\ exp\ [-(\frac{x}{\rho_x})^{\beta_x}]\ ;\ x > 0 \qquad (5)$$

where β_x and ρ_x denote the Weibull parameters of x. (The Rayleigh distribution corresponds to $\beta_x = 2$.)

The log-normal probability density distribution is given by

$$p(x) = \frac{1}{\sqrt{2\pi}\gamma_x x}\ exp\ [-\frac{(lnx-\theta_x)^2}{2\gamma_x^2}]\ ;\ x > 0 \qquad (6)$$

where θ_x and γ_x^2 denote the mean value and the variance of lnx, respectively.

The rms-values used for normalisation, ε_{rms} and H_{rms}, are related to wave spectral parameters by (Myrhaug and Kjeldsen [4])

$$\varepsilon_{rms} = 0.0202 + 32.4\ \kappa\ ;\ \kappa = \frac{m_2}{g\sqrt{m_0}} \qquad (7)$$

and

$$H_{rms} = 2.8582\ \sqrt{m_0} \qquad (8)$$

respectively. Equations (7) and (8) are obtained as the best fit to the data by linear regression analysis. m_0 and m_2 are the zeroth and second moment of the one-sided wave energy spectrum S(f), respectively, defined by $m_n = \int_0^\infty f^n S(f)df$, $n = 0,2$, where f is the frequency. κ is related to a steepness parameter based on the significant wave height $H_{mo} = 4\sqrt{m_0}$ and the average zero-crossing wave period $T_{mo2} = \sqrt{m_0/m_2}$, i.e. $\kappa = H_{mo}/4gT_{mo2}^2$.

Fig. 10a shows the joint distribution histogram and the corresponding isodensity curves of crest front steepness and wave height combined for all three locations, representing 6353 storm waves. This is the data to which the parametric models were fitted.

The Weibull distribution which was fitted to the marginal distribution histogram of $\hat{h}$ gave

$$\rho_{\hat{h}} = 1.05\quad and\quad \beta_{\hat{h}} = 2.39 \qquad (9)$$

The fitting of the Weibull and log-normal distributions to the conditional distribution of $\hat{\varepsilon}$ given $\hat{h}$ gave a set of Weibull and log-normal parameters, respectively, for each row of $\hat{h}$. These parameters as functions of $\hat{h}$ were then represented by estimated smooth curves which were used in the estimation of the joint probability density function. The functional relationships between the estimated parameter values for each row and the values of $\hat{h}$ corresponding to those rows were determined to be

NORMALIZED CREST FRONT STEEPNESS ê

(a)

$\epsilon = \frac{\eta}{\frac{g}{2\pi} \cdot T \cdot T}$

NORMALIZED CREST FRONT STEEPNESS ê

(b)

$\rho_{max} = 083$

NORMALIZED CREST FRONT STEEPNESS ê

(c)

$\rho_{max} = 099$
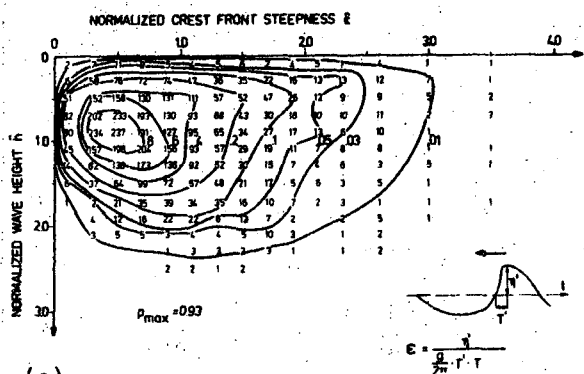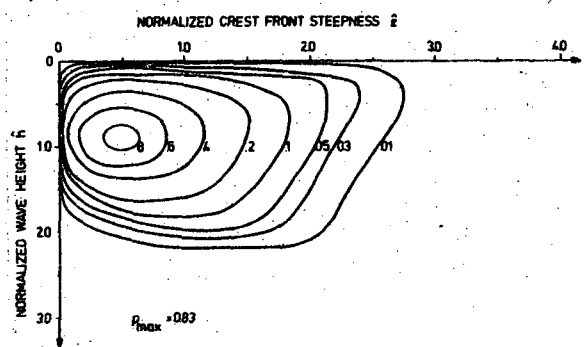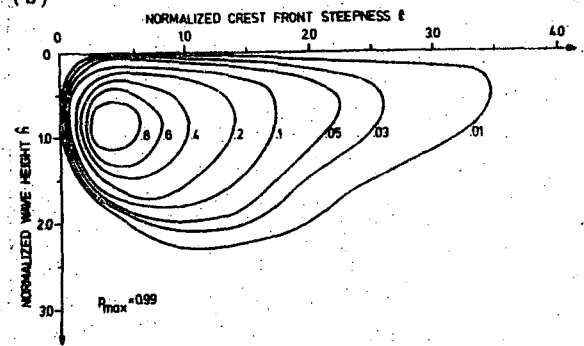
Fig. 10. Joint probability density distribution
of ê and ĥ, (a) observed joint distri-
bution; (b) and (c) fitted joint dis-
tributions based on Weibull and log-
normal model for p(ê|ĥ), respectively.

Weibull parameters:

$$\rho_{\hat\varepsilon}(\hat h) = \begin{cases} 1.37 - 1.10\ \hat h + 0.57\ \hat h^2 & \text{for } \hat h < 1.9 \\ 0.36\ \text{arctg}\ [2.80(\hat h-1.9)] + 1.34 & \\ & \text{for } \hat h > 1.9 \end{cases} \quad (10)$$

and

$$\beta_{\hat\varepsilon}(\hat h) = 0.56\ \text{arctg}\ [3.57(\hat h-1.7)] + 2.28 \quad (11)$$

log-normal parameters:

$$\theta_{\hat\varepsilon}(\hat h) = \begin{cases} 0.024 - 1.065\ \hat h + 0.585\ \hat h^2 & \text{for } \hat h < 1.7 \\ 0.32\ \text{arctg}\ [3.14(\hat h-1.7)] - 0.096 & \\ & \text{for } \hat h > 1.7 \end{cases} \quad (12)$$

and

$$\gamma_{\hat\varepsilon}^2(\hat h) = -0.21\ \text{arctg}\ [2.0(\hat h-1.4)] + 0.325 \quad (13)$$
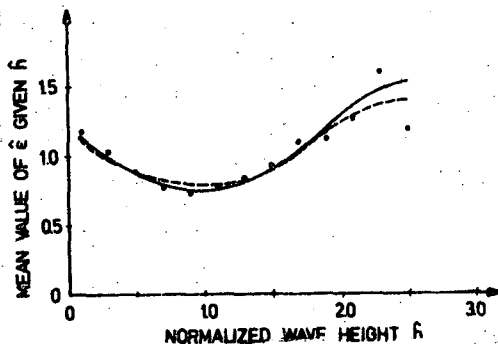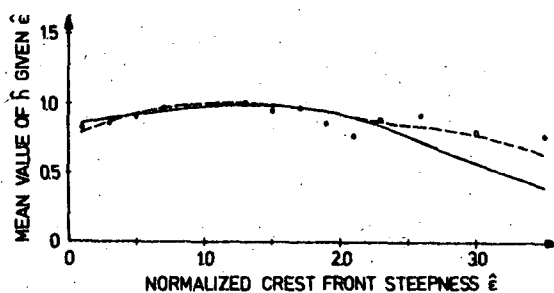
Fig. 11. Conditional mean values of ê and ĥ:
• estimated from data; — according to
Weibull model for p(ê|ĥ); --- according
to log-normal model for p(ê|ĥ).

The joint probability density distribution ob-
tained by this fitting to the data is then given by
Equations (4) and (5) where the Weibull parameters for
p(ĥ) and p(ê|ĥ) are given by Equations (9) and (10),
(11), respectively. This joint distribution is plot-
ted in Fig. 10b. A Pearson χ^2 goodness-of-fit test for
the joint density distribution resulted in a coeffi-
cient of 382 with 116 degrees of freedom.

The joint probability density distribution ob-
tained by this fitting to the data is then given by
Equations (4)-(6) where the Weibull parameters for
p(ĥ) and the log-normal parameters for p(ê|ĥ) are
given by Equations (9) and (12), (13), respectively.
This joint distribution is plotted in Fig. 10c. A
Pearson χ^2 goodness-of-fit test for the joint den-
sity distribution resulted in a coefficient of 354
with 122 degrees of freedom.

Fig. 11 shows the mean value of ê given ĥ vs.
ĥ and the mean value of ĥ given ê vs. ê. The dots
are based on the data, while the full and dashed
curves are based on the smoothed estimates of the
conditional Weibull and log-normal parameters,
respectively.

By comparing the results of the Pearson χ^2
goodness-of-fit test for the two joint density dis-
tribution models and the results in Fig. 11 they are
about equal in the goodness-of-fit to the data. How-
ever, there is a difference between the two models.
In Myrhaug and Kjeldsen [9] the resulting conditional
cumulative distributions of ê given ĥ,which were ob-
tained from the parametric models,were plotted to-
gether with the data. These plots showed that the

$$\varepsilon_c = 0.30., \quad H_c = H_{mo}$$

Left legend:
- $T_p = 3.6\sqrt{H_{mo}}$, $\alpha=0.016$, $\gamma=5$: $P_W = 5.3\cdot10^{-4}$, $P_{L-N} = 1.9\cdot10^{-3}$
- $T_p = 3.7\sqrt{H_{mo}}$, $\alpha=0.153$, $\gamma=4.5$: $P_W = 3.5\cdot10^{-4}$, $P_{L-N} = 1.6\cdot10^{-3}$
- $T_p = 3.8\sqrt{H_{mo}}$, $\alpha=0.147$, $\gamma=4.0$: $P_W = 2.4\cdot10^{-4}$, $P_{L-N} = 1.4\cdot10^{-3}$
- $T_p = 3.9\sqrt{H_{mo}}$, $\alpha=0.142$, $\gamma=3.4$: $P_W = 1.6\cdot10^{-4}$, $P_{L-N} = 1.2\cdot10^{-3}$
- $T_p = 4\sqrt{H_{mo}}$, $\alpha=0.136$, $\gamma=3.0$: $P_W = 1.2\cdot10^{-4}$, $P_{L-N} = 1.0\cdot10^{-3}$

Right legend:
- $T_p = 4.1\sqrt{H_{mo}}$, $\alpha=0.13$, $\gamma=2.6$: $P_W = 8.5\cdot10^{-5}$, $P_{L-N} = 9.1\cdot10^{-4}$
- $T_p = 4.3\sqrt{H_{mo}}$, $\alpha=0.119$, $\gamma=2.0$: $P_W = 4.0\cdot10^{-5}$, $P_{L-N} = 7.0\cdot10^{-4}$
- $T_p = 4.5\sqrt{H_{mo}}$, $\alpha=0.0108$, $\gamma=1.6$: $P_W = 1.8\cdot10^{-5}$, $P_{L-N} = 5.3\cdot10^{-4}$
- $T_p = 4.7\sqrt{H_{mo}}$, $\alpha=0.0097$, $\gamma=1.25$: $P_W = 7.5\cdot10^{-6}$, $P_{L-N} = 4.1\cdot10^{-4}$
- $T_p = 5\sqrt{H_{mo}}$, $\alpha=0.0081$, $\gamma=1$: $P_W = 1.5\cdot10^{-6}$, $P_{L-N} = 2.6\cdot10^{-4}$

Axes: H_{mo}(m) (vertical, 0 to 20); T_D (s) (horizontal, 0 to 20)

Fig. 12. Estimates for probabilities of occurrence of extreme steep waves with wave heights exceeding H_{mo}.

log-normal law does a better fitting to the data for $\hat{\varepsilon} > 2$ for $\hat{h}$ in the range from 1.3 to 1.9 than does the Weibull law. This suggests that the estimates of steep and high waves will depend on which model is used, since these results obviously will be sensitive to the fitting to the data in the tail of the distribution. By having these two models available a sort of sensitivity analysis of the result can be made. More discussions of the two models will be given below.

4. ESTIMATES FOR PROBABILITIES OF OCCURRENCE OF STEEP AND HIGH WAVES FOR GIVEN SEA STATES DESCRIBED BY A JONSWAP SPECTRUM

Estimates for probabilities of occurrence of steep and high waves by using the joint distribution of $\hat{\varepsilon}$ and $\hat{h}$ were given in Myrhaug and Kjeldsen [9]. These results will be summarized here. The probability of occurrence of waves with $\varepsilon > \varepsilon_c$ and $H > H_c$ for given rms-values of ε and H are given by

$$P[(\varepsilon > \varepsilon_c) \cap (H > H_c) \mid \varepsilon_{rms}, H_{rms}]$$

$$= \int_{\varepsilon_c}^{\infty} \int_{H_c}^{\infty} p(\varepsilon,H)dHd\varepsilon = \int_{\hat{\varepsilon}_c}^{\infty} \int_{\hat{h}_c}^{\infty} p(\hat{\varepsilon},\hat{h})d\hat{h}d\hat{\varepsilon} \qquad (14)$$

Since ε_{rms} and H_{rms} are coupled to spectral parameters this is a conditional probability given a sea state.

The sea states will here be specified by a JONSWAP spectrum, see Appendix.

For a given sea state, waves with heights exceeding the significant wave height will be considered, i.e. $H_c = H_{mo}$. Thus, according to Equation (8)

$$\hat{h}_c = 1.4 \qquad (15)$$

Further, the 3 following types of steep waves were considered

$$\varepsilon_c = \begin{cases} 0.10 \ ; \ \text{steep waves} \\ 0.20 \ ; \ \text{very steep waves} \\ 0.30 \ ; \ \text{extreme steep waves} \end{cases} \qquad (16)$$

Consider as an example the upper limit in Equation (A2) (in Appendix) corresponding to the Pierson-Moskowitz spectrum for fully developed sea where $\alpha= 0.0081$, $\gamma = 1$, $T_p = 5\sqrt{H_{mo}}$, $T_p = 1.40 \ T_{mo2}$ and accordingly $T_{mo2} = 3.57 \sqrt{H_{mo}}$. Thus $\kappa = 0.002$ and $\varepsilon_{rms} = 0.085$ according to Equation (7). With one of the values in Equation (16) $\hat{\varepsilon}_c$ is given and $\hat{h}_c$ is given in Equation (15). Thus, according to Equation (14) there will be a constant probability of occurrence of steep waves with a wave height exceeding the significant wave height in a sea state described by the Pierson-Moskowitz spectrum. This will also be the case for the lower limit in Equation (A2).

In Fig. 12 is given the estimates for probabilities of occurrence of extreme steep waves as defined

- 275 -

In Equation (16) and with wave heights exceeding H_{mo}. This probability is constant along each curve $T_p \sim \sqrt{H_{mo}}$ in the JONSWAP range as given in Equation (A2). The estimates of probabilities are given for both models of the joint ε-H distribution. P_W and P_{L-N} denotes the results based on the conditional Weibull and log-normal distributions, respectively. In Myrhaug and Kjeldsen [9] is shown that the estimates by the two models are in reasonable agreement for $\varepsilon_c = 0.10$ and $\varepsilon_c = 0.20$. This suggests that the estimates for probabilities of occurrence of steep waves and very steep waves (see Equation (16)) are reasonably reliable. However, the figure shows that for $\varepsilon_c = 0.30$ there is a significant difference between the two estimates showing that the model based on the log-normal model gives the highest value. The ratio between the two estimates, P_{L-N}/P_W, is in the range 4-20 for the most of the cases but as large as 170 for the Pierson-Moskowitz spectrum. This shows that the estimates are very sensitive to which model is used. The "correct" value is probably somewhere in this range. Judged from the previous discussions it seems reasonable to rely somewhat more on the estimates from the log-normal model than the Weibull model. However, this sensitivity study has demonstrated that the fitted ε-H distribution should be carefully applied for marginal values of ε and H. This means that estimates for probabilities of occurrence of extreme steep waves in deep water by application of this model should be taken as an approximation only. More data are needed for high values for both wave height and crest front steepness before such estimates can be improved and made with more confidence.

It is well known that a Waverider buoy provides a signal with less non-linear effects than the sea surface fluctuation itself. This is a result of the fact that, due to the local particle kinematics within the waves, the buoy stays at the wave crest for too long time and at the troughs for too short time. It is therefore obvious that wave steepness statistics obtained from Waverider buoys will be on the non-conservative side. Discussion of how corrections for such errors can be made are given in Kjeldsen et.al. [10].

5. EXAMPLE OF RESPONSES PLOTTED AS FUNCTIONS OF CREST FRONT STEEPNESS

Wave impacts on a tilted plate were measured in experiments performed by Kjeldsen [11]. Both experiments with non-breaking waves and with breaking waves were performed. Normalized impact pressures were then plotted as a function of a steepness ratio:

$$\frac{\varepsilon}{s}$$
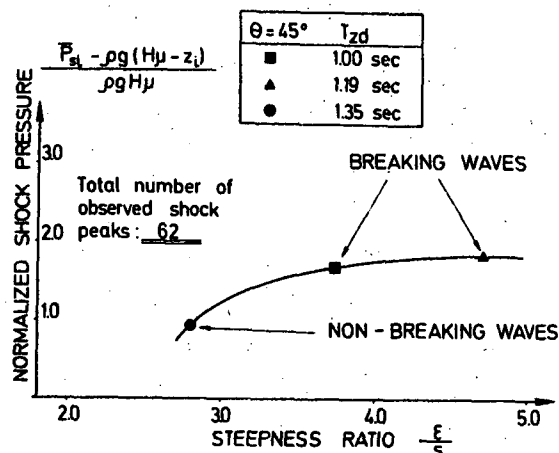
Fig. 13. Normalized mean shock pressure as a function of wave steepness ratio, ε/s, for a plate with tilt $\theta = 45^\circ$. Wave breaking occurs approximately at $\varepsilon/s = 3.5$.

Inception of breaking took place at $\varepsilon/s = 3.5$, see Fig. 13. It is then observed that there is a significant increase in wave impacts when wave steepness ratio increases. This is only one example where the new steepness and asymmetry parameters are relevant. Capsizing of small objects on the sea surface is another most relevant problem, where such parameters should be useful.

6. CONCLUSIONS

1. The wave spectrum alone is not sufficient to characterise the roughness of an irregular sea. Some time series have been found that contain steep asymmetric waves while others do not contain such waves, but they have in some cases identical wave spectra.
   Thus, additional information is required and the present study suggests an analysis in the time domain with the use of the following three parameters characterising single zero-downcross waves in a time series: crest front steepness ε, vertical asymmetry factor λ and horizontal asymmetry factor μ (Fig. 1). Steep asymmetric waves are uniquely defined by these parameters.

2. For a monochromatic train of sinusoidal waves the vertical and horizontal asymmetry factors are 1 and 0.5, respectively and $\varepsilon = 2s$. However, in the measured irregular seas consisting of a large number of Fourier components it is found that both "extreme waves" (as defined in (2) and (3)) and the highest waves in each 20 minutes record show a clear asymmetry. This asymmetry is most clearly demonstrated for waves having $\varepsilon > 2s$. For both "extreme waves" and the highest waves the crest is asymmetric in the direction of wave propagation considered in the time domain. "Extreme waves" with $\varepsilon > 2s$ had also a crest height which was higher than the corre-

sponding trough level below the mean water surface. This pronounced asymmetrical shape of wind waves in the time domain is probably also valid in the synoptic space for "extreme waves" and the highest waves.

3. Estimates for encounter probabilities of occurrence of steep and high waves in deep water for given sea states should be calculated by using the joint distribution of crest front steepness and wave height. The parametric model which should be used for such calculations is the model based on the fit of a log-normal distribution to the data for the conditional distribution of crest front steepness for given wave heights. This model seems to be closer to the trend in the data for higher values of the crest front steepness for given wave heights in the higher range, compared to a model based on the fit of a Weibull distribution for $p(\varepsilon|H)$. However, the parametric ε-H distribution model should be carefully applied for marginal values of ε and H, and estimates for probabilities for occurrence of extreme steep waves in deep water by application of the model should be taken as a first approximation only.

4. It is recommended to use the same approach for engineering structures in coastal areas. The three new parameters crest front steepness, horizontal wave asymmetry parameter and vertical wave asymmetry parameter are now recommended by the International Association for Hydraulic Research (IAHR) as international standard.

5. It is well known that the surface following properties of anchored ocean buoys are not perfect. In particular the response of an anchored ocean buoy to a large plunging breaker occurring in deep waters is unknown. Most probably the buoy will dive into the interior of the wave, and the recorded signal will later be taken away as unrealistic noise. Thus the naval architect and offshore engineer lose the extreme event which is most important to them, while they at the same time obtain a lot of data on less interesting events. Other measurements techniques should therefore be developed and applied.

7. ACKNOWLEDGEMENTS

8. NOMENCLATURE

f, f_p	frequency; spectral peak frequency
g	acceleration of gravity
$\hat{h} = H/H_{rms}$	normalized wave height
H	zero-downcross wave height
$H_{mo} = 4\sqrt{m_0}$	significant wave height
$m_n = \int_0^\infty f^n S(f) df$	nth moment of the spectrum
p	probability density function
s	total zero-downcross wave steepness
$S(f)$	one-sided wave energy spectrum
T	zero-downcross wave period
T'	time from zero-upcross point to wave crest
T''	time from wave crest to zero-downcross point
$T_p = 1/f_p$	spectral peak period
$T_{mo2} = \sqrt{m_0/m_2}$	average zero-crossing wave period
α, γ, σ	JONSWAP parameters
β, ρ	Weibull parameters
ε	crest front steepness
$\hat{\varepsilon} = \varepsilon/\varepsilon_{rms}$	normalized crest front steepness
η'	crest elevation
$\theta_\varepsilon, \gamma_\varepsilon$	log-normal parameters
$\kappa = H_{mo}/4gT_{mo2}^2$	spectral steepness parameter
λ	vertical asymmetry factor
μ	horizontal asymmetry factor
Index	
c	specific value
rms	root-mean-square

9. REFERENCES

[1] Longuet-Higgins, M.S., "On the statistical distribution of the heights of sea waves". J. Marine Res., Vol. XI, No. 3, 1952, pp. 245-266.

[2] Kjeldsen, S.P. and Myrhaug, D., "Kinematics and dynamics of breaking waves". Report No. STF60 A78100, "Ships in Rough Seas", Part 4. Norwegian Hydrodynamic Laboratories, Trondheim, Norway, 1978.

[3] Kjeldsen, S.P. and Myrhaug, D., "Wave-wave interactions, current-wave interactions and resulting extreme waves and breaking waves". Proc. 17th Conf. on Coastal Engineering, pp. 2277-2303, 1980.

[4] Myrhaug, D. and Kjeldsen, S.P., "Parametric modelling of joint probability density distributions for steepness and asymmetry in deep water waves". Applied Ocean Research, Vol. 6, No. 4, 1984, pp. 207-220.

[5] Kjeldsen, S.P., "2- and 3-dimensional deterministic freak waves". Proc. 18th Conf. on Coastal Engineering, Cape Town, South Africa, 1982.

[6] Kjeldsen, S.P. and Myrhaug, D., "Formation of wave groups and distribution of parameters for wave asymmetry". Report No. STF60 A79044, "Ships in

Rough Seas", Part 4. Norwegian Hydrodynamic Laboratories, Trondheim, Norway, 1979.

[7] Kjeldsen, S.P. and Myrhaug, D., "Wave-wave and wave-current interactions in deep water". Proc. 5th POAC Conference, Trondheim, Vol. III, 1979, pp. 179-200.

[8] Cokelet, E.D., "Steep gravity waves in water at arbitrary uniform depth". Phil. Trans. Roy. Soc. of London Ser. A, Vol. 286, No. 1335, 1977, pp. 183-230.

[9] Myrhaug, D. and Kjeldsen, S.P., "On the prediction of occurrences of steep and high waves in deep waters". Submitted for publication 1985.

[10] Kjeldsen, S.P., Lystad, M. and Myrhaug, D., "Forecast of breaking waves on the Norwegian continental shelf". Project report, "Ships in Rough Seas", The Norwegian Meteorological Institute and Norwegian Hydrodynamic Laboratories, Trondheim, Norway, 1981.

[11] Kjeldsen, S.P., "Shock pressures from deep water breaking waves". Int. Symp. on Hydrodynamics in Ocean Engineering, August 1981, The Norwegian Institute of Technology, Trondheim, Norway.

[12] Hasselmann, K. et. al., "Measurements of wind-wave growth and swell decay during the Joint North Sea Wave Project (JONSWAP)". Ergänsungsheft, Reihe A(8°), Nr. 12, Deutschen Hydrografischen Zeitschrift, 1973.

[13] Torsethaugen, K., Faanes, T. and Haver, S., "Characteristica for extreme sea states on the Norwegian continental shelf". Report No. STF60 A84123. Norwegian Hydrodynamic Laboratories, Trondheim, Norway, 1984.

[14] Haver, S., Private communication, 1985.

APPENDIX

The JONSWAP spectrum is given by (Hasselmann et. al. [12])

$$S(f) = \alpha g^2 (2\pi)^{-4} f^{-5} \exp[-1.25(T_p f)^{-4}]$$
$$\cdot \gamma^{\exp[-0.5(T_p f - 1)^2/\sigma^2]} \qquad (A1)$$

where σ determines the width of the spectral peak, and according to the JONSWAP experiment adopted as $\sigma = 0.07$ for $f < f_p$ and $\sigma = 0.09$ for $f > f_p$. α is an equilibrium range parameter governing the high frequency part of the spectrum, γ is a spectral peakedness parameter and $T_p = 1/f_p$ is the spectral peak period.

Since the sea states here are described by a JONSWAP spectrum wind sea is considered. If swell also should be considered an other spectral form has to be considered, or to consider a joint frequency table of H_{mo} and T_{mo2} where both wind sea and swell will be present.

Now, regarding wind sea described by a JONSWAP spectrum, this spectral formulation will only be valid in a subspace of the whole H_{mo}, T_{mo2} or H_{mo}, T_p space.

Following Torsethaugen et. al. [13] and Haver [14] the following representation of the JONSWAP parameters is used in this analysis: The JONSWAP spectrum is taken to be a reasonable good model for wind sea in a socalled JONSWAP range given by

$$3.6\sqrt{H_{mo}} < T_p < 5\sqrt{H_{mo}} \qquad (A2)$$

Assuming that α varies linearly with T_p over the JONSWAP range at a fixed H_{mo} then

$$\alpha = 0.036 - 0.0056 \frac{T_p}{\sqrt{H_{mo}}} \qquad (A3)$$

and γ is determined from

$$\gamma = \exp[3.484(1 - 0.1975\alpha \frac{T_p^4}{H_{mo}^2})] \qquad (A4)$$

Equations (A2)-(A4) are based on the use of $\sigma = 0.08$ for all frequencies, rather than the two values given above. Thus, for given values of H_{mo} and T_p in the JONSWAP range the corresponding values for α and γ can be found. Further, for a JONSWAP spectrum the ratio of T_p to T_{mo2} depends on the peakedness factor γ, and T_p/T_{mo2} versus γ is shown in Fig. A1 (Haver [14]).

The upper limit in the formulation above is taken to correspond to the Pierson-Moskowitz spectrum for fully developed sea, i.e. $\alpha = 0.0081$ and $\gamma = 1$. Introduction of these values in Equation (A3) gives $T_p = 5\sqrt{H_{mo}}$ and $T_p = 1.40 \ T_{mo2}$ according to Fig. A1.

The lower limit is assumed to be characterized by $\alpha = 0.016$ and $\gamma = 5$ and is taken to be representative for the dimensionless fetch of about 10^3. In most cases the dimensionless fetch will vary from about 10^3 to about $5 \cdot 10^4$ (Torsethaugen et.al. [13]). Introduction of these values in Equation (A4) gives $T_p = 3.6\sqrt{H_{mo}}$ and $T_p = 1.24 \ T_{mo2}$ according to Fig. A1.
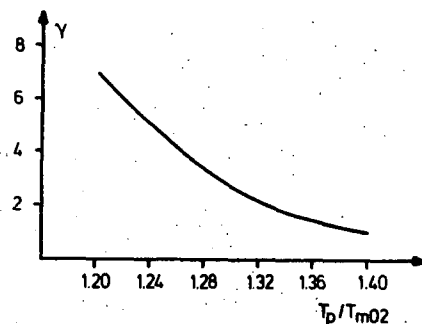

Fig. A1. γ vs T_p/T_{mo2} (from Haver [14]).

*) Division of Marine Hydrodynamics, Norwegian Institute of Technology, Trondheim, Norway.

**) MARINTEK A/S, SINTEF group. Trondheim, Norway.

ENVIRONMENTAL DATA FOR HIGH RISK AREAS
RELATING TO SHIP STABILITY ASSESSMENT

N. Hogben, J.A.B. Wills

ABSTRACT

This paper reviews very briefly the results of extensive investigations by the authors and a number of colleagues concerning environmental aspects of ship stability assessment.

The work is reviewed under 3 main headings. The first is concerned with definition of the relevant requirements for environmental data, including discussion of the ways in which they can be used for ship stability assessment. The second gives an account of a systematic compilation of data in terms of relevant wave and wind parameters and other information about environmental hazards, undertaken for a global selection of high risk areas. The third reviews an investigation of wind effects on ships in waves which included work concerned with the acquisition and use of full scale wind measurements as well as laboratory studies of the stability of models tested in a wind wave flume.

1. INTRODUCTION.

This paper is a highly condensed account of an investigation concerned with environmental aspects of ship stability assessment and provision of relevant data for areas of high risk. In undertaking this investigation it was important to begin by considering the forms of data required and how they should be used.

Stability assessment is concerned with studies of the risks associated with extreme rolling due to environmental forces which call for data to be used for numerical or physical modelling of these forces. The main causes of extreme rolling are wave forces but wind forces also play a key role and the worst conditions assumed for design purposes are commonly specified in terms of combinations of wave and wind parameters representing the most severe risks. In some cases consideration must also be given to currents and icing. Currents can significantly aggravate the severity of wave conditions and ice accretion can adversely affect roll stability both by raising the centre of gravity and by causing lopsided weight distribution. In this paper attention is concentrated on wave and wind data. A fuller account of the investigation including consideration of currents and icing may be found in the references [1] and [2].

2. REQUIREMENTS AND APPLICATIONS

The main requirement is for data to be used for numerical or physical modelling of wave and wind forces with emphasis on worst conditions for rolling, to be assumed for design purposes in the context of regulatory criteria. There are various ways of meeting these requirements which may be considered under the 2 headings, 'Design Case Approach' and 'Probabilistic Approach'.

2.1. The Design Case Approach

The design case approach involves the specification of worst case conditions in terms of particular values of the relevant parameters and is most commonly used for the framing of regulatory criteria. Fig. 1 shows an example of this approach to the defining of stability criteria (based on recommendations [3] adopted by the Intergovernmental Maritime Organisation, IMO). It involves the assumption that a steady moment M_v due to a specified extreme wind force is applied to a ship rolling in waves to a specified extreme angle to windward, ϕ_1. The criterion of acceptability is then that an area b representing work done by the restoring forces, which depend on the static stability characteristics of the ship, must be at least equal to an area a representing the kinetic energy imparted by the steady wind moment, in a roll to the limiting angle to leeward ϕ_f. There are of course other types of design case assessment which can be used. Their effectiveness must depend, however, on the validity of the choice of worst case parameters. Ideally these should represent conditions in which the rolling motion will be the most severe to be expected in a service life with some known level of risk.

2.2 The Probabilistic Approach

To assess the risks that given criteria for extreme rolling will be violated in service it is necessary to be able to describe the environmental conditions in terms suitable for use in a probabilistic analysis of the resulting roll motions. Ideally in undertaking such an assessment, the environmental data used should provide a basis for estimating the probabilities of occurrence in a service life


Figure 1 Weather Criterion [5]
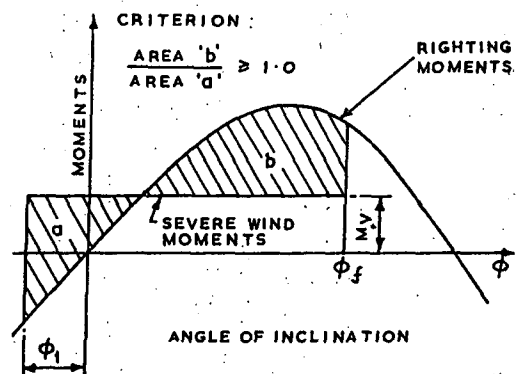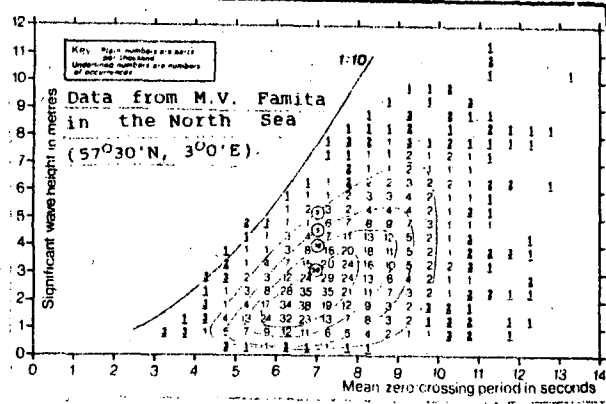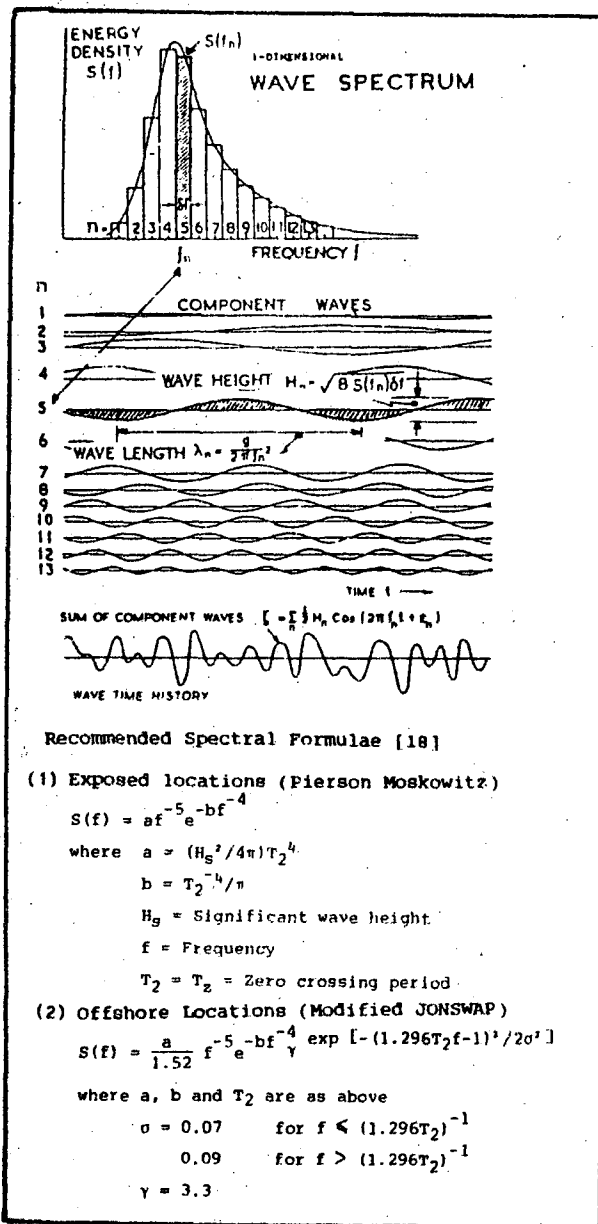
b) Height Period Scatter (Long Term) [19].

with relatively little damping. This means that extreme amplitudes of roll, though sometimes caused by a single catastrophic crest impact, will often develop over a time span covering several cycles of motion especially in waves with a period of encounter close to the natural roll period. Wave data to be used for assessing risks due to rolling must, therefore, provide a basis for realistic modelling of sequences or 'groups' of waves, with probability distributions of height and period representative of conditions to be encountered in service as well as individual waves of extreme height and steepness covering a range of periods.

Figure 2 indicates how these requirements can be met in terms of well established forms of data describing both the short term and long term wave conditions. Figure 2a illustrates the modelling of short term conditions, which may be referred to as 'Sea States', in terms of a concept known as the Wave Spectrum. As may be seen the spectrum describes a 'Sea State' as a linear sum of regular wave trains combining in random phase and is amenable to modelling in terms of characterising parameters such as the so called 'significant wave height', H_s and the 'mean zero crossing period', T_z. A spectrum offers a statistically realistic description of all the wave motions in a sea state specified by given values of H_s and T_z, including the grouping properties and the probability distributions of heights and periods and associated extreme values. It thus provides an effective basis for both numerical and physical modelling of waves which is widely used for the study of ship response motions.

Figure 2b illustrates a format commonly used for data defining the long term wave climate, sometimes referred to as a 'height/period scatter diagram'. It shows how the conditions over a period of years can be represented as a population of short term sea states with frequencies of occurrence classified according to range of significant wave height and zero crossing period. Such a diagram can be translated into a corresponding population of parametric wave spectra each representing a sea state with the appropriate significant height and zero crossing period using formulae such as those cited in the figure. Data in this format coupled with a suitable spectral model can thus provide a realistic statistical description of all the individual waves likely to be encountered by a ship in service over a period of years and is very suitable for use in assessment of risks due to extreme rolling. It has, therefore, been adopted as the format used for the wave data for high risk areas presented in this paper.

2.4 Requirements for Joint Wind and Wave Data
As discussed in more detail later, the wind

Recommended Spectral Formulae [18]

(1) Exposed locations (Pierson Moskowitz)

$$S(f) = af^{-5}e^{-bf^{-4}}$$

where $a = (H_s^2/4\pi)T_2^4$

$b = T_2^{-4}/\pi$

H_s = Significant wave height

f = Frequency

$T_2 = T_z$ = Zero crossing period

(2) Offshore Locations (Modified JONSWAP)

$$S(f) = \frac{a}{1.52} f^{-5}e^{-bf^{-4}} \gamma^{exp [-(1.296T_2f-1)^2/2\sigma^2]}$$

where a, b and T_2 are as above

$\sigma = 0.07$ for $f \leq (1.296T_2)^{-1}$

0.09 for $f > (1.296T_2)^{-1}$

$\gamma = 3.3$

a) The Wave Spectrum Concept (Short Term)

Figure 2 Forms of Wave Data

of all the possible types of risk situation due to waves, wind, currents and icing and the resulting probabilities of roll response. In practice, simplifying assumptions must be made and for the present attention will be concentrated on requirements for wave and wind data which offer a reasonably realistic and tractable basis for estimating the risks to be encountered in service. There is not space here to mention requirements for data on currents and icing but information on these questions may be found in reference [1].

In the light of the foregoing it follows that data suitable for use in probabilistic analysis will also meet the requirements for the design case approach. In considering these requirements it will be convenient to begin by discussing data on waves alone since waves are the main cause of rolling. An indication will then be given of how the effects of adding wind forces can be taken into account by use of data in terms of joint probabilities of waves and winds.

2.3 Requirements for Wave Data
The rolling of a ship in waves is a highly nonlinear response which is sharply tuned to the natural roll period of the ship concerned

effects on a vessel in waves can be estimated by use of data expressed in terms of some specified mean value of the wind speed making suitable assumptions regarding its variability in time and space. For assessing the risks due to rolling in wind and waves the requirement is for data in the form of joint probability distributions of the mean wind speed with the relevant wave parameters such as significant wave height and zero crossing period, discussed in the previous section.

The data for the high risk areas briefly reviewed in a later section is in the form of joint probability distributions of wind speed and wave height. Joint probabilities of wind speed and wave period are not included but in practice it is considered reasonable to choose an extreme level of wind speed by consideration of its joint probability of occurrence with wave height. Data on the joint probability of wind speed and wave period representative both of limited fetch and open ocean areas may be found in reference [4], indicating a relatively weak correlation between these paramaters.

2.5 Applications to Design Case Assessment

For design case purposes it must be appreciated that the most severe rolling will be associated with waves having a modal period T_p (the period corresponding to the peak energy of the spectrum) in the neighbourhood of the natural roll period T_c. This is recognised for example in the formulation of the IMO weather criterion from which fig.1 is cited. The criterion for determining the limiting windward roll angle ϕ_1, is in fact specified in terms which may be written (See Yamagata [5]) in notation matched to the present context in the form:

$$\phi_1 = M(X_n)\sqrt{S}$$

Where $M(X_n)$ may be interpreted as a magnification factor for rolling at the critical period T_c and is specified in terms of various ship design parameters X_n.

S defines a wave steepness (height H/length λ, where $\lambda = [g/(2\pi)]T^2)$ to serve as a measure of the maximum surface slope to be expected for waves of period $T=T_c$ and is specified as a function of T. For ocean going vessels S is given by the formula:

$$S=0.151-0.0072\ T_c$$

As an illustration of the application of data in the form shown in figure 2 it may be of interest to indicate briefly a simplified basis for estimating the expected maximum steepness S_m for a design wave of a given period $T=T_c$. Writing $S_m= H_m/\lambda$, the requirement is to determine a value for H_m the maximum height of an individual wave to be expected in the most severe sea state having a modal period $T_p=T_c$. In using the data in fig. 2 for this purpose it is a reasonable approximation to assume ([1] and [18]) that the zero crossing period $T_z=T_p/1.4$ and that H_m may be estimated from the significant height H_s using the relation $H_m=kH_s$ where $k= (1/2 \ln N)^{1/2}$ and N is the number of waves encountered in the sea state concerned. For a 12 hour storm assuming an average period of 10 seconds, N=4320 and k=2.

Consider for example the case $T_c=9$ seconds. The requirement is to estimate a maximum value for H_m for sea states with modal period $T_p=9$ seconds. The corresponding value of T_z is 6.4 seconds which lies in the range $6<T_z<6.5$ seconds defined in fig 2. As a rough estimate for illustrative purposes it may be seen by inspection of the data in fig 2 that the relevant maximum value for H_s is about 6_m and taking k=2 gives $H_m=12m$. Also the wave length

for a wave with period $T=T_c$ may be found using the above formula relating λ and T to be $\lambda=126m$, and hence $s_m=12/126=0.095$. This is slightly greater than the value S=0.086 given by the formula relating S and T cited above [5]

The foregoing is one highly simplified illustration of an application to one particular example of a design case formulation. In practice there are many other possibilities for defining design criteria for which such data can be used (See for example references [6] and [7]). Data in this form are also suitable for use in probabilistic analysis which is important for ensuring that design case criteria effectively cover all the worst case conditions at an appropriate risk level.

2.6 Applications to Probabilistic Assessment

As explained earlier the forms of wave data illustrated in fig.2 can be used to describe the long term wave climate in terms of a population of short term sea states each of which can be characterised by a parametric spectrum offering a realistic statistical description of all the relevant wave motions. In principle, therefore, they can offer a
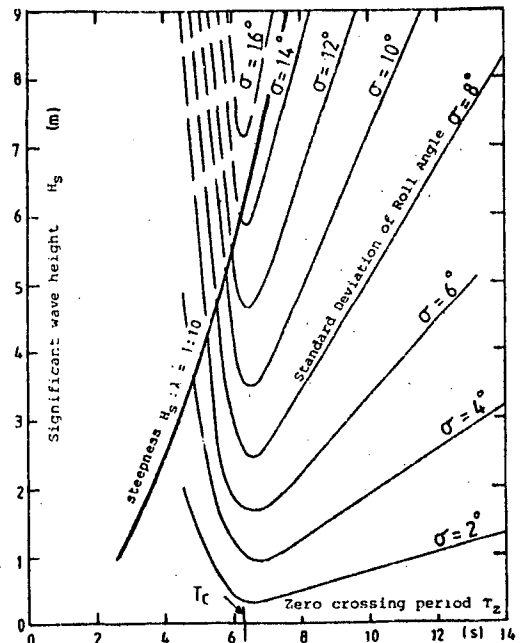
a) Standard Deviation of Roll Angle as a function of Wave Height and Period.
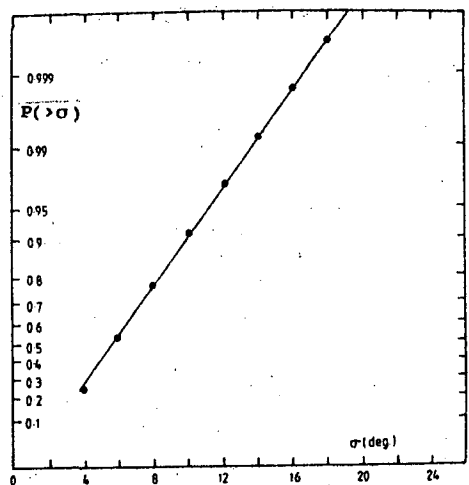
b) Exceedance Probability for the Standard Deviation of Roll Angle.

Figure 3 Roll Response Statistics

realistic statistical description based on a summation of all the spectra in the long term population, of all the individual wave motions likely to be encountered over a period of years spanning the life of a ship. Such a description moreover offers a basis for a corresponding modelling of the short term and long term statistics of all the individual roll motions experienced, for use in probabilistic assessment of stability.

There is only space here for a highly simplified indication of the ideas underlying such applications for the data and a brief reference to an example with which the author has been associated (See reference [8] and [9]).

It will be convenient to begin by considering applications to assessment of stability in individual sea states and then indicate how long term statistics can be derived by a process of summation of the behaviour in the individual sea states.

Roll motion in individual sea states can be investigated by use of theoretical or experimental modelling. In both cases the use of a spectral description of the waves ensures valid representation of the relevant statistical properties such as probability distributions and associated extreme values of wave heights, periods and slopes and the grouping of high waves. Most of these properties can be estimated theoretically and a number of formulae are available for modelling realistic spectra in terms of parameters such as significant height and zero crossing period (see fig 2).

Reference has already been made to a theoretical formula for estimating the most probable maximum height of an individual wave in a sequence of N waves. It may be of interest to refer here also to the estimation of grouping properties which can have a critical effect on extreme rolling, due to the cumulative build up of roll angle which can be caused by a sequence of high waves. Grouping properties can be studied either theoretically or by use of numerical or physical models [10] to [12]. A key parameter is the mean number of successive waves exceeding a given height threshold. This may be referred to as the 'run length' L_1, and may be estimated for a given height threshold H_1, by use of the formula [11].

$$L_1 = [1 - \exp(-2H_1^2/H_S^2)]^{-1}$$

An example of such a probabilistic analysis is described in detail in reference [8] (see also reference 9). It must suffice here for illustrative purposes to refer briefly to the sample of roll response data in fig. 3 to indicate how it can be used in association with the wave data in fig. 2 for deriving long term statistics of extreme rolling. Fig 3 shows contours of the standard deviation σ of roll motion determined for a particular ship by use of spectral modelling of individual sea states characterised by the respective values of H_S and T_Z. The probability P(σ) that σ will be in a given interval between 2 contours can be computed by integrating the probability density $P(H_S, T_Z)$ defined by the wave data in fig. 2 over the corresponding area of the H_S, T_Z plane. On this basis the long term wave data can be translated into long term statistics of roll motion, which may include as shown in fig. 3b) the probability P(>σ) that a given value of σ will be exceeded.

In practice it is of course important to ensure that the wave data used adequately represent

the conditions to be encountered in service. This question which calls for consideration of such factors as the duration of exposure in any given area and the effect of heading on the periods of wave encounter, is discussed in detail in reference [8].

3. DATA FOR HIGH RISK AREAS

In planning the provision of data for high risk areas it was first necessary to establish a clear criterion for identifying a suitable selection of such areas. A schedule for the scope of data to be provided to meet the practical requirements discussed in the previous chaper had then to be worked out.

3.1 Selection of Areas
In selecting the areas, it was assumed that in the context of stability assessment concern should be with high risks of loss due to capsize in severe weather. The criterion adopted for identifying such risks was based mainly on statistics for weather related casualties derived from the Department of Transport, Lloyds Shipping Information Services and a paper by Quayle [13].

Fig.4 shows a map of the global density distribution of weather related casualties per 15°square compiled using data from the above sources. After a careful study of all the relevant information including data on the global distribution of various environmental hazards, 5 main areas of high risk were selected as shown in fig 4b).

A detailed discussion of the basis of selection may be found in reference [1] and for the present some rather brief comments must suffice. A key point to be made about the selection criterion adopted is that the casualty incidence was assessed in terms of the actual number of weather related losses and not surprisingly it was found that this number is strongly correlated with traffic density. This means that areas selected by this criterion will not include regions of severe weather, where the traffic density is low. It may be noted for example that the 5 selected areas do not include the seas off Cape Horn where it is known that there is a high incidence of very severe weather, because the traffic density is relatively low.

The criterion adopted was nonetheless felt to be justified for two main reasons. The first is that it would be unrealistic to provide data for all areas of severe weather irrespective of the existence of traffic. The second is that severity in the context of stability assessment has widely different meanings for different ships and is not simply dependent on extreme values of specific weather parameters. It is thus difficult to define a relevant criterion of weather severity which is not somehow related to casualty risk information or some form of feedback from ship traffic.

It is recognised of course that there will be many requirements for assessment of the severity of weather conditions in areas not covered by the present investigation. Attention is, therefore, drawn to a book with the title 'Global Wave Statistics' [14] due for publication later this year which should meet most requirements.

3.2 Provision of Data
In chapter 2 it was explained how data in the form of joint probability distributions P(H,T) of wave height and period accompanied by joint probability distributions P(H,W) of wave height and wind speed can be used to meet most

Figure 4 Selection of High Risk Areas
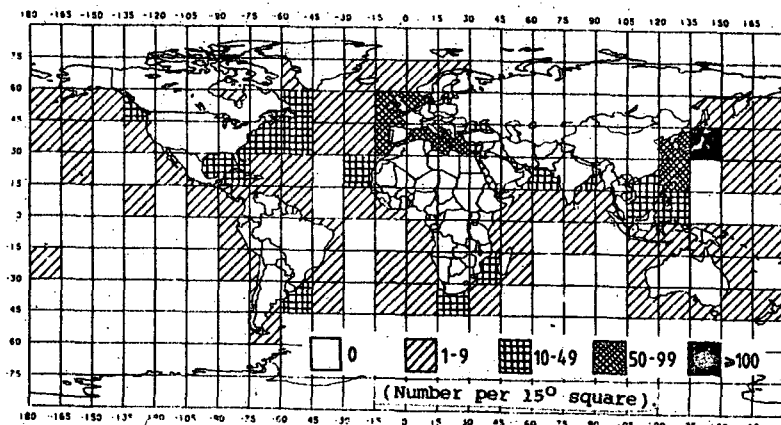
a) Incidence of Weather Related Losses
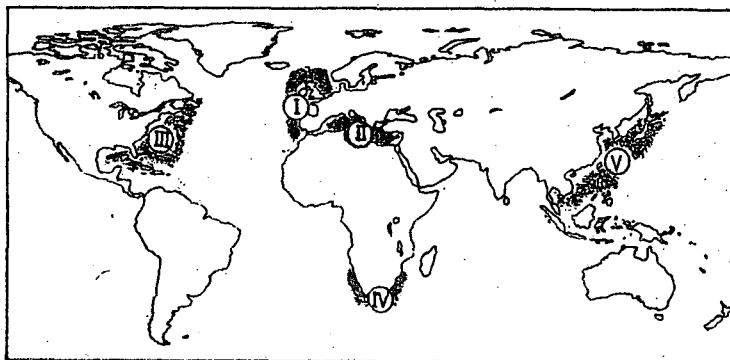
b) The 5 Selected High Risk Areas.

a) An Impression of the Global Distribution of Visual Observations.
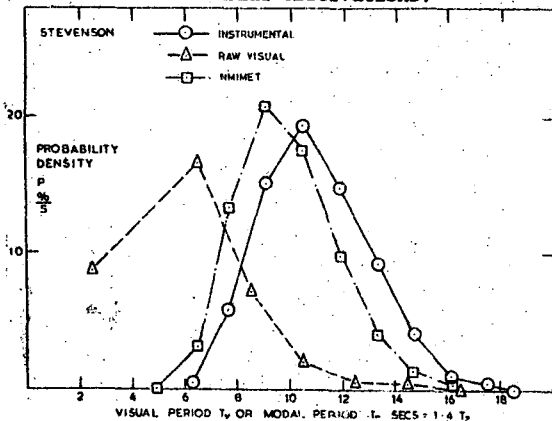
b) A Comparison of NMIMET and Visually Observed Wave Period Statistics with Measured Data (at Station Stevenson, 61°20'N, 0°).

Figure 5 NMIMET Wave Climate Data

requirements for wave and wind data. Brief mention was also made of the relevance to stability assessment of data on currents and on icing, citing reference [1] for more detailed information about the significance and availability of such data.

The present concern is with the provision of suitable data for the 5 high risk areas shown in fig 4b. A full account of the derivation of this data accompanies its presentation for all the chosen areas in reference [1]. There is only space here to offer some brief comments about derivation concentrating attention on the wave and wind statistics and to cite a small illustrative sample of such data presented for one of the selected areas.

There are various sources of wave and wind data which may be classified under the 3 main headings 'instrumental', 'hindcast' (derivation of wave data from wind field information) and 'visual observations'. The data for the 5 selected areas was derived from the global archive of visual observations of waves and

winds held by the UK Meteorological by use of a reliability enhancing program called NMIMET [15]to[17]. The reasons for this choice are explained in detail in reference [1]. the key advantages of the use of the NMIMET program are that it is an extensively validated capability offering data of homogeneous quality readily available in the required format, including both wave and wind data, for systematic coverage of all the 5 areas.

It is of course accepted that instrumental data are generally the most reliable but they are not suitable for the present purpose because of their limited availability. The reliability of the NMIMET data has been extensively documented by comparisons with instrumental data [15] to [17]. It is achieved by use of parametric modelling of the joint probability distributions of wave heights and wind speeds and of wave heights and periods. A key feature of the program is that it derives the statistics of wave period from the wave height observations by use of a joint probability model based on instrumental data and thus avoids any use of the visual observations of period which are notoriously unreliable. This point is particularly important because of the critical influence of wave period on ship rolling and its significance is underlined by the sample comparison of NMIMET and visually observed wave period statistics with instrumental data shown in fig 5b).

3.3. Sample of Data from Area V.

For each of the 5 areas a standard range of documentation is provided, supplemented as appropriate by additional information of special interest in specific areas. The standard items of documentation are:

1. A short commentary
2. Map of: 'Weather related casualties'
3.   'Bathymetry, wind climate and currents'
4.   'Instrumental data sites'
5.   'Observation counts for the NMIMET wave data'
6.   'Subareas covered by NMIMET wave and wind data'
7. Address list: 'Area representative with knowledge of instrumental wave data in the area'.
8. NMIMET Data: 'Wave height and period probabilities P(H,T)

     Wave height and wind speed probabilities P(H.W.)'

An illustrative selection of data from Area V is shown in the accompanying figures. It will be seen that in addition to samples of the above items 2,3,6,8 and 9, a map of 'Winter Gales and Tropical Storms' is also included.
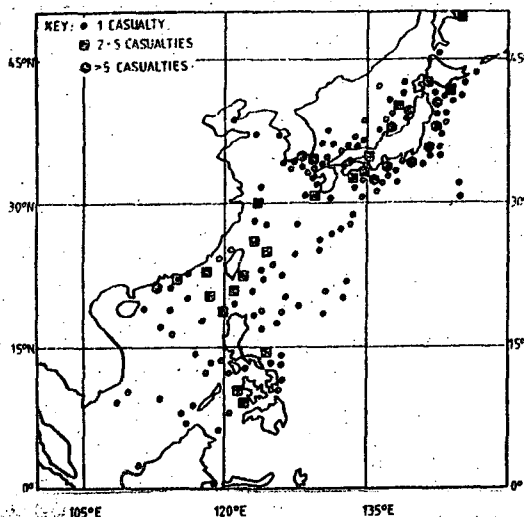
a) Weather Related Losses
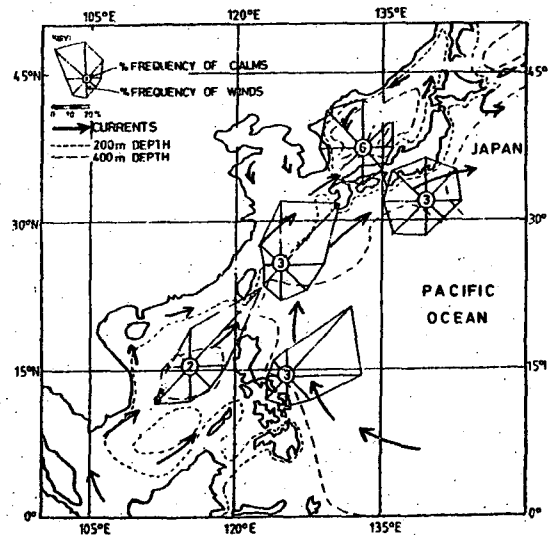
b) Bathymetry, Wind Climate and Currents
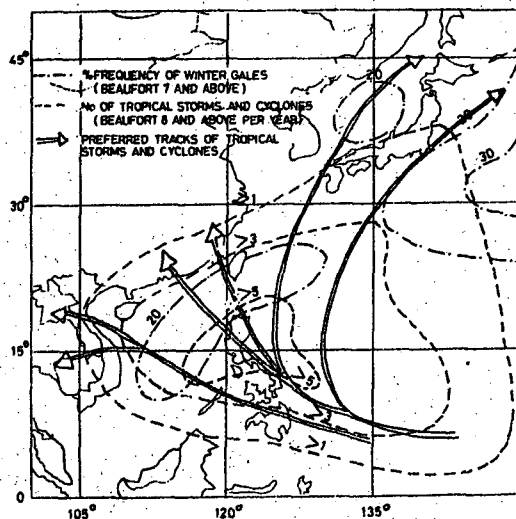
c) Winter Gales and Tropical Storms
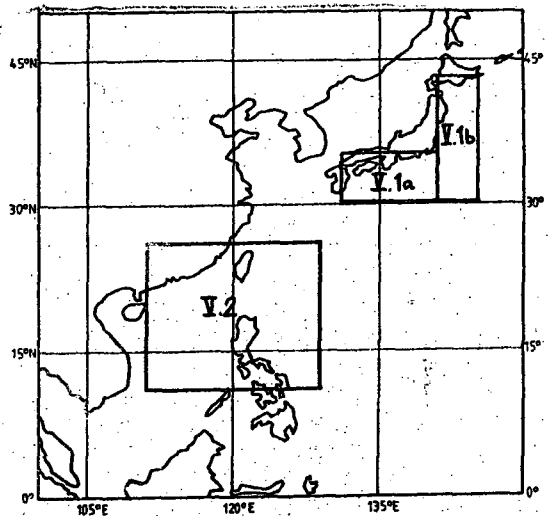
d) Map of Subareas covered by NMIMET data

Figure 6 Sample Selection of Data Provided for a High Risk Area (Area V)

SYNTHESIZED JOINT PROBABILITY DISTRIBUTION OF HEIGHT AND PERIOD DERIVED FROM SMOOTHED WAVE HEIGHTS (PARTS PER THOUSAND)

|	TOTAL	.0	3.8	96.2	202.1	295.2	237.9	128.1	92.3	17.6	5.1	1.4	.3	.1	.0	.0	.0	1000
W 15.0 TO 15.5	.0	.0	.0	.0	.0	.0	.0	.0	.0	.0	.0	.0	.0	.0	.0	.0	.0
A 14.5 TO 15.0	.0	.0	.0	.0	.0	.0	.0	.0	.0	.0	.0	.0	.0	.0	.0	.0	.0
V 14.0 TO 14.5	.0	.0	.0	.0	.0	.0	.0	.0	.0	.0	.0	.0	.0	.0	.0	.0	.0
E 13.5 TO 14.0	.0	.0	.0	.0	.0	.0	.0	.0	.0	.0	.0	.0	.0	.0	.0	.0	.1
13.0 TO 13.5	.0	.0	.0	.0	.0	.0	.0	.0	.0	.0	.0	.0	.0	.0	.0	.0	.1
H 12.5 TO 13.0	.0	.0	.0	.0	.0	.0	.0	.0	.0	.0	.0	.0	.0	.0	.0	.0	.1
E 12.0 TO 12.5	.0	.0	.0	.0	.0	.0	.0	.0	.0	.0	.0	.0	.0	.0	.0	.0	.2
I 11.5 TO 12.0	.0	.0	.0	.0	.0	.0	.0	.1	.0	.0	.0	.0	.0	.0	.0	.0	.2
G 11.0 TO 11.5	.0	.0	.0	.0	.0	.0	.1	.1	.0	.0	.0	.0	.0	.0	.0	.0	.2
H 10.5 TO 11.0	.0	.0	.0	.0	.0	.1	.1	.1	.0	.0	.0	.0	.0	.0	.0	.0	.3
T 10.0 TO 10.5	.0	.0	.0	.0	.0	.1	.1	.1	.0	.0	.0	.0	.0	.0	.0	.0	.4
9.5 TO 10.0	.0	.0	.0	.0	.1	.1	.2	.1	.1	.0	.0	.0	.0	.0	.0	.0	.7
C 9.0 TO 9.5	.0	.0	.0	.0	.1	.1	.3	.1	.1	.0	.0	.0	.0	.0	.0	.0	1.0
L 8.5 TO 9.0	.0	.0	.0	.0	.1	.3	.3	.3	.1	.1	.0	.0	.0	.0	.0	.0	1.4
A 8.0 TO 8.5	.0	.0	.0	.0	.1	.4	.5	.2	.1	.1	.0	.0	.0	.0	.0	.0	1.9
S 7.5 TO 8.0	.0	.0	.0	.0	.4	.6	.7	.5	.1	.1	.0	.0	.0	.0	.0	.0	2.5
S 7.0 TO 7.5	.0	.0	.0	.2	.1	.4	1.0	.7	.4	.1	.0	.0	.0	.0	.0	.0	3.5
E 6.5 TO 7.0	.0	.0	.0	.1	.6	1.2	1.0	.9	.4	.1	.0	.0	.0	.0	.0	.0	4.9
S 6.0 TO 6.5	.0	.0	.0	.0	.9	1.8	1.8	.9	.5	.2	.1	.0	.0	.0	.0	.0	6.8
5.5 TO 6.0	.0	.0	.0	.3	1.4	3.0	1.6	1.2	.6	.2	.1	.0	.0	.0	.0	.0	9.6
I 5.0 TO 5.5	.0	.0	.0	.3	2.2	3.8	3.0	1.6	.7	.3	.1	.0	.0	.0	.0	.0	13.6
N 4.5 TO 5.0	.0	.0	.1	.9	3.4	5.6	4.9	2.1	.9	.3	.1	.0	.0	.0	.0	.0	19.4
M 4.0 TO 4.5	.0	.0	.1	1.5	5.3	8.4	6.8	3.0	1.2	.4	.1	.0	.0	.0	.0	.0	28.0
E 3.5 TO 4.0	.0	.0	.2	2.7	9.0	12.4	9.4	4.6	1.7	.5	.1	.0	.0	.0	.0	.0	40.7
T 3.0 TO 3.5	.0	.0	.5	5.0	14.6	18.2	12.6	5.7	2.0	.5	.1	.0	.0	.0	.0	.0	59.3
R 2.5 TO 3.0	.0	.0	1.0	9.2	23.8	26.3	16.3	6.7	2.1	.5	.1	.0	.0	.0	.0	.0	86.2
E 2.0 TO 2.5	.0	.0	2.3	17.3	37.8	39.2	19.7	7.3	2.0	.5	.1	.0	.0	.0	.0	.0	123.3
S 1.5 TO 2.0	.0	.1	5.3	31.7	96.7	45.3	21.0	6.7	1.7	.3	.1	.0	.0	.0	.0	.0	168.8
1.0 TO 1.5	.0	.4	12.1	53.0	72.1	45.4	17.0	4.5	.9	.2	.0	.0	.0	.0	.0	.0	205.7
.5 TO 1.0	.0	1.4	22.8	62.6	57.3	25.4	7.1	1.4	.2	.0	.0	.0	.0	.0	.0	.0	178.5
.0 TO .5	.0	1.7	11.8	16.9	8.8	2.4	.4	.1	.0	.0	.0	.0	.0	.0	.0	.0	42.1
	2.5	3.5	4.5	5.5	6.5	7.5	8.5	9.5	10.5	11.5	12.5	13.5	14.5	15.5	16.5	17.5	TOTAL

MEAN ZERO-CROSSING PERIOD IN SECONDS

SMOOTHED BIVARIATE FREQUENCY OF VISUAL WAVEHEIGHT AND WINDSPEED

	TOTAL	1437.0	3192.0	5868.0	7484.0	7043.0	4626.0	2585.0	1330.0	565.0	204.0	89.0	21.0	7.0	34431		
15.5 TO 16.0	.0	.0	.0	.0	.0	.0	.0	.0	.0	.4	.5	.3	.2	1.3	H	.00
W 15.0 TO 15.5	.0	.0	.0	.0	.0	.0	.0	.0	.3	.5	.6	.3	.2	2.0	H	.01
A 14.5 TO 15.0	.0	.0	.0	.0	.0	.0	.0	.0	.4	.6	.8	.4	.2	2.5	E	.01
V 14.0 TO 14.5	.0	.0	.0	.0	.0	.0	.0	.0	.6	.8	1.0	.5	.2	3.2	I	.01
E 13.5 TO 14.0	.0	.0	.0	.0	.0	.0	.0	.9	1.1	1.2	.5	.3	4.0	G	.01
13.0 TO 13.5	.0	.0	.0	.0	.0	.0	.0	1.2	1.4	1.5	.6	.3	5.0	H	.01
W 12.5 TO 13.0	.0	.0	.0	.0	.0	.0	.9	1.7	1.8	1.8	.7	.3	7.2	T	.02
E 12.0 TO 12.5	.0	.0	.0	.0	.0	.0	1.3	2.3	2.1	.8	.3	9.2		.03
I 11.5 TO 12.0	.0	.0	.0	.0	.0	.9	3.1	3.0	2.5	1.9	.3	11.7	P	.03
G 11.0 TO 11.5	.0	.0	.0	.0	.0	2.8	4.1	3.7	3.0	1.0	.4	15.0	R	.04
H 10.5 TO 11.0	.0	.0	.0	.0	.0	4.0	5.5	4.6	3.4	1.1	.4	19.0	O	.06
T 10.0 TO 10.5	.0	.0	.0	.0	2.6	5.0	7.3	5.6	3.9	1.1	.4	26.7	B	.08
9.5 TO 10.0	.0	.0	.0	.0	4.1	8.2	9.5	6.8	4.4	1.2	.4	34.6	A	.10
C 9.0 TO 9.5	.0	.0	.0	.0	6.3	11.5	12.3	8.1	4.7	1.2	.3	44.6	B	.13
L 8.5 TO 9.0	.0	.0	.0	.0	9.5	16.0	15.7	9.6	5.3	1.2	.3	57.6	I	.17
A 8.0 TO 8.5	.0	.0	.0	6.0	14.4	21.9	19.7	11.0	5.7	1.2	.3	80.2	L	.23
S 7.5 TO 8.0	.0	.0	.3	10.0	21.5	29.6	24.3	12.5	5.9	1.2	.2	105.3	I	.31
S 7.0 TO 7.5	.0	.0	.0	16.5	31.7	39.5	29.6	13.8	6.0	1.1	.2	138.3	T	.40
E 6.5 TO 7.0	.0	.0	.0	27.0	46.0	51.6	34.9	14.9	5.9	1.0	.2	181.6	Y	.53
S 6.0 TO 6.5	.0	.0	.0	16.9	43.4	65.8	66.2	40.3	15.6	5.7	.9	.2	254.9		.74
5.5 TO 6.0	.0	.0	.0	31.0	68.7	92.1	82.8	45.3	15.8	5.2	.7	.1	341.8	P	.99
I 5.0 TO 5.5	.0	.0	13.3	56.0	106.8	126.1	100.7	49.1	15.4	4.5	.6	.1	472.7	E	1.37
N 4.5 TO 5.0	.0	.0	.9	29.5	99.3	162.4	167.9	118.3	51.2	14.3	3.8	.4	.1	647.1	R	1.88
4.0 TO 4.5	.0	.0	10.2	63.8	172.1	240.1	216.0	133.3	50.7	12.5	2.9	.3	.0	901.8		2.62
M 3.5 TO 4.0	.0	.0	30.7	133.8	283.7	343.2	266.4	142.5	47.2	10.1	2.1	.2	.0	1265.8	C	3.68
E 3.0 TO 3.5	1.4	12.1	89.1	269.8	469.5	465.4	311.0	142.4	40.4	7.5	1.3	.1	.0	1814.0	E	5.27
T 2.5 TO 3.0	12.1	58.5	239.2	515.1	723.8	605.4	337.6	130.1	31.1	4.9	.7	.0	.0	2659.6	N	7.72
R 2.0 TO 2.5	77.2	234.3	576.9	917.1	1040.0	718.9	330.7	104.8	20.6	2.4	.3	.0	.0	4024.0	T	11.69
E 1.5 TO 2.0	326.6	701.7	1182.9	1458.2	1364.3	754.0	277.7	69.7	10.8	1.1	.1	.0	.0	6127.0		17.80
S 1.0 TO 1.5	675.1	1290.0	1845.7	1923.1	1454.1	641.6	179.8	33.7	3.9	.3	.0	.0	.0	8047.3		23.37
.5 TO 1.0	326.0	873.5	1646.5	1729.7	1092.3	356.0	68.5	8.5	.6	.0	.0	.0	.0	6101.5		17.72
.0 TO .5	1.2	20.4	223.0	428.0	240.0	46.7	4.3	.2	.0	.0	.0	.0	.0	963.9		2.80
	0	1	2	3	4	5	6	7	8	9	10	11	12	TOTAL		

VISUAL WINDSPEED CLASSES IN BEAUFORT NUMBER

| .2 | 1.7 | 6.8 | 9.7 | 13.4 | 18.6 | 24.4 | 30.6 | 37.3 | 44.4 | 51.8 | 59.8 | 68.0 |

VISUAL WINDSPEED CLASSES IN KNOTS (MID-CLASS VALUES)

e) NMIMET Data

Figure 6 Sample Selection of Data Provided for a High Risk Area (Area V)

4. WIND EFFECTS ON VESSELS IN WAVES

A separate study of the combined effects of wind and waves on vessels was carried out, using both recently acquired wind data and model experiments. Especially where small vessels are concerned, it is dangerous to ignore wind forces and assume that wave forces, together with a safety factor to cover wind, can account for extreme motion and capsize. For example, some vessels have a much higher freeboard than others.

The IMO recommendations for stability [3] include the effects of wind (figure 1), assuming that this can be done by applying a worst case gust of 1.5 times the steady wind, from the time when the vessel is rolled farthest to windward. For stability, the net work done during a roll to the downflooding angle ϕ_f must be negative (area 'b' > area 'a'), as otherwise the roll will increase beyond the downflooding angle and the vessel capsize. With this in mind, BMT have studied recent offshore wind data, and carried out limited model tests in wind and waves.

4.1 Full-Scale Wind Measurements

Probably the most useful set of data available, in the present context, comes from the BMT wind measurement programme on BP's West Sole "A" gas platform (53°42'N, 1°9'E), a project supported by the UK Dept. of Energy. The advantages of this data set are that both processed and detailed raw data are available, and also that all the data are immediately available to BMT in a form that allows easy access to special purpose processing.

The BMT West Sole project [20] collects data from small cup anemometers mounted at 7 levels from 10m to 85m above sea level, and a single wave staff. The instruments are sampled twice per second, and the readings processed immediately to give the 3-minute mean value and turbulence intensity, and the maximum 3-second gust over 3 minutes. The wave staff samples are also processed to give the 20-minute mean level and rms level, together with the maximum height (peak-to-trough) in each 20 minutes. All these 3-minute values are then recorded on digital tape to provide a continuous record, interrupted only by so called "fast

experiments" or system failures. "Fast experiments" are 2½ hour periods of rapid data sampling (5 readings per second) where all the samples are stored. They occur under specified conditions of steady mean wind speed and direction, mainly at high wind speeds.

The data provided by this experiment are very pertinent to the problems of wind and wave loads on ships which call for information about the timewise and spatial variation of wind velocity. They can provide mean wind and turbulence level profiles over the range of heights important to vessels, as well as 3-second gust values, for a wide range of wind strengths. In addition, the samples from the fast experiments can be processed to provide additional information for the high wind speeds that represent the most important case. For instance, single- point spectra (figure 7) provide information on the energy levels in the turbulence at frequencies close to the natural roll frequency of the vessel. Likewise, two-point correlations of signals from different anemometers (figure 8) can yield estimates of the typical spatial extent of a gust, which could reduce the total wind load experienced by a vessel subjected to a sudden gust in, say, the Japanese weather criterion [5] if the correlated area were smaller than the exposed area of the vessel.

Detailed findings from the West Sole data relevant to the present context concern information about the vertical profile and the timewise and spatial variation of the wind velocity associated with a specified mean wind speed. Regarding the vertical profile it was found that the presently available analysed mean profile data (figure 9) cluster fairly well around a 1/8 power law curve, more or less independent of wind speed over the range 15-25m/s. Apart from West Sole, the best modern source of data seems to be the Draft extension of lattice tower code to Offshore Structures (hereafter called DOS, Reference [21]). DOS recommends a draft value of the exponent of 0.12 for $U_{10} < 30m/s$ and 0.13 for $U_{10} > 30m/s$. Over the very restricted range of heights (compared with the standard 10m measurement height), it is immaterial which exponent is chosen over which wind-speed range, but for convenience we suggest the uniform use of 0.12 at all wind speeds, giving a slight overestimate of the wind force at greater heights. This exponent is entirely consistent with our analysis of the West Sole data.
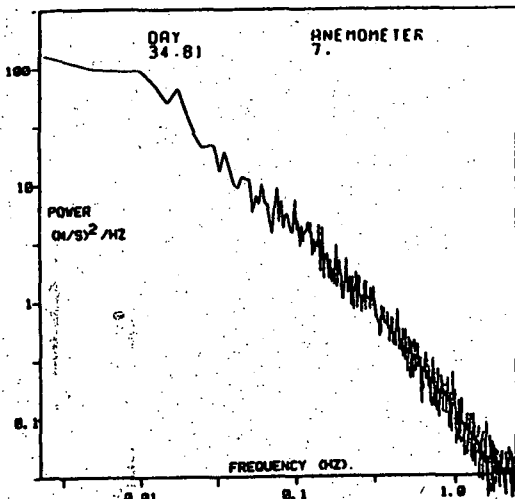

Figure 7   Turbulence spectrum of wind at height of 10m
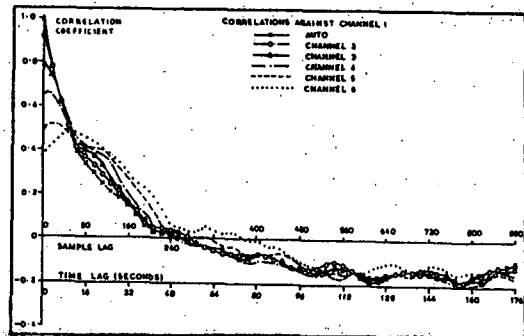
Figure 8   Wind velocity cross-correlation
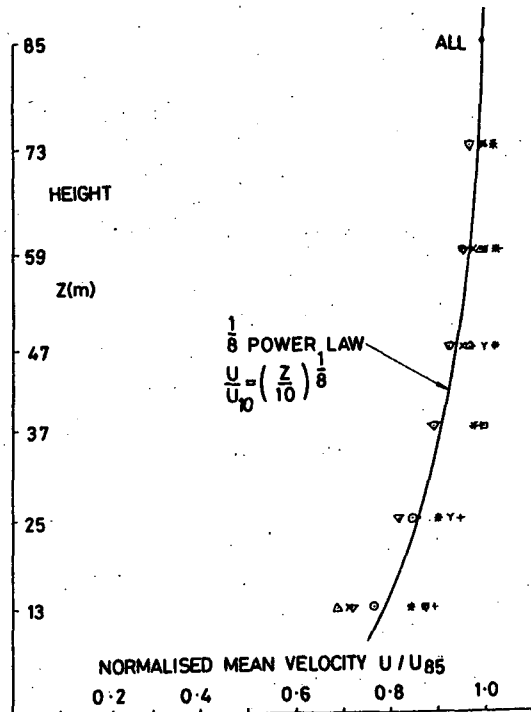
Figure 9   Mean wind velocity profile

Regarding the timewise variability, the turbulence intensity (rms velocity/mean velocity) obtained from the West Sole data averages about 9% of the local mean velocity at heights around 10-20m, and is again fairly independent of wind speed. Comparison of this figure with DOS is difficult because of the extremely complex method used to represent the recommended values, in which the turbulence level is normalised by a so called friction velocity u^*, which cannot be measured directly and must be inferred from mean velocity measurements for at least two heights. For engineering purposes it seems safe to assume a level of 10% based on the 10m height mean wind speed, U_{10}, the absolute intensity being constant with height.

In the present context the effect of the turbulence may be most simply estimated in terms of the widely accepted concept of the short duration uniform gust and associated gust factor. A common practice for example is to define a maximum 3 second gust as the maximum value of the 3 second running average of the instantaneous velocity. The gust factor is then this gust velocity normalised by the hourly mean velocity.

The West Sole experiment has produced 3-second gust values of $1.28U_{10}$ at 10m, decreasing slowly with height when normalised with the local mean velocity, and this appears to agree

with other offshore results obtained recently.
These values are significantly lower than those
generally assumed in the past, based on land
measurements where fluctuation levels are
usually higher, but are close to the Japanese
weather criterion, which assumes an effective
gust factor of 1.22 ($\sqrt{1.5}$).

The remaining question to be answered is that
of the spatial extent of the gusts. Figure 8
shows the correlation between wind speed
fluctuations at the 10m level and the higher
levels. This allows us to estimate both the
longitudinal and vertical scales of turbulent
motion directly, but not the lateral scale. The
vertical scale can be judged from the decay of
the maximum correlation between the 10m level
and greater heights. We see that the maximum
correlation remains greater than 0.7 even for a
vertical separation of 30m, so that as far as
small vessels are concerned, the gusts are
practically uniform in the vertical direction.
In the longitudinal direction, the
autocorrelation drops to 0.7 after 2 seconds
delay, and assuming that the mean time
variation is merely a spatial variation
convected at the local mean wind speed
(Taylor's hypothesis), this corresponds to a
longitudinal distance of about 40m. Although we
cannot estimate lateral scale from the West
Sole results, it seems reasonable to use the
ESDU data sheet on wind and turbulence data
(Reference [22]). These suggest a lateral scale
of 1.6 times the vertical scale at lower
levels, which would yield a lateral scale of
roughly 50m on our definition. Our definition,
however, is highly conservative; effectively,
the gusts are correlated over the whole side
area of a typical small vessel, so that any
gust applied to the vessel applies uniformly
over the whole exposed area. On a larger
vessel, say over 50m in length, some reduction
factor to allow for the finite volume of
correlated eddies might be possible, although
as the correlation lengths quoted are averages
over many eddies, we cannot be sure that a
larger eddy may not coincide with the most
unstable situation. It is therefore only safe
to assume fully correlated motion even over
larger vessels.

4.2   Application of Full-Scale Data to Capsize Prediction

Our study of the West Sole data and of existing
codes and those in preparation leads us to the
following recommendations:

(i)   The meteorological wind speed (that
referred to a height 10m above sea level) likely
to be encountered by a vessel very much depends
on the location of the vessel. In UK waters a
good estimate can be obtained from British
Standard 6235:1982 (Reference [23]), where
figure 2.2 shows the extreme 50-year hourly
mean at 10m. Close inshore, this may be as low
as 28m/s in some areas, but rises to 40m/s off
the West coast of Scotland. A commonly-assumed
value for North Sea installations is 38m/s, and
this should represent a safe value for exposed
areas around the UK. Over a wider area,
suitable figures can be obtained from our
comparison report on wave aspects (Reference
[1]), contained in the figures for joint
probability distributions of wind and waves for
different ocean areas.

(ii)   The variation of extreme mean
velocity with height, in those cases where it
is significant, can be represented by a power
law $U/U_{10} = (Z/10)^n$, with the exponent n equal
to 0.12.

(iii)   For conventional vessels, a gust
factor on velocity (running 3 second mean

velocity/overall mean velocity) of 1.28 should
be calculated (the corresponding factor on
force will be 1.28^2 or 1.64). For very high
vessels, the factor on velocity will be 1.28
$(Z/10)^{-0.03}$ in accordance with the behaviour
with height shown.

(iv)   The parts of the vessel exposed to a
beam wind should be considered separately as in
the IMO MODU Code 1980. For each part, a drag
coefficient C_D ("shape" coefficient in the
Code) should be assumed as follows:-

Shape	C_D
Spherical	0.4
Cylindrical	0.5
Large flat surface (hull, etc)	1.0
Isolated parts (cranes, masts)	1.5
Clustered structures	1.0

No allowance should be made for the fact that
the projected area reduces with heel angle,
since any reduction is roughly compensated by
increased exposed hull area.

The contributions to side force and overturning
moment should then be calculated, taking the
appropriate extreme mean at the centre of the
part, using

$$F = \tfrac{1}{2}C_D\rho U^2 A \quad N$$

$$M = \tfrac{1}{2}C_D\rho U^2 AZ \quad Nm$$

where Z is the distance from the centre of the
part to the centre of lateral resistance.
$\rho = 1.222kg\, m$ is the density of air.

(v)   Using the static stability curves,
the steady heel of the vessel may now be
calculated using the total heeling moment for
the extreme hourly mean wind.

(vi)   The roll amplitude appropriate to
the wave state should now be estimated. The
Japanese weather criterion[5] already cited in
an abbreviated form uses the formula
$\phi_1 = (138rs/N)^{\frac{1}{2}}$, where r is the effective
wave-slope factor $= 0.73 + 0.60\ OG_0/d$ (OG_0 is
the height of the C.G. above the water-line, d
is the mean draft), s the wave steepness can be
expressed in terms of vessel motion by:

$$s = 0.151 - 0.0072T \text{ for ocean-going ships}$$

$$s = 0.153 - 0.01T \text{ for coastal ships}$$

where T is the natural roll period of the ship,
and N is the assumed vessel damping of 0.02.
Clearly, other ways of estimating roll
amplitude are possible.

(vii)   The vessel is now assumed to start
from its extreme windward roll position, $\phi_1 -$
ϕ_0, and a gust load 1.64 times the steady wind
load is applied. For stability, area "b" in
figure 3 must remain larger than area "a" up to
the point of downflooding. We have applied this
analysis to the trawler model described in
Section 5.

The projected areas of the individual elements
of the model (hull, companion-way, wheelhouse,
masts and lifeboats) were measured from the
plans and scaled to full size. The wind force
acting on each area was then calculated,
assuming the appropriate C_D values and the wind
speed appropriate to the highest point of the
element. The wind force was assumed to act at
the centre of area of the element. For a range
of wind speeds, the wind moment arm was then
calculated using the gust factor of 1.28^2. The
static stability curve of the model was
measured, and after superimposing the constant
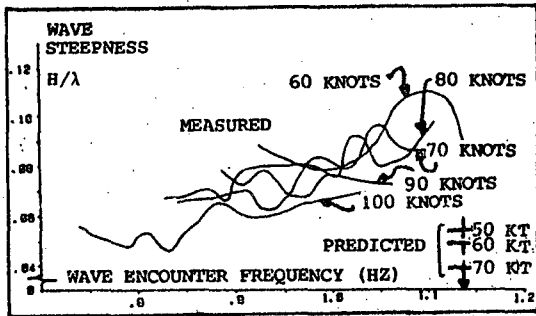
Figure 10   Measured and predicted capsize points

wind moment arm for different wind speeds, it was possible to estimate the wave steepness at the resonant wave frequency that would just make the vessel capsize, by finding the value of ϕ_1 that just makes area "a" equal to area "b". The results suggest the following:-

mean wind speed, kts	50	60	70
critical wave steepness	.055	.05	.04

These figures are compared in figure 10 with measured curves for different wave encounter frequencies, wind speeds and wave steepnesses. The results are difficult to compare because of the problem of generating good waves at the resonant wave encounter frequency, especially at higher wind speeds where the vessel is drifting quickly through the waves and lowering the wave encounter frequency below the resonant value. However, such evidence as has been gained shows that the predicted steepnesses are only about 60% of the values observed in the model tests. Several possible explanations present themselves, in addition to that of the difficulty of making representative tests on such a small model:

(i)   The effective wave steepness in the model tests is probably overestimated compared with that assumed in calculating the roll of the vessel. The model tests use very peaky wind-assisted waves whose steepness is calculated from the actual peak-trough height, whereas the "effective" wave height is that of a sinewave corresponding more to the trough shape.

(ii)   Although we were unable to estimate the damping coefficient of the small model accurately, it seemed to be much greater than the 0.02 assumed in the Japanese criterion. This coefficient is crucial in determining ϕ_1, and certainly in the model tests we never observed the large windward roll excursions that lead to such a large reduction in stability in the Japanese criterion.

Our conclusion from this comparison is that although the basis of the weather criterion for stability seems sound, great care is needed in determining the parameters that are fed into it, especially that on roll damping. The tests described in the next Section represent an attempt to clarify the situation by careful simulation of actual weather conditions.

4.3 Laboratory Model Tests

Tests were carried out on a 1:36 scale model of a typical small North Sea trawler in the BMT wind/wave facility (No. 9 tunnel) at Teddington. This type of model was chosen because (a) small vessels are in general more at risk, and (b) the small facility size requires a small vessel if excessively small scale modelling is to be avoided. The facility consists of a blower tunnel of 1.2m x 0.6m cross-section, blowing over a wave tank 12.5m

long x 1.2m wide x 1.4m deep. At the upwind end is a horizontal paddle wavemaker that can be programmed to produce any described motion, while the downwind end combines wind turning vanes and a beach. For these tests, the wavemaker was driven by a sinusoidal signal of various amplitudes and frequencies, producing regular waves of different wavelengths and steepness, while the windspeed could also be varied to simulate different wind strengths.

The model was a commercial kit with a vacuum-formed PVC hull whose lines and superstructure were typical of a small UK North Sea trawler. The model was fitted with a radio control of rudder and propeller, and ballasted to the fully-laden condition and a GM of 0.6m (full scale). The roll period was adjusted to the full-scale equivalent of 5.28 seconds.

An extensive series of tests was carried out on the effect of wind, wave height and wave period on the roll behaviour of the model in a regular beam sea. Some 300 combinations of wind and waves were set up, and for each the wave signal halfway along the tank was recorded. The model was then launched beam-on from a support cradle, the release time being chosen so that the model motion approached a free-rolling condition as rapidly as possible. The behaviour of the model was noted, and in roughly 90 cases the motion was recorded on video tape for later analysis of the development of rolling motion with time.

The wind and wave conditions investigated were chosen to represent a range of potentially dangerous situations that might be expected, say, in the North Sea. The conditions covered 60-100kt in wind speed, and wave periods from 4.5-7 seconds with associated heights in the range 1.5-4.5m.
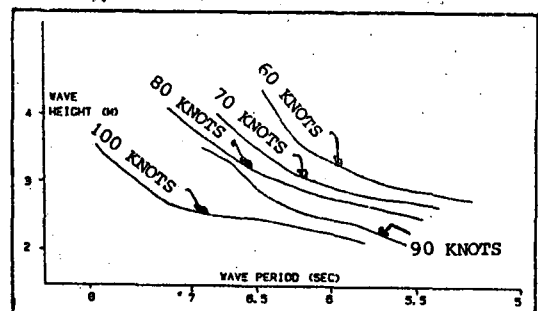

Figure 11   Effect of wind speed and wave height on capsize

Figure 11 shows the main result of the tests. The abscissa is the wave encounter frequency or period, and the ordinate the wave height. The curves show the boundary between the capsize and non-capsize regime for different wind speeds, and as the windspeed increases, the wave height needed to capsize the vessel decreases as expected. For example, whereas at 60kt a 6 sec wave of 3.5m is needed for capsize, at 90kt the necessary wave height is only 2.5m.

Some 20 capsize cases were analysed in detail from video recordings, to establish the sequence of events leading to capsize. A typical case is shown in figure 12. The heel angle shortly after launch is 12°, with a roll of ±13° superimposed. As time increases, the roll amplitude decreases, but the heel increases steadily. After four oscillations, water starts to be shipped over the lee rail as the vessel slides down the steep face of the wave before it has recovered from its maximum leeward roll. From this point on, the vessel is fighting a losing battle against water on deck

on the lee side, even though the freeing ports provide reasonable drainage. After the next wave peak, a smaller recovery allows more water to flood on deck, with a rapidly increasingly heel followed by capsize in the next trough. This mode of capsize is typical of conditions where the wave encounter frequency is slightly lower than the natural roll frequency, and the tests indicate, perhaps surprisingly, that the vessel is more unstable in these conditions than in the case where the wave encounter frequency is equal to the natural roll frequency. It is known that roll amplitude reaches a maximum at this coincidence. However, the position on the wave where the maximum roll occurs varies with the wave encounter/roll natural frequency ratio T_ϕ/T_W, and figure 13 shows how these results repeat well in our experiment. What is noteworthy is the fact that for T_ϕ/T_W less than 1, the maximum leeward roll occurs before the wave crest reaches the vessel, and similarly the maximum windward roll occurs before the wave trough. For T_ϕ/T_W greater than 1, the wave crest has passed before the maximum roll occurs. If we now add wind, observational evidence is more difficult because of the drift of the vessel and the non-stationary nature of the wave field, but the additional wind-induced heel puts the most vulnerable position just after the wave peak passes the vessel. For values of T_ϕ/T_W rather less than 1, say 0.9, what appears to happen is that the maximum leeward roll, occurring just before the crest passes, is greater because of the loss of restoring moment on the leeward face of the wave. The rapid passage of the wave crest under the vessel then floods the lee rail, holding the vessel at an angle from which it can escape only slowly as water drains from the freeing ports in the latter part of the wave cycle. Thus the heel is produced initially by the wind, but is later increased by the sustained effect of water on deck on the lee side, and eventually capsize results.
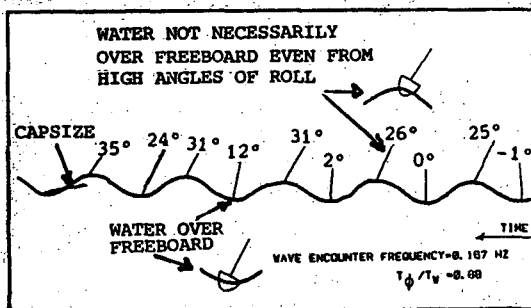

Figure 12 Capsize time history
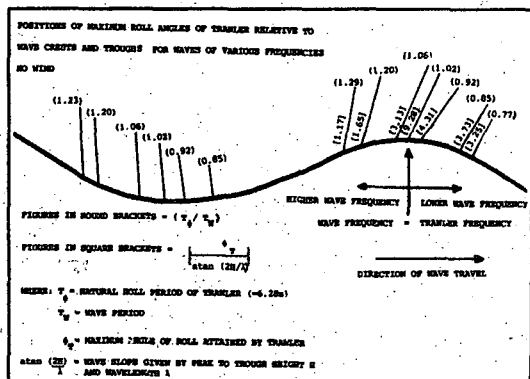
Figure 13 Maximum roll for different waves

5. CONCLUDING REMARKS

In this paper it has only been possible to present a very brief review of the investigations described more fully in reference [1] and [2]. Attention has here been concentrated on the derivation and use of wave and wind data for ship stability assessment in the context of regulatory criteria but in reference [1] information relating to data on currents and icing is also included.

The paper began with advice regarding the form and use of available wave and wind data, illustrated by some simple examples of applications under the headings of 'design case' and 'probabilistic analysis'. An account was then given of the compilation of systematic data provided in reference [1] for each of 5 selected areas of high risk, accompanied by a sample set of data for such an area including wave and wind statistics derived by use of a program called NMIMET. Finally an investigation of wind effects on vessels in waves including analysis of full scale measurements of winds over the sea and laboratory studies of models in a wind wave flume has been reviewed and procedures for application of the results to stability assessment have been summarised.

REFERENCES.

[1] ANDREWS, K.S.,DACUNHA,N.M.C and HOGBEN N. "SAFESHIP: Environmental Aspects. Part I Data for High Risk Areas" Report of NMI Ltd No. R185,1984.

[2] WILLS,J.A.B. COLE, L.R. and STOVOLD. A.J. "SAFESHIP:Environmental Aspects. PART 11 Wind Effects on Vessels" Report of NMI Ltd No. R186,1984.

[3] "Recommendation on Severe Wind and Rolling Criterion (Weather Criterion) for the Intact Stability of Passenger and Cargo Ships over 24 m in Length" Report of the Intergovernmental Maritime Organisation IMO MSC/circ 346, June 1983.

[4] HOGBEN. N. "Discussion of the Report of the Seakeeping Committee of the International Towing Tank Conference". Proc. 17th ITTC Vol. 2 pp 224 to 226, Gothenburg, September, 1984.

[5] YAMAGATA. M. "Standard of Stability Adopted in Japan". Trans. Royal Institution of Naval Architect. London 1959

[6] CALDEIRA-SARAIVA, F. "A Ship Stability Criterion based on Lyapunov's Direct Method" Paper presented to RINA Conference on the SAFESHIP Project, London, 1986.

[7] VASSALOS, D., KUO, C., ALEXANDER, G and BARRIE, D. "Using Theoretical Advances for Improving Ship Stability Criteria". Paper presented to RINA Conference on the SAFESHIP Project, London, 1986.

[8] ROBERTS, J.B. DACHUNHA, N.M.C. and HOGBEN N. 'The Estimation of the Long Term Roll Response of a Ship at Sea" Report of NMI Ltd No. R169 December 1983.

[9] ROBERTS, J. B. and STANDING R. G. 'A Probabilistic Model of Ship Roll Motion" Paper presented to RINA Conference on the SAFESHIP Project, 1986.

[10] Y. GODA. 'On Wave Groups" Proc BOSS'76 Conference vol.1,Trondheim, 1976.

[11] EWING. J.A. "Mean Length of Runs of High Waves" Jour.Geophys.Res.. VOL 78 No.12 pp 1933-1936,1973.

[12] RYE.H. "Ocean Wave Groups" Ph.D. Thesis,Division of Marine Hydrodynamics, Norwegian Institute of Technology Report No.82 18 Trondheim, November 1981.

[13] QUAYLE, R. G. "Weather and Maritime Casualty Statistics" Mariners Weather Log, March 1976.

[14] DACUNHA, N.M.C and HOGBEN N. "The Development of a New Global Atlas of Wave Statistics, "Journal of Navigation, London, January, 1985.

[15] HOGBEN. N. DACUNHA.N.M.C and ANDREWS K.S."Assessment of a New Global Capability for Wave Climate Synthesis" Proc. Oceans '83 Conference, San Francisco, September 1983.

[16] DACUNHA, N.M.C., HOGBEN. N. and ANDREWS K.S. "Waves Climate Synthesis Worldwide" Proc. RINA Symposium on Wave and Wind Climate Worldwide, London, April 1984.

[17] HOGBEN. N. and DACUNHA, N.M.C. "Wave Climate Synthesis: Some Recent Advances" Paper No. OTC 4938,Offshore Technology Conference, Houston, 1985.

[18] HOGBEN, N. "Basic Data Requirements: A Review with Emphasis on Wave and Wind Data" NMI Report No. R92, November 1980.

[19] FORTNUM, B.C.H. "Waves Recorded by M.V. Famita in the Northern North Sea (Winters 1969-1976)" IOS Report No. 59, 1978.

[20] WILLS, J.A.B. "Report on the West Sole wind structure project 1982". NMI Report R145, 1982.

[21] "Extension of lattice tower code to offshore mounted structures : Final Report". Dept. of Energy OT-R-82114, 1983.

[22] "Characteristics of wind speed in the lower layer of the atmosphere near the ground : strong winds (neutral atmosphere)". Engineering Services Data Item No. 72026, 1982.

[23] "Code of practice for fixed offshore structures". British Standard 6235 : 1982.

ZPPG/229/1/86/250